# THE JOURNAL OF

# PHYSICAL CHEMISTRY

# THE JOURNAL OF
# PHYSICAL CHEMISTRY

Notice to Authors last printed in the issue of June 10, 1971

**3A**

## AUTHOR INDEX

In papers with more than one author the name of the author to whom inquiries about
the paper should be addressed is marked with an asterisk in the by-line.

## ANNOUNCEMENT

On the last two pages of this issue you will find reproduced the table of contents of
the July 1971 issue of the *Journal of Chemical and Engineering Data.*

# The Reactions of Methylene with 1,2-Dichloroethane and Nonequilibrium

# Unimolecular HCl Elimination from 1,3-Dichloropropane,

# 1,4-Dichlorobutane, and 1-Chloropropane

## by K. Dees,[1] D. W. Setser,* and W. G. Clark

*Department of Chemistry, Kansas State University, Manhattan, Kansas 66502*   (*Received February 1, 1971*)

*Publication costs borne completely by The Journal of Physical Chemistry*

Methylene, produced by the photolysis of ketene, abstracts both H and Cl atoms from $1,2\text{-}C_2H_4Cl_2$. Experiments utilizing excess CO for removing $CH_2(^3\Sigma_g^-)$ revealed that $CH_2(^1A_1)$ mainly abstracts Cl atoms and $CH_2(^3\Sigma_g^-)$ mainly abstracts H atoms. Most products arising from monoradical combination reactions were identified, and their dependences on pressure (700–0.1 Torr) were investigated. The addition of small amounts of scavenger (butadiene or allene) was necessary at pressures below 1 Torr to alleviate complications, which were attributed to the presence of chlorine atoms. The half-quenching pressures with $1,2\text{-}C_2H_4Cl_2$ as the bath gas for the unimolecular reactions of the chemically activated molecules were: $1,2\text{-}C_2H_4Cl_2^*$, 11 Torr; $1,3\text{-}C_3H_6Cl_2^*$, 1.5 Torr; $1,4\text{-}C_4H_8Cl_2^*$, 0.40 Torr; and $1\text{-}C_3H_7Cl^*$, 6.5 Torr. The half-quenching pressure of CO for $1,3\text{-}C_3H_6Cl_2^*$ was 2.7 Torr. The experimental unimolecular reaction rates were interpreted according to the RRKM theory of unimolecular reactions; fair agreement was obtained between the calculated and experimental results providing that the threshold energy was permitted to decline from 60 to 52 kcal mol$^{-1}$ for the dichloroalkane series. There is some evidence that $C_3H_5Cl$ retained the major fraction of the vaailable energy from the $C_3H_6Cl_2^*$ elimination reaction.

## Introduction

The gas-phase reaction of methylene with a chloroalkane was first studied by Setser, Littrell, and Hassler;[2] $CH_3$ and $CH_2Cl$ radicals were produced by H and Cl abstraction from $CH_3Cl$. This reaction system and later work with methylene and $CH_2Cl_2$[3] permitted study of the nonequilibrium unimolecular HCl elimination reactions from $C_2H_5Cl$ and $1,2\text{-}C_2H_4Cl_2$ formed by radical combination. The rate constants were successfully interpreted by the RRKM theory of unimolecular reactions using a four-centered HCl elimination model for the activated complex which was defined by specifying the order of the bonds undergoing rearrangement. The usefulness of this four-centered complex was documented by additional studies of unimolecular eliminations from $C_2H_5Br$, $1,2\text{-}C_2H_4Br_2$, $1,2\text{-}C_2H_4Br\text{-}Cl$,[4] $1,2\text{-}C_2H_4F_2$,[5] and the kinetic isotope effects for $C_2H_5Cl$, $CD_3CH_2Cl$, $C_2D_5Cl$, $1,2\text{-}C_2H_4Cl_2$, and $1,2\text{-}C_2D_4Cl_2$.[6]

(1) Abstracted, in part, from the dissertation of K. Dees which was submitted in partial fulfillment for the Ph.D. degree, Kansas State University, 1970.

(2) (a) D. W. Setser, R. Littrell, and J. C. Hassler, *J. Amer. Chem. Soc.*, **87**, 2062 (1965); (b) J C. Hassler, D. W. Setser, and R. L. Johnson, *J. Chem. Phys.*, **45**, 3231 (1966).

(3) J. C. Hassler and D. W. Setser, *ibid.*, **45**, 3237, 3246 (1966).

(4) R. L. Johnson and D. W. Setser, *J. Phys. Chem.*, **71**, 4366 (1967).

(5) H. W. Chang and D. W. Setser, *J. Amer. Chem. Soc.*, **91**, 7648 (1969).

(6) (a) K. Dees and D. W. Setser, *J. Chem. Phys.*, **49**, 1193 (1968); (b) W. G. Clark, D. W. Setser, and K. Dees, submitted for publication in *J. Amer. Chem. Soc.*

The principal goal of this work was to measure the nonequilibrium unimolecular rate constants of chemically activated 1,3-$C_3H_6Cl_2$ and 1,4-$C_4H_8Cl_2$ produced by radical combination. A second goal was to study the overall reaction mechanism for $CH_2$ interacting with 1,2-$C_2H_4Cl_2$. The studies of Bamford and coworkers[7] have provided information about methylene reactions with 2 and 3 carbon monochloroalkanes; insertion into C–H bonds was competitive with H and Cl abstraction for the chloropropanes.

The photolysis of ketene gives a mixture of singlet ($^1A_1$) and triplet ($^3\Sigma_g^-$) methylene.[8] We attempted to use excess carbon monoxide to suppress[9,10] the reactions of $CH_2(^3\Sigma_g^-)$. Unfortunately this technique is not satisfactory at low pressures as shown by a complementary study of methylene with butane.[11,12] The excess CO technique was useful at high pressure for establishing the basic features of the interaction of $CH_2$-($^1A_1$) with 1,2-$C_2H_4Cl_2$, which is adequately described by abstraction of chlorine atoms followed by combination and disproportionation reactions of $CH_2Cl$ and $CH_2CH_2Cl$. In order to determine the nonequilibrium unimolecular rate constants low-pressure data were required and, under these conditions, singlet and triplet methylene as well as their associated secondary radical products simultaneously were present. A relatively complex overall mechanism then results.

## Experimental Section

Gas handling was done on a greaseless vacuum rack having either Hoke bellow valves or Springham valves utilizing viton-A diaphragms. Ground glass connections were made with Apiezon-W sealing wax. The vacuum system for the gas chromatograph inlet was also greaseless; the valves in this case were either Hoke or Nupro bellow valves. These precautions minimized absorption of reagents during sample preparation and recovery.

1,2-Dichloroethane, purchased from Matheson Coleman and Bell, was used without further purification. The carbon monoxide was Matheson CP grade. Ketene was prepared and purified as described previously.[6a] The reagents, which were condensable at 77°K, were measured in calibrated volumes using a spiral gauge to measure the pressure; these reagents subsequently were transferred into Pyrex vessels ranging in volume from 30 to 12,000 cc. Carbon monoxide was loaded by expanding the gas from a reservoir into the photolysis vessels, while maintaining the bottom tip of the vessel immersed in liquid nitrogen. The vessels contained glass beads and the filled vessels were warmed to room temperature and shaken by hand for 10 min before being photolyzed.

For experiments using carbon monoxide as the $CH_2$-($^3\Sigma_g^-$) scavenger, the 1,2-$C_2H_4Cl_2$:$CH_2CO$:CO ratios were 1.0:0.1–0.2:12; the quantity of 1,2-$C_2H_4Cl_2$ plus $CH_2CO$ was fixed at 2 cc (STP). Some experiments

utilized only $CH_2CO$ and $C_2H_4Cl_2$ as the reagents in the proportions just mentioned. For others 2–5% of 1,4-butadiene or allene was added.

The samples were photolyzed from 1 to 3 hr using the unfiltered light of a General Electric AH-6 high-pressure mercury arc. Previous calculations[9] for this lamp showed that the effective wavelength range is 3200 ± 200 Å for Pyrex vessels. Runs with no added ketene demonstrated that photolysis of $C_2H_4Cl_2$ was not important. After photolysis, the vessel was attached to the inlet system of the gas chromatograph and the entire contents were slowly pumped through a liquid nitrogen-cooled glass-wool packed trap. The condensable products were then transferred to the inlet of the gas chromatograph, a Perkin-Elmer 820 having a thermal conductivity detector.

The products from the photolysis were separated by a 12-ft 20% Apiezon-L column followed by a 15-ft 12% diisodecylphthalate column. Temperature programming was necessary.[12] Calibration factors for the compounds needed to obtain rate constants were obtained by checking with at least three independently prepared standards, which were nearly identical with actual reaction mixtures.

## Results

*High-Pressure Reaction Mechanism.* The high-pressure reaction mechanism was studied by adding excess CO to remove $CH_2(^3\Sigma_g^-)$. Experiments also were done in which $CH_2(^3\Sigma_g^-)$ was not scavenged and the additional products were attributed to $CH_2(^3\Sigma_g^-)$ reactions. By analogy with previous studies[7,9] the expected high-pressure reaction mechanism for the photolysis of ketene with 1,2-$C_2H_4Cl_2$ in which $CH_2(^3\Sigma_g^-)$ has been scavenged is

$$CH_2CO + h\nu\ (\sim 3200\ \text{Å}) \longrightarrow {}^1CH_2 + CO \quad (1)$$

$$^1CH_2 + ClCH_2CH_2Cl \longrightarrow CH_2Cl + CH_2CH_2Cl \quad (2)$$

$$CH_2Cl + CH_2Cl \longrightarrow ClCH_2CH_2Cl^* \quad (3)$$

$$CH_2Cl + CH_2CH_2Cl \longrightarrow ClCH_2CH_2CH_2Cl^* \quad (4)$$

$$CH_2CH_2Cl + CH_2CH_2Cl \longrightarrow$$
$$ClCH_2CH_2CH_2CH_2Cl^* \quad (5)$$
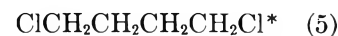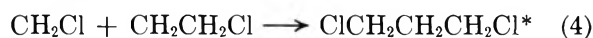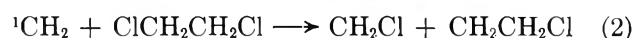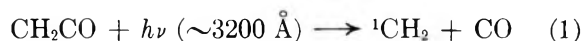
If triplet methylene is not removed, reactions 6–10 must be included.

(7) (a) C. H. Bamford, J. E. Casson, and R. P. Wayne, *Proc. Roy. Soc., Ser. A*, **289**, 287 (1966); (b) C. H. Bamford, J. E. Casson, and A. N. Hughes, *ibid.*, **306**, 135 (1968); (c) C. H. Bamford and J. E. Casson, *ibid.*, **312**, 141, 663 (1969).

(8) (a) A. N. Strachan and D. E. Thornton, *Can. J. Chem.*, **46**, 2353 (1968); (b) T. W. Eder and R. W. Carr, Jr., *J. Phys. Chem.*, **73**, 2074 (1969).

(9) W. G. Clark, D. W. Setser, and E. E. Siefert, *ibid.*, **74**, 1670 (1970).

(10) B. A. DeGraff and G. B. Kistiakowsky, *ibid.*, **71**, 3984 (1967).

(11) K. Dees and D. W. Setser, *ibid.*, **75**, 2240 (1971).

(12) K. Dees, Ph.D. Dissertation, Kansas State University, 1970.

$$CH_2CO + h\nu \; (\sim 3200 \; \text{Å}) \longrightarrow {}^3CH_2 + CO \quad (6)$$

$${}^3CH_2 + ClCH_2CH_2Cl \longrightarrow CH_3 + ClCHCH_2Cl \quad (7)$$

$$CH_3 + CH_3 \longrightarrow CH_3CH_3{}^* \quad (8)$$

$$CH_3 + ClCHCH_2Cl \longrightarrow CH_3CHClCH_2Cl{}^* \quad (9)$$

$$ClCHCH_2Cl + ClCHCH_2Cl \longrightarrow$$
$$ClCH_2CHClCHClCH_2Cl{}^* \quad (10)$$
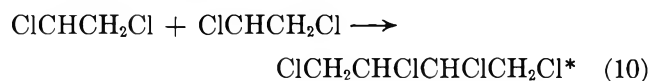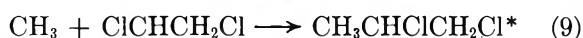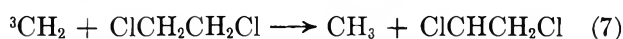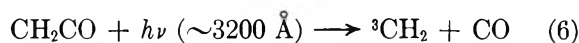
In addition there are the cross-combination reactions between the two sets of radicals.

$$CH_2Cl + CH_3 \longrightarrow CH_3CH_2Cl{}^* \quad (11)$$

$$CH_2Cl + ClCHCH_2Cl \longrightarrow CH_2ClCHClCH_2Cl{}^* \quad (12)$$

$$CH_3 + CH_2CH_2Cl \longrightarrow CH_3CH_2CH_2Cl{}^* \quad (13)$$

$$CH_2CH_2Cl + ClCHCH_2Cl \longrightarrow$$
$$CH_2ClCH_2CHClCH_2Cl{}^* \quad (14)$$
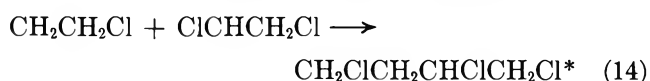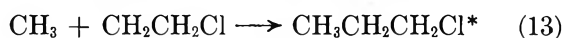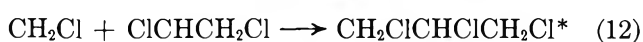
The formation of singlet and triplet methylene from the photolysis of ketene is more complicated[8] than indicated by (1) and (6), but for our purposes these reactions just denote the presence of $CH_2({}^3\Sigma_g{}^-)$ and $CH_2$-$({}^1A_1)$. The products from reactions 10 and 14 were not studied because of their extremely long retention times. No experiments were done to identify the reactions of $CH_2({}^3\Sigma_g{}^-)$ with ketene or with monoradicals; such reactions[11] may add to the complexity at lower pressures.

Although the products are vibrationally excited to $\sim 90$ kcal mol$^{-1}$, collisional stabilization occurs at high pressure and the products from the above mechanism can be measured. For nearly identical reaction conditions (but without any CO), we[9] found previously $\sim 28\%$ $CH_2({}^3\Sigma_g{}^-)$. The product distribution[12] in the present study is consistent with such a methylene composition and with the above mechanism. The presence of trace quantities of 1,2-dichloropropane in experiments with added CO could indicate a small amount of ($\leq 3\%$) C–H insertion by $CH_2({}^1A_1)$.[7] On the other hand, incomplete removal of $CH_2({}^3\Sigma_g{}^-)$ is another possibility.[9] Assuming that the chloroalkyl radicals have about the same rate constant, $\sim 10^{13}$ cc mol$^{-1}$ sec$^{-1}$, for combination,[13] the ratios of the product yields for 1,2-$C_2H_4Cl_2$, 1,4-$C_4H_8Cl_2$, and 1,3-$C_3H_6Cl_2$ should be 1:1:2 if $[CH_2Cl] = [CH_2CH_2Cl]$. The average 1,4-$C_4H_8Cl_2$:1,3-$C_3H_6Cl_2$ product ratio (including disproportionation products) for experiments with added CO at 1 atm pressure was 1.0:2.5. Since 1,2-$C_2H_4Cl_2$ was the reagent, the yield from reaction 3 could not be measured.

In addition to combination products, small yields of disproportionation products were found and three of the four possible disproportionation–combination ratios for $CH_2Cl$ and $CH_2CH_2Cl$ radicals were measurable from data obtained with added CO. The ratios, which are the average of three to five experiments, are given in Table I.

**Table I:** Disproportionation–Combination Ratios for $CH_2CH_2Cl$ and $CH_2Cl$ Radicals

| Radicals | Disproportionation products | Disproportionation–combination ratios[a] | | |
|---|---|---|---|---|
| | | This work | b | c |
| $CH_2CH_2Cl$ + $CH_2CH_2Cl$ | $ClCH_2CH_2Cl$ $CH_2CH_2$ | | 0.1 | 0.09 |
| $CH_2CH_2Cl$ + $CH_2CH_2Cl$ | $CH_3CH_2Cl$ $CH_2CHCl$ | 0.21 | 0.1 | 0.36 |
| $CH_2Cl$ + $CH_2CH_2Cl$ | $CH_3Cl$ $CH_2CHCl$ | 0.11 | | |
| $CH_2Cl$ + $CH_2CH_2Cl$ | $CH_2CH_2$ $CH_2Cl_2$ | 0.03 | | |

[a] Values are defined by disproportionation product yield/combination product yield. [b] B. C. Roquitte and M. H. J. Wijnen, *J. Chem. Phys.*, **38**, 4 (1963). [c] J. Heicklen, *J. Amer. Chem. Soc.*, **87**, 445 (1965).

*Unimolecular Reactions and the Low-Pressure Reaction Mechanism.* The HCl elimination reactions (15–19) are summarized in Table II. Three different experimental approaches were used to measure these unimolecular rate constants: (1) the pressure dependence of the product yields from photolysis of ketene and 1,2-dichloroethane with added carbon monoxide; (2) the pressure dependence of the product yields from photolysis of ketene and 1,2-dichloroethane; (3) the pressure dependence of the product yields from photolysis of ketene and 1,2-dichloroethane with small amounts of added butadiene or allene.

The original intent of using CO as a bath gas was to simplify the reaction mechanism. Although, the CO technique failed[11] to scavenge $CH_2({}^3\Sigma_g{}^-)$ at the lower pressures, it was possible to obtain the rate constant (2.2 Torr) for 1,3-$C_3H_6Cl_2{}^*$ using CO as the bath gas from the higher pressure data given in Figure 1. Data for $D/S > 0.8$ could not be obtained because lower pressures could not be achieved and still maintain a 12-fold excess of CO with a vessel of reasonable size. Furthermore, $CH_2({}^3\Sigma_g{}^-)$ was not scavenged at low pressures.[11] Figure 1 also contains some data obtained with *n*-butane added to the photolysis mixture. The intent was to use the product yields from $CH_2({}^1A_1)$ insertion into butane as an internal standard. This, however, failed because products arising from hydrogen abstraction by $CH_2({}^3\Sigma_g{}^-)$ interfered with the internal standard.

(13) (a) N. Basco, D. G. L. James, and R. D. Suart, *Int. J. Chem. Kinet.*, **2**, 215 (1970); (b) T. Ogawa, G. A. Carlson, and G. C. Pimentel, *J. Phys. Chem.*, **74**, 2090 (1970); (c) L. Bertrand, G. R. DeMare, G. Huybrechts, J. Olbregts, and M. Toth, *Chem. Phys. Lett.*, **5**, 183 (1970); (d) L. C. Dickey and F. F. Firestone, *J. Phys. Chem.*, **74**, 4310 (1970).

**Table II:** Summary of Unimolecular Reactions[a]

| Reaction | | Identification |
|---|---|---|
| $ClCH_2CH_2CH_2Cl^*$ $\xrightarrow{}$ $HCl + ClCH_2CHCH_2$ | (D) | 15 |
| $\xrightarrow{M}$ $ClCH_2CH_2CH_2Cl$ | (S) | |
| $ClCH_2CH_2CH_2CH_2Cl^*$ $\xrightarrow{}$ $HCl + ClCH_2CH_2$- $CHCH_2$ | (D) | 16 |
| $\xrightarrow{M}$ $ClCH_2CH_2CH_2CH_2Cl$ | (S) | |
| $CH_3CHClCH_2Cl^*$ $\xrightarrow{}$ $HCl + CH_2CHCH_2Cl$ | (D) | 17a |
| $\xrightarrow{}$ $HCl + CH_3CClCH_2$ | (D) | 17b |
| $\xrightarrow{}$ $HCl + CH_3CHCHCl$ | (D) | 17c |
| $\xrightarrow{M}$ $CH_3CHClCH_2Cl$ | (S) | |
| $CH_3CH_2CH_2Cl^*$ $\xrightarrow{}$ $HCl + CH_3CHCH_2$ | (D) | 18 |
| $\xrightarrow{M}$ $CH_3CH_2CH_2Cl$ | (S) | |
| $ClCH_2CH_2Cl^*$ $\xrightarrow{}$ $HCl + ClCHCH_2$ | (D) | 19 |
| $\xrightarrow{M}$ $ClCH_2CH_2Cl$ | (S) | |

[a] The apparent unimolecular rate constants[b] are defined as $k_{ai} = \omega D_i/S_i$, where $\omega$ is the collision frequency, $D_i$ is the unimolecular decomposition product yield, and $S_i$ is the stabilized product yield. [b] For cascade deactivation, $k_a$ becomes pressure dependent; however, for the higher pressure region, $D/S \leq 2$, linear $D/S$ vs. 1/pressure plots are found for moderately efficient bath gases.[5,9,15]

The $D/S$ plot for $1,3\text{-}C_3H_6Cl_2$ from photolysis of ketene with $1,2\text{-}C_2H_4Cl_2$ alone is shown in Figure 2. Reaction 17a,[14] which also gives 3-chloropropene, is a possible complication since the decomposition product is the same as from (15). The $1,2\text{-}C_3H_6Cl_2$ yield at high pressure was only $\sim 7\%$ of the $1,3\text{-}C_3H_6Cl_2$ yield; hence, this problem can be ignored. This small $1,2\text{-}C_3H_6Cl_2$ yield results because both $CH_3$ and $ClCHCH_2Cl$ arise from $CH_2(^3\Sigma_g^-)$ and, thus, are in lower concentration than $CH_2Cl$ and $CH_2CH_2Cl$. The high-pressure ($D/S < 1.0$) region of Figure 2 is linear and gives a rate constant of 0.9 Torr. The deviation from linearity at lower pressures arises from decomposition and/or other removal processes for $CH_2ClCH{=}CH_2$. Cascade deactivation, which becomes apparent at $D/S > 2$ for moderately efficient bath gases,[9,15] cannot account for the deviation since cascade would give a positive, rather than a negative, deviation from linearity. The addition of a small percentage of butadiene or allene to the photolysis sample gave slightly higher $D/S$ values for pressures above 2 Torr and significantly higher $D/S$ values below 2 Torr. The $ClCH_2CHCH_2$ was effectively protected from radical attack in such experiments since butadiene is probably more reactive toward radicals[16] or atoms, and because it was present in, at least, a ten- to 100-fold excess over $ClCH_2CHCH_2$. These scavenging results are consistent with other studies[5,17] which used olefins to protect olefinic decomposition products from chlorine atoms.

Figure 2 shows that even with the addition of butadiene a linear $D/S$ plot was not obtained at the lowest pressures. This raises the interesting possibility that
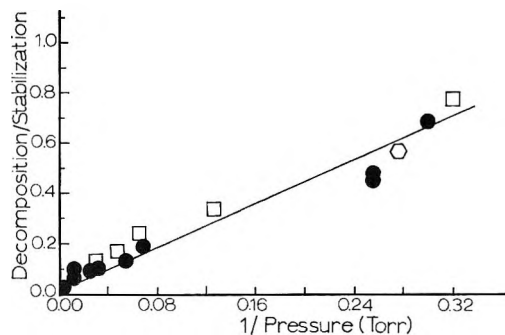
Figure 1. A decomposition/stabilization vs. pressure$^{-1}$ plot for 1,3-dichloropropane: ●, experiments having CO as the principal bath gas; □, experiments in which butane was added, but CO was still the main bath gas; ○, 2% butadiene was added prior to photolysis of $CH_2CO$ and $C_2H_4Cl_2$.
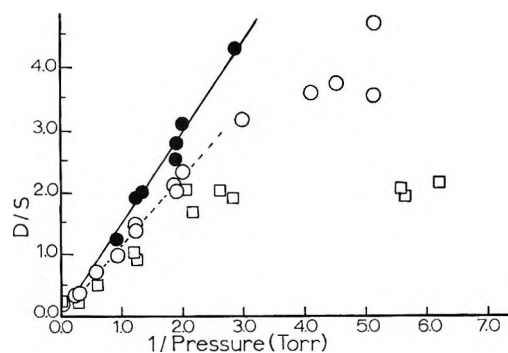


Figure 2. A decomposition/stabilization vs. pressure$^{-1}$ plot for 1,3-dichloropropane: □, $CH_2CO$ and $C_2H_4Cl_2$ as reagents; ○, 2–4%1,4-butadiene added to $CH_2CO$ and $1,2\text{-}C_2H_4Cl_2$; ●, the data obtained with added butadiene but corrected for decomposition of $ClCH_2CH{=}CH_2$ using a rate constant of 0.2 Torr.

$ClCH_2CHCH_2$ may undergo a unimolecular reaction from the retention of a large fraction of the 90 kcal mol$^{-1}$ of vibrational energy originally with $C_3H_6Cl_2^*$. A likely reaction channel for $ClCH_2CHCH_2$ is chlorine-atom rupture. If this interpretation is adopted, the data of Figure 2 may be corrected for $ClCH_2CHCH_2$ decomposition and $k_a(1,3\text{-}C_3H_6Cl_2) = 1.5$ Torr is obtained (shown by the solid points and solid line). For the present data a rate constant for 3-chloropropene of 0.2 Torr was deduced. The Discussion section contains further comment on the unimolecular decomposition of 3-chloropropene.

The foregoing discussion established that butadiene must be present in order to protect small quantities of olefinic products at low pressure. For this reason the

(14) (a) G. J. Martens, M. Godfroid, and L. Ramoisy, *Int. J. Chem. Kinet.*, **22**, 123 (1970); (b) K. A. Holbrook and J. S. Palmer, *Trans. Faraday Soc.*, **67**, 81 (1971).

(15) (a) J. D. Rynbrandt and B. S. Rabinovitch, *J. Phys. Chem.*, **74**, 1679 (1970); (b) D. W. Setser and J. C. Hassler, *ibid.*, **71**, 1364 (1967).

(16) S. Krzyzanowski and R. J. Cvetanović, *Can. J. Chem.*, **45**, 665 (1967).

(17) D. W. Setser, *J. Amer. Chem. Soc.*, **90**, 582 (1968).
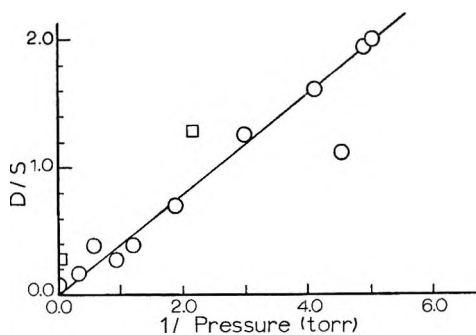
Figure 3. A decomposition/stabilization vs. pressure$^{-1}$ plot for 1,4-dichlorobutane: O, data obtained from photolysis of $CH_2CO$ and 1,2-$C_2H_4Cl_2$ with 1-2% of 2-4-butadiene; □, data from experiments containing only $CH_2CO$ and 1,2-$C_2H_4Cl_2$.



Figure 4. Comparison of propene and 1-3-$C_3H_6Cl_2$ (corrected for its own decomposition) yields vs. pressure. See text for method of obtaining the rate constant for $n$-$C_3H_7Cl$* from these data.

$D/S$ vs. $1/P$ plot for 1,4-$C_4H_8Cl_2$, Figure 3, was obtained with added butadiene. The plot, which is linear and apparently free of the complications encountered for the unimolecular decomposition of 1,3-$C_3H_6Cl_2$, gives $k_a$(1,4-$C_4H_8Cl_2$) = 0.40 Torr. However, the rate constant is surprisingly large and must be regarded with some suspicion.

The combination of $CH_3$ and $CH_2CH_2Cl$ radicals should be a minor, but significant, reaction for experiments without added CO. Unfortunately, the retention times for 1-$C_3H_7Cl$ and $CH_2Cl_2$ were the same. The $C_3H_6$ peak was, however, free from overlap, and the 1-$C_3H_7Cl$* decomposition rate was estimated by assuming this reaction to be the only pressure-dependent source of $C_3H_6$. An alternate source of $C_3H_6$ could be $CH_2$($^1A_1$) plus $C_2H_4$; however, the large amounts of 1,2-$C_2H_4Cl_2$ minimized such reactions as shown by the small $C_3H_6$ yield in high-pressure experiments with added CO. The butadiene also minimized the reactions of $CH_2$($^3\Sigma_g{}^-$) with $CH_2CO$ which might give $C_2H_4$.[11] Using the internal standard technique,[2-4] a plot of 1,3-$C_3H_6Cl_2$ yield (corrected for decomposition)/$C_3H_6$ yield vs. pressure gives the rate constant from (slope/intercept)$^{-1}$. Figure 4 illustrates the results which were obtained with added butadiene. The data give $k_a$(1-$C_3H_7Cl$) = 6.5 Torr. This technique assumes that the relative steady-state radical concentrations contributing to the $C_3H_6$, 1,3-$C_3H_6Cl_2$, and 1-$C_3H_7Cl$ yields were constant over the pressure range employed. From our previous experience this technique may have an error of ±50%. The nonequilibrium unimolecular decomposition rate constant for 1,2-$C_2H_4Cl_2$* was obtained in a similar manner and the results,[12] which are based on the yield of $C_2H_3Cl$ relative to 1,3-$C_3H_6Cl_2$, gave $k_a$(1,2-$C_2H_4Cl_2$) = 11 Torr. This value is consistent with results of previous studies.[2,3,6]

Other Reactions. For data obtained with butadiene added to the reaction mixture and at pressures above ~0.4 Torr, good mass balance between the sum of 1,3-$C_3H_6Cl_2$ plus $C_3H_5Cl$ and 1,4-$C_4H_8Cl_2$ plus $C_4H_7Cl$ was obtained. Furthermore the yields of other products
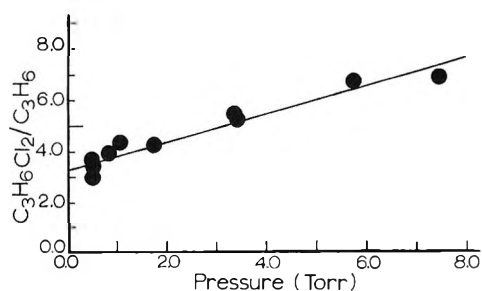
were in accord with the mechanism presented. However, at lower pressures the yields tended to become nonproducible, and such experiments were characterized by yields of $C_2H_3Cl$, $CH_2Cl_2$, and $CH_3Cl$ that became too large to be explained by the reactions already mentioned. The yield of $CH_3Cl$ often was especially large and probably originated from hydrogen abstraction by $CH_2Cl$ from $C_2H_4Cl_2$, which has an activation energy of 5-10 kcal mol$^{-1}$ and is preferred over chlorine abstraction.[13d,18] The H-atom abstraction reaction would be followed by disproportionation between $CH_2ClCHCl$ and $CH_2Cl$ giving $CH_2Cl_2$ and $CH_3Cl$. The low-pressure experiments were done in large vessels (up to 12 l.) and the low light intensity over the vessel volume and the low concentration of ketene may contribute to a reduced radical concentration, thus favoring abstraction reactions rather than radical-radical combination reactions. A possibility which adds to the complexity and cannot be eliminated is interaction between $CH_2Cl$ and $CH_2$($^3\Sigma_g{}^-$) yielding $C_2H_4$ + Cl.

Summary of Experimental Rate Constants. The experimental rate constants are summarized in Table III. The half-quenching pressures were converted to sec$^{-1}$ units using $\sigma^2$ and $\Omega^{(2,2)*}\sigma^2$. The Lennard-Jones diameters for 1,3-$C_3H_6Cl_2$ and 1,4-$C_4H_8Cl_2$ were estimated by adding 0.25 Å per $CH_2$ group[19] to $\sigma$ (1,2-$C_2H_4Cl_2$), which was taken as 5.5 Å.[9] In a similar way $\sigma$(1-$C_3H_7Cl$) was estimated from $\sigma$($C_2H_5Cl$) = 4.9 Å; $\sigma$(CO) was taken from Hirschfelder.[20a] The $\Omega^{(2,2)*}$ values were calculated from standard tables[20a] using $\epsilon/k$($C_2H_5Cl$) for all chloroalkanes.

Discussion

Experimental Measurements. Although the system is complex, a mechanism based on the characteristic

(18) D. M. Tomkinson and H. O. Pritchard, J. Phys. Chem., 70, 1579 (1966).

(19) (a) Y. N. Lin, S. C. Chan, and B. S. Rabinovitch, ibid., 72, 1932 (1968); (b) L. D. Spicer and B. S. Rabinovitch, ibid., 74, 2445 (1970).

(20) (a) J. O. Hirschfelder, C. F. Curtiss, and R. B. Bird, "Molecular Theory of Gases and Liquids," Wiley, New York, N. Y., 1965; (b) R. A. Svehla, NASA Technical Report R-132, Lewis Research Center, Cleveland, Ohio, 1962.

**Table III:** Experimental Nonequilibrium
Unimolecular Rate Constants

| Activated | $k_a$, Torr | $k_R(\sigma^2)$,[a] sec$^{-1}$ | $k_R(\Omega^{(2,2)*}\sigma^2)$,[b] sec$^{-1}$ | Bath gas |
|---|---|---|---|---|
| 1,4-C$_4$H$_8$Cl$_2$ | 0.40 | 4.5 × 10$^6$ | 1.1 × 10$^7$ | 1,2-C$_2$H$_4$Cl$_2$ |
| 1,3-C$_3$H$_6$Cl$_2$ | 1.5 | 1.7 × 10$^7$ | 4.3 × 10$^7$ | 1,2-C$_2$H$_4$Cl$_2$ |
| n-C$_3$H$_7$Cl | 6.5 | 7.1 × 10$^7$ | 1.8 × 10$^8$ | 1,2-C$_2$H$_4$Cl$_2$ |
| 1,2-C$_2$H$_4$Cl$_2$ | 11 | 1.2 × 10$^8$ | 3.0 × 10$^8$ | 1,2-C$_2$H$_4$Cl$_2$ |
| 1,3-C$_3$H$_6$Cl$_2$[c] | 2.7[c] | 3.5 × 10$^7$ | 5.7 × 10$^7$ | CO |

[a] Lennard-Jones collision diameters for 1,4-C$_4$H$_8$Cl$_2$, 1,3-C$_3$H$_6$Cl$_2$, 1,2-C$_2$H$_4$Cl$_2$, C$_3$H$_7$Cl, and CO are 6.0, 5.75, 5.5, 5.2, and 3.9 Å, respectively. [b] These rate constants were calculated using $[\Omega^{(2,2)*}\sigma^2]^{1/2}$ as the collision diameters with $\epsilon/k(CO) = 92°$ and $\epsilon/k$(chloroalkane) = 300°K. [c] The experimental rate constant from Figure 1 was corrected for ClCH$_2$CH=CH$_2$ decomposition to obtain the value in the table.

reactions of methylene[7,10] accounted for most of the experimental results. Carbon monoxide scavenged CH$_2$($^3\Sigma_g^-$) at high pressure[7,10,11] but not at low pressure. Four nonequilibrium unimolecular rate constants were measured and comparison between model calculations and experiment is made in the next section. The rate constants for 1,2-C$_2$H$_4$Cl$_2$* with various bath gases are worth summarizing. The half-quenching pressure with CO as the bath gas is 27 Torr;[9] whereas, with C$_2$H$_4$Cl$_2$ and CH$_2$Cl$_2$[9] it is 11 and 17 Torr. On a collision for collision basis the relative efficiencies are 1.0, 0.73, and 0.38 for C$_2$H$_4$Cl$_2$, CH$_2$Cl$_2$, and CO. Dichloromethane removes about 8 kcal mol$^{-1}$ per collision with C$_2$H$_4$Cl$_2$*, and the higher collisional efficiency of the parent, C$_2$H$_4$Cl$_2$, correlates with the removal of even a larger amount of energy per collision.[9] The relative efficiencies of CO and C$_2$H$_4$Cl$_2$ for deactivating dichloropropane, Table III, are in accord with those just listed for C$_2$H$_4$Cl$_2$*.

The experimental disproportionation–combination ratios of Table I show that hydrogen-atom transfer is favored by a factor of 4 over chlorine-atom transfer in encounters between CH$_2$Cl and C$_2$H$_4$Cl. For C$_2$H$_4$Cl with C$_2$H$_4$Cl, Heicklen (see footnote c, Table I) also found hydrogen-atom transfer to be faster by a factor of 4, although Roquitte and Wijnen (see footnote b, Table I) found comparable hydrogen- and chlorine-atom transfer rates. Wijnen and coworkers[21] reported only hydrogen-atom transfer in the disproportionation reaction between CCl$_3$ and CH$_2$CH$_2$Cl.

*RRKM Calculations.* The application of the RRKM theory has been presented in numerous places,[3,4] and it is sufficient to define the rate constant as $k_E = [\sigma/h][Z^\dagger/Z^*]\Sigma P^\dagger[E_{vr} - E_0)/N^*(E_{vr})$; $\sigma$ is the reaction-path degeneracy, $h$ is Planck's constant, $Z^\dagger/Z^*$ is the ratio of adiabatic partition functions of complex and molecule, $\Sigma P^\dagger(E_{vr} - E_0)$ is the total sum of internal energy states for the complex at energy $E_{vr} - E_0$, and $N^*(E_{vr})$ is the total density of internal energy states

for the molecule at energy $E_{vr}$. A summary of the vibrational frequencies and moments of inertia for the molecules and complexes is given in the Appendix. Fundamental frequencies for 1-C$_3$H$_7$Cl[22] and ClCH$_2$-CH=CH$_2$[23] were taken from the literature and those for 1,3-C$_3$H$_6$Cl$_2$ and 1,4-C$_4$H$_8$Cl$_2$ were estimated from 1-C$_3$H$_7$Cl and 1-C$_4$H$_9$Cl.[22] The ring frequencies for the HCl elimination complexes were calculated in the manner outlined previously;[3,4,6] i.e., the frequencies of the group attached to the ring were taken to be essentially the same as for that section of the chloroalkane molecule. The torsional degrees of freedom were treated as either vibrations or rotations in two separate computations. The overall rotations were considered to be adiabatic. The reduced moments of inertia for internal rotation were calculated using the method of Pitzer.[24] Each CH$_2$Cl rotor was considered to be attached to a rigid molecular unit; hence, no consideration was given to coupling with other rotors. Only the internal rotation that becomes the ring puckering vibration in the complex is important because the effects of other internal rotations tend to cancel in the $\Sigma P^\dagger(E_{vr} - E_0)$ and $N^*(E_{vr})$ ratio.

The threshold energy, $E_0$, and the average energy of the formed molecules, $E_{min} + \langle E\rangle_{thermal}$, are more important than details of the vibrational frequency patterns. Unfortunately the Arrhenius parameters have been measured[25] only for n-C$_3$H$_7$Cl: $k = 3.16 \pm 1.9 \times 10^{13} \exp(-55.1 \pm 0.7/RT)$. The Arrhenius preexponential factors for C$_3$H$_6$Cl$_2$ and C$_4$H$_8$Cl$_2$ can be estimated with reasonable certainty by analogy with other HCl elimination reactions; however, the $E_0$ values are not so easily estimated. Electron-withdrawing groups on the $\beta$ position tend[25] to raise $E_0$, and considering the remarkable increase in acidity upon substitution of Cl and CH$_2$Cl for H in CH$_3$COOH, the $E_0$ of 1,2-C$_2$H$_4$Cl$_2$ and 1,3-C$_3$H$_6$Cl$_2$ must be higher than for C$_2$H$_5$Cl. The threshold energies for n-C$_4$H$_9$Cl and 1,4-C$_4$H$_8$Cl$_2$ should be similar. The thermochemistry and calculated results for 1-C$_3$H$_7$Cl, 1,3-C$_3$H$_6$Cl$_2$, and 1,4-C$_4$H$_8$Cl$_2$ are given in Table IV along with a summary of earlier work.[6] The larger preexponential factor for the dichloroethane series arises from doubling of the reaction-path degeneracy.

The effect of anharmonicity on the vibrational sums and densities has been neglected in the calculations of Table IV. Anharmonic calculations[6b] based upon Harrhoff's treatment of Morse oscillators gave rate constants which were reduced by a factor of 2 to 3 relative to those in Table IV.

(21) W. H. S. Yu and M. H. J. Wijnen, *J. Chem. Phys.*, **52**, 2736, 4166 (1970).

(22) R. G. Snyder and J. H. Schachschneider, *J. Mol. Spectrosc.*, **30**, 290 (1969).

(23) R. D. McLachlan and R. A. Nyquist, *Spectrochim. Acta*, **24**, 103 (1968).

(24) K. S. Pitzer, *J. Chem. Phys.*, **14**, 239 (1946).

(25) A. Maccoll, *Chem. Rev.*, **69**, 33 (1969).

**Table IV:** Comparison of Experimental and Calculated Results[a]

| | $C_2H_5Cl$ | $n$-$C_3H_7Cl$ | 1,2-$C_2H_4Cl_2$ | 1,3-$C_3H_6Cl_2$ | 1,4-$C_4H_8Cl_2$ |
|---|---|---|---|---|---|
| $k_a$ (exptl),[b] sec$^{-1}$ | $3.4 \times 10^9$ | $7.1 \times 10^7$ $(1.8 \times 10^8)$ | $1.6 \times 10^8$ | $1.7 \times 10^7$ $(4.3 \times 10^7)$ | $4.5 \times 10^6$ $(1.1 \times 10^7)$ |
| $k_a$ (calcd),[c,d] vibration model | $2.39 \times 10^9$ $(2.29 \times 10^9)$ | $6.17 \times 10^7$ $(5.65 \times 10^7)$ | $1.99 \times 10^8$ $(1.81 \times 10^8)$ | $2.87 \times 10^7$ $(2.52 \times 10^7)$ | $2.48 \times 10^6$ $(2.05 \times 10^6)$ |
| $k_a$ (calcd),[c,d,e] internal rotation model | | $5.21 \times 10^7$ $(4.77 \times 10^7)$ | | $2.42 \times 10^7$ $(2.14 \times 10^7)$ | $1.96 \times 10^6$ $(1.64 \times 10^6)$ |
| Critical energy, kcal mol$^{-1}$ | $55.0^g$ | $53.0^g$ | $60.0^f$ | $55.0^f$ | $53.0^f$ |
| Thermal preexponential factor, sec$^{-1}$ [h] | $1.46 \times 10^{13}$ | $1.49 \times 10^{13}$ $(5.63 \times 10^{12})$ | $2.21 \times 10^{13}$ | $2.80 \times 10^{13}$ $(1.10 \times 10^{13})$ | $3.25 \times 10^{13}$ $(9.35 \times 10^{12})$ |
| $E_{min}$, kcal mol$^{-1}$ [i] | 88.4 | 85.9 | 85.3 | 84.5 | 83.5 |
| Average energy of formed molecules, kcal mol$^{-1}$ [g] | 91 | 89.5 | 88.0 | 88.4 | 88.0 |

[a] The calculations of Table IV are based on a model having ring bond orders of 1.9 (C–C), 0.9 (C–Cl), 0.1 (C–H), 0.1 (H–Cl); see Appendix for further details. [b] The rate constants for $C_2H_5Cl^*$ and $C_2H_4Cl_2^*$ have been measured with several relatively efficient quenching gases[6,9] and the values in the table are weighted averages, which we feel to be the most reliable estimates of the unit deactivation rate constants. The values for other molecules were taken from Table III. [c] The calculated value in parentheses is $k_a^0$ (the limiting low-pressure value); the other is $k_a^\infty$ (the high-pressure value). Our experimental error is too large for us to observe the variation in $k_a$ (which arises from the energy dispersion of the formed molecules) with change in pressure. [d] For the vibrational models the reaction-path degeneracies for 1-$C_3H_7Cl$ and $C_2H_5Cl$ are 2 and for 1,2-$C_2H_4Cl_2$, 1,3-$C_3H_6Cl_2$, and 1,4-$C_4H_8Cl_2$ are 4. For the internal rotational model the reaction-path degeneracy for $C_3H_7Cl$ is 4 and for the dichloroalkane series is 8. For internal rotors a $CH_3$ group has a symmetry number of 3 and a $CH_2Cl$ group has a symmetry number of 1. [e] All torsional motions in the molecule and complex were treated as free internal rotors. [f] See text for justification of these values. [g] Experimental values, see ref 25 for a review. [h] These tabulations are at 800°K; the numerical values are equal to $\sigma kT/hQ_{vr}^\dagger/Q_{vr}^*$. The values in parentheses are for the internal rotor models. The only experimental values are $1.2 \times 10^{13}$ sec$^{-1}$ for $C_2H_5Cl$ and $3.2 \times 10^{13}$ sec$^{-1}$ for $C_3H_7Cl$. [i] See Appendix for the thermochemistry and the definition of $E_{min}$. [j] Average energy of the formed chemically activated molecules at 300°K, which was calculated from the distribution function of the formed molecules, $f(E)dE$, and the value of $E_{min}$.

The internal rotational models gave rate constants that were virtually identical with those from the vibrational models. This results from interplay between $N^*(E_{vr})$, $\Sigma P^\dagger(E_{vr} - E_0)$, and the reaction-path degeneracy. Thus, at 90 kcal one $CH_2Cl$ rotor in the 1,3-$C_3H_6Cl_2$ complex raised the $\Sigma P^\dagger(E_{vr} - E_0)$ term by a factor of 4.3 relative to $\Sigma P^\dagger(E_v - E_0)$ for a 94-cm$^{-1}$ torsional vibration, but two $CH_2Cl$ rotors in the molecule raised $N^*(E_{vr})$ by a factor of 10.5 relative to $N^*$-$(E_{vr})$ for two 94-cm$^{-1}$ vibrations. These result in a lowering of $k_a$ by 0.41; however, the rotor model has a reaction-path degeneracy of 8 as contrasted to 4 for the vibrational model which puts $k_a$ back to approximately the same value as for the vibrational model. We[3,6] previously have argued against the importance of internal rotation models for $C_2H_5Cl$ and $C_2H_4Cl_2$.

*Comparison of Calculated and Experimental Rate Constants.* The calculated $k_a$ values for 1-$C_3H_7Cl$, 1,3-$C_3H_6Cl_2$, and 1,4-$C_4H_8Cl_2$ achieved the same degree of agreement with the experimental results as previously[4,6] obtained for $C_2H_5Cl$ and $C_2H_5Br$. At the present time the collision diameters are not known, but the agreement with calculations is best for the Lennard-Jones values and, in fact, identification of the correct collisional diameters for these polar molecules is essential before better testing of models or theory can be done. The individual agreement between theory and experiment for 1,3-$C_3H_6Cl_2$ and 1,4-$C_4H_8Cl_2$ is acceptable. However the relative change, a decline by a factor of $\sim$11

for the calculated rate constants and only a factor of 3 in the experimental values, points to some experimental error, which probably is for $k_a(C_4H_8Cl_2)$. Another possibility is that $E_0$ for 1,3-$C_3H_6Cl_2$ is even somewhat higher than 55.0 kcal mol$^{-1}$. Since a change of 2 kcal in $E_0$ affects the calculated rate constant by a factor of 2.1, raising $E_0$ to 57 kcal would substantially enhance the agreement between the calculated and experimental values.

*Unimolecular Decomposition Rate Constants and Number of Degrees of Freedom.* A basic postulate of RRKM theory is that the internal energy is randomly distributed among the internal degrees of freedom of the energized molecule. This basic idea has been tested by measuring rate constants for a homologous series[26] of molecules which have a common reaction channel. If the critical energy and the level of excitation stays constant throughout the series, the resulting decrease in the rate constants measures the quantum statistical weight changes incurred from $N^*(E_{vr})$ and $\Sigma P^\dagger(E_{vr} - E_0)$. The experimental demonstration of this often is hampered by variation of the threshold and average energies. The first series to be examined was a *sec*-alkyl radical homologous series.[26a] This was followed

(26) (a) M. J. Pearson and B. S. Rabinovitch, *J. Chem. Phys.*, **42**, 1624 (1965); (b) M. J. Pearson, B. S. Rabinovitch, and G. Z. Whitten, *ibid.*, **42**, 2470 (1965); (c) F. H. Dorer and B. S. Rabinovitch, *J. Phys. Chem.*, **69**, 1973 (1965); (d) F. H. Dorer and B. S. Rabinovitch, *ibid.*, **69**, 1952 (1965).
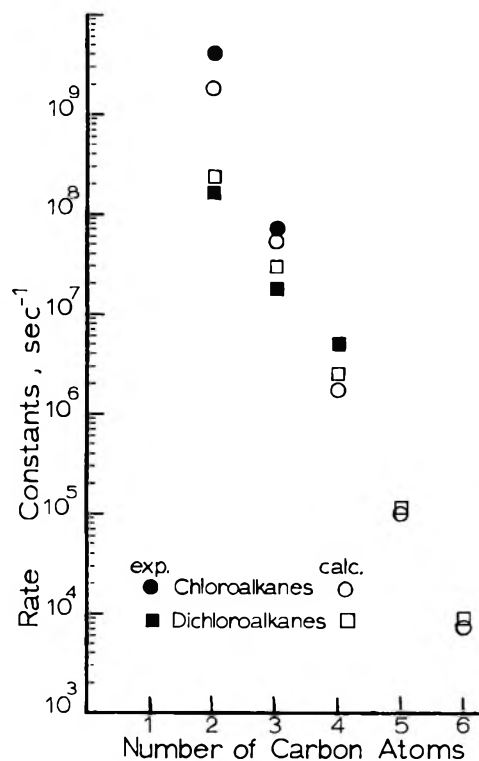
Figure 5. Comparison of calculated and experimental rate constants for the series of chemically activated mono- and dichloroalkanes at a common energy of 89 kcal mol$^{-1}$.

by studies of deuterated sec-alkyl radicals,[26b] alkylcyclopropanes,[26c] fluoroalkylcyclopropanes,[26c] and olefins.[26d] In general the experiments verified the basic assumption of the theory, although now some of the experiments are known to contain minor complications in mechanism.[27] Enough experimental data have accumulated so that a profitable comparison can be made for two new homologous series, the mono- and dichloroalkanes; the RRKM theoretical predictions are presented in Figure 5. The details of the models are given in Appendix I; the main features are that $E_0$ was taken as 53 kcal mol$^{-1}$ for all cases not explicitly listed in Table IV and that the preexponential factors for those not shown in Table IV were adjusted so as to be the same as for dichlorobutane or chloropropane. All calculations were done for an energy of 89 kcal mol$^{-1}$, which does not necessarily coincide with the average excitation energy in a real experiment. The calculated rate constants for the $C_5$ or $C_6$ mono- and dichloroalkanes are nearly equal, because the difference in reaction-path degeneracy nearly balances the difference in the $\Sigma P^\dagger(E_{vr} - E_0)/N^*(E_{vr})$ ratio at an $E_0$ of 53 kcal for both the mono- and dichloroalkane. The calculations for the larger members of the series (> three carbon atoms) give a statistical weight effect per added $CH_2$, which averaged $\sim$17 for both series. The largest change ($\sim$35) in $k_E$ per added $CH_2$ was for the $C_2$ and $C_3$ monochloroalkanes. The threshold energy for the first member of each series is higher than those of the subse-

quent members, which reduces the difference in $k_E$ between the $C_2$ and $C_3$ members. For example, lowering all the threshold energies to 53 kcal mol$^{-1}$ gives $k(C_2H_5Cl) = 3.16 \times 10^9$, $k(C_2H_4Cl_2) = 1.97 \times 10^9$, and $k(C_3H_6Cl_2) = 6.26 \times 10^7$ sec$^{-1}$; thus, the $C_2H_5Cl$ and $C_3H_7Cl$ ratio is 57, although the ratio for $C_2H_4Cl_2$ and $C_3H_6Cl_2$ is only 31. These calculations show that adding a $CH_2$ group has a greater influence upon the monochloroalkane series than upon the dichloroalkane series for the smaller molecules. This is simply a consequence of the larger total number of states for $C_2H_4Cl_2$* than for $C_2H_5Cl$*, thus adding a $CH_2$ has a stronger influence upon the latter.

The chemical activation rate constants for $C_2H_5F$ and n-$C_3H_7F$ formed by radical combination are claimed to differ by a factor of 100.[28] Calculations from our laboratory[5] using the same $E_0$ for $C_2H_5F$ and $C_3H_7F$ favor a factor nearer 50.

*Energy Partitioning by the 1,3-$C_3H_6Cl_2$ Reaction.* One of the objectives of this work was to study two successive unimolecular reactions; the magnitude of the second rate constant would permit the assignment of the energy distribution resulting from the first step. This was the reason for concentrating on the $C_3$ and $C_4$ dichloroalkanes rather than on the monochloroalkanes. If our interpretation for the loss of chloropropene displayed in Figure 2 is correct, then our goal was achieved. Unfortunately direct and quantitative confirmation that $ClCH_2CHCH_2$ decomposed to $Cl + CH_2CHCH_2$ is difficult to provide, although some 5-chloropentene-1 which could arise from combination of $C_3H_5$ with $CH_2CH_2Cl$ was identified as a reaction product. It is possible[12] to choose threshold energies and activated complex models to rationalize Cl rupture rather than HCl elimination from $ClCH_2CHCH_2$*. Recent infrared chemiluminescence emission studies have shown that little energy is partitioned as vibrational or rotational energy of HX by either four-[29a] or three-[29b] centered HX elimination reactions. Consequently, it is tempting to conclude that the majority of the available energy is retained by the olefin fragment. This would fit our observations for the 1,3-$C_3H_6Cl_2$ reaction. However, such a conclusion is of sufficient importance that it is wise to seek further evidence before offering a detailed discussion of energy partitioning for the 1,3-$C_3H_6Cl_2$ reaction. The implications of the energy partitioning data, with regard to the transition state of the four-centered HX elimination reaction, are discussed else-

(27) (a) Intramolecular H migration has been discovered for chemically activated alkyl radical studies; E. A. Hardridge, C. W. Larson, and B. S. Rabinovitch, *J. Amer. Chem. Soc.*, **92**, 3278 (1970); (b) for chemically activated fluorocyclopropanes having H atoms adjacent to the $CF_3$ group, HF elimination may have been in competition with cyclopropane isomerization.

(28) J. A. Kerr, B. V. O'Grady, and A. F. Trotman-Dickenson, *J. Chem. Soc. A*, 275 (1969).

(29) (a) P. H. Clough, J. C. Polanyi, and R. T. Taguchi, *Can. J. Chem.*, **48**, 2919 (1970); (b) D. W. Setser, Abstract presented at the CIC-ACS Joint Meeting at Toronto, May 1970.

where.[6b] For the $C_3$ and $C_4$ molecules any minor alteration of the frequency pattern associated with the four-atom ring cannot seriously affect the calculated rate constants.

## Conclusions

Although the reaction mechanism is complex and the thermochemistry of the unimolecular reactions is somewhat uncertain, the following conclusions can be drawn. (1) Singlet and triplet methylene interact with 1,2-$C_2H_4Cl_2$ by Cl and H abstraction, respectively. (2) Chloroethyl radical transfers a H atom approximately four times as fast as a Cl atom in disproportionation reactions. (3) Moderately good agreement between experimental and RRKM calculated unimolecular rate constants were obtained for $C_3H_7Cl$, 1,3-$C_3H_6Cl_2$, and 1,4-$C_4H_8Cl_2$. Additional knowledge about the collision diameters and threshold energies are needed before more detailed comparison with theory can be made. The statistical weight lowering of the HCl elimination rate constant per added $CH_2$ group was estimated as ~17 for $C_3$ and larger chloroalkanes. (4) Although tentative, the data provide some evidence that the olefin product (chloropropene) retained the majority of the excess energy from the HCl four-centered elimination reaction.

*Acknowledgments.* This work was supported by the National Science Foundation under Grant GP-9245 and by the Kansas State University Computing Center.

## Appendix

*Thermochemistry.* The heats of formation, which were taken from the literature and reduced to $0°K$, are summarized in Table V. $E_{min}$ is defined as $-[\Delta H_f°_0-(R_1R_2) - \Delta H_f°_0(R_1) - \Delta H_f°_0(R_2) - E_a]$; $E_a$ is the energy of activation for combination of radicals $R_1$ and $R_2$ to form $R_1$–$R_2$ and was set at 1 kcal mol$^{-1}$.

**Table V:** Standard Heats of Formation

| Molecule or radical | $\Delta H_f°_{298}$, kcal mol$^{-1}$ | $\Delta H_f°_0$,[a] kcal mol$^{-1}$ | Ref |
|---|---|---|---|
| $CH_3CH_2CH_2Cl$ | −31.2 | −26.3 | 30 |
| $ClCH_2CH_2CH_2Cl$[b] | −36.2 (34.8) | −31.7 (−30.3) | 30 (31) |
| $ClCH_2CH_2CH_2CH_2Cl$ | −41.1 | −34.9 | 30 |
| $CH_3$[c] | 34.1 | 34.9 | 32 |
| $CH_2Cl$[c] | 28.1 | 28.9 | 32 |
| $CH_2CH_2Cl$[d] | 21.2 | 23.8 | 33, 34 |

[a] The $\Delta H_f°_{298}$ were corrected to $H_f°_0$ by the appropriate statistical mechanical calculation; torsion degrees of freedom were treated as vibrations. [b] A compromise value ($-30.7$ kcal mol$^{-1}$) for $\Delta H_f°_0$(1,3-$C_3H_6Cl_2$) was used which gave an $E_{min}$($C_3H_6Cl_2$) intermediate between $E_{min}$($C_2H_4Cl_2$), and $E_{min}$($C_4H_8Cl_2$). [c] Calculated from bond energies of $CH_4$ and $CH_3Cl$ given in ref 32. [d] The $\Delta H_f°_{298}$($CH_2CH_2Cl$) is given as 20.2 kcal mol$^{-1}$ in ref 33. This was raised 1 kcal mol$^{-1}$ to conform with the slightly higher R–Cl bond strengths given by Kerr,[34] *i.e.*, $D$(ClCH$_2$CH$_2$-Cl) = 81.3 kcal mol$^{-1}$.

*Models of Molecules and Complexes.* The HCl elimination complex was viewed as a nearly planar, four-centered ring structure. A valence-force model with the Wilson *F-G* matrix method was used to calculate the frequencies of the four-atom ring; the atoms adjacent to the carbons of the ring were included as the mass of that corner of the ring. Bond orders were assigned to the four bonds undergoing rearrangement with the restraint that the sum of the bond order in the ring was 3. The C–C, C–Cl, H–Cl, and C–H stretch bond orders are 1.9, 0.9, 0.1, and 0.1, respectively. The bond lengths were calculated by Pauling's equation and the stretching force constants used for input into the *F-G* matrix program were derived from the bond lengths and bond

**Table VI:** Models for Molecules and Complexes

| Molecule[a] and complex | Frequencies,[a] cm$^{-1}$ | Moments of inertia,[a] amu-$\mathring{A}^2$ — Internal rotation | Overall rotation |
|---|---|---|---|
| 1-$C_3H_7Cl$[b] molecule | 2938 (7), 1365 (9), 1067 (3), 881 (2), 730 (2), 362 (1), 226 (2), 94 (1) | 2.70 ⟶ 8.03 | 19.4 ⟶ 207.9 ⟶ 218.2 |
| 1-$C_3H_7Cl$ complex | 2972 (6), 1429 (4), 1235 (3), 955 (4), 875 (2), 633 (2), 578 (2), 390 (2), 174 (1) | 2.70 | 30.2 ⟶ 180.4 ⟶ 202.6 |
| 1,3-$C_3H_6Cl_2$[c] molecule | 2951 (6), 1401 (5), 1266 (3), 1046 (3), 842 (3), 720 (2), 425 (1), 242 (2), 94 (2) | 12.2 (2) | 32.9 ⟶ 584.2 ⟶ 607.9 |
| 1,3-$C_3H_6Cl_2$ complex | 3016 (5), 1387 (3), 1140 (3), 920 (3), 882 (3), 739 (1), 629 (2), 520 (3), 400 (1), 250 (1), 94 (1) | 12.2 | 60.4 ⟶ 455.5 ⟶ 497.5 |
| 1,4-$C_4H_8Cl_2$[c] molecule | 2933 (8), 1449 (4), 1315 (4), 1247 (3), 1062 (5), 918 (1), 734 (4), 353 (3), 160 (1), 105 (1), 81 (2) | 25.4 (2) ⟶ [d] | 32.6 ⟶ 950.6 ⟶ 971.2 |
| 1,4-$C_4H_8Cl_2$ complex | 3010 (7), 1363 (6), 1093 (4), 927 (5), 830 (2), 664 (3), 537 (3), 400 (1), 250 (1), 200 (1), 105 (1), 81 (1) | 25.4 ⟶ [d] | 58.9 ⟶ 809.2 ⟶ 845.4 |

[a] The frequencies listed are for the vibrational model. For the rotational model the torsion frequencies were dropped (lowest frequencies) and the listed moments of inertia were used for the internal rotors. [b] Reference 22. [c] Estimated from $n$-$C_3H_7Cl$ and $n$-$C_4H_9Cl$ frequencies.[22] [d] The moment of inertia for rotation about the central carbon atoms was not calculated because it was taken to be the same in the molecule and complex; hence, the values cancelled from the calculations.

(30) S. W. Benson, F. R. Cruickshank, D. M. Golden, G. R. Haugen, H. E. O'Neal, A. S. Rodgers, R. Shaw, and R. Walsh, *Chem. Rev.*, 69, 279 (1969).

(31) J. L. Franklin, J. G. Dillard, H. M. Rosenstock, J. T. Herron, K. Draxl, and F. H. Field, Natl. Standard Reference Data System, NSRDS: NBS-26, 1969.

(32) S. Furuyama, D. M. Golden, and S. W. Benson, *J. Amer. Chem. Soc.*, 91, 7564 (1969).

(33) J. A. Franklin and G. H. Huybrechts, *Int. J. Chem. Kinet.*, 1, 3 (1969).

(34) J. A. Kerr, *Chem. Rev.*, 66, 465 (1966).

orders by the method of Johnston.[35] A ring-bending force constant also was required and $1 \times 10^{-4}$ dyn cm$^{-1}$ was used. The results consist of five modes, one was always ~30 cm$^{-1}$ and was assigned to the reaction coordinate. The ring-puckering frequency was set as 400 cm$^{-1}$ as in previous work. Recent energy partitioning data[6b,29] (see text) indicate the C–C bond is more nearly a single bond, but this change would not seriously affect the calculated values of $k_a$. The out-of-ring part of the complex was treated as a group attached to a carbon atom of the ring and the characteristic vibrational frequencies of the group were assigned by analogy to olefins and the parent molecule. Finally the bending frequencies of the group attached to the ring were adjusted to obtain the desired preexponential factor. The models are summarized in Table VI.

The models for the C$_5$ and C$_6$ chloroalkanes were obtained by assigning a basic set of frequencies for each CH$_2$ group; a 1260 twist, a 1300 wag, a 1058 C–C stretch, a 724 rock, a 460 deformation, and two 2900 C–H stretches. The torsional and bending modes were estimated individually for each molecule. For example,

a 119-cm$^{-1}$ bending mode was added for C$_5$H$_{10}$Cl$_2$ relative to C$_4$H$_8$Cl$_2$ and the C$_4$H$_8$Cl$_2$ torsional modes were changed from 105(1), 81(2) to 53(2), 105(1), and 120(1). The bending and torsion frequencies of the C$_5$ molecule were used in the complex, except for the 53-cm$^{-1}$ torsional frequency which became the ring-puckering mode. Minor adjustments were made to obtain the desired preexponential factors.

The overall rotational moments of inertia were calculated from a standard set of bond lengths and angles.[36] The complexes were similar in structure to the molecules except in the four-centered ring. The HCC and CCCl angles of the ring were set at 100°; the bond lengths, which are dictated by the bond order assignments, fixed the other two angles of the ring. The angles for the ring methylene or RCH group were 115° and the HCH and RCH plane was inclined 150° from the C–C bond.

(35) H. S. Johnston, "Gas Phase Reaction Rate Theory," Ronald Press, New York, N. Y., 1966.

(36) R. H. Schwenderman and G. D. Jacobs, J. Chem. Phys., 36, 1245 (1962).

# The Photolysis of Ketene–Butane Mixtures with and without

# Added Carbon Monoxide

## by K. Dees[1] and D. W. Setser*

*Department of Chemistry, Kansas State University, Manhattan, Kansas 66502* (*Received February 1, 1971*)

The photolysis of ketene with $n$-butane in the presence and absence of carbon monoxide was investigated. The presence of radical combination products, which are associated with C–H abstraction reactions by CH$_2$($^3\Sigma_g^-$), showed that excess CO did not adequately [combination products ≥3% of CH$_2$($^1$A$_1$) insertion products] suppress CH$_2$($^3\Sigma_g^-$) at pressures below 50 Torr. Furthermore, CO has decreasing scavenging ability for CH$_2$($^3\Sigma_g^-$) at lower pressures. The pressure dependence of various products and results of isotopic labeling experiments revealed that the total mechanism was quite complex at low pressures both with and without added CO; many of the complications arise from interaction of CH$_2$($^3\Sigma_g^-$) with ketene. The reaction of CH$_2$($^3\Sigma_g^-$) with $sec$-butyl radicals apparently competes with the reactions of CH$_2$($^3\Sigma_g^-$) and $n$-butane or ketene. Singlet methylene reacts one-half as fast with ketene (yielding C$_2$H$_4$) as with $n$-butane (C–H insertion). An RRKM treatment of the unimolecular decomposition of triplet ketene formed by CH$_2$($^3\Sigma_g^-$) + CO implies that the separation between the ground singlet and triplet states of ketene is less than 40 kcal mol$^{-1}$.

## Introduction

Recently, Braun, Bass, and Pilling[2] studied the reaction kinetics of triplet ($^3\Sigma_g^-$) and singlet ($^1$A$_1$) methylene by flash photolysis of ketene and diazomethane and, for the first time, measured a number of rate constants. In other recent studies, CH$_2$($^3\Sigma_g^-$) was found

to be relatively inert towards CD$_4$ and, instead, reacted with monoradicals;[3] a collision efficiency for CH$_2$($^3\Sigma_g^-$)

with $CD_4$ of $<10^{-9}$ was implied.[3a] The reactions of $CH_2(^3\Sigma_g^-)$ have been studied by mercury photosensitization of ketene[4] and by employing large excesses of inert gas to convert the $CH_2(^1A_1)$ to the ground $CH_2$-$(^3\Sigma_g^-)$ state.[5] The relative efficiencies[6] and absolute rate constants[2] for this process have been measured for several gases. The reactions which are characteristic of $CH_2(^1A_1)$ have been studied[7] by adding oxygen or nitric oxide to scavenge $CH_2(^3\Sigma_g^-)$ or other monoradicals produced by $CH_2(^3\Sigma_g^-)$ abstraction processes. The discovery[8] that carbon monoxide preferentially removed triplet methylene offered a particularly attractive way to isolate $CH_2(^1A_1)$ reactions because carbon monoxide does not remove monoradicals. Using this technique Bamford and coworkers[9] studied the abstraction reactions of $CH_2(^1A_1)$ with $C_2H_5Cl$ and $C_3H_7Cl$ and Setser and coworkers[10] studied $CH_2(^1A_1)$ with $CH_2Cl_2$.

In the present work the product yields from the photolysis of ketene and butane with and without added carbon monoxide were measured from 2 to 700 Torr. Isotopic labeling experiments using $CD_2CO$ were performed at different pressures with and without CO. The main goal was to determine whether CO was an effective scavenger of $CH_2(^3\Sigma_g^-)$ at low pressure. These experimental results were coupled with an RRKM analysis of the unimolecular decomposition of the triplet ketene formed by $CH_2(^3\Sigma_g^-)$ + CO in order to estimate the energy separation between the lowest singlet and triplet states of ketene. A second goal was to identify the overall reaction mechanism for the reactions of singlet and triplet methylene and formation of products. We found that the reaction mechanism was quite complex, especially at low pressure, and a complete characterization was not possible.

## Experimental Section

The gas samples were measured on a vacuum rack equipped with greaseless valves and were transferred to Pyrex photolysis vessels. The inlet system to the gas chromatograph also had only greaseless valves; Apiezon W sealing wax was used for ground glass joint connections. The noncondensable CO was metered into the vessel until the desired pressure of CO was obtained. Depending on the size of the vessel, either the entire vessel or just the very tip was immersed in liquid nitrogen before loading the CO. This latter procedure led to insignificant error in the total pressure since the cold part of the vessel was a small fraction of the total volume. The reactants were kept in nearly constant proportions ($n$-$C_4H_{10}$:$CH_2CO$:$CO$ = 1.0:0.1–0.2:12.0) and the pressure was changed by altering the vessel size. The quantity of $n$-$C_4H_{10}$ plus $CH_2CO$ was 1–2 cc (STP).

The $n$-$C_4H_{10}$ was Baker instrument grade and the CO was Matheson CP grade. Ketene-$d_0$ and ketene-$d_2$ were prepared by pyrolysis of acetone and acetone-$d_6$ over a hot wire. Purification was done by distillation and finally by collecting the ketene that was eluted from a fluoropak gas chromatography column. The deuterated ketene was $>99\%$ ketene-$d_2$. The samples were photolyzed for 1 to 2 hr at room temperature with the unfiltered light of a General Electric A-H6 high-pressure mercury arc. Nearly 100% of the methylene originated from the 3200 ± 200 Å range.[10] The condensable products were recovered by pumping the photolyzed sample through a glass wool packed trap at 77°K; they then were injected into the gas chromatograph. For analysis of ethane, ethene, acetylene, pentane, and isopentane a 3-ft Porapak S column in series with a 15-ft diisodecylphthalate column was used. For the heavier compounds a 12-ft Apiezon L column in series with the 15-ft diisodecylphthalate column gave adequate separation. Temperature programming was necessary for both cases. Gas chromatographic peaks were identified from retention times of pure samples and, in some cases, from the mass spectral cracking patterns. The response of the gas chromatograph was calibrated using, at least, two standard mixtures of known composition which nearly simulated the products of the photolyzed samples.

An EAI "Quad 250" mass filter was used for identification of photolysis products and for analysis of products in the isotopic labeling experiments. Samples were trapped from the glpc effluent and recycled through the columns until pure. These samples were transferred under vacuum to small vessels, which then were taken to the inlet of the "Quad 250." If available, pure compounds were used to obtain reference cracking patterns. The patterns for the deuterated ethanes were obtained from the literature.[11]

## Results

*Product Yields.* The significant products were pentane (P), isopentane (IP), 3,4-dimethylhexane (DMH), 3-methylpentane (3MP), propane, propene, ethane,

(3) (a) P. S. T. Lee, R. L. Russell, and F. S. Rowland, *Chem. Commun.*, 1, 18 (1970); (b) H. M. Frey and R. Walsh, *J. Chem. Soc. A*, 2115 (1970).

(4) (a) H. E. Avery and R. J. Cvetanović, *J. Chem. Phys.*, 48, 380 (1968); (b) H. M. Frey and M. A. Voisey, *Trans. Faraday Soc.*, 64, 954 (1968); (c) D. C. Montague and F. S. Rowland, *J. Phys. Chem.*, 72, 3705 (1968).

(5) (a) D. F. Ring and B. S. Rabinovitch, *Can. J. Chem.*, 46, 2435 (1968); (b) R. F. Bader and J. I. Generosa, *ibid.*, 43, 1631 (1965); (c) H. M. Frey, *J. Amer. Chem. Soc.*, 82, 5947 (1960).

(6) (a) R. A. Cox and K. F. Preston, *Can. J. Chem.*, 47, 3345 (1969); (b) T. W. Eder and R. W. Carr, Jr., *J. Chem. Phys.*, 53, 2258 (1970); (c) A. K. Dhingra and R. D. Koob, *J. Phys. Chem.*, 74, 4490 (1970).

(7) J. W. Simons, C. J. Mazac, and G. W. Taylor, *J. Phys. Chem.*, 72, 749 (1968), and references cited therein.

(8) B. A. DeGraff and G. B. Kistiakowsky, *ibid.*, 71, 3984 (1967).

(9) (a) C. H. Bamford and J. E. Casson, *Proc. Roy. Soc., Ser. A*, 312, 141, 163 (1969); (b) C. H. Bamford, J. E. Casson, and A. N. Hughes, *ibid.*, 306, 135 (1968); (c) C. H. Bamford, J. E. Casson, and R. P. Wayne, *ibid.*, 289, 287 (1966).

(10) W. G. Clark, D. W. Setser, and E. E. Siefert, *J. Phys. Chem.*, 74, 1670 (1970).

(11) J. A. Bell and G. B. Kistiakowsky, *J. Amer. Chem. Soc.*, 84, 3417 (1962).
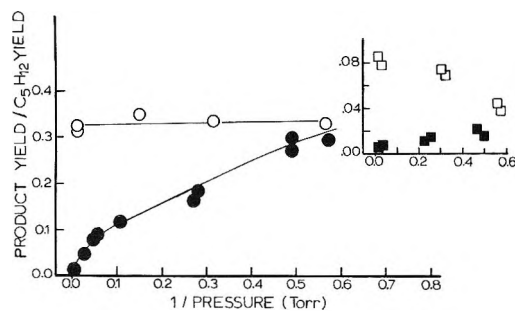
Figure 1. Ethane and dimethylhexane product yields, relative to $n$-pentane, for photolysis of ketene with $n$-pentane in the presence (filled symbols) and absence (open symbols) of added carbon monoxide: O, ethane; □, DMH. (The highest pressures were 700 and 70 Torr for experiments with and without added CO, respectively.)
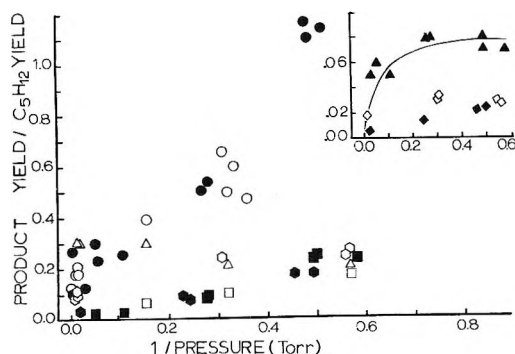


Figure 2. Product yields, relative to $n$-pentane, from photolysis of ketene with butane in the presence (filled symbols) and absence (open symbols) of carbon monoxide: O, ethene; □, acetylene; O, propene + propane; △, isopentane; ◇, 3-methylpentane. (The highest pressures were 700 and 70 Torr for experiments with and without added CO, respectively.) The isopentane yield shown in this plot is only that assigned to radical products, see text for further discussion. The purpose of the solid curve for isopentane is to indicate that the yield from the radical processes was negligible at the highest pressure (700 Torr) with added CO; the highest pressure shown by a point is 36 Torr.

ethene, acetylene, $n$-hexane, and other hexane isomers. Figures 1 and 2 summarize the product yields as a function of pressure. The yields are relative to the $n$-pentane yield, which was chosen as the internal standard because it is formed only from insertion of $CH_2(^1A_1)$ into the primary C–H bonds of butane. No attempt was made to study disproportionation reactions and, unless specifically stated otherwise, the yields associated with a given radical combination reaction do not include disproportionation.

The $CH_2(^1A_1)$ insertion products, isopentane and pentane, were the major reaction products at all pressures. The ratio of IP/P was 0.90 at 700 Torr in the presence of CO. Since only $CH_2(^1A_1)$ was present under these conditions, this ratio represents the relative rates of $CH_2(^1A_1)$ insertion into the primary and secondary C–H bonds. As the pressure was decreased, com-

bination of $CH_3$ and $sec$-butyl arising from C–H abstraction by $CH_2(^3\Sigma_g^-)$ increased the ratio of IP/P. The isopentane yield from radical combination alone (the difference between the measured ratio at a given pressure and the 0.90 ratio) is the quantity shown in Figure 2.

Propane, propene, 3,4-dimethylhexane, and 3-methylpentane were present in smaller yields. For experiments with added CO, the DMH yield increased from virtually zero to a plateau as the pressure was lowered; however, the yield decreased with diminishing pressure for experiments without CO. The 3MP yield is from two sources and is discussed separately. The yield of propane + propene (unresolved for most experiments) increased with decreasing pressure both with and without added CO. The propane and propene from one experiment without added CO at 2.2 Torr were resolved using a Porapak S column and $C_3H_8:C_3H_6$ was 0.6.

The $C_2$ hydrocarbons were ethane, ethene, and acetylene. Attention was focused upon ethane because it mainly arises from methyl combination and reflects the $CH_2(^3\Sigma_g^-)$ hydrogen abstraction reactions. The experiments without added CO have a relatively constant yield of ethane (and also isopentane) which was independent of pressure. At high pressure (700 Torr) carbon monoxide removed all of the ethane and virtually all of the DMH and IP; however, as the pressure was lowered, the ethane yield greatly increased. With added CO the ethene yield varied from a small amount at 700 Torr to yields comparable with pentane at 17 Torr. A similar trend was found in the absence of CO. Both with and without added CO the $C_2H_2$ yield varied from zero at high pressure to approximately one-half the ethane yield at 2 Torr.

A number of hexane isomers, including $n$-hexane and 3-methylpentane, were always present, although not shown in Figures 1 and 2. Since primary $CH_2$ insertion product yields were high ($\sim$2–4% butane conversion), secondary reactions of $CH_2(^1A_1)$ with pentane and isopentane are possible. This was checked by making several runs with traces of added $O_2$. The hexanes were still present; thus, confirming $CH_2(^1A_1)$ insertion into the pentanes.

The combination of ethyl and $sec$-butyl radicals also gives 3MP, and this contribution was found by subtracting the $CH_2$ insertion yield from the measured 3MP yield. Since radical combination was not important for experiments at 700 Torr with added CO, these were used to establish the $n$-hexane and 3MP relative ratio, which was 1.0, from insertion. Then the $n$-hexane yield was used to obtain the contribution to 3MP from insertion. At the lower pressures both with and without added CO, radical combination and insertion contributed equally to 3MP. The 3MP yields in Figure 2 are only the part attributed to radical combination.

**Table I:** Isotopic Composition for Ethane, Ethene,[a] and Propene

| Butane:ketene = 1.0:0.1 | | | | Butane:ketene:CO = 1.0:0.1:12 | | | |
|---|---|---|---|---|---|---|---|
| | 760 Torr | | | | 760 Torr | | |
| $C_2D_6$[b] | | $C_2D_4$ | 1.0 | $C_2D_6$ | | $C_2D_4$ | 1.00 |
| $C_2HD_5$ | 0.13 | $C_2HD_3$ | 0.22 | $C_2HD_5$ | | $C_2HD_3$ | 0.07 |
| $C_2H_2D_4$ | 1.0 | $C_2H_2D_2$[b] | | $C_2H_2D_4$ | | $C_2H_2D_2$ | 0.06 |
| | | $C_2H_3D$[b] | | | | $C_2H_3D$[b] | |
| | | $C_2H_4$ | 0.13 | | | $C_2H_4$ | 0.17 |
| | 88 Torr | | | | 1.9 Torr | | |
| $C_2D_6$ | 0.05 | $C_2D_4$ | 1.0 | $C_2D_6$ | 0.5 | $C_2D_4$ | 1.00 |
| $C_2HD_5$ | 0.24 | $C_2HD_3$ | 0.60 | $C_2HD_5$ | 1.0 | $C_2HD_3$ | 0.35 |
| $C_2H_2D_4$ | 1.0 | $C_2H_2D_2$ | 0.17 | $C_2H_2D_4$ | 0.8 | $C_2H_2D_2$ | 0.12 |
| | | $C_2H_3D$[b] | | | | $C_2H_3D$ | 0.15 |
| | | $C_2H_4$ | 0.17 | | | $C_2H_4$ | 0.35 |
| | 3 Torr | | | | 2.2 Torr | | |
| $C_2D_6$ | 0.25 | $C_2D_4$ | 1.0 | $C_3H_6$ | 0.28 | | |
| $C_2HD_5$ | 0.81 | $C_2HD_3$ | 0.60 | $C_3H_5D$ | 0.38 | | |
| $C_2H_2D_4$ | 1.0 | $C_2H_2D_2$ | 0.31 | $C_3H_4D_2$ | 1.0 | | |
| | | $C_2H_3D$ | 0.07 | $C_3H_3D_3$ | 0.13 | | |
| | | $C_2H_4$ | 0.16 | $C_3H_2D_4$ | 0.06 | | |
| | | | | $C_3HD_5$ | 0.09 | | |
| | | | | $C_3D_6$ | 0.22 | | |

[a] The relative abundance of $C_2H_4$ may include a small contribution by $N_2$ ($m/e$ 28) and is somewhat less reliable than the other measured values. All entries are the average of two or three experiments except the propene and the 1.9 Torr results with added CO, which are for only one experiment. [b] Below the detection limits of our instrument.

*Isotopic Labeling Results.* Ketene-$d_0$ was replaced with ketene-$d_2$ and photolyses were done at several pressures in the presence and absence of CO. The ethane and ethene products were trapped and analyzed for deuterium content; the results are shown in Table I. The ratio of the various ethene parent peaks from 20-eV spectra were taken as the relative abundance of these compounds. Isotopic analysis of the ethanes is more difficult because of cracking.[11] The 36, 35, and 34 mass peaks from 70-eV spectra were used to find the relative abundance of $C_2D_6$, $C_2HD_5$, and $C_2H_2D_4$. The yield of $C_2H_3D_3$ was insignificant. Propene was trapped from one run without added CO at 2.2 Torr, and the parent peaks from 20-eV spectra were used to obtain the relative abundance for $C_3H_6$ through $C_3D_6$.

## Discussion

*General Features.* The absence of ethane [or other products associated with $CH_2(^3\Sigma_g^-)$] at high pressure with added CO shows that CO effectively scavenged triplet methylene as previously claimed.[8-10] The ethane–pentane ratio summarized in Figure 1 is striking evidence that CO becomes less efficient at removing $CH_2(^3\Sigma_g^-)$ with decreasing pressure. This pressure dependence of $[CH_2(^3\Sigma_g^-)]$ can be understood in terms of formation of chemically activated triplet ketene molecules which either redissociate or are collisionally stabilized. At low pressures CO may collisionally convert[6] $CH_2(^1A_1)$ to $CH_2(^3\Sigma_g^-)$. The mechanism by

which $CH_2(^3\Sigma_g^-)$ generates methyl radicals is not limited to just hydrogen atom abstraction from butane as demonstrated by the labeling results of Table I. These details are discussed later; however, there is little doubt that $CH_2(^3\Sigma_g^-)$ is responsible for the increased ethane yield.

The expected source of $CH_3$ radicals was abstraction of H from the secondary position of $C_4H_{10}$ by $CH_2(^3\Sigma_g^-)$. Since *sec*-butyl radical gives DMH by radical combination, the DMH yield was monitored at various pressures in experiments with added CO. In contrast to $C_2H_6$, the DMH yield in the presence of CO (Figure 1) was not strongly pressure dependent. This implied that other reactions were removing *sec*-butyl radicals and/or that $CH_2(^3\Sigma_g^-)$ was reacting with ketene to give ethane. Our view of the mechanism is presented below.

*Reaction Mechanism for Methylene with Butane.* Our work provides no additional information on the formation steps[6,12-14] for $CH_2(^1A_1)$ and $CH_2(^3\Sigma_g^-)$. Under our conditions[10] with no added CO, the methylene is about 28% $CH_2(^3\Sigma_g^-)$; the proportions of singlet and triplet methylene are not strongly pressure dependent. The main reaction channel for $CH_2(^1A_1)$ is insertion

(12) A. N. Strachan and D. E. Thornton, *Can. J. Chem.*, **46**, 2353 (1968).

(13) S. Ho and W. A. Noyes, Jr., *J. Amer. Chem. Soc.*, **89**, 5091 (1967).

(14) (a) B. S. Rabinovitch, K. W. Watkins, and D. F. Ring, *ibid.*, **87**, 4960 (1965); (b) D. F. Ring and B. S. Rabinovitch, *J. Phys. Chem.*, **72**, 191 (1968).

into the C–H bond;[15] H abstraction is not important. The reactions of $CH_2(^3\Sigma_g^-)$ are not so well defined; Ring and Rabinovitch[5a] suggested that both insertion and abstraction may occur. Other laboratories[16,17] have found no evidence for $CH_2(^3\Sigma_g^-)$ insertion, and this reaction was certainly minor in our own work. The initial reaction with butane and the heats of reaction in kcal mol$^{-1}$ are listed. The collisional conversion of

$$^1CH_2 + CH_3CH_2CH_2CH_3 \longrightarrow \textit{n}\text{-}C_5H_{12}^*$$
$$\Delta H^\circ_{298} = -97 \quad (1)$$

$$^1CH_2 + CH_3CH_2CH_2CH_3 \longrightarrow$$
$$(CH_3)_2CHCH_2CH_3^* \quad \Delta H^\circ_{298} = -99 \quad (2)$$

$$^3CH_2 + CH_3CH_2CH_2CH_3 \longrightarrow$$
$$CH_3 + CH_3CHCH_2CH_3 \quad \Delta H^\circ_{298} = -15 \quad (3)$$
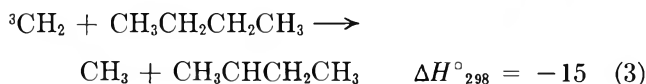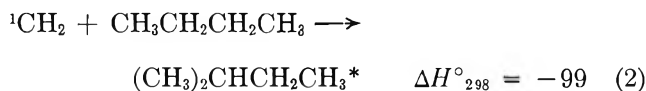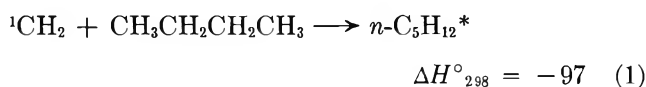
$CH_2(^1A_1)$ to $CH_2(^3\Sigma_g^-)$ by butane apparently competes[1,6] with insertion and is another contributing factor to the singlet–triplet methylene steady-state ratio. Based upon the absence of $n$-octane, the primary C–H abstraction reaction was omitted. Most investigators have found a primary–secondary abstraction ratio of $\sim1{:}10$,[5a,13,17] and the bulk of the evidence is opposed to Herzog and Carr's[18] ratio of $1{:}2$. Various radical–radical combination reactions are important.

$$CH_3 + CH_3 \longrightarrow CH_3CH_3^* \quad \Delta H^\circ_{298} = -88 \quad (4)$$

$$CH_3CH_3^* \xrightarrow{k_a} CH_3 + CH_3 \quad (5)$$

$$\xrightarrow{M} CH_3CH_3 \quad (6)$$

$$CH_3 + CH_3CHC_2H_5 \longrightarrow (CH_3)_2CHC_2H_5^*$$
$$\Delta H^\circ_{298} = -84 \quad (7)$$

$$CH_3CHC_2H_5 + CH_3CHC_2H_5 \longrightarrow$$
$$C_2H_5CH(CH_3)CH(CH_3)C_2H_5^*$$
$$\Delta H^\circ_{298} = -76 \quad (8)$$
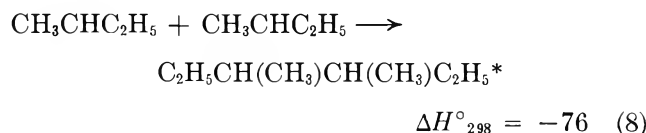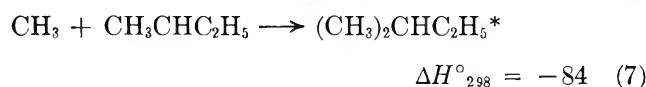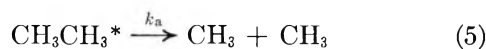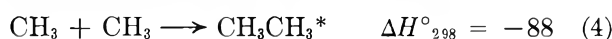
Of these chemically activated molecules, $C_2H_6^*$ has the largest unimolecular rate constant and its half-quenching pressure[15d,19] is $\sim1$ Torr for an efficient bath gas at 25°. Thus the maximum decomposition of $C_2H_6$ was $\sim50\%$, and the decomposition of IP and DMH was not important even at the lowest pressure.[15a]

The IP–P ratio at high pressure with and without added CO was 0.9 and 1.1–1.2; both are in excellent agreement with the results using $O_2$ and NO scavengers.[7,15d,17] Based on (4)–(8) one contradiction with experiment is the decline of the DMH yield with decreasing pressure for experiments having no added CO. This is attributed to the onset of new radical–radical reactions; one such reaction gives 3MP. Assuming

$$C_2H_5 + CH_3CHC_2H_5 \longrightarrow C_2H_5CH(CH_3)C_2H_5$$
$$\Delta H^\circ_{298} = -79 \quad (9)$$
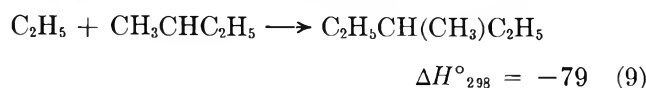
that (1)–(9) account for the main reactions, mass balance for methyl and $sec$-butyl radical products should exist. For 60-Torr experiments without added CO the methyl–butyl radical ratio was 1.0:0.7, even if disproportionation products[5a,20] were included. At 2 Torr with and without added CO the methyl–butyl ratio was 1.0:0.3 and 1.0:0.5, respectively. The combination–disproportionation values are not well established, but, even if mass balance was forced at 60 Torr, a loss of butyl radicals (or gain of methyl radicals) would occur at 2 Torr. Reactions 1–9 apparently do not fully describe the system.

Several additional observations must be considered. For experiments without CO the ethane yield was constant from 2 to 70 Torr. However, isotopic labeling experiments show this to be fortuitous, because the deuterium content of the ethane increased with decreasing pressure which implies that ketene is involved in the ethane formation mechanism. Even without added CO, the ethane composition at high pressure shows that nearly all the ethane originated from $CD_2H$. However, at 3 Torr the isotopic composition indicates that only 68% of the ethane can be attributed to reaction of $CD_2(^3\Sigma_g^-)$ with butane. If CO was added at 2 Torr, the fraction was even lower, $\sim50\%$. The yields and isotopic composition of ethene also are pressure dependent, which suggests the importance of pressure dependent reaction steps and reactions other than $CD_2(^1A_1) + CD_2CO$. Since the ethene yield is pressure dependent both with and without added CO, the pressure dependence of $[CH_2(^3\Sigma_g^-)]$ cannot fully explain the $C_2H_4$ yields.

The complexity of the products may partly arise from reactions of $CH_2(^3\Sigma_g^-)$ with monoradicals[3] and the following set of reactions could generate methyl radicals.

$$CH_2(^3\Sigma_g^-) + CH_3 \longrightarrow CH_2CH_3^*$$
$$\Delta H^\circ_{298} = -100 \quad (10)$$

$$CH_2CH_3^* \xrightarrow{k_a(C_2H_5)} CH_2CH_2 + H$$
$$\Delta H^\circ_{298} = 39 \quad (11)$$

$$H + CH_2CO \longrightarrow CH_3CO^* \quad \Delta H^\circ_{298} = -42 \quad (12)$$

$$CH_3CO^* \xrightarrow{k_a(CH_3CO)} CH_3 + CO \quad \Delta H^\circ_{298} = 12 \quad (13)$$
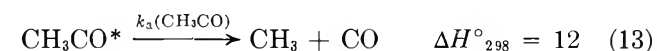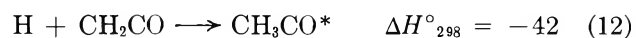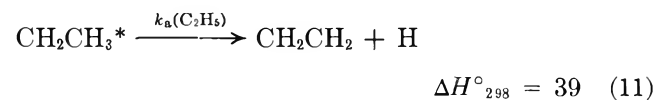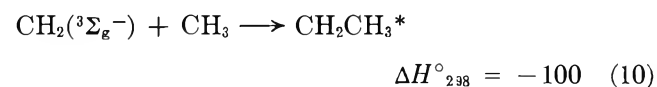
(15) (a) R. L. Johnson, W. L. Hase, and J. W. Simons, *J. Chem. Phys.*, **52**, 3911 (1970); (b) R. W. Carr and G. B. Kistiakowsky, *J. Phys. Chem.*, **70**, 118 (1966); (c) S. Y. Ho, I. Unger, and W. A. Noyes, Jr., *J. Amer. Chem. Soc.*, **87**, 2297 (1965); (d) M. L. Halberstadt and J. R. McNesby, *ibid.*, **89**, 3417 (1967).

(16) T. W. Eder and R. W. Carr, *J. Phys. Chem.*, **73**, 2074 (1969).

(17) G. B. Kistiakowsky and T. A. Walter, *ibid.*, **72**, 3952 (1968).

(18) B. M. Herzog and R. W. Carr, Jr., *ibid.*, **71**, 2688 (1967).

(19) B. S. Ravinovitch and D. W. Setser, *Advan. Photochem.*, **3**, 1 (1964).

(20) R. W. Carr, Jr., I. D. Gay, G. P. Glass, and H. Niki, *J. Chem. Phys.*, **49**, 846 (1968).

$$CH_3CO^* \xrightarrow{M} CH_3CO + M \qquad (14)$$
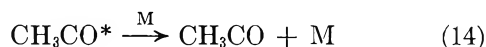
Since $k_a(C_2H_5) \geq 10^{12}$ sec$^{-1}$, $C_2H_5^*$ will be completely decomposed,[19] and the competition between (13) and (14) is the only possibility for explaining the pressure dependence of the $C_2H_4$ yield and the increase of methyl radical products relative to butyl radical products with declining pressure. Niki and coworkers[20] studied the H + $CH_2CO$ reaction but were unable to measure the unimolecular decomposition rate. Using RRKM theory we[21] estimated the rate constant as $\geq 10^{12}$ sec$^{-1}$; hence, stabilization of $CH_3CO^*$ is also unlikely. Assuming this to be true, the experiments with $CD_2CO$ favor perdeuterated ethene as the product of reactions 10–14. For statistical rupture of H or D in (11) and starting with $CD_2$, $CD_2H$, and $CD_2CO$, the predicted isotopic content of the ethene converges toward $C_2D_4$ after a few cycles. At 3 Torr without added CO, the $C_2D_3H$ yield is 0.6 of the $C_2D_4$ yield and other isotopically labeled ethenes are formed; hence, an explanation of ethene based *only on reactions 10–14* is unacceptable. Reactions 12–14 probably play a minor role in the production of methyl radicals under our conditions.

The reactions of *sec*-butyl radicals with $CH_2(^3\Sigma_g^-)$ should be considered. Reaction 16 giving propene and

$$CH_2(^3\Sigma_g^-) + CH_3CHCH_2CH_3 \longrightarrow$$

$$\cdot CH_2CH(CH_3)CH_2CH_3^* \qquad \Delta H°_{298} = -96 \quad (15)$$

$$\cdot CH_2CH(CH_3)CH_2CH_3^* \xrightarrow{k_a}$$

$$CH_2CHCH_3 + CH_2CH_3 \qquad \Delta H°_{298} = 22 \quad (16)$$

$$\xrightarrow{M} \cdot CH_2CH(CH_3)CH_2CH_3 + M \qquad (17)$$
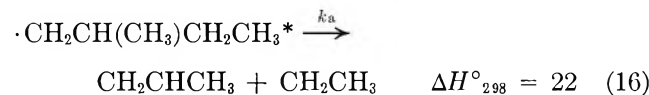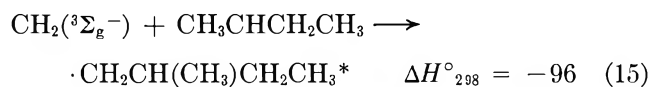
ethyl radicals is favored by a factor of $\sim 3$ over methyl rupture.[22] In order to test for (16) the deuterium content of propene was checked. The results from Table I indicate isotopic scrambling in the propene with a contribution from all possible deuterated species; however, propene-$d_2$ was the major product, which is evidence for (16). Although propene-$d_2$ can also originate from (18), the isotopic composition of the ethenes

$$CD_2(^1A_1) + CH_2CH_2 \longrightarrow CD_2HCHCH_2^*$$

$$\Delta H°_{298} = -100 \quad (18)$$
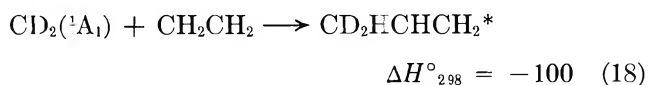
is quite mixed and reaction 18 would not give the observed proportion of propene-$d_2$. We conclude that the evidence supports the occurrence of reaction 15, although the small yield of propene shows that this reaction constitutes only a minor removal step for *sec*-butyl. Reaction 16 is one pressure-dependent source of ethyl radicals, and the small yields of radical combination products from $C_2H_5$ (propane and 3MP) are consistent with the yields of propene.

*Reactions of Methylene with Ketene.* Although the reactions of $CH_2(^3\Sigma_g^-)$ with monoradicals contribute to the mechanism, these reactions alone cannot account

for the isotopic composition and the pressure dependencies of ethene and ethane. The only recourse is to include the interaction of $CH_2(^3\Sigma_g^-)$ with ketene, which might have been expected considering its slow rate of reaction with alkanes.[2,3] Several proposals have been published,[4a,17] and the pressure-dependent biradical hypothesis[17] seems the most promising for explaining our data.

$$CH_2(^3\Sigma_g^-) + CH_2CO \longrightarrow$$

$$CH_2COCH_2^* \text{ or } CH_2CH_2CO^* \quad (19)$$

$$CH_2COCH_2^* \text{ or } CH_2CH_2CO^* \xrightarrow{k_a}$$

$$CH_3 + CHCO \text{ and } C_2H_4 + CO \quad (20)$$

$$\xrightarrow{M} C_2H_4CO + M \quad (21)$$
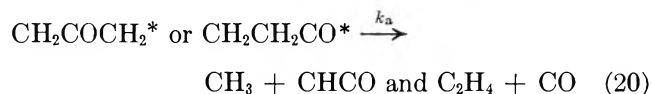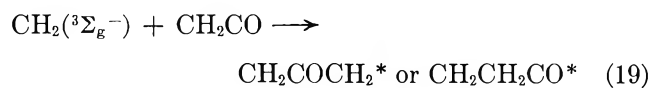
Assuming reactions 20 and 21 to be competitive, this mechanism can account for the increase in $C_2H_4$ with declining pressure either *via* (20) or by reaction of $CH_3$ with CHCO. Interaction between $CD_2H$ and CDCO could provide isotopic mixing for ethene.

The small amount of ethene at high pressure in the presence of CO must arise from

$$CH_2(^1A_1) + CH_2CO \longrightarrow C_2H_4^* + CO$$

$$\Delta H°_{298} = -91 \quad (22)$$
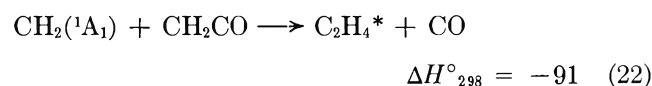
The high-pressure experiments with ketene-$d_2$, butane, and excess CO gave mostly $C_2D_4$ and verify (22). Since ethene:$n$-pentane $= 0.09$ for 1:10 ratio of ketene: butane, $k_{22}:k_1 = 0.9$ and $k_{22}:(k_1 + k_2) = 0.47$. The threshold energy[23] for elimination of $H_2$ from $C_2H_4^*$ is $\sim 80$ kcal mol$^{-1}$ and, depending on the excess energy provided by methylene and the energy partitioning character of (22), the $C_2H_4^*$ from reaction 22 may eliminate $H_2$ at low pressure. However, other reactions, such as interaction of two CHCO radicals also may give $C_2H_2$. The bimolecular combination of $CH_2(^3\Sigma_g^-)$ followed by elimination of $H_2$, which has been reported in a flash photolysis study,[1] is not likely to be important for our low intensity photolysis conditions.

(21) K. Dees, Ph.D. Dissertation, Kansas State University, 1970. The nonequilibrium unimolecular decomposition of $CH_3CO^*$ poses several questions. The reaction pathway may involve a nonadiabatic decomposition of the acetyl radical, which could account for the low $A$ factor (1.99 $\times$ 10$^{10}$) measured for this reaction [E. O'Neal and S. W. Benson, *J. Chem. Phys.*, **36**, 2196 (1962)]. On the other hand, other members of the acetyl radical series have normal $A$ factors. The calculated results quoted in the text were based on models having Arrhenius factors of 2.4 $\times$ 10$^{13}$ and $E_2$ of 14.7 kcal mol$^{-1}$. Thermal activation calculations based upon Arrhenius factors of 10$^{14.5}$ and 21.5 kcal mol$^{-1}$ for $CH_3CO$ have been published by Golden, Solly, and Benson [*J. Phys. Chem.*, **75**, 1333 (1971)]. Such a model gives even higher values for $k_a$ than the value quoted above.

(22) C. W. Larson, B. S. Rabinovitch, and D. C. Tardy, *J. Chem. Phys.* **47**, 4570 (1967). The chemically activated $CH_2CH(CH_3)C_2H_5$ radical can rearrange *via* a five-membered transition state to $CH_3CH$-$(CH_3)CH_2CH_2$ which gives only ethene and isopropyl radicals upon decomposition.

(23) A. W. Kirk and E. Tschuikow-Roux, *ibid.*, **51**, 2247 (1969); according to the RRKM calculations $k(C_2H_4) = 3 \times 10^8$ sec$^{-1}$ for an energy of 91 kcal mol$^{-1}$.

*Ethyl Radicals.* The $CH_2(^3\Sigma_g^-)$ + *sec*-butyl reaction is one probable source. Another possibility is the addition of methyl to ketene, which may proceed through a chemically activated acetyl radical.

$$CH_3 + CH_2CO \longrightarrow C_2H_5CO^*$$

$$\Delta H^\circ_{298} = -29 \quad (23)$$

$$C_2H_5CO^* \xrightarrow{k_a} C_2H_5 + CO \quad \Delta H^\circ_{298} = 9 \quad (24)$$

$$\xrightarrow{M} C_2H_5CO + M \quad (25)$$
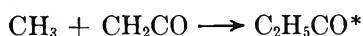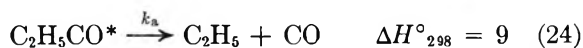
The $\Delta H_f^\circ_{298}(CH_3CH_2CO)$ was estimated as $-9.7$ kcal mol$^{-1}$ from $D(CH_3CH_2CO-H)^{24} = 88$ kcal mol$^{-1}$. Reaction 24 and the analogous $CH_3CO^*$ decomposition pose interesting questions for the kinetics of carbonyl compounds, and RRKM calculations were performed.[21] A model based on the thermal rate constant,[24] $k_{uni} = 2 \times 10^{13} \exp(-14,700/RT)$, predicted $k_a = 8 \times 10^{10}$ sec$^{-1}$ for an excitation energy of 29 kcal mol$^{-1}$. The activation energy of (23) would raise the available energy above 29 kcal mol$^{-1}$. On the other hand, the activation energy for (24) is probably higher than 14.7 kcal, but the complex is probably looser than implied by the $2 \times 10^{13}$ sec$^{-1}$ preexponential factor. These factors tend to make our estimate of $k_a$ a lower limit. Although this estimate of $k_a$ implies that (24) dominates over (25), the pressure dependence of $[C_2H_5]$ could be explained from that for $[CH_3]$. The activation energy for (23) may be sufficiently large to prevent the addition of $CH_3$ to $CH_2CO$ at room temperature,[25] and experiments specifically designed to study reactions 23–25 are needed to elucidate the chemistry of vibrationally excited $C_2H_5CO$ radicals.

*Reaction Rate Constants for Singlet Methylene.* Recently Braun, *et al.*,[2] measured the room temperature rate constant for insertion of $CH_2(^1A_1)$ into methane, $k = 1.9 \pm 0.5 \times 10^{-12}$ cm$^3$ molecule$^{-1}$ sec$^{-1}$. We already discussed the relative reaction rates of $CH_2(^1A_1)$ with ketene and butane: $k_{22}/(k_1 + k_2) = 0.47$. The relative rates of $CH_2(^1A_1)$ insertion with methane and *n*-butane and methane and propane have been measured[26,27] as 0.24 and 0.43, respectively. These relative rates can be combined to obtain rate constants for reaction of $CH_2(^1A_1)$ with butane, propane, and ketene, which are $8.0 \times 10^{-12}$, $4.4 \times 10^{-12}$, and $3.7 \times 10^{-12}$ cm$^3$ molecule$^{-1}$ sec$^{-1}$. It should be realized that the measurements of Braun and coworkers[2] have not been completely accepted by some laboratories.[6c]

*Unimolecular Decomposition Rate Constant for $CH_2CO(^3A_2)$.* If CO removes $CH_2(^3\Sigma_g^-)$ by forming $CH_2CO(^3A_2)$ in accordance with the potential energy diagram (Figure 3) first presented by DeGraff and Kistiakowsky,[8] and if the appearance of ethane is taken as diagnostic for $CH_2(^3\Sigma_g^-)$, an order of magnitude estimate can be given for the unimolecular decomposition rate constant of triplet ketene. Matching this estimated experimental value with the RRKM calculated
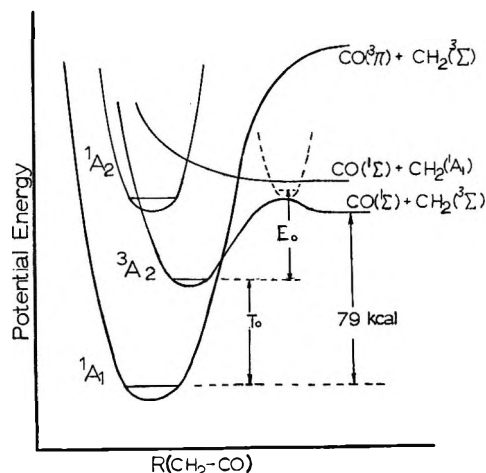
Figure 3. Potential energy diagram for ketene.[8] The separation between the $^1A_1$ and $^1A_2$ states now is thought[27b] to be $\leq 61$ kcal mol$^{-1}$. Bowers [*J. Chem. Soc. A*, 466 (1967)], estimated a 4–7-kcal activation energy for dissociation from $CH_2CO(^1A_1)$. The dotted curve denotes the transition state for $CH_2CO(^3A_2)$.

value by varying $E_0$ gives an estimate of the energy separation between the $^1A_1$ and $^3A_2$ states of ketene.

Ethane became measurable at $\sim 80$ Torr in experiments with added CO. For the sensitivity of our gas chromatographic apparatus, this is indicative of $\sim 10\%$ decomposition of $CH_2CO^*(^3A_2)$. An estimate of the half-quenching pressure can be made by noting that the RRKM theory calculations predict an increase from $10\%$ decomposition to $50\%$ decomposition with an order of magnitude change in pressure. The half-stabilization pressure for triplet ketene was therefore estimated as $\sim 8$ Torr, which is equivalent to a rate constant of $\sim 9 \times 10^7$ sec$^{-1}$. DeGraff and Kistiakowsky[8] noted that incomplete stabilization of triplet ketene occurred at 26 Torr and suggested a lifetime of $\sim 10^{-9}$ sec. Our estimate is a factor of 10 lower, but considering the uncertainties of both studies the disagreement is not serious.

The potential energy diagram[8] for ketene, altered to include a 3.5-kcal mol$^{-1}$ energy of activation for combination of $CH_2(^3\Sigma_g^-)$ and $CO(^1\Sigma_g^+)$, is shown in Figure 3. Using the $\Delta H_f^\circ$ from the Appendix, the separation between $CH_2CO(^1A_1)$ and $CH_2(^3\Sigma_g^-) + CO(^1\Sigma_g^+)$ is 78.6 kcal mol$^{-1}$. In their absorption studies Dixon and Kirby[27a] found broad diffuse bands between 3400–4735 Å, which appeared structureless under high resolution. The mean spacing between the maxima of the

(24) J. A. Kerr and A. C. Lloyd, *Trans. Faraday Soc.*, **63**, 2480 (1967).

(25) L. E. Endrenyi and D. J. LeRoy, *J. Phys. Chem.*, **71**, 1334 (1967): the activation energy for $CH_3 + CH_2CO$ may be similar to that for $CH_3 + C_2H_4$ which is $\sim 7$ kcal mol$^{-1}$.

(26) Private communication with Dr. J. W. Simons, New Mexico State University.

(27) (a) R. N. Dixon and G. H. Kirby, *Trans. Faraday Soc.*, **62**, 1406 (1966); (b) A. H. Laufer and R. A. Keller, *J. Amer. Chem. Soc.*, **93**, 61 (1971).

diffuse bands appeared to change at 3859 Å and this was interpreted as indicating different bending modes in two excited electronic states. These were thought to be the triplet $^3A_2$ and singlet $^1A_2$ electronic states, and predissociation was suggested as the cause of the diffuse nature of the $^1A_2$–$^1A_1$ and $^3A_2$–$^1A_1$ transitions. Laufer and Keller[27b] recently showed that the spacing between the diffuse bands changed regularly throughout the spectrum and suggest that the entire absorption spectrum is a singlet–singlet transition. Thus, the 61-kcal mol$^{-1}$ bond energy for ketene suggested by Dixon and Kirby can be discounted.[27b]

The RRKM equations are well known[19] and the following equation defines the unit deactivation rate constant for a nonequilibrium activation technique which has a distribution function, $f(E)$.

$$k_a = \omega D/S =$$

$$\omega \int_{E_{min}}^{\infty} \frac{k_E}{k_E + \omega} f(E) dE \bigg/ \int_{E_{min}}^{\infty} \frac{\omega}{k_E + \omega} f(E) dE$$

The vibrational frequencies for $CH_2CO(^3A_2)$ were assigned using the triplet states of aldehydes as a guide. The vibrational frequencies of the complex were taken to be the same as for the molecule, except that the C–C stretch served as the reaction coordinate. A looser complex would give larger values of $k_E$ than this tight complex and would require a larger $E_0$ to fit the same experimental rate constant. In this sense our calculations give a lower limit to $E_0$. The $k_E$ values were averaged over the distribution of formed triplet ketene molecules, and the high- and low-pressure limiting rate constants are summarized for various $E_0$ in Table II. An $E_0$ near 43 kcal mol$^{-1}$ is needed to fit the model calculation to the experimental data. No great emphasis should be placed on an exact fit, which would require a better calibration of the transition state and a better measurement of the nonequilibrium rate constant. Using 43 kcal mol$^{-1}$ as an estimate for $E_0$ and 3.5 kcal mol$^{-1}$ as the energy of activation, $T_0$ is 39.5 kcal mol$^{-1}$. This corresponds to a $^3A_2$–$^1A_2$ transition at 7250 Å, although phosphorescence has never been observed.[27b,28] Based upon the biacetyl-sensitized emission technique, Grossman, et al.,[28] concluded that photolysis of ketene in the 2800–3600-Å region gave no triplet ketene. Since the triplet state of biacetyl is 55 kcal mol$^{-1}$ above the singlet state, Grossman's work is consistent with the $^3A_2$–$^1A_2$ separation being less than 55 kcal mol$^{-1}$. We conclude, as did Laufer and Keller,[27b] that the earlier estimate[12,27a] of 61 kcal mol$^{-1}$ for this separation should be revised.

## Conclusions

(1) Nearly all reactions which can be associated with triplet methylene are suppressed at high pressure if carbon monoxide is added to butane–ketene mixtures that are photolyzed at 3200 Å. At lower pressures only partial suppression of $CH_2(^3\Sigma_g^-)$ was found with CO–

butane–ketene mixtures of 12:1:0.1–0.2, and at ~3 Torr the added CO seemed to have little influence on $[CH_2(^3\Sigma_g^-)]$. Recent high-pressure studies[29] by Montague and Rowland should be consulted for new information regarding reactions of both singlet and triplet methylene with CO. The mechanism for the singlet reaction also depends upon the pressure, but the interesting range of pressure (hundreds of Torr) is higher than for triplet methylene.

**Table II:** Calculated[b] Rate Constants for $CH_2CO(^3A_2)$

| $E_0$, kcal mol$^{-1}$ [a] | $k_a^{\infty}$, sec$^{-1}$ | $k_a^0$, sec$^{-1}$ | $\langle E \rangle$,[c] kcal mol$^{-1}$ |
|---|---|---|---|
| 21 | $3.52 \times 10^9$ | $1.66 \times 10^9$ | 22.3 |
| 26 | $1.30 \times 10^9$ | $5.80 \times 10^8$ | 27.3 |
| 31 | $5.39 \times 10^8$ | $2.31 \times 10^8$ | 32.3 |
| 35 | $2.85 \times 10^8$ | $1.19 \times 10^8$ | 36.3 |
| 39 | $1.59 \times 10^8$ | $6.43 \times 10^7$ | 40.3 |
| 43[b] | $9.21 \times 10^7$ | $3.65 \times 10^7$ | 44.3 |
| 47 | $5.54 \times 10^7$ | $2.15 \times 10^7$ | 48.3 |

[a] Includes 3.5-kcal mol$^{-1}$ activation energy for $CH_2(^3\Sigma_g^-)$ + CO. [b] The experimental rate constant was estimated as 9 ± 5 × 10$^7$ sec$^{-1}$. [c] Average energy of the formed molecules.

(2) Singlet methylene reacted with ketene approximately 0.5 times as fast as with butane. Triplet methylene reacts at least 20 times as fast with ketene as with butane.

(3) If triplet methylene is not removed, the reaction mechanism for the photolysis of ketene with butane is quite complicated and, in addition to the reactions of singlet methylene, consists of a competition between reactions of $CH_2(^3\Sigma_g^-)$ with butane, ketene, and, to a lesser extent, with monoradicals.

(4) If the CO removes $CH_2(^3\Sigma_g^-)$ by forming $CH_2CO(^3A_2)$, the data imply that the separation between $CH_2CO(^1A_2)$ and $(^3A_2)$ states is ≤40 kcal mol$^{-1}$.

(28) M. Grossman, G. P. Semeluk, and I. Unger, *Can. J. Chem.*, **47**, 3079 (1969).

(29) D. C. Montague and F. S. Rowland, submitted for publication in *J. Amer. Chem. Soc.* This work describes results from photolysis of $^{14}CH_2CO$ with added carbon monoxide. It was concluded that singlet $^{14}CH_2$ reacted with CO one-tenth as rapidly as with $CH_2CO$. The reaction with CO gave $^{14}CO$ at low pressure, but at a pressure of 840 Torr one-half of the $^{14}CH_2$ + CO adducts were stabilized. The authors found that $O_2$ was much more efficient than CO in suppressing the reactions of triplet methylene. The results obtained by Montague and Rowland do not conflict with the conclusions of this paper. However, further study using careful labeling techniques which encompasses the pressure ranges of both studies is desirable.

**Table III:** Heats of Formation

| Molecules | $\Delta H^{\circ}_{298}$ | Ref | Radicals | $\Delta H^{\circ}_{298}$ | Ref |
|---|---|---|---|---|---|
| $CH_3CH_3$ | −20.2 | c | $CH_3CH_2$ | 25.7 | d |
| $CH_3CH_2CH_2CH_3$ | −30.2 | c | $CH_2{}^a$ | 92.1 | f |
| $CH_3CH_2CH_2CH_2CH_3$ | −35 | c | $CH_3$ | 34.1 | g |
| $(CH_3)_2CHCH_2CH_3$ | −36.9 | c | $CH_3CHCH_2CH_3$ | 12.4 | d |
| $(C_2H_5CHCH_3)_2$ | −50.9 | c | H | 52.1 | e |
| $C_2H_5CHCH_3C_2H_5$ | −41.0 | d | $CH_2CH(CH_3)CH_2CH_3$ | 9.0 | b |
| $CH_2CO$ | −14.6 | e | $CH_3CO$ | −4.5 | e |
| $CH_3CHCH_2$ | 4.9 | c | $CH_3CH_2CO$ | −9.7 | h |
| $CH_2CH_2$ | 12.5 | e | | | |
| $CHCH$ | 54.2 | e | | | |
| $CO$ | −26.4 | e | | | |

$^a$ The difference in energy between $CH_2(^3\Sigma_g{}^-)$ and $CH_2(^1A_1)$ is not accurately known, and the experimental measurements may not be for the ground electronic state. In the present calculations the two $\Delta H_f{}^\circ$ were taken as being equal (but see $i$ for a summary). $^b$ Calculated from the data of this table by assuming the primary C–H bond energy to be 98 kcal mol$^{-1}$. $^c$ F. D. Rossini, "Selected Values of Physical and Thermodynamic Properties of Hydrocarbons and Related Compounds," Carnegie Press, Pittsburgh, Pa., 1953. $^d$ J. A. Kerr, *Chem. Rev.*, **66**, 465 (1966). $^e$ *Nat. Bur. Stand. Note*, **No. 270-273** (1968). For sale by Superintendent of Documents, U. S. Government Printing Office, Washington, D. C. 20402. $^f$ W. A. Chupka and C. Lifshitz, *J. Chem. Phys.*, **48**, 1109 (1968). $^g$ S. Furuyama, D. M. Golden, and S. W. Benson, *J. Amer. Chem. Soc.*, **91**, 7564 (1969). $^h$ See text. $^i$ R. W. Carr, Jr., T. W. Eder, and M. G. Topor, *J. Chem. Phys.*, **53**, 4716 (1970).

Health Service (Grant AP-00391). We thank Professor Rowland for sending us a preprint of the work described in ref 29.

**Appendix**

A summary of the heats of formation used in the text is given in Table III.

# Reactions of Recoil Carbon Atoms with Oxygen-Containing Molecules.

# II.  Structural Dependence of Carbon Monoxide Yields[1a]

## by A. F. Voigt,* G. F. Palino, and R. L. Williams[1b]

*Institute for Atomic Research and Department of Chemistry, Iowa State University, Ames, Iowa 50010*
*(Received December 21, 1970)*

Carbon-11 was produced by the reaction $^{12}C(\gamma,n)^{11}C$ in liquid alcohols and ethers, and the yield of $^{11}CO$ was determined by radiogas chromatography. The carbon monoxide yield is correlated with molecular structure by a simple bond and site counting model. Correlations are also shown between the yields and the Taft $\sigma^*$ parameter derived for inductive effects in aliphatic systems. Implications of the site model and the inductive effects of carbon-chain branching on the yields are discussed.

The study of the recoil chemistry of atomic carbon has received considerable attention in recent years and several reviews have appeared.[2-4] The observed chemistry in the simple hydrocarbons has been interpreted in terms of the insertion reactions of energetic carbon atoms, methyne, and methylene into C–H and C=C bonds. The subsequent reactions of the resultant adducts depend upon factors such as their internal energy and the phase and chemical composition of their environment.

(1) (a) Work was performed at the Ames Laboratory of the U. S. Atomic Energy Commission, Contribution No. 2759; (b) based in part on the Ph.D. Thesis submitted by R. L. Williams to Iowa State University, Ames, Iowa, 1970.

(2) A. P. Wolf, *Advan. Phys. Org. Chem.*, **2**, 201 (1964).

(3) R. Wolfgang, *Progr. React. Kinet.*, **3**, 97 (1965).

(4) R. Wolfgang, *Science*, **148**, 899 (1965).

The study of the reactions of atomic carbon with oxygen-containing molecules presents an interesting comparison and extension of the reactions observed in hydrocarbons. In general, nuclear recoil techniques prohibit the presence of elements other than carbon and hydrogen in view of the production of isotopes which would interfere with activity measurements and complicate the chemical situation by their own recoil chemistry. Oxygen-containing molecules may be subjected to $^{11}$C recoil studies without significant interference principally as a result of the short half-life (2.07 min) of the $^{15}$O isotope produced in the synchrotron irradiation. The presence of an oxygen atom in a small molecule substantially alters its electronic structure compared with a similar hydrocarbon, presenting a severely modified substrate for attack by the electrophilic carbon atom. Bonds with high charge density and nonbonding electron pairs should be very favorable attack sites and would be expected to lead to a variety of high yield products.

The reactions of recoil carbon atoms in methanol and ethanol have been presented by Palino and Voigt.[5] The product distribution was explained on the basis of reactions of $^{11}$C, $^{11}$CH, and $^{11}$CH$_2$ with the C–H and O–H bonds and of $^{11}$C with nonbonding electrons on oxygen. Iodine scavenger was used to effectively remove radiation effects attributed to the hydroxymethyl radical, the hydrogen atom, and the solvated electron. A major product from both methanol and ethanol was carbon monoxide, suggesting an efficient reaction in which these alcohols were deoxygenated by carbon atoms. Significant carbon monoxide yields were also obtained from an extended series of alcohols and ethers.[6,7] A simple bond counting model is presented in this paper which correlates the carbon monoxide yields with the structure of these oxygen-containing molecules. Correlation is also shown with the inductive effect of branched aliphatic chains as measured by the Taft $\sigma^*$ parameter.[8]

Skell, et al.,[9,10] have reported deoxygenation of some aldehydes, ketones, ethers, and alcohols by carbon atoms produced by a different method. A comparison of their results with the recoil results presented here may help clarify the nature of the fundamental deoxygenation process.

## Experimental Section

The experimental system has been described recently.[5] Recoil atoms of $^{11}$C are produced in situ by the nuclear reaction $^{12}$C($\gamma$,n)$^{11}$C using bremsstrahlung of 70-MeV maximum energy. The techniques used in these irradiations were described in a previous paper.[11] Although probably initially charged, the $^{11}$C atoms are neutral when they reach the energy for chemical reaction. Their distribution among electronic states is not known, but the ground $^3$P state and the excited singlet

states, $^1$D and $^1$S, are the most likely states in these solvents as had been postulated for hydrocarbons.[3]

The reagent chemicals used in the irradiations were: for methanol and the propanols, Fisher Certified reagent; for ethanol, Enjay Chemical Co., for the butanols, isopropyl ether, tetrahydrofuran, and dioxane, Matheson Coleman and Bell Chromatoquality; for ethyl ether, Baker and Adamson; for n-propyl ether, Matheson Coleman and Bell reagent. The iodine scavenger was J. T. Baker Analytical reagent, and isopentane, a calibration standard, was Phillips Petroleum Research grade. The alcohols were treated with H$_2$SO$_4$ and 2,4-dinitrophenylhydrazine to remove traces of aldehydes and ketones.[12] Methanol was dried by reaction with magnesium methoxide,[13] and the other alcohols were dried with Molecular Sieve 4A (Linde Co.) using an apparatus and technique similar to that described by Arthur, et al.[14] The ethers were purified by two distillations, the second from Drierite[15] to reduce water content. Samples were degassed by repeated freeze–thaw cycles under vacuum.

Carbon monoxide was separated from all the other $^{11}$C products by gas chromatography using a 30-ft column of 35% 2-ethylhexyl acetate (Eastman Organic) on Chromosorb P, 45–60 mesh (F & M Scientific). The product identity was verified with a 14-ft molecular sieve column, Linde Type 5A (Matheson Coleman and Bell), 40–60 mesh.

A FORTRAN computer program was written to aid in determining the site values, or reaction probabilities at a particular atom or bond, by solving a set of 13 equations in eight unknowns for the best values of the eight parameters. These equations were of the form

$$Y = \frac{x_j}{\sum_{n=1}^{8} p_i x_i} \tag{1}$$

in which $Y$ is the experimental $^{11}$CO yield, $x_i$ and $x_j$ are site values for specific bonds or atoms, and $p_i$ is the number of $x_i$ sites in the molecule.

(5) G. F. Palino and A. F. Voigt, J. Amer. Chem. Soc., 91, 242 (1969).

(6) G. F. Palino, Ph.D. Thesis, Iowa State University, Ames, Iowa, 1967.

(7) R. L. Williams, Ph.D. Thesis, Iowa State University, Ames, Iowa, 1970.

(8) R. W. Taft, Jr., in "Steric Effects in Organic Chemistry," M. S. Newman, Ed., Wiley, New York, N. Y., 1956.

(9) P. S. Skell, J. H. Plonka, and R. R. Engel, J. Amer. Chem. Soc., 89, 1748 (1967).

(10) P. S. Skell and R. F. Harris, ibid., 91, 4440 (1969).

(11) D. E. Clark and A. F. Voigt, ibid., 87, 5558 (1965).

(12) J. H. Baxendale and F. W. Mellows, ibid., 83, 4720 (1961).

(13) L. F. Fieser, "Experiments in Organic Chemistry," 3rd ed, D. C. Heath, Boston, Mass., 1957, p 289.

(14) P. Arthur, W. M. Haynes, and L. P. Uarga, Anal. Chem., 38, 1630 (1966).

(15) W. A. Hammond, "Drierite," Stoneman Press, Columbus, Ohio, 1961.

The equations are linearized using the constant and linear terms of a Taylor's series expansion about a set of initial values for the parameters. The set of 13 equations of the form

$$Y = Y_0 \bigg|_{x_0} + \sum_{n=1}^{8} \frac{\partial Y}{\partial x_i}\bigg|_{x_0} (x_i - x_0)$$

can be written simply as the matrix equation

$$\Delta Y = A \Delta x$$

where $\Delta Y = (Y - Y_0|_{x_0})$, $\Delta x = (x_i - x_0)$, $A$ = the matrix of partial derivatives. For an arbitrary set of initial $x_0$ values, the $\Delta x = x_i - x_0$ values can be determined. An improved set, i.e., making $\Delta Y$ smaller, is generated by $x_0 = x_0' - \Delta x$. Reiteration in this manner is repeated until $\Sigma(\Delta Y)^2$ is minimized. The final $x_0'$ values determined by this procedure are the molecular site values which result in the best agreement between observed and calculated yields of $^{11}CO$ from the alcohols and ethers studied. The iterative procedure in this program not only leads to a minimum value of $\Sigma(\Delta Y)^2$, i.e., converges, but results in the same normalized set of site values from a wide range of initial values indicating that this is a unique set, with no false minima.

The precision in the site values differs considerably. For two of them, O in a tertiary alcohol and in a secondary ether, only a single determination was made, in tert-butyl alcohol and isopropyl ether, respectively. The large error shown for the competing site value for the C–H bond of >CH– results from the fact that in each compound in which this group occurs its site value contributes a small part of the total denominator. Thus large variations in its value produce only small changes in the calculated yield and vice versa.

## Results

The carbon monoxide yields for the complete list of alcohols and ethers studied are given in Table I. As in previous work from this laboratory yields are on the basis of total $^{11}C$ produced in the sample. The yield of acetylene-$^{11}C$ from isopentane was used as an intercomparison with previous calibration experiments. For the pure, unscavenged compounds the $^{11}CO$ yields showed some dose dependence, but in the presence of iodine the variation of yield with dose was not outside the experimental error. Studies with varied iodine concentrations showed that above a minimum concentration, additional iodine did not change the yield. The strong dose dependence and sharp increase in yield in the presence of iodine which were observed in the case of methanol is the subject of another paper.[16] For the purpose of correlating the $^{11}CO$ yields with structure, all of the results with $\sim 1 \times 10^{-3}$ mol fraction of iodine were used regardless of dose.

The correlation of $^{11}CO$ yield with structure on the basis of a simple site model was successful for the full range of compounds studied in spite of its simplicity.

**Table I:** Carbon Monoxide Yields from Alcohols and Ethers

| Compd | Unscavenged a | Unscavenged b | Scavenged, 0.1 mol % I₂ a | Scavenged, 0.1 mol % I₂ b |
|---|---|---|---|---|
| Methanol | 19.1 | 9.63 | 24.1[c] | 24.9 |
| Ethanol | 14.5 | 14.6 | 16.9 | 17.5 |
| 1-Propanol | 11.3 | 10.2 | 12.7 | 12.7 |
| Isopropyl alcohol | 14.6 | 14.3 | 14.5 | 14.7 |
| 1-Butanol | 9.26 | 8.26 | 9.87 | 9.83 |
| Isobutyl alcohol | 10.3 | 10.3 | 10.1 | 10.7 |
| 2-Butanol | 11.8 | 11.8 | 12.5 | 12.3 |
| tert-Butyl alcohol | 13.2 | 12.2 | 16.1 | 15.9 |
| Ethyl ether | 9.38 | 9.45 | 9.40 | 9.40 |
| Propyl ether | 6.81 | 6.63 | 6.50 | 6.59 |
| Isopropyl ether | 10.2 | 10.2 | 9.90 | 9.94 |
| Tetrahydrofuran | 10.7 | 11.1 | 10.7 | 11.2 |
| p-Dioxane | 17.8 | 19.4 | 18.8 | 19.4 |

$^a$ Dose = 0.01 eV/molecule. $^b$ Dose = 0.05 eV/molecule. $^c$ Standard deviations of yields are of similar magnitude to those shown in Table III.

Other attempts at correlation, e.g., with polarizabilities as measured by refractivities and with fractional collision cross sections, were not successful. Within compounds with the same chemical composition and functional groups, e.g., the butanols, an interesting correlation was observed between these yields and the $\sigma^*$ values published by Taft.[8] This, as shown later in the Discussion, did not adequately correlate compounds of different functional groups, e.g., alcohols and ethers. Attempts to apply a correlation like the site model to the yields of other major products such as acetylene-$^{11}C$ were unsuccessful. The success of this model for $^{11}CO$ seems to indicate a degree of simplicity in the oxygen abstraction which is not present in the reactions producing acetylene or other products.

## Discussion

*A. The Site Model.* The various structural types of C–H bonds and O centers used in the site model calculations are listed in Table II. Site values, which can be considered as relative reaction probabilities, were determined using the FORTRAN computer program discussed in the Experimental Section and were normalized by assigning the value 1.00 to a C–H bond of a –CH₃ structural element. An illustrated calculation of CO yields appears below.

$$Yield_{CO} =$$

$$\frac{\text{sum of product site values}}{\text{sum of all site values in the molecule}} \times 100 \quad (2)$$

for 1-propanol, $CH_3CH_2CH_2OH$

$$Y_{CO} = \frac{1.00}{1.00 + 3 \times 1.00 + 4 \times 0.98} \times 100 = 12.6\%$$

(16) R. L. Williams and A. F. Voigt, J. Phys. Chem., **75**, 2253 (1971).

**Table II:** Molecular Sites and Site Values

| Molecular sites | Site value |
|---|---|
| CO production sites | |
| O in –CH$_2$OH | $1.00 \pm 0.01$ |
| O in >CHOH | $1.19 \pm 0.06$ |
| O in >C–OH | $1.71 \pm 0.05$ |
| O in –CH$_2$OCH$_2$– | $0.95 \pm 0.02$ |
| O in >CHOCH< | $1.49 \pm 0.09$ |
| Competing sites | |
| C–H bond of –CH$_3$ | $1.00 \pm 0.02$ |
| C–H bond of –CH$_2$ | $0.98 \pm 0.02$ |
| C–H bond of >CH– | $0.74 \pm 0.33$ |

The final site values are shown in Table II, and in Table III the [11]CO yields calculated as in eq 2 are compared with the experimental values. The difference between calculated and experimental values is approximately the same as the uncertainty in the experimental values.

**Table III:** Carbon Monoxide Yields and the Site Model

| Compd | Experimental CO yield, % | CO production sites | Total sites | Calculated CO yield, % |
|---|---|---|---|---|
| Methanol | $24.5 \pm 0.3$[a] | 1.00 | 4.00 | 25.0 |
| Ethanol | $17.3 \pm 0.6$ | 1.00 | 5.96 | 16.8 |
| 1-Propanol | $12.7 \pm 0.2$ | 1.00 | 7.92 | 12.6 |
| Isopropyl alcohol | $14.7 \pm 0.2$ | 1.19 | 7.93 | 15.0 |
| 1-Butanol | $9.9 \pm 0.2$ | 1.00 | 9.88 | 10.1 |
| Isobutyl alcohol | $10.4 \pm 0.2$ | 1.00 | 9.70 | 10.3 |
| 2-Butanol | $12.4 \pm 0.2$ | 1.19 | 9.89 | 12.0 |
| tert-Butyl alcohol | $16.0 \pm 0.4$ | 1.71 | 10.71 | 16.0 |
| Ethyl ether | $9.4 \pm 0.1$ | 0.95 | 10.87 | 8.7 |
| n-Propyl ether | $6.5 \pm 0.3$ | 0.95 | 14.79 | 6.4 |
| Isopropyl ether | $9.9 \pm 0.2$ | 1.49 | 14.97 | 9.9 |
| Tetrahydrofuran | $10.9 \pm 0.2$ | 0.95 | 8.79 | 10.8 |
| Dioxane | $19.1 \pm 0.3$ | 1.90 | 9.74 | 19.5 |

[a] Error limits are standard deviations from ten or more samples.

Differences in the site values for the oxygen groups are of interest. A constant value of 1.00 for the –OH group in the primary alcohols results from the regular decrease in the [11]CO yield as the chain length is increased. The secondary –OH group has a higher site value (1.19) indicating that it is 20% more productive in the deoxygenation reaction. The –OH site value for the tert-butyl alcohol is considerably higher (1.71). The site value for the oxygen center of unbranched ethers (0.95) is essentially the same as the primary –OH value while the effect of branching in the ethers is very pronounced as seen in the site value for oxygen in isopropyl ether, 1.49.

*B. Inductive Effects.* The effect of branching on the yields from a series like the butanols suggests a corre-
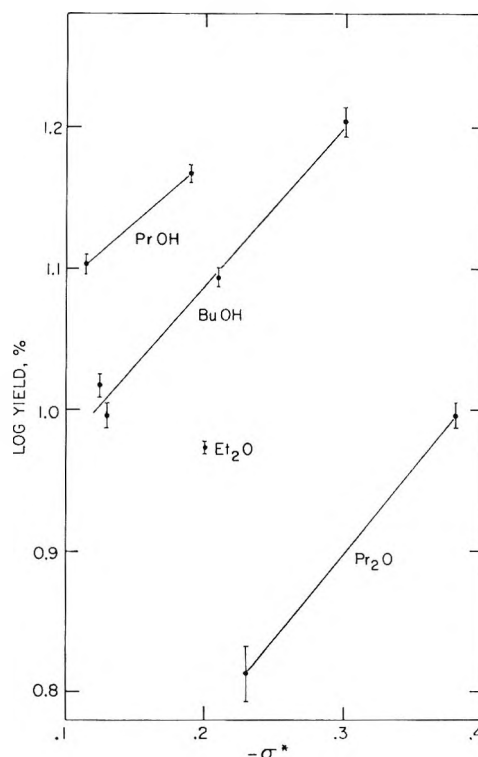


Figure 1. Yield [11]CO vs. inductive effect of alkyl groups, $\sigma^*$ for H atom is not included.

lation between yields and parameters describing the inductive effect, like the Hammett $\sigma$. The particular parameter which seems most likely to apply to these aliphatic reactions is Taft's $\sigma^*$.[8] In applying this concept an equation similar to the Hammett equation was used

$$\log Y_1/Y_2 = k(\sigma_1^* - \sigma_2^*) \qquad (3)$$

In applying this equation $Y$ is the yield of product from an alcohol ROH and $\sigma^*$ is the inductive parameter for the R group. The yields are assumed to reflect the relative rate constants for the deoxygenation reaction although competition studies were not conducted. Curves of the data on a $\log Y$ vs. $\sigma^*$ plot are given in Figure 1. The slope of the least-squares line for the butanols is quite close to that for the two points for the propanols. We would not expect these lines to have the same intercept since the fraction of the collisions between ^{11}C and the molecule which yield [11]CO must depend on the atomic fraction of oxygen in the molecule.

If the effect of the two alkyl groups in an ether are considered additive so that eq 3 becomes

$$\log Y_1/Y_2 = k(2\sigma_1^* - 2\sigma_2^*)$$

for the propyl ethers, the value of $k$ is remarkably close to that for the butanols as seen in Figure 1 and Table IV.

The role of hydrogen and the comparison of alcohols and ethers is, however, quite unclear. The addition of

**Table IV:** Carbon Monoxide Yields and $\sigma^*$

| Compd | CO yield, % | $\sigma^*$ for alkyl groups | $k$ |
|---|---|---|---|
| 1-Propanol | $12.7 \pm 0.2$ | $-0.115$ | $0.85 \pm 0.17^a$ |
| Isopropyl alcohol | $14.7 \pm 0.2$ | $-0.190$ | |
| 1-Butanol | $9.9 \pm 0.2$ | $-0.130$ | |
| Isobutyl alcohol | $10.4 \pm 0.2$ | $-0.125$ | $1.14 \pm 0.09^b$ |
| 2-Butanol | $12.4 \pm 0.2$ | $-0.210$ | |
| tert-Butyl alcohol | $16.0 \pm 0.4$ | $-0.300$ | |
| Ethyl ether | $9.4 \pm 0.1$ | $2(-0.100)$ | |
| n-Propyl ether | $6.5 \pm 0.3$ | $2(-0.115)$ | $1.22 \pm 0.22^a$ |
| Isopropyl ether | $9.9 \pm 0.2$ | $2(-0.190)$ | |

[a] Error estimated by using extreme values of yields. [b] Slope and error obtained using least-squares equations.

the Taft $\sigma^*$ value for the hydrogen atom ($+0.490$) to the $\sigma^*$ for the alkyl groups in the alcohols would displace all of these points by a large constant amount without, of course, changing the slopes of the lines. Data do not seem sufficient to attempt a correlation of the alcohol and ether results at this time.

*C. Conclusions.* It appears that much of the observed variations in yields can be correlated with the inductive effect as defined by Taft. On the other hand, the site model, although it does not at this time provide a mechanistic description of the process, does

succeed in correlating all of the yield data, including that for the two cyclic ethers. The evidence clearly indicates that deoxygenation is enhanced in proportion to the greater availability of electrons to the $^{11}C$ atom as the groups attached to the oxygen become better electron donors.

This is strong corroboration of the conclusion stated by Blaxell, MacKay, and Wolfgang[17] that electron-deficient species, such as $^{11}C$, will in abstraction and insertion reactions preferentially attack sites where electrons are most readily available. Their results, in which attack at C-F, C-H, and C=C sites were compared, gave clear evidence of this preference, and the present results provide the first quantitative measure of the effect.

The site model and inductive effect relations are not contradictory. From them a conclusion can be reached that the deoxygenation reaction is efficient and predictable. It is strongly dependent on electronic factors. An attractive possibility is a one-step process by direct collision with a site sufficiently reactive for the reaction to be probable even without excessive collision energy. This would account for the high yields, and the one-path simplicity of the mechanism would account for the effective calculation method involving simple site and bond counting.

(17) D. Blaxell, C. MacKay, and R. Wolfgang, *J. Amer. Chem. Soc.*, **92**, 50 (1970).

# Reactions of Recoil Carbon Atoms with Oxygen-Containing

# Molecules. III. Reaction Mechanisms in Methanol[1a]

## by R. L. Williams[1b] and A. F. Voigt*

*Institute for Atomic Research and Department of Chemistry, Iowa State University, Ames, Iowa 50010*
*(Received December 21, 1970)*

*Publication costs borne completely by The Journal of Physical Chemistry*

Carbon-11 was produced by the reaction $^{12}C(\gamma,n)^{11}C$ in liquid methanol, and the yields of labeled products were determined by radiogas chromatography. Reaction alternatives for the intermediate resulting from carbon atom insertion into a C–H bond of methanol are discussed. The dependence of the yields of carbon monoxide and acetaldehyde on the duration of the irradiation period is attributed to reactions of the solvated electron; kinetic expressions are developed.

The behavior of energetic carbon atoms produced in nuclear reactions has been studied rather extensively,[2–4] but only a few of the studies of organic systems have involved compounds containing alcoholic or ether groups. Voigt, et al.,[5] have recently discussed the structural dependence of carbon monoxide yields from alcohols and ethers. Deoxygenation and other reactions of vapor-deposited carbon atoms with oxygen-containing molecules have been reported by Skell, et al.[6–8]

Palino and Voigt[9] have presented a rather complete study of the methanol system. Additional studies of carbon atom reactions with methanol are reported in this paper in an attempt to clarify and evaluate some of the reaction schemes. Carbon-11 was produced by the reaction $^{12}C(\gamma,n)^{11}C$ and the yields were determined by radiogas chromatography. The strong dose dependence of the yields of carbon monoxide, acetaldehyde, and glycolaldehyde is discussed, and a brief kinetic treatment involving reactions of the methanolated electron is presented.

## Experimental Section

The experimental system has been described recently.[9] Recoil atoms of $^{11}C$ are produced *in situ* by the nuclear reaction $^{12}C(\gamma,n)^{11}C$ using the bremsstrahlung beam from a General Electric Model M electron synchrotron operating at a maximum energy of 70 MeV. The products were separated by gas chromatography using the columns reported previously. The purification of methanol with 2,4-dinitrophenylhydrazine and sulfuric acid was also reported.

The detection system for monitoring the total activity and for the radioactive effluent consisted of a 7.5 × 7.5 cm NaI(Tl) crystal (Isotopes, Inc.) with a 1.6-cm transverse hole through which the effluent was carried in an 8-mm quartz tube wound with iron resistance wire and heated. The crystal, which is very sensitive to thermal shock, was protected by a silvered air con-

denser placed between the heated counting tube and the crystal wall. With this configuration, the effluent tube could safely be heated to 160°.

*Yield and Dose Measurements.* Yields were calculated as previously described[9] and are based on the total $^{11}C$ produced. As before this activity was found to be directly proportional to the integrated dose as measured by cobalt glass dosimetry[9,10] which in turn was calibrated against Fricke dosimetry.

The integrated dose received by the sample can be calculated from eq 1

$$\text{dose (rads)} = \frac{9.09(\pm 0.88) \times 10^{21} M t_b e^{\lambda t_m}}{(1 - e^{-\lambda t_b})\rho_c} \quad (1)$$

in which the constant is determined from the dosimetry experiments,[11,12] $\rho_c$ is the carbon atom density (atoms/cm$^3$), and $t_b$ and $t_m$ are the irradiation time and time between the irradiation and monitor count $M$. The dose rate was taken as this dose divided by the irradiation time; thus the assumption was made that the synchrotron intensity was constant during the irradia-

(1) (a) Work was performed at the Ames Laboratory of the U. S. Atomic Energy Commission, Contribution No. 2787; (b) based on part of the Ph.D. Thesis submitted by R. L. Williams to Iowa State University.

(2) A. P. Wolf, *Advan. Phys. Org. Chem.*, **2**, 201 (1964).

(3) R. Wolfgang, *Progr. React. Kinet.*, **3**, 97 (1965).

(4) R. Wolfgang, *Science*, **148**, 899 (1965).

(5) A. F. Voigt, G. F. Palino, and R. L. Williams, *J. Phys. Chem.*, **75**, 2248 (1971).

(6) P. S. Skell, J. H. Plonka, and R. R. Engel, *J. Amer. Chem. Soc.*, **89**, 1748 (1967).

(7) P. S. Skell and R. F. Harris, *ibid.*, **91**, 4440 (1969).

(8) P. S. Skell and J. H. Plonka, *ibid.*, **92**, 836 (1970).

(9) G. F. Palino and A. F. Voigt, *ibid.*, **91**, 242 (1969).

(10) N. J. Kreidl and G. E. Blair, *Nucleonics*, **14** (3), 82 (1956); **17** (10), 58 (1959); G. E. Blair, *J. Amer. Ceram. Soc.*, **43**, 426 (1960).

(11) G. F. Palino, Ph.D. Thesis, Iowa State University, Ames, Iowa, 1967.

(12) R. L. Williams, Ph.D. Thesis, Iowa State University, Ames, Iowa, 1970.

**Table I:**  Yields (%) of Selected Products from Methanol Systems

| Product | Unscavenged a | Unscavenged b | Scavenged (concn i n mol %) 0.5 $I_2$ | Scavenged (concn i n mol %) 0.1 $Br_2$[c] | Other[d] |
|---|---|---|---|---|---|
| Methyl iodoacetate |  |  | 3.5 | 2.7 |  |
| Methyl acetate | 3.6 | 3.0 | ... | ... | N.D.[e] |
| Acetaldehyde | 2.4 | 0.8 | ... | ... | 7.3 |
| 1,2-Propanediol | 5.7 | 8.5 | ... | ... | 1.2 |
| 1,3-Propanediol | 1.1 | 1.3 | ... | ... | ... |
| 2,2-Dimethoxyethane | ... | ... | 3.0 | N.D. | N.D. |
| 2,2-Dimethoxyiodoethane |  |  | 9.4 | 9.4 |  |
| 2-Iodoethanol |  |  | 1.3 | 1.3 |  |
| Carbon monoxide | 16.3 | 10.2 | 24.8 | N.D. | 24.7 |
| Glycolaldehyde | 3.8 | 1.3 | ... | ... | ... |

[a] Dose = 0.009 eV molecule$^{-1}$.  [b] Dose = 0.036 eV molecule$^{-1}$.  [c] Yields of corresponding bromo products.  [d] Acetaldehyde or glycolaldehyde carrier present during irradiation.  [e] Yield not determined under these conditions.

tion period.  Dose rate and irradiation time are variables in the kinetic treatment.

*Bromine Scavenger Studies.*  Bromine was substituted for iodine as the scavenger in several experiments to aid in product identification and to verify the free-radical nature of particular reactions.  The product 2-iodoethanol is unstable toward thermal decomposition and has a long retention time on the columns used in these studies, but 2-bromoethanol can be handled more easily.  Identification of dimethoxybromoethane in the bromine-scavenged system led to laboratory preparations of the analogous iodo compound.  A synthesis method was suggested by the formation mechanism proposed for the recoil system, and its success lends considerable support to that proposal.  Methyl vinyl ether, the methoxy analog of a proposed enol intermediate, [$H_2C$=$CHOH$], and iodine were found to react in methanol at 0° yielding dimethoxyiodoethane.  Alternatively dimethoxyiodoethane was prepared by direct exchange of iodide for bromide by equilibration of a solution of NaI and $BrCH_2CH(OCH_3)_2$ in acetone.  In either preparation aliquots of the reaction mixture were injected onto the chromatograph column with an irradiated sample, and the unknown activity peak was identified by retention time without purification of the preparation product.

*Acetal Formation.*  The formation of an acetal from the corresponding aldehyde and alcohol under the conditions of these experiments was discussed previously.[9]  It appears that this reaction, which is usually considered to be an acid-catalyzed, high-temperature process, can also be catalyzed by elemental iodine, possibly through a halohydrin intermediate.

## Results

*Product Yields.*  Table I presents selected product yields observed in dose and scavenger studies.  Several of these yields show significant dose dependence in contrast to most products from methanol.[9]  In the presence of iodine or bromine the yields of methylace-

tate, acetaldehyde, glycolaldehyde, 1,2-propanediol, and 1,3-propanediol are reduced to below detection limits.  These products are replaced quantitatively by the new products methyl iodoacetate, dimethoxyethane, 2,2-dimethoxyiodoethane, 2-iodoethanol, and by the increased yield of carbon monoxide.  The yields of acetaldehyde, carbon monoxide, and 1,2-propanediol are also reported for samples to which carrier quantities of acetaldehyde or glycolaldehyde were added before irradiation.

*Dose and Dose Rate Effects.*  The yield of $^{11}CO$ from methanol is dependent on both dose and dose rate. The results are listed in Table II over the ranges of these two variables studied.  Fewer data were obtained for acetaldehyde, and the dose dependence is reported for samples irradiated over a range of dose rates.

**Table II:**  Dependence of Carbon Monoxide and Acetaldehyde Yields on Dose and Dose Rate

| Dose rate, eV molecule$^{-1}$ min$^{-1}$ × 10$^3$ | Dose, eV molecule$^{-1}$ × 10$^2$ 0.5 | 0.9 | 1.5 | 3.0 |
|---|---|---|---|---|
| Carbon Monoxide Yield | | | | |
| 1.5 | 19.3 | 15.8 | 13.3 | 11.2 |
| 1.9 | 19.4 | 16.1 | 13.7 | 10.8 |
| 2.2 | 19.2 | 16.3 | 14.0 | 10.4 |
| 2.7 | 18.5 | 14.8 | 12.5 | 10.2 |
| 3.2 | 17.8 | 14.2 | 11.6 | 9.1 |
| Acetaldehyde Yield | | | | |
| 1.9–2.6 | 4.0 | 2.4 | 1.2 | 0.9 |

## Discussion

*Reactions of the Insertion Intermediate.*  A primary concern is the behavior of the C–H insertion intermediate which is the precursor of several products. The proposed reaction scheme is shown in Figure 1.
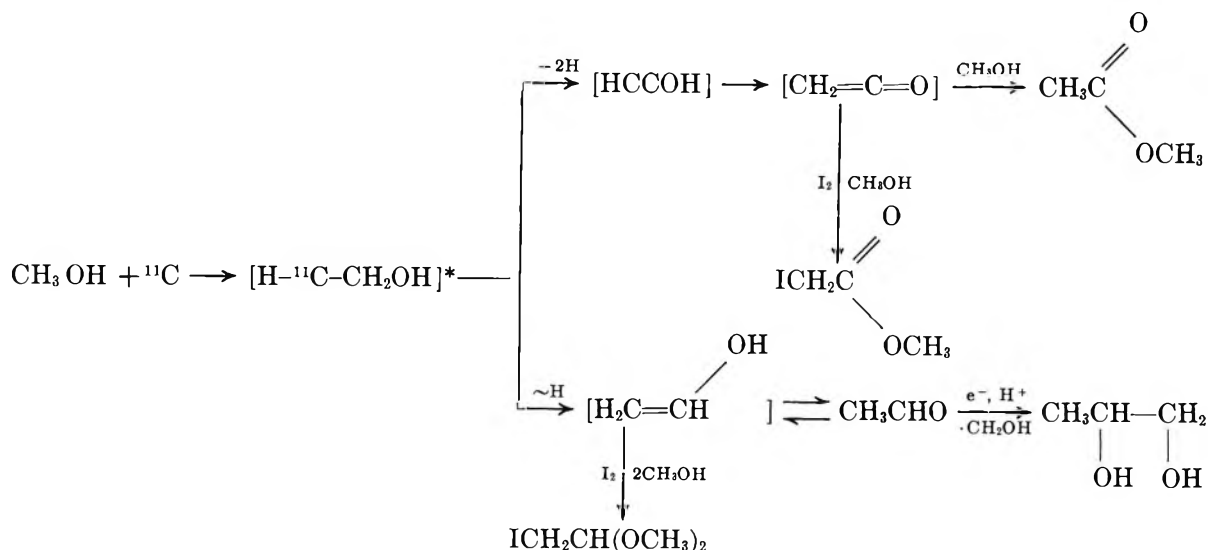
Figure 1. Proposed reaction sequence.

The insertion intermediate [H–$^{11}$C–CH$_2$OH]* can result from the interaction of methanol with carbon atoms over a wide range of energy. It is suggested that enough energy is deposited locally in some of the insertion processes to result in the loss of both hydrogen atoms from the methanol carbon atom producing an alkynol intermediate which rapidly collapses to ketene. In the unscavenged system the ketene is efficiently trapped by methanol to form the ester, methyl acetate. In the scavenged system iodine reacts with the ketene, and the product and solvent further react to produce methyl iodoacetate. The quantitative replacement of the ester by the iodo ester is shown in Table I.

If the insertion intermediate is produced with less energy, it can stabilize by molecular collision and intramolecular hydrogen transfer to the enol form of acetaldehyde which in the unscavenged system rapidly tautomerizes to the aldehyde. If iodine is present, the enol isomer is trapped and reacts with solvent to produce dimethoxyiodoethane, the dimethylacetal of iodoacetaldehyde. The acetaldehyde yield (Table II) is strongly dose dependent, an effect which Palino[11] attributed to reaction with the solvated electrons in the system to produce 1,2-propanediol. The addition of carrier quantities of acetaldehyde or glycolaldehyde to the sample before irradiation protects the trace amounts of labeled acetaldehyde and increases its yield to 7.3%, which we consider to be its undisturbed production value.

*Radical Reactions.* The yield of 1,2-propanediol was reduced from its dose dependent values of from 5.7 to 8.5% in the unscavenged system to zero in the presence of scavenger and to 1.2% with aldehyde carrier present. Several mechanisms apparently operate for its formation. Part of its yield is attributed to the free-radical mechanism shown in eq 2 (Figure 2 in ref 9). This is considered the mechanism responsible for the

1.2% yield of 1,2-propanediol observed in the irradiations with added aldehyde. The yield of 1,2-propanediol attributable to conversion of acetaldehyde would be the difference between its yield in the pure system and 1.2 or 4.5–7.3% depending on dose.

$$CH_3\dot{C}HOH \begin{cases} \xrightarrow{\cdot H} CH_3CH_2OH \\ \xrightarrow{\cdot CH_2OH} CH_3CHOHCH_2OH \\ \xrightarrow{I_2} CH_3CHI(OH) \xrightarrow{2CH_3OH} \end{cases} \quad (2)$$

$$CH_2CH(OCH_3)_2$$
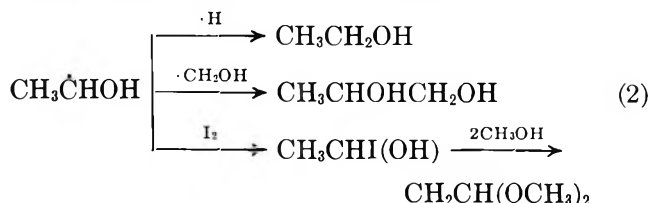
The yield of dimethoxyethane in the scavenged system (3.0%) is considerably greater than can be attributed to its replacement of the 1.2% yield of 1,2-propanediol which is considered to be produced by reaction 2. A proposed path for the additional 1.8% of dimethoxyethane is iodine assisted acetal formation, suggesting that the trapping of the acetaldehyde precursor [CH$_2$=CHOH] by iodine is incomplete.

It was proposed by Palino and Voigt[9] that $^{11}\dot{C}H_2$-CH$_2$OH combines with the radiation radical $\dot{C}H_2OH$ to produce 1,3-propanediol in a reaction analogous to the radical formation of 1,2-propanediol discussed previously. If this were the case, one would expect the replacement of 1,3-propanediol by 2-iodoethanol in the scavenged system. Since 2-bromoethanol is easier to handle chromatographically than the iodoethanol, bromine scavenger was used giving the results shown in Table I with 1.3% of 2-bromoethanol and no 1,3-propanediol. It was possible to repeat the experiment with iodine using a shorter column resulting in the same yield (1.3%) of 2-iodoethanol replacing the diol. The earlier proposal for the formation mechanism for 1,3-propanediol is substantiated.

*Dose and Dose Rate Studies.* Reactions of radiation-produced species with labeled products would appar-

ently account for systematic yield changes, the interference by radical reactions becoming more significant with increasing dose. Closer examination of the mathematics involved indicates that this explanation is not the most direct approach. The yield of any product is the fraction of the total activity of the sample measured after the irradiation. Carbon-11 is produced at a constant production rate dependent on the synchrotron beam intensity (dose rate), but decays by positron emission at a rate expressed by its decay constant $\lambda$. Thus the carbon activity does not increase linearly with irradiation time but instead follows the usual isotope production curve, $A = P(1 - e^{-\lambda t_b})$. Since the carbon-labeled products have the same decay constant, the yield of most products is not time dependent. However, if radical reactions remove some of the product molecules the yield must decrease, but the nature of the change is not obvious. During the beam burst the radicals are present at a steady-state concentration dependent on the reaction medium and the intensity of the radiation beam. The radical concentration is much higher than the concentration of $^{11}$C-labeled products. Radical reactions would then be expected to remove a constant fraction, $\alpha$, per unit time of the $^{11}$C-labeled product present at any time. Therefore the activity attributed to the product would increase during the irradiation by the modified production formula, $A = P(1 - e^{-(\lambda+\alpha)t_b})$ and the yield, given by eq 3 would

$$\text{yield} = \frac{\dfrac{P_1}{\lambda + \alpha}(1 - e^{-(\lambda+\alpha)t})}{\dfrac{P_2}{\lambda}(1 - e^{-\lambda t})} \tag{3}$$

show a nonlinear decrease with increasing irradiation time. Evidence for such nonlinearity will be presented.

*Solvated Electron Reactions.* The yields of carbon monoxide, glycolaldehyde, and acetaldehyde in the unscavenged methanol system show unusually strong dependence on dose and dose rate (Table II). Other products in the methanol system[9] show less pronounced dependences which are nearly linear with dose. Decreases in yields for unsaturated hydrocarbon products have been attributed[11] to reactions of hydrogen atoms resulting in increased yields of more-saturated products with increased time. The yields of some products, such as ethanediol, 1,3-propanediol, and ethanol, are attributed at least in part to combination of labeled radicals with the predominant radiation species in methanol,[13] $\cdot$CH$_2$OH and $\cdot$H, and show increases in yield with irradiation time. These minor dependences can be considered normal behavior for labeled products in methanol, and similar effects have been reported for other systems.[11,14]

A carbon monoxide production site model[5] was based on results of samples scavenged with iodine in which the

carbon monoxide yield is independent of irradiation time for all the compounds studied. In all cases the carbon monoxide yield is somewhat higher if iodine is present during the irradiation, but for unscavenged methanol the carbon monoxide yield falls from near the scavenged yield for short irradiation times to only one-third of this value for irradiation times of 20–30 min. The yields of acetaldehyde and glycolaldehyde show similar time dependencies in the same unscavenged system. The solvated electron, an important radiation product, appears to be a common reactant for all three of these species. The rate constants of reactions of $e_{aq}^-$ and other solvated electrons with a large number of compounds have been measured using the technique of pulse radiolysis and have been conveniently tabulated.[15] An intensive review of the current understanding of the solvated electron and its reactions has recently been prepared[16] and is recommended as an indepth summary of the subject.

The study of reactions of $e_{aq}^-$ with more than 300 compounds suggests that the reactivity of different chemical species toward $e_{aq}^-$ is a function of the availability of a vacant orbital on the substrate as well as of the change in free energy on incorporation of an additional electron. The compounds carbon monoxide and acetaldehyde are among the more reactive toward $e_{aq}^-$ with bimolecular rate constants $1 \times 10^9$ and $3.5 \times 10^9$ $M^{-1}$ sec$^{-1}$. The rate constant for glycolaldehyde has apparently not been determined although all the simple aldehydes and ketones show similar reactivities, with the exception that formaldehyde is about two orders of magnitude less reactive. The low reactivity of formaldehyde and its precursor radical $\cdot$CH$_2$OH in the radiolysis of methanol, coupled with the low reactivity of methanol itself toward $e_{solv}^-$ ($k < 10^4$ $M^{-1}$ sec$^{-1}$) makes methanol an ideal solvent for the study of the solvated electron. The anomalous behavior of formaldehyde provides the reason why reactions of the solvated electron have been observed with recoil products in methanol but not in other systems. In the radiation chemistry of ethanol, for example, large quantities of acetaldehyde are produced, $G = 3.14$.[13] Acetaldehyde effectively removes the solvated electron, thus eliminating its effects on yields in recoil studies. In methanol radiolysis the only product which can significantly reduce the concentration of solvated electrons is carbon monoxide, $G = 0.26$, which due to its low concentration would only be important in extended irradiations.

The rates of $e_{aq}^-$ reactions have been used in the pre-

(13) J. W. T. Spinks and R. J. Woods, "An Introduction to Radiation Chemistry," Wiley, New York, N. Y., 1964.

(14) D. E. Clark and A. F. Voigt, *J. Amer. Chem. Soc.*, **87**, 5558 (1965).

(15) M. Anbar and P. Neta, *Int. J. Appl. Radiat. Isotopes*, **16**, 227 (1965).

(16) (a) L. M. Dorfman, *Advan. Chem. Ser.*, No. **50**, 36 (1965); (b) M. Anbar, *ibid.*, **50**, 45 (1965).

ceding discussion since these values have been determined for a wide variety of compounds. Very similar rate constants for the solvated electron in methanol and ethanol have been reported for some of the same compounds. For example, the rate constants for $O_2$ with the various solvated electrons are $2.0 \times 10^{10}$ for water and $1.9 \times 10^{10}$ for both methanol and ethanol.[16a] Although such close agreement cannot be assumed for all compounds, no significant differences have been reported.

The subsequent reactions of the molecular ions formed in the $e_{solv}^-$ reaction have not been as thoroughly studied. The work of Weiss[17] is of particular interest and is the basis for the reaction proposals to be made here. He reported the formation of glycolic acid by the combination of the $\cdot CO_2^-$ radical ion with the methanol radical $\cdot CH_2OH$ in the radiolysis of solutions of methanol in water with a $G$ value of 2.7. Similarly, $\cdot COH$ combines with $\cdot CH_2OH$ to produce glycolaldehyde. The radical $\cdot COH$ could be formed by the reaction of $CO$ with $e_{solv}^-$ followed by neutralization, or by the combination of $CO$ with $\cdot H$. The hydrogen atom reaction is apparently unimportant in methanol since similar concentrations of $\cdot H$ are present during the irradiation of the other alcohols in which the carbon monoxide yields show little time dependence.

*Kinetic Analysis. Acetaldehyde.* The reaction of the methanolated electron with acetaldehyde accounts for the dose dependence of its yield by a simple kinetic analysis. The following reactions must be considered.

$$CH_3OH + \gamma \xrightarrow{k_1} {}^{11}C \text{ products} \quad (4)$$

$$CH_3OH + {}^{11}C \xrightarrow{k_2} CH_3{}^{11}CHO \quad (5)$$

$$CH_3{}^{11}CHO + e_{solv}^- \xrightarrow{k_3} \underset{\underset{OH \quad OH}{|}}{CH_2{}^{11}CHCH_3} \quad (6)$$
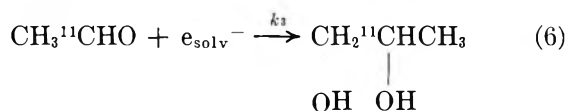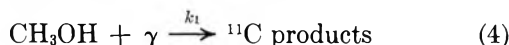
Equation 4 represents the total production of $^{11}C$ products by the synchrotron radiation. The rate of production denoted $R_1 = k_1[\gamma][CH_3OH]$ is independent of time and depends only on the beam intensity $[\gamma]$, i.e., dose rate. The rate of production of acetaldehyde, $R_2 = k_2[^{11}C][CH_3OH]$, will be a similar function of dose rate since $^{11}C$ is directly proportional to the beam intensity. The rate of loss of acetaldehyde by the electron reaction (cf. Figure 1) may be represented as $R_3 = k_3[e_{solv}^-][CH_3CHO] = K_3[CH_3CHO]$, since $[e_{solv}^-]$ is constant with time at a fixed dose rate.

The other reactants necessary to convert acetaldehyde into propanediol, $H^+$, and $\cdot CH_2OH$ will also be present in constant amounts at a fixed dose rate. However, the fate of the product of the reaction between $CH_3CHO$ and $e_{solv}^-$ does not affect the kinetic treatment as long as this reaction is not reversible.

The expected acetaldehyde yield as a function of dose at a fixed dose rate can be determined by solving the

prescribed rate equation. The last term must be included since the loss by decay is significant relative to loss by the electron reaction. The solution of eq 7 is

$$\frac{d[CH_3CHO]}{dt} =$$

$$R_2 - K_3[CH_3CHO] - \lambda[CH_3CHO] \quad (7)$$

$$[CH_3{}^{11}CHO] = \frac{R_2}{\lambda + K_3}[1 - e^{-(\lambda + K_3)t}] \quad (8)$$

and

$$\text{yield}(CH_3{}^{11}CHO) = \frac{\dfrac{R_2}{\lambda + K_3}[1 - e^{-(\lambda + K_3)t}]}{\dfrac{R_1}{\lambda}[1 - e^{-\lambda t}]} \quad (9)$$

The addition of carrier acetaldehyde eliminates the loss of labeled acetaldehyde by the electron reaction permitting direct evaluation of the ratio $R_2/R_1$ from the yield in the protected system, 7.3%. The value of $K_3$ in the unscavenged system can be determined from the data as shown in Figure 2. The best value is estimated as $0.75 \pm 0.10$ min$^{-1}$. Values for the bimolecular rate constant $k_3$ are dependent on estimates of $[e_{solv}^-]$.
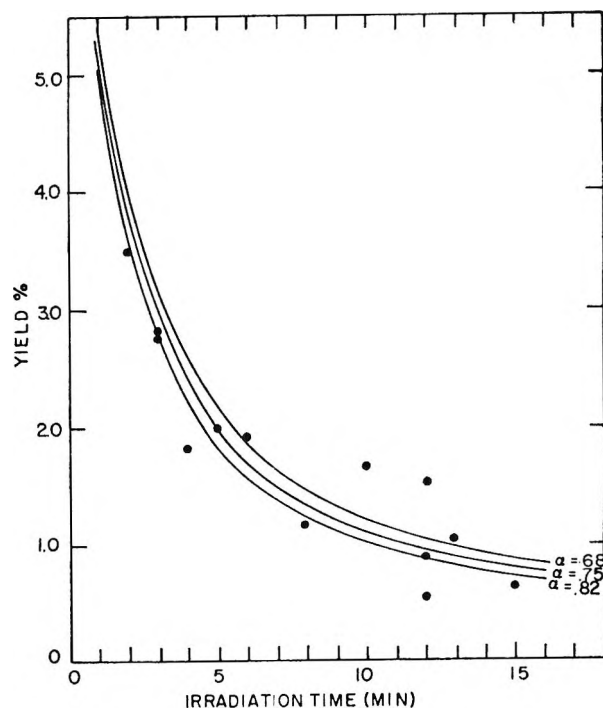


Figure 2. Acetaldehyde yield and calculated curves.

*Carbon Monoxide.* A similar treatment for the carbon monoxide yield using eq 10 and the reactions

(17) J. J. Weiss, *Radiat. Res., Suppl.*, **4**, 141 (1964).

proposed earlier provides a similar yield equation

$$^{11}CO + e_{solv}{}^{-} \xrightarrow{k_4} CH_2(OH)^{11}CHO \qquad (10)$$
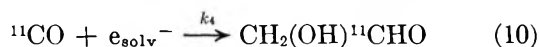
$$yield(^{11}CO) =$$

$$\frac{0.25\lambda}{\lambda + K_4}[1 - e^{-(\lambda + K_4)t}](1 - e^{-\lambda t})^{-1} \quad (11)$$

where the value 0.25 has been determined from the 25% yield of $^{11}CO$ in iodine-scavenged samples.

In Figure 3 the smooth curves result from substituting selected values of $K_4$ into eq 11 and the points are the carbon monoxide yields at a dose rate of $1.9 \times 10^{-3}$ eV molecule$^{-1}$ min$^{-1}$. Although the experimental results show considerable scatter, a relatively unique value of $K_4$ can be chosen by inspection to be $0.17 \pm 0.03$.

Repeating the analysis of the $^{11}CO$ yields for different dose rates results in a series of $K_4$ values; 0.15 at $1.5 \times 10^{-3}$ eV molecule$^{-1}$ min$^{-1}$, 0.20 at $2.2 \times 10^{-3}$, and 0.30 at $2.7 \times 10^{-3}$. Since $K_4 = k_4[e_{solv}{}^{-}][CO]$, this series reflects the relative concentration of solvated electrons with increasing dose rate.

The relative reaction rates of the methanolated electron with acetaldehyde and carbon monoxide determined by this method at $2.3 \times 10^{-3}$ eV molecule$^{-1}$ min$^{-1}$ are 0.75/0.25. Reactions of the methanolated electron significantly alter these recoil product yields, and the observed rates substantiate the similarity of this species with the hydrated electron, for which the ratio of rate constants is 3.5.
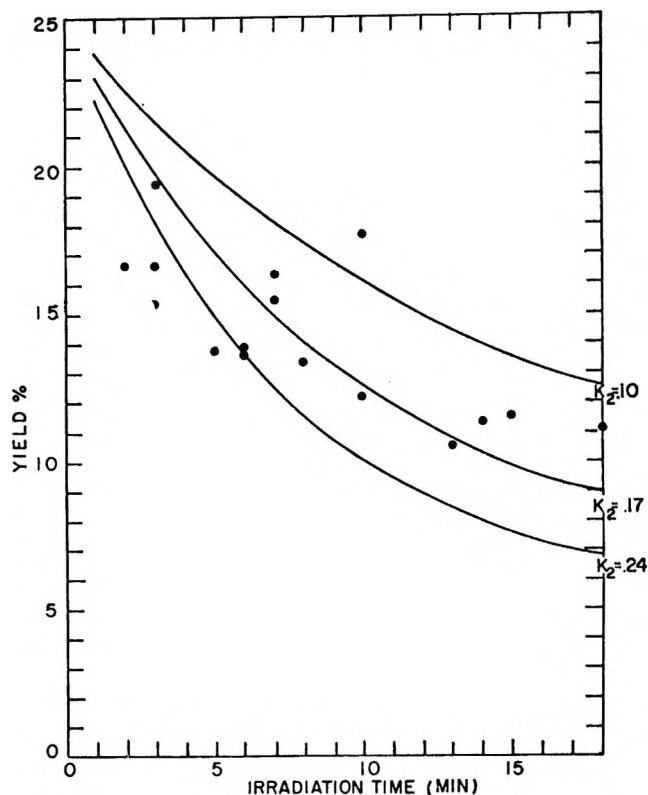


Figure 3.   Carbon monoxide yield and calculated curves.

# The Rate of Oxidation of Lead Vapor

## by P. R. Ryason* and E. A. Smith

*Chevron Research Company Richmond, California 94802 (Received March 8, 1971)*

*Publication costs assisted by the Chevron Research Company*

The rate of oxidation of lead vapor has been measured in a quartz fast-flow reactor. Atomic absorption spectrophotometry was used to measure lead atom concentrations. The kinetic data were interpreted according to the mechanism shown later in reactions 1, 2, and w. At 870°K, $k_1 = 3.4 \times 10^9$ l.$^2$/mol$^2$ sec. The wall reaction dominated Pb removal at 958 and 989°K. The rate constant for Pb agrees with those for other atom-oxygen molecule reactions, in particular, metal atom-oxygen reactions. An exception is the Na-O$_2$ and the Mg-O$_2$ rate constants measured by the diffusion flame method for which values are approximately 10$^3$ larger. There may be a systematic error in the diffusion flame method.

## Introduction

Few metal vapor-oxygen reaction rate constants have been reported. Two possible reactions of a metal atom, X, with molecular oxygen are

$$X + O_2 + M \longrightarrow XO_2 + M \qquad (a)$$

$$X + O_2 \longrightarrow XO + O \qquad (b)$$

Thermochemical data are useful in assessing which will dominate in a specified temperature range. For many metals, reaction b is endothermic, e.g., for lead, $\Delta H_0° = 30$ kcal/mol. Estimates of the rates of (a) and (b) at the temperatures used in this work suggested that (b) could be neglected. A fast-flow reactor method was used to measure the rate of (a), X = Pb. The ease with which PbO is reduced necessitated careful attention to materials and operation of the apparatus.

## Experimental Section

*A. Apparatus.* The experimental apparatus is shown schematically in Figure 1. In brief, it consists of two gas handling systems, a probe movement device, a controllable source of lead vapor, the reactor tube with an optical section for measurement of lead atom concentration, an optical train, and a pumping system.

Argon was supplied from a cylinder labeled "high purity dry" and was controlled by a regulator on the cylinder, a Matheson Model 149 low-pressure regulator, and a sapphire critical flow orifice. The low-pressure regulator maintained a constant pressure on the upstream side of the orifice. Mass flow through the orifice as a function of the upstream pressure was determined in a separate calibration, utilizing the method of pressure rise in a large vessel of known volume. Pressures in the calibration experiment were measured with a Wallace and Tiernan precision gauge (Model FA-129). The precision of this calibration was 2%, where this figure represents one relative standard deviation. Research grade Matheson oxygen was used and was controlled by a Matheson Model 150 valve. The

oxygen flow, approximately 1% of the argon flow, was measured by the method of pressure drop in a vessel of known volume.

Downstream of the flow control devices, the two gas streams were conducted by copper tubing to a manifold arranged to permit flushing of the probe with argon at the completion of a kinetic run. The argon was then passed over titanium sponge at 800° to purify it. Copper tubing was used to convey the gases from the manifold to the probe movement device, which was similar to that described by Westenburg and deHaas.[1] As indicated in Figure 1, the probe (a 6-mm o.d. quartz tube) was moved by an external solenoid acting on a gold-plated iron slug wired to the probe with silver wire. The probe was connected to the oxygen supply line by a length of Teflon tubing (3.2-mm o.d., 0.4-mm wall). The ends of this tubing were secured by silver wire. The tubing coiled up in a 5-l. flask when the probe was retracted. Argon was brought into the flask and swept its entire volume before passing *via* the annular space between the probe and its outer tube into the reactor. Of necessity, several joints were required. Sparingly greased standard taper joints were used, and great care was taken to avoid grease or any other reducing substance contacting the probe. Lead oxide is very readily reduced under the conditions of this experiment. The choice of the materials indicated minimizes the amount of reducing substances that might enter the gas streams. Thus, the wear particles from the gold-plated iron slug will be gold; the low coefficient of friction of Teflon should reduce wear of the tubing and the likelihood that carbon-containing particulates will enter the reactor.

Two different controllable sources of lead vapor, corresponding to two different versions of the reactor tube, were used. The first quartz reactor tube (28-mm o.d.) used was fitted with a boat containing a bead of lead (Mallinckrodt CP grade). This boat could be moved in

(1) A. A. Westenberg and N. deHaas, *J. Chem. Phys.*, **46**, 490 (1967).
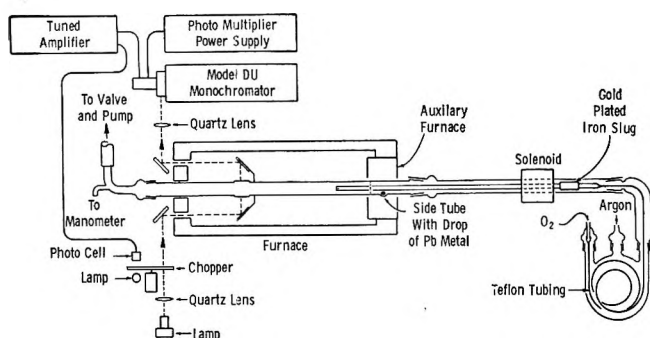
Figure 1. Diagram of reactor and detection apparatus.

and out of the Lindberg three-zone furnace by an external magnet. An iron slug on the boat was sealed in quartz. Plane quartz windows were fused on the tube at the point the optical beam passed through the tube. Sealing cane was used as an intermediate medium between the tube and the quartz flats to minimize distortion of the flats. Although this assured minimum distortion of the flats, on heating and cooling the seal developed small cracks which had to be sealed. Care was taken to avoid deposition of amorphous $SiO_2$ at all seals. Attempts to remove such material by HF solution in the early experiments resulted in exceedingly rapid fogging of the windows when they were subsequently exposed to lead vapor. The dimensions of this tube and the probe were such that the probe in its extreme position was 6 cm from the center of the windows. Two mirrors, platinum sputtered on quartz flats, were sealed on the tube to direct the radiation from the hollow cathode lamp through the tube.

The second quartz reactor tube (28-mm o.d.) shown in Figure 1 utilized a lead reservoir, the temperature of which could be separately controlled. Windows were sealed-on as in the first tube but so positioned that the end of the probe in its extreme position was 1.2 cm from the center of the windows. The mirrors on this tube were 5-cm square quartz flats sealed on to a post attached to the tube close to the windows to avoid fogging the exterior of the tube with amorphous silica. Liquid Platinum Bright No. 05, thinned with toluene, applied with an air brush, dried, and then fired provided the reflecting surface of these mirrors. The reflectivity of these mirrors decreased with time, and they were replaced by the sputtered platinum mirrors. A deflector plate was used in the tube just ahead of the lead reservoir, and a grid of rods was fused into the tube just downstream of the reservoir to promote mixing of lead vapor with the carrier gas.

Temperatures were measured at several points along the reactor tubes. Chromel–alumel thermocouples were used with an ice bath reference junction and a Leeds and Northrup No. 8667 potentiometer. The thermocouples were shielded from direct radiation from the furnace. In the case of the second version of the reactor tube, a thermocouple in a thermowell in the wall

of the side arm was used to measure the temperature of the lead (Mallinckrodt CP grade). Auxiliary furnace temperatures were regulated by a separate controller (API Instruments Co.).

The optical system consisted of a lead hollow cathode lamp (Techtron), a 13-cps chopper, a Beckman Model DU monochromator fitted with an EMI Type 9592D photomultiplier, and appropriate lenses and mirrors as indicated in Figure 1. The output of the photomultiplier was amplified by a Pederson Electronics phase-sensitive amplifier and displayed on an Electro Instrument digital voltmeter. The monochromator was set on a wavelength of 2833 Å; the slit width was 0.4 mm, corresponding to a spectral slit width of 20 Å, according to the dispersion curve given by the manufacturer. Photometric accuracy of the system was checked with a quartz neutral density filter (Special Optics, Inc.). The optical density of the filter measured by this system and that measured by a Cary Model 14 spectrophotometer agreed to within 1–2%.

*B. Procedure.* A set of preliminary experiments revealed an effect of the time of oxygen flow on the rate constant. To obtain consistent results, the procedure was adopted of allowing oxygen to flow at the rate of approximately $8 \times 10^{-7}$ mol/sec for 15 min prior to each experiment. The oxygen flow was followed by 5 min of argon flow. The intensity of the incident radiation, $I_0$, was measured with the lead source cold. Excess oxygen was added and the incident intensity again measured. If $I_0$ with and without excess oxygen differed by more than a few per cent, it was assumed there was an extraneous source of lead vapor in the reactant tube. Ordinarily, raising the tube temperature with the argon flowing for a period of time was sufficient to remove the extraneous lead. Occasionally, the tube had to be cleaned with dilute nitric acid.

The lead source was heated, either by pushing the boat forward into the furnace or heating the auxiliary furnace. The light intensity, $I$, was determined with no oxygen flow. Measurements of the light intensity with the oxygen flow on were then made for various probe positions, affording several quantities $I_{O_2i}$. The probe was always inserted its full length at the beginning of a run and then withdrawn stepwise during the run. It was found that if the probe were moved stepwise into the hot furnace during a run, enough lead condensed on the cold probe as it moved by the lead source to cause appreciable changes in $I$ when revolatilized as the probe warmed. The oxygen flow rate was measured during the period of kinetic measurements. At the completion of the kinetic measurements, the $O_2$ flow was halted, the probe flushed with argon, and $I$ again measured. The lead source was cooled and $I_0$ again determined. A variation on this procedure was found necessary at the highest temperature of these experiments. In this case, when the probe was withdrawn, the heat from the probe warmed the lead source
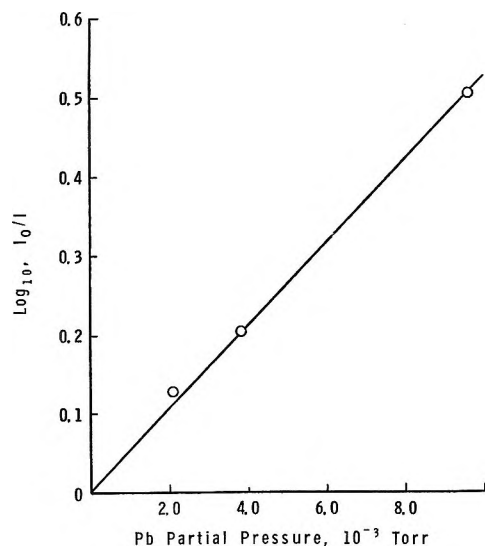
Figure 2. Extrapolated log $I_0/I$ vs. Pb partial pressure.

causing $I$ to change. The oxygen flow, therefore, was interrupted each time the probe was moved and $I$ remeasured to confirm it was stable. The oxygen flow rate was, in this case, determined at the completion of the kinetic measurements just prior to the determinations of $I_0$.

Beer's law was obeyed under the experimental conditions employed. This was established by measuring $I_0$ and $I$ at three different furnace temperatures at three flow rates for each temperature. The absorbance, log $(I_0/I)$, was plotted as a function of flow rate and found to vary linearly. Extrapolation to zero flow rate was carried out by a least-squares straight line fit to the absorbance-flow rate data. The absorbances obtained as intercepts in these plots were plotted as a function of the lead vapor pressure as shown in Figure 2. The vapor pressure-temperature results of Kim and Cosgarea[2] were used to determine the vapor pressure of lead from the known furnace temperature. Using the oscillator strength for this transition ($^3P_0 \leftarrow {}^3P_1{}^0$) of Pb given by deZafra and Marshall,[3] one can show that the absorption process here is the case of strong absorption.[4] The edges of the line dominate in this case. Within the precision of our measurements, over the restricted concentration range, this empirical demonstration of a linear dependence of log $I_0/I$ on lead atom concentration was deemed adequate for the purpose at hand. The lack of saturation of the argon stream resulted in sufficiently low partial pressures of PbO that it did not condense in the reactor tube. Lead oxide accumulated as a bright yellow ring on the reactor tube where it protruded from the furnace.

## Results and Discussion

Flow rates, probe positions, and values for $I_0$, $I$, and $I_{O_2i}$ were the primary experimental record. Plots of log $[\log (I_0/I)/\log (I_0/I_{O_2i})] = \log ([Pb]_0/[Pb])$ vs. time were linear, indicating first-order behavior. Illustra-
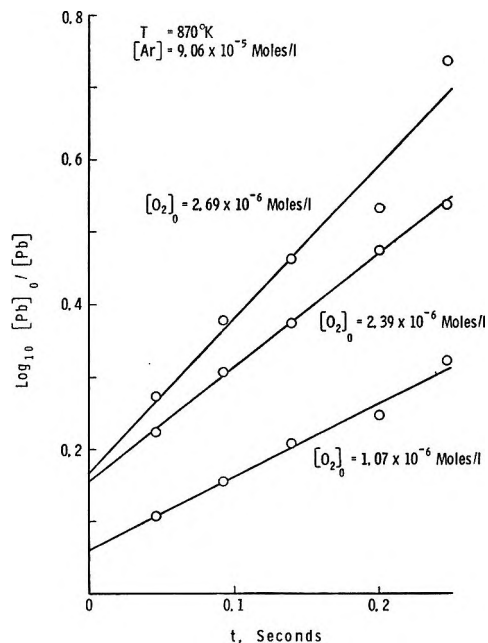


Figure 3. The removal of Pb by reaction with $O_2$, total pressure = 5 Torr.

tive data are shown in Figure 3. These data were obtained using the first version of the reactor tube. Least-squares straight lines were calculated for all experiments. In this series of experiments, there was a tendency, as indicated in Figure 3, for higher $O_2$ concentrations to result in larger intercepts. Check runs made later, using the second reactor, yielded slopes in good agreement with those measured in the first reactor. The slopes were used in computing rate constants.

Although the nonzero intercept may be a mixing effect, it may also be associated with the flow. Plug flow in low-pressure laminar viscous flow is presumably maintained by diffusion. Thus, one might expect an increased intercept for the runs made at the higher pressures. No such trend could be discerned in the intercepts although, with considerable scatter, the intercept increased as the $[O_2]_0$ increased. A referee has pointed out the nonzero intercept can result from a rapid removal of lead prior to the exponential decay. Two possibilities are: a temporary high local concentration of $O_2$ resulting from poor mixing at the tip of the injector; or an impurity in the $O_2$. Analytical results given on the $O_2$ cylinder label stated that all likely impurities were $\leq 20$ ppm. Poor mixing is the most likely explanation of the nonzero intercepts usually observed in these kinetic plots.

The most likely mechanism[5] for this reaction is

$$Pb + O_2 + M \longrightarrow PbO_2 + M \qquad (1)$$
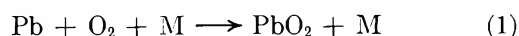
(2) J. H. Kim and A. Cosgarea, Jr., J. Chem. Phys., **44**, 806 (1966).

(3) R. L. deZafra and A. Marshall, Phys. Rev., **170**, 28 (1968).

(4) A. C. G. Mitchell and M. W. Zemansky, "Resonance Radiation and Excited Atoms," Cambridge University Press, New York, N. Y., 1961, pp 103–106.

(5) F. Haber and H. Sachsse, Z. Phys. Chem. Bodenstein Festband, 831 (1931).

$$PbO_2 + Pb \longrightarrow 2PbO \qquad (2)$$

$$Pb + O_2(ads), O(ads) \xrightarrow{wall} PbO \qquad (w)$$
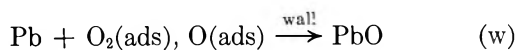
Assuming a steady state on $PbO_2$, the rate law is

$$\ln \frac{[Pb]_0}{[Pb]} = (2k_1[O_2][M] + k_w)t = k_{obsd}t \qquad (I)$$

assuming $[O_2] = [O_2]_0 \gg [Pb]_0$, a condition always satisfied in this work. The reaction

$$Pb + Pb \longrightarrow Pb_2 \qquad (3)$$
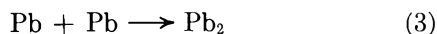
can be neglected because of the instability of $Pb_2$.[6]

All data could thus be summarized on plots of $k_{obsd}/[O_2]_0$ vs. [Ar] for three temperatures, 870, 960, and 992°K. Least-squares analysis of these data yielded $k_1$ and $k_w/[O_2]_0$. In turn, $k_w/[O_2]_0$ values were used to calculate the fraction of the reaction occurring on the wall for [Ar] $= 2 \times 10^{-4}$ mol/l. and $[O_2] = 1.5 \times 10^{-6}$ mol/l. For the reactions carried out at 960 and 992°K, 80–90% of the reaction occurred on the wall, and the standard deviations were very large. No values for $k_1$ at 960 and 992°K could be inferred.

For the same values of [Ar] and $[O_2]$ given above, 48% of the reaction occurred on the wall at 870°K. Figure 4 is the plot of $k_{obsd}/[O_2]_0$ vs. [Ar] for this temperature. Ranges of conditions used in obtaining the data of Figure 4 were: temperature, 865–886°K; standard deviation of temperature, 4°K; total pressure, 5–17 Torr; oxygen concentration, (1.09–2.61) $\times$ $10^{-6}$ mol/l.; and flow velocities, 130–175 cm/sec. The least-squares analysis of the 39 points of this plot resulted in $k_1 = (3.4 \pm 0.63) \times 10^9$ l.$^2$/mol$^2$/sec, where the uncertainty quoted is one standard deviation. The point in Figure 4 shown with error bars is the average value obtained in a number of determinations in which [Ar] was held constant and $[O_2]$ varied. It was intended to determine the order with respect to $[O_2]$ directly. Standard deviations of $k_{obsd}$ vs. $[O_2]$ and $k_{obsd}$ vs. $[O_2]^2$ were about equal. Therefore, the measurement was insufficiently precise to justify the model implied in eq I. However, second-order dependence on $[O_2]$ is very improbable.

The value found for $k_1$ is comparable with rate constants for gas phase reactions of atoms with oxygen molecules as shown in Table I below.

Our value for the rate constant of $Pb + O_2 + M \rightarrow PbO_2 + M$ is in agreement with those for similar reactions. In particular, the alkali metal vapor rate constants agree to within an order of magnitude. These were measured in lean $H_2$–$O_2$–$N_2$ flames by an atomic absorption method. Competing reactions are a matter of concern in this technique. Carabetta and Kaskan (see footnote $h$, Table I) have presented evidence to show that in lean flames the reaction is termolecular, though the alkali metal superoxides are not the final products.
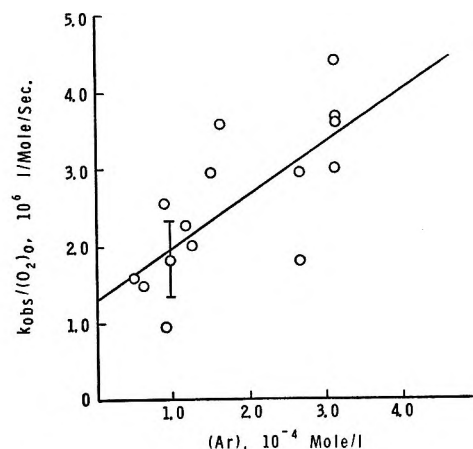
Figure 4. Plot of $k_{obsd}/[O_2]_0$ vs. [Ar]; $T = 870°K$.

**Table I:** Termolecular Rate Constants for Atom–Oxygen Molecule Reactions $A + O_2 + M \rightarrow AO_2 + M$

| A | $k$, l.$^2$/mol$^2$ sec | M | $T$, °K | Ref |
|---|---|---|---|---|
| H | $1.3 \times 10^9$ [a] | Ar | 870 | b |
| C | $1.5 \times 10^9$ | He | 300 | c |
| O | $(0.45–2.5) \times 10^8$ | $N_2$, $O_2$ | 298 | d |
| Cl | $6.2 \times 10^8$ | $O_2 + N_2$ | 293 | e |
| Na | $(3.3–2.6) \times 10^8$ | $H_2O + N_2$ | 1540–1720 | f |
| K | $(4.9–2.5) \times 10^8$ | $H_2O + N_2$ | 1375–1720 | f |
| Na | $(9.4–5.8) \times 10^8$ | $H_2O + N_2$ | 1380–2030 | g |
| K | $(1.1–0.83) \times 10^9$ | $H_2O + N_2$ | 1380–2030 | g |
| Na | $(3.1–2.7) \times 10^8$ | $H_2O + N_2$ | 1420–1600 | h |
| K | $(5.4–2.6) \times 10^8$ | $H_2O + N_2$ | 1420–1600 | h |
| Cs | $(9.8–5.1) \times 10^8$ | $H_2O + N_2$ | 1420–1600 | h |
| Pb | $3.4 \times 10^9$ | Ar | 870 | i |

[a] Calculated from the expression given in footnote b. [b] M. A. A. Clyne and B. A. Thrush, *Proc. Roy. Soc., Ser. A*, **275**, 559 (1963). [c] F. F. Martinotti, M. J. Welch, and A. P. Wolf, *Chem. Commun.*, 115 (1968). [d] Literature values quoted by P. D. Francis, *Brit. J. Appl. Phys.*, **2**, 1717 (1969). [e] J. E. Nicholas and R. G. W. Norrish, *Proc. Roy. Soc., Ser. A*, **307**, 391 (1958). [f] W. E. Kaskan, *Symp. (Int.) Combust. [Proc.], 10th*, 41 (1965). [g] M. J. McEwan and L. F. Phillips, *Trans. Faraday Soc.*, **62**, 1717 (1966). [h] R. Carabetta and W. E. Kaskan, *J. Phys. Chem.*, **72**, 2483 (1968). [i] This work.

The Polanyi diffusion flame technique has been used to determine the rate constants for the $Na$–$O_2$ reaction and the $Mg$–$O_2$ reaction. Haber and Sachsse[5] showed the $Na$–$O_2$ reaction to be termolecular and suggested the initial step was the formation of the moloxide $NaO_2$. Bawn and Evans[7] confirmed the termolecular nature of the $Na$–$O_2$ reaction but reported their rate constants as bimolecular rate constants. The termolecular rate constant computed from their data is $k = 1.3 \times 10^{12}$ l.$^2$/mol$^2$ sec for $Na + O_2 + M \rightarrow NaO_2 + M$. Mark-

(6) A. G. Gaydon, Dissociation Engeries, Chapman and Hall, London, 1953, p 229.

(7) C. E. H. Bawn and A. G. Evans, *Trans. Faraday Soc.*, **33**, 1580 (1937).

stein[8] used the diffusion flame method to measure the rate of oxidation of Mg vapor. He reports a value of $4 \times 10^8$ l./mol sec for a bimolecular rate constant. The endothermicity of $Mg + O_2 \rightarrow MgO + O$ is 22 kcal/mol. This implies a second-order rate constant three orders of magnitude less than the observed value. A third-order rate constant calculated from Markstein's data is $5 \times 10^{12}$ l.$^2$/mol$^2$ sec. The two diffusion flame results are higher by about a factor of $10^3$ than those obtained by other methods. Possibly the rate constant for the $Mg + O_2$ reaction should not be used in this comparison in view of the experimental difficulties encountered in that work.

One is left with the possibility that the rate constant for the $Na-O_2$ reaction measured by the diffusion flame method may be in error. The fast-flow method can be used to determine the rate constant for this reaction. The result would provide an independent check on the diffusion flame method and the lean $H_2-O_2-N_2$ flame method. Such a check would be of general interest in that comparison between rate constants calculated from molecular beam cross-section values and classical chemical rate constants are now being made for alkali metal-alkyl halide reactions.[9,10] Rate constants for such reactions have been measured only by the diffusion flame method. Evaluation by another method would put these comparisons on firmer ground.

*Acknowledgment.* The quartz reactors were made by Mr. R. F. Brennan and Mr. J. Wolford, whose careful work and constructive suggestions are gratefully acknowledged.

(8) G. H. Markstein, *Symp. (Int.) Combust. [Proc.]*, **9**, 137 (1963).

(9) J. P. Toennies, *Ber. Bunsenges. Phys. Chem.*, **72**, 927 (1968).

(10) K. R. Wilson and D. Herschbach, *J. Chem. Phys.*, **49**, 2676 (1968).

# Deuterium Isotope Effect on the Decay Kinetics of Perhydroxyl Radical[1]

## by Benon H. J. Bielski*

*Chemistry Departement, Brookhaven National Laboratory, Upton, New York 11973*

## and Eiichi Saito

*Centre d'Etudes Nucléaires de Saclay, Departement de Recherches et Analyse, B.P. n° 2, 91-Gif-sur-Yvette, France* (Received December 21, 1970)

Rate constants for the disproportionation of $HO_2$ in $H_2O$ and $DO_2$ in $D_2O$ have been determined as a function of acidity and temperature. The radicals were generated by pulse radiolysis and by oxidation of peroxide with ceric sulfate. It was found that the isotope effect on the decay rates of the two radicals varies with pH. The pK values for $HO_2$ and $DO_2$ were 4.8 and 4.9, respectively. Activation energies for the decay in 0.8 N $H_2SO_4$ and 0.8 N $D_2SO_4$ were 5.8 kcal/mol for $HO_2$ and 7.3 kcal/mol for $D_2O$.

## Introduction

Relatively high concentrations of the perhydroxyl radical can be generated in aqueous solutions by either high-energy ionizing radiations or by the oxidation of hydrogen peroxide by ceric sulfate.

In the field of radiation chemistry of aqueous solutions the perhydroxyl radical is of considerable interest, since it is probably the most important secondary product of the interaction between ionizing radiation and oxygenated water. Its formation can be described by the following equations.

$$H_2O \longrightarrow H, e_{aq}^-, OH, H_2O_2, H_2 \quad (1)$$

$$O_2 + H \longrightarrow HO_2 \quad (2)$$

$$O_2 + e_{aq}^- \longrightarrow O_2^- \quad (3)$$

$$O_2^- + H^+ \rightleftharpoons HO_2 \quad (4)$$
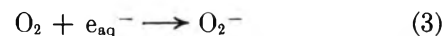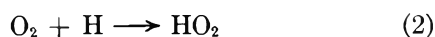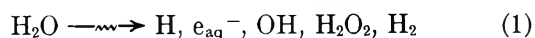
Formation of $HO_2$ as an intermediate in the oxidation of hydrogen peroxide by ceric sulfate was originally postulated by Baer and Stein[2] and later demonstrated by the studies of Saito and Bielski.[3,4] The following reactions account for the process.

$$Ce(IV) + H_2O_2 \rightleftharpoons Ce(III) + H^+ + HO_2 \quad (5)$$
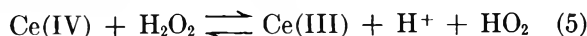
(1) Research performed under the auspices of the U. S. Atomic Energy Commission.

(2) S. Baer and G. Stein, *J. Chem. Soc.*, 3176 (1953).

(3) E. Saito and B. H. J. Bielski, *J. Amer. Chem. Soc.*, **83**, 4467 (1961).

(4) B. H. J. Bielski and E. Saito, *J. Phys. Chem.*, **66**, 2266 (1962).

$$Ce(IV) + HO_2 \longrightarrow Ce(III) + H^+ + O_2 \quad (6)$$
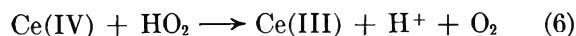
Bielski and Allen[5] have shown more recently that, in the range below pH 1.0, the perhydroxyl radical generated by either method was kinetically indistinguishable. Despite this agreement it was not clear whether in the Ce(IV)-$H_2O_2$ system the $HO_2$ was present as a free radical or complexed as Ce(III)–OOH, as suggested by Anbar.[6] Samuni and Czapski[7] solved this question recently by showing that $HO_2$ can exist either as a free radical or as a complex, depending upon the concentration of cerous ion in the system.

$$Ce(III) + HO_2 \rightleftharpoons Ce(III)\text{–}OOH \quad (7)$$

Their results suggest that Bielski and Allen studied the decay of the free form of the radical.

In the present study a comparison is made between the kinetics of $HO_2$ in $H_2O$ and $DO_2$ in $D_2O$ in order to establish the magnitude of the isotope effect on the decay rates of the light and heavy radicals.

## Experimental Section

*Chemicals.* $D_2O$, 99.7% in D, was further purified to ensure the removal of organic impurities. Two alternate methods of pretreatment were used. The $D_2O$ was mixed with oxygen in the vapor phase and passed through a silica tube at 800°, or it was preirradiated with $^{60}Co$ γ rays. In either case the heavy water was subsequently triple-distilled from acidic dichromate and alkaline permanganate solutions in an all-quartz distilling apparatus.

$D_2SO_4$ was prepared by the addition of $SO_3$ (Kuhlman, Paris) to $D_2O$.

$DClO_4$ was prepared by addition of $Ba(ClO_4)_2$ to $D_2SO_4$. After removal of excess $BaSO_4$, pure $DClO_4$ was obtained by distillation.

$D_2O_2$ and $H_2O_2$ solutions were prepared by the addition of $Na_2O_2$ (Prolabo Product R. P.) to $D_2O$ or $H_2O$ and subsequent acidification. Concentrations of the peroxide solutions were determined by the ceric sulfate method.[8]

Ceric sulfate solutions were prepared by dissolving the required amount of the anhydrous salt and checking the concentrations spectrophotometrically at 320 nm. The molar extinction coefficient in 0.8 $N$ sulfuric acid was taken as 5580 $M^{-1}$ cm$^{-1}$.

*Apparatus.* The apparatus for the pulse radiolysis experiments has been described in detail in an earlier publication.[9a] The 1.9-MeV electron pulses used in this study were of 2–20-msec duration with currents of 0.1 to 2 mA. The electron beam current striking the cell and cell holder was monitored and related to ferrous dosimetry. Total doses delivered to samples ranged from 0.3 to 2.5 krads. The corresponding perhydroxyl radical concentrations observed were of the order of 2 to 8 $\mu M$.

The pH measurements were taken on an ORION Research Ionalyzer Model 801.

For the esr studies, experimental equipment consisted of a Varian V-4502-13 electron spin resonance spectrometer, a 9-in. magnet with Fieldial, and a thermostated flow system. In order to be able to carry out corrections for variations in the microwave power in the cavity over a period of several hours, a double cavity was employed. With this equipment the signal of interest is constantly monitored against a standard KCl-pitch sample and corrections can easily be made.

The flow system consisted of a double-jet mixing chamber and a flow tube with an inner diameter of 0.86 mm. The flow tube itself was sealed into an 11-mm diameter quartz tube, and the space between them was evacuated. Tubes leading to the mixing chamber were jacketed by wider pipes through which the coolant was pumped from a thermostat bath by a circulating pump. Flow velocities were determined for each run. Temperature was monitored by thermometers embedded 15 cm above the mixing chamber. Average fluctuation during a run was about 0.2°.

## Results

*Pulse Radiolysis Studies.* Pulse radiolysis was used in the study of the decay rates in the pH range from 0 to 5.5. The change in concentration of the radical was followed spectrophotometrically at 241 nm. The molar extinction coefficients used for $HO_2$ and $O_2^-$ at this wavelength were 1100[9a] and 1950 $M^{-1}$ cm$^{-1}$,[9b] respectively. It was assumed that the values in $D_2O$ are the same.

Since under pulse radiolytic conditions a considerable quantity of hydrogen sesquioxide or deuterium sesquioxide, which decays by first-order kinetics, also forms, the contributions of the two decay processes were resolved by a computer program which was used in an earlier study by Bielski and Schwarz.[9a]

The numerical results of the observed second-order rate constants are given in Figure 1. The acidity scale was normalized by the Glasoe–Long relationship,[10] since pH measurements in $D_2O$ solutions are 0.4 pH units lower than in $H_2O$ solutions of comparable acidity.

The temperature dependence of the rate constants $k_{HO_2}$ and $k_{DO_2}$ was determined in 0.8 $N$ sulfuric acid solutions only. The corresponding activation energies, $E_{HO_2} = 5.8 \pm 0.5$ kcal/mol and $E_{DO_2} = 7.3 \pm 0.4$

(5) B. H. J. Bielski and A. O. Allen, Proceedings of the Second Tihany Symposium on Radiation Chemistry, Akad. Kiodo, Budapest, 1967.

(6) M. Anbar, *J. Amer. Chem. Soc.*, **83**, 2031 (1961).

(7) A. Samuni and G. Czapski, *Israel J. Chem.*, **7**, 375 (1969).

(8) C. J. Hochanadel and J. A. Ghormley, *J. Chem. Phys.*, **21**, 880 (1953).

(9) (a) B. H. J. Bielski and H. A. Schwarz, *J. Phys. Chem.*, **72**, 3836 (1968); (b) D. Behar, G. Czapski, L. M. Dorfman, J. Rabani, and H. A. Schwarz, *ibid.*, **74**, 3209 (1970).

(10) P. K. Glasoe and F. A. Long, *ibid.*, **64**, 188 (1960).
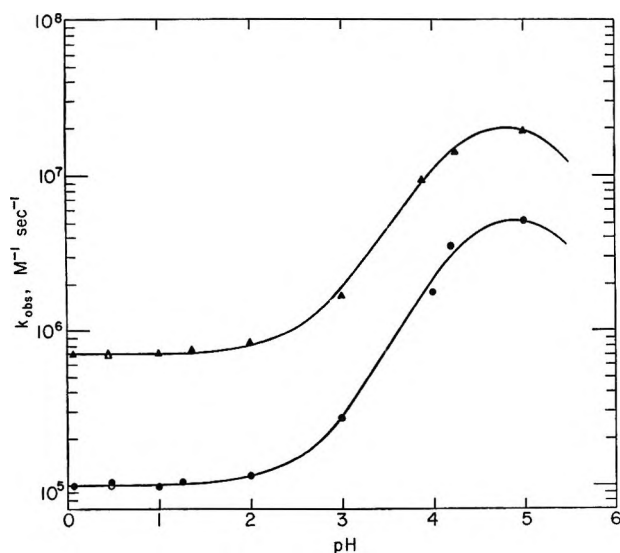
Figure 1. Plot of log $k_{obsd}$ as a function of acidity for the disproportionation of $HO_2$ in $H_2O$ and $DO_2$ in $D_2O$ (▲, $HO_2$, pulse radiolysis data; △, $HO_2$, esr data; ●, $DO_2$, pulse radiolysis data; ○, $DO_2$, esr data).
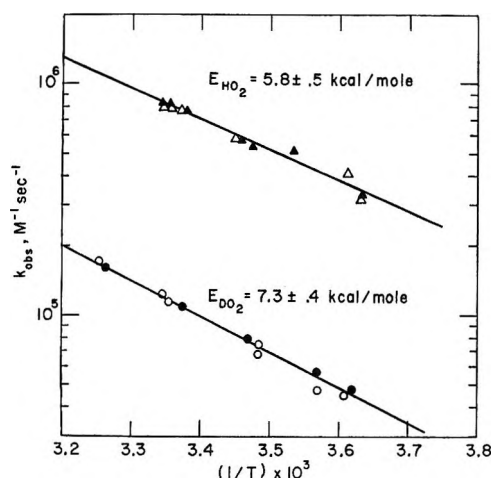


Figure 2. Plot of log $k_{obsd}$ for the disproportionation of $HO_2$ in $H_2O$ and $DO_2$ in $D_2O$ as a function of reciprocal temperature (▲, $HO_2$, pulse radiolysis data; △, $HO_2$, esr data; ●, $DO_2$, pulse radiolysis data; ○, $DO_2$, esr data).

kcal/mol, were calculated from the curves shown in Figure 2.

*Electron Spin Resonance Studies.* The generation of perhydroxyl radicals in the $Ce(IV)-H_2O_2$ system is limited to the strong acid region, since above pH 1.5 precipitation of the cations as hydroxides interferes with the experiment. For this reason, the esr experiments were carried out only in $0.8 N$ sulfuric acid.

The $HO_2$ and $DO_2$ radicals generated in a mixing chamber were transported to the spectrometer cavity by a flow apparatus. Flow velocities were about 380 cm/sec for $H_2O$ and 210 cm/sec for $D_2O$ solutions at 25°. The concentration of the Ce(IV) was $1.5 \times 10^{-3}$ $M$, while the $H_2O_2$ and $D_2O_2$ were always present in excess at a concentration of $0.3 M$. Under these conditions the steady-state concentration of the free radical
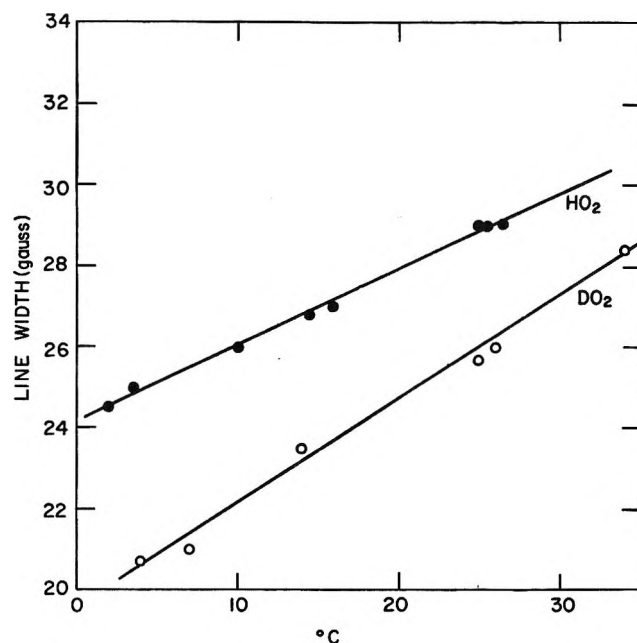


Figure 3. Change in line width for $HO_2$ in $0.8 N$ $H_2SO_4$ and for $DO_2$ in $0.8 N$ $D_2SO_4$ with temperature at 9.5 kMc.

was measured as a function of flow time from the mixing chamber to the center of the esr cavity. Calibrations were carried out after each run by replacing the ceric peroxide solutions by Mn(II) sulfate solutions (in $H_2O$ and $D_2O$) in order to determine the absolute number of spins and hence the concentration of the free radicals. The computation of the number of spins is based on the correspondence of the integrated surface areas of the spectra of $Mn^{2+}$, $HO_2$, and $DO_2$ at a given temperature. These calibrations had to be carried out at each temperature, as seen in Figure 3. The $g$ values for $HO_2$ and $DO_2$ radicals are 2.016 and 2.017, respectively. These values were computed with reference to the $g = 2.0036$ for $α,α$-diphenyl-$β$-picrylhydroxyl free radical.

Plots of reciprocals of concentrations of $HO_2$ and $DO_2$ against time gave in all cases straight lines, indicating that second-order kinetics were obeyed. The corresponding rate constants for the radical decay are average values from five experiments. The numerical values are given in Figure 1 as a function of pH and in Figure 2 as a function of temperature.

## Discussion

It has been shown by several research teams that the perhydroxyl free radical disproportionates by second-order kinetics to oxygen and peroxide.[9b],[11-17] The

(11) J. H. Baxendale, *Radiat. Res.*, **17**, 312 (1962).

(12) G. Czapski and B. H. J. Bielski, *J. Phys. Chem.*, **67**, 2180 (1963).

(13) G. Czapski and L. M. Dorfman, *ibid.*, **68**, 1169 (1964).

(14) Z. P. Zagorski and K. Schested, Risö Report No. 114 (1965).

(15) G. E. Adams, J. W. Boag, and B. D. Michael, *Proc. Roy. Soc.*, *Ser. A*, **289**, 321 (1966).

(16) J. Rabani and S. O. Nielsen, *J. Phys. Chem.*, **73**, 3736 (1969).

(17) D. Behar and G. Czapski, *Israel J. Chem.*, in press.

overall decay scheme, described by equations

$$HO_2 + HO_2 \xrightarrow{k_8} H_2O_2 + O_2 \qquad (8)$$

$$HO_2 + O_2^- \xrightarrow[H_2O]{k_9} H_2O_2 + O_2 + OH^- \qquad (9)$$

$$O_2^- + O_2^- \xrightarrow[2H_2O]{k_{10}} H_2O_2 + O_2 + 2OH^- \qquad (10)$$
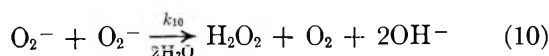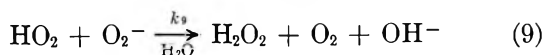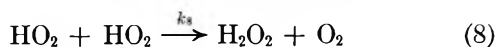
postulates a pH dependence based on the existence of two forms of the radical

$$HO_2 \underset{K_{HO_2}}{\overset{K_{HO_2}}{\rightleftharpoons}} O_2^- + H^+ \qquad (11)$$
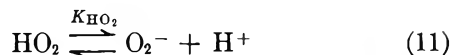
where small $k$'s are the various rate constants and $k_{HO_2}$ is the dissociation constant of $HO_2$.

Contrary to some earlier reports,[12,13,18] the rate constant for reaction 10 is now believed to be many orders of magnitude smaller ($k_{10} < 10^2 \ M^{-1} \ sec^{-1}$). Hence, neglecting reaction 10 for the pH range investigated in this study, the decay mechanism can be described by the following equation.

$$k_{obsd} = \frac{k_8}{\left[1 + \dfrac{K_{HO_2}}{[H^+]}\right]^2} +$$

$$\frac{k_9}{\left[1 + \dfrac{K_{HO_2}}{[H^+]}\right]\left[1 + \dfrac{[H^+]}{K_{HO_2}}\right]} \qquad (I)$$

The solid curves in Figure 1 were calculated from this equation using the following rate constants.
For $HO_2$

$$k_8 = 7.0 \times 10^5 \ M^{-1} \ sec^{-1}$$

$$k_9 = 8.50 \times 10^7 \ M^{-1} \ sec^{-1} \ ^{9b}$$

$$K_{HO_2} = 1.6 \times 10^{-5} \ or \ pK_{HO_2} = 4.8$$

For $DO_2$

$$k_8 = 1.0 \times 10^5 \ M^{-1} \ sec^{-1}$$

$$k_9 = 2.06 \times 10^7 \ M^{-1} \ sec^{-1}$$

$$K_{DO_2} = 1.26 \times 10^{-5} \ or \ pK_{DO_2} = 4.9$$

These values are in close agreement with figures given recently in two independent reports.[9b,16]
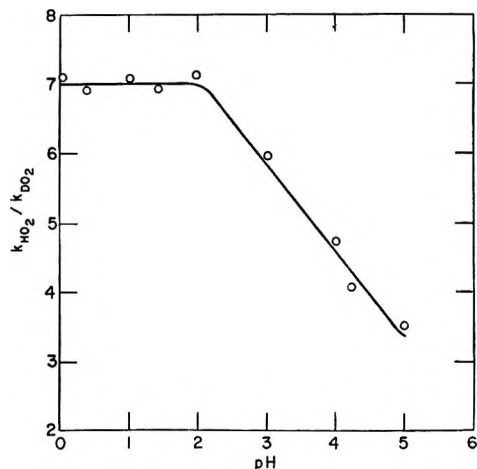


Figure 4. Plot of $k_{HO_2}/k_{DO_2}$ as a function of acidity.

Deuterium isotope effect upon the overall decay of the perhydroxyl radical is illustrated in Figure 4, where the solid line represents the ratio of $[k_{HO_2}/k_{DO_2}]_{obsd}$ computed from the rate constants and eq I. The experimental points are the ratios of the data shown in Figure 1. As expected, the isotope effect is most pronounced in the strong acid region ($k_{HO_2}/k_{DO_2}$ about 7.0), since the decay then takes place almost completely via reaction 8. With a shift in pH toward the neutral region this ratio decreases to a value of 3.5 at pH ~5.0. A smaller isotope effect in the less acid region could be explained by the fact that reaction 9, which is rate controlling, requires the breaking of one less bond than reaction 8.

The difference in the activation energies of 1.5 kcal/mol for the decay of $HO_2$ and $DO_2$ in 0.8 $N$ $H_2SO_4$ and 0.8 $N$ $D_2SO_4$ (Figure 2) is of reasonable magnitude.

(18) K. Schmidt, *Z. Naturforsch. B,* **16,** 206 (1961).

# Pulse Radiolysis of Liquid Amides

by N. Hayashi,[1] E. Hayon,[2]* T. Ibata,[1] N. N. Lichtin,[1] and A. Matsumoto[1]

Chemistry Department, Boston University, Boston, Massachusetts, and Pioneering Research Laboratory,
U. S. Army Natick Laboratories, Natick, Massachusetts 01760 (Received December 23, 1970)

The pulse radiolysis of the following liquid amides has been investigated: formamide (F), $N$-methylformamide (NMF), $N,N$-dimethylformamide (DMF), $N,N$-dimethylacetamide (DMA), and $N$-methylpropionamide (NMP). Radiation-induced ionization and excitation processes have been observed on irradiation of solutions of anthracene (A) and naphthalene (N), as indicated by the characteristic spectra of $A^-$, $N^-$, $A^T$, and $N^T$. The yields of these species have been determined, based on known extinction coefficients. Transient absorptions with $\lambda_{max}$ ~650 and 625 nm in DMF and DMA, respectively, have been assigned to the absorption spectra of solvated electrons in these liquid amides. Absorption bands at $\lambda_{max}$ ~350 nm due to the radicals $HCONH(\dot{C}H_2)$, $HCON(\dot{C}H_2)(CH_3)$, and $CH_3CON(\dot{C}H_2)(CH_3)$ have been observed and characterized. The nature of some of the other transient absorptions produced is discussed. It is concluded that the absorption with $\lambda_{max}$ at 540 nm which is produced in F is, contrary to a previous assignment, not due to solvated electrons.

Liquid amides are of great interest to the physical and physical organic chemist. They are polar liquids with high dielectric constants at room temperature, e.g., formamide $\epsilon$ = 109.5, $N$-methylformamide $\epsilon$ = 182.4, dimethylformamide $\epsilon$ = 36.7, dimethylacetamide $\epsilon$ = 37.8, and good solvents for a number of organic and inorganic solutes. For the radiation chemist, these solvents are of particular concern with respect to solvation of the electron produced in radiation-induced ionization processes. Such a solvation is expected to affect the escape probability of electrons and reduce the extent of geminate recombination of isolated ion pairs. In addition, amides are potentially of interest to the understanding of the radiation chemistry of polypeptides, proteins, and related molecules.

Relatively little attention has been given to the radiation or photochemistry of simple amides. Esr investigation of the radicals produced by electron irradiation of solid amides both in polycrystalline form and as single crystals has been carried out.[3] Some of the products produced in the radiolysis of $N,N$-dimethylformamide,[4] and of acetamide in the solid and liquid states,[5] have been reported. Recently, a rather detailed study of the radiolysis of formamide has been done.[6] The results obtained from the pulse radiolysis of liquid formamide, $N$-methylformamide, and $N,N$-dimethylformamide have recently been reported briefly.[7] The sites of attack of OH radicals in aqueous solution on formamides, acetamides, propionamides, isobutyramides, and pivalamides have been identified, and the transient absorption spectra of the resulting intermediates have been determined.[8]

This paper reports a pulse radiolysis investigation of neat liquid formamide (F), $N$-methylformamide (NMF), $N,N$-dimethylformamide (DMF), $N,N$-dimethylacetamide (DMA), and $N$-methylpropionamide (NMP). Some of the intermediates produced have been identified, and the results are discussed.

## Experimental Section

Most of the work was carried out using the Febetron 705 (Field Emission Corp.) pulsed radiation source. This machine produces single pulses of electrons of 2.3-MeV energy and ~30-nsec duration. The experimental conditions have been described elsewhere.[9] Initial experiments[10] were performed using a pulsed Van de Graaf accelerator at Brookhaven National Laboratory. A number of preliminary experiments, as well as the results presented in Figure 5, were obtained using the Natick linear accelerator. Electrons of 7-9-MeV energy were used and single pulses of 1.2-1.6 $\mu$sec employed. Details are given elsewhere.[11]

(1) Department of Chemistry, Boston University, Boston, Mass.

(2) U. S. Army Natick Laboratories, Natick, Mass.

(3) E. J. Burrell, Jr., J. Amer. Chem. Soc., 83, 571 (1961); M. T. Rogers, S. Bolte, and P. S. Rao, ibid., 87, 1875 (1965), and references cited therein: P. J. Hamrick, Jr., H. W. Shields, and S. H. Parkey, ibid., 90, 5371 (1968).

(4) N. Colebourne, E. Collinson, and F. S. Dainton, Trans. Faraday Soc., 59, 886 (1963).

(5) K. N. Rao and A. O. Allen, J. Phys. Chem., 72, 2181 (1968).

(6) A. Matsumoto, N. Hayashi, and N. N. Lichtin, Radiat. Res., 41, 299 (1970).

(7) N. S. Fel', P. I. Dolin, and V. I. Zolotarevskii, Khim. Vys. Energ., 1, 154 (1967); N. S. Fel', P. I. Dolin, and V. A. Sharpatyi, ibid., 2, 189 (1968).

(8) E. Hayon, T. Ibata, N. N. Lichtin, and M. Simic, J. Amer. Chem. Soc., 92, 3898 (1970); E. Hayon, T. Ibata, N. N. Lichtin, and M. Simic, ibid., in press.

(9) M. Simic, P. Neta, and E. Hayon, J. Phys. Chem., 73, 3794 (1969); E. Hayon, J. Chem. Phys., 51, 4881 (1969).

(10) A. Matsumoto and N. N. Lichtin, Advan. Chem. Ser., 82, 547 (1968).

(11) R. M. Danziger, E. Hayon, and M. E. Langmuir, J. Phys. Chem., 72, 3842 (1968); E. D. Black and E. Hayon, ibid., 74, 3199 (1970).
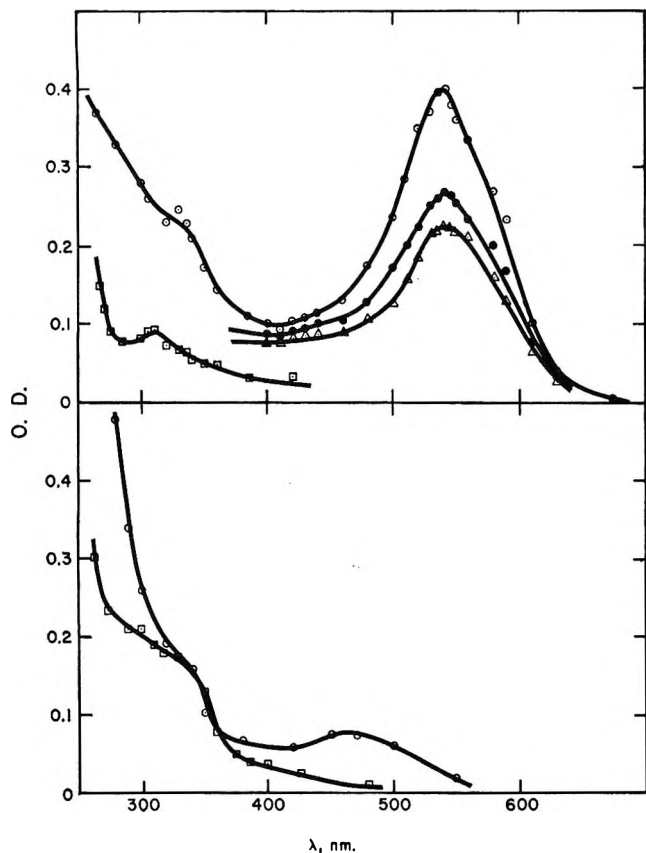
Figure 1.    Transient absorption spectra produced in the pulse radiolysis (dose ~41 krads/pulse) of formamide: top, in presence of argon (1 atm), OD read at 0.2 (○), 1.3 (●), 2.3 (△), and 28.0 (□) $\mu$sec after the 30-nsec electron pulse; bottom, in presence of $O_2$ (1 atm), (○), and 0.1 $M$ NH₄Cl (□), OD read at 0.2 $\mu$sec after the pulse.

Dosimetry was done using KCNS in aqueous solution as mentioned previously.[9]  The quartz optical cell used had an optical path of 2 cm, and fresh solutions were used for each electron pulse.

Formamide and $N$-methylformamide were purified as described in ref 6.  Spectrograde DMF and DMA gave similar results compared to the liquids used after multiple distillations at low pressure.  NMP was obtained from Eastman, distilled, bp 66° at 0.2 Torr.

The extinction coefficient of anthracene radical anion of Gill, et al.,[12] $\epsilon_{720} = 0.99 \times 10^4\ M^{-1}\ cm^{-1}$, was used.  The value for triplet excited naphthalene was that given by Land,[13] $\epsilon_{413} = 2.26 \times 10^4\ M^{-1}\ cm^{-1}$.

## Results

The purification of formamide presented some difficulties, and results varied from one purified batch to another.  In all cases, the transient optical absorption band, with $\lambda_{max}$ ~540 nm, was observed on pulse radiolysis of air-free formamide, see Figure 1.  However, the transient absorption below ~430 nm was found not to be reproducible.  Taking the conductivity of formamide as an indication of the purity of the solvent does not appear to be the only, or main, criterion of

purity.  In early experiments, an absorption band with $\lambda_{max}$ ~410 nm was observed (in addition to the 540-nm band) but could not be reproduced in later experiments.  The spectra shown in Figure 1 (top) are the results presently considered to be more reliable.  In the region below 420 nm, the overall absorption is made up of the overlap of two (or more) transients.  One of the transients with $\lambda_{max}$ ~320 nm could be due to the $\dot{C}ONH_2$ radical, its formation has been suggested[8] in the pulse radiolysis of aqueous solutions of formamide by the reaction

$$OH + HCONH_2 \longrightarrow \dot{C}ONH_2 + H_2O$$
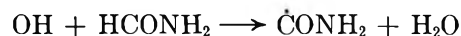
The transient absorption with $\lambda_{max}$ ~540 nm decays relatively quickly with $\tau = $ ~6 $\mu$sec.  Decay in this and other regions of the spectrum displayed in Figure 1 (top) follows neither first- nor second-order kinetics.  Neither the initial transient spectrum produced by pulse radiolysis of neat formamide nor its rate of decay is altered by saturating with 1 atm of $N_2O$ (~5 × 10⁻² $M^{6,14}$).  As shown in Figure 1 (bottom) however, pulsing of the solutions formed by saturation with 1 atm of $O_2$ or dissolution of 0.1 $M$ NH₄Cl gives a transient spectrum in which the 540-nm band is not detectable and in which other qualitative changes are also apparent.  Results identical with those obtained with 0.1 $M$ NH₄Cl are obtained with 0.1 $M$ $(NH_4)_2SO_4$.  Varying the concentration of $(NH_4)_2SO_4$ over the range down to 5 × 10⁻⁴ $M$ showed that the effect of this reagent is to accelerate the decay of the 540-nm peak.  The initial OD of this peak is not affected.

The pulse radiolysis of air-free $N$-methylformamide gives rise to two absorption bands, with maxima at ~360 and ~570 nm, Figure 2.  In the presence of 1 atm of $N_2O$, a slight overall decrease in transient absorption is observed, Figure 2, which could be due to trace amounts of $O_2$ in the $N_2O$ gas used.  The 570-nm band was found to decay by a first-order process, Table I, with $\tau = 2.5$ $\mu$sec.  The transient with $\lambda_{max}$ ~360 nm follows a second-order decay, with $2k/\epsilon \simeq 1.3 \times 10^6$.  This band and its decay are similar to those of a transient absorption produced by attack of OH radicals in the pulse radiolysis of aqueous solutions of NMF and assigned[8] to the $HCONH(\dot{C}H_2)$ radical.

Radiolysis of $N,N$-dimethylformamide produces transients with maxima at ~365 and 650 nm, Figure 3.  In the presence of $N_2O$ (1 atm) or 1.4 × 10⁻² $M$ NH₄Cl, the 650-nm band disappears, while the rest of the spectrum remains unchanged, Figure 3.  The 650-nm band decays by a first-order process with $\tau = 3.3$ $\mu$sec.  The transient with an absorption maximum at ~365 nm and with increasing absorption below 300 nm is closely similar to the spectrum assigned to the $HCON(\dot{C}H_2)$-

(12)  D. Gill, J. Jagur-Grodzinski, and M. Szwarc, Trans. Faraday Soc., 60, 1424 (1964).

(13)  E. J. Land, Proc. Roy. Soc., Ser. A, 305, 457 (1968).

(14)  D. A. Head and D. C. Walker, Can. J. Chem., 48, 1657 (1970).

**Table I:** Decay Kinetics of Transient Species Produced in the Pulse Radiolysis of Liquid Amides

| Amide | Suggested radical | $\lambda$, nm | $k$, $sec^{-1}$ | $2k/\epsilon^a$ | $\epsilon$, $M^{-1} cm^{-1}$ [b] | $2k$, $M^{-1} sec^{-1}$ |
|---|---|---|---|---|---|---|
| $N$-Methylformamide | $HCONH(\dot{C}H_2)$ | 360 | ... | $1.3 \times 10^6 (1.4 \times 10^6)$ | $1.0 \times 10^3$ | $1.3 \times 10^9$ |
| | $c$ | 570 | $4.1 \times 10^5$ | ... | ... | ... |
| | $c$ | 570 | $5.2 \times 10^{5\ d}$ | ... | ... | ... |
| $N,N$-Dimethylformamide | $HCON(\dot{C}H_2)(CH_3)$ | 365 | ... | $2.5 \times 10^6 (1.5 \times 10^6)$ | $1.6 \times 10^3$ | $4.0 \times 10^9$ |
| | $HCON(\dot{C}H_2)(CH_3)$ | 365 | ... | $2.8 \times 10^{6\ d}$ | ... | ... |
| | $e_{solv}^-$ | 650 | $3 \times 10^5$ | ... | ... | ... |
| $N,N$-Dimethylacetamide | $CH_3CON(\dot{C}H_2)(CH_3)$ | 350 | ... | $1.3 \times 10^6 (0.8 \times 10^6)$ | $2.0 \times 10^3$ | $2.6 \times 10^9$ |
| | $e_{solv}^-$ | 625 | $9.3 \times 10^5$ | ... | ... | ... |
| $N$-Methylpropionamide | $e_{solv}^-$ | $e$ | $1.3 \times 10^5$ | ... | ... | ... |

[a] Values given in parentheses were those obtained[8] for the same radical in the pulse radiolysis of the corresponding amides in aqueous solution.  [b] Extinction coefficients used are those derived in aqueous solutions, ref 8.  [c] See text.  [d] In the presence of 1 atm of $N_2O$ ($\sim 5 \times 10^{-2}$ $M$).  [e] Due to very broad absorptions in the 450–700-nm region, the absorption maximum cannot be given.
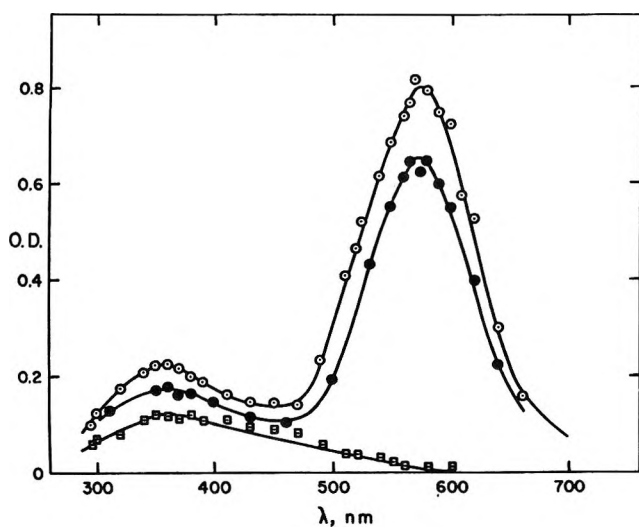


Figure 2. Transient absorption spectra produced in the pulse radiolysis (dose $\sim 19$ krads/pulse) of $N$-methylformamide: in presence of argon (1 atm), OD read at 0.2 (○) and 8.0 (⊡) $\mu$sec after the 30-nsec pulse; and in presence of $N_2O$ (1 atm), OD read at 0.2 $\mu$sec after the pulse (●).



Figure 3. Transient absorption spectra produced in the pulse radiolysis (dose $\sim 34$ krads/pulse) of dimethylformamide: top, in presence of Ar (1 atm) OD read at 0.2 (○) and 3.3 (●) $\mu$sec after the 30-nsec pulse; bottom, in presence of $N_2O$ (1 atm) (○) and in presence of $1.4 \times 10^{-2}$ $M$ $NH_4Cl$ (□), OD read at 0.2 $\mu$sec after pulse.

($CH_3$) radical in the pulse radiolysis of aqueous solution, by reaction with OH radicals (see Table I). The decay of the 365-nm absorption is second order with $2k/\epsilon$ equal to $2.5 \times 10^6$, similar to that observed in aqueous solution.

The pulse radiolysis of $N,N$-dimethylacetamide gives rise to a transient absorption, Figure 4, somewhat similar to that observed for DMF. The presence of $N_2O$ (1 atm) eliminates the formation of the band with $\lambda_{max} \sim 625$ nm, while it has little effect on the rest of the spectrum. The transient at 625 nm follows a first-order decay with $\tau = 10.7$ $\mu$sec. The shoulder at $\lambda \sim 350$ nm decays by a second-order process, with a value of $2k/\epsilon$ similar to that obtained[8] for the transient produced by attack of OH in the pulse radiolysis of DMF in aqueous solution and assigned to the radical $CH_3$-$CON(CH_3)(\dot{C}H_2)$ (see Table I).

Pulse radiolysis of $N$-methylpropionamide produces a



Figure 4. Transient absorption spectra produced in the pulse radiolysis (dose $\sim 34$ krads/pulse) of dimethylacetamide in presence of 1 atm of Ar (○) and $N_2O$ (●), OD read at 0.2 $\mu$sec after the pulse. Insert: transient absorption below $\sim 300$ nm, in Ar. Pulse width $\sim 30$ nsec.

**Table II:** Yield and Decay Rate of $A^-$ and $N^T$ Produced in the Pulse Radiolysis of Anthracene (A) and Naphthalene (N) in Liquid Amides

| Amide | [A], $M$ | $G_{A^-}$ | Decay $A^-$, $sec^{-1}$ | [N], $M$ | $G_{N^T}(Ar)$ | $G_{N^T}(N_2O)$ |
|---|---|---|---|---|---|---|
| Formamide | $<2 \times 10^{-3}$ | $>0.7^a$ | ... | $1 \times 10^{-2}$ | 0.19 | 0.08 |
| N-Methylformamide | $<4 \times 10^{-3}$ | $>1.5^a$ | ... | $1 \times 10^{-2}$ | 0.14 | 0.10 |
| N,N-Dimethylformamide | $5 \times 10^{-3}$ | 2.0 | $6.5 \times 10^4$ | $1 \times 10^{-2}$ | 0.43 | 0.24 |
| N,N-Dimethylacetamide | $5 \times 10^{-3}$ | 1.7 | $2.6 \times 10^5$ | $1 \times 10^{-2}$ | 0.32 | 0.11 |
| N-Methylpropionamide | $5 \times 10^{-3}$ | 2.6 | $2.2 \times 10^4$ | ... | ... | ... |

$^a$ Low $G_{A^-}$ values probably due to limited solubility of anthracene in these amides and/or presence of impurities.

transient spectrum with $\lambda_{max}$ ~340 nm and a weaker very broad absorption over the wavelength region 400–700 nm. Addition of $N_2O$ (1 atm) or 0.1 $M$ $NH_4Cl$ completely suppresses the absorption in the visible region of the spectrum and causes only a small decrease in the 340-nm region. Pulse radiolysis of NMP in aqueous solution[8] produces a transient absorption by attack of OH radicals, which has maxima at 242 and 350 nm and which has been assigned to the $CH_3CH_2$-$CONH\dot{C}H_2$ radical.

Based on the extinction coefficients derived[8] in aqueous solutions, the yields of the following radicals produced in the radiolysis of neat NMF, DMF, and DMA can be estimated: $G[HCONH(\dot{C}H_2)] \sim 2.0$, $G[HCON(\dot{C}H_2)(CH_3)] \sim 1.5$, and $G[CH_3CON(\dot{C}H_2)(CH_3)] \leq 2.0$.

## Discussion

Absorption of high-energy radiation is known to produce ionization and excitation processes in liquids, e.g.

$$RCONR_2 \xrightarrow{\quad\quad} RCONR_2^* + (RCONR_2)^+ + e^- \quad (1)$$
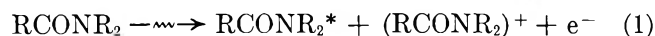
The isolated ion pairs produced in reaction 1 can undergo geminate combination and give rise to a further yield of excited molecules

$$(RCONR_2)^+ + e^- \longrightarrow RCONR_2^* \quad (2)$$
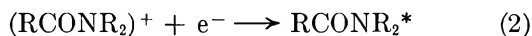
The extent of this combination is dependent on a number of factors, including the degree of solvation afforded by the solvent to the electron, the occurrence of proton transfer, ion–molecule reactions, the temperature, and the presence of solutes capable of reacting with either or both of the primary ions produced in the radiolysis. Recently, a marked dependence on the static dielectric constant of the liquid has been found[15] for the yield of electrons which escape primary combination. The free radicals produced on radiolysis (the precursors of many of the observed products) are presumed to be formed from the dissociation of the excited solvent molecules. They could also, however, be produced from the dissociation of the parent ions and/or in secondary reactions with free radicals.

The formation of electrons and excited state molecules in the radiolysis of the liquid amides studied can

be shown by irradiating amides containing anthracene (A), Figure 5. Here the characteristic transient spectra due to $A^-$ radical anions, with $\lambda_{max}$ ~720 nm (with shoulder and peak at ~650 and 570 nm) were observed and correspond to the reported[14] spectrum of $A^-$. From the known[12] extinction coefficient of $A^-$, and assuming it to be independent of the solvent, the yield of $A^-$, and therefore of $e^-$, produced was derived (see Table II)

$$e^- + A \longrightarrow A^- \quad (3)$$
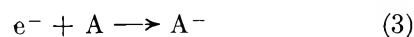
The values of $G_{e^-}$ observed in formamide and N-methylformamide are considered to be low due to the limited solubility of A in these solvents, the dependence of $G_{e^-}$ on [A] and/or the possible presence of electron-scavenging impurities (e.g., the corresponding acid, HCOOH, has a reactivity[17] with $e_{aq}^-$ of ~$10^8$ $M^{-1}$ $sec^{-1}$, and the presence of 0.1–1.0% of this impurity would compete effectively with A). The yield of $G_{e^-}$ in DMF and DMA of ~2.0 and ~1.7, respectively, is considered to represent the yield of free ions produced in these liquids. These yields are considerably lower than the limiting yield, $G_{e^-}$ ~4.0, expected for the total ionization yield in liquids. In the presence of high concentrations of electron scavengers, this optimum yield can be obtained. The limiting yield of $N_2$ produced from the radiolysis of formamide in the presence of up to ~8 $\times$ $10^{-2}$ $M$ $N_2O$ is reported[14] to be 3.3 $\pm$ 0.3 (see also ref 6), possibly corresponding to the reaction

$$e^- + N_2O \longrightarrow N_2 + O^- \quad (4)$$
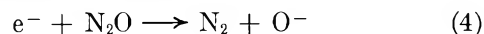
It is suggested that the transient absorptions with maxima at ~650 and ~625 nm obtained in the pulse radiolysis of neat DMF and DMA, respectively, Figures 3 and 4, are due to the solvated electron in these liquids: on addition of $N_2O$, $O_2$, or $NH_4^+$ ions these transient absorptions cannot be observed. These species also decay by first-order processes (see Table I). These results are usually characteristic for the behavior

(15) E. Hayon, J. Chem. Phys., 53, 2353 (1970).

(16) P. Balk, G. J. Hoijtink, and J. W. H. Schreurs, Recl. Trav. Chim. Pays-Bas, 76, 813 (1957); E. deBoer and S. I. Weissman, ibid., 76, 824 (1957).

(17) M. Anbar and P. Neta, Int. J. Appl. Radiat. Isotopes, 18, 493 (1967).
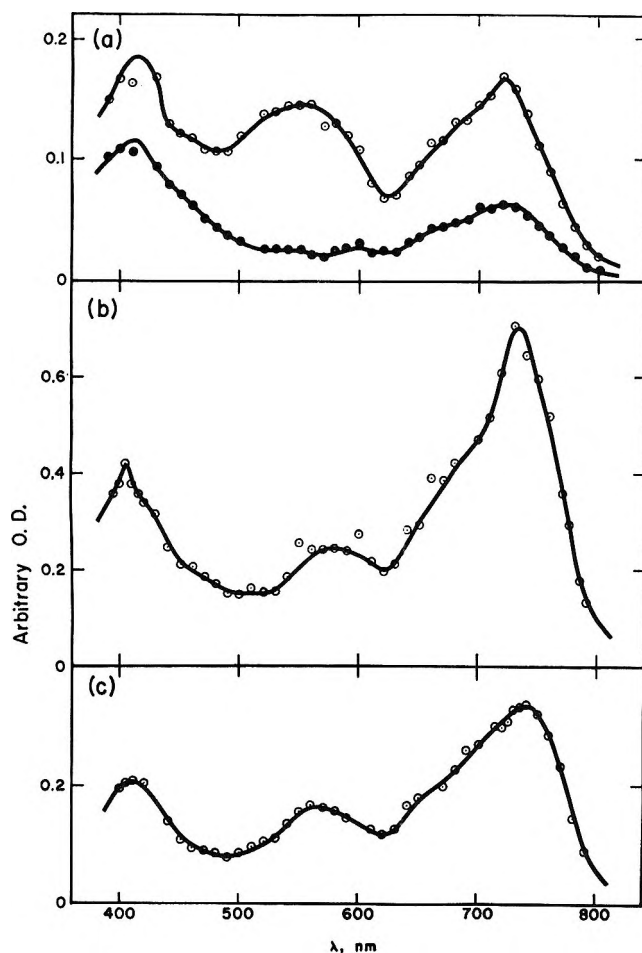
Figure 5. Transient absorption spectra produced in the pulse radiolysis of anthracene (A) in liquid amides: (a) $2 \times 10^{-3}$ $M$ A in formamide, OD read at 4.0 (○) and 8.0 (●) $\mu$sec after a 1.5-$\mu$sec pulse; (b) $1.8 \times 10^{-2}$ $M$ A in dimethylformamide, OD read at 3 $\mu$sec after a 1.5 $\mu$sec pulse; (c) $1 \times 10^{-2}$ $M$ A in dimethylacetamide, OD read at 3 $\mu$sec after a 1.5-$\mu$sec pulse.

of the solvated electron in polar liquids. Based on this interpretation, and the yields of $G_{e^-}$ given in Table II, one can determine the extinction coefficient of the solvated electron in DMF and DMA. Values of $\epsilon_{650} \sim 1000$ $M^{-1}$ cm$^{-1}$ for DMF and $\epsilon_{625} \sim 1500$ $M^{-1}$ cm$^{-1}$ for DMA were derived. It is to be noted that these values are considerably lower than those for the solvated electron in water or aliphatic alcohols, where extinction coefficients of $\sim 1$–2 $\times 10^4$ $M^{-1}$ cm$^{-1}$ were obtained.[18]

The absorptions with $\lambda_{max}$ $\sim 540$ and $\sim 570$ nm in F and NMF, Figures 1 and 2, do not appear to be those of the solvated electron in these liquids, contrary to the suggestion made by Fel', et al.,[7] for formamide. This conclusion is based primarily on (1) the presence of these bands in solutions containing $5 \times 10^{-2}$ $M$ N$_2$O, and (2) the almost quantitative formation of these bands in the presence of anthracene. The observation[14] that typical electron scavengers, e.g., acids and silver ions, sharply reduce the yields of N$_2$ produced by irradiation of their cosolutions with N$_2$O in formamide,

supports the view that N$_2$O either scavenges solvated electrons, eq 4, or some other highly reactive donor. Clearly, the transient absorption with $\lambda_{max}$ at $\sim 540$ nm cannot be such a donor. The nature of these transients formed in F and NMF is discussed further below.

The yield of free ions produced in the radiolysis of organic liquids appears to depend (among other factors) on the static dielectric constant of the liquid. The observed $G_{e^-}$ values for the liquid amides studied (Table II) are in accord with this approximate correlation. These results are further discussed elsewhere.[15]

The formation of excited solute molecules was observed in the pulse radiolysis of solutions of anthracene (A) or naphthalene in F, NMF, DMF, and DMA. The characteristic transient absorption with $\lambda_{max}$ $\sim 410$–420 nm for A$^T$ was found (see Figure 5). The yields of excited states were determined using N and are given in Table II. It is interesting to note that $G_{N^T}$ is significantly lower in the presence of the electron scavenger N$_2$O, indicating a decrease of reaction 2. For further discussion on these yields see ref 15.

In the pulse radiolysis of DMF and DMA the transient species absorbing at $\sim 365$ and $\sim 350$ nm, respectively, have spectra and decay rates which correspond closely to the radicals HCON($\dot{C}$H$_2$)(CH$_3$) and CH$_3$-CON($\dot{C}$H$_2$)(CH$_3$), see Table I, observed recently.[8] Similarly, the transient absorption with $\lambda_{max}$ $\sim 340$ nm produced by pulse radiolysis of NMP resembles that produced by attack of hydroxyl radical on aqueous NMP and ascribed[8] to CH$_3$CH$_2$CONH$\dot{C}$H$_2$. In the radiolysis of DMF, the following products were measured[4]: CO ($G = 2.6$), (CH$_3$)$_2$NH ($G = 2.6 \pm 0.5$), H$_2$ ($G = 0.14$), and CH$_4$ ($G = 0.93$). Of these products, the (CH$_3$)$_2$N$\cdot$ radical (the probable precursor of dimethylamine) due to the high electronegativity of the nitrogen atom should be electrophilic and, therefore, effectively abstract an H atom from DMF. No information is available on the spectrum of $\dot{C}$ON(CH$_3$)$_2$, but the R$\dot{N}$COCH$_3$ radical (R = H or CH$_3$) is expected[8] to absorb below $\sim 280$ nm.

Intermediates produced in the pulse radiolysis of F and NMF, Figures 1 and 2, are more difficult to characterize. If the 540- and 570-nm bands are not due to the solvated electron, then other possibilities such as one or more of the following species must be considered: HCO, $\cdot$CONH$_2$, $\cdot$CONHCH$_3$, HCO$\dot{N}$H, $\dot{N}$H$_2$, $\dot{N}$HCH$_3$, anions and cations of F and NMF. In aqueous solutions, the $\cdot$CO$\dot{N}$H$_2$ and HCO$\dot{N}$H radicals have been shown[8] to absorb with $\lambda_{max}$ $\sim 320$ nm and $\lambda_{max}$ $< 245$ nm, respectively. The formation of both of these radicals is supported by the observation of (CO-NH$_2$)$_2$ and (HCONH)$_2$ as products[6] in the radiolysis of neat formamide. The HCO radical is known to have

(18) L. M. Dorfman and M. S. Matheson, Progr. React. Kinet., 3, 237 (1960).

an absorption in the 550–600-nm region,[19] but no shift in absorption from 540 nm in F to 570 nm in NMF would be expected. The solvated electron could form electron adducts with the liquid amides. In aqueous solution, the corresponding ketyl radicals and radical anions have been found[20] to absorb in the uv region with $\lambda_{max}$ ~250 nm. Of the remaining possibilities, it is suggested that these bands might be due to amino/alkylamino radicals or to radical anions. The fact that both $NH_4Cl$ and $(NH_4)_2SO_4$ suppress the 540-nm peak of F indicates that $NH_4^+$ is the active reagent. Presumably ammonium ion acts by donating a proton. The fact that this effect consists in accelerating the decay of the 540-nm transient absorption, rather than

affecting its formation, indicates that the ammonium ion reacts with the transient species and not with its precursor(s).

(19) M. McCarty, Jr., and G. W. Robinson, *J. Chim. Phys.*, **56**, 723 (1959); F. S. Dainton, G. A. Salmon, and P. Wardman, *Proc. Roy. Soc., Ser. A*, **313**, 1 (1969).

(20) E. Hayon and M. Simic, Intra-Science Chemistry Report, Intra-Science Research Foundation, Santa Monica, Calif., in press.

# The Effect of Positive Ion Scavenging by Benzene in the Radiolysis of Propane

by Lester Y. Wei[1a] and Larry I. Bone*

*Department of Chemistry, East Texas State University, Commerce, Texas 75428* (*Received January 13, 1971*)

*Publication costs assisted by The Robert A. Welch Foundation*

Propane has been irradiated in the presence of small quantities of benzene at various total doses. It is deduced that propyl ions react readily with benzene and the final stable molecular products are cumene and diphenylpropane. It is observed that ethyl ions react with benzene approximately four times faster than they react with propane. In the presence of 1 mol % benzene the yields of all stable hydrocarbon products are independent of total dose. From this information it is deduced that in the gas-phase radiolysis of pure propane, the observed conversion dependence must result from ion interception by accumulated unsaturates.

## Introduction

Bone, Sieck, and Futrell[1b] have investigated the gas-phase radiolysis of propane at 1 atm pressure and were able to determine the complete ionic cracking pattern and the complete neutral molecule fragmentation pattern under the conditions of their experiment. Part of the argument of that particular study was based on a comparison of stable product yields in the presence and absence of 0.01 mole fractions of benzene. Benzene appeared to be serving as an ionic interceptor, as had been suggested by Ausloos and Lias.[2] At low concentrations of benzene, it was apparent that benzene was intercepting only propyl ions ($C_3H_7^+$) and propane ions ($C_3H_8^+$), since changes in the final stable molecular products could be correlated directly with the predicted yields of these ions. However, the authors[1b] were unable to determine the exact nature of these reactions, since no stable molecular products could be found which contained benzene.

Subsequently Bone and Futrell[3] investigated the reactions of propyl and propane ions with benzene in the

Aerospace Research Laboratories' tandem mass spectrometer. It was found that the predominant reaction of propane ion with benzene was charge transfer accompanied by a minor (<5%) contribution from proton transfer. It was found that propyl ion reacted with benzene to produce an excited $C_9H_{13}^+$ adduct ion, which required collisional stabilization. However, the lifetime of the excited $C_9H_{13}^+$ ion was sufficiently long that at pressures above a few Torr, $C_9H_{13}^+$ would be the only product produced. This observation was confirmed by a study by Munson and Field.[4] The mass spectrometric studies cannot predict the final stable neutral molecular products in the radiolysis experiments. In fact it is not clear whether the propyl ion

(1) (a) Submitted in partial fulfillment of the degree of Master of Science; (b) L. I. Bone, L. W. Sieck, and J. H. Futrell, "The Chemistry of Ionization and Excitation," Taylor and Francis, London, 1967, p 223.

(2) S. G. Lias and P. Ausloos, *J. Chem. Phys.*, **37**, 887 (1962).

(3) L. I. Bone and J. H. Futrell, *ibid.*, **47**, 4366 (1967).

(4) M. S. B. Munson and F. H. Field, *J. Amer. Chem. Soc.*, **89**, 1048 (1967).

actually reacts with the benzene ring or is simply electrostatically attached to the $\pi$ cloud of the benzene system. If the latter is the case, it is entirely possible that no benzene products would be expected in the gas-phase radiolysis of propane in the presence of benzene.

In the present study we have reinvestigated the gasphase radiolysis of propane in the presence of benzene at relatively high conversions of propane into products (a few tenths of a per cent) and at high benzene concentrations (up to 10 mol %) in order to systematically search for benzene-containing products. We have then determined the effects of benzene concentration and propane conversion on the yields of stable products.

## Experimental Section

All samples were irradiated at atmospheric pressure in a 250-cm³ cylindrical Pyrex flask with a thin bubble window. The X-ray source was a Siemens X-ray unit with a tungsten target. The unit was operated at 50 keV and 23 mA in all experiments. Five mole per cent xenon was added to all experiments to increase the dose rate, to take advantage of the strong dependence of the photoelectric process on the atomic number of the absorber. Five per cent xenon was sufficient to increase the dose rate by approximately an order of magnitude but undoubtedly insufficient to constitute sensitization, since only the initial photon interaction is inproportionately dominated by the xenon.

Gases used in the study include: Phillips Research grade propane which was further purified by preparative gas chromatography and outgassed *in vacuo*, Becker spectrometric grade benzene which was vacuum distilled below its boiling point such that only the middle three-fifths of each sample was retained, and Air Products research grade xenon which was outgassed at liquid nitrogen temperature.

The yields of hydrocarbon products were determined in a Hewlett–Packard Model 5750 gas chromatograph utilizing flame ionization. All aliphatic hydrocarbon products except propylene were analyzed on a 1.5-m 40–60 mesh activated alumina column. Propylene was analyzed on a 4-m squalane (20% by weight) on Chromosorb W column operated at $-10°$. The aromatic products were analyzed on a 2-m 10% UC, W98 Hewlett–Packard capillary column operated from room temperature to 300°.

In all cases gaseous samples were transferred from the radiolysis vessel to the chromatograph with a 5-cm³ gas syringe. A number of chromatographic analyses were made where the vessel and syringe were heated. The ratios of product yields were then observed in order to detect if any products had condensed in the vessel, since the relative yield of any condensed products would increase with temperature.

Hydrogen yields were determined on a Bell and Howell 21–440 residual gas analyzer which had been converted into a mass spectrometer in this laboratory.

The instrument was calibrated with propane-diluted hydrogen samples. In experiments where hydrogen yields were determined, no other product yields were measured. Yields were computed simply on the basis of radiation time.

Positive identification of all aromatic compounds was made by comparing their nmr spectra, uv spectra, and gas chromatographic retention times with known samples of various isomers of each compound synthesized at this institution.

The samples for nmr and uv analysis were collected from samples irradiated with 5 mol % benzene at 1% conversion of propane into products. Under these conditions, some condensed product could be observed on the sides of the vessel. After radiolysis the vessel was evacuated, the stopcock was broken off to avoid contaminating the sample with stopcock grease, and the condensate was dissolved in perdeuteriobenzene or deuteriochloroform.

## Results

Preliminary experiments at 5 mol % benzene, which were carried to near 1.0% conversion of propane into products, revealed that the following aromatic compounds were produced: ethylbenzene, isopropylbenzene, 3-phenyl-1-propene, 1,3-diphenylpropane, 2,2-diphenylpropane, and 1,2-diphenylpropane. In order to determine the mechanism of production of these products it was necessary to determine independently the variation of product yields with per cent conversion and with concentration of benzene. The most meaningful results are at low conversions where accumulated products cannot interfere with product yields and at low benzene concentration where benzene is only able to react with those intermediate species which are unreactive toward propane. The ion pair yields of all stable hydrocarbon products have been determined for 1, 5, and 10 mol % benzene at various percentages of conversion of propane into products.

All ion pair yields in this study are normalized to the ethane yield of the previous study,[1b] since no dosimetry or ion current measurements were made in conjunction with the present study.

Figure 1 shows the ion-pair yields of a few of the more important products as a function of per cent of conversion of propane into products at 1% benzene concentration. The behavior of all products at all benzene concentrations is very similar to that shown in Figure 1. That is, the yields of all stable molecular products appear to be independent of conversion in the gas-phase radiolysis of propane in the presence of 1 to 10 mol % benzene.

From a series of relationships similar to Figure 1, the ion-pair yields of all products were extrapolated to 0.01% conversion. Since no significant variation in yield was observed, this process was equivalent to averaging the yields for most products. The ion-pair yields
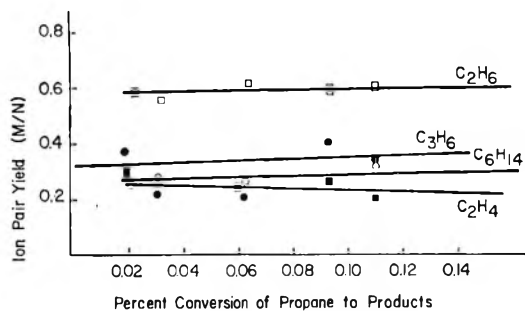
Figure 1. Propane radiolysis product yields at 1% benzene concentration: ●, propylene; ■, ethylene; □, ethane; ○, hexane.
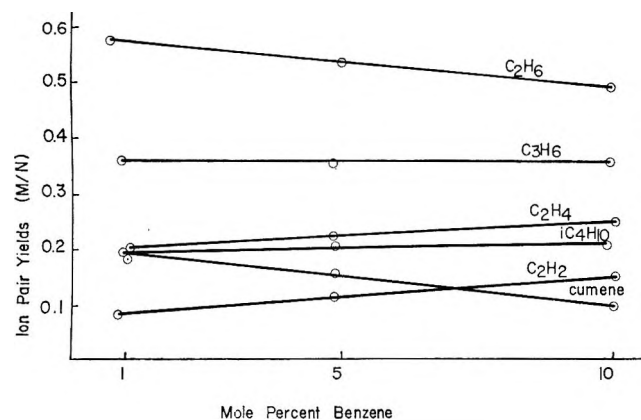


Figure 2. Propane radiolysis yields as a function of benzene concentration.

**Table I:** Product Yields from the Radiolysis of Propane with Added Benzene[a]

| Product | 1.0[b] | Mol % benzene 1.0 | 5.0 | 10 |
|---|---|---|---|---|
| Hydrogen | 1.15 | 1.2 | 1.2 | ... |
| Methane | 0.42 | 0.40 | ... | ... |
| Acetylene | 0.07 | 0.08 | 0.11 | 0.15 |
| Ethylene | 0.26 | 0.22 | 0.24 | 0.26 |
| Ethane | 0.58 | 0.58 | 0.54 | 0.49 |
| Propylene | 0.37 | 0.35 | 0.34 | 0.35 |
| Isobutane | 0.17 | 0.19 | 0.20 | 0.20 |
| n-Butane | 0.06 | 0.01 | 0.01 | 0.01 |
| Isopentane | 0.03 | 0.02 | 0.02 | 0.02 |
| Total hexane[c] | 0.24 | 0.26 | 0.25 | 0.24 |
| Ethylbenzene | ... | 0.014 | 0.015 | 0.016 |
| Cumene | ... | 0.18 | 0.15 | 0.10 |
| 3-Phenyl-1-propene | ... | 0.01 | 0.01 | 0.01 |
| Diphenylpropane[d] | ... | >0.35 | ... | ... |

[a] Yields defined as the observed yield of products divided by the total yield of ions deduced from the mechanism advanced in ref 1b. All numbers reported are an average of at least three separate radiolyses. [b] Yields reported in ref 1b at $10^{-2}$% conversion. [c] Includes yields of 2,3-dimethylbutane, 2-methylpentane, and n-hexane. [d] 60% 2,2-Diphenylpropane, 20% 1,2-diphenylpropane, and 20% 1,3-diphenylpropane.

of all products at 0.01% conversion were plotted as a function of benzene concentration. Figure 2 shows one of these plots for some of the most important products. The ion-pair yields of all products are shown in Table I at 1, 5, and 10 mol % benzene. The first column shows the yields reported by Bone, Sieck, and Futrell.[1b] The yield of diphenylpropane reported in Table I represents a lower limit, since this low vapor pressure product condensed on the sides of the vessel. Various methods were used to determine more accurate diphenylpropane yields, such as heating the vessel and the syringe or washing the sides of the vessel with solvents. None were particularly successful, and thus we are only able to measure a lower limit for the diphenylpropane yield. The same absolute quantity of this product was measured at every benzene concentration; thus the lower limit of the yield is reported for 1% benzene only. Three isomers of diphenylpropane were partially resolved by the chromatograph. The approximate percentages of each are reported in footnote d of Table I.

Hydrogen yields were measured in the presence of 1 and 5% benzene, and no variation in yield could be detected.

**Discussion**

We have observed that the yields of hydrocarbon

products produced in the radiolysis of propane in the presence of small quantities of benzene are very insensitive to the per cent conversion of propane into products. This is to be compared to the observation of Sieck, Blocker, and Futrell[5] of a strong conversion dependence of hydrocarbon yields in the radiolysis of pure propane. Since the difference in the two studies is the interception of propyl ions by benzene, this strengthens a previous suggestion[1b] that the conversion dependence observed in the gas-phase radiolysis of pure propane is primarily a result of ion interception by accumulated alkenes rather than free-radical scavenging as would be assumed from an earlier work of Back.[6] The slight decrease in propylene and ethylene yields as the conversion is increased is undoubtedly a result of hydrogen atom scavenging by these two alkenes. However, since propylene is the major alkene produced in the radiolysis and hydrogen atoms abstract from propane to produce propyl radicals in the absence of unsaturates, the product of the addition of a hydrogen atom to propylene is also a propyl radical. Thus, hydrogen atom scavenging has little effect on the yields of hydrocarbon products. The increase in acetylene yield observed from Table I undoubtedly results from direct energy absorption by benzene, since acetylene is the major product in benzene radiolysis.

The cumene yield holds the key to the determination of the mechanism of the reaction of propyl ions with

(5) L. W. Sieck, N. K. Blocker, and J. H. Futrell, J. Phys. Chem., 69, 900 (1965).

(6) R. A. Back, ibid., 64, 124 (1960).

benzene. It seems most logical to suggest that cumene is produced by the following mechanism.

$$C_3H_7^+ + C_6H_6 \longrightarrow C_9H_{13}^+$$

$$C_9H_{13}^+ + e^- \longrightarrow C_9H_{12} + H \cdot \qquad (1)$$

$$H \cdot + C_3H_8 \longrightarrow H_2 + C_3H_7 \cdot$$
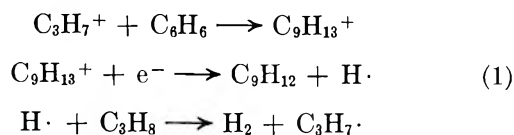
Diphenylpropane is produced by the following subsequent reaction sequence, which becomes more important as the benzene concentration is increased.

$$C_9H_{13}^+ + C_6H_6 \longrightarrow C_{15}H_{17}^+ + H_2$$

$$C_{15}H_{17}^+ + e^- \longrightarrow C_{15}H_{16} + H \cdot \qquad (2)$$

$$H \cdot + C_3H_8 \longrightarrow C_3H_7 \cdot + H_2$$
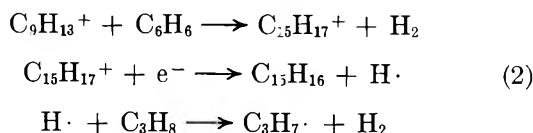
The yield of propyl ions can be calculated from the ionic cracking pattern reported previously.[1b]

$$C_3H_8^{+*} \longrightarrow \begin{cases} \xrightarrow{0.07} C_2H_3^+ + H_2 + CH_3 \cdot \\ \xrightarrow{0.07} C_3H_5^+ + H_2 + H \cdot \\ \xrightarrow{0.16} C_2H_4^+ + CH_4 \\ \xrightarrow{0.35} C_2H_5^+ + CH_3 \\ \xrightarrow{0.10} C_3H_7^+ + H \cdot \\ \xrightarrow{0.25} C_3H_8^+ \end{cases}$$
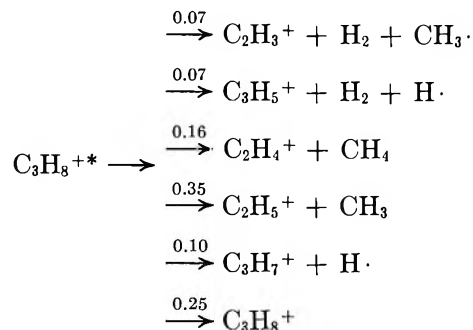
It has been shown[1b,7] that all fragment ions from propane undergo hydride transfer reactions with neutral propane. In some cases, notably $C_2H_4^+$ and $C_3H_6^+$, $H_2^-$ transfer from propane[8] is an important competitive process, but since the $C_3H_6^+$ produced will ultimately hydride transfer, the ionic daughter of all ions, except $C_3H_8^+$, is $C_3H_7^+$. With the exception of a small yield of 3-phenyl-1-propene, which probably results from the reaction of $C_3H_6^+$ with benzene, the hydride transfer reactions are too fast for reactions of benzene to compete. Thus the anticipated yield of propyl ions calculated from the cracking pattern above is 0.75. Since 0.18 propyl ions are accounted for by the observed ion pair yield of cumene, there remains a yield of 0.57 propyl ions which must yet be accounted for.

We suggest that the remainder of the propyl ions will ultimately appear as diphenylpropane. However, since we are only able to deduce a lower limit for the ion pair yield of diphenylpropane, we are forced into a less conclusive justification for our mechanism. This justification is based on a detailed accounting of propyl radicals, since they are produced concurrently with cumene and diphenylpropane by hydrogen atom abstraction.[9]

If one assumes the neutral molecule decomposition scheme reported previously[1b] along with the ionic cracking pattern already discussed

$$C_3H_8^* \longrightarrow \begin{cases} \xrightarrow{0.05} C_2H_4 + CH_4 \\ \xrightarrow{0.12} C_2H_4 + CH_3 \cdot + H \cdot \\ \xrightarrow{0.02} C_2H_6 + CH_2 : \\ \xrightarrow{0.14} C_3H_6 + H_2 \end{cases}$$
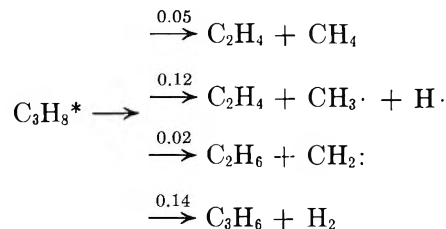
it is possible to predict a yield of 0.31 propyl radicals. This yield is primarily a result of hydrogen atom abstraction from propane by hydrogen atoms with a slight contribution from abstraction by "hot" methyls.[1b]

It is possible to calculate the observed yield of propyl radicals in any experiment by applying known disproportionation to combination ratios to the measured yields of hexane, pentane, and butane, since these products are produced almost exclusively by radical combination.[1b] In this manner one calculates that a yield of 1.05 propyl radicals was produced in experiments at low conversion with 1% added benzene. Since a yield of 0.31 propyl radicals was previously accounted for by primary processes and 0.18 was produced concurrently with cumene, there remains 0.56 propyl radicals unaccounted for. This is in excellent agreement with the propyl ions unaccounted for and strongly suggests that the actual ion-pair yield of diphenylpropane is 0.56 and that our mechanism for the reaction of propyl ions with benzene is correct.

We have been able to show that propyl ions actually react with benzene and the observed $C_9H_{13}^+$ ion is not simply an electrostatic adduct. Furthermore, the products of this reaction, after neutralization, are found to be cumene and diphenylpropane.

An attempt was made to correlate the yield of hydrogen with the mechanism advanced. This was not particularly successful.

The mechanism advanced suggests that the hydrogen yield should increase with benzene concentration. However, as the benzene concentration is increased some of the hydrogen atoms are undoubtedly scavenged by benzene. We were able to show in the earlier study[1b] that 1% benzene could not compete with the fast hydrogen abstraction reaction. Furthermore, this process cannot be too important as the benzene concentration is increased or a larger decrease in the hexane and butane yields would be observed, since these products result primarily from $C_3H_7$ radicals. Thus it was hoped that at least some increase in hydrogen yield could be observed as the benzene concentration was increased. We were unable to observe any difference in hydrogen yields between experiments with 1 and 5% benzene. The results are not surprising, since undoubtedly some of the hydrogen comes from the glass vessel

(7) L. I. Bone and J. H. Futrell, J. Chem. Phys., 46, 4084 (1967).

(8) L. W. Sieck and J. H. Futrell, J. Phys. Chem., 69, 888 (1965).

(9) L. I. Bone and R. F. Firestone, ibid., 69, 3652 (1965).

and it is impossible to explain the complete hydrogen yield even in the absence of any additives.

We feel that the decrease in the ethane yield observed as the benzene concentration is increased is worthy of comment. In the absence of benzene, ethyl ions are known to react rapidly with propane by

$$C_2H_5^+ + C_3H_8 \longrightarrow C_2H_6 + C_3H_7^+ \qquad (3)$$

The decrease in the yield of ethane as the benzene concentration is increased is attributed to competition by the following reaction which is analogous to the initial step in the propyl ion sequence

$$C_2H_5^+ + C_6H_6 \longrightarrow C_8H_{11}^+ \qquad (4)$$
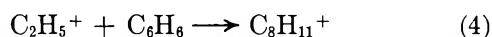
Some of the $C_8H_{11}^+$ is undoubtedly neutralized to ethylbenzene. The fact that we observe ethylbenzene and that it increases slightly with benzene concentration lends support to this conclusion, even though the increase in ethylbenzene does not correlate directly with the decrease in the ethane yield. The remainder of the $C_8H_{11}^+$ undoubtedly reacts further with benzene to produce products which we have not been able to observe.

From the ionic cracking pattern reported previously,[1b] the ion pair yield of $C_2H_5^+$ is 0.35. If we assume that the $C_8H_{11}^+$ ion does not react further with benzene at 1% benzene concentration, then the ethylbenzene yield, 0.014, represents a lower limit for the yield of ethyl ions reacting by reaction 4. Since in the absence of benzene ethyl ions react by reaction 3, one can calculate

$$k_4/k_3 = \frac{0.014}{0.35} \times \frac{\text{mole fraction propane}}{\text{mole fraction benzene}} = 4$$

In the experiments with 10% benzene the rate of reaction of ethyl ions with benzene should be $^4/_9$ the rate of the reaction with propane and the fraction which reacts with benzene is therefore

$$\frac{^4/_9}{1 + ^4/_9} \cong 0.3$$

Thus the ethane yield should decrease by $0.3 \times 0.35 = 0.105$ in the presence of 10 mol % benzene. The observed decrease is 0.09.

Therefore we suggest that the reaction of ethyl ions with benzene is approximately four times faster than the reaction of ethyl ions with propane.

# Electron Spin Resonance Study of Radicals Produced in Irradiated

# Aqueous Solutions of Thiols[1]

## by P. Neta and Richard W. Fessenden*

*Radiation Research Laboratories and Department of Chemistry, Mellon Institute of Science,
Carnegie-Mellon University, Pittsburgh, Pennsylvania 15213   (Received February 1, 1971)*

*Publication costs assisted by the Carnegie-Mellon University and the U. S. Atomic Energy Commission*

Radicals produced by reaction of hydrated electrons and hydroxyl radicals with several organic thiols in aqueous solutions have been studied by electron spin resonance. Irradiation with high-energy electrons was carried out directly in the esr cavity. Spectra of the radicals $\dot{C}H_2COO^-$ and $^-S\dot{C}HCOO^-$ ($g = 2.0086$, $a_{CH}{}^H = 13.4$ G) were obtained from alkaline solutions of mercaptoacetate. The variation in intensity of the two spectra when various scavengers were added shows that the two species were formed by reactions of $e_{aq}^-$ and OH, respectively. The radical $\dot{S}CH_2COO^-$ is also expected to be formed by reaction of OH but could not be observed under our experimental conditions. Similarly, the radicals $^-OOCCH_2\dot{C}HCOO^-$ ($g = 2.0033$, $a_{CH}{}^H = 20.4$ G, $a_{CH_2}{}^H = 23.6$ G) and $^-OOCCH_2\dot{C}(S^-)COO^-$ ($g = 2.0075$, $a_{CH}{}^H = 8.7$ G) in solutions of mercaptosuccinate were found to result from the reaction of $e_{aq}^-$ and OH, respectively. Substituted alkyl radicals produced by hydrogen abstraction from 3-mercaptopropionate, cysteine, thiodiglycolic acid, and dithiodiglycolic acid have also been observed.

## Introduction

The radiation chemistry of aqueous solutions of thiols has been the subject of several extensive investigations with particular emphasis on cysteine and related compounds (*cf.* ref 2–6). The radicals produced from these compounds have been studied both by pulse radiolysis[5,6] and by esr spectroscopy.[7,8] The esr studies, however, did not involve radiolytic production but relied on chemical oxidation using a mixing technique. It seemed, therefore, desirable to carry out an esr investigation of the radicals produced by *in situ* radiolysis of aqueous solutions of these compounds. This method has been developed and used in this laboratory for the study of the radiolysis of several groups of organic compounds in aqueous solutions,[9,10] and its application was expected to help elucidate the mechanism of reactions of OH and $e_{aq}^-$ with thiols.

Most of the studies of thiols have dealt solely with radicals of the type $R\dot{S}$, which are the main product of hydrogen abstraction. Rate constants for the different paths of abstraction have been measured for the reaction of hydrogen atoms with cysteine[11] but no measurements exist for the OH reactions. From the available data, abstraction is expected to take place from C–H at rates one to two orders of magnitude slower than from S–H. Although the radiobiological importance of mercaptoalkyl radicals may be less than that of thiyl radicals we wish to draw attention to their formation and to present esr data on some radicals of this type which have not been observed previously.

## Experimental Section

Mercaptoacetic acid, mercaptosuccinic acid, and thio-

diglycolic acid were Baker Grade reagents, 3-mercaptopropionic acid was obtained from Eastman, dithiodiglycolic acid from Aldrich, and cysteine from Cyclo. The inorganic materials were Baker Analyzed reagents. Water was doubly distilled. The pH was adjusted using potassium hydroxide, perchloric acid, or sodium tetraborate. Solutions were deoxygenated by bubbling with nitrogen or were saturated with nitrous oxide. The irradiation arrangement and other details of the experiment were as previously described.[9]

## Results and Discussion

The possible reactions of thiols with the primary

(1) Supported in part by the U. S. Atomic Energy Commission. Presented in part at the 161st National Meeting of the American Chemical Society, Los Angeles, Calif., March 28–April 2, 1971.

(2) V. G. Wilkening, M. Lal, M. Arends, and D. A. Armstrong, *Can. J. Chem.*, 45, 1209 (1967).

(3) A. Al-Thannon, R. M. Peterson, and C. N. Trumbore, *J. Phys. Chem.*, 72, 2395 (1968).

(4) J. E. Packer and R. V. Winchester, *Can. J. Chem.*, 48, 417 (1970).

(5) G. E. Adams, G. S. McNaughton, and B. D. Michael, "Chemistry of Ionization and Excitation," G. R. A. Johnson and G. Scholes, Ed., Taylor and Francis, London, 1967, p 281; *Trans. Faraday Soc.*, 64, 902 (1968).

(6) W. Karmann, A. Granzow, G. Meissner, and A. Henglein, *Int. J. Radiat. Phys. Chem.*, 1, 395 (1969).

(7) W. W. Wolf, J. C. Kertesz, and W. C. Landgraf, *J. Magn. Resonance*, 1, 618 (1969).

(8) W. A. Armstrong and W. G. Humphreys, *Can. J. Chem.*, 45, 2589 (1967).

(9) K. Eiben and R. W. Fessenden, *J. Phys. Chem.*, 72, 3387 (1968); 75, 1186 (1971).

(10) P. Neta and R. W. Fessenden, *ibid.*, 74, 2263, 3362 (1970); 75, 738 (1971).

(11) M. Anbar and P. Neta, *Int. J. Appl. Radiat. Isotop.*, 18, 493 (1967).

radicals of water radiolysis can be summarized

$$R_2CHSH + e_{aq}^- \longrightarrow R_2\dot{C}H + SH^- \qquad (1)$$

$$R_2CHSH + H \left[ \begin{array}{l} \longrightarrow R_2CH\dot{S} + H_2 \qquad (2) \\ \longrightarrow R_2\dot{C}SH + H_2 \qquad (3) \\ \longrightarrow R_2\dot{C}H + H_2S \qquad (4) \end{array} \right.$$

$$R_2CHSH + OH \left[ \begin{array}{l} \longrightarrow R_2CH\dot{S} + H_2O \qquad (5) \\ \longrightarrow R_2\dot{C}SH + H_2O \qquad (6) \end{array} \right.$$
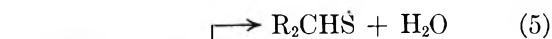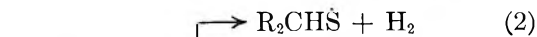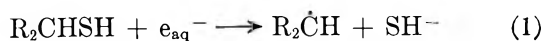
These reactions may be followed by

$$R_2\dot{C}H + R_2CHSH \longrightarrow R_2CH_2 + R_2CH\dot{S} \qquad (7)$$

$$R_2CH\dot{S} + R_2CHSH \rightleftarrows R_2CH\dot{S}SHCHR_2 \qquad (8)$$

$$2R_2CH\dot{S} \longrightarrow R_2CHSSCHR_2 \qquad (9)$$
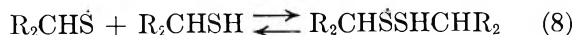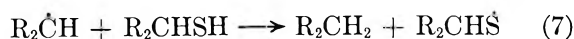
Rate constants for these reactions [excepting (6)] have been measured for cysteine and several other compounds.[5,6,11,12] The dissociated form of the thiol, $R_2$-$CHS^-$ (present at pH > 10), has been found to undergo reactions 1, 5, and 7 at rates lower than those for the acid form.[6,11,12] The dimeric complex in equilibrium 8 was observed by pulse radiolysis in both the acid $(R\dot{S}SHR)$[13] and the basic $(R\dot{S}SR)^-$ forms.[5,6] The radical recombination, eq 9 written specifically for $R_2CH\dot{S}$ can take place with all the types of radicals present.

Because the $g$ factors of sulfur-containing radicals potentially can vary more than those of their oxygen analogs this parameter can be of some use in identifying the radicals found. Values for two main types of radicals are known from studies on single crystals. Thiyl radicals typically have a large $g$-factor anisotropy (principal values such as 2.003, 2.025, and 2.053 found for $HOOCCH(NH_2)CH_2\dot{S}$ in L-cysteine dihydrochloride[14]) with an isotropic value of 2.027. The two mercaptoalkyl radicals which have been studied in crystals, $HO_2CCH_2S\dot{C}HCO_2H$[15] and $CH_3S\dot{C}HCH_2$-$CH(NH_3^+)CO_2^-$,[16] have moderate anisotropy (2.002 to 2.011 and 2.0017 to 2.0080, respectively) with an isotropic $g$ factor of about 2.0050. In the present work no radicals were encountered with $g$ factors above 2.01, and therefore it is likely that none of our spectra belong to thiyl radicals. It should be noted that the radicals reported by Wolf, et al.,[7] as thiyl radicals do not have $g$ factors as high as 2.027.

The simplest compound investigated was mercaptoacetic acid. Some of the spectra obtained with this compound are shown in Figure 1. Two radicals could be observed. The radical $\dot{C}H_2COO^-$ [2] formed by reaction with $e_{aq}^-$, eq 1, can be identified by its 21.2-G triplet with $g = 2.0032$ in agreement with previous measurements.[9,10] The 13.4-G doublet with $g = 2.0086$ can be assigned to the $^-S\dot{C}HCOO^-$ radical formed by reaction of OH, eq 6. Increasing the concentration of $^-SCH_2COO^-$ caused a decrease in the signal intensity of the spectrum of $\dot{C}H_2COO^-$ apparently as a result of
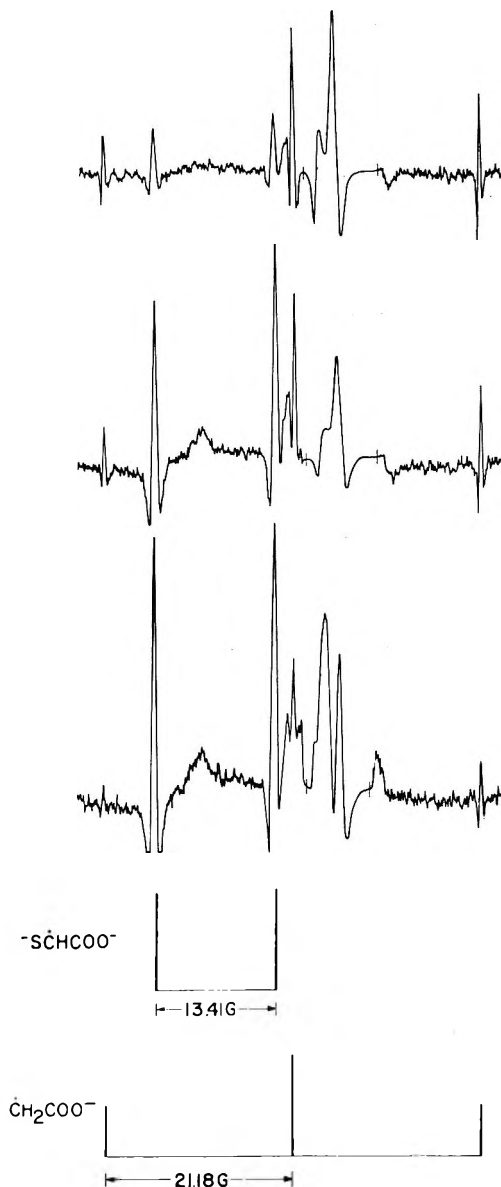
Figure 1. Second-derivative esr spectra from deoxygenated aqueous solutions of 0.01 $M$ mercaptoacetate at pH 12.4 during irradiation with 2.8-MeV electrons. Microwave power levels were 2.5 mW (top), 34 mW (center), and 100 mW (bottom). Magnetic field increases to the right. The stick spectra show the relationship of the lines. The large signal from the silica cell is seen just above the center of the spectrum and is recorded at a gain 100 times less than the other portions. Approximate positions of gain change indicated by vertical slash marks.

reaction 7. The addition of $N_2O$ to the solution caused the disappearance of the spectrum of $\dot{C}H_2COO^-$ and an increase in the intensity of the spectrum of $^-S\dot{C}H-$

(12) R. Braams, *Radiat. Res.*, **27**, 319 (1966).

(13) M. Simic and M. Z. Hoffman, *J. Amer. Chem. Soc.*, **92**, 6096 (1970).

(14) Y. Kurita and W. Gordy, *J. Chem. Phys.*, **34**, 282 (1961).

(15) Y. Kurita and W. Gordy, *ibid.*, **34**, 1285 (1961).

(16) D. G. Cadena, Jr., and J. R. Rowlands, *J. Chem. Soc. B*, 488 (1968).

COO$^-$. In the presence of another electron scavenger, acetone, the spectrum of $\dot{C}H_2COO^-$ was again absent. High concentrations of OH scavengers such as methanol or isopropyl alcohol had little effect on the spectrum of $\dot{C}H_2COO^-$. The fact that $\dot{C}H_2COO^-$ was not observed from solutions containing both $N_2O$ and $CH_3OH$ shows that $\dot{C}H_2O^-$ cannot react with $^-SCH_2$-COO$^-$ in the same way as $e_{aq}^-$.

It is seen in Figure 1 that the two radicals are affected differently by the change in microwave power. Whereas the signals of $\dot{C}H_2COO^-$ saturate similarly to those of other alkyl radicals (maximum peak height at ~5 mW), those of $^-S\dot{C}HCOO^-$ do not saturate up to the maximum power investigated (100 mW). (The line width for $^-S\dot{C}HCOO^-$ in Figure 1 is ~0.25 G and is noticeably larger than for $CH_2COO^-$. The implied decrease in relaxation time is probably a result of the $g$-factor anisotropy, see below.) This finding helps in distinguishing between the two types of radicals and prompted us to use high power levels for the study of sulfur-containing radicals. The studies of sulfur-centered radicals by Wolf, et al.,[7] utilized microwave power levels to 200 mW.

Spectra similar to those in Figure 1 were obtained from solutions of mercaptoacetate in the pH region 10–13.5. At pH 8.6 only $\dot{C}H_2COO^-$ was observed. In acid solutions (pH 4, 1, 0.3) no spectra could be observed. The absence of $\dot{C}H_2COOH$ in the acid region is probably a result both of a lower production rate and a more rapid recombination. The conversion of $e_{aq}^-$ to H replaces reaction 1 by reactions 2–4 of which reaction 2 is predominant (about 90% of the total). The absence of lines of $HS\dot{C}HCOOH$ or of $HS\dot{C}HCOO^-$ in both the acid and neutral regions can be a result of a low production rate in both pH regions although line broadening caused by proton exchange may also be a contributing factor to low line intensities. The production of $^-S\dot{C}HCOO^-$ in the basic region is probably also low but here the double negative charge will have a big effect on the recombination rate[17] and the steady-state concentration will be correspondingly higher. The moderate concentrations of $^-S\dot{C}HCOO^-$ observed are consistent with a relatively low production rate.

In all the experiments between pH 0.3 and 13.5 no spectrum could be observed from the $\dot{S}CH_2COOH$ or $\dot{S}CH_2COO^-$ radicals. These radicals are expected to undergo reaction 8 in the forward direction (with a rate constant higher than $10^9$ $M^{-1}$ sec$^{-1}$ for RS$^-$)[5] to form the complex ([RSSR$^-$]/[RS$^-$] [RS] ~ $10^4$ $M^{-1}$).[5] The $g$-factor anisotropy of such a radical might cause sufficient line broadening that the spectrum would be unobservable by esr spectroscopy at the concentrations existing. On the other hand, a spectrum attributed to the radical $\dot{S}CH_2COOH$ produced by mixing the thiol with Ce$^{4+}$ has been observed by esr spectroscopy in acid solution.[7] It is possible that the cerium prevents formation of the complex (RSSHR) by forming a stronger complex with $\dot{S}CH_2COOH$. We attempted to duplicate the experiment of Wolf, et al.,[7] using the same solution and spectrometer conditions, but utilizing radiation instead of Ce$^{4+}$ for the production of radicals. No spectrum could be observed even in the presence of Ce$^{3+}$. We conclude therefore that the steady-state concentration of radicals in our experiment is lower.

The results obtained with irradiated aqueous solutions of mercaptosuccinic acid are similar to those with mercaptoacetic acid. Two representative spectra are shown in Figure 2. Lines from more than three radicals are present. The reaction of $e_{aq}^-$ produces $^-OOC\dot{C}HCH_2COO^-$ according to reaction 1. This radical has previously been formed by H abstraction from succinate[18,19] and by H addition to fumarate[20] and the present hyperfine constants (see Table I) are in good agreement with the other values. The reaction of OH radicals with mercaptosuccinate produces the radical $^-OOC\dot{C}(S^-)CH_2COO^-$ according to reaction 6. This radical has a relatively high $g$ factor (2.0076) comparable to that of $^-S\dot{C}HCOO^-$ (2.0086). The third radical obtained from mercaptosuccinate (Figure 2) cannot be readily identified. The 20.15-G doublet with $g = 2.0048$ can possibly be assigned to the radical $^-OOC$-$\dot{C}HC(=S)COO^-$ formed by secondary reactions or by reaction with an impurity but no positive identification is suggested. Some additional lines which could not be analyzed are also present in the spectrum. In acid solutions, as in the case of mercaptoacetic acid, no spectrum could be observed.

A spectrum of only a single radical is observed from irradiated solutions of 3-mercaptopropionic acid (but only at high pH and high microwave power level). It has a 17.1-G doublet of 19.3-G triplets with $g = 2.0058$. This spectrum is assigned to the radical $^-S\dot{C}HCH_2$-COO$^-$ formed by hydrogen abstraction according to reaction 6. The $\alpha$-proton hyperfine constant (17.1 G) though higher than those of the radicals obtained from mercaptoacetate and mercaptosuccinate is nevertheless too low to be assigned to the radical $^-SCH_2\dot{C}HCOO^-$. It is expected that attack by OH radicals would be more favorable at the position adjacent to the sulfhydryl group than at that adjacent to the carboxyl group. The radical $\dot{C}H_2CH_2COO^-$ produced by reaction of $e_{aq}^-$ with 3-mercaptopropionate was not observed.

Cysteine behaved in a fashion similar to that of 3-mercaptopropionate in that a spectrum of a single radical was observed only from alkaline solution. This spectrum is a 10.0-G triplet, which is further split by

(17) The second-order decay rate constant of the radical HĊOH-COOH is two orders of magnitude higher than that of $^-O\dot{C}HCOO^-$ [M. Simic, P. Neta, and E. Hayon, J. Phys. Chem., 73, 4214 (1969)].

(18) H. Fischer, K.-H. Hellwege, and M. Lehnig, Ber. Bunsenges. Phys. Chem., 72, 1166 (1968).

(19) G. P. Laroff and R. W. Fessenden, submitted for publication in J. Chem. Phys.

(20) P. Neta, J. Phys. Chem., in press.
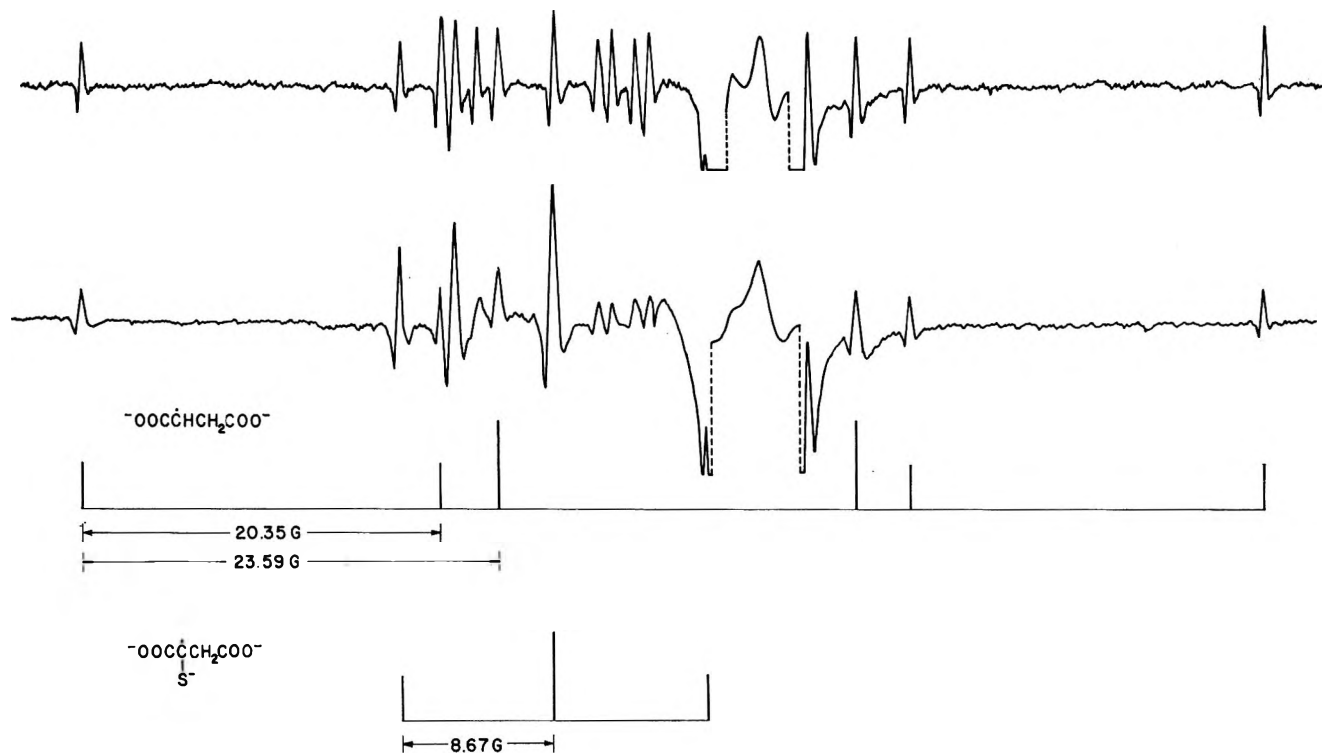
Figure 2. Esr spectra from deoxygenated aqueous solutions of 0.03 $M$ mercaptosuccinate at pH 13.1 during irradiation. Microwave power levels were 2.5 mW (top) and 34 mW (bottom). Two assigned sets of lines are indicated by the stick figures. The doublet mentioned in the text is composed of the fourth strong line from the low-field end and the line just above the signal from the cell. Other unassigned lines are present.
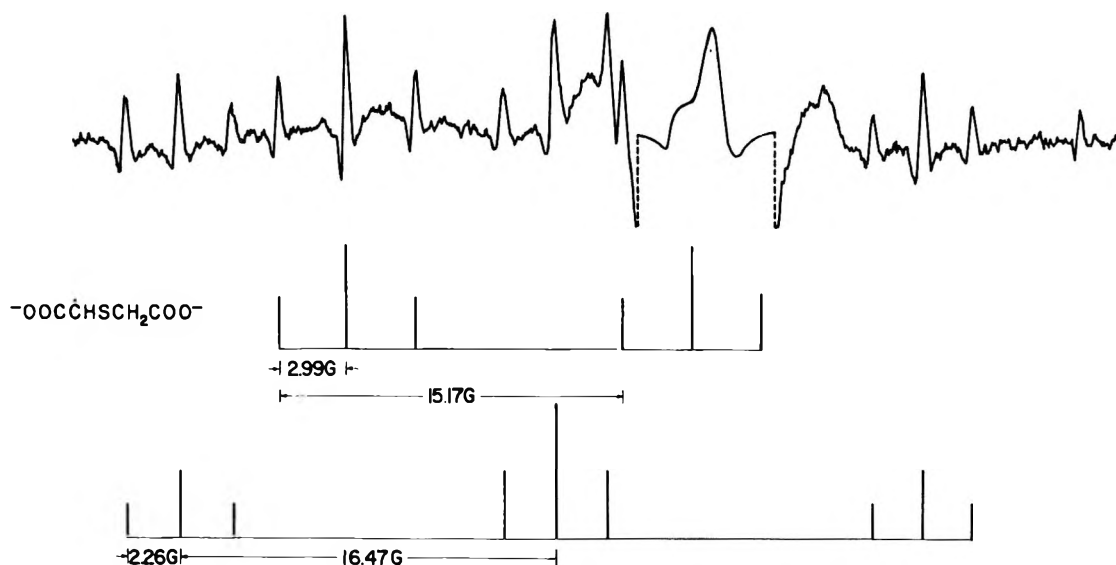


Figure 3. Esr spectrum from an $N_2O$ saturated aqueous solution of 0.003 $M$ thiodiglycolate at pH 8.5 (buffered with sodium tetraborate) during irradiation. Microwave power was 19 mW. The observed lines were considerably weaker at a power of 2.5 mW.

one nitrogen (5.4 G) and two unequivalent protons (0.5 and 1.2 G), and has $g = 2.0037$; it could be assigned to the radical $^-SCH_2\dot{C}(NH_2)COO^-$. Although both the $CH_2$ and CH positions are activated (by sulfhydryl and amino groups, respectively), the main OH attack evidently occurs at the more highly substituted or tertiary CH position. The two hydrogens of the

amino groups are not equivalent as was found in radicals obtained from other amino acids.[10c,21]

The spectrum obtained from irradiated solutions of thiodiglycolic acid is shown in Figure 3. Three different radicals are observed. The main species

(21) H. Paul and H. Fischer, Ber. Bunsenges. Phys. Chem., **73**, 972 (1969).

**Table I:** Structure and Hyperfine Constants of Radicals Produced in Irradiated Aqueous Solutions of Thiols

| Solute irradiated | Radical observed | $g$ factor[a] | Hyperfine constants[b] |
|---|---|---|---|
| $^-SCH_2COO^-$ | $\dot{C}H_2COO^-$ | 2.00322 | $a_{CH_2}{}^H = 21.18$ |
| | $^-S\dot{C}HCOO^-$ | 2.00861 | $a_{CH}{}^H = 13.41$ |
| $^-OOCCHCH_2COO^-$ <br> \| <br> $S^-$ | $^-OOC\dot{C}HCH_2COO^-$ | 2.00328 | $\begin{cases} a_{CH}{}^H = 20.35^c \\ a_{CH_2}{}^H = 23.59^c \end{cases}$ |
| | $^-OOC\dot{C}CH_2COO^-$ <br> \| <br> $S^-$ | 2.00755 | $a_{CH_2}{}^H = 8.67$ |
| $^-SCH_2CH_2COO^-$ | $^-S\dot{C}HCH_2COO^-$ | 2.00575 | $\begin{cases} a_{CH}{}^H = 17.08 \\ a_{CH_2}{}^H = 19.26 \end{cases}$ |
| $^-SCH_2CHCOO^-$ <br> \| <br> $NH_2$ | $^-SCH_2\dot{C}COO^-$ <br> \| <br> $NH_3$ | 2.00369 | $\begin{cases} a_{CH_2}{}^H = 10.01 \\ a_N = 5.43 \\ a_{NH_2}{}^{H^1} = 0.51 \\ a_{NH_2}{}^{H^2} = 1.24 \end{cases}$ |
| $^-OOCCH_2SCH_2COO^-$ | $\dot{C}H_2COO^-$ | 2.00320 | $a_{CH_2}{}^H = 21.17$ |
| | $^-OOC\dot{C}HSCH_2COO^-$ | 2.00562 | $\begin{cases} a_{CH}{}^H = 15.17 \\ a_{CH_2}{}^H = 2.99 \end{cases}$ |
| | (?) $\dot{C}H_2SCH_2COO^-$ | 2.00468 | $\begin{cases} a_{CH_2}{}^H = 16.47 \\ a_{CH_2}{}^H = 2.26 \end{cases}$ |
| $^-OOCCH_2SSCH_2COO^-$ | $^-OOC\dot{C}HSSCH_2COO^-$ | ~2.0046 | $a_{CH}{}^H \approx 11$ |
| $^-OOCCH_2SSCH_2COO^- + OH^-$ <br> (or $^-OOCCH_2S^- + H_2O_2 +$ <br> $OH^-$) | $^-OOCCH_2\dot{S}O_2$ | 2.00840 | $a_{CH_2}{}^H = 1.82$ |

[a] The $g$ factors are measured relative to the peak from the silica cell and are accurate to ±0.00005. Second-order corrections have been made [R. W. Fessenden, *J. Chem. Phys.*, **37**, 747 (1962)]. [b] Hyperfine constants are given in gauss and are accurate to ±0.03 G. [c] Hyperfine constants reported to be somewhat dependent on ionic strength; values in the presence of 1 $M$ Na$_2$SO$_4$: $a_{CH}{}^H = 20.41$, $a_{CH_2}{}^H = 22.75$ G (ref 18).



1.82G
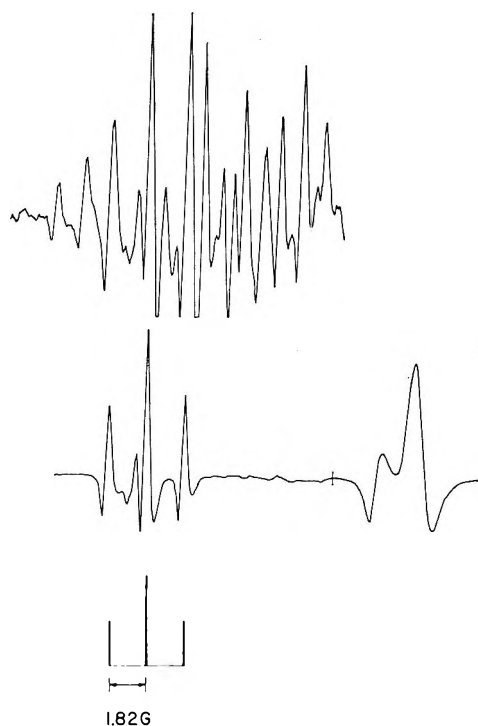
Figure 4. Esr spectra from N$_2$O-saturated solutions of 0.01 $M$ dithiodiglycolate at pH 12.8 during irradiation. Microwave power was 2.5 mW. Top spectrum—fresh solution, bottom spectrum—solution bubbled with oxygen for 65 hr and then oxygen removed by N$_2$O. Gain reduction by a factor of 10 at position of slash mark on lower trace.

formed by reaction of OH is $^-OOC\dot{C}HSCH_2COO^-$. It has a 15.17-G doublet of 2.99-G triplets with $g = 2.0056$. Two of the six lines are masked by the signal from the silica cell. The observed lines increased in the presence of N$_2$O and were also observed at pH 9.5 and 13.2. The second radical observed is $\dot{C}H_2COO^-$ formed by a reaction of $e_{aq}^-$ similar to reaction 1.

$$^-OOCCH_2SCH_2COO^- + e_{aq}^- \longrightarrow$$
$$^-OOCCH_2S^- + \dot{C}H_2COO^- \quad (10)$$
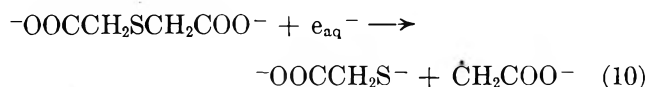
Although two lines of this triplet appear in the same position as lines of other radicals, they could be detected by the appropriate change in intensity when N$_2$O was present; the calculated hyperfine constant and $g$ factor agree very well with previous values. A third radical appears to be present in the spectrum in Figure 3. This radical has a 16.47-G triplet of 2.26-G triplets with $g = 2.0047$. A reasonable assignment is $\dot{C}H_2$-$SCH_2COO^-$, but the mechanism of formation is not clear.

Representative spectra obtained from irradiated solutions of dithiodiglycolic acid are shown in Figure 4. The results in this case are complicated by the fact that this compound undergoes hydrolysis and disproportionation in alkaline solutions.[22] The main reactions are (11) and (12).

$$^-OOCCH_2SSCH_2COO^- + OH^- \longrightarrow$$

$$^-OOCCH_2SOH + ^-SCH_2COO^- \quad (11)$$

$$2^-OOCCH_2SOH \longrightarrow$$

$$^-OOCCH_2SH + ^-OOCCH_2SO_2H \quad (12)$$
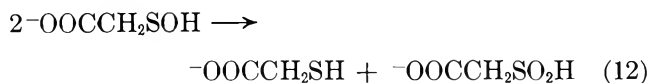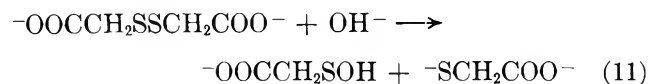
In mildly alkaline solutions (pH 9–11) the reaction of OH radicals with the solute is expected to form $^-OOC\dot{C}HSSCH_2COO^-$. This radical appears to show a doublet of about 11-G splitting with $g \approx 2.0046$ and no splitting ($<0.2$ G) by the $CH_2$ protons. Unfortunately, one line is masked by the signal from the cell and therefore these numbers must be regarded as approximate and the assignment as tentative. Additional weak lines were observed but could not be analyzed. At pH $> 12$ these weak lines increased in intensity as shown in the top spectrum of Figure 4 and a strong triplet appeared. All of these signals increased with time indicating that the slow reactions 11 and 12 were taking place. The spectrum obtained after a long hydrolysis time is shown at the bottom of Figure 4. The triplet observed has $a = 1.82$ G and $g = 2.0084$. Since the signal intensity was very high, it was possible to show that no other lines of this spectrum occur in the region of the signal from the cell. The additional lines in the top spectrum could not be interpreted and are probably formed from intermediates in the oxidation processes.

On the basis of reactions 11 and 12 the triplet observed in Figure 4 (bottom) can reasonably be assigned to the radical $^-OOCCH_2\dot{S}O_2$ formed by the reaction

$$^-OOCCH_2SO_2^- + OH \longrightarrow$$

$$^-OOCCH_2\dot{S}O_2 + OH^- \quad (13)$$
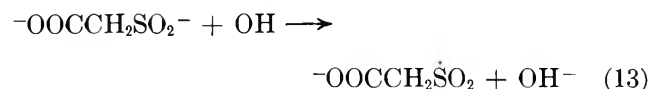
which is similar to the oxidation reaction of sulfite by OH. It should be noted that this radical has a structure which is isoelectronic with $^-OOCCH_2\dot{N}O_2^-$ ($a^H = 8.5$ G[19]). Aromatic radicals of this type have been observed in solution[23] and the ring proton splittings are rather small. The $g$ factor reported for $C_6H_5\dot{S}O_2$ is 2.0044. On this basis the parameters assigned here to $^-OOCCH_2\dot{S}O_2$ do not seem unreasonable. This radical is clearly different from the radical suggested by Wolf, et al.,[7] to be formed by the reaction of $^-OOCCH_2\dot{S}$ with $O_2$. This latter radical shows $g = 2.018$ (and no proton splittings), consistent with values for other peroxy radicals, and must have the structure $^-OOCCH_2-S-O-\dot{O}$.

The spectrum of $\dot{C}H_2COO^-$ was not observed from solutions of dithiodiglycolate. The reaction of $e_{aq}^-$ probably produces $^-OOCCH_2\dot{S}$ and $^-SCH_2COO^-$. However, if the compound was allowed time to hydrolyze according to reaction 11 and then irradiated, weak lines of $\dot{C}H_2COO^-$ were observed in addition to the bottom spectrum in Figure 4. Similar results to those obtained from very alkaline solutions of $(SCH_2-$

$COO^-)_2$ were also obtained from irradiated solutions of $^-SCH_2COO^- + H_2O_2$ at pH 13. The first reaction is of course the thermal oxidation of $^-SCH_2COO^-$ to $(SCH_2COO^-)_2$ by hydrogen peroxide which is then followed by hydrolysis and disproportionation.

No spectra could be observed with cystine, methyl mercaptan, dimethyl sulfide, dimethyl disulfide, and thiophenol. The reasons could be the lack of additional charged groups to lengthen the lifetime or the splitting into too many lines which decreases the intensity. Weak lines were observed from solutions of thioacetamide and thiourea, which appear to be due to $CH_3\dot{C}(S^-)NH_2$ and $NH_2\dot{C}(S^-)NH_2$, but no clear analysis could be made.

The structures of the radicals proposed to explain the various spectra and the corresponding spectral parameters are summarized in Table I. As mentioned above, two single crystal studies of mercaptoalkyl radicals have been reported. In both cases the isotropic value of $a_\alpha^H$ is about 15 G indicating considerable delocalization onto the sulfur. The isotropic $g$ factors in these two cases are about 2.0050. The parameters found here for $^-OOCC\dot{C}HSCH_2COO^-$ in aqueous solution are very similar. Adams[24] has also reported radicals of this type [$CH_3\dot{C}HSCH_2CH_3$ and $CH_3(CH_2)_2-\dot{C}HSCH_2(CH_2)_2CH_3$] in hydrocarbon solution as well as two of the type $R\dot{C}HSSR'$. The values of $a_\alpha^H$ are similar (17 G) but no $g$ factors were reported. He also observed splittings from $CH_2$ protons located across a single sulfur (but not from those across a disulfide group). Radicals of the type $R_2\dot{C}S^-$ have not been previously reported and their hyperfine constants are best discussed by reference to the oxygen analogs. The two direct comparisons which can be made are $^-S\dot{C}H-COO^-$ ($a^H = 13.4$ G) with $^-O\dot{C}HCOO^-$ ($a^H = 14.2$ G)[9] and $^-OOC\dot{C}(S^-)CH_2COO^-$ ($a^H = 8.7$ G) with $^-OOC\dot{C}(O^-)CH_2COO^-$ ($a^H = 8.4$ G).[19] In each case the hyperfine constants are remarkably similar. This result is a bit surprising in view of the results reported by Adams[24] on two thioether radicals. He found that for both radicals the value of $a_\alpha^H$ is 3 G higher than for the corresponding ether radical. The lack of any such difference for the radicals reported here suggests that $a_\alpha$ for the ether radical is unusually low. This effect may be related to a nonplanarity at the radical site.[25] With radicals like $^-O\dot{C}HCOO^-$ and $^-S\dot{C}HCOO^-$ an increased degree of conjugation may keep the radicals planar.

The $g$ factors for the mercaptoalkyl radicals reported here vary in a way which is very similar to that found

(22) "Organic Sulfur Compounds," N. Kharasch, Ed., Pergamon Press, Elmsford, N. Y., 1961.

(23) M. McMillan and W. A. Waters, J. Chem. Soc. B, 422 (1966).

(24) J. Q. Adams, J. Amer. Chem. Soc., 92, 4535 (1970).

(25) A. J. Dobbs, B. C. Gilbert, and R. O. C. Norman, Chem. Commun., 1353 (1969).

for the oxygen analogs but the deviations from the free-electron value are larger as a result of the larger spin-orbit coupling for sulfur. Sulfur in a $\beta$ position [$^-$SCH$_2$Ċ(NH$_2$)COO$^-$] shifts the $g$ factor very little. The two radicals of the type RĊHSR' have $g$ factors of about 2.0050 in agreement with the values found for such radicals in the solid (see above). The three radicals of the type R$_2$ĊS$^-$ do not show the same $g$ factor but show a markedly higher value if the carboxyl group is in the $\alpha$ position [$^-$SĊHCOO$^-$ and $^-$OOCĊ(S$^-$) CH$_2$COO$^-$ as compared with $^-$SĊHCH$_2$COO$^-$]. The increase with an $\alpha$-carboxyl group ($\sim$0.0025) is similar to but larger than the increase from, e.g., ĊH$_2$O$^-$ ($g = 2.0037$)[9] to $^-$OĊHCOO$^-$ ($g = 2.0044$).[9] Apparently there is some interaction of the S$^-$ and CO$_2$$^-$ groups.

The ratio of observed line widths (3.5[7] to 0.25) for thiyl and mercaptoalkyl radicals seems in accord with the known $g$-factor anisotropies and the idea that the width is a result of incomplete averaging of this anisotropy. The thiyl radicals have about a five times greater anisotropy and with similar tumbling rates the line width ratio should be the square of this or 25. The observed ratio (14) is in reasonable agreement with this rather crude calculation.

In conclusion, it was observed that thiols react with hydrated electrons to lose SH$^-$ and form alkyl radicals according to reaction 1. The reaction with hydroxyl radicals involves hydrogen abstraction from CH groups (reaction 6) in addition to abstraction from the SH group (reaction 5). Radicals of the types R$_2$ĊS$^-$, R$_2$ĊCH$_2$S$^-$, R$_2$ĊSR', R$_2$ĊSSR', and RṠO$_2$ were identified in this study and their hyperfine constants and $g$ factors were determined and discussed.

# The Infrared Spectrum of Matrix-Isolated Uranium Monoxide[1]

## by S. Abramowitz,* N. Acquista,

*National Bureau of Standards, Washington, D. C. 20234*

## and K. R. Thompson

*Department of Chemistry, University of Florida, Gainesville, Florida 32601* (*Received February 18, 1971*)

*Publication costs assisted by the National Bureau of Standards*

The infrared spectra of matrix-isolated uranium oxides have been observed. By varying the O/U ratio of the condensed phase from 1.5 to 3.0 and comparing the observed spectra of the matrix-isolated vapors in equilibrium with the condensed phases it has been possible to assign a frequency of 776.0 cm$^{-1}$ to U$^{16}$O. Verification of this assignment has been obtained in similar experiments using oxygen-18 enriched uranium oxides; a frequency of 736.2 cm$^{-1}$ has been observed for U$^{18}$O. This yields a force constant to the harmonic approximation of 5.32 mdyn/Å for this species. A stretching mode of UO$_2$ has also been assigned for U$^{16}$O$_2$, U$^{18}$O$_2$, and U$^{16}$O$^{18}$O.

## Introduction

Mass spectrometric studies of the vapors in equilibrium with the uranium–oxygen system coupled with Knudsen effusion techniques have yielded the vapor pressures of U, UO, UO$_2$, and UO$_3$.[2-6] It has also been shown in these studies that the ratios of the vapor pressures of these species at a given temperature can vary by several orders of magnitude as the O/U ratio changes between $1.5 < $ O/U $ < 3$. In particular these studies have shown that the vapor in equilibrium with substoichiometric UO$_2$ contains UO, UO$_2$, and some U. The ratio of the UO/UO$_2$ reaches about 15 at about 200°K in the three phase system of UO$_2$(s), U(l), and vapor. We have used these extensive data to pattern our matrix isolation studies of the uranium–oxygen system.

## Experimental Section

The electron beam furnace, cryogenic system consisting of an Air Products cryotip and Perkin-Elmer 99G monochromator and Perkin-Elmer 301 spectro-

(1) This research was supported in part by the Defense Atomic Support Agency, Washington, D. C., and in part by the National Science Foundation under Grant No. GP-9316.

(2) R. J. Ackermann, P. W. Gilles, and R. J. Thorn, *J. Chem. Phys.*, **25**, 1089 (1956).

(3) R. J. Ackermann and R. J. Thorn, *Int. At. Energy Ag., Tech. Rep. Ser.*, **39** (1965).

(4) A. Pattoret, J. Drowart, and S. Smoes, *Thermodyn. Nucl. Mater., Proc. Symp., 1967* (1968).

(5) R. J. Ackermann, E. G. Rauh, and N. S. Chandrasekharaiah, *J. Phys. Chem.*, **73**, 762 (1969).

(6) R. K. Edwards, M. S. Chandrasekharaiah, and P. M. Danielson, *High Temp. Sci.*, **1**, 98 (1969).

photometer have been previously described.[7,8] Tungsten Knudsen cells with 1-mm orifices were used. The temperature was measured with a W–3% Re vs. W–25% Re thermocouple inserted in a 0.030-in. hole drilled into and halfway up the length of the wall of the Knudsen cells. The total vapor pressure above the condensed uranium–oxygen systems studied was adjusted (by varying the temperature) to about $10^{-3}$ Torr using the data presented by Ackerman, Rauh, and Chandrasekharaiah[5] for the $UO_2(s) + U(l)$ condensed phase and by Ackermann and Thorn[3] for the urania condensed phase experiments. $U^{18}O_2$ (or some higher oxide of uranium such as $U_3O_8$ which by prolonged heating, is decomposed to $UO_2$) was synthesized by reacting outgassed uranium powder with $H_2$ to form $UH_3$ which is then thermally decomposed ($T \simeq 350°$) to form a chemically reactive uranium. The metal thus formed is then reacted with the isotopically enriched oxygen to form the uranium oxide. Some $U^{16}O_2$ is also found to be present in the synthesized product either because of the partial oxidation of the uranium metal used or the degree of enrichment of the $^{18}O_2$ (about 92% enrichment). The uranium metal, $UO_2$, $UO_3$, and $U_3O_8$ used in these experiments were obtained from commercial sources and were used without further purification or analysis. Therefore the $UO_2$ used could have been either sub- or superstoichiometric. From the observed spectra it appears that the $UO_2$ was substoichiometric. Argon was used as the matrix gas and concentrations of uranium oxide to matrix gas varied from about $^1/_{5000}$ to $^1/_{1000}$ as calculated from the effusion equation and the geometry of the apparatus used.

## Results and Discussion

The only region between 4000 and 100 cm$^{-1}$ which has significant absorption is shown in Figure 1. Curve a shows the spectrum of the vapors in equilibrium with the condensed phase $U^{18}O_2(s) + U(l)$ in an argon matrix at liquid hydrogen temperatures. The peak at 736.2 cm$^{-1}$ is $U^{18}O$ while that at 826.6 cm$^{-1}$ is $U^{18}O_2$. (These were run on a PE-99G monochromator. The 720-cm$^{-1}$ absorption band is due to atmospheric $CO_2$.) Curve b is a spectrum of the matrix-isolated vapors in equilibrium with the $U^{16}O_2(s) + U(l)$ condensed phase. The band at 776.0 is assigned to $U^{16}O$ while the band at 874.3 is assigned to $U^{16}O_2$. Confirmation of these results was also obtained by running infrared spectra of the matrix-isolated vapor in equilibrium with $U^{16}O_2$ and $U_3{}^{16}O_8$, and various oxygen-18-enriched uranium oxides. In these spectra the $UO_2$ band is much more prominent relative to the UO band, as one would expect from the mass spectrometric results.[2,6] There are several other bands in the $U^{16}O_2(s)$, U(l) spectra (a) and the $U^{18}O_2(s)$, U(l) spectra (b). A definitive assignment of these features is not yet available. Prolonged experimentation with the same starting sample of urania leads to an enhancement of the 870.4-cm$^{-1}$ fea-
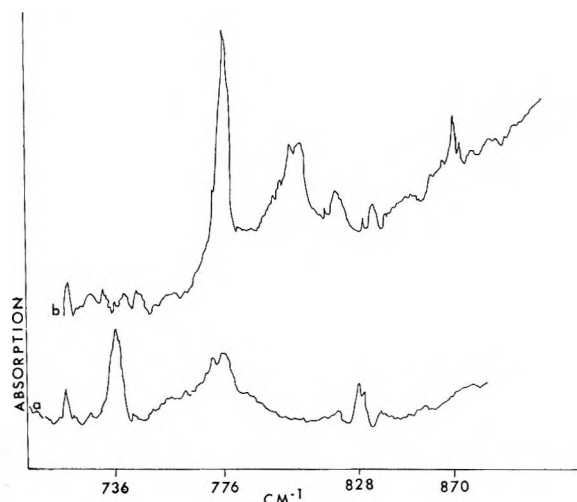


Figure 1. The infrared spectra of matrix-isolated uranium oxides: (a) $U^{18}O_2 + U^{18}O$ in an argon matrix; (b) $U^{16}O_2 + U^{16}O$ in an argon matrix.

ture relative to that at 776.0 cm$^{-1}$. This behavior is expected since with prolonged heating the condensed phase tends toward stoichiometric $UO_2$ at the temperature used in these experiments. The vapor above stoichiometric urania is known to be predominantly $UO_2$. These prolonged experiments also indicate that the features at about 800 cm$^{-1}$ in normal urania experiments and at about 776 cm$^{-1}$ in the oxygen-18-enriched urania runs are not due to $UO_2$ since these features diminish in intensity relative to the assigned $UO_2$ features at 874.3 and 826.6 cm$^{-1}$ for $U^{16}O_2$ and $U^{18}O_2$, respectively. Experiments with a synthesized $U^{16}O^{18}O$ sample do not show any significant features between 800 and 776 cm$^{-1}$ which is also consistent with the above interpretation. (The spectra of $U^{16}O^{18}O$ do have a feature about midway between $U^{16}O_2$ and $U^{18}O_2$ with a suitable relative intensity. They also do not show any features between 776.0 and 736.2 cm$^{-1}$ as would be expected.) A slower scan of the $U^{16}O$ and $U^{18}O$ is shown in Figure 2. Some residual $U^{16}O$ may be responsible for the absorption around 776.0 in the $U^{18}O$ spectrum. The ratio of the observed fundamental frequencies for $U^{18}O$ and $U^{16}O$ is 0.9487 in excellent agreement with the ratio of 0.9465 expected to the harmonic oscillator approximation for $[\nu^{238}U^{18}O/\nu^{238}U^{16}O]$. The observed frequency of 776.0 cm$^{-1}$ for $U^{16}O$ in an argon matrix corresponds to a harmonic force constant of 5.32 mdyn/Å for this diatomic molecule. A frequency of 776.0 cm$^{-1}$ for $U^{16}O$ in an argon matrix is lower than has been estimated for this species in the gas phase. Various workers have used esti-

(7) Certain commercial instruments are identified in this paper to specify completely the experimental procedure. In no case does such identification imply a recommendation or endorsement by the National Bureau of Standards.

(8) S. Abramowitz, N. Acquista, and I. W. Levin, J. Res. Nat. Bur. Stand., Sect. A, 74, 487 (1968).
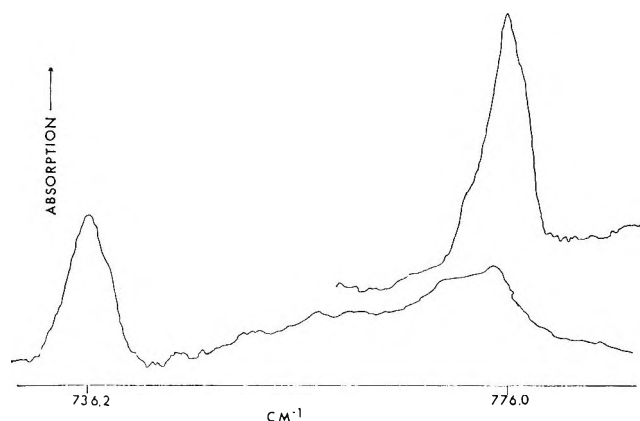
Figure 2. An expanded trace of the matrix-isolated spectra of $U^{16}O$ and $U^{18}O$.



Figure 3. The matrix-isolated spectra of $U^{16}O_2$, $U^{16}O^{18}O$, and $U^{18}O_2$. The prepared sample had an original ratio of $^{16}O_2/^{16}O^{18}O/^{18}O_2$ of about 1:4:4.

mated frequencies varying from 920[9] to 860 cm$^{-1}$ [5] for this species.

A summary of the results of this study for both UO and $UO_2$ in argon and neon matrices is given in Table I.

**Table I:** Assigned Matrix-Isolated Absorption Frequencies, cm$^{-1}$, for Uranium–Oxygen Species[a]

| Matrix | Frequency, cm$^{-1}$ | Assignment |
|--------|--------|------------|
| Neon | 881.5 | $U^{16}O_2$ |
|  | 786.3 | $U^{16}O$ |
| Argon | 874.3 | $U^{16}O_2$ |
|  | 776.0 | $U^{16}O$ |
|  | 826.6 | $U^{18}O_2$ |
|  | 736.2 | $U^{18}O$ |
|  | 854.6 | $U^{16}O^{18}O$ |

[a] Frequencies are correct to ±0.5 cm$^{-1}$.

The matrix-isolated infrared spectrum of $U^{18}O_2$, $U^{16}O^{18}O$, and $U^{18}O_2$ is shown in Figure 3 in the region of the observed stretching fundamental. The $U^{16}O$-$^{18}O$ band is at 854.6 cm$^{-1}$ and is closer to the corresponding feature observed for $U^{16}O_2$ than that of $U^{18}O_2$. This indicates that the unobserved fundamental stretching mode of $U^{16}O^{18}O$ is to lower frequency than the observed mode at 854.6 cm$^{-1}$. In a similar way one can conclude that the unobserved stretching modes of $U^{16}O_2$ and $U^{18}O_2$ both lie to lower frequencies than the observed bend. It would be interesting to speculate

on the assignment of the measured modes of $UO_2$. If they are assigned to $\nu_3$ the asymmetric stretching mode, then one can in principle calculate the bond angle from the observed shifts of $U^{16}O_2$ and $U^{18}O_2$ assuming negligible anharmonic contributions. The ratios of the $G$ matrix elements $G_{33} = \mu_O + \mu_U(1 - \cos \alpha)$ where $\mu_O$ and $\mu_U$ are the reduced mass of the oxygen and uranium atoms, respectively, and $\alpha$ is the band angle quantitatively describes the shift. For the case of $UO_2$ one has a poor "lever" on the system since $m_U/m_O = {}^{238}/_{16}$ or $\mu_U \sim \mu_O/15$. Hence one calculates a shift which varies by 2.9 cm$^{-1}$ for angles varying from 90 to 180°. In fact from 130 to 180° the calculated isotope shift varies by only 0.97 cm$^{-1}$. In those cases where the mass of the central atom is smaller as for $SO_2$ the isotope shift can indeed be used to estimate the bond angle.[10] (One calculates a shift of 13 cm$^{-1}$ for $SO_2$ angles varying from 90 to 180°.) In addition to these difficulties a definitive assignment of the one stretching mode observed for $U^{16}O_2$ and $U^{18}O_2$ at 874.3 and 826.6 cm$^{-1}$, respectively, to either the symmetric or asymmetric stretch of a bend $UO_2$ is not clear as yet. Observation of $\nu_2$ the bending mode of $UO_2$ may help in this regard. Experiments are in progress in an attempt to observe this fundamental at least for $U^{16}O_2$ and $U^{18}O_2$.[11]

(9) E. DeMaria, R. P. Burns, J. Drowart, and M. E. Inghram, J. Chem. Phys., 32, 1373 (1960).

(10) M. Allavena, R. Rysnik, D. White, V. Calder, and D. E. Mann, ibid., 50, 3399 (1969).

(11) NOTE ADDED IN PROOF. We have recently observed the far-infrared spectra of matrix isolated $U^{16}O_2$ and $U^{18}O_2$. An absorption band at 81 cm$^{-1}$ is assigned to $\nu_2$ of $U^{16}O_2$. A corresponding band assignable to $\nu_2$ of $U^{18}O_2$ is found at 73 cm$^{-1}$. This band center is somewhat uncertain due to the absorption of the thin polyethylene windows used for the outer windows of our cryostat. A more complete report of these observations will follow.

# Energy Parameters in Polypeptides. IV. Semiempirical Molecular

# Orbital Calculations of Conformational Dependence of Energy

# and Partial Charge in Di- and Tripeptides[1]

### by F. A. Momany,[2] R. F. McGuire,[3] J. F. Yan, and H. A. Scheraga*[4]

*Department of Chemistry, Cornell University, Ithaca, New York 14850* (*Received February 3, 1971*)

*Publication costs borne completely by The Journal of Physical Chemistry*

The results of semiempirical molecular orbital calculations on the conformational properties of oligopeptides of glycine and alanine are presented. The applicability of the Extended Hückel and Complete Neglect of Differential Overlap methods to these molecular systems is discussed (for example, the EHT method yields reliable torsional potentials, while the CNDO/2 procedure gives reasonable partial charges). cis and trans peptide conformations, as well as mixed D and L configurations, are investigated. Conformational $\phi-\psi$ energy maps are examined for each molecule, and comparisons are made with experimental data. The electronic distributions found by the CNDO/2 method in the regions of conformational space in which intramolecular hydrogen bonding may take place are analyzed.

## Introduction

This is a continuation of two previous papers[5,6] of this series (referred to as papers II and III), and a related one,[7] in which semiempirical molecular orbital methods [the Complete Neglect of Differential Overlap theory (CNDO/2) of Pople and Segal[8] and the Extended Hückel Theory (EHT) of Hoffmann[9]] are used to investigate the nature of the interactions which determine the molecular conformations of polypeptides and proteins; they are also used to improve and strengthen the physical basis of empirical methods[10] which are being applied to conformational energy calculations on biological macromolecules. The validity of the applicability of these molecular orbital methods to a *group* of related compounds was discussed in papers II[5] and III.[6]

In this paper, we explore the dependence of the energy and partial charge of several oligopeptides of glycine and alanine on their conformation, in order to identify the influence of such factors as orbital interactions, hydrogen bonding, etc., on the conformational states of these model systems. The molecular orbital methods used here[8,9] are clearly approximations to exact calculations of the electronic properties of molecules. Because of these approximations, it is unlikely that these methods will be able to account for the dependence of *all* molecular properties on changes in conformation; in fact, different molecular orbital methods give different conformational results when compared for the same molecules. Despite these difficulties, it was shown earlier[5-7] that both the EHT and CNDO/2 methods, applied to simple molecules and to intermolecular complexes, have their individual ranges of validity, as far as providing information

on the conformational dependence of various molecular properties is concerned.

The molecules treated in this paper are *N*-acetyl-*N'*-methylglycine amide (I) and *N*-acetyl-*N'*-methyl-L-alanine amide (II), shown in Figure 1; *N*-methyl-*C'*-methylglycylglycine (III) and *N*-methyl-*C'*-methyl-L-alanyl-L-alanine (IV), shown in Figure 2; the cis forms of molecule I (V) and molecule II (VI), respectively, shown in Figure 3; and *N*-methyl-*C'*-methyl-L-alanyl-D-alanine (VII), shown in Figure 4.

Because of the computer expense and machine core size necessary for molecular orbital calculations, there is a limitation on the size of the molecule which can

Figure 1. Computed CNDO/2 (ON) partial charges ($\sigma + \pi$) for the extended form with trans peptide units ($\phi = \psi = 180°$, $\omega_{1,2} = 180°$) of the molecules: (A) $N$-acetyl-$N'$-methylglycine amide (molecule I), and (B) $N$-acetyl-$N'$-methyl-L-alanine amide (molecule II). The values shown should be divided by 1000 to obtain electronic charge units. For convenience in identifying specific atoms, an atom numbering sequence is shown in B.



Figure 2. Computed CNDO/2 (ON) partial charges ($\sigma + \pi$) for the extended form with trans peptide units ($\phi_{1,2} = \psi_{1,2} = 180°$, $\omega = 180°$) of the molecules: (A) $N$-methyl-$C'$-methylglycylglycine (molecule III), and (B) $N$-methyl-$C'$-methyl-L-alanyl-L-alanine (molecule IV). The values shown should be divided by 1000 to obtain electronic charge units.

be studied in great detail by these methods. This is one of the reasons why we have applied molecular orbital procedures only to small-to-medium size molecules in order to improve the basis for the more rapid empirical procedures required to treat large polypeptides and proteins. In particular, it is hoped that more reliable concepts and insight into the equations and parameters used in empirical studies (which, in turn, will subsequently be refined by empirical calculations on crystals[10-13]) will emerge from results such as those reported here, in particular on the effect of changes in conformation on the distributions of partial charge and on the total energy.

While conformation (i.e., dihedral angles for internal rotation about single bonds) will be varied, the geometry (bond angles and bond lengths) will not be. However, the geometry of each amino acid residue, based on an exhaustive search of the recent structural lit-

erature, represents not only averages over many structures, but also departures from average values where these were judged to be significant;[14] the geometry used in these calculations is given in Table I.

The nomenclature and conventions used here are those recently adopted by a IUPAC–IUB commission;[15] the main difference between this nomenclature and that previously[16] used is that the cis conformation

(11) F. A. Momany, G. Vanderkooi, and H. A. Scheraga, Proc. Natl. Acad. Sci., U. S., 61, 429 (1968).

(12) H. A. Scheraga, Nobel Symposium 11 on "Symmetry and Function of Biological Systems at the Macromolecular Level," A. Engstrom and B. Strandberg, Ed., Stockholm, Aug 26–29, 1968, Almqvist and Wiksell, Stockholm, 1969, p 43.

(13) R. F. McGuire, G. Vanderkooi, F. A. Momany, R. T. Ingwall, G. M. Crippen, N. Lotan, R. W. Tuttle, K. L. Kashuba, and H. A. Scheraga, Macromolecules, 4, 112 (1971).

(14) R. F. McGuire, F. A. Momany, and H. A. Scheraga, unpublished work.

(15) IUPAC-IUB Commission on Biochemical Nomenclature, Biochemistry, 9, 3471 (1970).

(16) J. T. Edsall, P. J. Flory, J. C. Kendrew, A. M. Liquori, G. Nemethy, G. N. Ramachandran, and H. A. Scheraga, Biopolymers, 4, 121 (1966); J. Biol. Chem., 241, 1004 (1966); J. Mol. Biol., 15, 399 (1966).

A.

B.
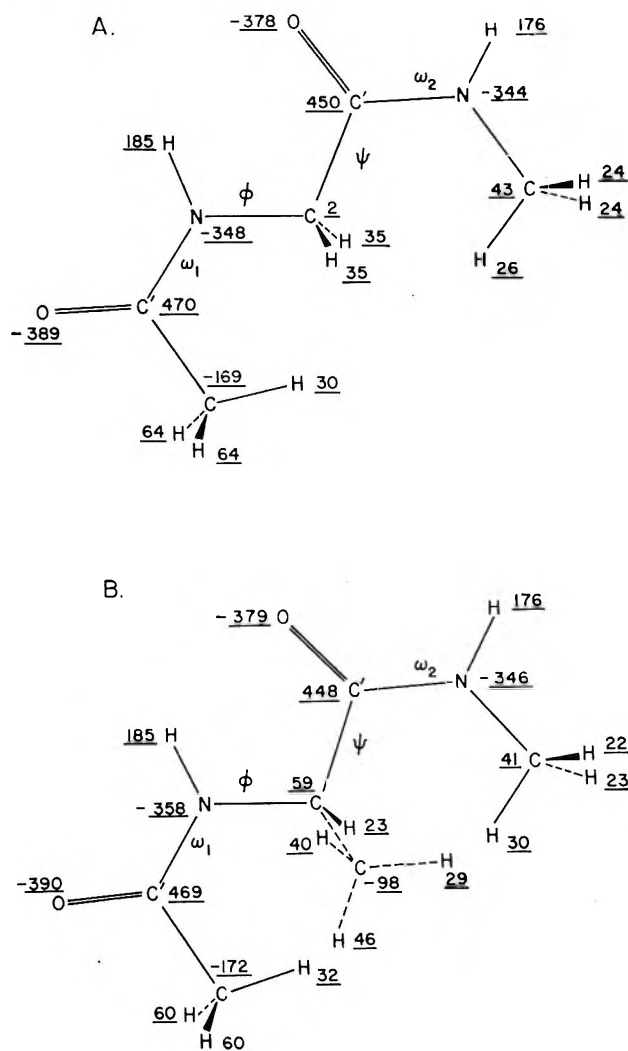
Figure 3.   Computed CNDO/2 (ON) partial charges ($\sigma + \pi$) for the extended form with cis peptide units ($\phi = \psi = 180°$, $\omega_{1,2} = 0°$) of the molecules:  (A) N-acetyl-N'-methylglycine amide (molecule V), and (B) N-acetyl-N'-methyl-L-alanine amide (molecule VI).  The values shown should be divided by 1000 to obtain electronic charge units.

is the one for which $(\phi,\psi) = (0,0)$ with the ranges of these angles being 0 to $\pm 180°$.

## Method

A brief description of the CNDO/2 and EHT methods was given in paper II.[5]  The input parameters for the computer programs[17] were the same as used previously.[5-7]  Because of limitations in computing time, bond lengths and bond angles were not varied, even though it is recognized that some changes in geometry could arise when the dihedral angles are varied.  It should be noted that the molecules considered in this paper represent upper limits of the size that can be treated practically with presently available computers and, further, that the computing time required in the CNDO/2 method considerably exceeds that for the EHT method.  For this reason, the CNDO/2 computations were not carried out for

**Table I:**   Molecular Geometry[a-d]

| Bond | Bond length, Å | Bond angle | Value, deg |
|---|---|---|---|
| C(methyl)–H | 1.090 | $\tau[\text{C}'\text{C}_{\text{methyl}}\text{H}]_{\text{acetyl}}$ | 109.5 |
| C(methyl)–N | 1.453 | $\tau[\text{C}^\alpha\text{C}'\text{O}]$ | 120.5 |
| C(methyl)–C' | 1.490 | $\tau[\text{C}^\alpha\text{C}'\text{C}_{\text{methyl}}]$ | 115.0 |
| C'$_{\text{amide}}$–O$_{\text{amide}}$ | 1.230 | $\tau[\text{C}_{\text{methyl}}\text{C}'\text{N}]$ | 115.0 |
| C'$_{\text{amide}}$–N | 1.325 | $\tau[\text{C}'\text{C}^\alpha\text{C}^\beta]$ | 112.4 |
| C$^\alpha$–C$^\beta$ | 1.530 | $\tau[\text{C}^\alpha\text{C}^\beta\text{H}]$ | 109.5 |
| C$^\alpha$–C' | 1.530 | $\tau[\text{C}'\text{NC}^\alpha]$ | 121.0 |
| C$^\alpha$–H | 1.000 | $\tau[\text{C}'\text{NH}]$ | 124.0 |
| C$^\beta$–H | 1.090 | $\tau[\text{C}^\alpha\text{NH}]$ | 115.0 |
| N–H | 1.000 | $\tau[\text{C}_{\text{methyl}}\text{NC}^\alpha]$ | 121.0 |
| N–C$^\alpha$ | 1.453 | $\tau[\text{C}_{\text{methyl}}\text{NC}']$ | 121.0 |
|  |  | $\tau[\text{NC}^\alpha\text{C}']$ | 109.3 (ala); 111.0 (gly) |
|  |  | $\tau[\text{NC}^\alpha\text{C}^\beta]$ | 109.5 |
|  |  | $\tau[\text{NC}'\text{O}]$ | 124.5 |
|  |  | $\tau[\text{NC}_{\text{methyl}}\text{H}]$ | 109.5 |

[a] The geometry in this table was maintained fixed for all values of the dihedral angles of internal rotation.  [b] The H$^\alpha$ atom of the alanine residue was positioned on the vector perpendicular to the plane made by the N, C$^\beta$, and C' atoms, and passing through the C$^\alpha$ atom.  [c] The H$^\alpha$ atoms of the glycine residue were positioned in the plane bisecting the $\tau[\text{NC}^\alpha\text{C}']$ angle at an angle $\tau[\text{H}_1^\alpha\text{C}^\alpha\text{H}_2^\alpha] = 107°$, and at an equal distance above and below the plane formed by the NC$^\alpha$C' atoms.  [d] The dihedral angles[15] maintained fixed were: $\chi_1 = \chi_2 = -60°$, $\omega_1 = \omega_2 = 180°$ for trans and $0°$ for cis peptide bonds.  All methyl end groups are fixed as shown in Figures 1–4.  All $\phi$ and $\psi$ values were varied, and, in those cases where applicable, $\phi_1 = \phi_2$ and $\psi_1 = \psi_2$.  See Figures 1–4 for definitions of these angles.

as large a range of $(\phi,\psi)$ values for the different molecules as would have been desired.  As in previous papers,[5-7] greater reliability is attached to CNDO/2 rather than to EHT partial charges because of the excessive charge separation which arises when polar molecules are treated by the EHT method.

## Results and Discussion

For each of the molecules of Figures 1–4, the overlap normalized (ON) CNDO/2 partial charges for the extended conformation and the EHT total energy for varying $\phi$ and $\psi$ (with $\omega = 180°$ for trans or $0°$ for cis peptide bonds) have been computed; in addition the CNDO/2 (ON) partial charges and total energy for varying $\phi$ and $\psi$ (with $\omega = 180°$) for molecule II have been computed.  The variation of the total energy with $\phi$ and $\psi$ are expressed in terms of contour diagrams, with the energy normalized to zero at the lowest minimum-energy value; in this way, all contours correspond to positive energies.

(17)  We are indebted to Professor R. Hoffmann for making the EHT and CNDO/2 computer programs available to us.
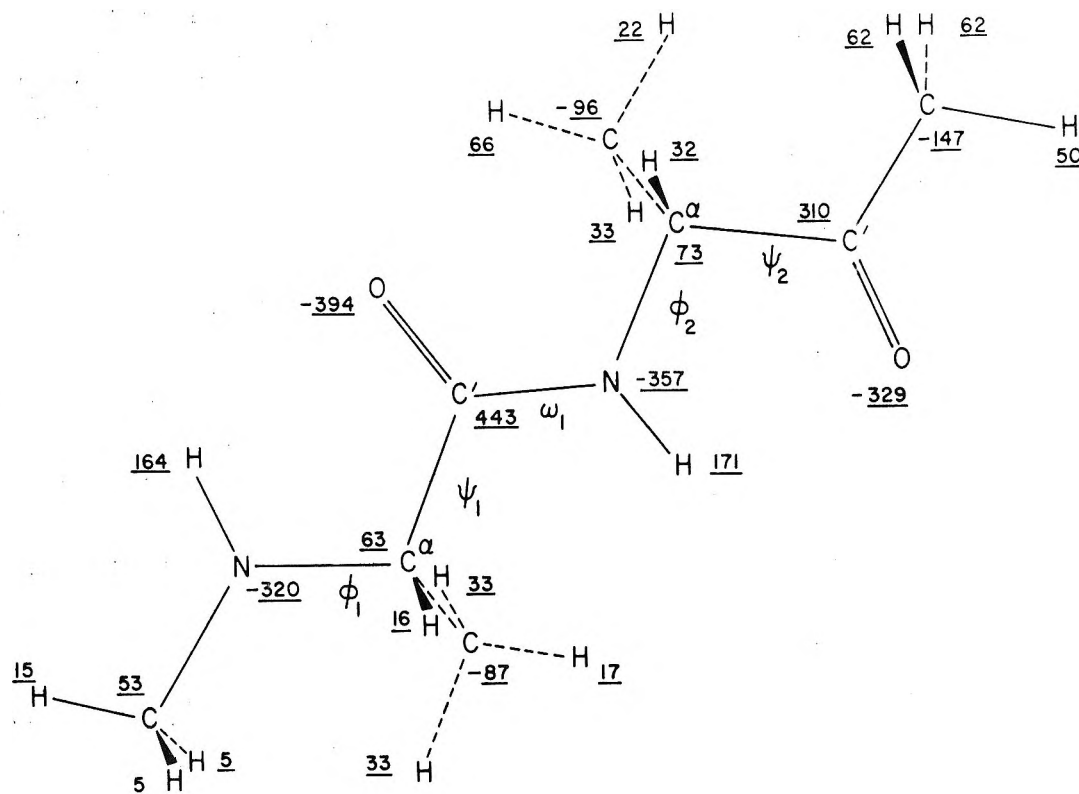
Figure 4. Computed CNDO/2 (ON) partial charges ($\sigma + \pi$) for the extended form with trans peptide units ($\phi_{1,2} = \psi_{1,2} = 180°$, $\omega = 180°$) of the molecule $N$-methyl-$C'$-methyl-L-alanyl-D-alanine (molecule VII). The values shown should be divided by 1000 to obtain electronic charge units.
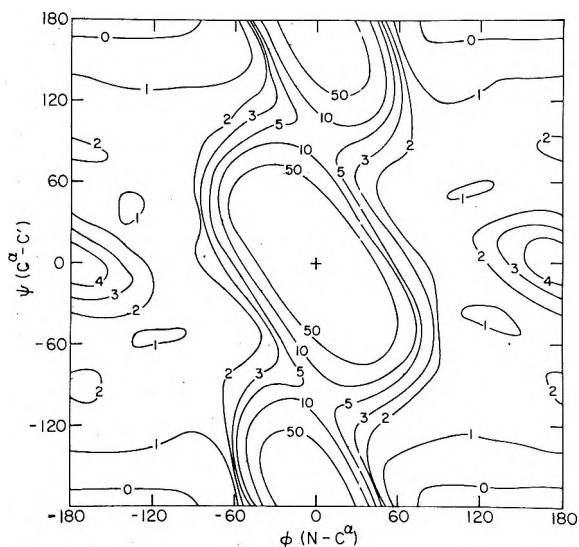


Figure 5. Conformational energy contour diagram (EHT) for $N$-acetyl-$N'$-methylglycine amide (I) with $\omega_{1,2} = 180°$. The methyl end groups were held fixed as shown in Figure 1A. The energies are in units of kilocalories per mole relative to zero at the lowest energy minimum (at $\phi = 180°$, $\psi = 180°$). The energies were computed at 10° intervals in $\phi$ and $\psi$.
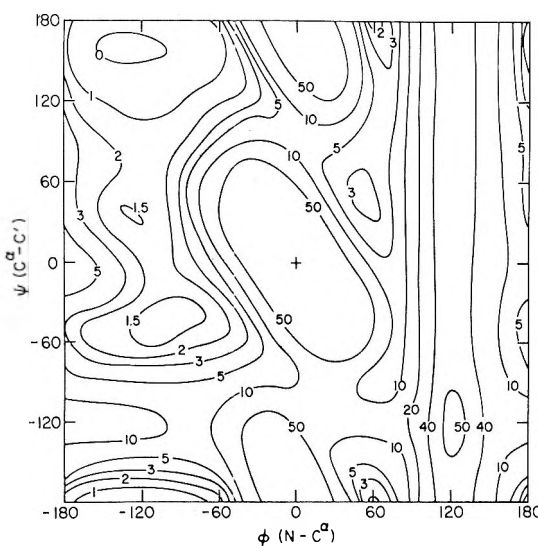


Figure 6. Conformational energy contour diagram (EHT) for $N$-acetyl-$N'$-methyl-L-alanine amide (II) with $\omega_{1,2} = 180°$ and $\chi = -60°$. The methyl end groups were held fixed, as shown in Figure 1B. The energies are in units of kilocalories per mole relative to zero at the lowest energy minimum (at $\phi = -130°$, $\psi = +160°$). The energies were computed at 10° intervals in $\phi$ and $\psi$.

*1. Molecules I and II.* We consider first molecules I and II, shown in Figure 1 together with their CNDO/2 (ON) partial charges (for the extended form) and with sequence numbers appended to the atoms of

molecule II for convenience in identifying atom–atom interactions. EHT conformational energy maps for molecules I and II are shown in Figures 5 and 6, re-
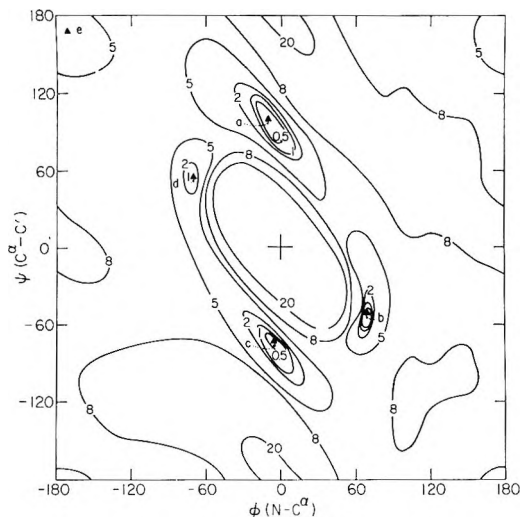
Figure 7. Conformational energy contour diagram (CNDO/2)
for $N$-acetyl-$N'$-methyl-L-alanine amide (II) with $\omega_{1,2} = 180°$
and $\chi = -60°$. The methyl end groups were held fixed, as
shown in Figure 1B. The energies are in units of kilocalories
per mole relative to zero at the lowest energy minimum
(at $\phi = -10°$, $\psi = +100°$). The energies were computed
at 10° intervals in $\phi$ and $\psi$. The solid triangles a, b, c, d,
e refer to the minima of increasingly higher energy.

**Table II:** Energy Minima in the Map Computed
for Molecule II by the CNDO/2 Method

| Mini-mum | Conformation $\phi$, deg | $\psi$, deg | Energy,[a] kcal/mol |
|---|---|---|---|
| a | −10 | +100 | 0.0 |
| b | +70 | −50 | 0.3 |
| c | −5 | −75 | 0.6 |
| d | −70 | +55 | 1.0 |
| e | −170 | +170 | 4.1 |

[a] Energy normalized to zero at minimum a.

spectively, and a CNDO/2 conformational energy map
for molecule II is shown in Figure 7. Similar maps
for these molecules had been calculated earlier by the
EHT method[18,19] and by the method of Perturbative
Configuration Interaction using Localized Orbitals
(PCILO);[20,21] also limited data (with no map re-
ported) on the same molecules, using the EHT method,
were obtained by Kier and George.[22] Differences
among the various maps will be discussed later.

In the maps of Figures 5 and 6, and also in those[19]
of ref 18, the lowest energy minimum arises for the
conformation for which $\phi \sim 180°$, $\psi \sim 180°$ (extended
form), with higher local minima near $\phi = -120°$, $\psi =
-50$ and $+50°$ (and the symmetry-related positions $\phi
= +120°$, $\psi = -50$ and $+50°$) for molecule I;
for molecule II the lowest energy minimum is at $\phi =
-130°$, $\psi = 160°$, with local minima near $\phi = -100°$,
$\psi = -50°$, and $\phi = -120°$, $\psi = +40°$.

The CNDO/2 map of Figure 7 is quite different
from the EHT map of Figure 6 for molecule II, as
expected (because of the reasons cited here and in
papers II and III). The five low-energy minima found
by the CNDO/2 method are compared in Table II.

The lowest energy conformation (a of Figure 7)
has not been reported previously in either empirical
or quantum mechanical calculations.[23] Because of its
unusual position on the $\phi$-$\psi$ map, we have attempted
to find the origin of this stabilization by a study of
the molecular orbital overlap coefficients and the elec-
tronic polarization (i.e., charge redistribution). We
could not isolate any particular feature which could
be held responsible for the stabilization; for this reason,

we can only conjecture as to its origin. For example,
in the language of the empirical approach,[10] this in-
teraction can be thought of as an attraction between a
partial negative charge on $O_6$ and a partial positive
charge on $C'_{12}$. A somewhat similar attractive energy
was found in the plane-to-plane stacking of the $N$-
methylacetamide and formamide dimers[6] which appear
to be stabilized by overlap of the $\pi$ orbitals as well
as by favorable electrostatic interactions when the
two NHCO groups are oppositely aligned. Since con-
formation a has not been found to be of low energy
by empirical calculations, because of the short contact
distance between the $O_6$ and $C'_{12}$ atoms (viz., 2.3 Å,
in this conformation) leading to a repulsive nonbonded
interaction, these molecular orbital calculations seem
to indicate that the parameters of the empirical non-
bonded energy functions, which dominate the energy
in this conformational region, may need to be revised
to remove this discrepancy.

The second minimum (b of Figure 7) corresponds
to a conformation which contains a seven-membered
ring in which $H_{18}$ serves as a hydrogen bond link be-
tween atoms $N_{17}$ and $O_6$, with the $C^\beta$ methyl group
occupying a position axial to the ring. For this con-
formation, the hydrogen bond is nonlinear with an
$H \cdots O$ distance of 1.56 Å and angles of $\angle N–H \cdots O$
of 148° and $\angle H \cdots O=\!\!=C$ of 100°. The third minimum
(c of Figure 7) corresponds to a conformation closely
similar to a, with the $O_6 \cdots C'_{12}$ interaction favoring
the stabilization. The slight destabilization of c with

(18) R. Hoffmann and A. Imamura, *Biopolymers*, **7**, 207 (1969).

(19) Since the Hoffmann–Imamura EHT calculations were carried
out at 30° intervals in $\phi$ and $\psi$, the calculations of Figures 5 and 6
were performed at 10° intervals to reduce the possibility of over-
looking any minima in the energy surface. While the maps of
Figures 5 and 6 differ slightly from those of ref 18 (probably because of
slight differences in geometry), the same minima appear in the maps
of Figures 5 and 6 and in those of ref 18.

(20) B. Maigret, B. Pullmann, and M. Dreyfus, *J. Theor. Biol.*, **26**,
321 (1970).

(21) B. Pullmann, B. Maigret, and D. Perahia, *Theor. Chim. Acta*,
**18**, 44 (1970).

(22) L. B. Kier and J. M. George, *ibid.*, **14**, 258 (1969).

(23) This conformation does not appear in the map of ref 20. How-
ever, when only the *higher* energy contours of ref 20 were reproduced
in ref 21, a minimum was marked on the map, even though the *low*-
energy contours of ref 20 give no indication of the existence of such
a minimum.

respect to a arises from the close $H_{18}$ contact with the $C^\beta$ hydrogens.

The fourth minimum (d of Figure 7) corresponds to a conformation which also contains a seven-membered hydrogen-bonded ring, involving atoms $O_6$ and $H_{18}$, with the $C^\beta$ methyl group occupying a position *equatorial* to the ring.

We have listed the fifth minimum (e of Figure 7) in Table II, even though it is of considerably higher energy than the others, because of its importance for the extended $\beta$ conformations taken by many poly-amino acids and polypeptides in films and crystals. We would not expect this conformation to contribute much to the average equilibrium conformation of molecule II.

Before turning to the interpretation of available experimental results on alanine peptides, we must examine the conformational differences between D and L isomers since these differences have not always been appreciated when assigning conformations on the basis of experimental data. For example, in Figure 7, the L isomer in the seven-membered hydrogen-bonded conformation is found to be axial at minimum b, and equatorial at minimum d while, for the D isomer, the equatorial conformation occurs at minimum b and the axial one at minimum d. The relative order of the energies of the minima also changes in going from the L to D isomer. It is important to keep these differences between the D and L conformations in mind since the experimental results to be examined were obtained for both the mixed DL and the D isomers. For a comparison of the results of Figure 7 with experimental ones, there are two kinds of data which provide conformational information. First, a study of the infrared absorption spectrum, specifically the N–H stretching frequency, can indicate the fraction of the molecules having conformations in which the N–H group is hydrogen bonded. Second, the $^3J_{NH-CH}$ constant, arising from the coupling of the spins of NH and $C^\alpha$H protons, has been taken as an indication of conformation. For example, Bystrov, et al.,[24] relate this constant to $\phi'$ (the dihedral angle for rotation about the N–$C^\alpha$ bond, but defined by the group of atoms HN–$C^\alpha$H rather than by standard nomenclature) by the equation

$$^3J_{NH-CH},\ cps\ =\ 8.9\ \cos^2\phi' -$$

$$0.9\cos\phi' + 0.9\sin^2\phi' \quad (1)$$

where $\phi'$ is taken as $0°$ for the conformation in which NH is cis to $C^\alpha$H. When this equation was used with the coupling constants determined for N-acetyl-D-ala-nyl-D-alanine methyl ester and other similar dipeptides in the mixed solvent $CDCl_3 + CCl_4$ (*viz.*, 7.3 to 7.8), Bystrov, et al.,[24] obtained a $\phi'$ value of $\sim 0°$. On the basis of these nmr results and their infrared data on the N–H stretching frequencies, they concluded that a large fraction ($\sim 70\%$) of these molecules are

in a seven-membered hydrogen-bonded ring. Since, of the three possible conformations considered by Bystrov, et al. (*viz.*, conformations b, d, and e), only conformation d for the D isomer (which is equivalent to conformation b for the L isomer) leads to a high coupling constant (conformations b and e for the D isomer have negative values of $\phi'$ and hence would lead to coupling constants less than 6), they were able to conclude that conformation d is the most predominant one (even though the values $\phi = +60°$, $\psi = -60°$ given by Bystrov, et al., pertain to the L rather than the D isomer). Very little discussion was given concerning the conformation of the remaining fraction ($\sim 30\%$) of the molecules. When their model compounds were then transferred to a polar solvent (*i.e.*, $H_2O$), the coupling constants were found to decrease to between 5 and 6, indicating that a conformational change had occurred. Although Bystrov, et al., indicated that this new conformation may be close to the right-handed $\alpha$-helix, our CNDO/2 calculations suggest that conformations a and c, which expose the backbone groups to the solvent, would be favorable. Furthermore, since both conformations a and c have negative values of $\phi'$, they would yield coupling constants below 6.

On the other hand, Mizushima, et al.,[25,26] interpreted their infrared data on the NH-stretching frequencies of N-acetyl-N'-methyl-DL-alanine amide and similar derivatives in nonpolar solvents (*viz.*, in $CCl_4$ and $CHCl_3$) as representing the conformation $\phi = -60°$, $\psi = +60°$, which is similar to conformation d. More recently, Avignon, et al.,[27-29] found that their infrared spectra on the molecule N-acetyl-N'-methyl-DL-alanine amide and similar derivatives corresponded to mixtures of both the extended (assumed to be a five-membered hydrogen-bonded structure as shown in Figure 1B) and the seven-membered hydrogen-bonded ring conformations. Their conclusion was that the folded conformation is the *equatorial* form (our d conformation for the L isomer). However, in the interpretation of their results, both Mizushima, et al.,[25,26] and Avignon, et al.,[27-29] overlooked the presence of both D and L isomers in their systems.

While we have no access to the original experimental data, it should be noted that none of the above authors[24-29] considered conformations a or c of Figure 7 in their interpretation. Our results imply that a

(24) V. F. Bystrov, S. L. Portnova, V. I. Tsetlin, V. T. Ivanov, and Y. A. Ovchinnikov, *Tetrahedron*, **25**, 493 (1969).

(25) S. Mizushima, T. Shimanouchi, M. Tsuboi, and T. Arakawa, *J. Amer. Chem. Soc.*, **79**, 5357 (1957).

(26) M. Tsuboi, T. Shimanouchi, and S. Mizushima, *ibid.*, **81**, 1406 (1959).

(27) M. Avignon, P. V. Huong, and J. Lascombe, *Biopolymers*, **8**, 69 (1969).

(28) M. Avignon and P. V. Huong, *ibid.*, **9**, 427 (1970).

(29) M. Marraud, J. Neel, M. Avignon, and P. V. Huong, *J. Chim. Phys. Physicochim. Biol.*, **67**, 959 (1970).

search for these apparently stable conformations should be carried out.

It is interesting at this point to consider the EHT map for molecule II (Figure 6). There are no low-energy regions on this map, except the extended conformation, that can be associated with hydrogen bonding. Thus, if one considers only the proton coupling constant $^3J_{NH-CH}$ for the L isomer, the three low-energy regions at $\phi = -130°$, $\psi = +160°$; $\phi = -100°$, $\psi = -50°$; and $\phi = -120°$, $\psi = +40°$, all give $\phi'$ values of 130 to 160° which would fit the observed coupling constants of 7.3 to 7.8 very well. However, since the infrared data[24-29] *strongly* suggest the existence of a seven-membered hydrogen-bonded conformation, one must be particularly careful in using nmr data of this kind in order to justify or confirm conformational calculations. An example of the coupling of nmr results with empirically calculated conformational maps may be found in papers by Tonelli, *et al.*,[30] and by Silverman and Scheraga.[31]

Other theoretical calculations on similar molecular systems have also been carried out. Maigret, *et al.*,[20,32] studied molecules I and II using the PCILO–MO method, and found low-energy minima near $\phi = -80°$, $\psi = +40°$ and $\phi = +80°$, $\psi = -40°$ for molecule I, and a low-energy minimum near $\phi = 80°$ and $\psi = -40°$ with a second minimum (about 1 kcal/mol higher) near $\phi = -80°$ and $\psi = +40°$, followed by the region $\phi = \psi = 180°$ for molecule II. These results correspond to our CNDO/2 minima b, d, and e shown in Figure 7. From their results, Maigret, *et al.*,[20] predicted that the folded seven-membered ring postulated by Bystrov, *et al.*,[24] is the most stable conformation for molecule II; however, they failed to distinguish between D and L isomers in their interpretation of the data of Bystrov, *et al.*[24] They also found the conformation postulated by Mizushima, *et al.*,[25,26] at somewhat higher energy. It is interesting to note that, in this paper,[20] they did not find the minima in regions a and c of Figure 7, but, in a later paper,[21] these regions are shown with minima but without explanation. It is not clear why the PCILO treatment, which uses CNDO/2 parameterization, and the usual hypothesis of complete neglect of differential overlap, should give such a different result from the CNDO/2 method; it is also not clear why the same group[20,21] obtained two different maps, using the same method on the same molecule.

Several other computational studies of these molecules have also been carried out. Scott and Scheraga,[33] Crippen and Scheraga,[34] and Popov, *et al.*,[35] used empirical energy calculations to study the conformational space of these molecules, and Ramachandran, *et al.*,[36] and Leach, *et al.*,[37] used the hard-sphere approach on similar molecules. In these empirical approaches only Crippen and Scheraga[34] and Popov, *et al.*,[35] found the *axial* seven-membered hydrogen-bonded conformation

as a low-energy region. In summary, it appears that we must wait for further critical experimental data on these dipeptide systems, before we will be able to judge the correctness of our conformational calculations.

Having considered the conformational energies of molecules I and II, we turn now to the dependence of the partial charges on conformation. The CNDO/2 (ON) partial charges for these two molecules in the extended conformation are shown in Figure 1. It can be seen that the partial charges of identical atoms in a given "tripeptide" differ from each other; *e.g.*, in molecule II, the charges on $C'_5$ differ from those on $C'_{12}$. The reason for this difference is that the two carbon atoms are in different environments because the molecule possesses methyl end groups. If, on the other hand, the molecule were an infinitely long homopolymer, then of course the charges on corresponding atoms would be identical. Hence, we would expect the low-energy conformations of the oligopeptides studied here to differ somewhat from those of similar segments in infinite polyamino acids. Consequently, the role of the end groups must be taken into account in interpreting experimental results purporting to show that the carbonyl groups of different amino acids are supposedly protonated to different extents. When molecule I is compared with molecule II, *i.e.*, when a $C^\alpha$ hydrogen is replaced by a methyl group, the charges on $C_9^\alpha$ and $N_7$ change considerably, but that on $C'_{12}$ changes very little; in other words, the side chain influences the charges on the $C^\alpha$ and neighboring N atoms more than that on the neighboring C=O group.

Turning to the seven-membered hydrogen-bonded ring structures, Figure 8 shows how the partial charges change as the conformation changes in the region of $\psi = -120$ to 0° for $\phi$ held fixed at $+70$ and $+80°$, respectively, and $\psi = 0$ to $+120°$ for $\phi = -70$ and $-80°$, respectively (see minima b and d of Figure 7); those atoms whose charges vary by $\leq 1\%$ are not included in Figure 8. The variation in charge shown in Figure 8 arises from the mutual approach of polar

(30) (a) A. E. Tonelli and F. A. Bovey, *Macromolecules*, **3**, 410 (1970); (b) A. E. Tonelli, A. I. Brewster, and F. A. Bovey, *ibid.*, **3**, 412 (1970).

(31) D. N. Silverman and H. A. Scheraga, *Biochemistry*, **10**, 1340 (1971).

(32) We should note that the results of our paper confirm the choice of intrinsic potential function for rotation about the N–C$^\alpha$ bond used by Scott and Scheraga,[33] rather than that found in ref 20.

(33) R. A. Scott and H. A. Scheraga, *J. Chem. Phys.*, **45**, 2091 (1966).

(34) G. M. Crippen and H. A. Scheraga, *Proc. Natl. Acad. Sci., U. S.*, **64**, 42 (1969).

(35) E. M. Popov, G. M. Lipkind, S. F. Arkhipova, and V. G. Dashevskii, *Mol. Biol.*, **2**, 622 (1968).

(36) G. N. Ramachandran, C. M. Venkatachalam, and S. Krimm, *Biophys. J.*, **6**, 849 (1966).

(37) S. J. Leach, G. Nemethy, and H. A. Scheraga, *Biopolymers*, **4**, 369 (1966).
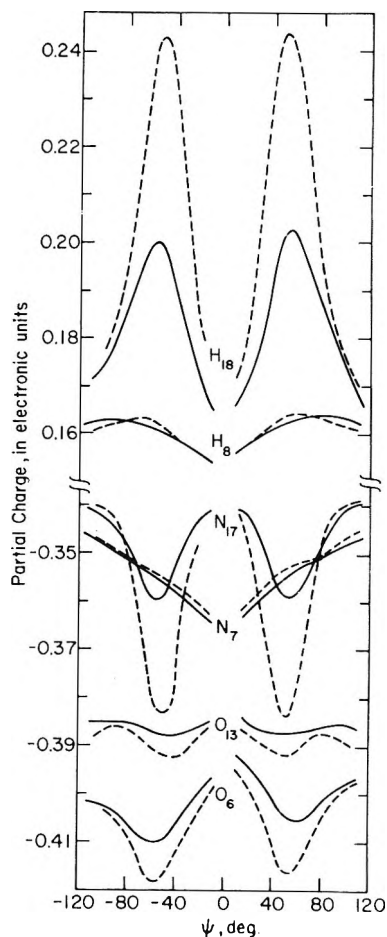
Figure 8. Variation of the CNDO/2 (ON) partial charges with conformation for the atoms of molecule II, as designated in Figure 1B, with $\chi = -60°$ and $\omega_{1,2} = 180°$. $\psi$ varies from $-120$ to $0°$ for $\phi = +70°$ (dashed lines) and $+80°$ (solid lines) and $\psi$ varies from 0 to 120° for $\phi = -70°$ (dashed lines) and $-80°$ (solid lines). In this conformational region in which the seven-membered hydrogen-bonded ring structures occur (b and d of Figure 7), those atoms whose charges vary by less than 1% are not included.

groups to form "hydrogen bonds," or energetically favored orientations of oppositely charged atoms. For example, $H_{18}$ and $O_6$ pass closest to one another (for $\phi = \pm 70°$) at $\psi \sim \mp 55°$, which correspond to minima b and d, respectively. As $\phi$ changes from $\pm 80$ to $\pm 70°$ (*i.e.*, as it moves closer to the positions of minimum energy), the changes in charge become more pronounced, as shown. The variation in the charge of $N_{17}$ follows the change in charge of $H_{18}$, and is also maximal in this region. Even though $O_{13}$ and $N_7$ do not participate in "hydrogen bonding" in this region, their charges show some variation which arises from various other interactions. The charges on the $C'$ atoms (not shown) show very little variation in this conformational region.

Moving away from the region of the seven-membered hydrogen-bonded ring structures, we consider first the region around minimum a. For $\psi = +100°$, and $\phi$ varying from $-40$ to $+40°$, we find that the $C'_{12}$

atom undergoes a noticeable change of charge, becoming more positive by 0.03 electronic units in this range of $\phi$. The charge of $O_6$ changes by about 0.015 electronic units over this same range, and no other significant changes of charge were observed. These changes in charge near minimum a may be compared with the large changes found near minima b and d in which hydrogen bonds are formed. The changes in charge near minimum c are similar to those near minimum a. Aside from the regions discussed above, no significant variation of charge occurs as the conformation changes, except in those high-energy regions (which involve atom–atom overlap) which are of no interest as far as the location of stable conformations is concerned.

From the above results, we see that the partial charges depend on the conformation, and show significant variation in regions of energy minima. This implies that the results of measurements of physical properties such as dipole moments, infrared spectra, ORD, etc., should be interpreted in terms of these "polarized" states of the molecule, particularly if the conformation involves a hydrogen bond. Hence, work is now in progress[14] to incorporate these polarization effects in the empirical functions[10] used for conformational energy calculations.

*2. Molecules III and IV.* The extended conformations and the CNDO/2 (ON) partial charges of molecules III and IV are shown in Figure 2. These molecules differ from molecules I and II in two respects. First, they contain only one peptide bond, whereas molecules I and II both contain two peptide bonds. Second, molecule IV is obtained from III by the addition of two side-chain methyl groups, whereas molecule II is obtained from I by the addition of only one side-chain methyl group. In essence, molecules III and IV are "dipeptides," whereas molecules I and II are "tripeptides."

The CNDO/2 (ON) partial charges of the amide ($CH_3NH-$) and the carboxyl ($-COCH_3$) end groups of molecules III and IV (Figure 2) differ slightly from those of I and II (Figure 1), when all four molecules are in the extended conformation. These differences in charge appear to arise primarily from the fact that the environments of the end groups differ, *i.e.*, the amide ends ($CH_3NH-$) of molecules III and IV are attached to $C^\alpha$ atoms, whereas those of molecules I and II are attached to $C'$ atoms; similarly, the environments of the carbonyl ends ($-COCH_3$) also differ, in that they are attached to different backbone atoms in the peptide chain. As stated in section 1, differences in partial charges probably influence the conformations.

It was not practical to carry out CNDO/2 computations for molecules III and IV, other than in the extended conformation, because of the large amount of computer time required. Therefore, we have resorted
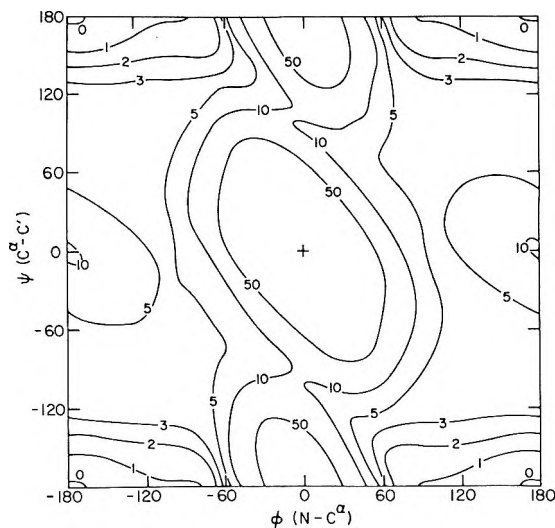
Figure 9. Conformational energy contour diagram (EHT) for
$N$-methyl-$C'$-methylglycylglycine (III) with $\omega_1 = 180°$, $\phi_1 = \phi_2$, and $\psi_1 = \psi_2$. The methyl end groups were held fixed, as shown in Figure 2A. The energies are in units of kilocalories per mole relative to zero at the lowest energy minimum (at $\phi = 180°$; $\psi = 180°$). The energies were computed at 10° intervals in $\phi$ and $\psi$.

Figure 10. Conformational energy contour diagram (EHT) for $N$-methyl-$C'$-methyl-L-alanyl-L-alanine (IV) with $\omega_1 = 180°$, $\phi_1 = \phi_2$, $\psi_1 = \psi_2$, and $\chi_1 = \chi_2 = -60°$. The methyl end groups were held fixed, as shown in Figure 2B. The energies are in units of kilocalories per mole relative to zero at the lowest energy minimum (at $\phi = -140°$; $\psi = +160°$). The energies were computed at 10° intervals in $\phi$ and $\psi$.

to a consideration of the more rapidly attainable EHT conformational energy maps, since a comparison of these maps for the various molecules treated here gives some indication as to which interactions are important in determining the low-energy conformations of these molecules. It is important to remember that, while the EHT method does not predict a stable hydrogen bond,[6] it does reproduce very well the non-bonded and torsional properties of these molecules.[5,6] Hence, the EHT computations were carried out only for conformations in which hydrogen bonding cannot occur. This was accomplished by the restriction that $\phi_1 = \phi_2$ and $\psi_1 = \psi_2$ (with $\chi_1 = \chi_2$ for molecule IV); with this restriction, conformations such as b and d of Figure 7 cannot arise. This restriction of conformational equivalence of residues is usually, but not always, made in treating homopolymers.[10] The EHT conformational energy maps for molecules III and IV, computed on the basis of this restriction, are shown in Figures 9 and 10, respectively.

Recalling that molecules III and IV have only one peptide bond, whereas I and II each have two, we may examine the region of conformational space in which peptide–peptide interactions are important. From a comparison of Figures 5 and 9, we see that the local minima of Figure 5 at $\phi \sim \pm120°$, $\psi \sim \pm60°$ do not appear in Figure 9; instead, these regions are relatively flat and of several kilocalories/mole higher in energy in Figure 9. Also, the heights of the "passes" in going between regions of negative $\phi$ and positive $\phi$ are about 7 kcal/mol in Figure 5, but greater than 10 kcal/mol in Figure 9. From a comparison of Figure 6 and Figure 10, we see that the general shapes of the energy

contours are similar except for the disappearance of the local minimum at $\phi \sim -120°$, $\psi \sim +40°$ of Figure 6. However, the depths of the other local minima are significantly altered. For example, the energy of the $\alpha_R$-helical region ($\phi \sim -80°$, $\psi \sim -50°$) has more than doubled, being 1.5 kcal/mol in Figure 6 and 4.0 kcal/mol in Figure 10. Since this relative increase in energy in the $\alpha_R$-helical region also appears in a comparison of Figures 5 and 9, i.e., for glycine as well as for alanine, it seems that peptide–peptide interactions, rather than interactions involving side-chain methyl groups, may be responsible for these differences in the $\alpha_R$-helical region in the two sets of maps. This conclusion must be accepted with the possible reservation that differences in end groups between the two sets of molecules (whose effects cannot be estimated, even qualitatively) may play a role in this region of conformational space. A second reservation is that the peptide–peptide interaction (in the EHT calculation) could be repulsive in nature when the peptides are stacked parallel to each other, as found[6] for stacked dimers of $N$-methylacetamide and -formamide, respectively, and could be attractive (or less repulsive) in the $\alpha_R$-helical region, where they are offset and in a perpendicular arrangement to one another. While the EHT maps of Figures 5, 6, 9, and 10 provide indications of those regions of conformational space, in which peptide–peptide interactions are important, the quantitative features of
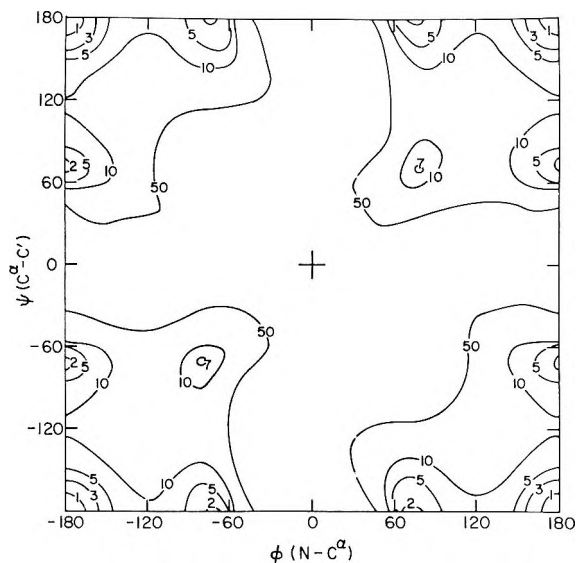
Figure 11. Conformational energy contour diagram (EHT) for cis-N-acetyl-N'-methylglycine amide (V) with $\omega_1 = \omega_2 = 0°$. The methyl end groups were held fixed, as shown in Figure 3A. The energies are in units of kilocalories per mole relative to zero at the lowest energy minimum (at $\phi = 180°$; $\psi = 180°$). The energies were computed at 10° intervals in $\phi$ and $\psi$.



Figure 12. Conformational energy contour diagram (EHT) for cis-N-acetyl-N'-methyl-L-alanine amide (VI) with $\omega_1 = \omega_2 = 0°$ and $\chi = -60°$. The methyl end groups were held fixed, as shown in Figure 3B. The energies are in units of kilocalories per mole relative to zero at the lowest energy minimum (at $\phi = -70°$, $\psi = +160°$). The energies were computed at 10° intervals in $\phi$ and $\psi$.

these interactions must await a more refined (e.g., CNDO/2) treatment.

*3. Molecules V and VI.* Since cis peptide units exist in small cyclic peptides,[38–40] in N-methylated polypeptides,[41] and in poly-L-proline (I),[42] it appeared desirable to calculate the conformational maps for cis peptides of glycine and alanine, specifically for cis-N-acetyl-N'-methylglycine amide (V) and cis-N-acetyl-N'-methyl-L-alanine amide (VI). The CNDO/2 (ON) partial charges of the extended forms of these two molecules are shown in Figure 3, and the EHT energy maps in Figures 11 and 12, respectively.

A comparison of these cis peptides (in Figure 3) with those of the trans conformations (in Figure 1) shows that there is no significant difference in the partial charges arising from the cis–trans conversion. The most noticeable change in charge is associated with atom $H_8$ which is situated between two oxygens when in the cis conformation.

As in the case of molecule I, the low-energy regions of molecule V are located near the extended conformation ($\phi = 180°$, $\psi = 180°$). Otherwise the maps for the two molecules are quite different, there being other local minima in Figure 11 near $\phi = \pm70°$, $\psi = 180°$ and $\phi = 180°$, $\psi = \pm70°$ (all with energies of about 2 kcal/mol), and some higher-energy minima at $\phi = -80°$, $\psi = -70°$ and $\phi = 80°$, $\psi = 70°$ (of about 7 kcal/mol). In the map for the cis alanine form (Figure 12), there is a low-energy minimum at $\phi = -70°$, $\psi = +160°$, with a second local minimum at $\phi = -160°$, $\psi = +160°$ (of about 1.0 kcal/mol), and a third

minimum at $\phi = -160°$, $\psi = +70°$ (of about 3.0 kcal/mol).

It is interesting to note that, even though the EHT method does not give reliable results for "hydrogen-bonding" conformations, it does lead to regions of low energy which are in excellent agreement with experimental data for these cis peptides (where no hydrogen bonding can occur). For example, the poly-L-proline I helix is observed to have a conformation near $\phi = -80°$, $\psi = +160°$,[42] which is near the low-energy minimum of Figure 12. Figure 12 also compares favorably with "hard-sphere"[10,12,36] calculations on cis peptides.[39] For the cyclic cis dipeptide

$$\begin{array}{ccc} S & \text{------} & S \\ | & & | \\ \text{L-Cys} & \text{-} & \text{L-Cys} \end{array}$$
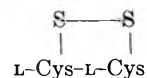
the "hard-sphere" calculations of Chandrasekharan[43] give the allowed conformation as $\phi \sim -140°$, $\psi \sim +135°$, by varying $\omega$ up to $+30°$ (nonplanar peptide). On the other hand, for the molecule represented in Figure 12, we obtain a minimum for a cis conformation near these values of $\phi$ and $\psi$ by keeping $\omega$ fixed at $0°$, i.e., with a planar peptide group.

(38) R. Degeith and R. E. Marsh, *Acta Crystallogr.*, **12**, 1007 (1959).

(39) G. N. Ramachandran and C. M. Venkatachalam, *Biopolymers*, **6**, 1255 (1968).

(40) E. Sletten, *J. Amer. Chem. Soc.*, **92**, 172 (1970).

(41) P. Groth, *Acta Chem. Scand.*, **24**, 780 (1970).

(42) W. Traub and U. Shmueli, "Aspects of Protein Structure," G. N. Ramachandran, Ed., Academic Press, New York, N. Y., 1963, p 81.

(43) R. Chandrasekharan, *Proc. Indian Acad. Sci., Sect. A*, **68**, 13 (1968).
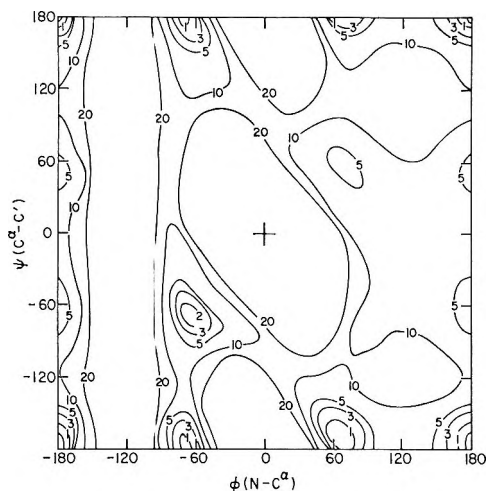
Figure 13. Conformational energy contour diagram (EHT) for
$N$-methyl-$C'$-methyl-L-alanyl-D-alanine (VII) with $\omega_1 = 180°$,
$\phi_1 = \phi_2$, $\psi_1 = \psi_2$, and $\chi_1 = \chi_2 = -60°$. The methyl end
groups were held fixed, as shown in Figure 4. The energies
are in units of kilocalories per mole relative to zero at the
lowest energy minimum (at $\phi = 180°$, $\psi = 180°$). The
energies were computed at 10° intervals in $\phi$ and $\psi$.

A comparison of Figures 11 and 12 shows clearly
the conformational space made inaccessible by the
addition of a methyl side chain (for a cis peptide).

*4. Molecule VII.* Finally, it was of interest to
examine a molecule, $N$-methyl-$C'$-methyl-L-alanyl-D-
alanine (VII), containing both an L and a D residue.
The CNDO/2 (ON) partial charges for the extended
conformation of molecule VII are shown in Figure 4,
and the EHT energy map for $\phi_1 = \phi_2$, $\psi_1 = \psi_2$, $\omega_1 =$
$180°$, and $\chi_1 = \chi_2$ is shown in Figure 13.

The considerable differences in the conformational
maps of L-ala-D-ala (Figure 13) and of L-ala-L-ala (Fig-
ure 10) are due primarily to the interaction of the
side-chain methyl group of the D residue with the
backbone oxygen of the L residue. The extended con-
formation of molecule VII is that of lowest energy,
followed closely by two local-minimum conformations
at $\phi = -70°$, $\psi = -180°$ and $\phi = +70°$, $\psi = -170°$
(each of about 1.0 kcal/mol), and one at $\phi = -70°$,
$\psi = -70°$ (of about 2.0 kcal/mol). The latter confor-
mation is close to that found to be favorable by empirical
calculations for LDLD mixed residues of cyclotetralanyl[44]
with trans peptides.

## Conclusions

In conclusion, extreme care must be exercised in
the interpretation of results from calculations on peptide
systems by the EHT, CNDO/2, or other molecular
orbital methods. While these methods are more rig-
orous than empirical ones, they still require consider-
able improvement before they can yield unambiguous
conformational information, which is in agreement
with experimental results. Further, the large core size
required and the large expense of the computations

make them of little practical value for large polypep-
tides or proteins, at the present time. For these rea-
sons, we expect that refined[10-13] empirical methods,
improved by the knowledge gained from the results
of the molecular orbital methods, will be the most
fruitful ones for use on macromolecules. Work along
these lines is in progress in this laboratory.

From the results presented in this paper, as well
as in our previous ones,[5-7] we may formulate some
approximate rules as to which properties of peptides
are best accounted for by the EHT method, and which
by the CNDO/2 method. Considering first the EHT
procedure, three rules emerge. (1) It is clear that
this theory is not applicable to regions of conformational
space in which hydrogen bonds are formed (see paper
III[6]). Indeed, the results of the present paper confirm
those of paper III, *i.e.*, that the EHT method does
not lead to the stabilization of favorable hydrogen
bonds, either intermolecular ones in model com-
pounds[6,45] or intramolecular N—H⋯O=C hydrogen
bonds in oligopeptides. (2) There is some experi-
mental evidence that stabilized peptide–peptide (*i.e.*,
plane-to-plane) interactions may occur. For example,
some nmr results for benzene–NMA complexes[46] and
observations from X-ray studies indicate that ring-to-
ring and ring-to-peptide conformations occur in pro-
teins and hence that some type of $\pi$–$\pi$ interactions
must be important in stabilizing certain conformations.
Yet, no evidence of a preferential attractive potential
for this type of stacking interaction is obtained by
the EHT method. However, the EHT results pre-
sented here (see section 2) do indicate that $\alpha$-helical
conformations are stabilized. (3) Nonpolar repulsive
interactions, and potential functions for rotation about
bonds, seem to be reasonably well accounted for by
the EHT method (see paper II[5]), for the molecules
studied here, and in a previous paper.[7] Thus, we
may expect to obtain reliable values for rotational
barriers in *nonpolar* side chains of amino acids; such
calculations have been carried out and will be reported
elsewhere.

Turning now to the CNDO/2 results, the following
three rules emerge. (1) In contrast to the EHT pro-
cedure, the CNDO/2 method does account for the
formation of stable hydrogen-bonded intermolecular
complexes (see paper III[6]) and also intramolecular
hydrogen-bonded structures in the oligopeptides studied
in this paper. (2) Also, the CNDO/2 method accounts
for $\pi$–$\pi$ and n–$\pi$ types of interaction (see paper III[6]).
(3) As shown previously,[5-7] and in the present paper,
the CNDO/2 (ON) partial charges are reasonable

(44) C. Ramakrishnan and K. P. Sarathy, *Biochim. Biophys. Acta,*
**168,** 402 (1968).
(45) A. S. N. Murthy, K. G. Rao, and C. N. R. Rao, *J. Amer.*
*Chem. Soc.,* **92,** 3544 (1970).
(46) M. Davies and D. K. Thomas, *J. Phys. Chem.,* **60,** 767 (1956).

ones,[47,48] since they account for observed dipole moments.[6] We have examined the polarization effects which accompany changes in conformation and find significant changes in charge when hydrogen bonding occurs. These results are being used[14] to formulate a potential function for hydrogen bonding. They are also being used in the crystal structure refinements[10-13] of empirical potentials.

To summarize, neither the quantum mechanical theory (EHT or CNDO/2) nor the empirical calculations give unequivocal agreement with the experimental results found in nonpolar and polar solvents. Although it has been shown that one theory is as good or better than another for certain specific interactions (*e.g.*, the EHT theory yields reliable torsional potentials, while the CNDO/2 method gives reasonable partial charges),

there is not at the present time any justification for selecting any one theory (either quantum mechanical or empirical) over all others to obtain the most stable conformation. Hopefully, the insight gained from these calculations, and the refinement of the parameters of the energy functions by calculations of crystal structures,[11-13] will provide a suitable basis for conformational energy calculations on polypeptides.

(47) Hehre and Pople[48] have compared CNDO/2 and *ab initio* charge distributions and dipole moments for a series of organic molecules and have shown that both methods give similar results.

(48) W. J. Hehre and J. A. Pople, *J. Amer. Chem. Soc.*, 92, 2191 (1970).

# A Semicontinuum Model for the Hydrated Electron. II.

# Configurational Stability of the Ground State

**by Kenji Fueki,**

*Department of Synthetic Chemistry, Faculty of Engineering, Nagoya University, Nagoya, Japan*

**Da-Fei Feng, Larry Kevan,*[1]**

*Department of Chemistry, Wayne State University, Detroit, Michigan 48202*

**and Ralph E. Christoffersen**

*Department of Chemistry, University of Kansas, Lawrence, Kansas 66044* (*Received December 22, 1970*)

*Publication costs assisted by the U. S. Atomic Energy Commission and the Air Force Office of Scientific Research*

A semicontinuum model is further developed for the hydrated electron in water at 300°K and in ice at 77°K. Both short-range charge-dipole and long-range polarization interactions between the electron and the solvent molecules are calculated self-consistently. The configurational stability for the ground state of the hydrated electron has been established by applying the variational procedure to the total energy of the system. This allows the prediction of a unique cavity radius within the framework of the approximations used. Various physical properties of the electron in water and ice are calculated and discussed. The difference between water and ice is basically that the long-range interactions of the electron are weaker in ice. The calculated results are generally in semiquantitative agreement with experimental values, but discrepancies remain with regard to absorption bandwidth and relaxation processes following optical excitation.

## I. Introduction

The hydrated electron has become a well-known species in chemistry,[2] but a quantitative theoretical understanding of its spectrum and properties is far from complete. In a previous paper,[3] we presented a semicontinuum model calculation on the hydrated electron which includes both short- and long-range interactions between the hydrated electron and the solvent or ma-

trix. A principal conclusion from that study was that short-range attractive interactions must be included to properly account for the absolute values of the electron

(1) John Simon Guggenheim Fellow, 1970-1971.

(2) E. J. Hart and M. Anbar, "The Hydrated Electron," Wiley-Interscience, New York, N. Y., 1970.

(3) K. Fueki, D.-F. Feng, and L. Kevan, *J. Phys. Chem.*, 74, 1976 (1970).

energy levels. In brief, the inclusion of a short-range charge-dipole potential tends to move the energy levels toward the continuum so that the levels are less strongly bound. Satisfactory agreement between the calculated and experimental properties of the hydrated electron was obtained by arbitrarily choosing a cavity radius to give the best fit with experiment.

It is obviously more fundamental to *predict* a cavity radius by minimizing the total energy of the hydrated electron with respect to a configurational coordinate such as the cavity radius. This has recently been done by Copeland, *et al.*,[4] for the solvated electron in liquid ammonia. It turns out that an energy minimum cannot be found if only long-range interactions are included in the potential. So short-range interactions are included by a charge-dipole potential in analogous fashion to the semicontinuum model. This is another example of the necessity for including short-range interactions when describing solvated electrons.

Within the approximations involved in their model, Copeland, *et al.*,[4] could establish the configurational stability of the electron cavity in ammonia but not in water, because no energy minimum was found in water. They used a self-consistent treatment only for short-range interactions and a Landau-type potential for long-range interactions. Also, the variational procedure was applied only to the electronic energy and the wave functions obtained in this way were used for the calculation of the medium rearrangement energy.

Our objective has been to establish the configurational stability for the ground state of the hydrated electron. This has been achieved by performing a somewhat more elaborate calculation on our semicontinuum model. In particular, (1) we treat both short- and long-range interactions self-consistently, and (2) we apply the variational procedure to the total energy (the sum of the electronic energy and the medium rearrangement energy) of the system.

We also extend this type of calculation to the trapped electron in ice at 77°K. In addition, we carry out the first calculations of the relaxed excited state for the electron in both water and ice in connection with the relaxation problem of the optically excited state.

## II. Outline of Calculation

*A. The Model.* The model used in the present calculation is essentially the same as that in the previous paper.[3] We assume that the solvated electron interacts with the dipoles of specifically oriented water molecules in the first solvation shell by a short-range attractive potential. The solvent molecules beyond the first solvation shell are treated as a continuous dielectric medium with which the electron interacts by a long-range polarization potential. The number of the solvent molecules in the first solvation shell is taken to be four or six, which are arranged symmetrically around

the center of the cavity. We assume that the water dipoles are allowed to reach thermal equilibrium.

*B. Ground State.* The total ground-state energy, $E_t(1s)$, for the solvated electron is given by the sum of the electronic energy, $E_e(1s)$, and the medium rearrangement energy, $E_m(1s)$.

$$E_t(1s) = E_e(1s) + E_m(1s) \tag{1}$$

The electronic energy for short-range attractive interactions can be written as

$$E_e{}^s(1s) = -\int_{r \leq r_d} \psi_{1s}\left(\frac{Ne\mu_0\langle\cos\theta\rangle_{1s}}{r_d{}^2} + \frac{Ne^2\alpha_4 C_{1s}}{2r_d}\right)\psi_{1s}d\tau \tag{2}$$

$$\langle\cos\theta\rangle_{1s} = \coth\chi - \frac{1}{\chi}, \chi = \frac{e\mu_0 C_{1s}}{kTr_d{}^2}, C_{1s} = \int_{r \leq r_d}\psi_{1s}{}^2 d\tau$$

where $\mu_0$ and $\alpha$ are the magnitudes of the permanent dipole moment ($\mu_0 = 1.85$ D) and of the isotropic polarizability ($\alpha = 1.51$ Å³) for the water molecule, respectively, and $N$ is the number of the water molecules in the first solvation shell ($N = 4$ or 6); $\theta$ is the angle between the dipole moment vector and the line joining the center of the cavity to the center of the dipole; $r_d$ is the distance between the center of the cavity and the dipole; $C_{1s}$ is the charge enclosed within radius $r_d$; $\psi_{1s}$ is a hydrogen-like 1s wave function for the ground state;[3] $k$ is Boltzmann's constant; and $T$ is the absolute temperature.

The dipole-dipole interaction energy between the oriented dipoles in the first solvation shell is given by

$$E_{dd}(1s) = \frac{D_N\mu_{1s}{}^2}{r_d{}^3}$$

$$\mu_{1s} = \mu_0\langle\cos\theta\rangle_{1s} + \frac{e\alpha C_{1s}}{r_d{}^2} \tag{3}$$

where $D_4 = 2.2964$ and $D_6 = 7.1140$.[5]

The short-range interaction part, $E_{1s}{}^s$, of the total ground-state energy is

$$E_{1s}{}^s = E_e{}^s(1s) + E_m{}^s(1s) = E_e{}^s(1s) + E_{dd}(1s) \tag{4}$$

The long-range interaction part, $E_{1s}{}^1$, of the total ground-state energy is given by

$$E_{1s}{}^1 = E_e{}^1(1s) + E_m{}^1(1s) =$$

$$\frac{e}{2}\left(1 - \frac{1}{D_s}\right)f_{1s}(R)\int_{r \leq R}\psi_{1s}{}^2 d\tau +$$

$$\frac{e}{2}\left(1 - \frac{1}{D_s}\right)\int_{r \geq R}f_{1s}(r)\psi_{1s}{}^2 d\tau \tag{5}$$

where $D_s$ is the static dielectric constant of the medium

(4) D. A. Copeland, N. R. Kestner, and J. Jortner, *J. Chem. Phys.*, **53**, 1189 (1970).

(5) A. D. Buckingham, *Discuss. Faraday Soc.*, **24**, 151 (1967).

$(D_s = 80$ for water at 300°K and 3 for ice at 77°K[3]); $R$ is the distance between the center of the cavity and the inner boundary of the continuous medium; $R = r_d + r_s$ where $r_s$ is the radius of the solvent molecule, 1.4 Å. The long-range polarization potential, $f_{1s}$, is a self-consistent field potential which is obtained by solving Poisson's equation for the ground-state electron density.

In order to take into account short-range repulsive interactions, we include in the calculation a Wigner–Seitz potential, which was discussed by Copeland, *et al.*, in some detail.[4] The contribution of this term to the electronic energy is given by $V_0(1 - C_{1s})$, where $V_0$ is the energy of the quasi-free electron state and is actually treated as a parameter whose value is varied near zero. For $V_0 = 0$ this correction vanishes.

The energy, $E_v$, required to form a void in the medium also contributes to the medium rearrangement energy. $E_v$ is approximately given by

$$E_v = 4\pi(r_d^2 - r_s^2)\gamma \tag{6}$$

where $\gamma$ is the surface energy of the medium ($\gamma = 72$ ergs cm$^{-2}$ for water and 100 ergs cm$^{-2}$ for ice[6]).

Thus, the total ground-state energy is

$$E_t(1s) = E_k(1s) + E_{1s}{}^s +$$
$$E_{1s}{}^l + V_0(1 - C_{1s}) + E_v \tag{7}$$

where $E_k(1s)$ is the kinetic energy of the electron in its ground state.

In order to get the best wave function and energy value, $E_t(1s)$ is minimized with respect to a variational parameter in $\psi_{1s}$ for a fixed cavity radius. Such variational calculations are performed for various cavity radii to construct configuration coordinate diagrams for the solvated electron in its ground state.

The heat of solution, $\Delta H$, of the electron is given by

$$\Delta H = -E_t(1s)_{R = R_0} \tag{8}$$

where $E_t(1s)_{R = R_0}$ is the total ground-state energy at the minimum $(R = R_0)$ in its configuration coordinate curve.

The totally symmetric vibrational frequency, $\bar{\nu}_s$, of the ground state is obtained from the configuration coordinate curve[4]

$$\bar{\nu}_s = (^1/_2\pi c)(K/\mu)^{1/2} \tag{9}$$

where the force constant $K$ is $^1/_2(\partial^2 E_t/\partial R^2)_{R = R_0}$ and $c$ is the velocity of light. The effective mass, $\mu$, is taken to be $Nm_{H_2O}$ where $m_{H_2O}$ is the mass of the water molecule.

*C. Excited State.* The lowest optically excited state is the 2p state. This excited state is not an equilibrium state because of Franck–Condon restrictions. We choose a hydrogen-like 2p wave function for the excited state.[3]

The electronic energy for short-range attractive inter-

actions is given by

$$E_e{}^s(2p) = -\int_{r \leq r_d} \psi_{2p}\left(\frac{Ne\mu_0\langle\cos\theta\rangle_{1s}}{r_d{}^2} + \frac{Ne^2\alpha C_{2p}}{2r_d{}^4}\right)\psi_{2p}d\tau \tag{10}$$

$$C_{2p} = \int_{r \leq r_d} \psi_{2p}{}^2 d\tau$$

The dipole–dipole interaction energy between the oriented dipoles in the first solvation shell is

$$E_{dd}(2p) = \frac{D_N\mu_{2p}{}^2}{r_d{}^3} \tag{11}$$

$$\mu = \mu_0\langle\cos\theta\rangle_{1s} + \frac{e\alpha C_{2p}}{r_d{}^2}$$

The short-range interaction part, $E_{2p}{}^s$, of the total excited-state energy is given by

$$E_{2p}{}^s = E_e{}^s(2p) + E_{dd}(2p) \tag{12}$$

The long-range interaction part, $E_{2p}{}^l$, of the total excited-state energy is

$$E_{2p}{}^l = \frac{e}{2}\left(1 - \frac{1}{D_{0p}}\right)f_{2p}(R)\int_{r \leq R}\psi_{2p}{}^2d\tau +$$
$$\frac{e}{2}\left(1 - \frac{1}{D_{0p}}\right)\int_{r \geq R}f_{2p}(r)\psi_{2p}{}^2d\tau +$$
$$e\left(\frac{1}{D_{0p}} - \frac{1}{D_s}\right)f_{1s}(R)\int_{r \leq R}\psi_{2p}{}^2d\tau +$$
$$e\left(\frac{1}{D_{0p}} - \frac{1}{D_s}\right)\int_{r \geq R}f_{1s}(r)\psi_{2p}{}^2d\tau -$$
$$\frac{e}{2}\left(\frac{1}{D_{0p}} - \frac{1}{D_s}\right)f_{1s}(R)\int_{r \leq R}\psi_{1s}{}^2d\tau -$$
$$\frac{e}{2}\left(\frac{1}{D_{0p}} - \frac{1}{D_s}\right)\int_{r \geq R}f_{1s}(r)\psi_{1s}{}^2d\tau \tag{13}$$

Here $D_{0p}$ is the optical dielectric constant ($D_{0p} = 1.78$), and $f_{2p}$ is a self-consistent field potential which is obtained from Poisson's equation for the excited-state electron density.

Thus, the total excited-state energy is

$$E_t(2p) = E_k(2p) + E_{2p}{}^s + E_{2p}{}^l +$$
$$V_0(1 - C_{2p}) + E_v \tag{14}$$

where $E_k(2p)$ is the kinetic energy of the electron in its excited state and $V_0(1 - C_{2p})$ is the energy term arising from a Wigner–Seitz potential. $C_{2p}$ is the charge enclosed within radius $r_d$. $E_v$ is the same as that for the ground state.

$E_t(2p)$ is minimized with respect to a variational parameter in $\psi_{2p}$ for a fixed cavity radius. Such vari-

(6) N. H. Fletcher, "The Chemical Physics of Ice," Cambridge University Press, London, 1970, p 123.

ational calculations are carried out for various cavity radii to obtain configuration coordinate diagrams for the solvated electron in its excited state.

The 1s → 2p transition energy is given by

$$h\nu = E_t(2p)_{R=R_0} - E_t(1s)_{R=R_0} \quad (15)$$

where $E_t(2p)_{R=R_0}$ is the total excited-state energy at $R = R_0$.

The half-width, $\Delta$, of the absorption line arising from the 1s → 2p transition in the Franck–Condon region is obtained from the configuration coordinate diagrams for the ground and excited states.[4]

We can also calculate from the diagrams the energy difference, $h\nu_e$, between $E_t(1s)$ and $E_t(2p)$ at the cavity radius which gives the minimum excited-state energy; $h\nu_e$ corresponds to the transition energy for the 2p → 1s emission process, if it occurs.

*D. Conduction State.* The optically excited conduction state is not an equilibrium state, as is the case with the optically excited 2p state. The energy of the conduction state at its threshold, $E_t(\text{cond})$, is given by

$$E_t(\text{cond}) = V_0 + E_{dd}(\text{cond}) + \pi + E_v \quad (16)$$

Here only the permanent dipoles contribute to the short-range interaction energy, $E_{dd}(\text{cond})$, because the electron is completely delocalized in this state.

$$E_{dd}(\text{cond}) = \frac{D_N\mu_0^2\langle\cos\theta\rangle_{1s}^2}{r_d^3} \quad (17)$$

The long-range medium polarization energy, $\pi$, is

$$\pi = -\frac{e}{2}\left(\frac{1}{D_{0p}} - \frac{1}{D_s}\right)\int_{r\geq R} f_{1s}(r)\psi_{1s}^2 d\tau \quad (18)$$

Both $E_{dd}(\text{cond})$ and $\pi$ are determined by the ground-state wave function because of Franck–Condon restrictions.

The photoconductivity threshold energy, $I$, is obtained as

$$I = E_t(\text{cond})_{R=R_0} - E_t(1s)_{R=R_0} \quad (19)$$

*E. Relaxed Excited State.* The relaxed excited 2p state will be attained upon medium relaxation following an optical transition. The total energy, $E_t'(2p)$, of the relaxed excited state is given by

$$E_t'(2p) = E_k'(2p) + E_{2p}^{s'} +$$
$$E_{2p}^{1'} + V_0(1 - C_{2p}') + E_v \quad (20)$$

Here

$$E_{2p}^{s'} = E_e^{s'}(2p) + E_{dd}'(2p) \quad (21)$$

$$E_e^{s'}(2p) = -\int_{r\leq r_d}\psi_{2p}'\left(\frac{Ne\mu_0\langle\cos\theta\rangle_{2p}}{r_d^2} + \frac{Ne^2\alpha C_{2p}'}{2r_d^4}\right)\psi_{2p}'d\tau \quad (22)$$

$$\langle\cos\theta\rangle_{2p} = \coth y - \frac{1}{y}, \quad y = \frac{e\mu_0 C_{2p}'}{kT r_d^2}$$

$$E_{dd}'(2p) = \frac{D_N\mu_{2p}^{2'}}{r_d^3} \quad (23)$$

$$\mu_{2p}' = \mu_0\langle\cos\theta\rangle_{2p} + \frac{e\alpha C_{2p}'}{r_d^2}$$

$$E_{2p}^{1'} = \frac{e}{2}\left(1 - \frac{1}{D_s}\right)f_{2p}'(R)\int_{r\leq R}\psi_{2p}^{2'}d\tau +$$
$$\frac{e}{2}\left(1 - \frac{1}{D_s}\right)\int_{r\geq R}f_{2p}'(r)\psi_{2p}'d\tau \quad (24)$$

The 1s ground state which corresponds to the relaxed 2p state in the Franck–Condon region is not an equilibrium state. The total energy, $E_t'(1s)$, of the nonequilibrium ground state is given by the equation which is obtained by interchanging the 1s wave function with the 2p wave function in eq 14.

The energy of the 2p → 1s transition between the relaxed excited state and the nonequilibrium ground state is

$$h\nu_e' = E_t'(2p)_{R=R_e'} - E_t'(1s)_{R=R_e'} \quad (25)$$

where $E_t'(2p)_{R=R_e'}$ is the relaxed excited-state energy at the minimum $(R = R_e')$ in its configuration coordinate curve, and $E_t'(1s)_{R=R_e'}$ is the corresponding nonequilibrium ground-state energy.

## III. Results and Discussion

The results of the calculations are given in Figures 1–4 and in Tables I–VII. In the tables, $f$ is the oscillator strength and $r_v$ is the void radius defined as $r_v = r_d - r_s$. At the minimum of the configuration coordinate curve $r_v = r_v^0$. $C_{1s}(r)$ and $C_{2p}(r)$ are the charges enclosed within radius $r$ for the 1s and 2p states, respectively. Other symbols were defined in the previous section.

*A. Solvated Electron in Water.* Figure 1 shows configuration coordinate diagrams calculated for the solvated electron in water and $V_0 = 0$. The general features of the configuration coordinate diagrams for other values of $V_0$ are essentially the same as those in Figure 1 and are not shown here. The configurational stability of the electron cavity is established for the ground state at finite cavity radii for both $N = 4$ and 6. The configuration coordinate curves for the ground and excited states are asymmetric about their energy minima. The cavity radius for the 2p state at its energy minimum is considerably greater than that for the 1s state. The 2p state in the Franck–Condon region lies above the quasi-free electron state $[E_t(2p)_{R=R_0} > V_0]$ and below the conduction state (the curves indicated by "continuum" in Figure 1 show the bottom of the conduction bands). There is no minimum in the configuration coordinate curves (dashed line) for the relaxed 2p state, and the total energy decreases with de-

**Table I:** Calculated Properties for the Solvated Electron in Water at 300°K

| $N$ | $V_0$, eV | $h\nu$, eV | $f$ | $I$, eV | $h\nu_e$, eV | $\Delta H$, eV | $r_v^0$, Å | $\bar{\nu}_a$, cm$^{-1}$ | $\Delta$, eV | $\langle\cos\theta\rangle$ |
|---|---|---|---|---|---|---|---|---|---|---|
| 4 | +0.5 | 2.37 | 0.77 | 2.97 | 1.50 | 1.76 | 0.68 | 90 | 0.22 | 0.968 |
|   | 0.0 | 2.11 | 0.78 | 2.67 | 1.38 | 1.94 | 0.67 | 88 | 0.18 | 0.967 |
|   | −0.5 | 1.90 | 0.79 | 2.42 | 1.28 | 2.14 | 0.67 | 83 | 0.16 | 0.966 |
| 6 | +0.5 | 2.23 | 0.91 | 3.26 | 1.48 | 1.65 | 1.18 | 62 | 0.26 | 0.956 |
|   | 0.0 | 2.08 | 0.88 | 2.94 | 1.33 | 1.79 | 1.18 | 61 | 0.24 | 0.955 |
|   | −0.5 | 1.86 | 0.86 | 2.61 | 1.25 | 1.95 | 1.17 | 58 | 0.21 | 0.954 |

**Table II:** Various Energy Contributions to the Total Energy of the Solvated Electron in Water at 300°K and $V_0 = 0$ at $R_0$

Ground State

| $N$ | $E_k(1s)$, eV | $E_e^s(1s)$, eV | $E_e^1(1s)$, eV | $E_m^s(1s)$, eV | $E_m^1(1s)$, eV | $E_v$, eV | $E_t$, eV |
|---|---|---|---|---|---|---|---|
| 4 | 2.198 | −3.542 | −2.131 | 1.230 | 0.168 | 0.137 | −1.940 |
| 6 | 1.903 | −3.901 | −1.863 | 1.684 | 0.121 | 0.262 | −1.794 |

Excited State

| $N$ | $E_k(2p)$, eV | $E_e^s(2p)$, eV | $E_e^1(2p)$, eV | $E_m^s(2p)$, eV | $E_m^1(2p)$, eV | $E_v$, eV | $E_t$, eV |
|---|---|---|---|---|---|---|---|
| 4 | 1.376 | −0.546 | −1.842 | 0.607 | 0.438 | 0.137 | 0.170 |
| 6 | 1.773 | −1.354 | −1.798 | 1.119 | 0.286 | 0.262 | 0.288 |
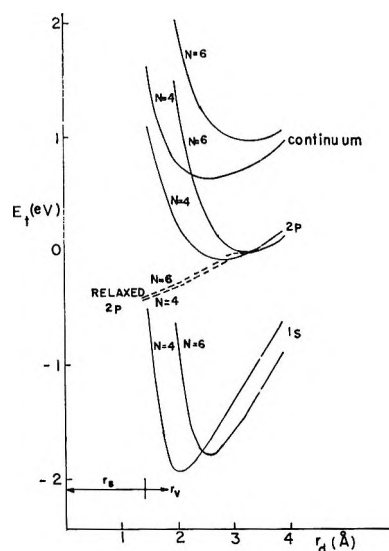


Figure 1. Configuration coordinate diagram for the solvated electron in water at 300°K for $V_0 = 0$.

creasing cavity radius. The energy difference between the relaxed 2p states for $N = 4$ and 6 is very small.

Table I shows various properties of the solvated electron in water at 300°K obtained in the present calculation. Table II shows the various energy contributions to the total energy. It is clear that the short-range interactions make very large contributions. The calculated 1s → 2p transition energies, $h\nu$, are compared reasonably to the observed transition energy, 1.73 eV,[7] at the absorption maximum, although they

tend to overestimate the experimental value. The calculations on the solvated electron in liquid ammonia overestimate $h\nu$ by a similar amount.[4] The value of $h\nu$ increases with increasing $V_0$ for both $N = 4$ and 6. It is also seen in Table I that the values of $h\nu$ for $N = 4$ and 6 are close to each other for the same value of $V_0$. Thus a distribution of different short-range molecular configurations is probable. The oscillator strength, $f$, is not very sensitive to the values of $V_0$ and $N$. The calculated $f$ is in reasonable agreement with the experimental value, 0.71,[7] which is a lower limit.[8]

The calculated threshold energy for photoconductivity, $I$, is significantly higher than the 1s → 2p transition energy. The difference between $h\nu$ and $I$ is greater for $N = 6$ than for $N = 4$. At present, there are no available experimental data on the photoconductivity threshold of the solvated electron in water. The energy difference, $h\nu_e$, between the 2p state at the energy minimum on its configuration coordinate curve and the corresponding 1s state is around 1.4 eV, which is considerably less than the calculated $h\nu$. Thus, if emission occurs from this 2p state at all, a significant Stokes shift would be observed in the spectrum. However, since the dielectric relaxation time of water is very short ($\sim$10$^{-11}$ sec) compared with the lifetime of the luminescent state, the 2p state would relax to yield the relaxed 2p state before emission occurs. We shall discuss the relaxed 2p state later.

(7) Reference 2, pp 40, 62.

(8) H. Hase and L. Kevan, J. Chem. Phys., 54, 908 (1971).

The calculated half-width, $\Delta$, of the absorption line arising from the 1s → 2p transition is about 0.2 eV and it is much narrower than the observed bandwidth, 0.93 eV,[7] of the absorption spectrum of the solvated electron in water. Transitions to higher excited states or directly to the continuum may possibly account for the observed bandwidth. However, it seems more probable that a distribution of short-range molecular configurations may account for the absorption bandwidth. From Figure 1 it can be seen that a distribution between $N = 4$ and $N = 6$ configurations will increase the bandwidth. Further theoretical work on the bandwidth and band shape is clearly of importance.

The calculated heats of solution, $\Delta H$, are in reasonable agreement with the experimental value, 1.7 eV.[7] The value of $\Delta H$ decreases with increasing $V_0$. For the same value of $V_0$, the value of $\Delta H$ for $N = 4$ is slightly greater than that for $N = 6$. In other words, the electron cavity for $N = 4$ is energetically more stable than that for $N = 6$. A similar result was obtained by Copeland, et al.,[4] for the solvated electron in liquid ammonia.

The void radius, $r_v{}^0$, depends on $N$, but it is insensitive to $V_0$. The value of $r_v{}^0$ for $N = 6$ is greater than that for $N = 4$. It should be noted that $r_v{}^0$ is different from the "effective" cavity radius defined in ref 4. The effective cavity radius includes the fact that the first solution shell around the cavity has a lower density than the bulk medium. The effective volume of the hydrated electron is estimated to be 25 ml mol$^{-1}$ for $N = 4$ and 40 ml mol$^{-1}$ for $N = 6$. The former value is close to a recent experimental estimate[9] for the upper limit of the hydrated electron volume, 20 ml mol$^{-1}$, while earlier experimental estimates give lower values.[10] Although a good experimental value of the molal volume is not available, the $N = 4$ model seems strongly favored over the $N = 6$ model for this particular hydrated electron property.

The vibrational frequency, $\bar{\nu}$, of the cavity for the ground state is also given in Table I. The value of $\bar{\nu}_s$ for $N = 4$ is somewhat higher than that for $N = 6$, and it is not very sensitive to $V_0$ over the range of $V_0$ studied.

The average angle of orientation of the water dipoles in the first solvation shell is obtained from $\langle \cos \theta \rangle$ in Table I to be ~15° for $N = 4$ and ~17° for $N = 6$.

Figure 2 shows the fraction of the solvated electron in water within radius $R$ plotted as a function of radius $r_d$. The fraction, $C_{1s}(R)$, of the solvated electron in its ground state within $R$ (curve a for $N = 4$ and curve a′ for $N = 6$) has a maximum at a value of $r_d$ which is somewhat smaller than the radius corresponding to the configurational minimum, and decreases gradually with increasing $r_d$ for greater values of $r_d$. The fraction, $C_{2p}(R)$, of the solvated electron in its excited state within $R$ (curve b for $N = 4$ and curve b′ for $N = 6$) increases with increasing $r_d$ and approaches a constant value at large values of $r_d$.
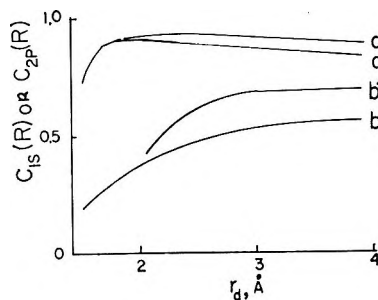


Figure 2. Fraction of the solvated electron in water at 300°K within radius $R$ vs. cavity radius for $V_0 = 0$: a, $C_{1s}$, $N = 4$; b, $C_{2p}$, $N = 4$; a′, $C_{1f}$, $N = 6$; b′, $C_{2p}$, $N = 6$.

Table III shows the charge distributions of the hydrated electron in the ground and excited states at $R_0$ and corresponding other radii. The charges enclosed within radii $r_v{}^0$, $r_d{}^0$, and $R_0$ increase with increasing $V_0$, respectively. The charge enclosed within a specified radius for $N = 6$ is greater than that within the same radius for $N = 4$. It is seen in Table III that a major fraction of the electron population in the ground state is found in a spherical shell between $r_v{}^0$ and $R_0$, i.e., in the first solvation shell. The charge distribution of the excited state is much more diffuse than that of the ground state. The charge enclosed within $r_v{}^0$ is very small for the excited state. About half of the electron population in the excited state is outside the first solvation shell.

We now consider the relaxed excited state. Table IV shows some properties of the hydrated electron in the relaxed excited state at its energy minimum ($r_v = 0$ or $r_d = 1.4$ Å) for $V_0 = 0$ and in the corresponding nonequilibrium ground state. The relaxed 2p state is much lower in energy than the unrelaxed 2p state for small cavity radii (see Figure 1), and it lies below the quasi-free electron state ($V_0 = 0$) by about 0.4 eV. Thus, once the optically excited 2p state relaxes to yield the completely relaxed 2p state, this state would not autoionize into the conduction state. We caution that this conclusion is based on the approximations inherent in our model and that the 2s state, which has not yet been calculated, may complicate the relaxation processes. Since the calculated transition energies, $h\nu_e'$, between the relaxed 2p state and the corresponding 1s state are 0.3–0.4 eV, the emission spectrum would not be observed in the visible and near-infrared region, if such a transition occurs at all. It is seen in Table IV that the charge distribution of the hydrated electron in the relaxed 2p state is very diffuse and the electron is almost completely outside the first solvation shell. Such a large electron orbital in the relaxed 2p state is responsible for lowering its energy, because a very weak

(9) U. Schindewolf, H. Kohramann, and G. Lang, *Angew. Chem., Int. Ed. Engl.*, **8**, 512 (1969).

(10) R. R. Hentz, Farhataziz, and D. J. Milner, *J. Chem. Phys.*, **47**, 5381 (1967).

**Table III**: Charge Distribution of the Solvated Electron in Water at 300°K at Radii
Corresponding to the Configurational Minimum Energy of the Ground State

| N | $V_0$, eV | Ground state $C_{1s}(r_v^0)$ | $C_{1s}(r_d^0)$ | $C_{1s}(R_0)$ | Excited state $C_{2p}(r_v^0)$ | $C_{2p}(r_d^0)$ | $C_{2p}(R_0)$ |
|---|---|---|---|---|---|---|---|
| 4 | +0.5 | 0.101 | 0.645 | 0.914 | 0.002 | 0.132 | 0.458 |
|   | 0.0 | 0.089 | 0.616 | 0.899 | 0.002 | 0.111 | 0.410 |
|   | −0.5 | 0.070 | 0.578 | 0.881 | 0.001 | 0.086 | 0.345 |
| 6 | +0.5 | 0.259 | 0.727 | 0.928 | 0.037 | 0.347 | 0.707 |
|   | 0.0 | 0.243 | 0.703 | 0.918 | 0.027 | 0.275 | 0.629 |
|   | −0.5 | 0.213 | 0.676 | 0.904 | 0.017 | 0.222 | 0.553 |

**Table IV**: Calculated Properties for Solvated Electrons in the Relaxed, Excited,
and Nonequilibrium Ground States for $V_0 = 0$ at $r_d = 1.4$ Å

| N | $E_t'(1s)$, eV | $E_t'(2p)$, eV | $h\nu_e'$, eV | $C_{1s}'(r_d)$ | $C_{1s}'(R)$ | $C_{2p}'(r_d)$ | $C_{2p}'(R)$ |
|---|---|---|---|---|---|---|---|
| | | | Water at 300°K | | | | |
| 4 | −0.829 | −0.424 | 0.405 | 0.057 | 0.250 | 0.002 | 0.031 |
| 6 | −0.740 | −0.411 | 0.329 | 0.040 | 0.190 | 0.001 | 0.023 |
| | | | Ice at 77°K | | | | |
| 4 | −0.426 | −0.193 | 0.233 | 0.036 | 0.171 | 0.000 | 0.007 |
| 6 | −0.390 | −0.187 | 0.203 | 0.026 | 0.134 | 0.000 | 0.005 |

local-field strength on the water dipoles in the first solvation shell results in a remarkable decrease in the effective dipole–dipole repulsion energy. It is noted that a very diffuse charge distribution has also been calculated for the relaxed excited state of the F-center.[11]

*B. Trapped Electron in Ice.* Figure 3 shows configuration coordinate curves for the trapped electron in ice at 77°K at $V_0 = 0$. The general features of the curves are similar to those in Figure 1. It is seen, however, that the total energies of trapped electrons in ice in the ground and excited states are significantly higher than those of solvated electrons in water. This difference arises from the weaker long-range interactions characterized by $D_s = 3$ for ice compared with $D_s = 80$ for water. The 2p state lies well above the quasi-free electron state in the Franck–Condon region. This 2p state is closer in energy to the bottom of the conduction band than is the case with the solvated electron in water.

Table V shows various properties of the trapped electron in ice at 77°K. Table VI shows the various energy contributions to the total energy. If Table VI is compared to Table II the effect of decreasing the long-range contributions to the trapping potential by decreasing the static dielectric constant can be directly seen. The short-range interactions become relatively much more important in ice at 77°K compared with water at 300°K. The 1s → 2p transition energy calculated for $V_0 = 0$ in ice is in quantitative agreement with the ob-
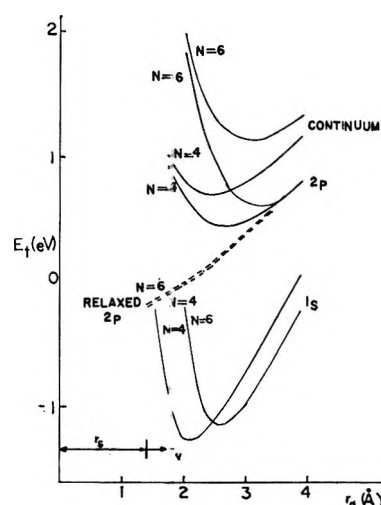


Figure 3. Configuration coordinate diagram for the trapped electron in ice at 77°K for $V_c = 0$.

served transition energy 1.97 eV.[7] It is true that $h\nu$ (water) $> h\nu$ (ice) at $V_0 = 0$, which is opposite to experiment, but both $h\nu$ values are comparable so small differences are hard to predict. The oscillator strength for $N = 4$ is significantly smaller than that for $N = 6$. The same trend was observed for the hydrated electron in water, but the results in ice are much more pronounced. No experimental value of $f$ has been reported for the trapped electron in pure ice, but a value of $f \geq 0.86$

(11) W. B. Fowler, *Phys. Rev.*, **135**, A1725 (1964).

**Table V: Calculated Properties for the Trapped Electron in Ice at 77°K**

| N | $V_0$, eV | $h\nu$, eV | $f$ | $I$, eV | $h\nu_e$, eV | $\Delta H$, eV | $r_v{}^0$, Å | $\bar\nu_s$, cm⁻¹ | $\Delta$, eV | $\langle \cos\theta \rangle$ |
|---|---|---|---|---|---|---|---|---|---|---|
| 4 | +0.5 | 2.15 | 0.55 | 2.33 | 1.55 | 1.10 | 0.72 | 83 | 0.07 | 0.991 |
|   | 0.0 | 1.90 | 0.50 | 2.09 | 1.41 | 1.29 | 0.71 | 82 | 0.06 | 0.991 |
|   | −0.5 | 1.62 | 0.51 | 1.77 | 1.26 | 1.49 | 0.71 | 77 | 0.06 | 0.991 |
| 6 | +0.5 | 2.28 | 0.86 | 2.78 | 1.55 | 1.02 | 1.21 | 64 | 0.11 | 0.985 |
|   | 0.0 | 2.00 | 0.82 | 2.51 | 1.42 | 1.16 | 1.21 | 63 | 0.10 | 0.988 |
|   | −0.5 | 1.75 | 0.76 | 2.06 | 1.27 | 1.32 | 1.20 | 60 | 0.09 | 0.988 |

**Table VI: Various Energy Contributions to the Total Energy of the Trapped Electron in Ice at 77°K and $V_0 = 0$ at $R_0$**

Ground State

|  | $E_k(1s)$, eV | $E_e{}^s(1s)$, eV | $E_e{}^1(1s)$, eV | $E_m{}^s(1s)$, eV | $E_m{}^1(1s)$, eV | $E_v$, eV | $E_t$, eV |
|---|---|---|---|---|---|---|---|
| 4 | 2.144 | −3.550 | −1.444 | 1.256 | 0.118 | 0.190 | −1.286 |
| 6 | 1.822 | −3.831 | −1.242 | 1.621 | 0.083 | 0.385 | −1.162 |

Excited State

| N | $E_k(2p)$, eV | $E_e{}^s(2p)$, eV | $E_e{}^1(2p)$, eV | $E_m{}^s(2p)$, eV | $E_m{}^1(2p)$, eV | $E_v$, eV | $E_t$, eV |
|---|---|---|---|---|---|---|---|
| 4 | 0.732 | −0.196 | −1.092 | 0.562 | 0.416 | 0.190 | 0.612 |
| 6 | 1.499 | −1.146 | −1.234 | 1.060 | 0.271 | 0.385 | 0.835 |

for the electron in alkaline ice (10 $M$ NaOH) has been determined.[8] This compares well with the calculated values for $f$ with $N = 6$.

The photoconductivity threshold is not far from the 2p state for $N = 4$. The calculated results show that the photoconductivity threshold for the trapped electron in ice is considerably lower than that for the solvated electron in water. Recent photoconductivity[12] and optical bleaching[13] studies of trapped electrons in alkaline ice indicate that there are no stable bound excited states for the trapped electron in alkaline ice. The present model does not explain satisfactorily this observation. The difference in energy between the 2p state at the energy minimum on its configuration coordinate curve and the corresponding 1s state is about 1.4 eV, which is considerably less than $h\nu$. If emission occurs from this 2p state, the emission spectrum would be observed at ~900 nm. However, no emission was found in this region for photoexcited electrons in alkaline ice.[14]

The calculated half-width of the absorption line arising from the 1s → 2p transition is about 0.1 eV and is much narrower than the observed bandwidth, 0.29 eV.[7]

The void radius and the vibrational frequency of the cavity for the trapped electron in ice are about the same as those for the solvated electron in water. It is interesting that the vibrational frequency of the cavity is of about the same magnitude as the frequency, 65 cm⁻¹, of the lowest translational mode of lattice vibration in an ice crystal.[15]
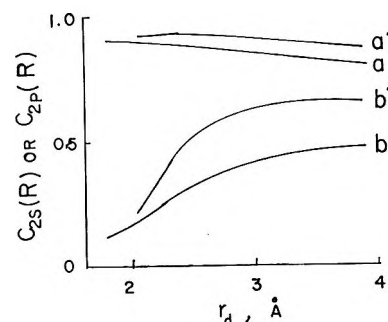
Figure 4. Fraction of the trapped electron in ice at 77°K within radius $R$ vs. cavity radius for $V_0 = 0$; a, $C_{1s}$, $N = 4$; b, $C_{2p}$, $N = 4$; a′, $C_{1s}$, $N = 6$; b′, $C_{2p}$, $N = 6$.

Figure 4 shows the fraction of the trapped electron in ice within radius $R$ plotted as a function of radius $r_d$. The general behavior of the curves in Figure 4 is similar to that in Figure 2.

Table VII shows the charge distributions of trapped electrons in ice. The charge distribution of the trapped electron in ice in its ground state is similar to that of the solvated electron in water, while the charge distribution of the excited state is more diffuse for ice than for water. Such a difference in the excited-state charge distribution arises from the weaker long-range interactions for the

(12) I. Eisele and L. Kevan, *J. Chem. Phys.*, **53**, 1867 (1970).

(13) P. Hamlet and L. Kevan, *J. Amer. Chem. Soc.*, **93**, 1102 (1971).

(14) H. Hase and L. Kevan, unpublished results.

(15) Reference 6, p 137.

**Table VII:** Charge Distribution of the Trapped Electron in Ice at 77°K at Radii
Corresponding to the Configurational Minimum Energy of the Ground State

| $N$ | $V_0$, eV | Ground state | | | Excited state | | |
|---|---|---|---|---|---|---|---|
| | | $C_{1s}(r_v{}^0)$ | $C_{1s}(r_d{}^0)$ | $C_{1s}(R_0)$ | $C_{2p}(r_v{}^0)$ | $C_{2p}(r_d{}^0)$ | $C_{2p}(R_0)$ |
| 4 | +0.5 | 0.109 | 0.641 | 0.909 | 0.001 | 0.063 | 0.272 |
| | 0.0 | 0.087 | 0.607 | 0.894 | 0.001 | 0.039 | 0.195 |
| | −0.5 | 0.078 | 0.569 | 0.871 | 0.000 | 0.031 | 0.162 |
| 6 | +0.5 | 0.245 | 0.724 | 0.929 | 0.026 | 0.296 | 0.655 |
| | 0.0 | 0.240 | 0.702 | 0.915 | 0.020 | 0.236 | 0.568 |
| | −0.5 | 0.222 | 0.673 | 0.900 | 0.014 | 0.162 | 0.447 |

electron in ice. The long-range interactions play a more important role in the excited state.

The relaxed 2p state at its energy minimum at $r_d = r_s$ lies below the quasi-free electron state by about 0.2 eV (Table IV). The transition energy between the relaxed 2p state and the corresponding nonequilibrium 1s state is calculated to be about 0.2 eV. If the time for this process is long, the optically excited 2p state may decay *via* other pathways. The relaxation time in bulk ice is not appropriate to this problem because the strong electric field of the electron greatly shortens this time. Recent pulse radiolysis work on trapped electrons in various glassy matrices demonstrates this.[16,17] Further work is required on the relaxation processes following optical excitation of trapped or solvated electrons and the formation of mobile conducting states.

In summary, the model used herein demonstrates a configurational minimum in the ground-state energy for electrons in water and ice. This allows the prediction of a unique cavity radius within the framework of the approximations used. The calculated results are generally in semiquantitative agreement with experimental values, but certain discrepancies remain with regard to absorption bandwidth and relaxation processes following optical excitation.

(16) J. T. Richards and J. K. Thomas, *J. Chem. Phys.*, **53**, 218 (1970).

(17) L. Kevan, to be published.

# Corresponding States and the Glass Transition for Alkali Metal Nitrates

## by C. A. Angell* and D. B. Helphrey

*Department of Chemistry, Purdue University, Lafayette, Indiana 47907*   *(Received August 10, 1970)*

*Publication costs assisted by the National Science Foundation*

In order to establish a set of corresponding temperatures for the much-studied molten alkali metal nitrates, estimates of the "ideal" glass transition temperatures for $NaNO_3$ and $KNO_3$ are made from available thermodynamic data and shown consistent with "experimental" glass transition temperatures obtained by extrapolation from binary solution (hydrate melt) data. $T_g$ values are obtained in the same manner for the other alkali metal nitrates, Li, Rb, and $CsNO_3$, the spread of values among the five salts found being only 18°, thereby largely justifying isothermal comparisons of their properties despite the 160° spread in melting points. The order–disorder transition in sodium nitrate is examined and the relation of this class of transition to the glass transition phenomenon is considered. Equations from a zeroth-order, order–disorder theory for the glass transition are used to give a qualitative account of the change in heat capacity at the glass transition for sodium nitrate.

The alkali metal nitrates are among the most studied of molten salts. Since it has proved possible to correlate, and simplify interpretation of, a number of aspects of the physicochemical behavior of binary fused salt solutions by recognizing that these liquids all tend on cooling towards a glassy condition reached at a characteristic temperature for each liquid,[1] it is of interest to decide whether definite glass transition temperatures can be measured or inferred for the pure alkali nitrates. The purpose of this short paper is to affirm that such temperatures can be assigned, by predicting theoretical glass transition temperatures using only equilibrium thermodynamic data, and then showing that very reasonable extrapolations of measured glass transition temperatures in appropriate binary solutions are in good accordance with the thermodynamic predictions. These values turn out to conflict with previous estimates based on cation charge/radius ratios, while confirming a previously noted parallel in the relaxational behavior of lithium and sodium ions in their nitrate melts.

According to our ideas these studies define a useful set of corresponding temperature bases for use in interpreting other physicochemical properties of the solutions. That they also provide a novel means of detecting interactions between ionic species in these melts will be shown in subsequent papers.

The thermodynamic estimates of the alkali metal nitrate glass transition temperatures are based on the observation, first made by Kauzmann,[2] that the rate at which entropy is lost from a supercooling liquid is generally so much greater than that at which entropy is lost from the stable crystalline phase cooling in the same temperature region, that were it not for the intervention of the glass transition phenomenon the liquid would reach a state of lower entropy than the crystal well before the temperature could fall to 0°K. The glass transition phenomenon, at which the heat capacity changes rather abruptly under nonequilibrium condi-

tions to a value essentially that of the crystal, always intervenes before this interesting equilibrium problem can be resolved.

Although Kauzmann considered the resolution of the equilibrium problem to lie in an impending irreversible crystallization, Gibbs and Dimarzio[3] argued that the intervention of the glass transition was no accident but rather a direct consequence of the approach of the system to a configurational ground state. Their theory indicated a second order-thermodynamic transition at a temperature $T_0$ consequent on the vanishing of the liquid excess entropy.

Regardless of whether the normal liquid regime is terminated by such a second-order transition or by a (dynamically more appealing) rapid decrease in heat capacity, as for an "Einstein" crystal, as $kT$ falls below some critical energy related to the energy spacing of the implied configurational microstates (see Discussion), it is clear that in the metastable equilibrium phase $C_p$ and $C_v$ must change value before 0°K, and that the lower limit on the temperature at which the change has to occur during cooling can be determined from known heat capacity data for the liquid and crystalline states and the entropy of fusion. A suitable graphical method of finding this limiting temperature,[4] called in this work the "ideal glass transition temperature," is shown in Figure 1 for the cases of $NaNO_3$, and $KNO_3$, for which excellent thermodynamic data are available in the work of Shmidt.[5] It is assumed that the supercooled liquid retains the same temperature-independent heat capacity as its exhibits above the melting point. This

(1) (a) C. A. Angell, *J. Phys. Chem.*, **70**, 2793 (1966); (b) *J. Chem. Phys.*, **46**, 4673 (1967).

(2) W. Kauzmann, *Chem. Rev.*, **43**, 219 (1948).

(3) J. H. Gibbs and E. A. Dimarzio, *J. Chem. Phys.*, **28**, 373 (1958).

(4) C. A. Angell and C. T. Moynihan, "Molten Salts: Characterization and Analysis," G. Mamantov, Ed., Marcel Dekker, New York, N. Y., 1969, p 315.

value of $C_p$ is extrapolated into the supercooled region to a point ($T_0$) at which the area between the crystalline heat capacity curve and the extrapolated liquid heat capacity curve is exactly equal to the total area representing the entropy of fusion plus the entropies of all solid-state transitions occurring above $T_0$. By this construction, then, the supercooled liquid would have the same total entropy as the stable crystalline phase at $T_0$. Discounting the unlikely case in which the amorphous phase has a lower vibrational heat capacity than the stable crystalline form (usually it is observed to be slightly larger), $T_0$ therefore stands as a lower limit of the temperature range through which the supercooled liquid could persist with constant heat capacity.
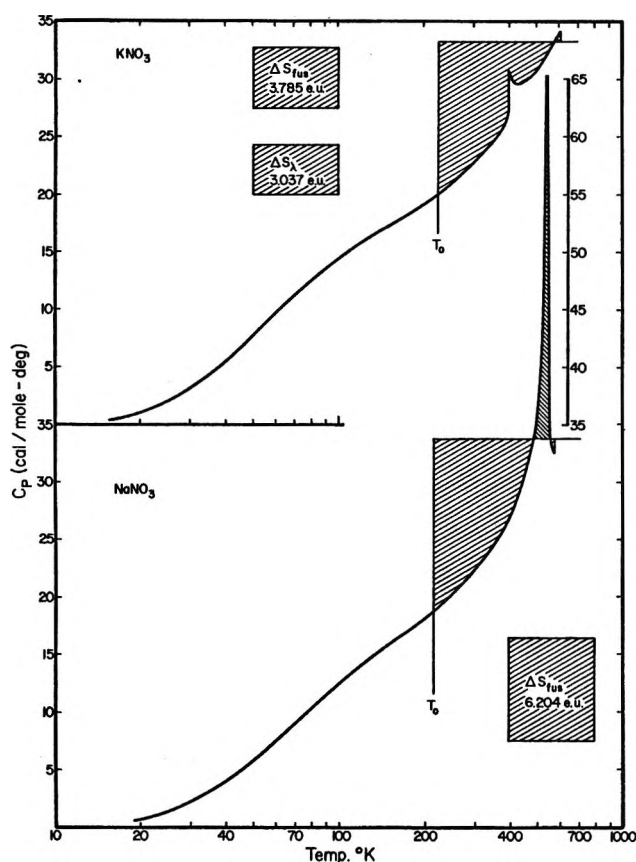


Figure 1. Heat capacity plots for $KNO_3$ and $NaNO_3$ crystal and liquid, showing estimation of "ideal" glass temperatures.

Only for $NaNO_3$ and $KNO_3$ among the alkali nitrates are sufficient heat capacity data available for this calculation to be performed. Suitable data are also available for $AgNO_3$[5c] and $NH_4NO_3$[6] although the anomalous increasing liquid heat capacity for $AgNO_3$, and the presence of no less than four solid state transitions, and some uncertainty in the liquid heat capacity for $NH_4$-$NO_3$, make the calculation less reliable in these cases. The "ideal" glass temperatures for sodium and potassium nitrates are found (from Figure 1) to lie at 218

and 224°K, respectively. That for $NH_4NO_3$ falls lower at 165°K, while for $AgNO_3$ a higher $T_0$, $\sim 260$°K, is indicated for the improbable case in which $C_p$ (liquid) continues to increase well below $T_F$.

Measurement of an experimental quantity to compare with these calorimetric "ideal" glass temperatures presents problems. Although the formation of glasses from pure $NaNO_3$ and $KNO_3$ by quenching tiny liquid droplets has been reported by Tammann and Elbrachter,[7] our attempts to produce useful experimental amounts of such glasses for glass transition temperature determinations have not to date been successful. Low-melting mixtures of nitrates may be obtained as thin sheets of glassy appearance by pressure pulse splat quenching onto copper sheet at $-196°$; however, except for some compositions in the $LiNO_3$–$NH_4NO_3$ system these preparations exhibited a succession of irreversible crystallizations rather than a glass transition during warm-up.[8] There is also some doubt that glass transition temperatures measured in the eutectic regions of such systems would provide an accurate guide to the glass temperatures of the pure salts because of deviations from $T_g$ additivity indicated by electrical conductance measurements.[1b] Finally we have chosen to estimate $T_g$ for pure nitrates by extrapolations of glass temperatures measured over substantial glass-forming composition regions in "hydrate melt" type binary solutions,[9] in which $T_g$ seems to be a quite linear function of composition. Changes in $T_g$ across these systems are small and molar volumes in a representative case, Ca-$(NO_3)_2 \cdot 4H_2O$ + $KNO_3$, are found to be additive within experimental error.[10] Thus although calorimetric data are not available to establish ideal mixing behavior, it seems the extrapolations should be fairly reliable.

For the present work the hydrate $Cd(NO_3)_2 \cdot 4H_2O$ was chosen as the second component. This salt has properties very similar to those of $Ca(NO_3)_2 \cdot 4H_2O$ but the $Cd^{2+}$ ion appears, from pmr studies,[11] to bind the water molecules somewhat more strongly than $Ca^{2+}$ thus reducing the effects of constitutional changes due to water displacement into the alkali metal cation coordination with increasing alkali nitrate concentration.[12]

(5) (a) V. A. Sokolov and N. E. Shmidt, Izv. Sekt. Fiz. Khim. Anal. Inst. Obshch. Neorg. Khim. Akad. Nauk SSSR, 26, 123 (1955); (b) V. A. Sokolov and N. E. Shmidt, ibid., 27, 217 (1956); (c) The results of these authors for sodium nitrate have been confirmed to 0.2% by the more recent work of W. C. Reinsborough and F. W. Wetmore, Aust. J. Chem., 20, 1 (1967). AgNO_3 was also studied by the latter authors.

(6) M. Nagatani, T. Seiyama, M. Sakiyama, H. Suga, and S. Seki, Bull. Chem. Soc. Jap., 40, 1833 (1967).

(7) G. Tammann and E. Elbrachter, Z. Anorg. Allg. Chem., 267, 268 (1932).

(8) D. B. Helphrey, unpublished work. LiNO_3 (40%) + NH_4NO_3 (60%) yielded a T_g of 231°K, while for 1:1 AgNO_3 + TlNO_3 eutectic, T_g was found, surprisingly, at a higher temperature, 242°K.

(9) C. A. Angell, J. Electrochem. Soc., 112, 1225 (1965).

(10) J. Braunstein, L. Orr, and W. Macdonald, J. Chem. Eng. Data, 12, 415 (1967).

(11) C. T. Moynihan, C. R. Smalley, C. A. Angell, and E. J. Sare, J. Phys. Chem., 73, 2287 (1969).
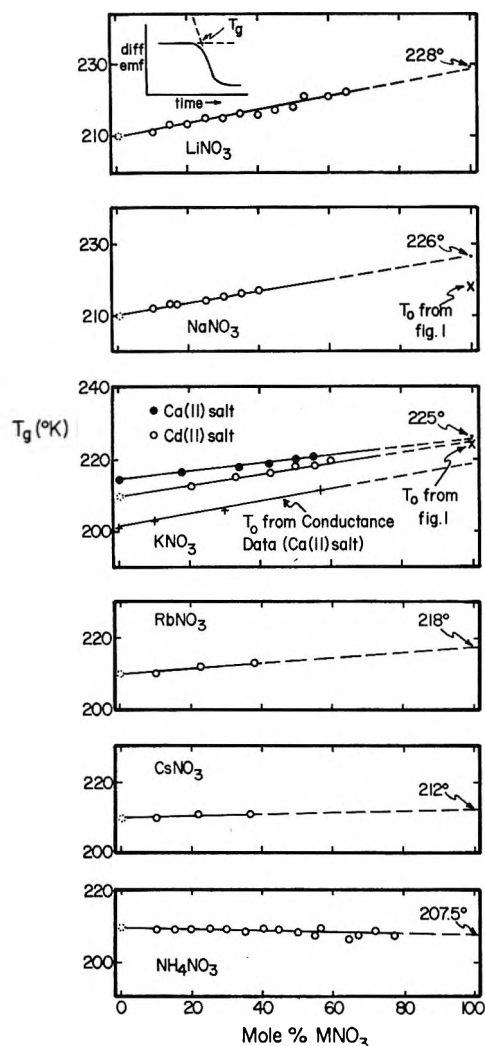
Figure 2. Experimental glass transition temperatures for
$Cd(NO_3)_2 \cdot 4H_2O$ + alkali metal nitrate and ammonium
nitrate showing extrapolations to obtain estimates for $T_g$ of
pure alkali nitrates. Also included are $T_g$ and $T_0$ (from
conductance measurements) values for $Ca(NO_3)_2 \cdot 4H_2O$ +
$KNO_3$ solutions (see ref 9 and 14). Inset, differential emf–time
trace showing definition of $T_g$.

## Experimental Section

*Materials.* $Cd(NO_3)_2 \cdot 4H_2O$ was the Mallinckrodt
reagent grade product. $LiNO_3$, $NaNO_3$, and $KNO_3$
were Baker Analyzed materials while $RbNO_3$ and $Cs$-
$NO_3$ were "99.9% pure" products from Alfa Inorganics.
All salts were used without further purification.

*Procedure.* All test solutions were made up individ-
ually, to avoid the possibility of systematic errors in
composition or possible cumulative losses of water from
the solutions. $T_g$ values were determined by a simple
dta method described elsewhere,[13] differential and
absolute temperatures being recorded as chromel-
alumel thermocouple output using a Honeywell Elec-
tronic 19 two-pen recorder. A full-scale sensitivity of
0.1 mV was utilized to record the differential thermo-
couple output. A heating rate of 8° min⁻¹ was adopted
for all determinations. $T_g$ was assessed from the data

trace as indicated in the inset to Figure 2, and values
are believed accurate to $\pm 1°$.

## Results

Results for the five $Cd(NO_3)_2 \cdot 4H_2O$ + $M(1)NO_3$
systems studied and an independently obtained set of
data for the system $Ca(NO_3)_2 \cdot 4H_2O$ + $KNO_3$,[14] are
displayed in Figure 2. The value for $Cd(NO_3)_2 \cdot 4H_2O$
(which is not itself glass-forming) is interpolated from
data on $Cd(NO_3)_2$ + $H_2O$ solutions both richer and
poorer in $H_2O$ than the stoichiometric compound.[11]

There seems no reason to doubt that the linear repre-
sentation of the data is correct, and the extrapolations
to the pure $M(1)NO_3$ component accordingly appear
very reasonable. The case most open to question on
grounds of complications due to possible alkali metal
hydration in the binary solutions is, of course, $LiNO_3$,
yet next to $NH_4NO_3$ this salt with $Cd(NO_3)_2 \cdot 4H_2O$
provides the greatest range of glass-forming solutions,
hence best established case of linear composition de-
pendence for $T_g$. Furthermore, the extrapolated $T_g$
value for $LiNO_3$ lies within 4° of the directly measured
value for the $LiNO_3$–$NH_4NO_3$ anhydrous eutectic (see
ref 8): the excess of measured $T_g$ for this eutectic
over the additive value, based on component $T_g$ values
from Figure 2, is in the direction expected from ref 1b.
(It is hoped to explore this matter in more detail when
improved splatting techniques become available, since
a single result for a $LiNO_3$–$KNO_3$ eutectic, indicates $T_g$
only 3° in excess of the value expected from additivity
of component $T_g$ values.)

## Discussion

The extrapolations of $T_g$ (also $T_0$ in the $KNO_3$ case)
yield $T_g$ (also $T_0$) values for the pure $NaNO_3$ and $KNO_3$
components in quite surprising accord with the vanish-

(12) Although evidence against any marked effect of added $KNO_3$
on such displacement is available for $Ca(NO_3)_2 \cdot 4H_2O$ + $KNO_3$ solu-
tions at room temperature [C. T. Moynihan and A. Fratiello, *J.
Amer. Chem. Soc.*, **89**, 5546 (1967)] there are a number of indications,
from studies of the room temperature water concentration depen-
dence of vibration spectra [D. E. Irish, C. Chang, and D. L. Nelson,
*Inorg. Chem.*, **9**, 425 (1970); V. S. Ellis and R. E. Hester, *J. Chem.
Soc. A*, 607 (1969)], and fixed composition temperature dependence
of pmr chemical shifts (C. T. Moynihan, E. J. Sare, and C. A.
Angell, unpublished work), that at molten hydrate compositions
there occurs an exchange equilibrium involving nitrate anions and
water molecules in the first cation coordination sheath. Some
effects, on this exchange, of added alkali metal nitrate are to be
expected. Their importance, however, is not easily anticipated
since, at these molten salt like compositions, the nitrate ion concen-
tration is little affected by additions of more nitrate ion; the nitrate–
water ratio in the immediate divalent cation environment need not
change. Although structural complications due to such possible
exchanges may be in principle undesirable to the present purposes,
the fact is that composition-dependent constitutional changes will
not affect our ability to make reliable extrapolations provided they
occur progressively with, and in proportion to, composition changes.
It is fortunate in this respect that the two cases of maximum glass-
forming composition range (both of which show linear $T_g$-composi-
tion relations) involve almost opposite extremes, $NH_4^+$ and $Li^+$,
in competition for $H_2O$ coordination.
(13) C. A. Angell and E. J Sare, *J. Chem. Phys.*, **52**, 1058 (1970).
(14) We are grateful to Dr. E. J. Sare for permission to include his
data for this system in support of the present measurements.

ing excess entropy temperature $T_0$ obtained from the thermal data. In each case $T_0$ lies below $T_g$ as it should if $T_g$ is set not by the actual vanishing of the excess entropy but by its reaching some relaxation-time-limited small positive value.[15] We consider, then, that this work establishes for alkali metal nitrates a set of corresponding temperatures at which the excess entropy reaches some fixed small positive value. If we take $T_0$ literally, maintaining that in a hypothetical equilibrium experiment $C_p$ would actually change value discontinuously at this temperature as drawn in Figure 1 (see discussion below), or alternatively if we define $T_0$ operationally according to Figure 1, we can give a set of zero excess entropy temperatures which although less definite in value, are in some ways more satisfying to use than the experimental time-scale-dependent $T_g$ values. Since we have found[16] many cases of glass-forming liquids for which the $T_0$ assessed from thermal data as in Figure 1 falls within 5° or less of the best fit value of $T_0$ obtained from transport data by VTF eq 4, we will use the transport $T_0$ values known for the $KNO_3$–$Ca(NO_3)_2$· $4H_2O$ case[9] (see Figure 2c) to assign $T_0$ values for the alkali nitrates. These are taken to lie 10° (approx 5%) below the extrapolated $T_g$ values; both $T_g$ and $T_0$ thus defined are collected in Table I, where they are compared with the erratically ordered melting points, $T_F$, for this series.

**Table I:** Experimental (8°/min) and Ideal Glass Temperatures for Alkali Metal Nitrates

| Salt | $T_g$ | $T_0$ | $T_F$ |
|------|-------|-------|-------|
| $LiNO_3$ | 228 | 218 | 527 |
| $NaNO_3$ | 226 | 216 | 583 |
| $KNO_3$ | 225 | 215 | 610 |
| $RbNO_3$ | 218 | 208 | 589 |
| $CsNO_3$ | 212 | 202 | 690 |

The dependence of these corresponding temperatures on cation type is unexpectedly small and is in sharp conflict with corresponding temperatures previously assigned to alkali metal nitrates on the basis of cation radii[17] and anion–cation radius sums[18] (according to which largest differences should occur between the $Li^+$, $Na^+$, and $K^+$ cases). On the other hand, the near identity of $T_0$ values for $LiNO_3$ and $NaNO_3$ is quite consistent with observations made above $T_m$ that $LiNO_3$ is in some respects similar to $NaNO_3$ in its transport behavior.[17,19] In particular, a discrepancy between $LiNO_3$ and $KNO_3$ in the correlation,[17] with $T/T_0$, of deviations from the Nernst–Einstein relation between equivalent conductance, $\Lambda$, and ionic diffusivity, $D_i$

$$\Lambda = \frac{F^2}{RT}(Z_+D_+ + Z_-D_-)$$

(where $Z$ is the ionic charge), is largely removed by the

new assignments. An interesting consequence of the new correlation is the indication that the Nernst–Einstein equation should be obeyed at $T/T_0$ ratios of about 2.0 or temperatures of about 180°, and that the conductance calculated from the diffusion coefficients should be less than the measured value in some common two-component molten salt systems, such as $LiNO_3 + KNO_3$, near their eutectic temperatures. Such an observation would require the recognition of correlation effects[20] in liquids. It should be noted that a very small correlation coefficient has been found for sodium ion migration in sodium silicate glass[21] and has been valuable in understanding the mechanism of sodium-ion migration in this case.[22]

In support of the small cation effect seen in Table I, we note that identical $T_g$ spacings are observed by direct measurement for solutions of constant composition in the anhydrous systems $M(I)NO_3 + Cd(NO_3)_2$.[8]

To summarize, our findings support the view[4] that the melting points provide a very poor corresponding states basis for comparison of liquid nitrate properties. Rather, a justification is given for the various isothermal comparisons of such properties which have been made in the past.[23]

Finally, we note that the values of $T_g$ found for alkali nitrates in this study are not those which an extrapolation of $T_0$ or $T_g$ values measured in the glass-forming composition regions of alkali metal + divalent metal nitrate systems [~30 to 60 mol % $M(II)(NO_3)_2$] would indicate.[1,8,24] This apparent discrepancy probably originates in the presence of an interaction maximum occurring around 20% $M(II)(NO_3)_2$[25] which invalidates extrapolations based on measurements at higher $M(II)(NO_3)_2$ contents. $T_g$ would evidently exhibit a maximum deviation from additivity at this

(15) Actually neither difference can be considered significant in view of the long extrapolations, based on an unproven assumption (that $C_p$ remains temperature independent), which are involved in the estimates. The constancy of heat capacity, which seems common for fused salts above $T_m$, could however be checked down to 130° by studies of $LiNO_3$–$KNO_3$ or $LiNO_3$–$NH_4NO_3$ eutectics, and at the glass transition by studies on splat-quenched $LiNO_3 + NH_3NO_3$ glasses.

(16) C. A. Angell and K. J. Rao, submitted to *J. Chem. Phys.*

(17) C. A. Angell, *J. Phys. Chem.*, **69**, 399 (1965).

(18) H. Reiss, S. W. Mayer, and J. L. Katz, *J Chem. Phys.*, **35**, 820 (1961).

(19) B. de Nooijer (Thesis, Amsterdam 1965), showed Tabolosky parameter correlations for excess equivalent conductivities in binary alkali nitrate solutions required the radius assigned to $Li^+$ to be almost as large as that for $Na^+$.

(20) J. Bardeen and C. Herring, "Imperfections in Nearly Perfect Crystals," Wiley, New York, N. Y., 1952.

(21) Y. Haven and B. Verkerk, *Phys. Chem. Glasses*, **6**, 38 (1965).

(22) P. L. Spedding and R Mills [*J. Electrochem. Soc.*, **112**, 594 (1965)], found a small negative deviation also for molten $Na_2CO_3$ near the melting point, but C. T. Moynihan (private communication) has pointed out that this is a result of computational errors.

(23) *E.g.*, A. S. Dworkin, R. B. Escue, and E. R. VanArtsdalen, *J. Phys. Chem.*, **64**, 872 (1960).

(24) C. A. Angell, *ibid.*, **68**, 218 (1964).

(25) O. J. Kleppa and L. S. Hersh, *Discuss. Faraday Soc.*, **No. 32** (1962).

composition, though direct observation of the maximum must await development of suitable splat-quenching techniques.

## Thermodynamics of Glass Transition and Relation to Solid–Solid and Solid–Liquid Phase Transitions

Since in addition to the previously studied complex salt melts, we now find even the simple alkali metal nitrates behaving as if their liquid properties are acquired only when the temperature exceeds a characteristic (configurational ground state) temperature, it seems important to inquire more closely about the molecular energetic origin of these liquid properties. In this connection it is a clear advantage to have glass transition thermodynamic data on substances which are simple enough for their crystalline forms to have been well studied; indeed current knowledge on the interesting solid-state transitions observed for $NaNO_3$ and $KNO_3$ proves very relevant to our purpose.

Apart from the property of fluidity, the most striking distinction between the supercooled liquid and crystalline nitrates lies in the difference in their heat capacities. According to Figure 1 this difference may reach values of about 15 cal mol$^{-1}$ deg$^{-1}$, a value which, it should be noted, is supported by changes in heat capacity directly measured at the glass transition for cases of alkali metal + alkaline earth nitrate mixtures,[26] and $Ca(NO_3)_2 \cdot 4H_2O$.[27] Such changes are some 70% greater than the change in heat capacity on fusion of water, and as such are of considerable theoretical interest. We therefore consider briefly the application of a simple order–disorder model which seems to provide a satisfactory first approximation explanation of the observations.

We note firstly that $NaNO_3$ exhibits a $\Lambda$-type second-order transition with critical temperature at 276°. $KNO_3$ is evidently commencing a similar transition at 3–400° but this is cut out by the first-order transition to the rhombohedral phase. Whether this transition could be bypassed, and a $\Lambda$ transition observed, by the technique of treating the crystal with surfactant additives,[6] is not known. In each case, at least, the high temperature phase has a structure best described as a statistical mixture of calcitelike and aragonitelike structures.[28] No rotational freedom of the nitrate ion is involved in the $NaNO_3$ transition, although the increasing anharmonicity of the in-phase librational mode of motion is evident in the continuous decrease in frequency of the associated Raman band from 183 to ~160 cm$^{-1}$ through the transition,[29] and the considerable broadening of the band which accompanies the shift. A further decrease in the frequency of this band occurs on melting without significant further change in bandwidth.[30] Thus as Ubbelohde and coworkers,[31] have suggested, the nitrate ion in these melts is evidently by no means freely rotating, even in two dimensions, in the liquid state near the melting point,

but may be participating in structural interchanges between sites which offer different librational barriers.

The following discussion will utilize what is known about $\Lambda$ transitions, in particular the present one in $NaNO_3$, to suggest a line of thought on the glass transition phenomenon, for nitrates (and other ionic melts), without meaning to imply that the energy states involved in the two transitions are necessarily the same or even very closely related.

The $\Lambda$ transitions are widespread in nature (Curie point, Néel point, gas–liquid, and liquid–liquid critical points, etc.) and are often discussed in terms of some form of order–disorder theory. The disordering of distinct configurations of local minimum energy occurs continuously with increasing temperature, and the $\Lambda$ shape arises because the energy required to cause the basic rearrangement decreases in proportion to the number of rearrangements already existing, thus producing a snowball effect. The critical temperature is related to the 0°K rearrangement energy parameter. The similarity between the ir spectra of high temperature crystal phase $NaNO_3$ and liquid $NaNO_3$[22] suggests the short-range liquid structure is not greatly different from that of the solid, and that on a local scale the same or similar alternative high- and low-energy configurations probably are still available. The liquid can in this case lose energy on decrease of temperature by progressively populating the lower of these two, or few, energetically distinct configurations. However, in the disordered rapidly relaxing liquid, the energies of the neighboring configurations are presumably no longer coupled in the same manner as in the solid, and in the absence of the necessary degree of cooperation, the $\Lambda$-type transition cannot be recovered. On the other hand, some related phenomenon might be anticipated, and we view the glass transition in this light.

The manner in which some features of the glass transition can be explained by structural state mixture models (well known for their application to water) has been pointed out by Macedo, Litovitz, and coworkers,[33]

(26) K. J. Rao, private communication; see also the results of J. de Neufville (unpublished data); quoted in C. A. Angell, L. J. Pollard, and W. Strauss, *J. Chem. Phys.*, **50**, 2694 (1969).

(27) J. Tucker, private communication.

(28) K. Stromme, *Acta Chem. Scand.*, **23**, 1616 (1969).

(29) J. H. R. Clarke, *Chem. Phys. Lett.*, **4**, 39 (1969).

(30) Low-frequency Raman spectral studies of the consequences of solid–solid and solid–liquid phase transitions have also been made in some details by D. W. James and W. H. Leong, *J. Chem. Phys.*, **51**, 640 (1969), and J. P. Devlin and D. W. James, unpublished work.

(31) (a) W. J. McAuley, E. Rhodes, and A. R. Ubbelohde, F.R.S., *Proc. Roy. Soc., Ser. A*, **289**, 151 (1966); (b) E. Rhodes, W. E. Smith, and A. R. Ubbelohde, *ibid.*, **285**, 263 (1965).

(32) G. H. Wegdam, R. Bonn, and J. Van der Elsken, *Chem. Phys. Lett.*, **2**, 182 (1968).

(33) P. B. Macedo, W. Capps, and T. A. Litovitz, *J. Chem. Phys.*, **44**, 3357 (1966); H. W. Leidecker, P. B. Macedo, and T. A. Litovitz, ONR Technical Report No. 1, N00014-68-A-0506-0002, 1969.

and one of us[34] has recently shown how equations similar to those of the mixture models can be derived by a *zeroth-order* treatment of a "bond-lattice" representation of the liquid.

The bond-lattice treatment leads in the simplest case to two-state thermodynamic equations for the excess heat capacity of the liquid and appears to give a very good description of the excess thermodynamic properties (and also transport properties) of water[34] which, with liquid $H_2SO_4$ and the group IV monatomic amorphous solids, appears to be one of the few cases where the constituent particles are bonded in tetrahedral coordination through single bonds. The more familiar case is the bridge-bonded network, *e.g.*, $SiO_2$, $BeF_2$, $ZnCl_2$, where the thermodynamic treatment leads one to expect three-state thermodynamics. Evidence for the three states in the case of $ZnCl_2$ was recently presented by Angell and Wong.[34] In the case of molten nitrates, there are no clear-cut bonds to break since all attractive interactions are ionic, thus the conceptual simplicity of the bond-lattice model is lost. However, in energetic terms the rearrangement of ions from disordered calcite-like to disordered aragonite like or other disordered local packings is the equivalent of breaking a bond, since the forces "locking in" the alternative configurations are repulsive in nature and therefore of short range. We assume the thermodynamic relations will be similar perhaps with modifications to permit a large number of high-energy states. It should be noted that the "lattice" or ground-state packing envisioned here may be seen as a formal representation of the "clustered state" which has been discussed by Ubbelohde and coworkers[31b] in their investigations of the behavior of molten nitrates.

To obtain the thermodynamic parameters characteristic of the difference per mole of "broken" and "unbroken" bonds, (excited- and ground-state configurations) one may fit the theoretical expressions to some suitable fraction (based on the number of bonds per mole) of the measured molar excess quantities. If the coordination number of the bonded particles or groups is $Z$, then there are $Z/2$ bonds per mole; the factor 2 avoids counting each bond twice. While it is clear that for $SiO_2$ and $ZnCl_2$ the appropriate coordination number is 4 (each Si or Zn coordinated to four others through [-O-] or [-Cl-] bridge bonds), it is not as obvious what coordination number should be assigned to the $NaNO_3$ quasilattice.

For purposes of illustration, we choose a coordination number of 6, and will determine energy parameters for the high–low energy configuration change from the two-state expression[33,34]

$$\frac{1}{3}\Delta C_{p(conf)} = R\left(\frac{\Delta H}{RT}\right)^2 \times$$

$$\frac{\exp(\Delta H - T\Delta S)/RT}{[1 + \exp(\Delta H - T\Delta S)/RT]^2} \quad (1)$$
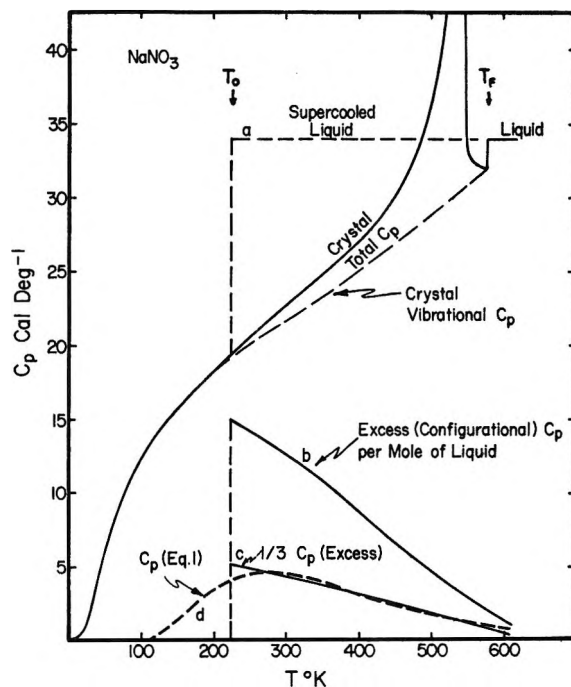
Figure 3. Heat capacity of crystalline and liquid $NaNO_3$, curve a; configurational heat capacity of liquid; curve b, $C_{p(conf)}/3$, curve c; and theoretical $C_{p(conf)}$ curve for two-state bond-lattice model, curve d. The configurational heat capacity maximum of 15 cal mol$^{-1}$ deg$^{-1}$ may be compared with the directly measured increase in molar heat capacity at the glass transition, 15 cal mol$^{-1}$ deg$^{-1}$, for a 60% $KNO_3$ + 40% $Ca(NO_3)_2$ solution (ref 26). The latter $\Delta C_p$ corresponds to (11 cal (mol of $NO_3^-)^{-1}$ deg$^{-1}$.

where $\Delta C_{p(conf)}$ is the change in heat capacity at $224°K$ indicated in Figure 1, $\Delta H$ is the enthalpy change associated with the breaking of 1 mol of "bonds," and $\Delta S$ is the increase in lattice vibrational entropy consequent on the rupture of 1 mol of "bonds." The factor $1/3$ is a consequence of the coordination number choice.

Figure 3 shows the molar excess heat capacity, $\Delta C_{p(conf)}$ (curve b) separated from the total liquid heat capacity (curve a), the quantity $\Delta C_p/3$ (curve c), and the theoretical heat capacity according to eq 1, with the parameters $\Delta H = 2000$ cal/mol of "bonds" and $\Delta S = 5.0$ eu (curve d). $\Delta H$ per mole of salt is thus 6000 cal and $\Delta S$ per mole is 15 eu. For a choice of coordination number of 4, a slightly poorer fit to the excess heat capacity per 0.5 mol of salt can be obtained with $\Delta H = 2000$ cal/mol of bonds and $\Delta S = 6.5$ eu, implying $\Delta H$ per mole of salt of 4000 cal and $\Delta S$ of 13 eu.

That the model in the above form is defective can be seen from the fact that both sets of parameters yield overestimates (4–5 eu) of the combined entropies of fusion + Λ transition,[35] although the ability of eq 1

(34) C. A. Angell, submitted for publication in *J. Phys. Chem.* See also C. A. Angell and J. Wong, *J. Chem. Phys.*, **53**, 2053 (1970), concluding section and note added in proof.

(35) $\Sigma\Delta S_{trans}$ is taken to be $\Delta S$ per mole × the fraction, $N_x$, of "bonds" excited into "off" condition at $T_{fusion}$ + entropy of distribution of "on" and "off" "bonds" on lattice $(= -1/2ZR[N_x \ln N_x + (1 - N_x) \ln (1 - N_x)])$.

to reproduce the general form of the excess heat capacity curve (Figure 3) suggests this sort of approach is worthy of development. The overestimates of $\Sigma \Delta S_{trans}$ can be attributed to the complete neglect of cooperative effects which, one surmises, should play an important role at low temperatures as the lattice "tightens up," and the manner in which refinements based on this idea lead to a sharpened heat capacity–temperature plot and much improved entropy estimates will be described in a separate publication.[36]

## Concluding Remarks

It is notable that the solid–solid transition in both the nitrates discussed here, in $NH_4NO_3$, and also in many other salts, occur at temperatures above the glass temperature for the substance. It seems that the glass temperature is probably the lowest temperature at which significant rearrangement of particles in the condensed state of any substance can occur. Again[37] we note that this temperature lies in the vicinity of the Debye temperature assessed from the low-temperature (acoustic modes) crystal heat capacities ($\theta_D(NaNO_3)$ = 206°K,[38] $\theta_D(KNO_3)$ = 178°K,[39] $\theta_D(NH_4NO_3)$ = 192°K.[39] $\theta_D$ values, but evidently not $T_g$ values,[8] are distinctly lower for $AgNO_3$ and $TlNO_3$.

In substances in which solid-state transitions with substantial entropy changes occur, ease of glass formation will unfortunately be uncommon. For most cases glass formation requires a high viscosity at the melting point, which in turn requires a melting point not more than $1.7 T_g$. By reducing the entropy difference between solid and liquid states, solid-state transitions help to postpone the melting phenomenon to temperatures $>1.7 T_g$ and thus make glass-forming ability improbable. It may be that the methods of estimation of glass temperatures utilized in this work will prove helpful in seeking more general correlations between the energetic characteristics of solid-state transition phenomena and those of the glass transition, and thereby assist in developing a better understanding of the liquid state.

(36) K. J. Rao and C. A. Angell, 3rd International Conference on Physics of Non-Crystalline Solids, Sheffield, England, Sept 1970, to be published as "Amorphous Material," Douglas and Ellis, Ed., Wiley, New York, N. Y., 1971.

(37) C. A. Angell, *J. Amer. Ceram. Soc.*, **51**, 117 (1968), however, see U. E. Schnaus, C. T. Moynihan, R. W. Gammon, and P. B. Macedo, *ibid.*, in press.

(38) J. C. Southard and R. A. Nelson, *J. Amer. Chem. Soc.*, **55**, 4865 (1933).

(39) C. C. Stephenson, D. R. Bentz, and D. A. Stevenson, *ibid.*, **77**, 2161 (1955).

# Freezing Points, Osmotic Coefficients, and Activity Coefficients of Salts

# in N-Methylacetamide.  I.  Alkali Halides and Nitrates[1]

## by R. H. Wood,* R. K. Wicker, II, and R. W. Kreis

*University of Delaware  Newark, Delaware 19711  (Received June 2, 1970)*

*Publication costs assisted by the National Science Foundation*

The freezing points of N-methylacetamide solutions of most of the chlorides, bromides, iodides, and nitrates of lithium, sodium, potassium, and cesium have been measured at concentrations from 0.1 to 0.8 m. Osmotic and activity coefficients were calculated from the freezing points and the molal freezing point depression constant. The osmotic and activity coefficients are much higher than in water due to the high dielectric constant of N-methylacetamide. The order of osmotic coefficients is similar to the order in water. This can be explained by the relative ease with which oppositely charged ions can displace solvent from the immediate neighborhood of an ion. The strong structure making action of alkali metal halides in N-methylacetamide indicates that solvent structure breaking is not a necessary condition for observing the order of osmotic coefficient found in both water and N-methylacetamide.

## Introduction

Water is the only solvent with a high dielectric constant that has been thoroughly investigated. However, aqueous solutions show many anomalous properties such as the expansion of water on freezing, the formation of clathrate compounds, and the formation of "icebergs" around nonpolar solutes.[2] It is recognized that the unique structure of water may have an important influence on the thermodynamic properties of aqueous electrolytes.[3-7] In particular, structural ideas have been used to explain the relative positions of the activity coefficients of aqueous alkali halides.[6]

In order to understand properties of electrolytes in high dielectric solvents and how they are influenced by the properties of the solvent, it will be necessary to have extensive series of measurements on more than one solvent. The present results represent a step towards the collection of this kind of data.

The solvent N-methylacetamide (NMA) was chosen for the present measurements because it has a very high dielectric constant ($\epsilon$ = 178 at 30.5°)[8] which should ensure that effects of ion pairing will be minimized. In addition, NMA has a chain like hydrogen-bonded structure[8-15] rather than the branched three-dimensional hydrogen-bonded structure of water. Gas solubility measurements have shown[16] that small amounts of nonpolar solutes in NMA dissolve without appreciably disrupting the linear hydrogen-bonded chains of solvent molecules. The solutes are in contact with the nonpolar groups of the NMA polymer and this explains why NMA is capable of dissolving large amounts of nonpolar solutes.

The present paper presents the results of the measurements of the freezing points and thus activity coefficients of some alkali halides and nitrates in NMA.

Dawson and coworkers,[17-20] and also French and Glover,[21] have measured the conductances of many strong electrolytes in NMA and have shown that there is a negligible association of normal strong electrolytes.

(1) Presented in part at the 154th National Meeting of the American Chemical Society, Chicago, Sept 1967. This study was aided by a grant from the National Science Foundation, Grant No. GP5239.

(2) For a review see J. L. Kavenau, "Water and Solute-Water Interaction," Holden-Day, San Francisco, Calif., 1964.

(3) H. S. Frank and A. L. Robinson, *J. Chem. Phys.*, 8, 933 (1940).

(4) H. S. Frank and M. W. Evans, *ibid.*, 13, 507 (1945).

(5) H. S. Frank and W.-Y. Wen, *Discuss. Faraday Soc.*, 24, 133 (1957).

(6) R. W. Gurney, "Ionic Processes in Solutions," McGraw-Hill, New York, N. Y., 1953, p 256.

(7) H. S. Frank, *Z. Phys. Chem. (Leipzig)*, 228, 364 (1965).

(8) S. J. Bass, W. I. Nathan, R. M. Meighan, and R. H. Cole, *J. Phys. Chem.*, 68, 509 (1964).

(9) J. L. Katz and B. Post, *Acta Crystallogr.*, 13, 624 (1960).

(10) S. Mizushima, T. Simanouti, S. Nagakura, K. Kuratani, M. Tsuboi, H. Baba, and O. Fujioka, *J. Amer. Chem. Soc.*, 72, 3490 (1950).

(11) G. R. Leader and J. F. Cormley, *ibid.*, 73, 5731 (1951).

(12) R. Linn and W. Dannhauser, *J. Phys. Chem.*, 67, 1805 (1963).

(15) L. A. Planche, H. B. Thompson, and M. T. Rogers, *ibid.*, 69, 1482 (1965).

(14) M. Davies and D. K. Thomas, *ibid.*, 60, 767 (1956).

(15) I. M. Klotz and J. S. Frazen, *J. Amer. Chem. Soc.*, 84, 3461 (1962).

(16) R. H. Wood and D. DeLaney, *J. Phys. Chem.*, 72, 4651 (1968).

(17) L. R. Dawson, P. G. Sears, and R. H. Graves, *J. Amer. Chem. Soc.*, 77, 1986 (1955).

(18) L. R. Dawson, E. D. Wilhoit, and P. G. Sears, *ibid.*, 78, 1569 (1956).

(19) L. R. Dawson, E. D. Wilhoit, R. R. Holmes, and P. G. Sears, *ibid.*, 79, 3004 (1957).

(20) L. R. Dawson, G. R. Lester, and P. G. Sears, *ibid.*, 80, 4233 (1958).

(21) C. M. French and K. H. Glover, *Trans. Faraday Soc.*, 51, 1427 (1955).

In another series of papers, Dawson and coworkers have measured the activity coefficients of HCl in NMA up to 0.1 $M$ and have shown that the HCl behaves as a strong electrolyte in agreement with Debye–Hückel theory.[22,23] Bonner and coworkers[24-26] have reported some activity coefficients which change very rapidly at low concentrations. However, the freezing point depression constant used by these workers has been shown to be off by 15%.[27] Recent results[26] on NaI and KI when corrected for the new freezing point depression constant are consistent with the present results ($\pm 2\%$) from 0.1 to 0.005 $m$. Apparently there was an error in the early measuring technique of these authors at low concentrations. Holleck, Cogley, and Butler[28] have found that large errors are possible with the warming curve technique used by Bonner, et al.

## Experimental Section

The lithium bromide and the cesium salts used in this work were analyzed for sodium and potassium with a flame photometer. Impurities were negligible except for the lithium bromide which contained 0.2% sodium. All other salts were of reagent grade. After being dried in an appropriate manner, the salts were stored in a drybox. In addition, the dryness of those salts of a particularly hygroscopic nature was analyzed by a Karl Fischer titration. $N$-Methylacetamide, obtained commercially, was vacuum distilled after being dried over calcium hydride. The final purification of the solvent is described below.

The experimental procedure has been described previously in detail and, therefore, is only briefly summarized here.[29,30] Two different freezing point cells were used. The first set of measurements used a dewar flask fitted with a rubber stopper containing openings for the salt inlet tube, thermistor well, sample port, and nitrogen inlet. The freezing point cell used in the later experiments consisted of a solvent well which was sealed at the top by a specially constructed cap fitted with three ground-glass joints and a stopcock which served, respectively, as a salt inlet, thermistor well inlet, sample port, and nitrogen inlet. Stirring was achieved by means of a magnetic stirring bar placed into the solvent well. During an experiment the solvent well was inserted into a strip silvered dewar around which was wound a copper coil through which thermostated water was circulated to minimize heat exchanges with the surroundings.

In the first experiments the final purification of the solvent was achieved by slow recrystallization in a drybox. The solvent was then transferred to the freezing point cell with a dry syringe. The major impurity was water and initial freezing points and Karl Fischer titrations show the water content varied from 0.03 to 0.001 $m$. The freezing point of pure NMA was determined to be 30.56°.

In later experiments the NMA was refined by zone melting in a side tube of the freezing cell. Prior to each experiment the entire apparatus was dried at 120° and assembled while hot. The entire cell and zone purification tube were evacuated through the stopcock and flamed with a Bunsen burner. Upon cooling, the cell was put under a slight positive pressure of dry nitrogen and this was maintained until the end of the experiment. Approximately 135 ml of NMA was then transferred from the drybox in a syringe and loaded into the zone melting tube. After purification by repeated zone melting the top 25 ml of NMA was melted and poured into the freezing point cell. In these experiments the concentration of impurities varied from 0.001 to about 0.0002 $m$ as determined by fractional freezing experiments. Karl Fischer titrations showed that the water content was less than 0.001 $m$. Calorimetric measurements on a sample prepared in the same way showed a total impurity of 0.0005 $m$.[27]

Temperatures were measured by a thermistor connected to a resistance bridge.

After temperature equilibration, the freezing point of the solvent was taken and a small amount of salt was added from the salt pistol. After equilibration at the new temperature, a sample was removed using a heated syringe with a long needle and more salt was added. The process was repeated until saturation was reached. Karl Fischer titrations indicated that no appreciable water was introduced during an experiment. The actual freezing point of the solvent in each run was used to calculate the freezing point depression. In this way any water present in the solvent would affect the initial and final freezing points by the same amount provided the water did not preferentially solvate the salts and the amount of solid in the equilibrium mixture stayed constant.

The halide concentrations of the samples were determined by titrating with standard AgNO₃ from a micropipet, using an absorption indicator. Synthetic standards showed results accurate to 0.1%. The nitrate solutions were analyzed by evaporating to dryness at 140°. Synthetic samples showed that this procedure was accurate to 1%.

(22) L. R. Dawson, R. C. Sheridan, and H. C. Eckstrom, *J. Phys. Chem.*, 65, 1829 (1961).

(23) L. R. Dawson, W. H. Zuber, Jr., and J. C. Eckstrom, *ibid.*, 69, 1335 (1965).

(24) O. D. Bonner, C. F. Jordan, and K. W. Bunzl, *ibid.*, 68, 2450 (1964).

(25) O. D. Bonner, K. W. Bunzl, and G. B. Woolsey, *ibid.*, 70, 778 (1966).

(26) O. D. Bonner, S. J. Kim, and A. L. Torres, *ibid.*, 73, 1968 (1969).

(27) R. W. Kreis and R. H. Wood, *J. Chem. Thermodyn.*, 1, 523 (1969).

(28) G. Holleck, D. R. Cogley, and J. N. Butler, *J. Electrochem. Soc.*, 116, 952 (1969).

(29) R. K. Wicker, Ph.D. Thesis, University of Delaware, 1966.

(30) R. W. Kreis, Ph.D. Thesis, University of Delaware, 1969. (Note that the molecular weight used for CsBr is incorrect.)

## Results

The activity coefficients were represented by an extended form of Guggenheim's[31] equation

$$\log \gamma_{\pm} = -Am^{1/2}/(1 + m^{1/2}) + Bm + Cm^{3/2} \quad (3)$$

The Debye–Hückel coefficient, $A$, was calculated using the dielectric constant of Bass, Nathan, Meighan, and Cole[8] and the density of Dawson and Griffith.[32] The result was $A = 0.14128$ for NMA. Integration of eq 3 in the normal manner yields the following expression for osmotic coefficients, $\phi$

$$\phi = 1 - \frac{2.303}{3}Am^{1/2}\sigma(m^{1/2}) +$$
$$\frac{2.303}{2}Bm + 2.303(5/6)Cm^{3/2} \quad (4)$$

where

$$\sigma(m^{1/2}) = (3/m^{3/2})[1 + m^{1/2} -$$
$$1/(1 + m^{1/2}) - 2 \ln (1 + m^{1/2})] \quad (5)$$

The practical osmotic coefficient, $\phi$, of a solvent as a function of temperature depression, $\theta$, is given by[33]

$$vKm\phi = \left(1 + \frac{\bar{L}_1}{H^\circ_f}\right)\theta +$$
$$\left(\frac{1}{T_f} - \frac{\Delta C_p{}^\circ_f}{2\Delta H^\circ_f} + \frac{\bar{L}_1}{T_f\Delta H^\circ_f} - \frac{\bar{J}_1}{2\Delta H^\circ_f}\right)\theta^2 +$$
$$\left(\frac{1}{T^\circ_f} - \frac{2\Delta C_p{}^\circ_f}{3T_f\Delta H^\circ_f} + \frac{\Delta b}{6\Delta H^\circ_f} + \frac{\bar{L}_1}{T_f{}^2\Delta H^\circ_f} -$$
$$\frac{2\bar{J}_1}{3T_f\Delta H^\circ_f}\right)\theta^3 + \cdots \quad (6)$$

$\bar{L}_1$, the relative partial molal enthalpy, and $\bar{J}_1$, the relative partial molal heat capacity, are not available for NMA solutions.[34] The term in $\Delta b$ takes into account the change in heat capacity, $\Delta C_{pf}$, with temperature and is negligible relative to other uncertainties. Ignoring terms contributing less than 0.1% of $\phi$ at $\theta = 10°$ or less and omitting those terms which presently are not available, eq 6 reduces to

$$vKm\phi = \theta + \left(\frac{1}{T_f} - \frac{\Delta C_p{}^\circ_f}{2\Delta H^\circ_f}\right)\theta^2 + \frac{\theta^3}{T_f{}^2} \quad (7)$$

Substituting eq 4 in eq 7 yields

$$vKm\left[1 - \frac{2.303}{3}Am^{1/2}\sigma(m^{1/2})\right] +$$
$$2.303KBm^2 + 2.303(6/5)KCm^{3/2} =$$
$$\theta + \left(\frac{1}{T_f} - \frac{\Delta C_p{}^\circ_f}{2\Delta H^\circ_f}\right)\theta^2 + \frac{\theta^3}{T_f{}^2} \quad (8)$$

and upon rearrangement

$$\theta + \left(\frac{1}{T_f} - \frac{\Delta C_p{}^\circ_f}{2\Delta H^\circ_f}\right)\theta^2 + \frac{\theta^3}{T_f{}^2} -$$
$$2Km\left(1 - \frac{2.303}{3}Am^{1/2}\sigma(m^{1/2})\right) =$$
$$2.303KBm^2 + 2.303(6/5)Cm^{5/2} \quad (9)$$

where the heat of fusion ($\Delta H_f = 31.78 \pm 0.16$ cal/g), change in heat capacity ($\Delta C_p{}^\circ_f = 0.12 \pm 0.03$ cal/g °K), and freezing point constant ($K = 5.77 \pm 0.02°$K/$m$) are taken from Kreis and Wood.[27]

The experimental data[29,30] were fit to eq 9 by the method of least squares to calculate values of $B$ and $C$. In the case of NaCl, KCl, and CsCl where the solubility was low, the $C$ term was set equal to zero since it was not needed for a good fit. The results of the calculations are given in Tables I–III and Figure 1. The osmotic and activity coefficients were calculated by eq 4 and 3, respectively. The results in Table I and examination of the data indicate that the great majority of the differences between the least-squares fit and the experimental osmotic coefficients are less than 0.01 indicating an accuracy better than 1% in $\phi$. The data for NaI are not as good as the rest, and errors as high as 2% would be possible. The first measurements of NaCl, KCl, and LiBr and LiNO₃ showed errors much higher than this so the osmotic coefficient was remeasured using the redesigned apparatus. The new measurements changed the

**Table I:** Results of the Least-Squares Fit

| Salt | $B$ | $C$ | Standard[a] error of $\theta$ | Standard error of $\phi$ |
|---|---|---|---|---|
| LiCl | 0.5555 | −0.4089 | 0.017 | 0.006 |
| NaCl[b] | 0.2101 | | | 0.011 |
| KCl[b] | 0.1406 | | | 0.017 |
| CsCl | 0.0835 | | | 0.021 |
| LiBr[b] | 0.2872 | 0.0034 | 0.015 | 0.003 |
| NaBr | 0.3087 | −0.0685 | 0.028 | 0.005 |
| KBr | 0.1415 | −0.0070 | 0.031 | 0.007 |
| CsBr | 0.3284 | −0.4363 | 0.008 | 0.003 |
| NaI | 0.3776 | −0.0498 | 0.071 | 0.024 |
| KI | 0.1084 | 0.0859 | 0.046 | 0.004 |
| CsI | 0.1516 | −0.0828 | 0.012 | 0.004 |
| LiNO₃[b] | 0.2127 | 0.0474 | 0.048 | 0.014 |
| NaNO₃ | −0.0481 | 0.0069 | 0.023 | 0.006 |
| KNO₃ | −0.0498 | −0.1051 | 0.024 | 0.010 |

[a] This is the standard deviation of the left-hand side of eq 9. [b] Remeasured using zone melted NMA.

(31) E. A. Guggenheim, *Phil. Mag.*, 19, 588 (1935).

(32) L. R. Dawson and E. J. Griffith, *J. Phys. Chem.*, 56, 281 (1952).

(33) G. N. Lewis and M. Randall, "Thermodynamics," K. S. Pitzer and L. Brewer, Ed., McGraw-Hill, New York, N. Y., 1961, p 406.

(34) By analogy with aqueous solutions, the inclusion of $\bar{L}_1$ and $\bar{J}_1$ in eq 6 would result in a correction to $\phi$ of less than 1% over the concentration range studied.

**Table II:** Osmotic Coefficients, $\phi$

| m | LiCl | NaCl | KCl | CsCl | LiBr | NaBr | KBr | CsBr | NaI | KI | CsI | LiNO₃ | NaNO₃ | KNO₃ |
|---|------|------|------|------|------|------|------|------|------|------|------|-------|-------|-------|
| 0.01 | 0.996 | 0.993 | 0.992 | 0.992 | 0.994 | 0.994 | 0.992 | 0.994 | 0.995 | 0.992 | 0.992 | 0.993 | 0.990 | 0.990 |
| 0.05 | 1.008 | 0.994 | 0.990 | 0.987 | 0.999 | 0.999 | 0.990 | 0.994 | 1.003 | 0.990 | 0.990 | 0.995 | 0.979 | 0.978 |
| 0.10 | 1.023 | 1.001 | 0.994 | 0.987 | 1.011 | 1.010 | 0.993 | 0.996 | 1.019 | 0.994 | 0.991 | 1.004 | 0.972 | 0.967 |
| 0.20 | 1.050 | 1.020 | | | 1.039 | 1.035 | 1.004 | 0.994 | 1.053 | 1.008 | 0.997 | 1.027 | 0.962 | 0.948 |
| 0.30 | 1.068 | 1.042 | | | 1.070 | 1.061 | 1.017 | | 1.089 | 1.027 | 1.003 | 1.054 | 0.955 | |
| 0.40 | | | | | 1.101 | 1.086 | 1.030 | | 1.124 | 1.048 | 1.009 | 1.082 | 0.948 | |
| 0.50 | | | | | 1.133 | 1.111 | | | 1.159 | 1.071 | | 1.112 | 0.942 | |
| 0.60 | | | | | 1.166 | 1.135 | | | 1.194 | 1.095 | | 1.143 | 0.937 | |
| 0.70 | | | | | | 1.158 | | | 1.228 | 1.122 | | | 0.931 | |
| 0.80 | | | | | | | | | 1.262 | | | | 0.926 | |

**Table III:** Activity Coefficients, $\gamma_\pm$

| m | LiCl | NaCl | KCl | CsCl | LiBr | NaBr | KBr | CsBr | NaI | KI | CsI | LiNO₃ | NaNO₃ | KNO₃ |
|---|------|------|------|------|------|------|------|------|------|------|------|-------|-------|-------|
| 0.01 | 0.982 | 0.976 | 0.974 | 0.973 | 0.977 | 0.977 | 0.974 | 0.977 | 0.979 | 0.973 | 0.974 | 0.975 | 0.970 | 0.969 |
| 0.05 | 0.993 | 0.966 | 0.958 | 0.952 | 0.974 | 0.974 | 0.957 | 0.968 | 0.983 | 0.956 | 0.956 | 0.966 | 0.937 | 0.934 |
| 0.10 | 1.020 | 0.971 | 0.955 | 0.943 | 0.988 | 0.988 | 0.955 | 0.966 | 1.005 | 0.954 | 0.952 | 0.974 | 0.915 | 0.907 |
| 0.20 | 1.073 | 0.996 | | | 1.033 | 1.028 | 0.964 | 0.962 | 1.065 | 0.968 | 0.953 | 1.007 | 0.886 | 0.864 |
| 0.30 | 1.120 | 1.031 | | | 1.088 | 1.075 | 0.980 | | 1.135 | 0.993 | 0.959 | 1.051 | 0.864 | |
| 0.40 | | | | | 1.151 | 1.126 | 1.000 | | 1.213 | 1.025 | 0.966 | 1.102 | 0.847 | |
| 0.50 | | | | | 1.220 | 1.179 | | | 1.296 | 1.062 | | 1.160 | 0.832 | |
| 0.60 | | | | | 1.295 | 1.235 | | | 1.386 | 1.105 | | 1.224 | 0.818 | |
| 0.70 | | | | | | 1.293 | | | 1.482 | 1.154 | | | 0.805 | |
| 0.80 | | | | | | | | | 1.584 | | | | 0.794 | |
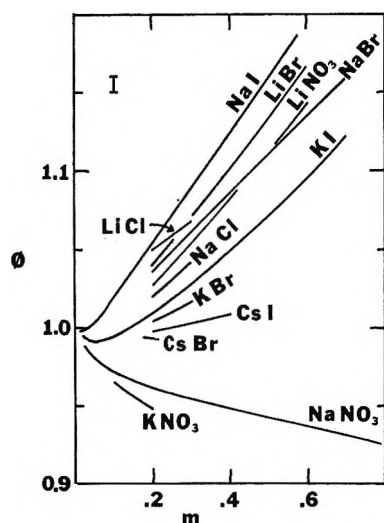


Figure 1. Osmotic coefficients in $N$-methylacetamide vs. m.

values of $\phi$ by less than 1% for NaCl, 1.5% for KCl, 1.5% for LiNO₃, and 4% for LiBr. Points which differed from the final least-squares fit more than about $2\sigma$ were rejected. This resulted in the dropping of one point from the KBr data and one from the CsBr data. The points above about 0.8 m tended to have larger random errors so they were not included in the least-squares fit.

Measurements on LiI solutions had very high random errors in both sets of measurements for unknown reasons.[30] These data are not reported.[35]

At low concentrations the osmotic coefficients are much higher than in water, and this is due to the high dielectric constant of NMA which results in a Debye–Hückel slope that is one-fourth as large as the Debye–Hückel slope for water.

At the highest concentrations where the most accuracy is obtained, the order of osmotic coefficients is NaI > LiBr > LiCl > LiNO₃ > NaBr > NaCl > KI > KBr > CsI > CsBr > CsCl > NaNO₃ > KNO₃ with KCl close to KI and KBr. This order is consistent with Li⁺ > Na⁺ > K⁺ > Cs⁺ and I⁻ > Br⁻ > Cl⁻ > NO₃⁻. The low-concentration data for LiCl and CsBr do not follow this order but this could easily be due to the greater experimental error at low concentrations. The unusually large values of $C$ (Table I and eq 3) for these two salts also suggests this kind of error. The solubility of KCl is not high enough to see if it fits this order. The order observed at high concentrations in NMA is the same as the order in water except that in water the cesium salts show the reverse anion order. It should be noted that although the cesium salts do show a reversal

(35) The measurements show LiI to have the highest value of $\phi$ measured and this is consistent with the interpretation presented.

in order in water and NMA, the osmotic coefficients of the cesium salts in both solvents are very close to each other. This similarity in trends is brought out by a plot of $\phi_{NMA}$ vs. $\phi_{H_2O}$ which shows that there is a rough correlation. Although the data are limited, it looks as if a similar rough correlation will hold for alkali halides in formamide.[36,37] These regularities indicate that the same factors are important in both the water and the NMA solutions (and possibly in formamide) and that the effects depend in roughly the same way on the sizes of the ions. It may be that this similarity will hold for any strongly hydrogen-bonded solvent with a high dielectric constant. At moderate concentrations the osmotic coefficients of the alkali metal halides and the nitrates will depend mostly on the interactions of the two oppositely charged ions although like-charged ion interactions will also contribute.[38,39] The interactions between ions are influenced by the solvation of the ions,[40-43] the relative ease with which ions of opposite charge displace solvent from the coordination sphere of an ion,[44-46] the structure of the solvent in the solvation spheres of the ions,[3,6,7,47] and the "localized solvolysis" induced by weak acids.[48,49] All of these effects and others effects not listed may be important, and the problem is that it is impossible to distinguish between effects which predict the observed experimental results. For this reason the present discussion will be limited to showing how the competition of oppositely charged ions and solvent for the immediate company of an ion can account for the data and how the evidence indicates that solvent structure breaking is not an important factor.

Prue[45,46] has proposed that the competition of solvent and oppositely charged ions for the immediate company of an ion is an important effect of the solvent. A crude model predicts that ions that are both small or both large can more easily come into contact. This can be understood by comparing the interaction energy of a small ion with a coordinated solvent molecule and with an oppositely charged ion. If the oppositely charged ion is much larger than the solvent molecule, the interaction energy of the two ions is less than the interaction energy of the ion with the solvent dipole. Because of this, a large ion cannot easily enter the coordination sphere of a small ion and direct ion–ion contacts do not often occur. In the case of two small ions or two large ions the ion–ion interaction is larger than the ion–solvent dipole interaction so that in these cases ion–ion contact is more frequent.[45,46]

The cation order in the osmotic coefficients of NMA solutions, $Li^+ > Na^+ > K^+ > Cs^+$, and the anion order, $I^- > Br^- > Cl^- > NO_3^-$, are explained by this model with the assumption that the alkali metal cations are small strongly solvated ions and the anions are relatively weakly solvated. As the cation gets smaller and the anion gets larger, it is more difficult for the solvent displacement to occur, ion–ion repulsion increases, and

the osmotic coefficient goes up. The nitrate ion acts as an ion that is smaller than the chloride ion because its coordinating groups, the oxygen atoms, are about the same size as a fluoride ion.

The hydration association model of Frank[44] is an early attempt to put some of these effects on a more quantitative basis. A calculation of the energy of displacing two solvent molecules and forming a contact ion pair in an aqueous solution predicts the correct trends in activity coefficients. Specifically, there is evidence for the reversals that occur in water as the anion gets smaller and as the cation gets larger. The model takes into account dielectric saturation, ion–ion, ion–dipole, and Van der Waals forces in calculating the energy of the displacement reaction. The following paper shows that with an ion that is able to displace solvent from the coordination sphere of the alkali metals, the order of osmotic coefficients is reversed in NMA. This is just what would be predicted by the theory.

Recent calculations on a charged square-well model[50] show that very small changes in the energy of the ions at contact $(E < kT)$ are adequate to account for the osmotic coefficients of aqueous solutions. These small energy changes do not greatly affect the pair correlation function, and thus do not change the probability of an ion–ion encounter to any great extent. It appears that osmotic coefficients are a very sensitive measure of ion–ion interactions.

Frank and Wen[5] picture the water around an ion as being divided roughly into three regions: strongly hydrated water near the ion; a transition region where the normal water structure is broken; and an outer region of relatively undisturbed water. This picture of

(36) E. N. Vassenko, Zh. Fiz. Khim., 21, 361 (1947); 22, 999 (1948); 23, 959 (1949).

(37) The data of E. Luksha and C. M. Criss [J. Phys. Chem., 70, 1496 (1966)] in N-methylformamide indicate trends opposite to those in water but in view of the difficulty of cell measurements this is not certain.

(38) R. H. Wood and R. W. Smith, J. Phys. Chem., 69, 2974 (1965).

(39) R. H. Wood and H. L. Anderson, ibid., 70, 992 (1966).

(40) N. Bjerrum, Z. Anorg. Allg. Chem., 109, 275 (1920).

(41) R. H. Stokes and R. A. Robinson, J. Amer. Chem. Soc., 70, 1870 (1948).

(42) E. Glueckauf, Trans. Faraday Soc., 51, 1235 (1955).

(43) D. G. Miller, J. Phys. Chem., 60, 1296 (1956).

(44) H. S. Frank, J. Amer. Chem. Soc., 63, 1789 (1941).

(45) (a) J. E. Prue, "Chemical Physics of Ionic Solutions," B. E. Conway and R. G. Barradas, Ed., Wiley, New York, N. Y., 1966, p 163; (b) J. E. Prue, "The International Encyclopedia of Physical Chemistry and Chemical Physics," Vol. 3, "Ionic Equilibria," Pergamon Press, Oxford, 1966, Chapter 10, Topic 15.

(46) R. Garnsey and J. E. Prue, Trans. Faraday Soc., 64, 1206 (1968).

(47) R. H. Wood and H. L. Anderson, J. Phys. Chem., 71, 1869 (1967).

(48) R. A. Robinson and H. S. Harned, Chem. Rev., 28, 419 (1941).

(49) R. M. Diamond, J. Amer. Chem. Soc., 80, 480 (1958).

(50) R. F. Rasaiah and H. L. Friedman, J. Phys. Chem., 72, 3352 (1968).

the structure of water around an ion explains the viscosity, conductance, and heats of interaction of the ions very nicely.[2-7,47] Gurney[6] proposed that the relative amounts of structure making or structure breaking present were responsible for the trends of the activity coefficients of the alkali halides. The similarity of the trends of activity coefficients in water and NMA raises the question of whether the structural properties of water and NMA are similar. All of the evidence indicates that structure breaking is not important in solutions of alkali halides in any of the N-methylamides. Viscosity measurements of electrolytes in N-methylformamide,[51] N-methylacetamide,[17] and N-methylpropionamide[52] indicate that structure making is the predominant effect for alkali halides. The transference numbers of KCl in NMA led Gopal and Bhatnagar[53] to conclude that the potassium ion has no appreciable structure breaking. Engle and Hertz[54] conclude from nuclear magnetic relaxation studies on alkali halides that there is no structure breaking in N-methylformamide. However, French and Glover[21] and Singh, Rastogi, and Gopal[55] conclude from conductance measurements that tetraalkylammonium ions depolymerize NMA. Similarly Millero[52b] has shown that benzene and pyridine depolymerize N-methylpropionamide solutions. Apparently the alkali halides are all net structure makers while some nonelectrolytes and perhaps the tetraalkylammonium ions are structure breakers.

This strong structure-making effect of the alkali metal halides is just what might be expected from the properties of the solvent. Each ion in NMA should act as a cross-linking agent for the chains of hydrogen-bonded solvent molecules that occur in the pure solvent,[9-16] because each ion would serve as a starting point for four to six chains, depending on its coordination number. The chains would be fairly long because coordinated NMA molecules would be strongly polarized and thus have an increased tendency to hydrogen bond.[13]

The fact that NMA solutions of the alkali halides show no evidence of structure breaking together with the similarity[56a] in the order of osmotic coefficients in water and NMA indicates that net structure breaking[56b] is not a necessary condition for observing this order.

Frank and Kerwin[57] measured osmotic coefficients of alkali halides in $D_2O$ and showed that the osmotic coefficients of the alkali halides were not sensitive to the structural differences between $D_2O$ and $H_2O$.[58] Similarly, Robinson[59] showed that the osmotic coefficients of a mixture of NaCl and KCl are very similar in $H_2O$ and $D_2O$. It may be that osmotic coefficients in both NMA and water are not sensitive to small changes in the structure of the solvent. In contrast to this the enthalpies and entropies of dilution[60,61] appear to be very sensitive to the structural difference between $H_2O$ and $D_2O$.

(51) D. Feakins and K. G. Lawrence, *J. Chem. Soc.*, 212 (1966).

(52) (a) T. B. Hoover, *J. Phys. Chem.*, 68, 876 (1964); (b) F. J. Millero, *ibid.*, 72, 3209 (1968).

(53) R. Gopal and O. N. Bhatnagar, *ibid.*, 69, 2382 (1965).

(54) G. Engel and H. G. Hertz, *Ber. Bunsenges, Phys. Chem.*, 72, 808 (1968).

(55) R. D. Singh, P. P. Rastogi, and R. Gopal, *Can. J. Chem.*, 46, 3525 (1968).

(56) (a) The anion order for cesium salts is the only difference between the two solvents (see above). (b) It is probably true that there will always be at least a small transition region between the solvated ion and the solvent which will have less structure than the solvent. The term net structure breaker is used here to denote an ion where the structure-breaker region is small compared with the region where structure-making predominates.

(57) R. E. Kerwin, Ph.D. Thesis, University of Pittsburgh, 1964.

(58) G. Nemethy and H. A. Scheraga, *J. Chem. Phys.*, 41, 680 (1964).

(59) R. A. Robinson, *J. Phys. Chem.*, 73, 3165 (1969).

(60) Y. C. Wu and H. L. Friedman, *ibid.*, 70, 2020 (1966).

(61) R. H. Wood, R. A. Rooney, and J. N. Braddock, *ibid.*, 73, 1693 (1969).

# Freezing Points, Osmotic Coefficients, and Activity Coefficients of Salts

# in N-Methylacetamide. II. Tetraalkylammonium Halides and

# Some Alkali Metal Formates, Acetates, and Propionates[1]

## by R. W. Kreis and R. H. Wood*

*Department of Chemistry, University of Delaware, Newark, Delaware 19711*     *(Received June 2, 1970)*

*Publication costs assisted by the National Science Foundation*

The freezing points of N-methylacetamide solutions of the acetates and propionates of lithium, sodium, and potassium, the formates of lithium and sodium, and the chlorides, bromides and iodides of some n-tetraalkylammonium ions have been measured at concentrations from 0.1 to 0.8 m. Osmotic and activity coefficients were calculated from the freezing points. The similarity of the order of osmotic coefficients in water and N-methylacetamide, observed for the alkali metal halides and nitrates, also holds for the alkali metal formates, acetates, and propionates. It is unlikely that "localized solvolysis" is an important factor in determining the order of osmotic coefficients. At low concentrations, the order of osmotic coefficients of the n-tetraalkylammonium halides, $Cl^- > Br^- > I^-$, is the same as in water. With the smaller ions the order is $Bu_4N^+ > Pr_4N^+ > Et_4N^+ > Me_4N^+$ in both water and N-methylacetamide. As the anion increases in size the order reverses in water and becomes less pronounced in N-methylacetamide. In both solvents the osmotic coefficients of the iodides of the larger cations are below the Debye–Hückel limiting law. The similarity in trends shows that the water-structure enhancing properties of the larger tetraalkylammonium ions are not responsible for the trends. The results in water and NMA can be explained by the penetration of the larger, weakly solvated anions into the hydrocarbon portion of the cation. Very small distances of closest approach are possible and the effective dielectric constant should be small. For aqueous solutions at higher concentrations, the effects of the water structure enhancement around the larger tetraalkylammonium ions become apparent.

## Introduction

The previous paper[2] showed that order of the osmotic coefficients of alkali metal halides and nitrates in water and N-methylacetamide were similar. This could be explained by the relative ease with which oppositely charged ions displace solvent from the primary coordination sphere of an ion. The results also showed that solvent structure breaking is not responsible for the similarity of the order of osmotic coefficients. This paper extends the measurements to the osmotic coefficients of a variety of salts in order to see if the similarity to aqueous solutions is still present.

Gopal and Siddiqi[3] have measured the apparent molal volumes of a series of tetraalkylammonium iodides as a function of concentration and temperature. Their results show a great similarity between aqueous solutions and NMA solutions. On this basis, Gopal and Siddiqi concluded that the behavior could not be due to lyophopic structure making. The present paper reports measurements of the osmotic coefficients of some tetraalkylammonium halides which show the same similarity between aqueous and NMA solutions.

## Experimental Section

The details of the experimental procedure have been reported previously.[2,4] Lithium formate, lithium acetate, and lithium propionate were prepared by reacting

the appropriate metal carbonate with either formic, acetic, or propionic acid. The resulting solutions were recrystallized from the appropriate pure acid and then from water. Sodium formate, sodium acetate, sodium propionate, and potassium acetate were obtained commercially and used without further purification. These salts were dried under vacuum for 24 hr, the formates at 130° and the acetates and propionates at 180°. As a rough check on purity, 1 M solutions of the acetates and propionates were titrated with 1 M HCl. The results were accurate to about 1% and showed purities from 98.6 to 99.1%. The initial pH's of 1 M aqueous solutions were: lithium acetate 8.60, sodium acetate 9.60, potassium acetate 8.78, lithium propionate, 8.48, sodium propionate 8.40, and potassium propionate 7.88. These pH values indicate that residual weak acid in the sample is less than 0.2%. The results of a carbon analysis of the formates were: lithium formate 23.12 calcd, 22.71 found; sodium formate 17.60 calcd, 17.52 found.

(1) Presented at the 5th Middle Atlantic Meeting of the American Chemical Society, Newark, Del., April 1970.

(2) R. H. Wood, R. K. Wicker, and R. W. Kreis, *J. Phys. Chem.*, **75**, 2313 (1971).

(3) R. Gopal and M. A. Siddiqi, *ibid.*, **73**, 3390 (1969).

(4) R. W. Kreis, Ph.D. Thesis, University of Delaware, Newark, Del., June 1969.

Samples of these solutions in equilibrium with solid NMA were analyzed for salt by evaporating to dryness at 140°, and weighed. Synthetic solutions of the salts analyzed in the same way showed that the procedure was accurate to ±0.5% for the acetates and propionates and ±1.0 for the formates.

The n-tetraalkylammonium salts were obtained commercially, purified and dried according to Unni, Elias, and Schiff.[5] The per cent purity of the individual salts based on an analysis for halide was: $(CH_3)_4$-NCl, 100.13; $(C_2H_5)_4NCl$, 100.26; $(C_3H_7)_4NCl$, 99.94; $(C_4H_9)_4NCl$, 99.99; $(CH_3)_4NBr$, 99.70; $(C_2H_5)_4NBr$, 99.97; $(C_3H_7)_4NBr$, 99.95; $(C_4H_9)_4NBr$, 100.12; $(C_2H_5)_4$-NI, 100.30; $(C_3H_7)_4NI$, 99.95; and $(C_4H_9)_4NI$, 100.12. All samples were stored in a drybox (dewpoint, −50°) until transferred to the salt pistol of the freezing point apparatus. Samples taken from the freezing point cell were analyzed for halide by adding 2–5 ml of water and titrating with silver nitrate solution using dichlorofluorescein as an indicator and a few drops of Triton CF21 polyethyl eneoxide[6] as an anticoagulant. Titration of known amounts of tetraalkylammonium halides under similar conditions were accurate to 0.3% or better. This is true even for the iodides which are known to form mixed salts with silver iodide.

The all-glass cell was used for all measurements. Based on the variation of the initial freezing points of the solvent, the total impurity was 0.001 to 0.0002 $m$ for zone melted samples. To save time, some of the experiments were conducted using NMA recrystallized in the drybox or a second sample of solvent from the zone melting tube. The total solvent impurity in these runs varied from 0.001 to 0.03 $m$. No systematic differences between the results of the two methods were detected. Zone melted solvent was normally used for the lowest concentration points where it gave more reproducible results. The temperature was measured by a thermistor calibrated against a standard platinum resistance thermometer.

### Treatment of Data

The treatment of the data has been described previously.[2,4] Briefly the measured osmotic coefficients are fit to the equation

$$\phi = 1 - (2.303A/3)m^{1/2}\sigma(m^{1/2}) + (2.303/2)Bm + 2.303(^5/_6)Cm^{3/2} \quad (1)$$

where

$$\sigma(m^{1/2}) = (3/m^{3/2})[1 + m^{1/2} - 1/(1 + m^{1/2}) - 2\ln(1 + m^{1/2})] \quad (2)$$

and $B$ and $C$ are determined by the method of least squares. The coefficient $A$ is the Debye–Hückel slope ($A = 0.14128$ was used).[2] The activity coefficients are then given by

$$\log \gamma = Am^{1/2}/(1 + m^{1/2}) + Bm + Cm^{3/2} \quad (3)$$

### Results and Discussion

*I.  Formates, Acetates, and Propionates.*  The results of the least-squares fit of the data for the formates, acetates, and propionates are given in Tables I–III and Figure 1. The standard deviation of both the temperature differences and the osmotic coefficients are given in Table I. The standard deviations indicate that the osmotic coefficients are accurate to about 1%.

**Table I:**  Results of the Least-Squares Fit

| Salt | B | C | Standard[a] error of $\theta$ | Standard error of $\phi$ |
|------|------|------|------|------|
| Li form | −0.4992 | 0.3709 | 0.020 | 0.008 |
| Na form | −0.0321 | −0.3373[b] | 0.018 | 0.012 |
| LiOAc | −0.2272 | 0.0254 | 0.046 | 0.012 |
| NaOAc | −0.1668 | −0.0251 | 0.035 | 0.015 |
| KOAc | 0.0466 | −0.0422 | 0.031 | 0.008 |
| LiOPr | −0.0926 | −0.0669 | 0.023 | 0.007 |
| NaOPr | 0.0052 | −0.1399 | 0.029 | 0.004 |
| KOPr | 0.1776 | −0.1522 | 0.052 | 0.014 |

[a] This is the standard deviation of the freezing point depression.  [b] If $C$ is set equal to zero, the fit is almost as good if the $B$ coefficient is −0.2035.

At the highest concentrations where the measurements are the most accurate, the order of osmotic coefficients is potassium propionate > potassium acetate > sodium propionate > lithium propionate > sodium acetate > sodium formate = lithium acetate > lithium formate. This order is consistent with the cation order $K^+ > Na^+ > Li^+$ and the anion order propionate > acetate > formate.

The osmotic coefficients of sodium formate and sodium acetate are within experimental error of each other at all concentrations and the order changes between 0.1 and 0.2 $m$. The high concentration data are more accurate and these are consistent with the order of the rest of the salts. In addition the least-squares fit for sodium formate is almost as good with the $C$ term set equal to zero and $B = -0.2035$. With this change the $B$ coefficients of Table I and the osmotic coefficients have the order propionate > acetate > formate. Also with this change sodium formate fits better into the family of curves in Figure 1.

This cation order is the reverse of the order of the alkali metal halides and nitrates in both water[7] and NMA.[2] Similarly the order in aqueous solutions is propionate > acetate > formate.[7] Thus the similarity of the order of the osmotic coefficients in water and NMA observed for the alkali metal halides and nitrates

(5) A. K. R. Unni, L. Elias, and H. I. Schiff, *J. Phys. Chem.*, **67**, 1216 (1963).

(6) Rohm and Haas Co.

(7) R. A. Robinson and R. H. Stokes, "Electrolyte Solutions," 2nd ed, Butterworths, London, 1965, Appendices 8.7 and 8.10.

**Table II:** Osmotic Coefficients, $\phi$

| $m$ | Li form | Na form | LiAc | NaAc | KAc | LiPr | NaPr | KPr |
|------|---------|---------|-------|-------|-------|-------|-------|-------|
| 0.01 | 0.985 | 0.990 | 0.988 | 0.989 | 0.991 | 0.989 | 0.990 | 0.992 |
| 0.05 | 0.959 | 0.975 | 0.969 | 0.972 | 0.984 | 0.976 | 0.980 | 0.990 |
| 0.10 | 0.936 | 0.959 | 0.952 | 0.957 | 0.981 | 0.964 | 0.972 | 0.991 |
| 0.20 | 0.903 | 0.923 | 0.923 | 0.931 | 0.978 | 0.943 | 0.956 | 0.995 |
| 0.30 | 0.881 |       | 0.897 | 0.906 | 0.976 | 0.922 | 0.940 | 0.996 |
| 0.40 | 0.867 |       | 0.872 | 0.882 | 0.974 | 0.902 |       | 0.996 |
| 0.50 |       |       |       |       | 0.973 |       |       | 0.994 |
| 0.60 |       |       |       |       | 0.970 |       |       |       |
| 0.70 |       |       |       |       | 0.968 |       |       |       |
| 0.80 |       |       |       |       | 0.965 |       |       |       |

**Table III:** Activity Coefficients, $\gamma_{\pm}$

| $m$ | Li form | Na form | LiAc | NaAc | KAc | LiPr | NaPr | KPr |
|------|---------|---------|-------|-------|-------|-------|-------|-------|
| 0.01 | 0.961 | 0.969 | 0.966 | 0.967 | 0.972 | 0.969 | 0.971 | 0.974 |
| 0.05 | 0.898 | 0.931 | 0.919 | 0.924 | 0.946 | 0.931 | 0.939 | 0.958 |
| 0.10 | 0.847 | 0.896 | 0.879 | 0.888 | 0.932 | 0.901 | 0.917 | 0.953 |
| 0.20 | 0.776 | 0.831 | 0.819 | 0.833 | 0.916 | 0.855 | 0.881 | 0.951 |
| 0.30 | 0.726 |       | 0.769 | 0.787 | 0.906 | 0.815 | 0.848 | 0.951 |
| 0.40 | 0.691 |       | 0.726 | 0.745 | 0.898 | 0.779 |       | 0.950 |
| 0.50 |       |       |       |       | 0.891 |       |       | 0.947 |
| 0.60 |       |       |       |       | 0.884 |       |       |       |
| 0.70 |       |       |       |       | 0.878 |       |       |       |
| 0.80 |       |       |       |       | 0.872 |       |       |       |
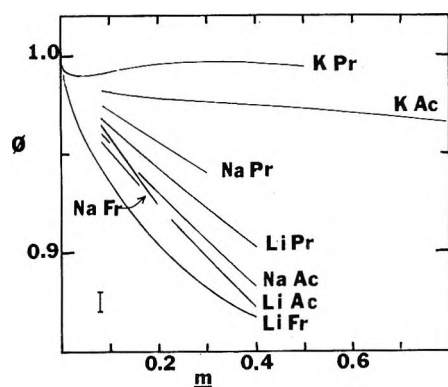


Figure 1. Osmotic coefficients of alkali metal formates (Fr), acetates (Ac), and propionates (Pr) in NMA as a function of molality.

also holds for the alkali metal formates, acetates, and propionates.

Robinson and Harned[8] suggested that cations polarize the coordinated solvent molecules and make them stronger acids. In the presence of a basic anion, association can occur through the intermediacy of a solvent molecule. This "localized solvolysis" was used to explain the cation order $K^+ > Ni^+ > Li^+$ for the salts of weak acids in water since the smaller cations polarize the solvent more and thus cause greater association. Diamond[9] suggested that this same mechanism was responsible for the order $I^- > Br^- > Cl^-$ for the smaller alkali metal cations.

The use of the "localized solvolysis" concept to explain the present results is not very plausible for the following reason. We must compare the relative free energy of an outer sphere complex in which "localized solvolysis" is present with an inner sphere complex. Comparing the acetate ion with a solvent molecule as ligands it is clear that the acetate ion has less steric hindrance, has the same coordinating atom (oxygen),[10-15] and is a much stronger base due to the negative charge on the oxygen. Thus, there is every reason to believe that the acetate ion would preferentially displace solvent from the primary coordination sphere of the alkali metal cations. The same arguments apply to the formate and propionate ions. It is doubtful that the stabilization through an intervening solvent molecule would be anywhere near as large an effect since one must compare the acidity of the alkali metal cation with acidity induced by the alkali metal cation in a solvent molecule. This argument receives some

(8) R. A. Robinson and H. S. Harned, *Chem. Rev.*, **28**, 419 (1941).

(9) R. M. Diamond, *J. Amer. Chem. Soc.*, **80**, 4808 (1958).

(10) R. A. Y. Jones and A. R. Katritzky, *Chem. Ind. (London)*, 772 (1961).

(11) R. J. Gillespie and T. Birchall, *Can. J. Chem.*, **41**, 148 (1963).

(12) S. J. Kuhn and J. S. McIntyre, *ibid.*, **43**, 375, 995 (1965).

(13) J. Bello and H. R. Bello, *Nature*, **194**, 681 (1962).

(14) P. Piret, L. Rodrique, Y. Gobellin, and M. van Meerssche, *Acta Crystallogr.*, **20**, 482 (1966).

(15) R. A. Mackay and E. J. Poziomeck, *Inorg. Chem.*, **7**, 1454 (1968).

confirmation from the observation that all of the lithium and sodium salts in this study have osmotic coefficients that fall on or below the Debye–Hückel limiting slope. This is just what would be expected if cation–anion contact was favored.

Frank[16] and Prue[17,18] have explained the order of activity coefficients in water on the basis of the ease with which ions displace solvent molecules and come into contact. This model was able to account for the order of the osmotic coefficients of the alkali metal halides and nitrates in NMA.[2] The previous discussion has shown that formate, acetate, and propionate anions should displace solvent molecules from the inner coordination sphere of the alkali metal cations. The strongest interaction should occur with the smallest alkali metal cation, $Li^+$, so the order of osmotic coefficients $Li^+ < Na^+ < K^+$ is expected. The anion order is not easily predicted. Data on aqueous solutions show that propionate ion is the strongest base but it also has the highest steric requirements. The present results indicate that the steric requirement is the more important in this case. It is expected that for much stronger bases steric requirements will have less relative influence.

*II. Tetraalkylammonium Halides.* The results of the least-squares fit of the data for the tetraalkylammonium halides are given in Tables IV–VI and Figure 2. The standard deviations of both the temperature differences and the osmotic coefficients are given in Table IV. The standard deviations indicate that the osmotic coefficients are accurate to about 1%. In the final least-squares fit two experimental points, one for $Me_4NBr$ and one for $Et_4NBr$, were rejected because their deviations from the best fit were more than twice the standard deviation. Tetramethylammonium iodide was too insoluble to permit accurate measurements. Tetraethylammonium iodide and tetramethylammonium bromide have limited solubilities and only the $B$ term in eq 1 was necessary to fit the data.

**Table IV**

| Salt | $B$ | $C$ | Standard[a] error of $\theta$ | Standard error of $\phi$ |
|---|---|---|---|---|
| $Me_4NCl$ | 0.0153 | −0.1249 | 0.020 | 0.007 |
| $Et_4NCl$ | 0.1212 | −0.0835 | 0.031 | 0.010 |
| $Pr_4NCl$ | 0.1401 | −0.0629 | 0.025 | 0.007 |
| $Bu_4NCl$ | 0.2045 | −0.0963 | 0.055 | 0.010 |
| $Me_4NBr^b$ | −0.2341 | | | 0.004 |
| $Et_4NBr$ | −0.0875 | −0.0302 | 0.051 | 0.009 |
| $Pr_4NBr$ | −0.1427 | 0.0511 | 0.035 | 0.007 |
| $Bu_4NBr$ | −0.1064 | 0.0481 | 0.044 | 0.009 |
| $Et_4NI^b$ | −0.4082 | | | 0.007 |
| $Pr_4NI$ | −0.4981 | 0.2042 | 0.028 | 0.006 |
| $Bu_4NI$ | −0.5182 | 0.2419 | 0.044 | 0.010 |

[a] This is the standard deviation of the freezing point depression. [b] For these salts $C$ was set equal to zero and only $B$ calculated.
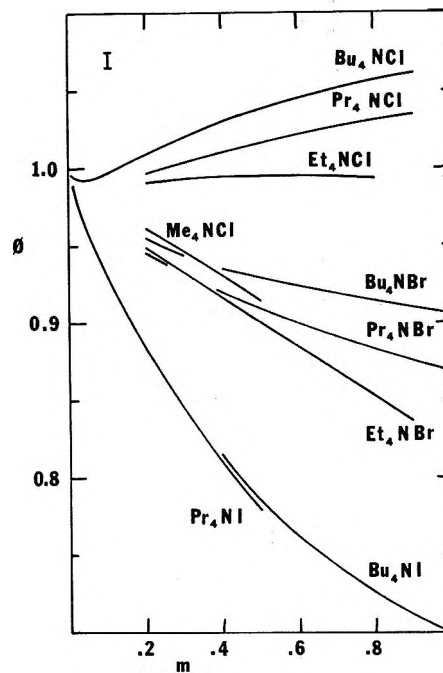
Figure 2. Osmotic coefficients in NMA *vs.* molality.

The osmotic coefficients of the iodides are below the Debye–Hückel limiting law [$\phi(DH) = 0.957$ at $0.2\ m$]. The same salts are below the limiting law in water.[19,20] The order of osmotic coefficients in Table II is $Bu_4NCl > Pr_4NCl > Et_4NCl > Me_4NCl > Bu_4NBr > Pr_4NBr > Et_4NBr > Me_4NBr > Bu_4NI > Pr_4NI$. The $Pr_4NBr$–$Et_4NBr$ order is reversed below $0.3\ m$ where the data are not as accurate. Similarly the $Pr_4NI$–$Bu_4NI$ order is reversed below $0.2\ m$, and the position of $Et_4NI$ is not certain. The anion order is $Cl^- > Br^- > I^-$ and this is exactly the same as the low concentration order of aqueous tetraalkylammonium solutions. It is also the reverse of the anion order of the alkali metals in water and NMA. In NMA the order is $Bu_4N^+ > Pr_4N^+ > Et_4N^+ > Me_4N^+$ and this order is less pronounced as the anion size increases. In the case of aqueous solutions the order is the same for the fluorides[21] and reverses with the chlorides[21,22] and bromides.[19] The same trend seems to be present in both water and NMA but while the iodide is apparently not big enough to cause a reversal in NMA, the reversal

(16) H. S. Frank, *J. Amer. Chem. Soc.,* **63,** 1789 (1941).

(17) J. E. Prue, "Chemical Physics of Ionic Solutions," B. E. Conway and R. G. Barradas, Ed., Wiley, New York, N. Y., 1966, p 163; (b) J. E. Prue, "Ionic Equilibria," Pergamon Press, Oxford, 1966, Chapter 10.

(18) J. E. Prue, A. J. Read, and G. Romeo, "Hydrogen Bonded Solvent Systems," A. K. Covington and P. Jones, Ed., Taylor and Francis, London, 1968, p 155.

(19) S. Lindenbaum and G. E. Boyd, *J. Phys. Chem.,* **68,** 911 (1964).

(20) S. Lindenbaum, L. Leifer, G. E. Boyd, and J. W. Chase, *ibid.,* **74,** 761 (1970).

(21) W. Y. Wen, S. Saito, and C. M. Lee, *ibid.,* **70,** 1244 (1966).

(22) J. P. Rupert and H. S. Frank, Abstracts, 5th Middle Atlantic Regional Meeting of the American Chemical Society, Newark, Del., April 1970.

**Table V:** Osmotic Coefficients, $\phi$

| $m$ | Me4NCl | Et4NCl | Pr4NCl | Bu4NCl | Me4NBr | Et4NBr | Pr4NBr | Bu4NBr | Et4NI | Pr4NI | Bu4NI |
|---|---|---|---|---|---|---|---|---|---|---|---|
| 0.01 | 0.991 | 0.992 | 0.992 | 0.993 | 0.988 | 0.990 | 0.989 | 0.989 | 0.986 | 0.985 | 0.985 |
| 0.05 | 0.981 | 0.988 | 0.989 | 0.992 | 0.969 | 0.977 | 0.975 | 0.977 | 0.959 | 0.957 | 0.956 |
| 0.10 | 0.974 | 0.988 | 0.991 | 0.997 | | 0.966 | 0.963 | 0.967 | 0.930 | 0.929 | 0.928 |
| 0.20 | 0.961 | 0.990 | 0.997 | 1.008 | | 0.949 | 0.946 | 0.954 | | 0.883 | 0.883 |
| 0.30 | 0.947 | 0.993 | 1.004 | 1.018 | | 0.932 | 0.932 | 0.944 | | 0.844 | 0.846 |
| 0.40 | 0.931 | 0.994 | 1.010 | 1.028 | | 0.917 | 0.920 | 0.935 | | 0.810 | 0.814 |
| 0.50 | 0.914 | 0.995 | 1.016 | 1.037 | | 0.901 | 0.909 | 0.929 | | 0.779 | 0.786 |
| 0.60 | | 0.995 | 1.022 | 1.044 | | 0.885 | 0.900 | 0.923 | | | 0.763 |
| 0.70 | | 0.995 | 1.027 | 1.051 | | 0.870 | 0.891 | 0.918 | | | 0.743 |
| 0.80 | | 0.993 | 1.031 | 1.057 | | 0.853 | 0.883 | 0.913 | | | 0.726 |
| 0.90 | | | 1.034 | 1.061 | | 0.837 | 0.876 | 0.910 | | | 0.712 |
| 1.00 | | | | | | | 0.869 | 0.907 | | | 0.701 |

**Table VI:** Activity Coefficients, $\gamma_{\pm}$

| $m$ | Me4NCl | Et4NCl | Pr4NCl | Bu4NCl | Me4NBr | Et4NBr | Pr4NBr | Bu4NBr | Et4NI | Pr4NI | Bu4NI |
|---|---|---|---|---|---|---|---|---|---|---|---|
| 0.01 | 0.971 | 0.973 | 0.974 | 0.975 | 0.967 | 0.969 | 0.968 | 0.969 | 0.962 | 0.960 | 0.959 |
| 0.05 | 0.941 | 0.953 | 0.956 | 0.962 | 0.917 | 0.932 | 0.928 | 0.932 | 0.899 | 0.894 | 0.893 |
| 0.10 | 0.920 | 0.945 | 0.951 | 0.963 | | 0.904 | 0.898 | 0.906 | 0.842 | 0.837 | 0.835 |
| 0.20 | 0.888 | 0.940 | 0.952 | 0.974 | | 0.863 | 0.856 | 0.870 | | 0.750 | 0.749 |
| 0.30 | 0.859 | 0.939 | 0.959 | 0.990 | | 0.829 | 0.823 | 0.843 | | 0.683 | 0.683 |
| 0.40 | 0.831 | 0.939 | 0.967 | 1.006 | | 0.799 | 0.796 | 0.822 | | 0.628 | 0.630 |
| 0.50 | 0.803 | 0.939 | 0.976 | 1.022 | | 0.771 | 0.773 | 0.804 | | 0.582 | 0.586 |
| 0.60 | | 0.938 | 0.984 | 1.038 | | 0.744 | 0.752 | 0.788 | | | 0.549 |
| 0.70 | | 0.937 | 0.993 | 1.052 | | 0.719 | 0.734 | 0.775 | | | 0.518 |
| 0.80 | | 0.934 | 1.001 | 1.066 | | 0.694 | 0.717 | 0.763 | | | 0.492 |
| 0.90 | | | 1.008 | 1.078 | | 0.671 | 0.702 | 0.752 | | | 0.469 |
| 1.00 | | | | | | | 0.688 | 0.743 | | | 0.450 |

occurs with at least two of the chlorides in water.[22] The reversal of the cation order in water and the low osmotic coefficients of the iodides have been ascribed to the unique structural properties of the water in the hydration spheres of the ions.[19-21 23] In the case of the iodides an increased structure-enforced ion pairing as the cation increases in size was postulated.[23] For the fluorides an increased structural salting-out was assumed[21] because of the incompatability of the kinds of structure making occurring in the ions. The unique structural properties of aqueous solutions are not present in NMA since nonpolar molecules do not enforce solvent structure in NMA.[24] In addition, the conductance[24,25] and surface tension[26] of the larger tetraalkylammonium ions in NMA do not show effects attributed to water-structure enhancement in aqueous solutions.[27-29] This means that the previous explanations for the low-concentration data in water are probably not correct since they fail to explain the similarity of the results in NMA.

At higher concentrations, the osmotic coefficients of some of the tetraalkylammonium halides in water show very irregular behavior.[19] This is quite probably due to the unique properties of aqueous solutions since the effects are not evident in NMA solutions. It is well known that cation-cation interactions have very large effects on the excess heats, entropies, and volumes of

tetraalkylammonium ions,[30-36] but relatively small effects on the free energies.[19]

Frank[16] has shown that the effects of dielectric saturation near an ion in water would greatly increase the attraction between ions so that cation-anion contacts would be common. In order to explain the activity coefficients of the alkali halides in water, it was neces-

(23) R. M. Diamond, *J. Phys. Chem.*, **67**, 2513 (1963).

(24) R. H. Wood and D. E. Delaney, *ibid.*, **72**, 4651 (1968).

(25) C. M. French and K. H. Glover, *Trans. Faraday Soc.*, **51**, 1427 (1955).

(26) (a) R. E. Singh, P. P. Rastogi, and R. Gopal, *Can. J. Chem.*, **46**, 3525 (1968); (b) R. Gopal and O. N. Bhatnagar, *J. Indian Chem. Soc.*, **44**, 1082 (1967).

(27) D. F. Evans and R. L. Kay, *J. Phys. Chem.*, **70**, 366 (1966).

(28) R. L. Kay and D. F. Evans, *ibid.*, **70**, 2325 (1966).

(29) R. L. Kay, T. Vituccio, C. Zawoyski, and D. F. Evans, *ibid.*, **70**, 2336 (1966).

(30) W. Y. Wen and S. Saito, *ibid.*, **68**, 2639 (1964).

(31) S. Lindenbaum, *ibid.*, **70**, 814 (1966).

(32) R. H. Wood and H. L. Anderson, *ibid.*, **71**, 1871 (1967).

(33) R. H. Wood, H. L. Anderson, J. D. Beck, J. R. France, W. E. DeVry, and L. J. Soltzberg, *ibid.*, **71**, 2149 (1967).

(34) W. Y. Wen and K. Nara, *ibid.*, **71**, 3907 (1967); **72**, 1137 (1968).

(35) W. Y. Wen, K. Nara, and R. H. Wood, *ibid.*, **71**, 3048 (1967).

(36) It also should be noted that the cation-anion interactions proposed in this paper cannot explain the large heat and volume changes observed on mixing tetraalkylammonium halides with the corresponding alkali metal halide[1-21] because there is no change in the cation-anion interaction during the mixing process.

sary to postulate that the hydration of the alkali metals resulted in a decreased tendency for cation–anion contacts. The balance between these two forces then accounts for the experimental results in water. These same effects will explain the present results. Models show that a halide ion can bury itself in the hydrocarbon portion of the n-tetraalkylammonium cation and that when this happens the radius of *closest approach* of the tetraalkylammonium ion is about 1.7 Å (this is the radius of the Cs+ ion). This distance does not vary much as the alkyl groups increase in length. In contrast the *average* radius of the $Bu_4N^+$ ion is about 4.9 Å.[37] This means that from some angles of approach this ion will have a very large radius while from other angles of approach it will be much smaller.[38] At a distance of 1.7 Å, the effective dielectric constant would be expected to be very low because of the very low dielectric constant of the hydrocarbon chains in the cation as well as the effect of dielectric saturation. This would result in very high attractive forces between the oppositely charged ions. Add to this the fact that the tetraalkylammonium ions are not strongly solvated and it is easy to account for an appreciable decrease in osmotic coefficients due to the occasional penetration of the anion to within 1.7 Å of the positively charged nitrogen atom.[39] Another way of saying this is that these effects make the effective Bjerrum radius[40] much larger than what would be expected on the basis of the macroscopic dielectric constant and also allow very low distances of closest approach. The order of osmotic coefficients in water can be explained by the very low effective radius of the tetraalkylammonium ions together with the ion–solvent competition principle.[17,18] It is postulated that the fluoride ion has strong enough solvation to prevent it from losing its solvation layer and coming into direct contact with the tetraalkylammonium ions. The osmotic coefficients are high and the butyl ion is the highest because of its larger effective size. In the case of the bromide and iodide where the solvation of the anion is weaker, the effective radii of the tetraalkylammonium ions are reduced to about 1.7 Å and appreciable cation–anion contact takes place. The iodide with its weaker solvation would have the lowest osmotic coefficients. The $Bu_4N^+$ ion would have the lowest osmotic coefficients because it would have about the same distance of closest approach and a lower effective dielectric constant (because of its larger alkyl groups).[41] The order of osmotic coefficients in NMA is explained in a similar way by assuming the iodide ion still has enough solvation so that cation–anion contacts are about equally frequent with all of the tetraalkylammonium ions.

In a series of papers Hughes and coworkers[42,43] have presented evidence from conductance measurements that interpenetration of anions and tetraalkylammonium cations occurs in some ketone solvents. The present results indicate that this is a more general phenom-

ena and that the effective radius of the tetraalkylammonium ions could be as low as 1.7 Å. Adams and Laidler[44] showed that the pressure and temperature dependence of the conductivity of some tetraalkylammonium halides in acetone indicated the presence of the two kinds of ion pairs. The authors concluded that solvent-shared and solvent-separated ion pairs were present. However, the ion size parameters derived in this study are more consistent with the conclusion that one of the two kinds of ion pairs that are formed is the contact ion pair postulated here. More recently Darbari and Petrucci[45] reported ultrasonic absorption data which support the conclusion that two kinds of ion pairs are present in acetone solutions.

It is interesting to note that the behavior of the tetraalkylammonium halides dissolved in water,[46] some alcohols,[47,48] and formamide[49-51] show some similarities to the present results. The amount of association increases as the size of the halide increases. This has been explained by Evans and Gardam[47] by the increase in solvation of the lower halides that is expected in hydrogen-bonding solvents like water, NMA, and the alcohols. In addition, the amount of association is relatively independent of cation size. In some cases the larger cations even have higher association constants. For instance the association constant for tetraheptylammonium iodide is larger than that for tetrabutylammonium iodide in ethanol, 1-propanol, and 1-butanol.[47] In 1-pentanol the association constants are equal.

(37) Reference 7, p 125.

(38) The small effective radius of the tetraalkylammonium ions postulated here explains why the trialkylsulfonium halides have similar properties to the tetraalkylammonium halides in aqueous solutions. The structural effect of the hydrocarbon chains is similar and the distances of closest approach are similar. See S. Lindenbaum, *J. Phys. Chem.*, **72**, 212 (1968), and D. F. Evans and T. L. Broadwater, *ibid.*, **72**, 1037 (1968), for details.

(39) It will require some force to push the hydrocarbon chains out of the way because their freedom of movement (free volume) will become somewhat more restricted. What is postulated here is that this is a small force compared with the attraction between the cation and anion.

(40) N. Bjerrum, *Kgl. Dan. Vidensk. Selsk.*, **7**, No. 9 (1926).

(41) Recent evidence suggests that the tetramethylammonium ion does not often come into contact with the iodide ion [D. W. Larsen, *J. Phys. Chem.*, **74**, 3380 (1970)].

(42) S. R. C. Hughes and S. H. White, *J. Chem. Soc. A*, 1216 (1966).

(43) S. R. C. Hughes and D. H. Price, *ibid.*, 1093 (1967).

(44) W. A. Adams and K. J. Laidler, *Can. J. Chem.*, **46**, 1977, 1989, 2005 (1968).

(45) G. S. Darbari and S. Petrucci, *J. Phys. Chem.*, **74**, 268 (1970).

(46) R. L. Kay, C. Zawoyski, and D. F. Evans, *ibid.*, **69**, 4208 (1965).

(47) D. F. Evans and P. Gardam, *ibid.*, **72**, 3281 (1968); **73**, 158 (1969).

(48) R. L. Kay, F. F. Evans, and G. P. Cunningham, *ibid.*, **73**, 3322 (1969).

(49) R. Gopal and M. M. Husain, *J. Indian Chem. Soc.*, **43**, 204 (1966).

(50) R. Gopal and M. A. Siddiqi, *Z. Phys. Chem. (Frankfurt am Main)*, **67**, 122 (1969).

(51) R. Gopal and K. Singh, *ibid.*, **69**, 81 (1970).

The conductance studies also show that the distances of closest approach necessary to fit the data are very low and independent of the cation. Evans and co-workers concluded that contact as well as solvent-separated ion pairs were involved[47] and that at least part of the particular concentration dependence of aqueous solutions was a general feature of hydrogen-bonding solvents.[52] This behavior is consistent with the very low distances of closest approach that are possible with the large tetraalkylammonium ions.

Solvents which solvate cations very strongly would be expected to solvate the tetraalkylammonium ions. Models show that a low distance of closest approach is possible for at least one solvent molecule. With these solvents close cation–anion contacts might not occur and the tetraalkylammonium ions would behave as ordinary large ions. Some examples of solvents exhibiting this type of behavior are acetonitrile,[53] nitromethane,[54] and nitrobenzene.[53,55,56] In order to predict the behavior of a solvent, it will be necessary to know more about the energy of the process

$$R_4N^+ \cdot nS + X^- \cdot mS \longrightarrow$$
$$R_4N^+X^- \cdot pS + (n + m - p)S$$
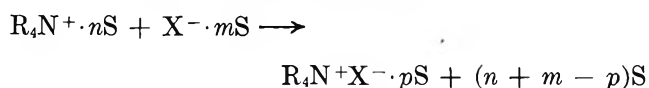
where S denotes a solvent molecule. This equation shows that the relative ease of displacement of solvent from a tetraalkylammonium ion will depend on the difference between the solvation energy of the cation and the solvation energy of a solvent molecule. The normal behavior of acetonitrile, nitrobenzene, etc., could be due to a reasonably high energy of solvation of the cations together with a low energy of solvation of the solvent. In water, the alcohols, and NMA the energy of solvation of the solvent is much higher and this favors cation–anion contact.

(52) T. L. Broadwater and D. F. Evans, *J. Phys. Chem.*, **73**, 3985 (1969).

(53) D. F. Evans, C. Zawoyski, and R. L. Kay, *ibid.*, **69**, 3878 (1965).

(54) R. L. Kay, S. C. Blum, and H. I. Schiff, *ibid.*, **67**, 1223 (1963).

(55) E. G. Taylor and C. A. Kraus, *J. Amer. Chem. Soc.*, **69**, 1731 (1947).

(56) C. T. Witschonke and C. A. Kraus, *ibid.*, **69**, 2474 (1947).

# Solvation Studies. II. Some Alkaline Earth Halides in High Dielectric Solvents

## by A. Finch, P. J. Gardner,* and C. J. Steadman

*Moore Laboratory, Chemistry Department, Royal Holloway College, Surrey, United Kingdom* (Received September 15, 1970)

*Publication costs borne completely by The Journal of Physical Chemistry*

The standard enthalpies of solution of the chlorides and bromides of calcium, strontium, and barium in formamide (F), N-methylformamide (NMF), and N,N-dimethylformamide (DMF) are reported (excepting barium chloride in NMF and DMF and barium bromide in DMF). Debye–Hückel limiting law slopes are compared with those obtained experimentally. Structural implications of enthalpies of transfer and combined ion solvation enthalpies are discussed. Individual ionic entropies are estimated from a correspondence principle.

## Introduction

In part I,[1] corresponding data for alkaline earth chlorates and bromates in F, NMF, and DMF were reported. Since then there have been several calorimetric studies using these[2-5] and other[6-9] nonaqueous solvents (*e.g.*, N-methylacetamide, dimethyl sulfoxide, and propylene carbonate). Usually salts of the alkali metals or alkylammonium halides have been employed. Data for diunivalent electrolytes remain scarce.

In this work an isoperibol (constant-temperature environment) solution calorimeter was used to measure

(1) A. Finch, P. J. Gardner, and C. J. Steadman, *J. Phys. Chem.*, **71**, 2996 (1967).

(2) D. V. S. Jain, B. S. Lark, S. P. Kochar, and V. K. Gupta, *Indian J. Chem.*, **7**, 256 (1969).

(3) L. Weeda and G. Somsen, *Recl. Trav. Chim. Pays-Bas*, **85**, 159 (1966).

(4) R. P. Held and C. M. Criss, *J. Phys. Chem.*, **71**, 2487 (1967).

(5) C. M. Criss and E. Luksha, *ibid.*, **72**, 2966 (1968).

the enthalpies of solution of the chlorides and bromides of calcium, strontium, and barium in F, NMF, and DMF (excepting barium chloride in NMF and DMF and barium bromide in DMF) within the concentration range 0.003–0.06 $m$ and at 25°.

## Experimental Section

*Solvents.* These were purified and assayed for conductivity and water content as described in part I.[1]

*Solutes.* These were rarely obtainable commercially in anhydrous form and direct thermal dehydration often resulted in decomposition.

(i) AnalaR (BDH) samples of $CaCl_2 \cdot 6H_2O$, $SrCl_2 \cdot 6H_2O$, and $BaCl_2 \cdot 2H_2O$ were dehydrated in a slow stream of hydrogen chloride gas over a period of 7 days, the sample temperature gradually being increased from ambient to 500°. The samples were then purged with a fast stream of dry oxygen-free nitrogen. Conventional halide analysis gave: $CaCl_2$, 99.8; $SrCl_2$, 99.6; $BaCl_2$, 100.2% purity.

(ii) Calcium bromide dihydrate (Hopkins and Williams) was dehydrated as above in a stream of hydrogen bromide (purified by passing through a trap at $-65°$) in an all-glass apparatus. Halide analysis gave: $CaBr_2$, 99.8% purity.

(iii) Strontium bromide hexahydrate and $BaBr_2 \cdot 2H_2O$ (BDH) were dehydrated at 14 mm and at 180° (12 hr), followed by 300° (*ca.* 3 hr). Halide analysis gave: $SrBr_2$, 100.6; $BaBr_2$, 100.0.

Handling subsequent to dehydration was performed in a dry nitrogen-filled glove bag. Water content determinations (Karl Fischer) of the solutions at the conclusion of typical calorimetric runs showed an increase of *ca.* 0.01% by weight.

*Calorimeter.* An isoperibol solution calorimeter of all-glass construction[10] and operating at 25° was used. Temperature sensing was by thermistor and calibration was electrical. Errors[11] in the experimental $\Delta H$ data derive from two sources. First, a constant proportional error in $\Delta H$ due to uncertainties in electrical standards, thermal leakage corrections etc., and second, a variable proportional error in $\Delta H$ due to the limits imposed by thermometer sensitivity, variations in ampoule fracture energy, etc. The former error was assessed *via* the reproducibility of a typical electrical calibration and was *ca.* 0.1%. The latter error is inversely proportional to the temperature rise ($\Delta T$ in °C), and hence to $m$ in a series of runs on one substance, and is given by $\delta(\Delta H)/\Delta H \sim 0.3\%/\Delta T$ for the calorimeter used in this work. Alternatively expressed, this error is inversely proportional to $\Delta H$ and $m$. The maximum error from this source was *ca.* 1% and commonly 0.5%. The precision and accuracy of the system was checked by two standard reactions: (i) for the enthalpy of solution of potassium chloride in water, the mean of eight observations was $\Delta H$ (25°, $N = 200$) = 4.213 ± 0.005 kcal mol$^{-1}$ (lit.[12] 4.196 to 4.204 kcal mol$^{-1}$ de-

pending on sample pretreatment and 4.196 ± 0.010 kcal mol$^{-1}$ from a literature survey[13] up to 1965, both data at $N = 200$ and 25°) and (ii) for the neutralization of tris(hydroxymethyl)aminomethane (THAM) in excess 0.1 $M$ aqueous hydrochloric acid, the mean of 11 observations was $\Delta H$ (25°, $670 < N < 1030$) = $-7.15$ ± 0.01$_5$ kcal mol$^{-1}$ (lit.[14] $-7.116$ ± 0.001 kcal mol$^{-1}$ at 25° and $1180 < N < 1570$). $N$ is the mole ratio of water to solute. The heat of dilution correction for potassium chloride was taken from Parker[13] and is negligible[15] for THAM. The uncertainty interval for the above data is $\pm \bar{s}$, where $\bar{s}$ is the standard deviation of the mean. All thermochemical results are given in terms of the defined calorie, 1 cal = 4.1840 J.

**Table I:** Enthalpies of Solution of Some Alkaline Earth Halides in Nonaqueous Solvents at 25°[a]

| Salt–solvent | Molality, $m$ | $\Delta H_s(m)$, kcal mol$^{-1}$ |
|---|---|---|
| CaBr$_2$–F | 0.0073 | $-29.58$ |
| | 0.0080 | $-29.89$ |
| | 0.0123 | $-29.27$ |
| | 0.0191 | $-27.63$ |
| CaBr$_2$–NMF | 0.0053 | $-32.27$ |
| | 0.0062 | $-31.79$ |
| | 0.0088 | $-31.51$ |
| | 0.0089 | $-31.00$ |
| | 0.0155 | $-30.72$ |
| CaBr$_2$–DMF | 0.0063 | $-37.63$ |
| | 0.0096 | $-37.46$ |
| | 0.0102 | $-37.21$ |
| | 0.0153 | $-36.57$ |
| | 0.0215 | $-36.27$ |

[a] A complete tabulation of the enthalpy of solution data in the style of the typical data given in Table I will appear immediately following this article in the microfilm edition of this volume of the journal. Single copies may be obtained from the Reprint Department, ACS Publications, 1155 Sixteenth St., N.W., Washington, D. C. 20036. Remit $3.00 for photocopy or $2.00 for microfiche.

## Results

Some typical enthalpy of solution data are given in

(6) L. Weeda and G. Somsen, *Recl. Trav. Chim. Pays-Bas,* **86,** 263 (1967).

(7) H. L. Friedman, *J. Phys. Chem.,* **71,** 1723 (1967).

(8) C. V. Krishnan and H. L. Friedman, *ibid.,* **73,** 1572 (1969).

(9) C. V. Krishnan and H. L. Friedman, *ibid.,* **73,** 3934 (1969).

(10) A. Finch and P. J. Gardner, *J. Chem. Soc. (London),* 2985 (1964).

(11) We are indebted to a referee for drawing our attention to this analysis.

(12) S. R. Gunn, *J. Phys. Chem.,* **69,** 2902 (1965).

(13) V. B. Parker, "Thermal Properties of Aqueous Uni-univalent Electrolytes," NSRDS-NBS 2, National Bureau of Standards, 1965.

(14) J. O. Hill, G. Öjelund, and I. Wadsö, *J. Chem. Thermodyn.,* **1,** 111 (1969).

(15) R. J. Irving and I. Wadsö, *Acta Chem. Scand.,* **18,** 195 (1964).

**Table II**

| Salt | Solvent | $\Delta H_s(m)$, kcal mol$^{-1}$ | Molality, $m$ | $\Delta H_s^\circ$, kcal mol$^{-1}$ | $a$,[a] kcal mol$^{-1/2}$ kg$^{1/2}$ |
|------|---------|------|------|------|------|
| CaCl$_2$ | H$_2$O | | | $-19.38 \pm 0.01$†[b] | 1.5 |
| SrCl$_2$ | H$_2$O | | | $-12.05 \pm 0.01$† | 1.4 |
| BaCl$_2$ | H$_2$O | | | $-3.38 \pm 0.01$† | 1.4 |
| CaCl$_2$ | F | $-21.9 \pm 0.1$ ($-19.1$) | 0.025–0.033 | $-22.7 \pm 0.8$ | $5 \pm 5$ |
| SrCl$_2$ | F | $-17.5_5 \pm 0.2$ ($-17.7$) | 0.008–0.023 | $-17.6 \pm 0.5$ | $0 \pm 4$ |
| BaCl$_2$ | F | $-10.4 \pm 0.2$ ($-11.4$) | 0.01–0.04 | $-10.0 \pm 0.3$ | $-2 \pm 2$ |
| CaCl$_2$ | NMF | $-22.0 \pm 0.7$ | 0.008–0.02 | $-24.3 \pm 0.9$ | $20 \pm 8$ |
| SrCl$_2$ | NMF | $-17.3 \pm 0.3$ | 0.01–0.017 | $-16.2 \pm 1.3$ | $-9 \pm 11$ |
| CaCl$_2$ | DMF | $-20.4 \pm 0.9$ | 0.006–0.05 | $-23.8 \pm 2.2$ | $25 \pm 15$ |
| SrCl$_2$ | DMF | | | $-15.8 \pm 0.6$† | $14 \pm 4$ |
| CaBr$_2$ | H$_2$O | | | $-24.61 \pm 0.01$† | 1.3 |
| SrBr$_2$ | H$_2$O | | | $-16.82 \pm 0.01$† | 1.2 |
| BaBr$_2$ | H$_2$O | | | $-5.61 \pm 0.01$† | 1.2 |
| CaBr$_2$ | F | $-29.6 \pm 0.3$ ($-26.8$) | 0.008–0.019 | $-29.9 \pm 0.8$ | $3 \pm 7$ |
| SrBa$_2$ | F | $-25.3 \pm 0.2$ | 0.007–0.012 | $-26.0 \pm 0.6$ | $7 \pm 6$ |
| BaBr$_2$ | F | $-15.4 \pm 0.2$ ($-14.4$) | 0.016–0.026 | $-16.3 \pm 0.6$ | $7 \pm 4$ |
| CaBr$_2$ | NMF | | | $-34.0_5 \pm 0.7$† | $28 \pm 7$ |
| SrBr$_2$ | NMF | | | $-28.0 \pm 0.3$† | $22 \pm 2$ |
| BaBr$_2$ | NMF | $-17.5 \pm 0.1$ | 0.008–0.027 | $-18.0 \pm 0.4$ | $4 \pm 3$ |
| CaBr$_2$ | DMF | | | $-39.6 \pm 0.3$† | $22 \pm 3$ |
| SrBr$_2$ | DMF | | | $-34.1 \pm 0.4$† | $29 \pm 4$ |

[a] The random error in $a$ for aqueous solutions is ca. $\pm 4\%$.  [b] †, cases where linear dependence was significant.

Table I for the reaction

$$\Delta H_s(m) = \Delta H_f^\circ [\text{M}^{II}\text{X}_2, \text{ solution of molality } m] - \Delta H_f^\circ [\text{M}^{II}\text{X}_2, \text{ cryst}]$$

where M is Ca, Sr, or Ba and X = Cl or Br. All experiments were performed at $25.0 \pm 0.1°$. Barium chloride and bromide had a low solubility in DMF and, in addition, barium chloride dissolved very slowly in NMF. These factors precluded measurements for these combinations. All other reactions were complete within 5 min except for calcium chloride in DMF for which the duration of the main period was ca. 15 min.

The experimental data were fitted to the Debye–Hückel limiting law[16] and values of $\Delta H_s^\circ$ and $a$, with

$$\Delta H_s = \Delta H_s^\circ + am^{1/2}$$

their associated uncertainties, are collected in Table II. Only in those cases where the linear dependence was significant (those marked † in Table II) was the value of $\Delta H_s^\circ$ so calculated used in subsequent calculations. For all remaining cases a mean value of the experimental data [$\Delta H_s(m)$ in Table II] was taken and identified with $\Delta H_s^\circ$ in subsequent calculations. In tabulating this mean, the uncertainty interval is the range for four or less observations and is $\pm \bar{s}$ for five or more observations, where $\bar{s}$ is the standard deviation of the mean.

These data are collected and compared with the corresponding data for aqueous solutions[17-19] in Table II. Some literature data[2] for some of the salts in F are given in parentheses. The agreement is poor in most cases.

**Discussion**

The theoretical value of the limiting-law constant is given by

$$a = \frac{2}{3}\sqrt{6}\mathcal{S}_H d_0^{1/2}$$

(where $d_0$ = solvent density at $25°$) and has the following values at $25°$: 2.4 (H$_2$O),[19] 0.7 (F),[20,21] 4.1 (NMF),[22,23] and 10.1 (DMF)[24-26] kcal mol$^{-1/2}$ kg$^{1/2}$, using

(16) H. S. Harned and B. B. Owen, "The Physical Chemistry of Electrolytic Solutions," 3rd ed, Reinhold, New York, N. Y., 1958, p 334.

(17) P. Ehrlich, K. Peik, and E. Koch, Z. Anorg. Allg. Chem., 324, 113 (1963).

(18) F. D. Rossini, et al., Nat. Bur. Stand. (U. S.) Circ. No. 500 (1952).

(19) Reference 16, Appendix A, Table (8-2-1A), p 707.

(20) L. R. Dawson, T. M. Newell, and W. J. McCreary, J. Amer. Chem. Soc., 76, 6024 (1954).

(21) G. R. Leader, ibid., 73, 356 (1951).

(22) Yu. I. Sinyakov, A. I. Gorbanev, Yu. M. Povarov, and Yu. Mo. Kesslev, Izv. Akad. Nauk SSSR, Otd. Khim. Nauk, 1514 (1961).

(23) S. J. Bass, W. I. Nathan, R. M. Meighan, and R. H. Cole, J. Phys. Chem., 68, 509 (1964).

(24) J. R. Ruhoff and E. E. Reid, J. Amer. Chem. Soc., 59, 401 (1937).

(25) B. V. Ioffe, Zh. Obshch. Khim., 25, 902 (1955).

(26) G. R. Leader and J. F. Gormley, J. Amer. Chem. Soc., 73, 5731 (1951).

**Table III:** Lattice Enthalpies ($\Delta H_L$), Combined Ion Solvation Enthalpies ($\Phi$),
and Enthalpies of Transfer ($\Delta\Phi$) in kcal mol$^{-1}$ at 25°

| Salt | $-\Delta H_L$ | $-\Phi_{D_2O}(\Delta\Phi)$ | $-\Phi_{H_2O}$ | $-\Phi_F(\Delta\Phi)$ | $-\Phi_{NMF}(\Delta\Phi)$ | $-\Phi_{DMF}(\Delta\Phi)$ |
|------|------|------|------|------|------|------|
| CaCl$_2$ | 540.1 | 558.4 ($-1.1$)$^a$ | 559.5 | 562.0 (2.5) | 562.1 (2.6) | 560.5 (1.0) |
| SrCl$_2$ | 514.7 | 525.6 ($-1.1$)$^a$ | 526.7 | 532.2 (5.5) | 532.0 (5.3) | 530.5 (3.8) |
| BaCl$_2$ | 490.5 | 492.3 ($-1.6$)$^a$ | 493.9 | 500.9 (7.0) | | |
| CaBr$_2$ | 519.3 | | 543.9 | 548.9 (5.0) | 553.3 (9.4) | 558.9 (15.0) |
| SrBr$_2$ | 494.4 | | 511.2 | 519.7 (8.5) | 522.4 (11.2) | 528.5 (17.0) |
| BaBr$_2$ | 472.8 | | 478.4 | 488.2 (9.8) | 490.3 (11.9) | |

$^a$ These enthalpies of transfer are slightly different to those given in the original reference[34] due to the use of different data for $\Delta H_s$
(MX$_2$ in H$_2$O).

physical constants from the references indicated. Although the experimental data for $a$ are associated with considerable uncertainty intervals, it appears that the experimental slopes for aqueous solutions are lower and those for nonaqueous phases are higher than the theoretical slopes. This is in contrast to the alkaline earth halates where there was good agreement for the solvents NMF and DMF. In the case of the positive deviations, the most likely cause is incomplete dissociation at the concentration under study. This has been noted previously for certain uni-univalent salts in NMF.[27] Gunn[28] has discussed the earlier literature concerning Debye–Hückel slopes from enthalpy of solution measurements in nonaqueous solvents with dielectric constants less than that of water and notes positive deviations in ammonia and methanol for several valence types. Young and Seligmann[29] have commented that experimental slopes for diuniivalent electrolytes in aqueous solutions are usually in agreement with theoretical slopes, but with less precision than the corresponding slopes for uni-univalent electrolytes.

Combined ion solvation enthalpies ($\Phi$) are obtained from $\Delta H_L = \Phi - \Delta H_s{}^\circ$, where $\Delta H_L$, the lattice enthalpy at 25°, is calculated from

$$\Delta H_L = \Delta H_f{}^\circ[\text{MX}_2, \text{cryst}]^{17} -$$
$$\Delta H_f{}^\circ[\text{M,g}]^{30} - 2\Delta H_f{}^\circ[\text{X,g}]^{31} +$$
$$2[A + {}^5\!/_2 RT]^{32} - [I_1 + I_2 + 5RT]^{33}$$

with the numerical data from the references indicated. Enthalpies of transfer ($\Delta\Phi$) for the following reaction

$$[\text{M}^{2+} + 2\text{X}^-](\text{solv}, a_\pm = 1) =$$
$$[\text{M}^{2+} + 2\text{X}^-](\text{aq}, a_\pm = 1)$$
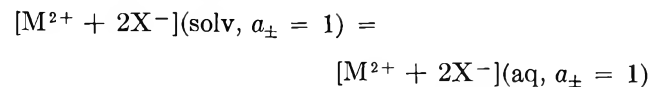
are given by the difference between the combined ion enthalpies of aquation and solvation

$$\Delta\Phi = \Phi(\text{aq}) - \Phi(\text{solv}) = \Delta H_s{}^\circ(\text{aq}) - \Delta H_s{}^\circ(\text{solv})$$

Combined ion solvation enthalpies, lattice enthalpies, and enthalpies of transfer (in parentheses) are compared with some corresponding literature data[34] for D$_2$O in Table III.

The precision of the combined ion solvation enthal-

**Table IV:** Ionic Partial Molal Entropies at 25°
(Hypothetical Unit Molal Solution as Standard
State) in cal °$K^{-1}$ mol$^{-1}$

| Ion | $\bar{S}_2{}^\circ(\text{H}_2\text{O})$ [conv]$^a$ | $\bar{S}_2{}^\circ(\text{H}_2\text{O})$ [abs]$^b$ | $\bar{S}_2{}^\circ(\text{F})$ | $\bar{S}_2{}^\circ(\text{NMF})$ | $\bar{S}_2{}^\circ(\text{DMF})$ |
|-----|------|------|------|------|------|
| Ca$^{2+}$ | $-13.2$ | $-23.2$ | $-15.4$ | $-22.5$ | $-35.3$ |
| Sr$^{2+}$ | $-9.4$ | $-19.4$ | $-13.0$ | $-19.8$ | $-32.3$ |
| Ba$^{2+}$ | 3 | $-7$ | $-5$ | $-11$ | $-22.5$ |
| Cl$^-$ | 13.2 | 18.2 | 11.1 | 7.3 | $-2.6$ |
| Br$^-$ | 19.29 | 24.29 | 15.0 | 11.7 | 2.2 |

$^a$ From ref 39.   $^b$ See text.

pies is $ca. \pm 0.8$ kcal mol$^{-1}$ and for the enthalpies of transfer $ca. \pm 0.3$ kcal mol$^{-1}$. Some trends (in terms of $-\Phi$) are: (i) a decrease with increasing cation size; (ii) a decrease with increasing anion size; and (iii) an increase with decreasing "structure" of the solvent in the case of the bromides. The relative extent of internal structural order has been rationalized for the nonaqueous solvents[1] and for deuterium oxide.[35] The sequence is D$_2$O > H$_2$O > F > NMF > DMF in decreasing structural order. Observations (i) and (iii) are confirmed[1] for the corresponding alkaline earth halates. Observations (i) and (ii) are in qualitative accord with the Born electrostatic solvation model although the enthalpies of transfer conflict with this model as do corresponding data for the halates.[1] In the interpretation of enthalpies of transfer for the al-

(27) R. P. Held and C. M. Criss, *J. Phys. Chem.*, **69**, 2611 (1965).

(28) S. R. Gunn and L. G. Green, *ibid.*, **64**, 1066 (1960).

(29) T. F. Young and P. Seligmann, *J. Amer. Chem. Soc.*, **60**, 2379 (1938); see also ref 16, p 339.

(30) H. A. Skinner and G. Pilcher, *Quart. Rev. Chem. Soc.*, **17**, 264 (1963).

(31) D. D. Wagman, W. H. Evans, V. B. Parker, I. Halow, S. M. Bailey, and R. H. Schumm, *Nat. Bur. Stand. (U. S.) Tech. Note*, No. 270-3 (1968).

(32) R. S. Berry and C. W. Reimann, *J. Chem. Phys.*, **38**, 1540 (1963).

(33) C. E. Moore, *Nat. Bur. Stand. (U. S.) Circ.*, No. 467 (1949–1958) (Vol. I, 1949; Vol. II, 1952; Vol. III, 1958).

(34) J. Greyson and H. Snell, *J. Phys. Chem.*, **73**, 3208 (1969).

(35) G. Nemethy and H. A. Scheraga, *J. Chem. Phys.*, **41**, 680 (1964).

**Table V:** Crystalline Entropies, $S°$(cryst), Entropies of Solution, $\Delta S_s°$, and Gibbs Energies of Solution, $\Delta G_s°$, at 25°

| Salt | $S°$(cryst), cal °K$^{-1}$ mol$^{-1}$ | $\Delta S_s°$(F), cal °K$^{-1}$ mol$^{-1}$ | $\Delta G_s°$(F), kcal mol$^{-1}$ | $\Delta S_s°$(NMF), cal °K$^{-1}$ mol$^{-1}$ | $\Delta G_s°$(NMF), kcal mol$^{-1}$ | $\Delta S_s°$(DMF), cal °K$^{-1}$ mol$^{-1}$ | $\Delta G_s°$(DMF), kcal mol$^{-1}$ |
|---|---|---|---|---|---|---|---|
| CaCl$_2$ | 27.2 | $-20.4$ | $-15.8$ | $-35.1$ | $-11.5$ | $-67.7$ | $-0.2$ |
| SrCl$_2$ | 28 | $-19$ | $-12$ | $-33$ | $-7.5$ | $-65.5$ | $+4$ |
| BaCl$_2$ | 30 | $-13$ | $-6.5$ | $-26$ | | $-58$ | |
| CaBr$_2$ | 31 | $-16$ | $-25$ | $-30$ | $-25.1$ | $-62$ | $-21$ |
| SrBr$_2$ | (33.8)$^a$ | $-16.8$ | $-20.3$ | $-30.2$ | $-19.0$ | $-61.7$ | $-15.7$ |
| BaBr$_2$ | (35.5)$^a$ | $-10.5$ | $-12.3$ | $-23.5$ | $-10.5$ | $-53.5$ | |

$^a$ Estimates.[39]

kali halides from F,[36] NMF,[3] and $N$-methylacetamide,[6] Somsen successfully applies a solvation model due to van Eck.[36] This model requires that $\Delta\Phi$ for salts with a common anion is a constant dependent only on the nonaqueous phase and is independent of the cation. Only for lithium salts does van Eck's model conflict with Somsen's data. It is clear from the data in Table III that this model is not applicable to the alkaline earth halides.

Criss[37] has derived partial molal entropies for univalent ions in several nonaqueous solvents using a correspondence principle[38] in the form

$$\bar{S}_2°(A) = a + b\bar{S}_2°(H_2O)$$

where $a$ and $b$ are constants depending on the solvent A. It is of interest to see if this expression, using Criss' constants, is applicable to divalent ions. A rough test is to use the derived partial molal entropies with crystal entropies to obtain entropies of solution, whence Gibbs energies of solution follow on combination with the experimental enthalpies of solution. It may be seen whether these Gibbs energies are of sensible magnitude and conform to known solubility trends. Taking the hypothetical unit molal solution as standard state, Criss' equation becomes

$$\bar{S}_2°(A) = (a + c_A - bc_{H_2O}) + b\bar{S}_2°(H_2O)$$

where $c_i = R \ln (1000/M_i)$, $M$ = molecular weight. Values for $\bar{S}_2°(H_2O)$ were taken from Latimer[39] and converted to "absolute" entropies via $\bar{S}_2°$(abs) = $\bar{S}_2°$ (conventional) $- 5z$, the value of $-5$ cal °K$^{-1}$ mol$^{-1}$ being used by Criss[37] and being close to the latest estimation[40] of the partial molal entropy of the aquated proton ($-4.8 \pm 1.2$ cal °K$^{-1}$ mol$^{-1}$). Partial molal entropies for the ions are given in Table IV. Crystalline entropies from Latimer,[39] derived entropies and Gibbs energies of solution are given in Table V.

As all of the $\Delta G_s°$ data in the above table are numerically reasonable in the light of known solubilities, the estimates of the ionic entropies for the divalent ions in Table IV are acceptable.

(36) G. Somsen and J. Coops, *Recl. Trav. Chim. Pays-Bas*, **84**, 985 (1965).

(37) C. M. Criss, R. P. Held, and E. Luksha, *J. Phys. Chem.*, **72**, 2970 (1968).

(38) J. W. Cobble, *Annu. Rev. Phys. Chem.*, **17**, 27 (1966).

(39) W. M. Latimer, "The Oxidation States of the Elements and their Potentials in Aqueous Solutions," 2nd ed, Prentice-Hall, Englewood Cliffs, N. J., 1952.

(40) C. L. de Ligny, M. Alfenaar, and N. G. van der Veen, *Recl. Trav. Chim. Pays-Bas*, **87**, 585 (1968).

# The Enthalpy of Solution of Some Molecules in Aqueous Tetraalkylammonium

# Bromide Solutions and the Apparent Expansion Coefficient

# of the Aqueous Salt Solution

### by Michel Lucas* and André Feillolay

*Département de Chimie, Centre d'Etudes Nucléaires, Fontenay-aux-Roses, France*   (*Received January 18, 1971*)

*Publication costs assisted by the Commissariat à l'Energie Atomique*

The enthalpy of solution of liquid chloroform, butanol, and isopropyl alcohol in various aqueous tetraalkyl-ammonium bromide solutions has been measured at 15°. A few measurements have been done at 25°. The density of some of the salt solutions at 5.7 and 24.2° has also been determined. The thermal expansion coefficients have been calculated for the salt solution. The experimental values of the enthalpies have been compared with values calculated by means of equations derived from the scaled particle theory. The fit between calculated and experimental values is only qualitative. However, a correlation exists between the enthalpy and the expansion coefficient of the solution. The molar heat capacity change for the solution process of gaseous chloroform in aqueous tetrabutylammonium bromide solution has also been calculated and compared with the experimental one.

## Introduction

The scaled particle theory has been used rather successfully by Pierotti,[1] to predict the values of free energy and enthalpy of solution for nonpolar molecules in pure water.

Lebowitz and Rowlinson,[2] extended the Percus–Yevick theory to mixtures of hard spheres, and it has been found possible to extend the calculations of Pierotti to mixtures of water and another solvent.

Experimental data of the enthalpy of solution of some nonpolar molecules in aqueous ethanol solutions have been compared with the data calculated by means of the equations derived from the extended theory.[3] Then the peculiar shape of curves of enthalpy when plotted aginst the ethanol molar fraction could be explained.

Our purpose in the present paper is to compare experimental data of enthalpy and calculated ones for molecular solutes in the aqueous tetraalkylammonium solutions. From the theory, a close relationship should exist between the enthalpy and the apparent thermal expansion coefficient of the solution $\alpha$ given by the equation

$$\alpha = -\frac{1}{d}\frac{\partial d}{\delta T} \tag{1}$$

where $d$ is the density of the salt solution at a given temperature $T$.

From measurements of apparent molal volumes of the tetraalkylammonium bromides in water at various temperatures,[4,5] it has been possible to calculate $\alpha$ for some aqueous salt solutions.

The plots of $\alpha$ against the salt molality show unusual features. According to the scaled particle theory,

similar characteristics should be observed when the enthalpy of solution for a molecule is plotted against the salt molality. This research has been undertaken in order to examine if such a correlation does really exist. The equations derived from the scaled particle theory[1,3] are strictly valid only when the solutes under consideration are nonpolar molecules. Owing to the limited sensitivity of our calorimetric apparatus, measurements have been done with more soluble polar solutes: chloroform, 1-butanol, and isopropyl alcohol. Arnett[6] has studied the enthalpy of solution of many polar and nonpolar molecules in aqueous ethanol solutions. The plots of the enthalpy against the ethanol molar fraction are very similar for nonpolar and moderately polar solutes. Thus it is hoped that our results will be significant.

The solvents were aqueous solutions of tetrabutyl, tetrapropyl, and tetraethylammonium bromides at 15°. Some measurements have been done at 25°. Also, for values of $m$ smaller than 1, some density measurements have been done in order to get the expansivity coefficients with the required accuracy.

## Experimental Section

*Chemicals.* The tetraethyl and tetrabutylammo-

(1) R. A. Pierotti, *J. Phys. Chem.*, **69**, 281 (1965).

(2) J. L. Lebowitz and J. S. Rowlinson, *J. Chem. Phys.*, **41**, 133 (1964).

(3) M. Lucas and A. Feillolay, *Bull. Soc. Chim. Fr.*, 1267 (1970).

(4) W. Y. Wen and S. Saito, *J. Phys. Chem.*, **68**, 2639 (1964).

(5) M. Lucas and A. de Trobriand, *ibid.*, in press.

(6) E. M. Arnett, P. M. Dugglesby, and J. J. Burke, *J. Amer. Chem. Soc.*, **85**, 1351 (1963).
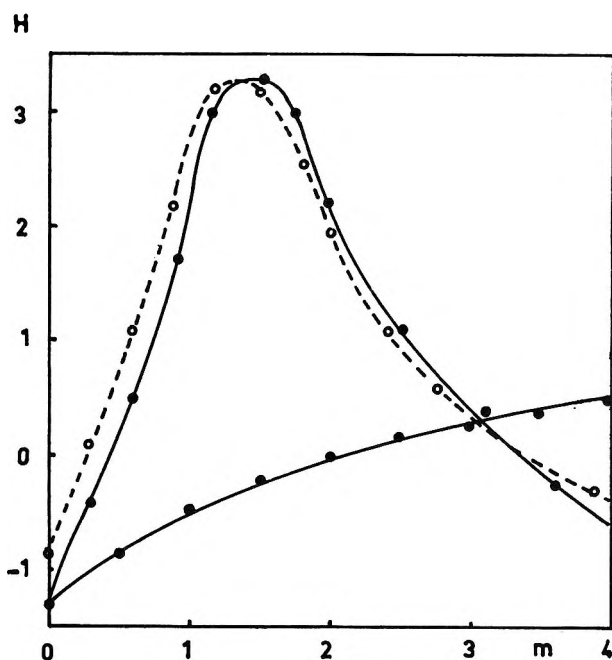
Figure 1. Enthalpy of solution of liquid chloroform in
aqueous salt solution against salt molality: units, kcal/mol.
Solid circles, temperature 15°; salts, tetraethyl and
tetrabutylammonium bromides; open circles, 25°,
tetrabutylammonium bromide.



Figure 2. Enthalpy of solution of liquid butanol and isopropyl
alcohol and gaseous methane and propane in aqueous salt
solutions at 15°: open circles, tetrabutylammonium
bromide; solid circles, tetrapropylammonium bromide.
Right ordinate for propane only: units, kcal/mol.

nium bromides, Carlo Erba, Polarographic grade, were
dried at 70° *in vacuo* for days before use. The tetra-
propylammonium bromide (Eastman Kodak) was
purified according to the procedure given in ref 4.
The chloroform, butanol, and isopropyl alcohol, R.P.
grade, Prolabo, were purified by distillation.

*Measurements.* (a) *Enthalpy Measurements.* The
procedure and the calorimeter have been described else-
where.[7] Both are generally similar to those followed by
Arnett.[6]

(b) *Density Measurements.* Absolute densities were
measured with a digital high-precision densimeter
DMA 02 manufactured by Anton Paar K.G., Austria.
The density is determined from the measured deviation
of resonant frequency of a hollow mechanical oscillator
which is filled with the sample material when compared
with a material of known density.[8] An ultrathermostat
allowing the temperature to be controlled within 0.01°
was used with a sample of liquid of 1.4 ml. Distilled
water according to the procedure of ref 9 was used as
the main standard.

The apparatus was standardized from separate mea-
surements with water and dry air. Absolute ethanol
was used as a check. The value of the density was
found to differ from the literature value from less than
$1 \times 10^{-5}$ g cm³.

## Results

(a) In Figure 1 is plotted the enthalpy of solution
of liquid chloroform in tetraethyl and tetrabutylam-
monium bromide aqueous solution at 15 and 25°. In

Figure 2 similar plots are shown for butanol and 2-
propanol from our data and for methane and propane
from literature data.[10]

Units are kilocalories per mole. The solute concentra-
tions are about $3 \times 10^{-3}$ mol/l. For the alcohols the
reproducibility of measurements is better than 0.02
kcal/mol and for the chloroform about 0.07 kcal/mol.
It should be noticed that all values increase with the
salt concentration but that the dependence on molality
of the enthalpy is nonlinear in every case. A striking
fact is the break which occurs at a molality of about
0.2 with the tetrapropylammonium bromide solutions.

(b) *Density Measurements.* Measurements have
been done at 5.70 and 24.20° in order to calculate the
expansivity coefficient cf the salt solution at 15°. The
results are given in Table 1. The accuracy is about
$1 \times 10^{-5}$ g/cm³.

The thermal expansion coefficients for the aqueous salt
solutions have been calculated from our present density

(7) M. Lucas, *Bull. Soc. Chim. Fr.*, 2902 (1970).

(8) O. Kratky, H. Leopold, and H. Stabinger, *Z. Angew. Phys.*, **27**, 273 (1969).

(9) "Physical Methods of Organic Chemistry," A. Weissberger, Ed., Vol. 1, 2nd ed, Interscience Publishers, New York, N. Y., 1949, Part 1.

(10) W. Y. Wen and J. Hung, *J. Phys. Chem.*, **74**, 170 (1970).

**Table I:** Absolute Density of Solutions of Alkylammonium Bromides at 5.7° and 24.2° against Salt Molality

| Concn, $m$ | Bu$_4$NBR 5.7° | 24.2° | Concn, $m$ | Pr$_4$NBR 5.7° | 24.2° |
|---|---|---|---|---|---|
| 0 | 0.99995 | 0.99725 | 0.100 | 1.00300 | 1.00003 |
| 0.102 | 1.00274 | 0.99960 | 0.199 | 1.00582 | 1.00276 |
| 0.213 | 1.00572 | 1.00216 | 0.300 | 1.00879 | 1.00549 |
| 0.301 | 1.00816 | 1.00420 | 0.400 | 1.01177 | 1.00816 |
| 0.504 | 1.01370 | 1.00882 | 0.502 | 1.01481 | 1.01090 |
| | | | 0.707 | 1.02078 | 1.01630 |

measurements and from densities calculated from literature[6,7] data. The equation

$$\alpha = \frac{1}{d_{15°}} \frac{\Delta d}{\Delta T} \qquad (2)$$

has been used. For the aqueous tetrabutylammonium bromide solutions at 15° the expansion coefficient has been extrapolated from the calculated data at 20° and 30° for the molality higher than 0.6. The reason is the limited solubility of the salt in water at 5.70°.

Plots of $\alpha$ against the salt molality are shown in Figure 3. It should be noticed that when the salt under consideration is tetrapropylammonium bromide, a sharp break in the curve appears at a molality of about 0.3.

## Discussion

(a) *Enthalpy of Solution.* In the process of solution of a molecular solute from the gaseous state, Pierotti[1] considers two steps. In the first a cavity with the same dimension as the solute has to be made in the solvent in order to accomodate the solute. In the second step, interactions between the solute and the molecular and ionic species, through dispersion forces, polarizability, etc., are taken into account.

The enthalpy of solution of a gaseous solute is given by the equation

$$H = H_c + H_i + \alpha R T^2 - RT \qquad (3)$$

where $H_c$ is the cavity formation enthalpy, $H_i$ the interaction enthalpy, $T$ the absolute temperature, and $R$ is the gas constant. According to the scaled particle theory, the value of $H_c$ is given by the equations[2,3]

$$H_c = \frac{RT^2\alpha}{1-\xi}\left(\frac{3DX + 3D^2Y}{1-\xi} + \xi + \frac{9D^2X^2}{(1-\xi)^2}\right) \qquad (4)$$

with

$$\xi = \left(\frac{\pi N}{6}\right)\frac{55.5a^3 + m(b^3 + c^3)}{55.5V_{H_2O} + mV_2} \qquad (5)$$

$$X = \left(\frac{\pi N}{6}\right)\frac{55.5a^2 + m(b^2 + c^2)}{55.5V_{H_2O} + mV_2} \qquad (5')$$

and

$$Y = \left(\frac{\pi N}{6}\right)\frac{55.5a + m(b + c)}{55.5V_{H_2O} + mV_2} \qquad (5'')$$
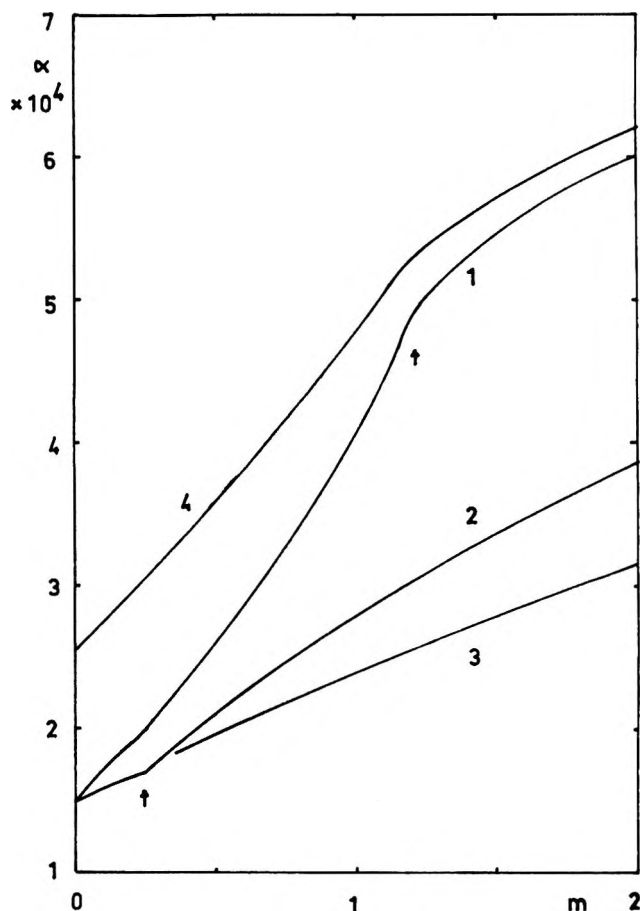
Figure 3. Apparent expansivity coefficients of aqueous salt solutions plotted against the salt molality: curve 1, tetrabutylammonium bromide, 15°; curve 2, tetrapropylammonium bromide, 15°; curve 3, tetraethylammonium bromide, 15°; curve 4, tetrabutylammonium bromide, 25°.

where $m$ is the molality of the aqueous salt solution, $N$ the Avogadro number, $V_{H_2O}$ and $V_2$ are the molar volume of pure water and the apparent molal volume of the salt, respectively. $a, b, c$ are the hard-sphere diameters of the water, of the anion, and the cation of the salt. Finally, $D$ is the hard-sphere diameter of the solute (for the justification of the equations, ref 5 should be consulted).

If the dispersion and repulsive interactions are approximated by a Lennard-Jones (6–12) potential,[1] then the value of $H_i$ is given by the relation

$$H_i = -\frac{32R\pi N}{k}\left\{55.5\left(\frac{D+a}{2}\right)^3(\epsilon\epsilon_a)^{1/2} + m\left(\left(\frac{D+b}{2}\right)^3(\epsilon\epsilon_b)^{1/2} + \left(\frac{D+c}{2}\right)^3(\epsilon\epsilon_c)^{1/2}\right)\right\} \times$$
$$(55.5V_{H_2O} + mV_2)^{-1} \qquad (6)$$

derived in a straightforward manner from the equation given in ref 3 modified to include terms calculated on a molality scale. Here $K$ is the Boltzmann constant;

$\epsilon_a$, $\epsilon_b$, $\epsilon_c$, are the energy parameters for the water, the ions, and the molecular solute, respectively.

The enthalpy of solution in pure water $H°$ is given by the same equations where $m$ is set up equal to zero. It is apparent from eq 5 that there is a direct relation between $H_c$ hence $H$ and $\alpha$. Indeed the examination of Figures 1–3 shows that both sets of curves are similar at least for the molalities smaller than 1.3.

Now we should examine the correlation between experimental and calculated data. The apparent molal volumes of the salts are taken from ref 4 and 5. The hard-sphere diameters of the particles are given in Table II. The values of the energy parameters are not known for the alkylammonium ions. For this reason we may calculate $H_c$ but not $H_i$.

**Table II:** Values of the Hard-Sphere Diameters of the Particles

| Particle | Diameter, Å |
|---|---|
| Br⁻ | 3.92[a] |
| Et₄N⁺ | 7.0[b] |
| Pr₄N⁺ | 8.0[b] |
| Bu₄N⁺ | 8.7[b] |
| H₂O | 2.76[c] |
| CH₄ | 3.80[d] |
| C₃H₆ | 5.30–5.60[d] |
| CHCl₃ | 5.40 |

[a] Crystal ionic diameter. [b] From B. E. Conway, R. E. Verrall, and J. E. Desnoyers, *Trans. Faraday Soc.* **62**, 2738 (1966). [c] See ref 4. [d] J. O. Hirschfelder, C. F. Curtiss, and S. B. Bird, "Molecular Theory of Gases and Liquids," Wiley, New York, N. Y. 1967, p 1110 ff.

In a first approximation and only for a nonpolar solute, we shall assume tentatively that the equation

$$H_i = H_i° + k_1 m \qquad (7)$$

where $H_i°$ is the value of $H_i$ in pure water and $k_1$ a suitable constant, holds for moderate concentrations.[11] Then we shall compare the experimental values of $(H - H°/m)$ with the calculated values of the term

$$\frac{H_c - H_c° + RT^2(\alpha - \alpha°)}{m}$$

where $H_c°$ and $\alpha°$ are the values of $H_c$ and $\alpha$ for pure water. If the assumption is valid, then the values of $(H - H°)/m$ and of the calculated term should differ only by a constant.

Figure 4 shows the plots of $(H - H°)/m$ and of the calculated term against the salt molality for the solutes: methane, propane, isopropyl alcohol, and the salt tetrapropylammonium bromide. Bars of error are given; they are calculated from the literature[10] and our claimed accuracy. It is apparent from the plots that the features of the experimental curves are qualitati-



Figure 4. Plots of $(H - H°)/m$ against the salt molality, 15°; salt, tetrapropylammonium bromide: --O--, experimental; ——, calculated.

vely, but not quantitatively, reproduced by the calculated ones for the nonpolar solutes. For the polar solute isopropyl alcohol, no calculation has been attempted as the eq 7 is certainly not valid. However, the plot for this solute is shown as it exhibits the same minimum at about 0.25 $m$ as the plots for the nonpolar solutes.

Figure 5 shows similar plots for chloroform, methane, isopropyl alcohol, and aqueous tetrabutylammonium bromide solutions at 15°. The main features of the experimental curves are the initial decrease with an increasing molality and the existence of a sharp maximum at a molality around 1.2. The calculated curves show the same characteristics, and the order of magnitude of the calculated variation with the salt molality is good for the nonpolar solute. For other solutes there are some discrepancies, especially at the higher molalities. They should be ascribed to the influence of their polarity.

Figure 6 shows the plots for chloroform and tetrabutyl or tetraethylammonium bromide solutions.

Figure 7 shows the plots of $\alpha - \alpha°/m$ against $m$ for the different aqueous salt solutions. There is a strong analogy between this set of curves and the curves shown in Figures 4–6, at least for the nonpolar solutes and the moderately polar chloroform. Then a correlation between the enthalpies of solution of molecular solutes and the expansivity coefficient of the solutions really exists in our opinion. This correlation should be inferred from the equations derived from the scaled particle

(11) Equation 7 is easily derived if eq 6 is replaced by the first and second term of a Taylor series, assuming that $V_2$ is independent of $m$.
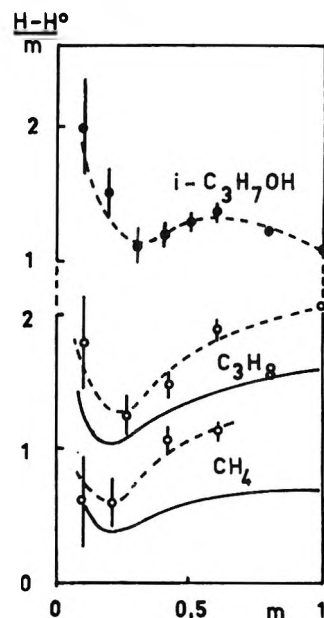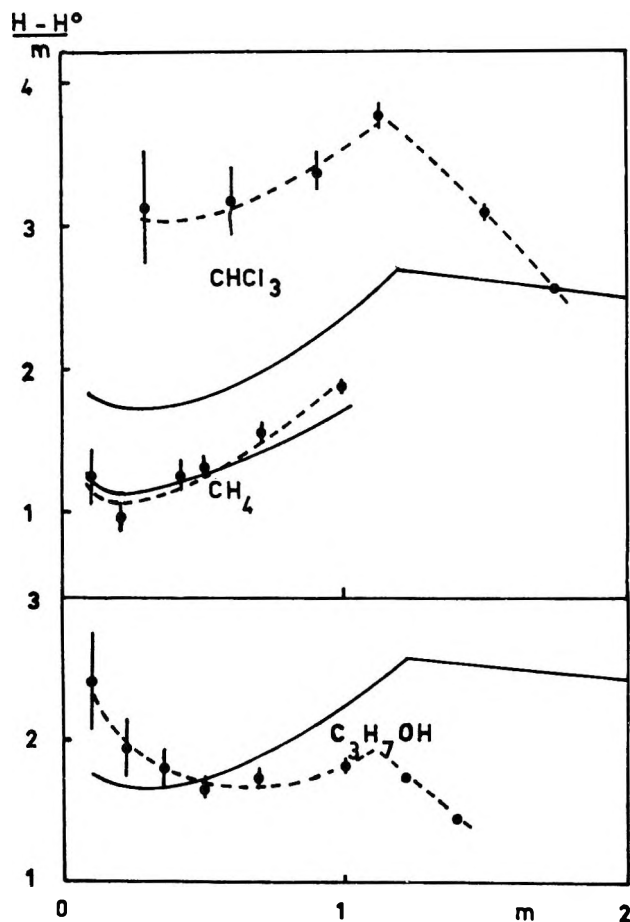
Figure 5. Plots of $(H - H°)/m$ against the salt molality, 15°; salt, tetrabutylammonium bromide: - -O- -, experimental; ———, calculated.
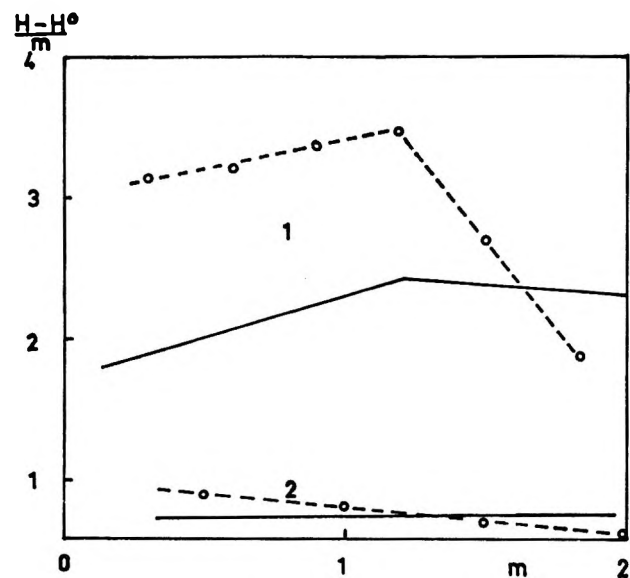


Figure 6. Plots of $(H - H°)/m$ against the salt molality for CHCl₃ and various aqueous salt solutions: curve 1, 25°, salt, tetrabutylammonium bromide; curve 2, 15°, salt, tetraethylammonium bromide; - -O- -, experimental; ———, calculated.
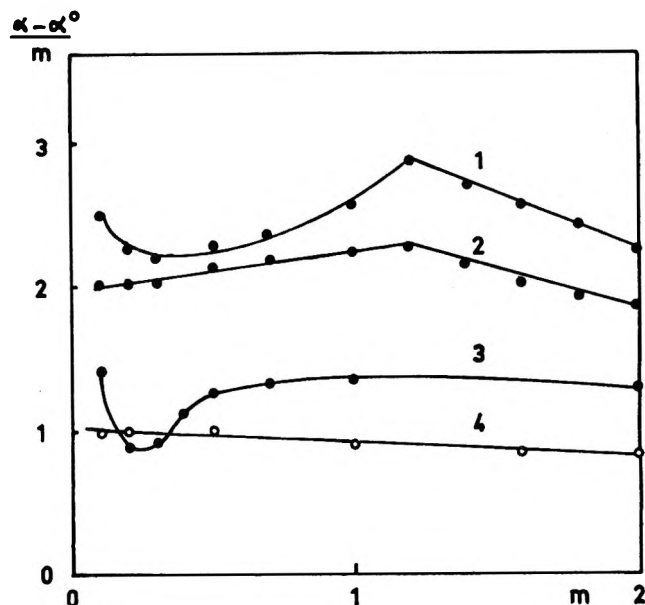
Figure 7. Plots of $(\alpha - \alpha°)/m$ against the salt molality for various aqueous salt solutions: curve 1, 15°, tetrabutylammonium bromide; curve 2, 25°, tetrabutylammonium bromide; curve 3, 15°, tetrapropylammonium bromide; curve 4, 15°, tetraethylammonium bromide.

theory, but the fit between the calculated and experimental values is not so good as expected. If other values are taken for the cationic diameters, the fit is not much improved.

(b) *Heat Capacity Change for the Solution Process.* From our data, it is possible to compute the experimental molar heat capacity change for the solution process for the solute chloroform in aqueous tetrabutylammonium bromide solutions.

The molar heat capacity change for the solution process from the gaseous state is given by eq 4 of ref 1

$$\Delta C_p = \left(\frac{\delta H}{\delta T}\right)_p = C_c + C_i - $$

$$R + 2\alpha RT + RT^2 \left(\frac{\delta \alpha}{\delta T}\right)_p \quad (8)$$

where $C_c$ and $C_i$ are the partial molar heat capacity for cavity for cavity formation and interaction, respectively.

If $C_i$ is neglected the heat capacity change may be calculated from the theory by means of the eq 8 and 9

$$C_c = \frac{H_{c(T)} - H_{c(T°)}}{T - T°} \quad (9)$$

where $H_c$ at the two temperatures $T$ and $T°$ is calculated as shown before.

From our data, the experimental value of $\Delta C_p'$ at 20° for the solution process of pure liquid chloroform

in aqueous tetrabutylammonium bromide solutions is calculated by means of the equation

$$\Delta C_p{}' = \frac{H_{25°} - H_{15°}}{10} \qquad (10)$$

The heat capacity change for the solution process of gaseous chloroform is the sum of $\Delta C_p{}'$ and of the difference between the heat capacity of liquid and gaseous chloroform. This difference may be calculated from ref 12.

Figure 8 shows the plots for experimental and calculated $\Delta C_p$. The agreement between the two quantities is not very good but the main features of the experimental curve are reproduced by the calculated one.

Finally, we should emphasize that the scaled particle theory is merely providing the form for the equation relating the variation of the cavity formation enthalpy with the thermal expansion coefficient.

The experimental enthalpy appears to be really related to the thermal expansion coefficient but there is some discrepancy between the calculated and experimental data. This may be ascribed in part to the existence and importance of the enthalpy of interaction $H_i$ especially with polar solutes; another reason for the discrepancy may be the uncertainties on the hard sphere diameters of solutes and ions.

Then no definite conclusion on the fit of the scaled particle theory can be drawn until measurements have been done with gases of low polarizability as helium or neon, in order to reduce the importance of the term $H_i$.



Figure 8. Plots of $\Delta C_p$ against the salt molality at 20°:
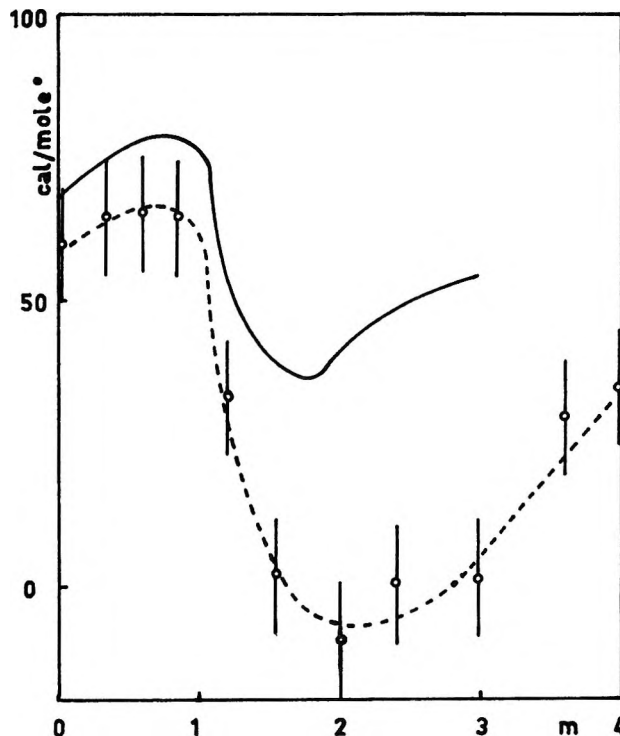- -O- -, experimental; ———, calculated.

(12) R. R. Dreisbach, *Advan. Chem. Ser.*, No. 15 (1955); No. 22 (1959); No. 29 (1961).

# Ultrasonic Velocity in Nonelectrolyte–Water Mixtures

## by Erwin K. Baumgartner and Gordon Atkinson*

*Department of Chemistry, University of Maryland, College Park, Maryland   20740*   (*Received October 26, 1970*)

*Publication costs borne completely by The Journal of Physical Chemistry*

Aqueous solutions of propylene oxide, acetone, tetrahydrofuran, *p*-dioxane, and *tert*-butyl alcohol exhibit marked nonideal thermodynamic behavior in the concentration range 3–8 mol % organic solute.   All of these solutes form solid clathrate hydrates of the well characterized "17 hydrate" structure.   In order to investigate the possibility of a water stabilization into ordered, clathrate-like shells in these dilute solutions, we have measured the ultrasonic velocity in aqueous propylene oxide, tetrahydrofuran, and *tert*-butyl alcohol solutions at 10 and 25°.   All systems show a maximum in the sound velocity in the mentioned concentration range.   The adiabatic compressibilities were calculated from the measured velocities and known densities and show a minimum very near the clathrate composition ($X_2 = 0.0556$).   It is shown that a simple two-state model suffices to explain the behavior seen in such systems in the low-concentration range.

## Introduction

It has been observed by several workers that aqueous solutions of propylene oxide (PO), acetone (A), tetrahydrofuran (THF), *p*-dioxane (D), and *tert*-butyl alcohol (TBA) exhibit anomalous water properties near 3–8 mol % solute.   A very good account of these results can be found in a paper by Glew and coworkers.[1]   Since these solutes all form solid clathrates with water at concentrations near 5 mol % solute,[2] corresponding to a composition consisting of (1 organic molecule)·17-$H_2O$, it has been suggested that the dilute aqueous solutions consist of solute molecules stabilizing adjacent water into ordered, hydrogen-bonded shells, similar to clathrate "cages."[1,3]   Using these ideas, Glew was able to explain, at least qualitatively, the marked nonideal behavior of these solutions in this concentration range.[1,3]

The velocity of ultrasound, *v*, in a solution is related to the adiabatic compressibility through eq 1

$$v^2 = 1/\beta_s d \tag{1}$$

where *d* is the density of the solution and $\beta_s$ is the adiabatic compressibility.

$$\beta_s = -1/V(\partial V/\partial P)_s \tag{2}$$

The stabilization of water molecules by the organic solute would be expected to decrease the compressibility of the solution[1] and since the density in these systems changes very smoothly with the concentration,[4,5] it could be expected that the ultrasonic velocity would show a maximum at the concentration where the stabilization of water into clathrate shells is a maximum ($X_2 = \frac{1}{18}$).   In fact, this behavior has been observed in A–$H_2O$,[6] D–$H_2O$,[6,7] and TBA–$H_2O$[6] solutions.

In order to further investigate these ideas about water stabilization in nonelectrolyte–water mixtures, we have measured the velocity of ultrasound in the PO–$H_2O$ and THF–$H_2O$ systems at 25 and 10° and in the TBA–

$H_2O$ system at 10°.   We have also examined equimolar ternary mixtures of two clathrate formers with water at 25 and 10°.

## Experimental Section

*Apparatus.*   The sound velocity was determined by the "sing-around" technique,[8] using a NUS Laboratory Velocimeter Model 6100, which works at a fixed frequency of 3.6 MHz, together with a Beckman Universal EPUT Meter Model 7350R.   The temperature of the solutions was maintained constant to better than ±0.002° by means of a Leeds and Northrup thermostatic oil bath (Model 4956).   The error in velocity measurements has been estimated to be less than 0.03%.

*Solutions.*   All solutions were made up with deionized water.   They were prepared at the required concentrations by weight.

The organic solutes, tetrahydrofuran (Chromato quality from Matheson Coleman and Bell), propylene oxide (Eastman), and certified *tert*-butyl alcohol (Fisher Scientific Co.) were used without further purification.   The data in tabular form can be obtained on request from the senior author (G. A.).

(1) D. N. Glew, H. D. Mak, and N. S. Rath in "Hydrogen-Bonded Solvent Systems," A. K. Covington and P. Jones, Ed., Taylor and Francis, London, 1968.

(2) TBA does not form solid clathrates with water, but it does form them in the presence of a help gas like $H_2S$.   The formula is $2H_2S \cdot$ TBA·$17H_2O$.[1]

(3) M. J. Blandamer, D. E. Clarke, N. J. Hidden, and M. C. R. Symons, *Trans. Faraday Soc.*, **64**, 2691 (1968).

(4) J. Timmermans, "The Physico-Chemical Constants of Binary Systems," Vol. 4, Interscience, New York, N. Y., 1960.

(5) R. Signer, H. Arm, and H. Daeniker, *Helv. Chim. Acta*, **52**, 2347 (1969).

(6) Ch. J. Burton, *J. Acoust. Soc. Amer.*, **20**, 186 (1948).

(7) K. Arakawa and N. Takenaka, *Bull. Chem. Soc. Jap.*, **42**, 5 (1969).

(8) R. Garnsey, R. J. Boe, R. Mahoney, and T. A. Litovitz, *J. Chem. Phys.*, **50**, 5222 (1969).
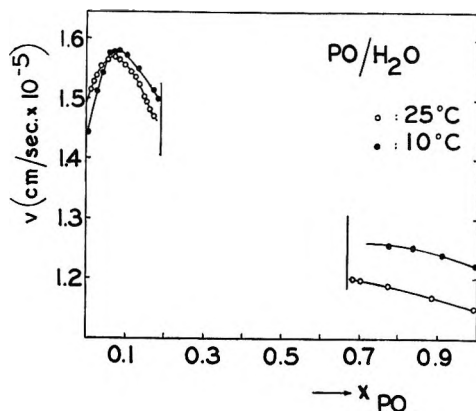
Figure 1. Concentration dependence of ultrasonic velocity for the propylene oxide–water system at 25 and 10°.
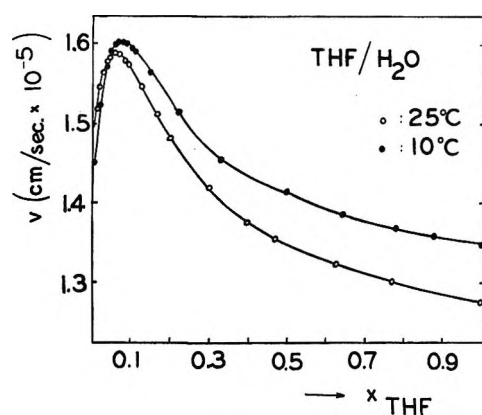


Figure 2. Concentration dependence of ultrasonic velocity for the tetrahydrofuran–water system at 25 and 10°.
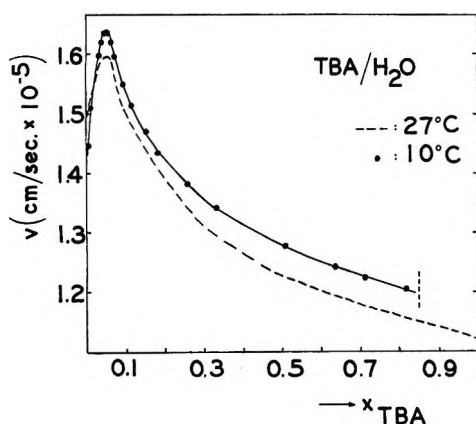


Figure 3. Concentration dependence of ultrasonic velocity for the tert-butyl alcohol–water system at 27[6] and 10°.

## Results

The concentration dependence of ultrasonic velocity for the systems PO–H$_2$O and THF–H$_2$O at 10 and 25° and at 10° for TBA–H$_2$O is given in Figures 1–3. We have included in Figure 3 Burton's data[6] measured at 27°. The curve corresponding to TBA–H$_2$O at 10° has been interrupted at $X_2 = 0.85$ because of the appearance of two phases.
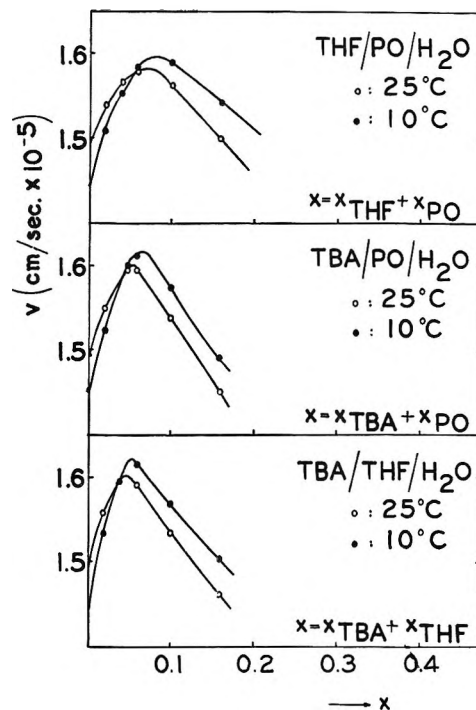


Figure 4. Concentration dependence of ultrasonic velocity for ternary mixtures of organic solutes in water at 25 and 10°.

The concentration dependence of ultrasonic velocity in the water-rich region for ternary mixtures of organic solutes in water, using equimolar concentrations of both solutes, is depicted in Figure 4. The mixtures studied were: THF–PO–H$_2$O, TBA–PO–H$_2$O, and TBA–THF–H$_2$O at 25 and 10°.

## Discussion

Using very extensive nuclear relaxation data, Hertz[9] has pointed out that clathrates certainly do not exist in solution as rigid, long-lived hydration spheres. Yet Hertz's results also show a marked decrease in the diffusion coefficient of the water near the solute. At the same time the organic molecule is freer to rotate in the water than it was in the pure solute. It seems useful then to consider that the "guest" solute molecule causes fluctuations in the thermodynamic properties of the "host" water in the region near the "guest." It should be emphasized that for both ultrasonic velocity and absorption, the effects seen are maximized by solutes with the greatest ratio of hydrocarbon group to hydrophilic group.

The ultrasonic absorption peak in dilute aqueous TBA solutions has been explained with the clathrate water-shell model,[3] but the same explanation seems to fail in A–H$_2$O, THF–H$_2$O, and D–H$_2$O solutions, where the ultrasonic absorption peak occurs at a molar fraction

(9) E. von Goldammer and H. G. Hertz, J. Phys. Chem., 74, 3734 (1970).

near 0.5.[6,10-12] The same problem seems to arise in the PO–$H_2O$ system, since we have found[13] that there is no maximum in the 3–8 mol% concentration range. The ultrasonic absorption in this system tends toward a maximum at higher concentrations but since there is a phase separation at $X_2 \simeq 0.15$, there is no way to tell at which concentration the real maximum would occur. An interpretation in terms of concentration fluctuation gives an explanation of this apparent inconsistency. Ultrasonic absorption phenomena due to concentration fluctuations have been analyzed by Solovyev and co-workers.[14] They find that the amplitude of the excess sound absorption as a function of $X_2$ is a complex function of the second derivatives of the volume, enthalpy, and free energy of the system with respect to $X_2$. Only when the volume factor is dominant, as it has been shown to be in TBA–$H_2O$ solutions,[15] does the ultrasonic absorption give a peak at around the same concentration as does the ultrasonic velocity. In the other systems, the situation is much more complicated and the absorption is a result of the combination of the three mentioned thermodynamic properties. Ultrasonic velocity is easier to interpret, since it depends only on the compressibility of the system. As is shown in Figure 1, we have indeed found a distinct maximum for the PO–$H_2O$ system at $X_2 \simeq 0.08$. The same behavior has also been observed for THF–$H_2O$ and TBA–$H_2O$ solutions, as depicted in Figures 2 and 3. It can be observed in these figures that the velocity maxima are always higher and sharper at lower temperatures. This is entirely consistent with the water-shell stabilization model.

It has been suggested by Hertz[9] that the structuring in the water-rich region might be due to association of organic molecules. In order to test this possibility, we have measured the concentration dependence of ultrasonic velocity in the dilute concentration region for ternary mixtures of organic solutes in water, where the concentrations of both organic solutes were equimolar. The results, shown in Figure 4, do not seem to indicate the suggested association of organic molecules, since the observed maxima correspond quite well to a linear superposition of the maxima corresponding to each solute, at the same total concentration, measured separately. If there were distinct association between organic molecules at low concentrations, one should expect that the ultrasonic velocity maxima would depend much more on the nature of the solute.

We have tried to explain the obtained ultrasonic velocity vs. concentration curves with a simple two-state model. In the concentration range $0 \leq X_2 \leq 0.0556$ we assume that each solute molecule is surrounded by water molecules forming a clathrate-like structure, in the sense discussed above, and that the water molecules not involved in the host structures behave like ordinary water. It is assumed also in this model that the compressibility of the guest molecule is zero

since it occupies a "hole" in the water but does not fill it.

Basically, this model implies that we are dealing with an ideal two-state solution. Our aim is to calculate the isoentropic compressibility for it. The expression commonly used for this purpose is the following[16a-c]

$$\beta_s{}^{id} = \sum_i \varphi_i \beta^0{}_{si} \qquad (3)$$

where $\varphi_i$ is the volume fraction of the $i$th component and $\beta^0{}_{si}$ the isoentropic compressibility for the pure component $i$. It has been recently shown[17] that this expression is only an approximate one and that the correct one is

$$\beta_s{}^{id} = \beta_T{}^{id} - TV_{id}(\alpha_{id})^2/C_{p id} \qquad (4)$$

where $\beta_T{}^{id}$ is the isothermal compressibility for an ideal solution, which is correctly calculated by an averaging over volume fractions (eq 3), and $V_{id}$, $\alpha_{id}$, and $C_{p id}$ are the molar volume, the thermal expansivity, and the heat capacity at constant pressure for ideal solutions. $V_{id}$ and $C_{p id}$ are calculated by a molar fraction average and $\alpha_{id}$ by a volume fraction average.

The use of correct eq 4 requires the knowledge of $\alpha$ and $C_p$ for a clathrate structure and for the components PO, THF, etc., which are not known at the present. Therefore, having estimated an error in $\beta_1{}^c$ (see below) by using the approximate expression less than 2%, which is smaller than the extent of our trust in the primitive model, we decided to use approximate eq 3 for our purposes.

By means of the described two-state model, we compute the molar volume $\bar{V}$ and the approximate adiabatic compressibility for the solution

$$\bar{V} = [(1 - X_2) - 17X_2]\bar{V}_1{}^0 + 17X_2\bar{V}_1{}^c \qquad (5)$$

where $\bar{V}_1{}^0$ = molar volume of "free" water and $\bar{V}_1{}^c$ = molar volume of "cage" water.

$$\beta_s = 1/\bar{V}[(1 - 18X_2)\bar{V}_1{}^0\beta_1{}^0 + 17X_2\bar{V}_1{}^c\beta_1{}^c] \qquad (6)$$

where $\beta_1{}^0$ = adiabatic compressibility of "free" water and $\beta_1{}^c$ = adiabatic compressibility of "cage" water. It follows immediately from eq 5 and 6 that

$$\beta_s = \beta_1{}^c \qquad (7)$$

when $X_2 = {}^1/_{18}$.

(10) J. H. Andreae, P. D. Edmonds, and J. F. McKellar, *Acustica,* **15,** 74 (1965).

(11) Unpublished results from this laboratory.

(12) G. Hammes and W. Knoche, *J. Chem. Phys.,* **45,** 4041 (1966).

(13) E. Baumgartner and G. Atkinson, unpublished results.

(14) V. P. Romanov and V. A. Solovyev, *Sov. Phys.-Acoust.,* **11,** 68, 219 (1965).

(15) M. J. Blandamer and D. Waddington in "Advances in Molecular Relaxation Processes," Elsevier, Amsterdam, 1970.

(16) (a) G. H. Findenegg and F. Kohler, *Trans. Faraday Soc.,* **63,** 870 (1967); (b) O. Kiyohara and K. Arakawa, *Bull. Chem. Soc. Jap.,* **43,** 3037 (1970); (c) J. Thamsen, *Acta Chem. Scand.,* **19,** 1939 (1965).

(17) G. L. Bertrand and L. E. Smith, *J. Phys. Chem.,* **74,** 4171 (1970); G. L. Bertrand, private communication.

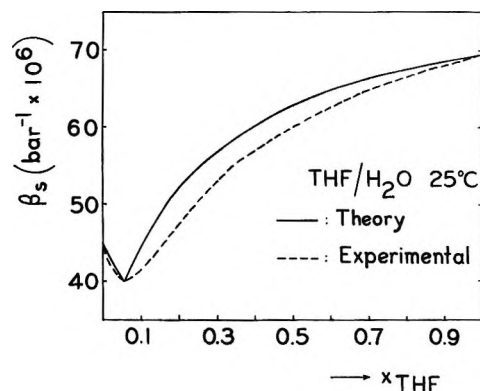Figure 5. Concentration dependence of adiabatic compressibility for the tetrahydrofuran–water system at 25°.

In the remaining concentration range $0.0556 < X_2 \leq 1$ and with assumptions based on the same model, part of the solute molecules form guest–host structures with water and part of them are free. In this case, the expressions for the molar volume of the solution and its adiabatic compressibility become

$$\bar{V} = (1 - X_2)\bar{V}_1^c + \left(\frac{18X_2 - 1}{17}\right)\bar{V}_2^0 \qquad (8)$$

where $V_2^0$ = molar volume of solute.

$$\beta_s = \frac{1}{\bar{V}}\left[(1 - X_2)\bar{V}_1^c\beta_1^c + \left(\frac{18X_2 - 1}{17}\right)\bar{V}_2^0\beta_2^0\right] \qquad (9)$$

where $\beta_2^0$ = adiabatic compressibility of pure solute.

Through eq 5, 6, 8, and 9 we are able to evaluate the adiabatic compressibility for the entire range of concentration. We have shown this for the system THF–$H_2O$ at 25° as an example. The value for $\bar{V}_1^c$ has been obtained from crystallographic data: 22.5 cc/mol.[18,19] The only unknown in this treatment then is $\beta_1^c$. We have used the value obtained from eq 7, which means that we have fitted the theoretical and experimental curves at the concentration where the minimum in compressibility occurs. The densities used to calculate $\beta_s$ from velocity measurements have been taken from the literature.[4,5] The experimental and calculated adiabatic compressibilities against $X_{THF}$ have been plotted in Figure 5. The agreement is very good at low concentrations, whereas at higher molar fractions it is rather poor.[20] This is not surprising since we did not expect this simple model to be valid at higher organic solute concentrations where a breakdown of the structured water shell is very likely.[1]

We have listed in Table I the $\beta_1^c$ values necessary to fit experimental curves at the minima for several solutes, at 25 and 10°. Several interesting conclusions can be drawn from an examination of this table. The values of $\beta_1^c$ are practically the same for all the different solutes. This fact and the relative temperature insensitivity of $\beta_1^c$, compared with liquids,[21] are in very good agreement with the clathrate solid-like explanation.

Another fact gives even stronger support to this interpretation: the values of $\beta_1^c$ are very close to the solid clathrate compressibility calculated by von Stackelberg[22,23] using phase diagrams: $40 \times 10^{-6}$ bar$^{-1}$.

Table I: Fitted Values of $\beta_1^c$ for Several Solutes

| Organic solute | $\beta_1^{c,a}$ bar$^{-1} \times 10^6$ (eq 7) | Temp, °C | Source |
|---|---|---|---|
| THF | 40 | 25 | This work |
| | 39 | 10 | This work |
| A | 41 | 27.5 | Burton[6] |
| TBA | 40 | 27 | Burton[6] |
| | 38 | 10 | This work |
| D | 39 | 25 | Burton[6] |
| | | | Arakawa, et al.[7] |
| PO | 41 | 25 | This work |
| | 41 | 10 | This work |

$^a$ $\beta_1^0$ (25°): $44.7 \times 10^{-6}$ bar$^{-1}$; $\beta_1^0$ (10°): $47.7 \times 10^{-6}$ bar$^{-1}$; $\beta_s$ (clathrate) (von Stackelberg):[22,23] $40 \times 10^{-6}$ bar$^{-1}$.

We are aware of the fact that the model used for our calculations is a very simple one which does not take account of the probable dynamic nature of the formation and dissociation of the clathrates. The model chosen is essentially that of an ideal associated solution with an infinite association constant. We have done some preliminary derivations, considering a finite association constant, but this would introduce another fitting parameter, whose real physical meaning is impossible to know at present.

We believe that the data presented in this paper support the water cage stabilization model. It is the simplest explanation for the striking regularities seen, and it seems only reasonable that the particular interactions that give rise to the "17 hydrate" structure in the solid clathrates should persist in the liquid state, albeit in a dynamic form. This last point is the factor that so many opponents and proponents of the model persist in ignoring. The "clathrate" model does not envisage the existence of long-lived cages in the liquid state, only short-lived structures observable as thermodynamic fluctuations and minor variations in spectral properties. It is clear that the short lifetime of the "cage" structures (as inferred from the nmr relaxation data) means that only spectral measurements with the same time scale will see anything but an average.

(18) A. S. Quist and H. S. Frank, J. Phys. Chem., 65, 560 (1961).

(19) M. von Stackelberg and B. Meuthen, Z. Elektrochem., 62, 130 (1958).

(20) Molar volumes, calculated through eq 5 and 8, give a very good fit with experimental data also.

(21) Landolt-Börnstein, N. S., Gruppe II, Band 5, "Molekularakustik," Springer Verlag, Berlin, 1967.

(22) M. von Stackelberg, Naturwissenschaften, 36, 327 (1949).

(23) M. von Stackelberg and W. Jahns, Z. Elektrochem., 58, 162 (1954).

The "fluctuating cage" model (not to be confused with the "flickering cluster" model) is being examined further in a number of ways in our laboratory. We are attempting to describe quantitatively the ultrasonic absorption in the systems discussed in this paper in terms of the fluctuation approach. We are also examining solutions of nonelectrolytes that are known to form clathrates of different composition. Finally, we are looking at the scattering spectra of solutions of "cage" formers. We are extremely hopeful that pur-

suit of this line of research may lead to some quantitative information on the dynamics of hydrophobic interaction.

# Miscibility of Liquid Metals with Salts. X. Various Studies in Alkaline Earth Metal–Metal Fluoride and Rare Earth Metal–Metal Difluoride and Trifluoride Systems[1]

## by A. S. Dworkin* and M. A. Bredig

*Chemistry Division, Oak Ridge National Laboratory, Oak Ridge, Tennessee 37830* (*Received January 25, 1971*)

*Publication costs borne completely by The Journal of Physical Chemistry*

The phase diagrams Ba–BaF$_2$, Sm–SmF$_2$, and Yb–YbF$_2$ were determined. The Ba–BaF$_2$ and Yb–YbF$_2$ systems are similar to Ca–CaF$_2$ in that they exhibit complete miscibility. In Sm–SmF$_2$, at 1216°, a large miscibility gap extends from the liquid monotectic, 32 mol %, to almost 100% Sm. The solubilities of Mg in MgF$_2$, of La, Ce, and Nd in their respective trifluorides and of Th in ThF$_4$ were found to be very low, less than 0.5 mol %. Determination of the melting point depression of calcium metal caused by the dissolution of CaF$_2$ and of the solubility of CaF$_2$ in solid Ca metal yielded the not unexpected result that in the solution the fluoride ions form separate particles.

## Introduction

Lichter and Bredig[2] have shown earlier that the original data[3] on the phase relations in the calcium metal–calcium fluoride system required a reinterpretation in terms of complete miscibility of the metal with the salt in the liquid state. The CaF$_2$–Ca system, then, was the first metal–metal halide system other than the alkali metal systems for which no monotectic reaction and no equilibria between two liquid phases were observed. This suggested that barium fluoride, because of its lower lattice energy compared with calcium fluoride, would be considerably more soluble in liquid barium metal than CaF$_2$ in Ca. Furthermore, it seemed likely that some of the rare earth metal–metal difluoride systems (Eu, Yb, and perhaps Sm) also might exhibit complete miscibility since the metals have similar heats of vaporization to calcium and barium. We therefore have measured and report here the phase diagrams of

the barium–barium fluoride, samarium–samarium difluoride, and ytterbium–ytterbium difluoride systems. This work is an extension of our previous measurements of the miscibility of the alkaline earth metals with their halides.[4]

An application of the principles governing the miscibility of the most electropositive mono- and divalent metals, the alkali and alkaline earth metals, with their fluorides to the behavior of the trivalent rare earth

(1) Research sponsored by the U. S. Atomic Energy Commission under contract with the Union Carbide Corp.

(2) B. D. Lichter and M. A. Bredig, *J. Electrochem. Soc.*, **112**, 506 (1965).

(3) P. S. Rogers, J. W. Tomlinson, and F. D. Richardson, "Proceedings of the International Symposium on the Physical Chemistry of Process Metallurgy, Pittsburgh, 1959," G. R. St. Pierre, Ed., Interscience, New York, N. Y., 1961, p 909.

(4) A. S. Dworkin, H. R. Bronstein, and M. A. Bredig, *J. Phys. Chem.*, **72**, 1892 (1968).

metals which form many subhalides with the other halogens[5] seemed to be somewhat uncertain. Therefore we have made some qualitative measurements of the solubility of lanthanum, cerium, and neodymium in their respective molten fluorides. We also measured the solubility of magnesium in molten magnesium fluoride and of thorium in molten thorium tetrafluoride.

A determination of the freezing point depression of calcium metal produced by dissolving $CaF_2$ and of the solubility of $CaF_2$ in solid Ca was made to examine the hitherto little-explored mechanism of the dissolution of a salt in a liquid metal or the "structure" of that solution.

## Experimental Section

(a) The phase diagrams were delineated by the method of thermal analysis (heating and cooling curves). It was necessary to modify the apparatus used for our previous measurements.[4] A platinum-wound Marshall tube furnace 40 cm in length with a 6.3-cm bore was employed to attain the necessary high temperatures. The salts and metals were loaded into tantalum capsules in a drybox under a helium atmosphere. The capsules were then sealed by welding in a drybox. The capsules were mounted on a tantalum frame in a 5-cm o.d. Morganite impervious recrystallized alumina tube, 45 cm in length. The top of the tube, 15 cm above the top of the furnace, was fitted with a water-cooled stainless steel head which also sealed the tube with a silicone rubber gasket. Fittings in the head made it possible to pump a vacuum of a few microns in the tube or alternatively to perform the experiment in an inert atmosphere of argon. Special fittings in the head allowed for the entrance of a Pt— Pt–10% Rh thermocouple which was placed in a well extending about 1.5 cm into the tantalum capsule from the bottom. The entire furnace assembly could be rocked about the horizontal position to obtain mixing.

The apparatus used to obtain the freezing point depression of calcium metal produced by dissolving $CaF_2$ was essentially the same as that described above except that a regular nichrome-wound Marshall furnace was used and the outer tube and mount were constructed of stainless steel.

(b) The solid solubility of calcium fluoride in calcium metal was obtained as follows. Calcium was melted in an inert atmosphere in a tantalum capsule similar to those used for the thermal analysis experiments. Upon solidification, the surface of the calcium was machined flat. A crystal of $CaF_2$ with a flat surface was placed on the calcium and a molybdenum weight was used to press the crystal against the metal. The capsule was then sealed by welding under helium, placed in the apparatus described above, and equilibrated for approximately 1 week at 815 ± 1°, i.e., a few degrees below the eutectic temperature. The capsule was then cooled, opened, and the calcium cut into several sec-

tions. The calcium was dissolved in a dilute HCl solution and the insoluble calcium fluoride was filtered and weighed. The filtrate was also analyzed for the small amount of soluble fluoride. The calcium fluoride crystal was also weighed for loss as an extra check.

(c) The rare earth trifluorides were prepared by gradually heating an intimate mixture of the rare earth oxide (Lindsay Chemical, 99.9%) with ammonium hydrogen fluoride in a platinum dish under an inert atmosphere to a temperature of 500°. The samarium and ytterbium difluorides were prepared by heating to a temperature of 1000° a stoichiometric mixture of the trifluoride and 200-mesh metal (Lindsay Chemical, 99.9%). The difluorides analyzed 79.8% Sm (theoretical 79.82%) and 82.0% Yb (theoretical 82.0%). Their X-ray patterns agreed with the literature[6] as did their melting points (see Table I).[7-13]

**Table I:** Melting Points of Fluorides and Metals

| | Melting point, °C | | |
| | Measured | Literature | Ref |
|---|---|---|---|
| $MgF_2$ | 1256 | 1261, 1263 | 7, 8 |
| $CaF_2$ | 1416 | 1423, 1418 | 7, 8 |
| $BaF_2$ | 1354 | 1355, 1354 | 7, 9 |
| $SmF_2$ | 1425 | 1417 | 10 |
| $YbF_2$ | 1407 | 1407 | 10 |
| $LaF_3$ | 1495 | 1493, 1490 | 10, 9 |
| $CeF_3$ | 1429 | 1430, 1437 | 10, 9 |
| $NdF_3$ | 1372 | 1374 | 10 |
| $ThF_4$ | 1110 | 1110, 1102 | 11, 9 |
| Ca | 839 | 836 | 12 |
| Ba | 731 | 729 | 12, 13 |
| Sm | 1086 | 1072 | 10 |
| Yb | 843 | 824 | 10 |

Calcium fluoride and barium fluoride were Harshaw optical grade single crystals and were used without further purification. Calcium and barium metal were purified by vacuum distillation at 900° under dynamic vacuum. The metal was distilled from a molybdenum cup and collected on a stainless steel cold finger. Melting points of 731° for barium and 839° for calcium are in good agreement with the literature (see Table I).

(5) E.g., J. D. Corbett, "Fused Salts," B. Sundheim, Ed., McGraw-Hill, New York, N. Y., 1964.

(6) (a) E. Catalano, R. G. Bedford, V. G. Silveira, and H. H. Wickman, J. Phys. Chem. Solids, 30, 1613 (1969); (b) J. J. Stezowaki and H. A. Eick, Inorg. Chem., 9, 1102 (1970).

(7) H. Kojima, S. G. Whiteway, and C. R. Masson, Can. J. Chem., 46, 2968 (1968).

(8) B. F. Naylor, J. Amer. Chem. Soc., 67, 150 (1945).

(9) B. Porter and E. A. Brown, J. Amer. Ceram. Soc., 45, 49 (1962).

(10) F. H. Spedding and A. H. Daane, Met. Rev., 5, 297 (1960).

(11) R. E. Thoma, H. Insley, B. S. Landau, H. A. Friedman, and W. R. Grimes, J. Phys. Chem., 63, 1266 (1959).

(12) D. T. Peterson and J A. Hinkebein, ibid., 63, 1360 (1959).

(13) D. T. Peterson and M. Indig, J. Amer. Chem. Soc., 82, 5645 (1960).

All the fluorides and metals used were analyzed spectrographically and were found to have only trace amounts of foreign cations. A comparison of our melting points ($\pm 3^c$) with the "best" literature values is given in Table I. Our melting point of MgF$_2$ is low because of the presence of about 1 mol % oxygen. Our values for the melting points of ytterbium and samarium metals are somewhat higher than those found in the literature (Table I). This may be caused by small quantities of oxygen and/or hydrogen in the metals forming solid solutions with melting points higher than the pure metal. Such behavior is known in the systems barium–barium hydride,[13] neodymium–neodymium hydride,[14] and yttrium–yttrium oxide.[15]

## Results and Discussion

The phase equilibria data are given in Table II and illustrated in Figure 1. As expected, barium fluoride is considerably more soluble in liquid barium metal than calcium fluoride in calcium by as much as a factor of 4. Furthermore, ytterbium also exhibits complete miscibility in the liquid state with ytterbium difluoride, the extent of the solubility being between that for the calcium and barium cases. There is a large monotectic solubility of samarium in samarium difluoride (32%) but from that concentration to almost 100% samarium, a large miscibility gap exists. The dotted solid solution lines are estimated except for the calcium case which was measured previously.[2] The estimations were made on the basis of (1) ideal activity for MF$_2$ in the solid phase, (2) a two-particle effect, i.e., dissociation according to M → M$^{2+}$ + 2e$^-$ in both the liquid and solid phases, and (3) an average literature value[16] for the entropy of fusion of BaF$_2$ of 3.3 eu and a value for the rare earth difluorides of 4 eu. This latter figure is based on our assumption that the rare earth difluorides, having the fluorite type of structure, are similar to the alkaline earth fluorides in that they have a diffuse transition in the solid and a low entropy of fusion.[17]

Corbett and coworkers[18] have correlated the solubilities of the rare earth metals in their respective trichlorides with the sum of the sublimation energy and ionization energies of the metals. They found that the sublimation energies appear primarily responsible for the observed trends while the ionization energies and the other terms in the complete Born–Fajans–Haber cycle[19] had only relatively small effects. A similar scheme with vapor pressure as the prime factor was proposed by Topol.[20] The overall effect is that of increasing solubility with decreasing sublimation energy of the metals. This correlation also seems to apply to the metal–difluoride systems with the sublimation energy of samarium being about 12 to 14 kcal higher than the other three metals. We would then predict that the europium–europium difluoride system is somewhat similar to the calcium–calcium fluoride system and that, if thulium difluoride is stable, the solubility

**Table II:** Equilibrium Phase Compositions in the Ba–BaF$_2$, Sm–SmF$_2$, and Yb–YbF$_2$ Systems

| Composition, mol % metal | Liquidus, °C | Monotectic, °C | Eutectic, °C |
|---|---|---|---|
| **Ba–BaF$_2$** | | | |
| 0 | 1354 | | |
| 3.9 | 1321 | | |
| 9.4 | 1282 | | 724 |
| 19.6 | 1231 | | |
| 27.5 | 1192 | | 729 |
| 35.1 | 1166 | | 728 |
| 55.3 | 1098 | | 728 |
| 69.6 | 1045 | | 729 |
| 85.0 | 948 | | 730 |
| 91.9 | 862 | | 730 |
| 100 | 731 | | |
| **Sm–SmF$_2$** | | | |
| 0 | 1425 | | |
| 5.2 | 1375 | | |
| 10.3 | 1332 | 1212 | |
| 24.4 | 1253 | 1216 | 1080 |
| 48.7 | | 1217 | 1080 |
| 68.7 | | 1214 | 1083 |
| 85.5 | | 1211 | 1085 |
| 95.3 | | 1211 | 1087 |
| 100.0 | 1086 | | |
| **Yb–YbF$_2$** | | | |
| 0 | 1407 | | |
| 9.4 | 1347 | | 810 |
| 25.3 | 1282 | | 820 |
| 49.9 | 1244 | | 827 |
| 73.0 | 1186 | | 832 |
| 90.5 | 1029 | | 837 |
| 100 | 843 | | |

of thulium metal in liquid thulium difluoride is less than that of samarium in samarium difluoride, since the heat of sublimation of thulium exceeds that of samarium by 8 kcal/mol.

Figure 2 is a (nonisothermal) plot of the partial molar excess free energy or excess chemical potential of BaF$_2$, $\Delta\mu^E_{(BaF_2)}$, vs. the square of the barium metal mole fraction, $N_{Ba}$. In this test of the most simple form of the dependence of the activity coefficient on concentration according to regular solution theory, the experimental

(14) D. T. Peterson, T. J. Poskie, and J. A. Straatmann, *J. Less-Common Metals*, **23**, 177 (1971).

(15) R. C. Tucker, Jr., E. D. Gibson, and O. N. Carlson, *Nucl. Met.*, **10**, 315 (1964).

(16) (a) G. Petit and F. Delbove, *C. R. Acad. Sci. Paris*, **254**, 1388 (1960); (b) D. F. Smith, University of Alabama, private communication, 1969; (c) R. I. Efremova and E. V. Matizen, *Izv. Sib. Otd. Akad. Nauk SSSR, Ser. Khim. Nauk*, (1), 3 (1970).

(17) A. S. Dworkin and M. A. Bredig, *J. Phys. Chem.*, **72**, 1277 (1968).

(18) J. D. Corbett, D. L. Pollard, and J. E. Mee, *Inorg. Chem.*, **5**, 761 (1966).

(19) D. F. C. Morris and E. L. Short, *Nature*, **224**, 950 (1969).

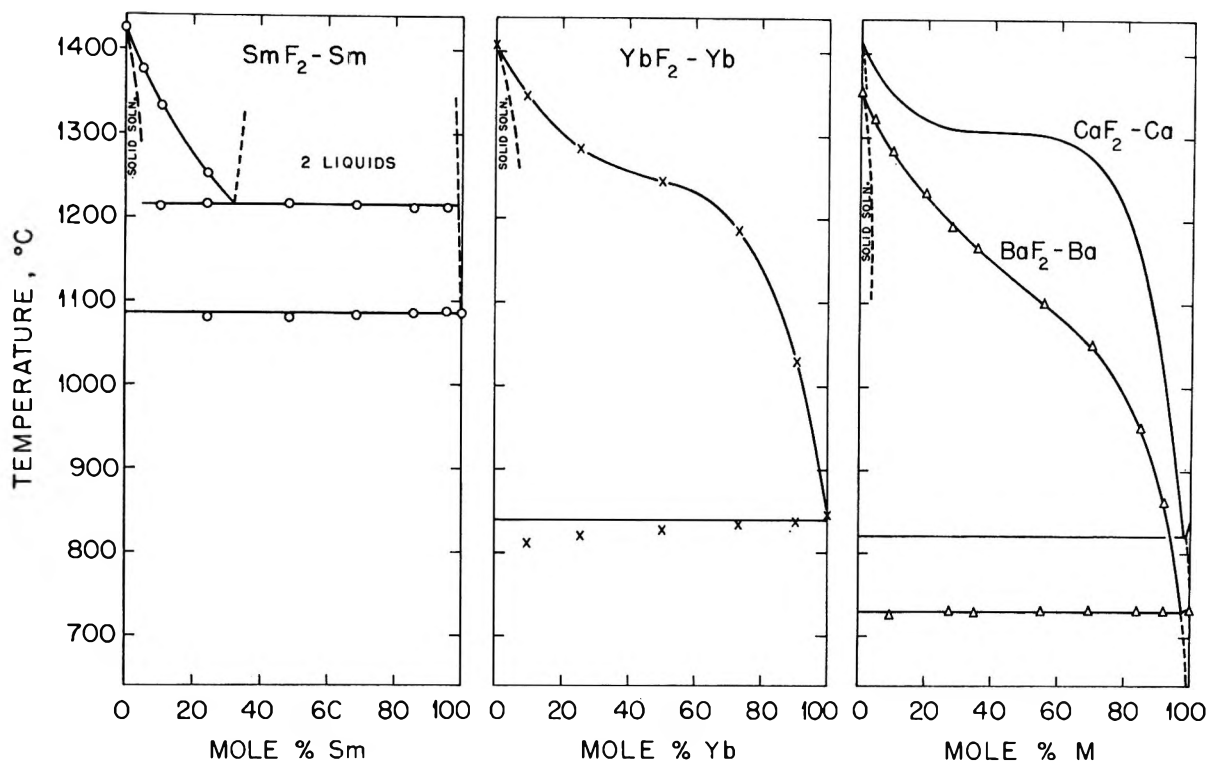(20) L. Topol, *J. Phys. Chem.*, **69**, 11 (1965).

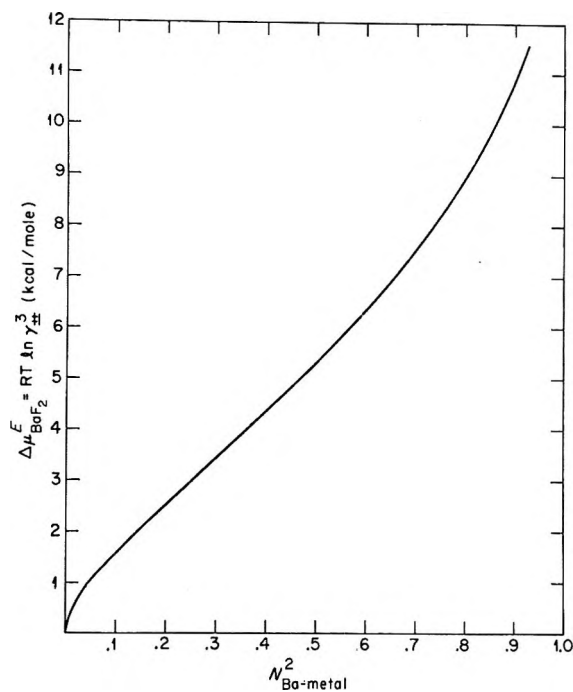Figure 1. Equilibrium phase diagrams of metal fluoride–metal systems, $MF_2$–M (M = Sm, Yb, Ca, or Ba).



Figure 2. Excess chemical potential of $BaF_2$ as a function of concentration.

points should have fallen on a straight line. Its slope and intercept at $N_{Ba} = 1$ would equal the parameter $B$ in $\ln \gamma_{BaF_2} = (B/RT)N_{Ba}^2$. This plot for the $BaF_2$–Ba solutions (the Ca and Yb solutions are slightly higher but similar) greatly resembles earlier plots for several alkali metal–metal halide systems, Rb–RbBr, Cs–CsI,

and the other cesium systems.[21] The actual nonlinear character of the curve indicates considerable deviation from simple regular solution behavior,[22] i.e., nonideal entropy of mixing and very likely also a temperature dependence of this entropy. The value of $B$ from an approximate straight line through the experimental points, ~6 kcal per equivalent of $BaF_2$, compares with the 3.5 to 4.5 kcal/mole for the alkali metal systems above.

A qualitative determination of the solubilities of Mg in $MgF_2$, La, Ce, and Nd in their respective trifluorides, and Th in $ThF_4$ was made by determining the melting point depression of the fluoride produced by dissolving the metal. The measurements were qualitative because the melting points were depressed only a few degrees in all the above cases despite additions of up to more than 20 mol % metal. The maximum lowering was 3 ± 1° for $MgF_2$, 4 ± 3° for the rare earth trifluorides, and 2 ± 1° for $ThF_4$. Assuming the metal dissolves as $M = M^{n+} + ne^-$, a monotectic solubility of 0.3 to 0.6 mol % for Mg ($n = 2$) in $MgF_2$, 0.1 to 0.5 mol % for La, Ce, and Nd ($n = 3$) in their trifluorides, and 0.1 to 0.3 mol % for Th ($n = 4$) in $ThF_4$, is calculated from the melting point depression equation $\Delta T/N = nRT/\Delta S_m$. These low solubilities indicate that there is essentially no tendency toward formation of lower valent fluorides in any of the above systems.

(21) M. A. Bredig, "Molten Salt Chemistry," M. Blander, Ed., Interscience, New York, N. Y., 1964.

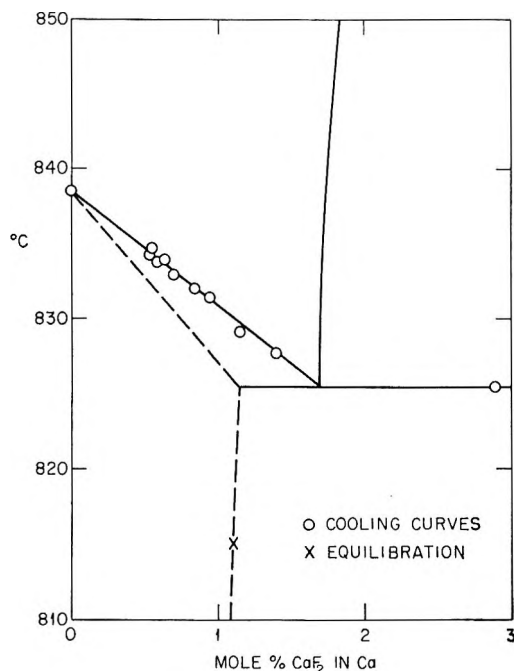(22) K. S. Pitzer, J. Amer. Chem. Soc., 84, 2025 (1962).

Figure 3. Melting point depression of calcium metal by calcium fluoride.

Phase diagram, vapor pressure, and electrical conductance data for solutions of alkali metal halides in liquid alkali metals were interpreted[21,22] in terms of substitution of electrons by single halide ions. In these cases, colligative properties would not allow distinction between dissociation of MX into $M^+$ and $X^-$ and dissolution as MX molecules, since the $M^+$ ions introduced by the salt would be indistinguishable from those of the metal. On the other hand, in $M-MX_n$ systems with $n > 1$, dissociation into individual $M^{n+}$ cations and $nX^-$ anions could be reflected into the colligative properties of the solution. Figure 3 shows both the melting-point depression of calcium metal produced by dissolving $CaF_2$ and the solubility of $CaF_2$ in solid Ca metal. The latter is shown as an estimated dotted line since the solid solution determination was made at only one temperature. The observed solid solubility of 1.1 ± 0.1 mol % Ca comes from three determinations at 815 ± 1° and permits the estimate of the solidus curve which brings the melting point depression in agreement with an

$$n = \frac{\Delta T \Delta S}{RT(N_{CaF_2(in\ liq)} - N_{CaF_2(in\ solid)})} = 2$$

corresponding to the expected separation of the $F^-$ ions. Without the solid solubility, the limiting slope for the melting point depression would suggest the highly unlikely occurrence of association rather than dissociation of the $CaF_2$. In the $BaF_2-Ba$ system a relatively high solubility of $BaF_2$ in solid Ba metal, $N_{BaF_2(in\ solid)}$, of approximately 2.5 mol % is estimated from the above equation. $N_{BaF_2(in\ liquid)}$ is the intercept of the liquidus with the eutectic horizontal at ~2.5 mol %, $\Delta T$ is the difference of ~1° between the eutectic temperature and the melting point of pure barium, $\Delta S$ is the entropy of fusion of Ba metal, 1.86 cal $deg^{-1}$ $mol^{-1}$, and the number of particles, $n$, is taken as 2 in the $CaF_2-Ca$ system. The high solubility as compared with the calcium system is ascribed to the lower lattice energies of the components in the barium system ($CaF_2$, 617; Ca, 456; $BaF_2$, 547; Ba, 393 kcal $mol^{-1}$).[23]

(23) "Gmelins Handbuch Der Anorganische Chemie," 8th ed, 1957, 1960.

# Solubilities of Hydrocarbons and Carbon Dioxide in

# Liquid Methane and in Liquid Argon

by G. T. Preston,[*1] E. W. Funk, and J. M. Prausnitz

*Department of Chemical Engineering, University of California, Berkeley,
Berkeley, California 94720 (Received December 21, 1970)*

Solubility data in liquid methane and in liquid argon were obtained for carbon dioxide, *n*-pentane, cyclopentane, neopentane, 1,3-butadiene, and 2,3-dimethylbutane in the temperature region 90-125°K. Activity coefficients for the solutes, referred to the pure subcooled liquid, were interpreted with the Scatchard–Hildebrand equation allowing for deviations from the geometric-mean assumption for the cohesive energy density of unlike molecular pairs. Attention is given to the importance of pure-component solid transitions in solid–liquid equilibrium calculations for binary mixtures. For saturated hydrocarbons, activity coefficients at 120°K and "total" entropies of fusion decline sharply as the extent of hydrocarbon branching rises. Methane and cyclopentane form two liquid phases at about 123°K. The upper consolute point for this system is estimated to be 166°K and 76 mol % methane.

A recent review of solubility data for solids in cryogenic solvents[2] showed that very little experimental information is available on solubilities in liquid argon. While solubility data in liquid methane are somewhat more plentiful, few measurements have been made at low temperatures for hydrocarbons larger than propane. In this work, we report solubility data for carbon dioxide and five hydrocarbons in liquid argon and in liquid methane. Particular attention is given to the effect of hydrocarbon molecular structure on solubility at low temperatures.

## Experimental Section

The experiments were carried out in a cylindrical stainless steel vacuum cryostat 3 ft high and 1 ft in diameter. Suspended from the cover plate of the cryostat was a massive heat sink assembly consisting of a copper bar partially immersed in a reservoir of liquid nitrogen boiling at atmospheric pressure. Figure 1 shows the basic features of the cryostat.

The cryostat was evacuated to $<10^{-5}$ mm pressure by a 4-in. oil diffusion pump, backed up by a large mechanical vacuum pump. The pumps were separated from the cryostat by a large liquid nitrogen cold trap. To minimize radiative heat transfer from the environment, two concentric heat shields made of copper sheet were located between the heat-sink assembly and the cryostat walls. The heat shields and the heat-sink assembly were highly polished and chrome plated. Thin cross-section stainless steel tubing and supports were used where large temperature gradients could exist in order to minimize conductive heat transfer.

To permit visual observation of the mixtures, the equilibrium cell was constructed from a thick-walled Pyrex tube 3 cm in diameter and 20 cm long. It was located in a cylindrical cavity in the upper end of the copper bar. For good thermal contact with the copper bar, the ends of the cell were made of copper; they were sealed to the Pyrex tube by a pure indium soldering procedure.

The upper end of the cell was bolted to the copper bar and the bolts were spring-loaded to allow for differences in thermal expansion. The cell contained a movable liquid-sampling probe, a pressure tap, an inlet and an outlet for recirculation of the vapor phase, and a thermocouple well. The cell construction is shown in Figure 2.

Temperatures in the liquid phase were measured with a calibrated copper–constantan thermocouple, a Leeds and Northrup K-3 potentiometer, and a Honeywell galvanometer. The thermocouple and potentiometer leads were joined by soft-solder connections at a ceramic seal on the cryostat cover plate; the seal was elevated above the cover plate to decrease thermal gradients between the solder joints.

Temperature control was maintained by a low gain, proportional mode temperature controller. Its platinum sensor was located in a cavity in the copper bar, just below the cell.

To accelerate attainment of equilibrium between the liquid and solid phases and to assure a uniform temperature in the liquid phase, the vapor in the cell was recirculated at about 100 cm³/min with a peristaltic pump outside the cryostat. The returning vapor was cooled by countercurrent heat exchange with the vapor leaving the cell. The vapor reentered the cell near the bottom

(1) Garrett Research & Development Co., La Verne, Calif.

(2) G. T. Preston and J. M. Prausnitz, *Ind. Eng. Chem., Process Des. Develop.*, 9, 264 (1970).
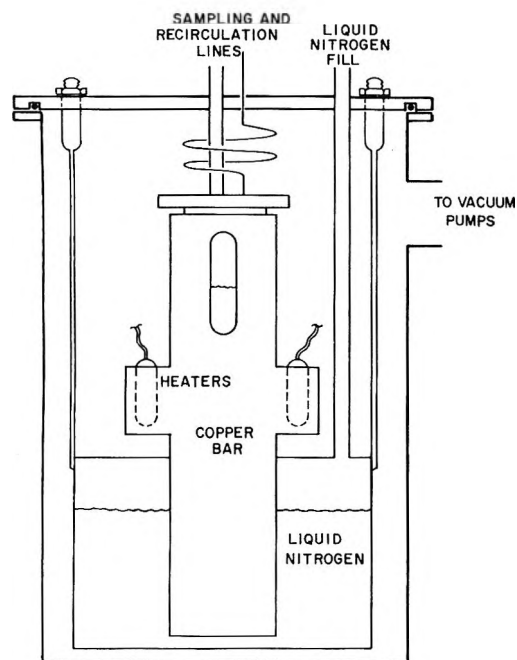
Figure 1.   Schematic of cryostat.



Figure 2.   Solid–liquid equilibrium cell.



Figure 3.   Liquid-sampling valve.

raised or lowered, to open or close the valve, by turning a threaded handle at the top of the valve, outside the cryostat.   Another threaded handle was used to raise and lower the entire probe in the cell.   The valve body was wrapped with heating wire to achieve complete vaporization of the liquid sample as it entered the valve; a vacuum jacket served to decrease heat loss into the cell.   The temperature in the valve was monitored by means of a thermocouple in the valve stem, near the tip.   The inlet to the valve was a 0.006-in. i.d. needle extending down about 1 in. below the vacuum jacket. Thermal expansion or contraction was taken up by a kink in the needle between the valve seat and the vacuum jacket.   The valve seat was copper.   The valve stem tip was "Rulon" (Dixon Corp.), a filled Teflon which is elastic and thus does not cold-flow.   All other parts of the valve were stainless steel.

Analysis of the samples was carried out using a gas chromatograph equipped with a thermal conductivity detector and a hydrogen flame-ionization detector in series.

Whereas the amount of the solvent component was determined from the response of the thermal conductivity detector, the amount of the solute component was determined from the response of the flame detector, which is several orders of magnitude more sensitive to hydrocarbons than the thermal conductivity detector. Both signals were observed on a 1-mV recorder and integrated by a ball-and-disk mechanical integrator.

and bubbled up through the liquid, providing vigorous agitation.

The probe used to sample the liquid phase was functionally equivalent to a very tall vee-tip valve; it is shown schematically in Figure 3.   The valve stem was

Details concerning the apparatus and its operation are given by Preston[3] and Funk.[4]

## Materials

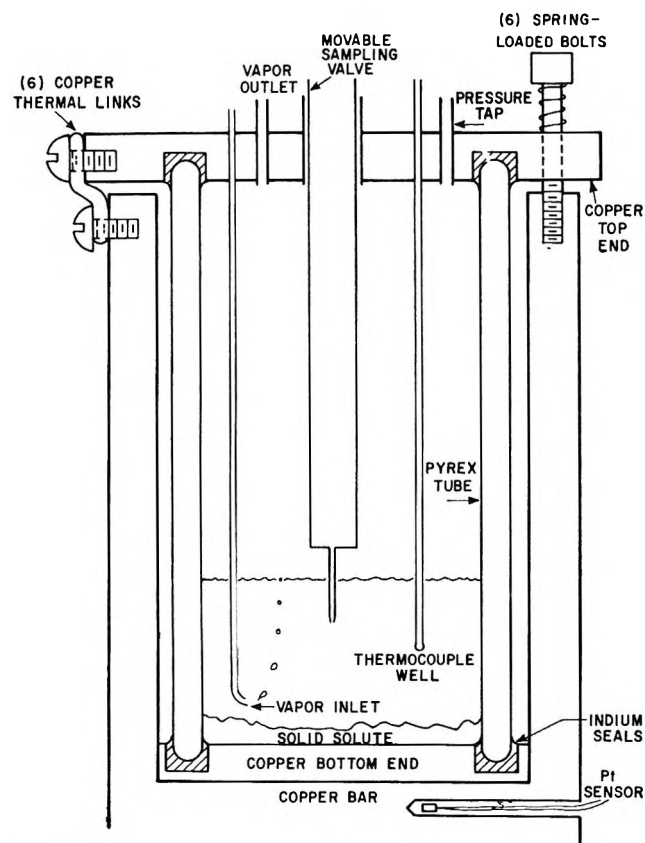The solvents and solutes were purchased from the suppliers listed in Table I; the purities shown are the manufacturers' specifications. A trace of carbon dioxide in the methane was removed by passing the methane through an Ascarite trap.

**Table I**

| Material | Supplier | Purity, % |
|---|---|---|
| Methane | Matheson Co. | 99.97 |
| Argon | Matheson Co. | 99.995 |
| n-Pentane | Phillips Petroleum Co. | 99.90 |
| 1,3-Butadiene | Phillips Petroleum Co. | 99.89 |
| Carbon dioxide | Matheson Co. | 99.8 |
| Cyclopentane | Phillips Petroleum Co. | 99.90 |
| Neopentane | Matheson Co. | 99.90 |
| 2,3-Dimethylbutane | Phillips Petroleum Co. | 99.95 |

## Results

The experimental results are summarized in Table II. The solubility $x_2$ is the mole fraction of solute in the liquid phase. Since it was only possible to maintain desired temperatures to $\pm 0.50°K$, the temperatures given in Table II are averages calculated by

$$\bar{T} = \left(\sum_i T_i\right)/N \tag{1}$$

where $T_i$ is the experimental temperature and $N$ is the number of samples taken at the desired temperature. For each average temperature, the average solubility in Table II was calculated by

$$\bar{x}_2 = \left(\sum_i x_{2,i}\right)/N \tag{2}$$

where $x_{2,i}$ is the experimental solubility. The precision, or scatter, of the solubilities was calculated from

$$\text{precision} = \sqrt{\left[\sum_i \left(\frac{x_{2,i} - \bar{x}_2}{\bar{x}_2}\right)^2\right]/N} \times 100\% \tag{3}$$

For the cyclopentane–methane system it was observed that at about 123°K the system split into two liquid phases.

Solubilities of carbon dioxide in methane shown in Table II are in good agreement with those reported by Davis[5] and by Cheung and Zander.[6]

## Thermodynamics of Solid–Liquid Equilibria

Assuming that the solid phase is pure solute and that the liquid phase is a saturated solution of the solute in the solvent, the equation of equilibrium is

$$f_2^s = \gamma_2 x_2 f_2^l \tag{4}$$

where subscript 2 refers to the solute, $f^s$ is the fugacity

of the pure solid, $f^l$ is the fugacity of the pure subcooled liquid, $x$ is the mole fraction in solution, and $\gamma$ is the activity coefficient of the solute in the liquid, referred to the pure subcooled liquid, all at system temperature $T$.

For temperatures not much below the melting temperature and for normal pressures, the fugacity ratio $f_2^s/f_2^l$ can be estimated by

$$\ln \frac{f_2^s}{f_2^l} = \frac{\Delta S_f}{R}\left[1 - \frac{T_m}{T}\right] \tag{5}$$

where $R$ is the gas constant, $T_m$ is the melting temperature of the solute, and $\Delta S_f$ is the molar entropy of fusion of the solute.[7]

Some substances undergo solid-phase transitions from one crystal structure to another. For these solutes, if the temperature of interest is less than the transition temperature, $T_{trans}$, the expression for the fugacity ratio $f_2^s/f_2^l$ becomes

$$\ln \frac{f_2^s}{f_2^l} = \frac{\Delta S_f}{R}\left[1 - \frac{T_m}{T}\right] + \frac{\Delta S_{trans}}{R}\left[1 - \frac{T_{trans}}{T}\right] \tag{6}$$

where $\Delta S_{trans}$ is the molar entropy of transition. If there is more than one solid-phase transition above the temperature of interest, further terms must be added to eq 6.

Table III gives the melting temperatures and entropies of fusion for carbon dioxide and 45 hydrocarbons. Also, transition temperatures and entropies of transition are given for those hydrocarbons for which experimental data are available. If no transition data are given for a particular hydrocarbon in Table III, we cannot assume that the hydrocarbon does not exhibit transitions in the solid phase. For many hydrocarbons, the desired experimental information has not been obtained.

The thermodynamics of solid–liquid equilibria becomes complicated if a solid solution is formed. In this experimental work the solid-phase composition was not determined. However, there was no visual indication of any formation of a solid solution. Using semiquantitative calculations, Funk shows[4] that the solubilities of the hydrocarbon solutes are negligible in solid methane or solid argon. Equation 5 was used in these calculations to estimate the ratio of the pure-component fugacities of methane in the liquid and solid phases, and regular solution theory[7] was used to esti-

(3) G. T. Preston, Ph.D. Dissertation, University of California, Berkeley, 1970.

(4) E. W. Funk, Ph.D. Dissertation, University of California, Berkeley, 1970.

(5) J. A. Davis, N. Rodewald, and F. Kurata, AIChE J., **8**, 537 (1962).

(6) H. Cheung and E. H. Zander, Chem. Eng. Progr., Symp. Ser., **64**, No. 88, 34 (1968).

(7) J. H. Hildebrand and R. L. Scott, "Solubility of Nonelectrolytes," Dover Publications, New York, N. Y., 1964.

**Table II:**   Summary of Experimental Results

| System Solvent | System Solute | $T$, °K | $10^3 x_2$ | No. of samples | Precision, rel % | Recommended $l_{12}$ |
|---|---|---|---|---|---|---|
| Methane | n-Pentane | 100.4 | 1.380 | 9 | 6 | 0.03 |
| | | 112.7 | 6.16 | 7 | 3 | |
| | | 124.5 | 17.86 | 8 | 13 | |
| Argon | n-Pentane | 92.3 | 0.0158 | 7 | 6 | 0.07 |
| | | 99.8 | 0.0326 | 7 | 5 | |
| | | 104.8 | 0.0563 | 8 | 8 | |
| | | 110.5 | 0.1729 | 9 | 7 | |
| Methane | 1,3-Butadiene | 101.8 | 0.200 | 14 | 26 | 0.05 |
| | | 113.3 | 1.071 | 8 | 7 | |
| | | 128.4 | 4.504 | 7 | 9 | |
| Argon | 1,3-Butadiene | 92.7 | 0.00147 | 7 | 4 | 0.11 |
| | | 102.2 | 0.00722 | 6 | 4 | |
| | | 110.8 | 0.02241 | 7 | 6 | |
| Methane | Carbon dioxide | 126.4 | 0.732 | 3 | 7 | −0.02 |
| | | 137.5 | 2.366 | 7 | 15 | |
| Argon | Carbon dioxide | 109.0 | 0.0797 | 10 | 46 | −0.04 |
| | | 115.9 | 0.2059 | 9 | 11 | |
| Methane | Cyclopentane | 100.2 | 3.52 | 6 | 6 | 0.007 |
| | | 112.5 | 12.9 | 7 | 9 | |
| Argon | Cyclopentane | 92.6 | 0.151 | 7 | 7 | 0.023 |
| | | 104.0 | 0.325 | 8 | 5 | |
| | | 110.4 | 0.651 | 8 | 8 | |
| Methane | Neopentane | 99.9 | 10.1 | 6 | 8 | 0.015 |
| | | 112.0 | 16.9 | 7 | 8 | |
| | | 123.2 | 26.5 | 4 | 12 | |
| Argon | Neopentane | 92.7 | 0.901 | 7 | 8 | 0.035 |
| | | 104.6 | 1.30 | 8 | 4 | |
| | | 110.2 | 1.51 | 4 | 10 | |
| Methane | 2,3-Dimethylbutane | 100.2 | 3.98 | 7 | 10 | 0.025 |
| | | 111.9 | 10.0 | 5 | 9 | |
| | | 123.4 | 43.1 | 5 | 9 | |
| Argon | 2,3-Dimethylbutane | 92.3 | 0.278 | 5 | 15 | 0.045 |
| | | 104.6 | 0.638 | 5 | 9 | |
| | | 109.3 | 0.801 | 4 | 11 | |

mate the activity coefficients of methane in both liquid and solid phases.

## Activity Coefficients

For many nonpolar systems, the theory of regular solutions[7] can be used to estimate the activity coefficients. For a binary system, the equation of Scatchard[7] for the activity coefficient of the solute is

$$RT \ln \gamma_2 = v_2 A_{12}\Phi_1^2 \tag{7}$$

where $v_2$ is the molar volume of the subcooled liquid solute, $A_{12}$ is the exchange energy density, and $\Phi_1$ is the volume fraction of the solvent in solution, defined by

$$\Phi_1 = \frac{x_1 v_1}{x_1 v_1 + x_2 v_2} \tag{8}$$

The exchange energy density is related to the cohesive energy densities, $C_{ij}$, by

$$A_{12} = C_{11} + C_{22} - 2C_{12} \tag{9}$$

where $C_{11}$ is the cohesive energy density of the solvent, $C_{22}$ is the cohesive energy density of the subcooled liquid solute, and $C_{12}$ is the cohesive energy density

characterizing the interaction between solute and solvent. The most serious weakness of regular solution theory, as with most solution theories, lies in its inability to relate accurately interactions between unlike molecules to those between like molecules. The Scatchard–Hildebrand theory[7] makes the assumption that the cohesive energy density for unlike-molecule interactions is given by the geometric mean of the cohesive energy densities of the like molecules.

$$C_{12} = [C_{11}C_{22}]^{1/2} \tag{10}$$

Since results are very sensitive to this mixing rule, for quantitative application, the geometric-mean mixing rule is relaxed by writing

$$C_{12} = [C_{11}C_{22}]^{1/2}(1 - l_{12}) \tag{11}$$

where $l_{12}$ is a binary constant, whose magnitude is of the order of $10^{-2}$, characteristic of the solute–solvent pair. This constant, to a good approximation, is independent of composition and varies little with temperature. From London's theory of dispersion forces, an approximate expression for $l_{12}$ can be derived; this expression shows that $l_{12}$ can be positive or negative, but it seldom

**Table III:** Temperatures and Entropies for Fusion and Other Solid-Phase Transitions[a]

| Hydrocarbon | $T_m$, °K | $\Delta S_f$, cal/mol-°K | Hydrocarbon | $T_m$, °K | $\Delta S_f$, cal/mol-°K |
|---|---|---|---|---|---|
| 1. Methane | 90.6 | 2.26 | 20. 3-Ethylpentane | 154.5 | 14.63 |
|  | (20.5)[b] | (0.88)[b] | 21. Methylcyclohexane | 146.6 | 11.00 |
| 2. Butane | 134.8 | 8.32 | 22. Octane | 216.3 | 22.80 |
|  | (107.6) | (4.62) | 23. 2-Methylheptane | 164.1 | 14.94 |
| 3. 2-Methylpropane | 113.5 | 9.55 | 24. 3-Methylheptane | 152.6 | 17.81 |
| 4. Pentane | 143.5 | 14.02 | 25. 4-Methylheptane | 172.2 | 15.05 |
| 5. Isopentane | 113.2 | 10.88 | 26. 2,2-Dimethylhexane | 152.0 | 18.20 |
| 6. Neopentane | 256.5 | 3.03 | 27. 2,5-Dimethylhexane | 181.9 | 16.89 |
|  | (140.0)[c] | (4.43)[c] | 28. 3,3-Dimethylhexane | 147.0 | 11.58 |
| 7. Cyclopentane | 179.3 | 0.81 | 29. 2,2,3-Trimethylpentane | 160.9 | 12.82 |
|  | (138.0) | (0.60) | 30. 2,2,4-Trimethylpentane | 165.8 | 13.28 |
|  | (122.4) | (9.53) | 31. 2,3,3-Trimethylpentane | 172.4 | 2.12[d] |
| 8. Hexane | 177.8 | 17.51 | 32. 2,3,4-Trimethylpentane | 163.9 | 13.51 |
| 9. 2-Methylpentane | 119.5 | 12.55 | 33. 2,2,3,3-Tetramethylbutane | 373.8 | 4.55 |
| 10. 2,2-Dimethylbutane | 173.4 | 0.80 |  | (148.0) | (2.56) |
|  | (141.1) | (0.57) | 34. Decane | 243.1 | 28.26 |
|  | (127.1) | (10.16) | 35. Dodecane | 263.5 | 33.15 |
| 11. 2,3-Dimethylbutane | 144.7 | 1.34 | 36. Eicosane | 309.5 | 47.46 |
|  | (136.1) | (11.40) | 37. 1-Butene | 87.8 | 10.47 |
| 12. Cyclohexane | 279.8 | 2.28 | 38. 2-Methylpropene | 132.8 | 10.67 |
|  | (186.1) | (8.59) | 39. 1-Pentene | 105.8 | 11.14 |
| 13. Methylcyclopentane | 130.7 | 12.67 | 40. 2-Methylbutene-2 | 139.4 | 13.02 |
| 14. Heptane | 182.6 | 18.39 | 41. Heptene-1 | 154.1 | 19.64 |
| 15. 2-Methylhexane | 154.9 | 13.69 | 42. Butadiene-1,3 | 164.2 | 11.62 |
| 16. 2,2-Dimethylpentane | 149.4 | 9.38 | 43. Pentadiene-1,4 | 125.0 | 11.73 |
| 17. 2,4-Dimethylpentane | 153.9 | 10.40 | 44. 2-Methylbutadiene-1,3 | 126.3 | 9.05 |
| 18. 3,3-Dimethylpentane | 138.7 | 12.18 | 45. 1,2-Dimethylacetylene | 140.6 | 15.70 |
| 19. 2,2,3-Trimethylbutane | 248.2 | 2.12[d] | 46. Carbon dioxide | 216.5 | 4.86 |

[a] J. Timmermans, "Physico-Chemical Constants of Pure Organic Compounds," Elsevier, Amsterdam, 1950; R. H. Perry, C. H. Chilton, and S. D. Kirkpatrick, Ed., "Chemical Engineers' Handbook," 4th ed, McGraw-Hill, New York, N. Y., 1963; J. G. Aston and G. H. Messerley, *J. Amer. Chem. Soc.*, **58**, 2354 (1936). [b] Parentheses denote solid-phase transition data. [c] Solid-phase transition data determined by indirect experiment (data of Aston and Messerly). [d] These low entropies of fusion suggest the possibility of transitions to more stable solid forms at temperatures below the melting temperature.

gives good quantitative results. Preston and Prausnitz[2] and Cheung and Zander[6] discuss methods for obtaining rough estimates of $l_{12}$ for use in solid–liquid equilibria.

If we introduce the solubility parameter $\delta$ into eq 7, 9, and 11, the expression for the activity coefficient of the solute is

$$RT \ln \gamma_2 = v_2 \Phi_1{}^2 [(\delta_1 - \delta_2)^2 + 2l_{12}\delta_1\delta_2] \quad (12)$$

where $\delta_1 = C_{11}{}^{1/2}$ and $\delta_2 = C_{22}{}^{1/2}$. When $l_{12} = 0$, eq 12 reduces to the familiar Scatchard–Hildebrand equation.

Experimental solubility data were used to calculate $l_{12}$ for each binary system. the results are shown in Table II. In these calculations, solubility parameters and liquid molar volumes were obtained from a corresponding-states correlation.[2]

Equation 12, coupled with eq 4 and 6, enables us to estimate the fugacity of each component in the binary liquid mixtures as a function of temperature and composition. In such calculations, solubility parameters and liquid molar volumes are functions of temperature

as indicated in the corresponding-states correlation,[2] but $l_{12}$ is considered to be independent of temperature.

## Correlation of Activity Coefficients and Entropies of Fusion

The values of $l_{12}$ given in Table II show that $l_{12}$ generally increases with difference in molecular size and chemical nature. It is impractical, however, to attempt any quantitative correlation of $l_{12}$ because the values of $l_{12}$ are sensitive to the extrapolation of solubility parameters to low temperatures. We attempt to correlate instead the activity coefficients of the saturated hydrocarbon solutes at infinite dilution in the solvent.

Activity coefficients at infinite dilution in methane and argon were first calculated at 120°K for a variety of saturated hydrocarbons using eq 12 and assuming $l_{12} = 0$. These calculated activity coefficients are given in Table IV. Figure 4 shows the activity coefficients plotted against a solute parameter $r$, which is a measure of the extent of branching in the hydrocarbon.

**Table IV:** Activity Coefficients at 120°K of Hydrocarbons at Infinite Dilution in Liquid Methane and in Liquid Argon

| Solute | $\delta_2,{}^a$ (cal/cm³)$^{1/2}$ | In methane[b] | | In argon[b] | |
|--------|------|------|------|------|------|
| | | $\gamma_2^\infty(l_{12}=0)$ | $\gamma_2^\infty(\text{exp})$ | $\gamma_2^\infty(l_{12}=0)$ | $\gamma_2^\infty(\text{exp})$ |
| 1. Cyclohexane | 9.60 | 41.2 | | 597.6 | |
| 2. Cyclopentane | 9.92 | 46.1 | 62.1 | 538.1 | 1291.0 |
| 3. Methylcyclohexane | 9.25 | 29.7 | | 492.9 | |
| 4. Methylcyclopentane | 9.15 | 15.4 | | 164.0 | |
| 5. Octane | 8.80 | 17.4 | | 329.0 | |
| 6. Heptane | 8.70 | 10.5 | | 134.7 | |
| 7. Hexane | 8.63 | 6.7 | | 57.4 | |
| 8. Pentane | 8.60 | 5.2 | 21.5 | 35.7 | 602.0 |
| 9. 3-Methylhexane | 8.58 | 7.9 | | 88.1 | |
| 10. 2-Methylpentane | 8.52 | 5.6 | | 46.5 | |
| 11. 3-Methylpentane | 8.52 | 5.4 | | 45.7 | |
| 12. Isopentane | 8.49 | 4.4 | | 27.8 | |
| 13. Isooctane | 8.48 | 8.6 | | 126.0 | |
| 14. 2,3-Dimethylbutane | 8.46 | 5.2 | 19.4 | 40.5 | 311.0 |
| 15. Neopentane | 8.26 | 3.2 | 6.42 | 16.5 | 64.1 |
| 16. 1,3-Butadiene | 9.45 | 21.2 | 140.0 | 136.0 | 8000.0 |

$^a$ Solubility parameters calculated using the correlation given in G. T. Preston and J. M. Prausnitz, *Ind. Eng. Chem., Process Des. Develop.*, **9**, 264 (1970). $^b$ At 120°K, the solubility parameter of methane is 6.61 and that for argon is 5.68 (cal/cm³)$^{1/2}$.

$$r = \frac{\text{Number of CH}_3 \text{ groups in saturated hydrocarbon}}{\text{Total number of carbon atoms in saturated hydrocarbon}}$$

Figure 4 shows that there is a strong decrease in the predicted activity coefficient at infinite dilution with an increase in the extent of branching in the saturated hydrocarbon; Figure 5 shows results when argon is the solvent.
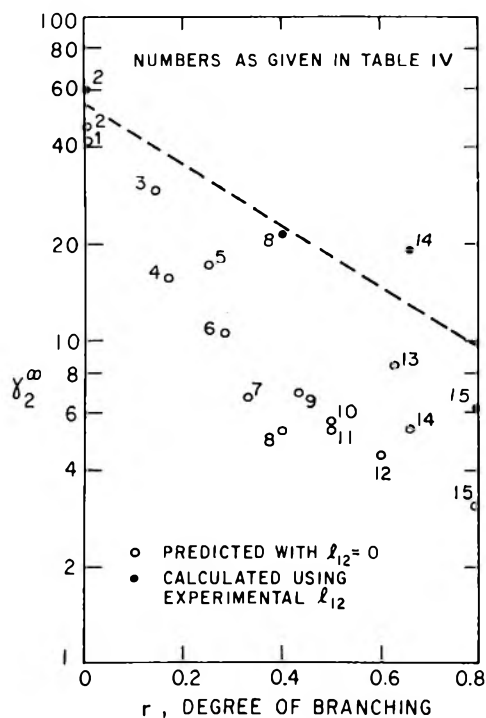


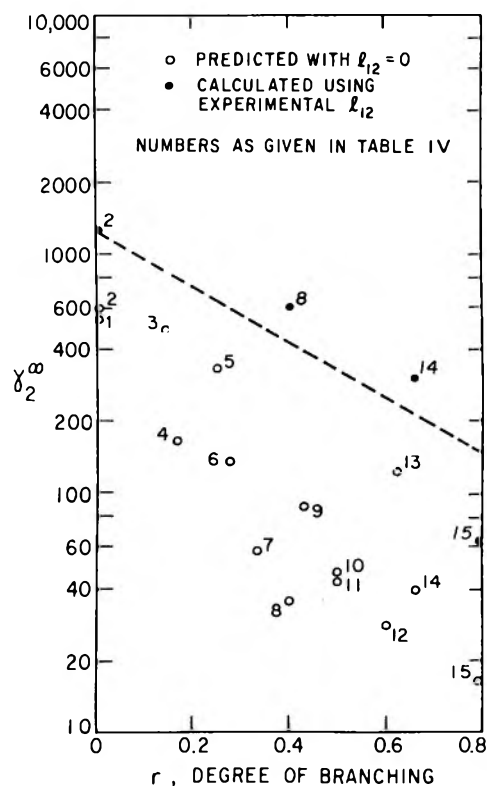Figure 4. Activity coefficients at 120°K of saturated hydrocarbons at infinite dilution in methane.



Figure 5. Activity coefficients at 120°K of saturated hydrocarbons at infinite dilution in argon.

Using experimental values of $l_{12}$, activity coefficients at infinite dilution were again calculated at 120°K using eq 12, and these are also given in Table IV. Figure 4 shows experimental activity coefficients of the saturated hydrocarbons at infinite dilution in methane and Figure 5 shows similar results in argon. For both solvents, the experimental activity coefficients define a line above that predicted with $l_{12} = 0$ and with a smaller
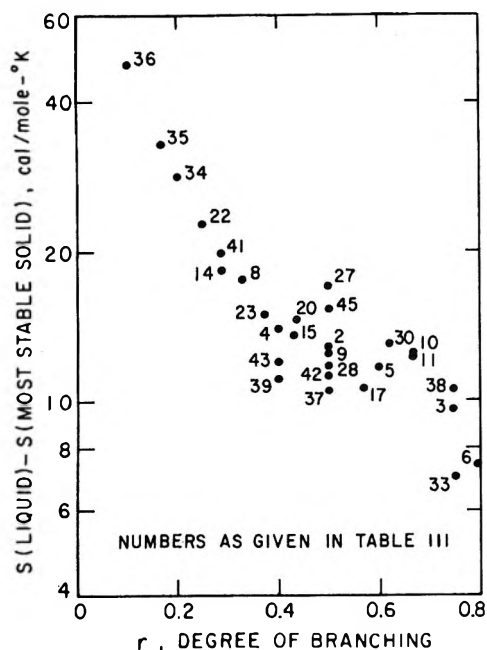
Figure 6. Total entropies of fusion (from most stable solid to liquid) for aliphatic hydrocarbons.

slope. (The experimental activity coefficients of 1,3-butadiene at infinite dilution in liquid methane and in liquid argon are much larger than those predicted by Figures 4 and 5.)

Figures 4 and 5 can be used to obtain estimates of activity coefficients at infinite dilution for those saturated hydrocarbons that have not been determined experimentally. For temperatures not far removed from 120°K, we can assume that the logarithm of the activity coefficient varies inversely with temperature. If the solubility of the solute is not small, eq 7 for the activity coefficient can be written

$$\ln \gamma_2 = (\ln \gamma_2^\infty)\Phi_1^2 \qquad (13)$$

The solubility is then calculated using eq 4, 5 or 6, and 13.

Entropies of fusion of aliphatic hydrocarbons can also be correlated as a function of the extent of branching. Figure 6 shows the entropy of fusion (or the "total" entropy change from the most stable solid to liquid for those substances with transition points) from Table III plotted against $r$; there is a sharp decrease in the entropy of fusion with an increase in branching. For unsaturated hydrocarbons, the value of $r$ for the saturated hydrocarbon of the same chain structure is used. Cyclic hydrocarbons, such as cyclopentane, do not fall on the same line as aliphatic hydrocarbons. Several of the aliphatic hydrocarbons given in Table III are not shown in Figure 6 because it is likely that they have solid-phase transitions that have not been reported. Bondi[8] gives a thorough discussion of entropies of transition and shows that while it is often possible to give a reasonable prediction of the "total" entropy of fusion, it is seldom possible to predict what part of the "total" entropy appears at the transition temperature, and it is almost never possible to give an accurate prediction of transition temperatures.

Figure 6 can be used to obtain reasonable estimates of the "total" entropy of fusion of saturated and unsaturated aliphatic hydrocarbons. With an estimated entropy of fusion from Figure 6, the fugacity ratio can be estimated by

$$\ln \frac{f_2^s}{f_2^l} = \frac{\Delta S(\text{total})}{R}\left[1 - \frac{T_m}{T}\right] \qquad (14)$$

where $\Delta S(\text{total})$ is the "total" entropy of fusion. This approximate equation tends to underestimate the fugacity ratio for two reasons. First, the effect of considering that the "total" entropy change occurs at the melting point is to predict a fugacity ratio which is too small; this effect becomes large only when the temperature of interest and the transition temperatures are far below the melting temperature. For example, the fugacity ratio predicted for neopentane (melting temperature 256.5°K and transition temperature 140°K) at 120°K using eq 14 is 0.014 and the value predicted using transition data from Table III in eq 6 is 0.120. Second, eq 14 gives an unrealistically low value of the fugacity ratio if the transition temperature is below the temperature of interest. The uncertainty in the fugacity ratio can be estimated by taking as a lower limit the fugacity ratio calculated by eq 14 and as an upper limit the value calculated by eq 5, which neglects the lowering of the fugacity ratio due to phase transitions.

## Phase Diagram for the Cyclopentane–Methane System

In the experimental work, it was observed that at about 123°K the cyclopentane–methane binary changed from a solid–liquid to a liquid–liquid system. Using the $l_{12}$ found from the solid–liquid equilibrium data, it is possible, using regular solution theory, to give a reasonable prediction of the phase diagram of the cyclopentane–methane system.

Prausnitz[9] has shown that for a system described by the Scatchard–Hildebrand equation, the coordinates of the upper consolute point are

$$T_c = \frac{2x_1 x_2 A^2/B}{R\left[\frac{A}{B}x_1 + x_2\right]^3} \qquad (15)$$

$$x_1 = \frac{\left[\left(\frac{A}{B}\right)^2 + 1.0 - \left(\frac{A}{B}\right)\right]^{1/2} - \frac{A}{B}}{1 - \frac{A}{B}} \qquad (16)$$

(8) A. Bondi, "Physical Properties of Molecular Crystals, Liquids, and Glasses," Wiley, New York, N. Y., 1968.

(9) J. M. Prausnitz, "Molecular Thermodynamics of Fluid-Phase Equilibria," Prentice-Hall, Englewood Cliffs, N. J., 1969.
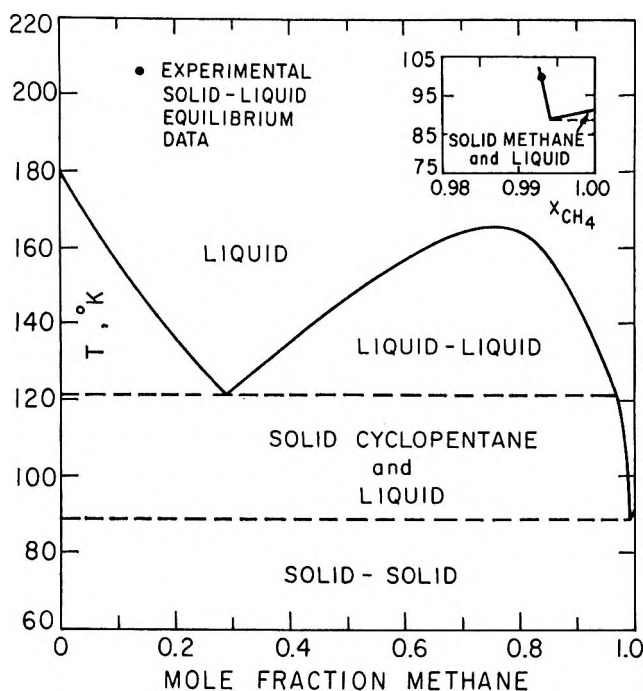
Figure 7. Calculated phase diagram for the system methane–cyclopentane.

where $A = v_1[(\delta_1 - \delta_2)^2 + 2l_{12}\delta_1\delta_2]$ and $A/B = v_1/v_2$. For cyclopentane–methane, $A = 200$ and $B = 880$ cal/mol; the consolute point is estimated to be $T = 166°K$ and $x_1 = 0.76$, where subscript 1 refers to methane.

The estimated phase diagram for the cyclopentane–methane system at temperatures up to the consolute point is shown in Figure 7. The phase diagram for the cyclopentane–methane system differs from a simple freezing-point diagram because there is a range of compositions where the liquid solutions are unstable. Starting at pure cyclopentane, the solid–liquid equilibrium curve for cyclopentane as the solid exists until a liquid composition is reached where the liquid solution is unstable. No solid–liquid equilibrium occurs in the composition range where two liquid phases are formed because, by the phase rule, the composition of a binary system cannot vary when four phases are in equilibrium. However, over the composition range where liquid solutions are unstable, we have liquid–liquid equilibria. The compositions of these liquid phases were estimated by constructing detailed plots of the Gibbs energy change of mixing vs. composition and finding the compositions that have a common tangent; these are equilibrium compositions since they have the same partial molar Gibbs energy for each component. At a methane mole fraction of 0.96, the liquid solutions are once again stable, and we have solid–liquid equilibrium with cyclopentane as the solid until the eutectic point.

Solid–liquid equilibrium for methane as the solid is observed only at high mole fractions of methane.

Davenport and Rowlinson[10] have studied several methane–hydrocarbon systems and found lower consolute temperatures above the critical temperature of methane. From the rough correlation they give for the lower consolute temperatures, it appears that the cyclopentane–methane system consists of a single phase above 166°K, but again shows a miscibility gap at a temperature slightly above 200°K.

## Conclusions

In the temperature range 90–125°K, solubilities in liquid methane and in liquid argon have been measured for carbon dioxide and for several hydrocarbons of different chain structure. From the measured solubilities, activity coefficients were calculated and regular solution theory was used to estimate values of $l_{12}$, the deviation from the geometric-mean cohesive energy density.

For both methane and argon as solvents, it was found that the activity coefficients of the saturated hydrocarbons adjusted to infinite dilution decreased with the extent of branching of the saturated hydrocarbon. This agrees qualitatively with the prediction of regular solution theory, since the solubility parameters of the hydrocarbons decrease with the extent of branching and approach the solubility parameters of methane and argon. However, the activity coefficients of saturated hydrocarbons do not decrease with the extent of branching in all solvents. For example, the predicted and observed[11] activity coefficients of saturated hydrocarbons at infinite dilution in benzene increase with the extent of branching of the saturated hydrocarbon, since benzene has a solubility parameter greater than that of any of the saturated hydrocarbons.

The entropy of fusion of aliphatic hydrocarbons also decreases with the extent of branching. Qualitatively this indicates that the difference between the solid and liquid free volumes decreases as the extent of branching rises.

The correlations for activity coefficients at infinite dilution and "total" entropies of fusion can be used to estimate the solubilities of saturated hydrocarbons in liquid methane or in liquid argon.

(10) A. J. Davenport and J. S. Rowlinson, Trans. Faraday Soc. 59, 78 (1963).

(11) E. W. Funk and J. M. Prausnitz, Ind. Eng. Chem., 62, 8 (1970).

# Polyion Hydration. I. Partial Molar Volumes and

# Electrostriction of Polyimine Salts

## by J. Lawrence and B. E. Conway*

*Chemistry Department, University of Ottawa, Ottawa, Canada    (Received March 25, 1970)*

*Publication costs borne completely by The Journal of Physical Chemistry*

With the purpose of continuing investigations on the relation between molecular configuration and hydration of organic ions, studies on polyion hydration, by measurements of apparent molar volumes, are reported for the hydrobromides of polyethylenimines having varying degrees of ionization and polymerization. Emphasis has been placed on evaluation of the individual ionic behavior since this approach allows a clearer insight into the specificity of electrostriction and other solvent structural effects caused by the polymers in aqueous solution. Comparison of the volumes of the salts with those of the corresponding neutral bases allows the volumes of ionization to be calculated. Studies over a range of degrees of ionization enable the relative effects of the ionic and nonionic parts of the molecule on solvent structure and volume to be evaluated. Radioactive tracer diffusion measurements with the higher molecular weight polymers allowed the extent of counterion association to be determined.

## Introduction

Although the hydration behavior of monomeric ions has been extensively studied for several decades,[1] the hydration of polymeric ions has hitherto received relatively little attention. Investigations with such materials allow relations between molecular configuration and hydration, of great importance with organic ions,[2–5] to be demonstrated. Previous experimental and theoretical work of Conway, Desnoyers, and Smith in this field is referred to below. The hydration of polymeric ions, like that of their monomeric analogs, is of primary importance in determining their properties and interactions in solution and the kinetics of their reactions in aqueous and other media. For example, Ise and Matsui[2] have found that small additions of various polysulfonic acids to systems in which reactions between like-charged ionic species are occurring have a substantial catalytic influence on the reaction kinetics; they concluded that the enhancement of rates was the result of hydrophobic and electrostatic interactions causing an abnormally high local concentration of reactant species around the polyelectrolyte. The effect is thus analogous to adsorption, *e.g.*, at a charged electrode interface, or salting-in. A large variety of more complex hydrated polycations, polyanions, and polyampholytes are also of great interest in biophysics and biochemistry and consequently the question of the nature of their hydration is of current interest. However, before such molecules can be quantitatively investigated in a useful way with respect to their hydration, the behavior of simpler model substances must first be studied. In the present work, based on measurements of polyion volumes and compressibilities in solution, we have therefore selected a series of well characterized polyethylenimine (PEI) oligomers, and several corre-

sponding polymers, in order to determine the hydration behavior as a function of degree of polymerization and ionization. This series is of particular interest since: (a) the charge-bearing centers form part of the backbone of the polymer rather than being located on side groups, as for example, in the case of ions derived from polyvinylpyridine or polymethacrylic acid; (b) several of the low molecular weight oligomers may also be obtained so that the transition from simple electrolyte to polyelectrolyte behavior may be examined; and (c) apart from the small differences in bond length between C–C and C–N atoms in the chain, the molecules are microscopically uniform. This work also provides a logical extension of our own[3] and other[1] previous work on the study of structural effects in solvation of organic ions and the ionization of organic acids and bases.

In order to relate the overall experimental results for the polyelectrolyte salts to *specific* ion–solvent interactions for the individual polycations and the coanions, it is necessary to separate the partial molar thermodynamic quantities for the salts into individual ionic components.[3] Any separation of this nature must to some extent be empirical, but for certain homologous series of organic ions, there is now considerable justification for supposing that gram ionic volumes and com-

(1) For recent reviews see (a) B. E. Conway, *Annu. Rev. Phys. Chem.* **17**, 481 (1966); (b) J. E. Desnoyers and P. Joliecoeur, "Modern Aspects of Electrochemistry," Vol. 5, J. O'M. Bockris and B. E. Conway, Ed., Plenum Press, New York, N. Y., Chapter 1; (c) F. J. Millero, *Chem. Rev.*, **71**, 147 (1971).

(2) N. Ise and F. Matsui, *J. Amer. Chem. Soc.*, **90**, 4242, (1968).

(3) B. E. Conway, R. E. Verrall, and J. E. Desnoyers, *Trans. Faraday Soc.*, **62**, 2738 (1966); see also B. E. Conway and R. E. Verrall, *J. Phys. Chem.*, **70**, 3952, 3961 (1966).

(4) R. Zana and E. Yeager, *ibid.*, **70**, 954 (1966).

(5) B. E. Conway and L. H. Laliberte, *Trans. Faraday Soc.*, **66**, 3032 (1970); *J. Phys. Chem.*, **74**, 4116 (1970).

pressibilities[5] of completely coordinated charge centers are a simple function of ionic radii or molecular weight. Thus, Conway, Verrall, and Desnoyers[3] have shown that for the tetraalkylammonium halides, which do not electrostrict the surrounding water, the partial molar volumes at infinite dilution, $\bar{V}_s{}^\circ$, are directly proportional to the molecular weight of the cation. Hence a graph of $\bar{V}_s{}^\circ$ plotted against cation molecular weight when extrapolated to zero molecular weight yields the gram-ionic volume of the coanion.[3] Evaluation of individual ionic volumes by the completely different method of Zana and Yeager[4] yielded results in excellent agreement with those of Conway, et al.[3] Using a similar method, Conway and Laliberte[5] have shown that the partial molar compressibilities of these salts can also be separated into individual ionic components.

In the present papers (see also part II), precise measurements of apparent molar volumes, $\phi_v$, and adiabatic compressibilities, $\phi_K$, are reported for the hydrobromides of polyethylenimines having varying degrees of ionization at the nitrogen centers. The choice of the bromide salts was dictated by (a) their facile preparation and easier purification than in the case of chloride salts; and (b) the prior work[3] on other types of organic bromide salts. The degree of polymerization, $z$, ranged from 1 to 2300. Radioactive tracer diffusion measurements were also carried out for all the imines with $z > 4$ in order to allow the extent of counterion association to be estimated, since ion-binding can affect the hydration of the polyion.

**Experimental Section**

(i) *Apparent Molar Volumes.* Values of $\phi_v$ were calculated from density measurements in the usual way[3,6] by means of the following relationship

$$\phi_v = \frac{-10^3(d - d_0)}{cd_0} + \frac{M}{d_0} \qquad (1)$$

where $d$ and $d_0$ are the densities of the solution and pure solvent, respectively, $M$ is the molecular weight of the solute, and $c$ is the molar concentration. Densities were measured at 25° by means of a previously described[3] differential buoyancy balance using techniques for optimum accuracy reported earlier.[3,6] Densities were reproducible to 3 in the sixth decimal place which enabled $\phi_v$ to be determined to $\pm 0.05$ ml monomol$^{-1}$, i.e., 0.1%.

For solutions more dilute than 0.02 $M$, $\phi_v$ was determined dilatometrically[5] using the 500-ml instrument recently described.[5] The dilatometer was immersed in a water thermostat controlled at 25 $\pm$ 0.001° in a room controlled at 24.5 $\pm$ 0.2°. This technique allowed $\phi_v$ to be determined in the concentration range 0.001 to 0.02 $M$ with a precision of approximately 0.1%, at moderate concentrations, to 0.3% at the lowest concentration.[5]

(ii) *Molecular Weights and Nature of the Polymers.* Synthetically prepared ethylenediamine, ED, diethylenetriamine, DT, triethylenetetramine, TT, and tetraethylenepentamine, TP, were obtained from Eastman Organic Chemical Co. as the reagent grade bases and were purified by double distillation under reduced pressure in an atmosphere of nitrogen. The polymers designated as PEI 6, PEI 12, PEI 18, PEI 600, and PEI 1000 having number average molecular weights of 600, 1200, 1800, 50,000, and 75,000, respectively (see below), were obtained from the Dow Chemical Co. The three lowest molecular weight compounds were supplied as pure bases (assay min 99%) and the two highest molecular weight compounds as 33% aqueous solutions. The latter, after analysis, were used without further purification. The fully ionized salts of ED, DT, TT, and TP were prepared by dissolving the corresponding purified synthetic bases in aqueous ethanol mixtures cooled in an ice bath and then bubbling in an excess of HBr. The salts were then recrystallized twice from aqueous ethanol and analyzed for bromide content by Volhard's method. The salt preparations analyzed were better than 99% pure. All the other polymeric salts were prepared by titrating the required stoichiometric amount of aqueous analytical grade HBr into a cooled aqueous solution of the corresponding polybase. The pH of the solutions at the formal equivalence point for a weak base (since p$K_a$ increases with increasing degree of ionization in polycation acids) was always referred to a control, potentiometric titration curve previously run on a small sample of the material. All solutions were prepared volumetrically (sometimes by dilution of a more concentrated, standard solution) using doubly distilled water.

The molecular weight determination for PEI polymers presents a number of difficulties. The procedures used for the Dow polymers employed in the present work were described and applied by Dick.[7] Synthesized PEI oligomers of approximate numbers which average molecular weights of 600, 1200, 1800, 5000, and 10,000 were made and the number average molecular weights were evaluated by ebullimetry in 2-propanol.[7] These PEI oligomers were then used to standardize a gel permeation chromatographic system[7] using an 8-ft column with a polyacrylamide packing and an eluent of 1 wt % $CH_3COONa$ + 1 wt % $CH_3COOH$ in distilled water (pH 4.2 ~ 4.3) at 26°. The higher polymers PEI 600 and PEI 1000 were run on the same column and the molecular weight was estimated by employing the extrapolated standardization curve. Ranges of molecular weights 50 ($\pm$10) $\times$ 10$^6$ and 90 ($\pm$10) $\times$ 10$^3$ were assigned to these two higher molecular weight polymers.

(6) H. E. Wirth, *J. Amer. Chem. Soc.*, **55**, 2549 (1937); see also F. Vaslow, *J. Phys. Chem.*, **70**, 2286 (1966).

(7) C. R. Dick, Dow Chemical Co. Amines Research Laboratory, private communication; see also J. C. Moore, *J. Polym. Sci., Part A-2*, 835 (1964); J. Cazes, *J. Chem. Educ.*, **47**, A461, A505 (1970).

Difficulties arise in the precise assignment of molecular weights to the higher polymers owing to cross-linking or chain branching.

Since obvious uncertainties arise in the use of gpc columns, standardized by means of low molecular weight polymers, for evaluation of the molecular weights of higher polymers, a column of Sephadex 200 G was also employed, standardized with 5, 10, and $20 \times 10^3$ molecular weight PEI materials. The PEI 600 and 1000 materials were then run and the same ranges of molecular weights were obtained as in the first method. In the case of PEI 600, light-scattering measurements gave a confirming value of 36 to $37 \times 10^3$ for the molecular weight.

Although the PEI polymers are difficult to characterize precisely with respect to molecular weights and molecular weight distribution, the present studies of hydration of the N-ionized polyelectrolytes will, it is considered, not be made uncertain on this account since the hydration effects studied through the partial molar volumes and compressibilities are quite short range effects with respect to the polymer chains and the charged $N^+$ centers which they bear.

(iii) *Estimation of Counterion Binding.* The fraction of $Br^-$ counterions likely to be bound to the polyions could only be investigated by reference to studies of the self-diffusion of radioactive *chloride* ion in otherwise-identical solutions of PEI–HCl. The experiments were carried out under steady-state conditions by a method similar to that used by Huizenga, Grieger, and Wall,[8] the details having been described in that paper. Unfortunately, it was not possible to measure reliably the extent of ion-binding in the series of hydrobromide salts by this method since the half-life of the commonly available isotope $^{82}Br$ is only 36 hr, while the duration of a typical experiment is 48 hr. The two-compartment cells were filled and rotated for about 4 hr to allow a uniform concentration gradient of $^{36}Cl^-$ to be established across the frit,[8] after which time they were emptied and refilled with their respective solutions and the experiment continued for a further period of about 2 days. At the end of this time, a sample from one compartment of the cell together with a sample of the original solution in the other compartment was analyzed for $^{36}Cl^-$ in a liquid scintillation counter.

If a quantity $R$ is defined as

$$R = \frac{\text{counts min}^{-1}\text{ cm}^{-3}\text{ in compartment b at time} = t}{\text{counts min}^{-1}\text{ cm}^{-3}\text{ in compartment a at time} = 0}$$

then the fraction of *free* chloride ions, $f$, can be calculated from the expression

$$-fDKt = \log\left[1 - R(1 + V_b/V_a)\right]$$

where $V_a$ and $V_b$ are the volumes of compartments a and b, respectively, $t$ is the duration of the experiment, $D$ the diffusion coefficient of $Cl^-$ ion, and $K$ the cell constant. The latter was obtained from measurements (cf.

**Table I:** $(1 - f)$, the Fraction of Chloride Ions Bound to Polyimine Cations

PEI 6 (HCl)

| $c$ | 0.80 | 0.60 | 0.40 | 0.20 |
|------|------|------|------|------|
| 0.14 | 0.75 | 0.75 | 0.71 | 0.51 |
| 0.08 | 0.51 | 0.47 | 0.38 | 0.24 |
| 0.05 | 0.39 | 0.34 | 0.25 | 0.15 |
| 0.01 | 0.21 | 0.20 | 0.19 | 0.14 |

PEI 12 (HCl)

| $c$ | 0.77 | 0.55 | 0.35 | 0.25 |
|------|------|------|------|------|
| 0.07 | 0.72 | 0.70 | 0.66 | 0.64 |
| 0.03 | 0.54 | 0.50 | 0.44 | 0.38 |
| 0.008 | 0.50 | 0.45 | 0.37 | 0.30 |
| 0.002 | 0.42 | 0.39 | 0.32 | 0.25 |

PEI 18 (HCl)

| $c$ | 0.70 | 0.50 | 0.30 | 0.20 |
|------|------|------|------|------|
| 0.047 | 0.83 | 0.83 | 0.78 | 0.71 |
| 0.010 | 0.50 | 0.49 | 0.41 | 0.31 |
| 0.005 | 0.49 | 0.48 | 0.38 | 0.30 |
| 0.001 | 0.48 | 0.43 | 0.32 | 0.25 |

PEI 600 (HCl)

| $10^3c$ | 0.70 | 0.50 | 0.30 | 0.20 |
|------|------|------|------|------|
| 0.90 | 0.70 | 0.70 | 0.70 | 0.56 |
| 0.30 | 0.62 | 0.62 | 0.58 | 0.48 |
| 0.06 | 0.61 | 0.60 | 0.55 | 0.48 |
| 0.01 | 0.60 | 0.60 | 0.52 | 0.40 |

PEI 1000 (HCl)

| $10^4c$ | 0.70 | 0.50 | 0.30 | 0.20 |
|------|------|------|------|------|
| 4.00 | 0.70 | 0.70 | 0.69 | 0.52 |
| 1.00 | 0.65 | 0.64 | 0.61 | 0.44 |
| 0.20 | 0.67 | 0.67 | 0.58 | 0.43 |
| 0.07 | 0.67 | 0.67 | 0.58 | 0.40 |

Stokes[9]) of the diffusion of $^{36}Cl^-$ in 0.005 $m$ sodium chloride solution taking $D = 1.65$ cm$^2$ day$^{-1}$.[9]

## Results

(i) *Ion Association.* In Table I are recorded the fractions of chloride ions $(1 - f)$ bound to the polyimine cations at four concentrations and for four apparent degrees of ionization, the latter being based on the stoichiometric ratio of monomole N centers and moles of HBr added (cf. ref 10). With the exception of the most concentrated solutions of PEI 6, 12, and 18, the results, for $1 - f$, like those found by other authors

(8) J. R. Huizenga, P. F. Grieger, and F. T. Wall, *J. Amer. Chem. Soc.*, **72**, 4228 (1950); see also R. H. Stokes, *ibid.*, **72**, 763 (1950).

(9) R. A. MacInnes, T. Shedlovsky, and L. G. Longsworth, *ibid.*, **54**, 2758 (1932).

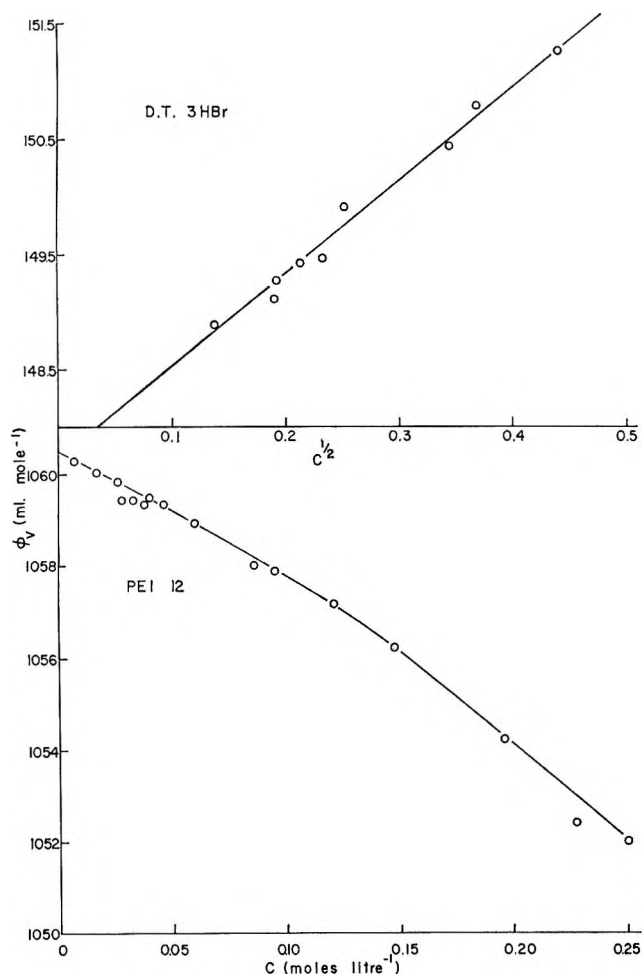(10) N. Ise and T. Okubo, *ibid.*, **90**, 4527 (1968).

Figure 1. Relations between apparent molar volume, $\phi_v$, and concentration for DT(3HBr) salt and polymer PEI 12.



Figure 2. Relations between apparent molar volume, $\phi_v$, and concentration for the polyion salts PEI 1000 (HBr)$_{0.7}$ and PEI 600 (HBr)$_{0.7}$.

for different polyelectrolytes,[11] show only a small concentration dependence but a stronger dependence on charge. That the data for $Cl^-$ binding can be used as an indication of the $Br^-$ binding in the apparent molar volume measurements receives support from the work of Lapanje, et al.,[12] who showed that counteranion ($Cl^-$) association at polyimine ions was loose and nonspecific on a site for site basis. However, with other polycations, degrees of association of $Br^-$ are some 20% greater than those of $Cl^-$. Corrected degrees of ionization were estimated from the stoichiometric apparent degrees of ionization, $\alpha$, defined above by applying a correction for the degree of anion association, $1 - f$.

(ii) *Apparent and Partial Molar Volumes.* The apparent molar volumes of each compound studied were fitted to a quadratic equation in concentration $c$ by means of a computer and the resulting coefficients are listed in Table II. For some of the solutions, a comparison can be made with the somewhat less accurate results (cf. their experimental conditions) of Ise and Okubo,[10] who measured $\phi_v$ of the low molecular weight imine hydrochlorides without corrections for ion association. The results of these authors are consistently
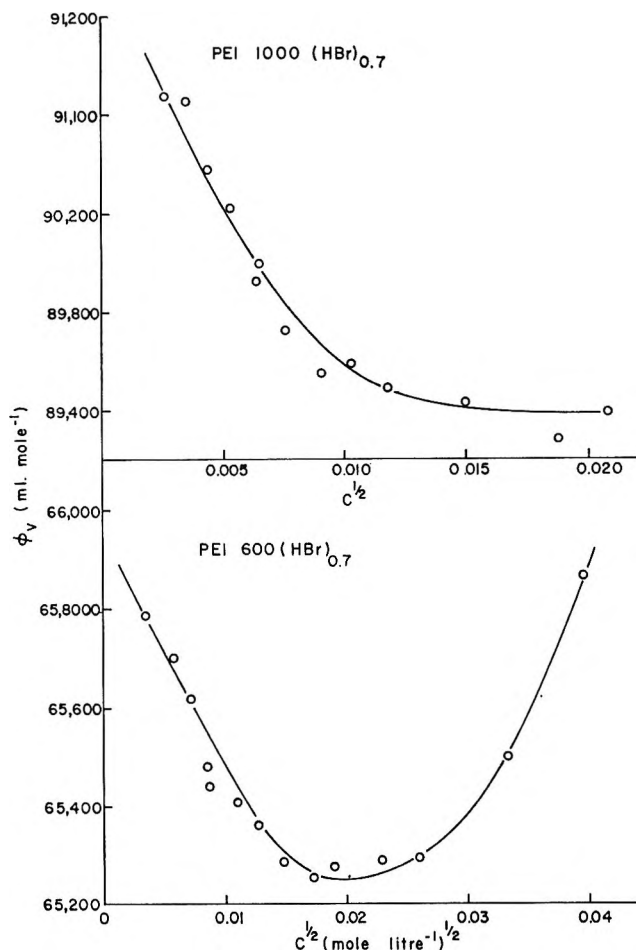
higher than ours by up to 5% but part of this small but significant discrepancy could be due to the somewhat uncertain difference between $\bar{V}_{Br^-}{}^\circ$ and $\bar{V}_{Cl^-}{}^\circ$. Plots of $\phi_v$ against $c^{1/2}$ (or $c$ for the neutral bases) show the expected linearity with positive slopes for the salts and negative or near zero slopes for the bases. The plots for DT(3HBr) and the neutral polybase PEI 12 are shown in Figure 1 as two typical examples. The only two significant exceptions to this behavior are exhibited by the salts PEI 600 (HBr)$_{0.7}$ (where the fractional subscripts denote the apparent degree of ionization $\alpha$) and PEI 1000 (HBr)$_{0.7}$; the results for these materials are shown in Figure 2. The distinct minimum at $c^{1/2} = 0.018$ for PEI 600 (HBr)$_{0.7}$ and that which appears to exist at some higher concentration for PEI 1000 (HBr)$_{0.7}$ could be accounted for in terms of a change in configuration of the polymeric chain.[13] At infinite dilution the cations (or sections between branching

(11) J. R. Huizenga, P. F. Grieger, and F. T. Wall, *J. Amer. Chem. Soc.*, 72, 2636 (1950).

(12) S. Lapanje, J. Harebig, H. T. Davis, and S. A. Rice, *ibid.*, 83, 1590 (1961).

(13) R. M. Fuoss and W. N. Maclay, *J. Polym. Sci.*, 6, 305 (1951).

**Table II:** Coefficients of Molar Concentration Dependence of $\phi_v$ Data Expressed as $\phi_v = A + Bc + Cc^2$ ml mol$^{-1}$

| Solute | $A$ | $B$ | $C$ |
|---|---|---|---|
| HBr | $26.0 \pm 0.2$ | 3.15 | $-5.24$ |
| ED (2HBr) | $94.8 \pm 0.4$ | 15.9 | $-32.9$ |
| DT (2HBr) | $143.6 \pm 0.4$ | 19.9 | $-36.9$ |
| DT (3HBr) | $149.4 \pm 0.4$ | 20.1 | $-26.5$ |
| TT (2HBr) | $185.9 \pm 0.6$ | 10.4 | $-8.88 \pm 2\%$ |
| TT (3HBr) | $205.3 \pm 0.6$ | $23.5 \pm 1\%$ | $-24.7$ |
| TT (4HBr) | $214.7 \pm 0.6$ | 18.9 | $-20.8$ |
| TP (2HBr) | $215.5 \pm 0.6$ | 13.2 | $-17.4$ |
| TP (3HBr) | $230.1 \pm 0.6$ | 34.4 | $-64.0$ |
| TP (4HBr) | $243.2 \pm 0.6$ | 46.4 | $-87.6$ |
| PEI 6 (2HBr) | $577.5 \pm 6$ | 15.6 | $-40.4$ |
| PEI 6 (7HBr) | $481.4 \pm 5$ | 287.9 | $-1,791$ |
| PEI 6 (HBr)$_{0.8}$[a] | $749.5 \pm 8$ | 95.4 | $-6.09$ |
| PEI 12 (HBr)$_{0.77}$ | $1,486 \pm 10$ | $257 \pm 2\%$ | $-82.6 \pm 5\%$ |
| PEI 18 (HBr)$_{0.7}$ | $2,171 \pm 20$ | 1,406 | $-13,789$ |
| PEI 600 (HBr)$_{0.7}$ | $65,627 \pm 50$ | $-1,190$ | 881 |
| PEI 1000 (HBr)$_{0.7}$ | $90,498 \pm 50$ | $-994$ | 177 |
| ED | $63.1 \pm 0.4$ | $-0.72$ | 1.18 |
| DT | $101.2 \pm 0.4$ | 1.05 | $-3.05$ |
| TT | $137.6 \pm 0.5$ | $2.12 \pm 1\%$ | $-2.83 \pm 2\%$ |
| TP | $175.9 \pm 0.6$ | $-0.235$ | $-3.72$ |
| PEI 6 | $537.9 \pm 1$ | $-8.39$ | $-7.09$ |
| PEI 12 | $1,061 \pm 1$ | $-53.8$ | 67.2 |
| PEI 18 | $1,582 \pm 1$ | $-62.1 \pm 2\%$ | $63.0 \pm 5\%$ |
| PEI 600 | $43,133 \pm 15$ | 57.5 | $-23.2$ |
| PEI 1000 | $65,171 \pm 20$ | $-108.0$ | $-6.47$ |

[a] The numerical subscripts used in the nomenclature for the solute salts represent the apparent degree of ionization, $\alpha$. The numbers in brackets in the first 11 entries in column 1 for the polyimine oligomers refer to the stoichiometry of the hydrobromide salts prepared from the corresponding bases by controlled additions of HBr. The anomalously high values of the coefficient, $C$, for PEI (HBr)$_{0.7}$ and PEI 6 (7HBr) have been specially investigated but no particular explanation can at the moment be given except that they may be due to chain branching. The experimental results are as accurate as those for the other materials studied in the same apparatus, so the high values are not experimental artefacts. The last nine entries in the table refer to the neutral bases. Uncertainties in $A$ values depend not only on the accuracy of the primary $\phi_v$ data but on the extrapolation to $c \rightarrow 0$. "$A$" hence depends on the shape of the curve of $\phi_v$ vs. $c$ at low concentrations[b] and the accuracy of $A$ is weighted by the accuracy of $\phi_v$ at the low concentrations. The coefficients $B$ and $C$, being based on all the points for a given polysalt, are quoted less specifically.

points at tertiary N centers) will tend to assume a "stretched rod-like" configuration as a result of the electrostatic repulsion between the charged N centers, but as the concentration is increased, anions tend to come into closer proximity[12] to the polyions and partially screen the positive charges. As a result, the intramolecular repulsion decreases allowing the polyion to become more loosely coiled with interpolyion attraction.[14] An apparent insensitivity of $\phi_v$ to changes of $c$ with PEI (HCl)$_{0.8}$ [$z = 770$] was reported by Ise and Okubo[10] (Figure 2 of ref 10) but on closer examination the results also exhibit a definite minimum at ca. $c = 0.5$ monomol l.$^{-1}$ which corresponds well with the minimum found in our results at $c = 0.00032$ mol l.$^{-1}$ (0.38 monomol l.$^{-1}$.) Extrapolation of the $\phi_v$ against $c^{1/2}$ or $c$ plots to zero $c$ gives values for the apparent molar volume at infinite dilution $\phi_v°$, which correspond to within 1% (and usually to better than 0.5%) with the empirical coefficients $A$ in Table II calculated by curve fitting.

While the empirical extrapolations of $\phi_v$ to zero concentration (Figures 1 and 2) raise the same problems as arise in the case of R$_4$N$^+$ salts, owing to persistence of nonideality to very low concentrations,[3,5] the additivity of the extrapolated $\phi_v$ data (Figures 3 and 4) is nevertheless rather satisfactory, indicating adequacy of the dilatometric results at low concentrations.

The dependence of the empirical coefficient $B$ (Table II) of the linear term in $c$ in the equation for $\phi_v$, on degree of polymerization, is shown in Figure 3 for oligomer cations of various charges. All values are positive in accordance with the behavior of simple electrolytes. The sign of $B$ at low concentration for the higher molecular weight cations, however, becomes rapidly negative (Table II) and we presume this arises from the appreciable degree of ion association by site binding and looser association within the polycation

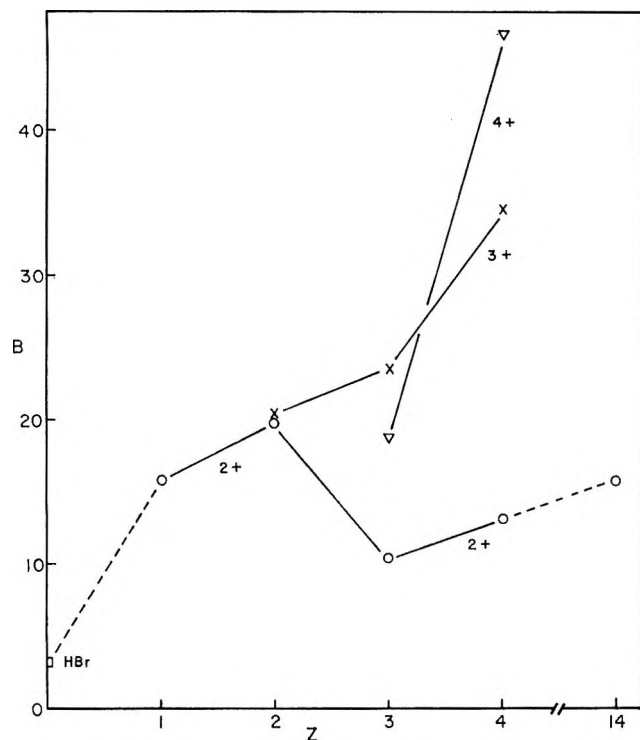(14) J. A. V. Butler, B. E. Conway, and D. W. F. James, *Trans. Faraday Soc.*, **50**, 612 (1954).

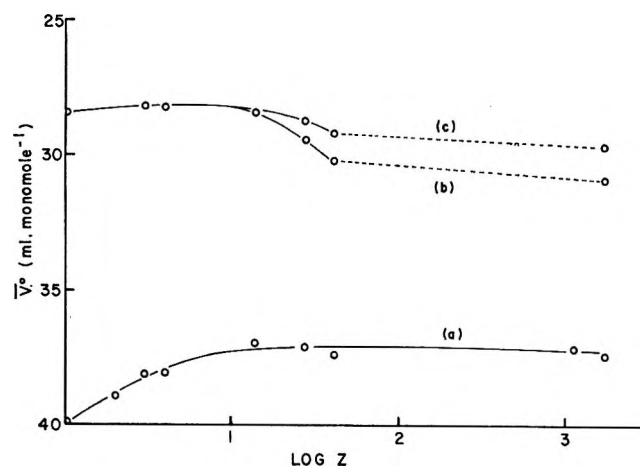Figure 3. Values of the $B$ coefficient (Table II) as a function of $z$ for the oligomer ions.



Figure 4. Partial molar volume at infinite dilution, $\bar{V}^\circ$, per *monomole* of the polyimines as a function of degree of polymerization: curve a, volume per monomer group of neutral bases as a function of log $z$; curve b, approximate volume per monomer group of the polycations ($a = 0.7$–$0.8$) as a function of log $z$; curve c, corrected volumes per monomer group of the polycations ($a = 0.7$–$0.8$) as a function of log $z$, allowing for effects of ion association.

random coil which occurs when the molecular weight becomes high enough for random coil configurations to be adopted (polymers PEI 600 and PEI 1000) (see Table I). Also, with the higher molecular weight polymers, appreciable chain branching is known to arise.

In the case of the neutral bases, hydrolysis was suppressed in all measurements by making the solutions 0.1 $m$ with respect to KOH in addition to the working concentration of imine and employing 0.1 $m$ KOH as the reference solvent in the second float vessel. The tendency of the salts to hydrolyze in aqueous solutions more dilute than about 0.01 $m$ would prevent the relevant (see below) Debye–Hückel limiting slope from being attained even though experimental values for $\phi_v$ were measured down to at least 0.001 $m$. However, it is unlikely, of course, that these salts would give the normally expected limiting slopes for 1:1, 2:1, 3:1, 4:1, etc., electrolytes[15] since the charge is not localized at any single point on the molecule.

## Discussion

*1. Additivity of Volumes and the Individual Polycation Volumes.* The infinite dilution volume, $\bar{V}^\circ{}_{-C_2H_4NH-}$, per monomer group ($-C_2H_4NH-$) for the neutral bases was calculated from $\bar{V}^\circ{}_{base}$ by subtracting 23.5 ml mol$^{-1}$ for the volume of one of the terminal $-NH_2$ groups[16] and dividing by $z$. The results are shown in Figure 4a as a function of $z$ and it can be seen that except for the slight increase for $z \leq 4$, $\bar{V}^\circ{}_{-C_2H_4NH-}$ is almost independent of chain length, a result which indicates reasonable additivity of $\bar{V}^\circ$ contributions per monomer. The small increase in $\bar{V}^\circ$ indicated in curve a of Figure 4 is presumably the result of a structure-forming interaction of the remaining terminal N being greater than that associated with the intermediate N atoms in the chain, an effect which must become relatively negligible on a $\bar{V}^\circ$ monomol$^{-1}$ basis for the higher polymers.

The $V^\circ{}_{-C_2H_4NH-}$ value derived by Ise and Okubo[10] for the neutral base PEI with $z = 770$ is 10% lower than that obtained in the present work, but this is probably because these authors did not suppress the hydrolysis of the weak base by using 0.1 $N$ aqueous KOH as "solvent." The results are illustrated in another way in Figure 5 (line a) where $\bar{V}^\circ{}_{base}$ is plotted against $z$. Good linearity is observed with a slope of 36.8 which is consistent with the constant value of $\bar{V}^\circ{}_{-C_2H_4NH-}$ of Figure 4, line a. Extrapolation to $z = 0$ gives a value of 24 ml mol$^{-1}$ for the volume of the terminal $-NH_2$ group and this agrees well with the value of 23.5 referred to earlier. The constancy of $\bar{V}^\circ{}_{-C_2H_4NH-}$ indicates that the volumes of the bases are directly proportional to the lengths of the polymer chains and therefore suggests that these systems, when ionized, can be adequately represented with regard to the short-range interactions involved in hydration by the uniform linear rod model of Alfrey, Berg, and Morawetz[17] employed

(15) L. A. Dunn, *Trans. Faraday Soc.*, **62**, 2348 (1966).

(16) R. E. Verrall, Ph.D. Thesis, University of Ottawa, 1966, p 245.

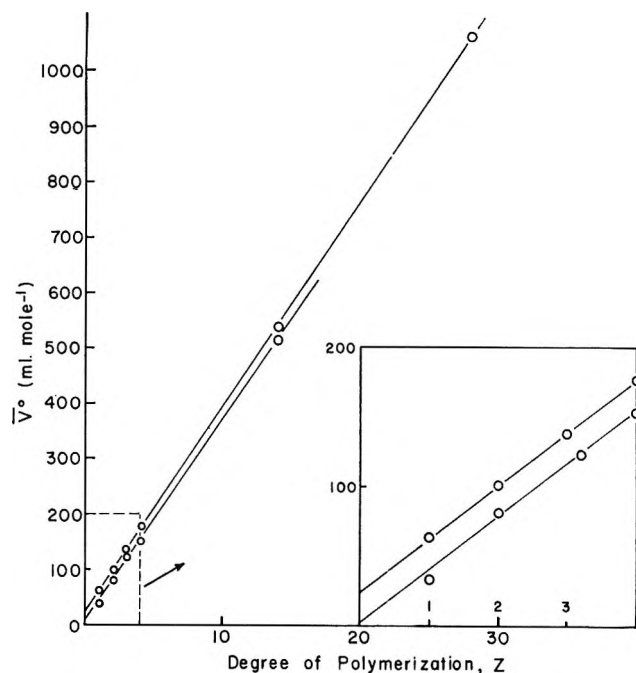(17) T. Alfrey, P. W. Berg, and H. Morawetz, *J. Polym. Sci.*, **7**, 543 (1951).

Figure 5. Additivity of partial molar volumes at infinite dilution of the polyimines as expressed by the dependence of $\bar{V}^\circ$ (per mole) on degree of polymerization for the oligomers: curve a, values for the neutral bases; lower curve, b, values for the divalent cations derived from the bases. Inset: behavior in polymers with $Z = 1-4$.

by Conway, Desnoyers, and Smith[18] in their treatment of the salting-out and volume behavior of other ionized polymeric species (polyphosphates and salts of poly-methacrylic acid).

The partial gram-ionic volume of the bromide ion at infinite dilution was estimated from the apparent molar volume of HBr taking[1,3] the gram-ionic volume of $H^+$ as $-5.7$ ml (g-ion)$^{-1}$. The resulting value of 31.6 ml (g-ion)$^{-1}$ was then used to calculate the individual partial gram-ionic volumes of the polymeric cations. The volumes of the divalent cations are shown in Figure 5 (lower curve, b). The same linear relationship is observed as was found for the neutral bases and the two lines are virtually parallel since the slopes have the same significance because the repeating group within the chain $-CH_2CH_2NH-$ is the same. Extrapolation to zero $z$ leads to a value of $\bar{V}^\circ_{-NH_3^+}$ of 2 ml mol$^{-1}$ for the end group, in the absence of chain branching.

The approximate volume per monomer for the poly-cations with apparent degree of ionization $\alpha = 0.7$ to 0.8 (i.e., $-NH_2-C_2H_4-$) was first calculated in the usual way

$$\bar{V}^\circ_{(BH_n)^{n+}} = (\bar{V}^\circ_{salt} - n\bar{V}^\circ_{Br^-} - \bar{V}^\circ_{NH_3^+})/z \quad (2)$$

The results are shown in Figure 4 (curve b) where it can be seen that, unlike the behavior of the neutral bases, there is a substantial increase in volume as $z$ increases in the case of the higher molecular weight polymers; i.e., there is a relative decrease in electrostriction per $N^+$

center for the longer chain molecules, an effect which probably arises from ion association.

*2. Ion Binding and the Electrostriction.* More reliable evaluation of $\bar{V}^\circ_{(BH_n)^{n+}}$ must therefore take into account the ion-binding associated with these larger ions. Hamann, Pearce, and Strauss[19] obtained a value for the volume change $\Delta V_d$ which occurs when ion pairs of $Mg^{2+}SO_4^{2-}$ and $La^{3+}[Fe(CN)_6]^{3-}$ dissociate: $\Delta V_d$ was evaluated from the pressure dependence of the (overall) ion-pair dissociation constant (cf. Eigen and Tamm[20]) and these measurements together with those of Padova[21] suggest that most ($>85\%$) of the electrostriction associated with hydration is *maintained* when ion association occurs; i.e., the ion pairs are hydrated-ion pairs and not contact pairs. The electrostriction associated with the salt $TP(HBr)_{0.8}$ was calculated from the experimental volume of the TP base and that of its salt by considering $\bar{V}^\circ$ to be composed of three contributions

$$\bar{V}^\circ = \bar{V}_I + \bar{V}_S + \bar{V}_E \quad (3)$$

where $\bar{V}_I$ is the intrinsic volume of the compound, $\bar{V}_S$ is the volume due to a change in structure of the surrounding water (i.e., the hydrophobic or structure-breaking term,[1] including the cavity volume), and $\bar{V}_E$ is the volume change due to electrostriction of the surrounding water.[18] $\bar{V}_E$ for the neutral bases is equal to zero and therefore $\bar{V}^\circ_{base} = \bar{V}_I + \bar{V}_S$. A difficulty arises with the quantity $\bar{V}_S$ for the base and the conjugate cation; if $\bar{V}_S$ were assumed to be the same for the cation as for the base, then $\bar{V}_E$ could be simply expressed as

$$\bar{V}_E = \bar{V}^c_{(BH_n)^{n+}} - \bar{V}^\circ_{base} \quad (4)$$

The validity of the above assumption for $\bar{V}_S$ receives some justification from the previously published results of Conway and Laliberte[22] on the ionization of 2,6-lutidine which indicate specific structural effects in the apparent molar volume $\phi_v$ which are largely independent of whether the lutidine is present as the neutral molecule or in the form of the protonated base.

The above relation for $\bar{V}_E$, derived on the basis of this now rationalized assumption, then enables a value of $\bar{V}_E$ for the salt $TP(HBr)_{0.8}$ to be derived from the experimental results as $-8.8$ ml monomol$^{-1}$. This value was then used to calculate first the apparent volume change $\Delta V_d$, resulting from dissociation of ions bound to a monomole of polycation at a degree of ionization $\alpha$, for the polysalt PEI 6 $(HBr)_{0.8}$, viz. eq 5.

(18) B. E. Conway, J. E. Desnoyers, and A. C. Smith, *Phil. Trans. Roy. Soc. London*, 256, 389 (1964).

(19) S. D. Hamann, P. F. Pearce, and W. J. Strauss, *J. Phys. Chem.*, 68, 375 (1964).

(20) M. Eigen and K. Tamm, *Z. Elektrochem.*, 66, 107 (1962).

(21) J. Padova, *J. Chem. Phys.*, 39, 1552 (1963); 40, 691 (1964).

(22) B. E. Conway and L. H. Laliberte in "Hydrogen Bonded Solvent Systems," A. Covington and P. Jones, Ed., Taylor and Francis, London, 1968, p 139.

$$\Delta V_\mathrm{d} = \bar{V}^\circ{}_{(\mathrm{PEI}\ 6)^{n+}} - \bar{V}^\circ{}_{(\mathrm{PEI}\ 6)} + 8.8 \qquad (5)$$

Then, taking account of the apparent degree of ionization $\alpha$ and the fraction $1 - f$ of counterions bound (measured as $\mathrm{Cl}^-$, see above), the true volume change $\Delta V^\circ{}_\mathrm{d}$ arising from the dissociation of a monomole ion pair is given by

$$\Delta V^\circ{}_\mathrm{d} = \Delta V_\mathrm{d}/(1 - f)\alpha \qquad (6)$$

which, upon introducing the appropriate values for $\alpha$ and $f$, and noting the individual $\bar{V}^\circ{}_{\mathrm{Br}^-}$ value,[3,4] gives $\Delta V^\circ{}_\mathrm{d} = 2.5$ ml monomol$^{-1}$ for the PEI 6 salt. In eq 5 and 6, all volume terms are calculated per monomole in order to facilitate comparisons between the various data. This value for $\Delta V^\circ{}_\mathrm{d}$ (per monomole) was assumed to be independent of $z$ and then used to calculate a corrected volume (i.e., for the fully dissociated polysalts) for the other polymeric cations by means of the relation

$$\bar{V}^\circ{}_{(\mathrm{BH}_n)^{n+}{}_\mathrm{cor}} = \bar{V}^\circ{}_{(\mathrm{BH}_n)^{n+}{}_\mathrm{exptl}} - \Delta V^\circ{}_\mathrm{d}\alpha(1 - f) \qquad (7)$$

The corrected volumes (curve c in Figure 4) still show a small but significant increase with increasing $z$ and this could be explained, within the limitation of the correction described above,[23] by a decrease in $\bar{V}_\mathrm{E}$ resulting from a decrease in $E$, the electric field at a point near the axis of the ion, with increasing $z$. Thus, it has been shown in ref 18 that for the "linear charged rod" model of a polyion, the average field at a distance $r$ from the polyion axis is given approximately by $E = -2ae/\epsilon\lambda r$ (from the logarithmic potential function) where $\lambda$ is the distance between the ionizable groups on the chain, and $\epsilon$ is the dielectric constant, whereas the field at a distance $r$ from a simple ion is $E = -ze/\epsilon r^2$.

The increase of electrostriction about the charged nitrogen centers which arises with increasing cationic charge is well illustrated in Figure 6 where $\bar{V}^\circ{}_{(\mathrm{BH}_n)^{n+}}$ (written as $\bar{V}^\circ{}_\mathrm{cation}$) is plotted against the net and apparent charge for each of the oligomeric imines up to PEI 6. In this plot, the results are most conveniently expressed in ml g-ion$^{-1}$ to illustrate the progressive change of $\bar{V}^\circ$. The nonlinear decrease of volume with net charge is presumably mainly the result of interaction of primary hydration shells when, progressively, more and more "adjacent" N atoms become ionized, although a small contribution to the curvature might be expected[3,22] to arise from the fact that the terminal N atoms are more accessible for hydration than are the inner N atoms. Such steric effects have already been examined by Conway and Laliberte[4,22] with simpler N-containing molecules, e.g., pyridine and its homologs.

*3. Volume of Ionization.* The volume change $\Delta \bar{V}^\circ{}_\mathrm{ioniz}$ (associated with hydration) accompanying the ionization process was examined directly for the lower molecular weight imines by calculating the volume change occurring in the reaction
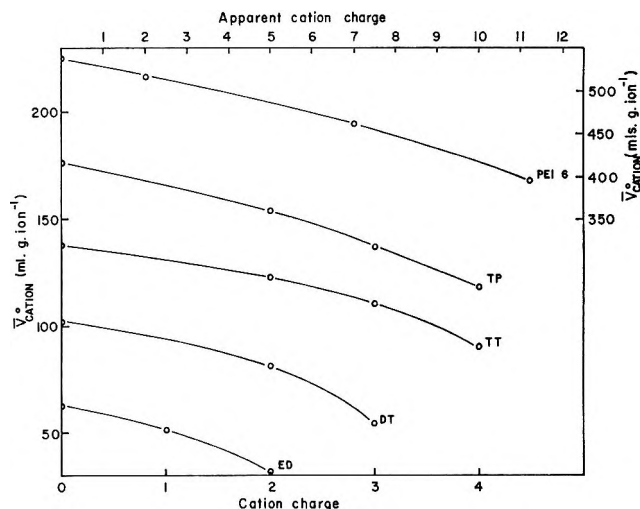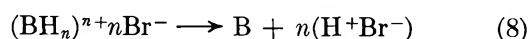
$$(\mathrm{BH}_n)^{n+}{}\!+\!n\mathrm{Br}^- \longrightarrow \mathrm{B} + n(\mathrm{H}^+\mathrm{Br}^-) \qquad (8)$$

Figure 6. Partial molar volume at infinite dilution, $\bar{V}^\circ$, per g-ion as a function of cation charge for a series of polyimine cation oligomers.
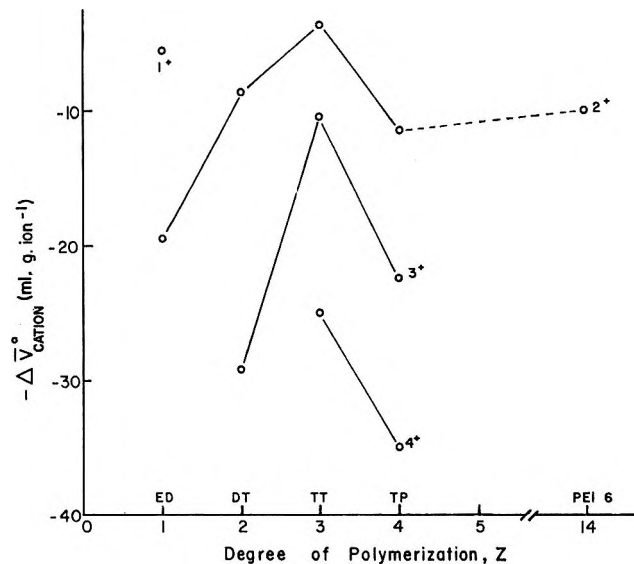


Figure 7. Volume of ionization, $\Delta \bar{V}^\circ{}_\mathrm{ionization}$, per mole as a function of degree of polymerization for polyimine cation oligomers having various charges.

Therefore, without any thermodynamic ambiguity, $\Delta \bar{V}^\circ{}_\mathrm{ioniz}$ can be expressed as

$$\Delta \bar{V}^\circ{}_\mathrm{ioniz} = \bar{V}^\circ{}_\mathrm{base} + n\bar{V}^\circ{}_{\mathrm{H}^+\mathrm{Br}^-} - \bar{V}^\circ{}_{(\mathrm{BH}_n)^{n+}{}\!+\!n\mathrm{Br}^-} \qquad (9)$$

It might have been expected that $\Delta \bar{V}^\circ{}_\mathrm{ioniz}$ for the divalent ions would be independent of $z$ since the only hydration changes that occur would tend to arise at the terminal N atoms. However, it can be seen from Figure 7 that this is evidently not the case for $z \leq 4$. The minimum at $z = 3$ suggests that the hydration sheaths

(23) If values of $1 - f$ for $\mathrm{Br}^-$ are taken as 20% larger than the measured values for $\mathrm{Cl}^-$, the corrected values of $\bar{V}^\circ{}_{(\mathrm{BH}_n)^{n+}}$ are somewhat smaller but might be more independent of $z$ if $1 - f$ for $\mathrm{Br}^-$ increased with $z$ at a greater rate than do the data for $\mathrm{Cl}^-$. This is the general trend with polyions of increasing molecular weight and anions of increasing polarizability and decreasing hydration.[1,2,5]

have least interaction in the case of the triethylene-tetramine salts and only the longer chain divalent ions tend to behave as bolaform[24] electrolytes and thus possess sufficient flexibility to allow the $N^+$ center at one end of the chain to interact with the counterion atmosphere and solvent-influenced region surrounding the ionized center at the further end.[13,25] Consequently, above $z = 4$, the addition of extra uncharged monomer units to the chain has little effect on the $\Delta \bar{V}^\circ_{ioniz}$. Figure 7 also shows the data for singly, triply, and quadruply charged ions.

It is of interest to compare $\Delta \bar{V}^\circ_{ioniz}$ for the various oligomer ions with the values for the $(CH_3)_nH_{3-n}N^+H$ series investigated previously[3] ($n \leq 3$). The data are listed in Table III.

**Table III**

| | $\Delta \bar{V}^\circ_{ioniz}$, ml mol$^{-1}$ | | $\Delta \bar{V}^\circ_{ioniz}$, ml mol$^{-1}$ |
|---|---|---|---|
| $CH_3NH_3^+$ | $+4.1 \pm 0.4$ | $ED^+$ | $+5.5$ |
| $(CH_3)_2NH_2^+$ | $+4.0 \pm 0.4$ | $ED^{2+}$ | $+11.5$ |
| $(CH_3)_3NH^+$ | $+5.2 \pm 0.4$ | $DT^{2+}$ | $+8.7$ |
| $(C_2H_5)_3NH^+$ | $-1 \pm 0.4$ | $TT^{2+}$ | $+3.7$ |
| | | $TP^{2+}$ | $+11.5$ |

The $\Delta \bar{V}^\circ_{ioniz}$ for the first ionization ($ED^+$) is a little larger than that for the primary aminium ion $CH_3$-$NH_3^+$ and the second ionization ($ED^{2+}$) contributes a further 6 ml mol$^{-1}$. The contributions per $+$ charge in the TP series increase in the order 5.8, 7.5, and 8.8 ml mol$^{-1}$, respectively, in going from the $2+$

to the $4+$ ion (Figure 7), as they do in the TT series (from 1.9 to 3.5 to 6.3 ml mol$^{-1}$). This is the effect predicted[18] when a linear array of charges is accumulated on a chain. Also, with the longest chain divalent ion derived from PEI 6, $\frac{1}{2} \bar{V}^\circ_{ioniz} = 5.0$ while the value for $ED^+$ is 5.5; hence intercharge effects are almost attenuated to zero in a chain of this length (cf. ref 24) and also to a large extent already at $z = 4$ (TP, Figure 7).

The electrostriction for various types of charge situation on the chains may also be estimated from the data of Table II using the absolute value for $\bar{V}^\circ_{H^+} = -5.7$ ml g-ion$^{-1}$.[3] (cf. ref 4). Consequently, as $z$ increases, the field and therefore the electrostriction tends to change its functional dependence on distance from $r^{-2}$ to $r^{-1}$. Since an independent value for $\Delta \bar{V}^\circ_d$ is not available, it is not possible to calculate the volumes of the cations in their fully dissociated state by an absolute approach.

In paper II, the adiabatic compressibility behavior will be reported.

(24) R. M. Fuoss and D. Edelson, *J. Amer. Chem. Soc.*, **73**, 266 (1951).

(25) B. E. Conway, *Rev. Macromol. Chem.*, in press.

# Polyion Hydration. II. Compressibility Behavior of Polyimine Salts

## by J. Lawrence and B. E. Conway*

*Department of Chemistry, University of Ottawa, Ottawa, Canada    (Received March 25, 1970)*

*Publication costs borne completely by The Journal of Physical Chemistry*

Apparent molar adiabatic compressibilities have been derived from differential measurements of ultrasonic velocity for a series of aqueous solutions of the hydrobromides of polyethylenimines. Results were obtained over a wide range of degrees of polymerization and extents of neutralization. The compressibilities of the salts at infinite dilution have been separated into their individual ionic components since these can be related to specificity of ion–solvent interactions. The change in compressibility caused by the electrostriction around the polyion has been calculated from the compressibility change occurring in the ionization process and is discussed in terms of overlap of hydration sheaths as more adjacent N atoms become ionized.

## Introduction

The apparent molar adiabatic compressibilities, $\phi_K$, of a variety of electrolytes in aqueous solutions have been reported in previous publications[1-6] and related to electrostrictive and structural hydration effects associated with the solute ion. All of these studies, however, have been confined to simple electrolytes for which the theoretical interpretation is, in principle, straightforward since the ions can be considered as isolated entities, i.e., free of a counterion atmosphere, if data are measured down to sufficiently low concentrations and the appropriate relations[1,3] extrapolated to infinite dilution. Interesting structural effects are manifested particularly with organic ions.[1,3,7]

In the present paper, precise measurements of $\phi_K$ are reported for the hydrobromides of some polyethylenimines and for the bases themselves over a wide range of polymerization, $z$, starting with $z = 1$ in order to study progressively the change in hydration on going from simple to polymeric ions. Results were also obtained at varying degrees of ionization to allow the compressibility change occurring in the ionization process to be related to changes in the fraction of ionic and nonionic parts of the molecule and to modification of the solvent structure. A method which has recently been proposed by Conway and Laliberte[7] for separating the experimental compressibilities of the salts into individual ionic components has facilitated this study, since the measured compressibilities of the salts can then be related to contributions associated with individual ion–solvent interactions as in the case of the partial g-ionic volumes.[8] Similarly, changes of these quantities with degree of ionization and polymerization can be evaluated. The $\phi_K$ data have been compared with the volume behavior for these compounds reported in paper I of this work[9] and the relationships are discussed in terms of electrostriction and solvent structure effects.

## Experimental Section

The apparent molar adiabatic compressibilities were calculated from differential measurements of ultrasonic velocity using the relationship[1]

$$\phi_K = \frac{10^3(\beta - \beta_0)}{c} + \beta_0\phi_v \quad (1)$$

where $\beta = 10^6/u^2d$, $u$ is the velocity of ultrasound in the solution, $\beta$ and $\beta_0$ are the coefficients of specific compressibility for the solution and solvent, respectively, $d$ is the density of the solution, $c$ the molar concentration, and $\phi_v$ the apparent molar volume. Ultrasonic velocities were measured by the differential interferometric method of Carstensen[10] as developed further by Conway and Verrall.[1] Improvements to the apparatus described in the latter paper have been reported by Laliberte and Conway[7] elsewhere and the modified and more sensitive apparatus was employed in the present work. The operating principles have been described previously.[1,11] A 100-cm cell was used and surrounded by a special large water thermostat controlled over its entire length to $25 \pm 0.01°$ by means of a series of stirrers and independently operated heaters.

Basically, the method compares the signal that has passed through two sections of the bath containing solvent and solution with that directly received from the acoustic signal generator, so that the resultant signal amplitude, displayed on a cathode ray oscilloscope,

(1) B. E. Conway and R. E. Verrall, *J. Phys. Chem.*, 70, 3952 (1966).

(2) F. T. Gucker, C. L. Chernick, and P. Roy-Chowdhury, *Proc. Nat. Acad. Sci. U. S.*, 55, 12 (1966).

(3) B. E. Conway and L. H. Laliberte in "Hydrogen Bonded Solvent Systems," A. Covington and P. Jones, Ed., 1968, p 139 (1968).

(4) D. S. Allam and W. H. Lee, *J. Chem. Soc.*, 6049 (1964).

(5) D. A. Allam and W. H. Lee, *J. Chem. Soc. A*, 1, 5 (1966).

(6) D. S. Allam and W. H. Lee, *ibid.*, 1, 426 (1966).

(7) B. E. Conway and L. H. Laliberte, *J. Phys. Chem.*, 74, 4116 (1970); see also *Trans. Faraday Soc.*, 66, 3032 (1970); L. H. Laliberte, see Ph.D. Thesis, University of Ottawa, 1969.

(8) B. E. Conway, R. E. Verrall, and J. E. Desnoyers, *Trans. Faraday Soc.*, 62, 2738 (1966).

(9) J. Lawrence and B. E. Conway, *J. Phys. Chem.*, 75, 2353 (1971).

(10) E. L. Carstensen, *J. Acoust. Soc. Amer.*, 26, 858 (1954).

(11) R. E. Verrall, Ph.D. Thesis, University of Ottawa, 1966.

is at a minimum when the two signals are 180° out of phase. Movement of the two transducers at a fixed distance apart, relative to the membrane separating solvent and solution, changes the number of acoustic wavelengths between them and therefore the distance $\Delta y$ which the rack has to be moved between successive signal minima; $\Delta y$ is related to the difference between the ultrasonic velocities in solvent and solution, $\Delta u$, by

$$\Delta u = \frac{u_0{}^2}{\omega \Delta y - u_0} \qquad (2)$$

where $u_0$ is the ultrasonic velocity in pure water and $\omega$ is the frequency of the signal. Accuracy of the measurements was discussed in a previous paper[1] but the improved experimental arrangement[7] enabled data to be obtained with rather higher accuracy than that in the earlier work.

The preparation, purification, and molecular weight characterization of the polymers, oligomers, and their bromide salts were described in paper I.

## Results and Discussion

Plots of the apparent adiabatic compressibility against $c^{1/2}$ for the salts, or $c$ for the neutral bases, show good linearity with positive slopes for all the compounds studied except PEI 600 $(HBr)_{0.7}$ for which the results exhibit a maximum at $c^{1/2} = 0.016$ and PEI 1000 $(HBr)_{0.7}$ for which $\phi_K$ exhibits a constant negative slope
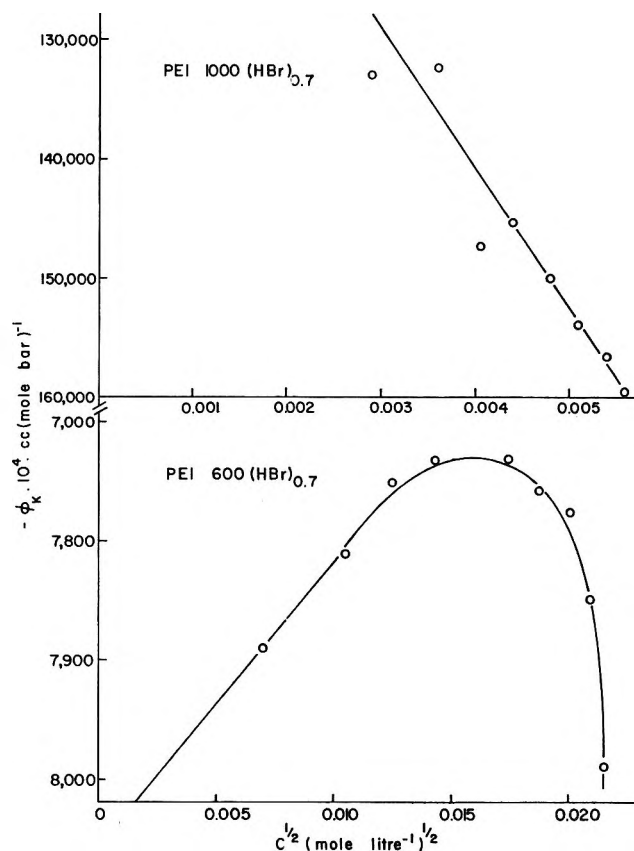


Figure 2. Plots of $-\phi_K \times 10^4$ cc (mol bar)$^{-1}$ for 70% hydrobromide salts of polyimines PEI 600 and PEI 1000 as a function of concentration in aqueous medium.

with respect to $c^{1/2}$ over the entire concentration range examined. The plots for PEI 18 $(HBr)_{0.7}$ and PEI 12 are shown in Figure 1 as typical examples of the results, while the behavior of the bromide salts of PEI 600 (which shows a maximum in $\phi_K$ at ca. 0.00025 mol l.$^{-1}$) and PEI 1000 is illustrated in Figure 2. As in the case of the data for $\phi_v$ reported in paper I, the $\phi_K$ values for all polysalts have been plotted empirically as a function of $c^{1/2}$ although, for the polyions, there is no a priori basis for the $c^{1/2}$ plot as there is for monomeric ions.

Since it has been suggested in paper I that the ions can assume a more loosely coiled configuration at ca. 0.0003 mol l.$^{-1}$, this maximum compressibility may be associated with the critical condition of overlap of the polymer coil cospheres at this concentration. Under these conditions, polymer–polymer association may increase due to gegenion sharing.[12] All the compressibility results are summarized in Table I in terms of the slopes and intercepts of the plots of $\phi_K$ against $c^{1/2}$ or $c$. As in the determination of apparent molar volumes, the hydrolysis of the neutral bases was suppressed by using 0.1 $M$ aqueous KOH as solvent instead of water for these solutions.



Figure 1. Typical plots of $-\phi_K \times 10^4$ cc (mol bar)$^{-1}$ for 70% hydrobromide salts of polyimine PEI 18 and for the polyimine base PEI 12 as a function of concentration in aqueous medium.

(12) F. T. Wall and J. W. Drennan, J. Polym. Sci., 7, 83 (1951); cf. B. E. Conway, J. Chem. Educ., 31, 477 (1954).

Table I:   Adiabatic Compressibility Data for Imine Polymers and Oligomers and Their Hydrobromide Salts:  Slopes and Intercepts of the Linear Plots of $\phi_K$ against $c^{1/2}$ or $c$ and $\phi^\circ_K$ per Monomer Unit for the Neutral Bases

| Salt | $-10^4 \times \phi^\circ_K$, cc (mol bar)$^{-1}$ | $d\phi_K/dc^{1/2}$ | Base | $-10^\circ \phi^\circ_K$, cc (mol bar)$^{-1}$ | $d\phi_K/dc$ | $-10^4\phi^\circ_K$, per monomer |
|---|---|---|---|---|---|---|
| | Salts[a] | | | Neutral bases | | |
| ED (2HBr)[b] | $49.3 \pm 0.5$ | 22.6 | ED[b] | $-0.36 \pm 0.05$ | 0.80 | $(-0.36)$ |
| DT (2HBr) | $32.1 \pm 0.5$ | 26.0 | DT | $4.86 \pm 0.05$ | 2.4 | 2.43 |
| DT (3HBr) | $74.5 \pm 0.5$ | 37.5 | TT | $11.08 \pm 0.2$ | 3.7 | 3.67 |
| TT (2HBr) | $30.3 \pm 0.5$ | 22.5 | TP | $14.6 \pm 0.2$ | 4.7 | 3.66 |
| TT (4HBr) | $78.3 \pm 0.5$ | 28.0 | PEI 6 | $48.8 \pm 0.5$ | 12.5 | 3.13 |
| TP (2HBr) | $41.1 \pm 0.5$ | 27.5 | PEI 12 | $93.5 \pm 0.5$ | 46.0 | 3.35 |
| TP (4HBr) | $88.0 \pm 0.5$ | 54.0 | PEI 18 | $135.3 \pm 1.0$ | 15.0 | 3.24 |
| PEI 6 (2HBr) | $70.5 \pm 0.5$ | 45.5 | PEI 600 | $3559 \pm 30$ | 1.28 | 3.26 |
| PEI 6 (HBr)$_{0.8}$ | $203.9 \pm 1$ | 133 | PEI 1000 | $6268 \pm 100$ | 2.5 | 3.60 |
| PEI 12 (HBr)$_{0.77}$ | $341.4 \pm 2$ | 349 | | | | |
| PEI 18 (HBr)$_{0.7}$ | $388.3 \pm 2$ | 484 | | | | |
| PEI 600 (HBr)$_{0.7}$ | $8,540 \pm 100$ | Graph not linear | | | | |
| PEI 1000 (HBr)$_{0.7}$ | $89,400 \pm 4000$ | $-1.09 \times 10^6$ | | | | |

[a] The $\phi^\circ_K$ values for the salts must be regarded only as *apparent* values owing to the difficulty of obtaining measurements of $\phi_K$ below ca. 0.01 monomol l.$^{-1}$ at low concentrations comparable with those that can be reached with the $\phi_v$ measurements.   [b] Abbreviations as defined in paper I.

The $\phi^\circ_K$ values derived by empirical extrapolation of the $\phi_K$ values as a function of $c^{1/2}$ must be regarded as apparent values (see Table I) owing to the difficulties of obtaining accurate values of $\phi_K$ below 0.01 monomol l.$^{-1}$ concentration even by the differential technique[10] (*cf.* ref 13) and on account of the persistence of appreciable nonideality of organic salt solutions down to very low concentrations.[7]   In this respect, the extrapolations of the $\phi_v$ data are more justified and reliable.   However, the sound velocity is relatively insensitive to coulombic interaction effects[13] so that a linear representation[13] of $\phi_K$ as f(c) or $c^{1/2}$ is not so unsatisfactory at these concentrations as might at first seem to be the case.

An unexpected result of the present studies is that the compressibilities of these polymeric salts ($\phi^\circ_K \doteq -25 \times 10^{-4}$ cc (monomol bar)$^{-1}$), are higher (less negative) in comparison with the values for 1:1 inorganic electrolytes such as KBr for which $\phi^\circ_K = -30.5 \times 10^{-4}$ cc (mol bar)$^{-1}$.   This result implies that the polymeric cations must be apparently more compressible than a potassium ion.  A similar effect was observed with the tetraalkylammonium cations[1] but the compressibility becomes more *negative* with increasing length of the alkyl chains.   Similar effects are apparent with the neutral polybases with increasing z (Table I).  Since the intrinsic compressibility of an ion is normally only a relatively small part of the overall apparent compressibility, the above effect was explained[1] in terms of water having limitingly different types of compressibility behavior in the hydration layers around "hydrophilic" [*e.g.*, (Me)$_3$NH$^+$, (Me)$_2$NH$_2^+$ etc.] and "hydrophobic" types of ions.  Although the polybases have progressively more negative $\phi_K$ values with increasing z, ionization causes relatively large changes to even more nega-

tive values (Table I), consistent with electrostriction as in the case of the protonated ions derived from secondary bases (*e.g.*, (Me)$_2$NH$_2^+$, ref 1, *i.e.*, with secondary structures similar to that at N atoms within the polymer chain).   For example, the change of compressibility upon ionization of interchain N atoms at $z = 4$ (Figure 6) may be estimated as $-24$ cc (g-ion bar)$^{-1}$ noting that as $z \geqslant 4$, $\Delta\phi^\circ_K$ (Figure 6) becomes independent of z, while the corresponding value for ionization of Me$_2$NH ions[1] $-19.4$ cc (g-ion bar)$^{-1}$.   In the polymer, the overall $\Delta\phi^\circ_K$ will be determined by the balance between this type of electrostriction effect and any structure promotion effect (change to a relaxationally less mobile situation in H$_2$O) in the water brought about by the un-ionized parts of the partially ionized chain.

The neutral polymer bases have, as expected, higher $\phi_K$ values due to lack of electrostriction and their small tendency (*e.g.*, in relation to R$_4$N$^+$ ions[1]) to cause structure promotion with resulting negative $\phi_K$ contributions.  This is presumably due to the hydrophilic character of the exposed –NH– centers as found previously[1] with neutral secondary bases.

Figure 3 shows $\phi_K$ for the neutral bases, extrapolated to infinite dilution, as a function of the degree of polymerization, z; logarithmic scales have been used in order to accommodate the data for $z > 14.2$.   A good linear relationship is observed which is also illustrated by the constancy of the compressibilities calculated *per monomer unit* (–C$_2$H$_4$NH–) and listed in Table I.   Figure 4 shows the compressibilities of the bases as a function of their respective apparent molar volumes, again on a

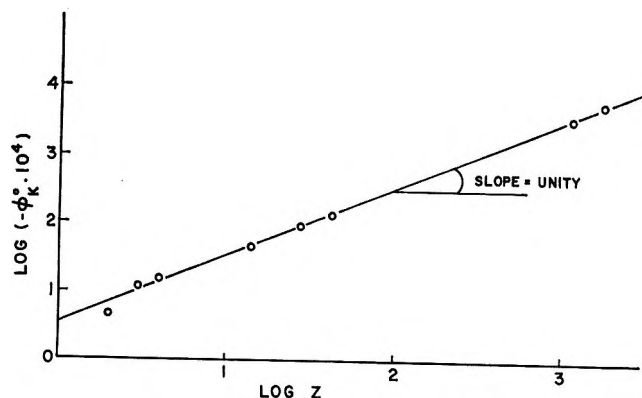(13) R. Garnsey, R. J. Moe, R. Mahoney, and T. A. Litovitz, *J. Chem. Phys.*, **50**, 5222 (1969).

Figure 3. Logarithmic plot of $\phi^\circ{}_K$ values for the neutral polyimine bases as a function of log $z$, the degree of polymerization (unit slope indicates proportionality of $\phi^\circ{}_K$ to $z$).
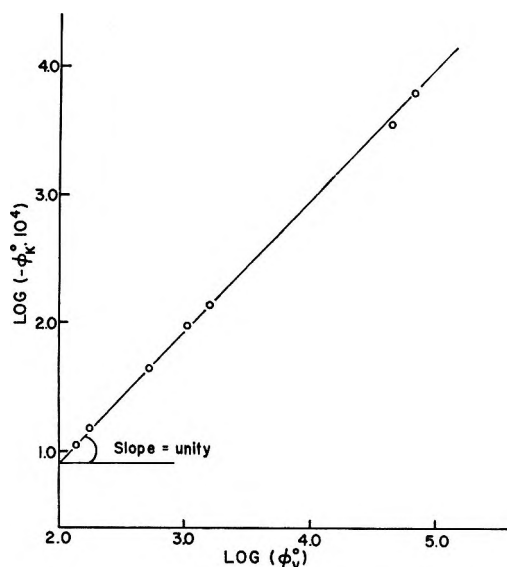


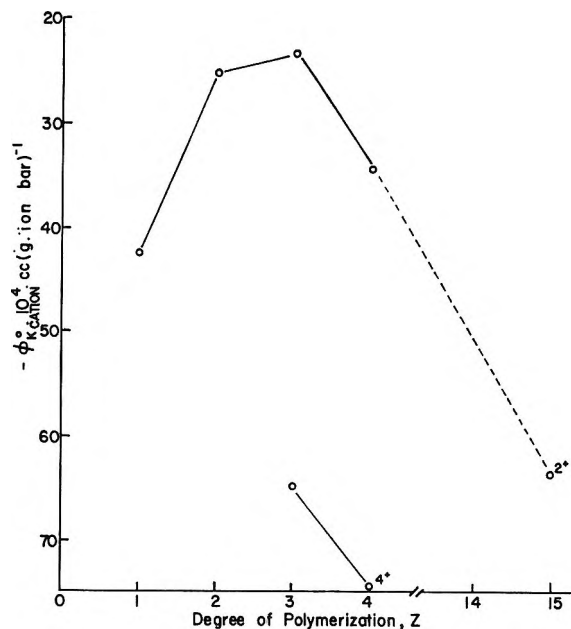Figure 4. Log–log plot for proportionality between $\phi^\circ{}_K$ and $\phi^\circ{}_V$ for the PEI bases.



Figure 5. Relation between $\phi^\circ{}_{K,cation}$, for di- and tetravalent oligomeric polyimine cations, and $z$, the degree of polymerization. Maximum compressibility occurs at $z = 3$.
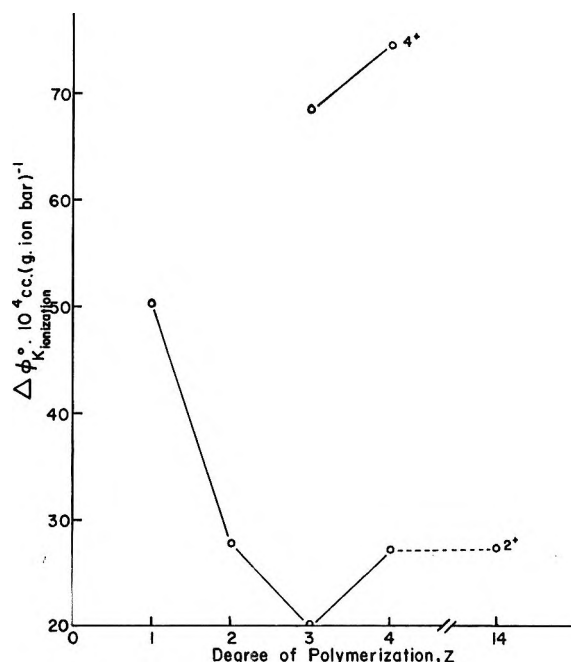


Figure. 6. Compressibility change on ionization $\Delta\phi^\circ{}_{K,ioniz}$ for di- and tetravalent cations as a function of degree of polymerization $z$.

logarithmic scale, and this linearity illustrates that the hydration of these compounds is a strictly additive effect, independent of any random coiling (or chain branching) in the higher molecular weight polymers; such behavior may be expected since the hydration of the bases arises essentially from short-range H-bonding interactions. On the other hand, the behavior is, of course, quite different with the ionized polymers (Figures 5 and 6). The higher (less negative) compressibility of DT and ED bases is due partly to the lack of correction for the compressibility contribution of one of the terminal $NH_2$ or OH groups and partly to the possibly smaller relative extents of hydrophobic hydration associated with the smaller molecules.

A value for $\phi^\circ{}_K$ of the iodide ion has been derived by Conway and Laliberte,[7] who found that $\phi^\circ{}_K$ values for four substituted $N$-methylpyridinium iodides and four tetraalkylammonium iodides were a linear function of

molecular weight so that the data could be extrapolated to zero molecular weight (ref 8). They obtained a value for $\phi^\circ{}_{KI^-}$ of $+6.9 \times 10^{-4}$ cc (g-ion bar)$^{-1}$ and this, combined with the known difference $\Delta\phi^\circ{}_{K(Br^- I^-)}$, leads to $\phi^\circ{}_{KBr^-} = -3.4 \times 10^{-4}$ (g-ion bar)$^{-1}$. The $\phi^\circ{}_K$ for the polyethylenimine cations were then estimated from the salt compressibilities assuming additivity of the ionic contributions. The plot of $\phi^\circ{}_{K_{cation}}$ against $z$

at constant cation charge in Figure 5 shows a distinct maximum at $z = 3$ which is consistent with the minimum volume of ionization observed (paper I) at this chain length because once interaction of the hydration sheaths between neighboring $N^+$ centers occurs, a greater and more cylindrical region of solvation about the oligomeric ion tends to arise and lead to an overall decrease in compressibility as is evident with the $4+$ ions ($z = 3$ or 4) referred to in Figure 5. The overlap of hydration sheaths about adjacent charged centers evidently prevents the compressibility of the cations corresponding to the partially ionized polybases from being estimated from a simple additivity expression of the type

$$\phi_{K_{cation}} = \alpha\phi_{K^+} + (1 - \alpha)\phi_{K_{base}} \qquad (3)$$

involving the compressibility of the corresponding neutral base, the compressibility $\phi_{K^+}$ of the fully ionized cation, and $\alpha$ the degree of ionization. Some chain branching, corresponding to the presence of tertiary $N^+$ centers, would enhance this effect.

The compressibility changes, $\Delta\phi^\circ_{K,ioniz}$, occurring in the ionization process were calculated by a method analogous to that used for the evaluation of $\Delta\bar{V}^\circ_{ioniz}$, i.e., by considering the change in compressibility associated with the reaction

$$(BH_n)^{n+}nBr^- \longrightarrow B + nHBr$$
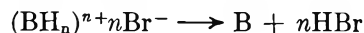
that is, $\Delta\phi^\circ_{K,ioniz}$ can be expressed as

$$\Delta\phi^\circ_{K,ioniz} = \phi^\circ_{K_{base}} \pm n\phi^\circ_{KHBr} - \phi^\circ_{K(BH_r)^{n+}nBr^-} \qquad (4)$$

The adiabatic compressibility of HBr was estimated from the corresponding isothermal compressibility assuming that the latter is, in the usual way, 7–10% more negative than the former.[14] The resulting values of $\Delta\phi^\circ_{K,ioniz}$, plotted in Figure 6 as a function of $z$, show a sharp minimum at $z = 3$ which is consistent with the maximum in Figure 5 at the same $z$ since the compressibility of the neutral bases is directly proportional to $z$.

The relation between $\Delta\phi^\circ_{K,ioniz}$ and $\Delta\bar{V}^\circ_{ioniz}$ as plotted previously[1] for ionization of methylamine bases and more recently by Lown, Thirsk, and Wynne-Jones[15] for ionization of weak acids, bases, and water is shown in Figure 7 and provides a basis for the close relation often assumed and demonstrated theoretically[16] between the changes of volume and compressibility associated with electrostriction.[17] The relation between the field and electrostriction at polyions is considered theoretically in the Appendix.

*Acknowledgments.* Grateful acknowledgment is made to the National Research Council, Canada, for support in this work. One of us (J. L.) acknowledges the award of a postdoctoral Fellowship supported on N. R. C. funds. The senior author wishes to make acknowledgment to the Association of Commonwealth Universities for his nomination as Commonwealth
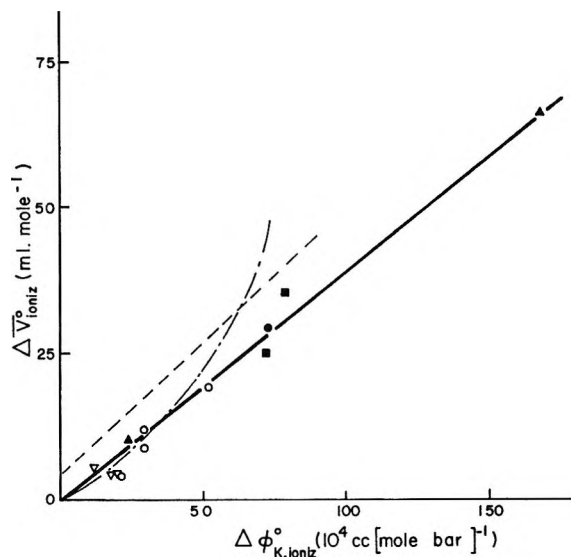


Figure 7. Relation between $\Delta\phi^\circ_{K,ioniz}$ and $\Delta\bar{V}^\circ_{ioniz}$ for ionization of oligomeric and polymeric imines. ⊙, divalent ions; ●, trivalent ions; □, tetravalent ions; ∇, $Me_3H_{n-3}NH^+$ ions; ▲, PEI 6, $HBr_{0.8}$; - - -, line of ref 15 for acids and $H_2O$; ·——·——·, intermediate field, theoretical limiting relation from ref 16 calculated per mole of $H_2O$. (For unknown reasons, the line for data of ref 15 do not pass through the origin. This may be due to structural contributions in $\Delta\bar{V}^\circ$ not exhibited in $\Delta\phi^\circ_K$; *cf.* ref 7.)

Visiting Professor at the Universities of Southampton and Newcastle, England, where this work was completed.

## Appendix

*Field and Electrostriction at a Linear Array of Charges.* For a linear array of charges separated by a distance $2\lambda$ the field vector can be calculated at a distance $r$ from the chain. For the case of two charges on a chain (or at the midpoint of an array of charges), the field at points along a line normal to the chain midway between the charges will also be directed normally (and radially) to the chain and will have the magnitude

$$E = 2er/(r^2 + \lambda^2)^{3/2}\epsilon \qquad (A-1)$$

In the general case of an array of like charges, the net field at a point midway along the chain will be

$$E = \sum_0^n 2er/[r^2 + (2n - 1)^2\lambda^2]^{3/2}\epsilon \qquad (A-2)$$

where $(2n - 1)\lambda$ is the distance of the $n$th charge from the midpoint of the chain. At other points, the field vector will not be normal to the chain but can be evaluated numerically by trigonometric procedures.

(14) B. B. Owen and J. S. Simons, *J. Phys. Chem.*, **61**, 479 (1957).

(15) D. A. Lown, H. R. Thirsk, and Lord Wynne-Jones, *Trans. Faraday Soc.*, **64**, 2073 (1969).

(16) J. E. Desnoyers, R. E. Verrall, and B. E. Conway, *J. Chem. Phys.*, **43**, 243 (1965).

(17) B. E. Conway, *Rev. Macromol. Chem.*, in press.

For the ion with two charges at various separations (cf. Figure 5 and the case of bolaform electrolytes) it is of interest to evaluate the variation of $E$ with $\lambda$ and $r$.

Differentiating (A-1) gives

$$dE = (2e(\lambda^2 - 2r^2)/\epsilon(r^2 + \lambda^2)^{2.5})\, dr -$$

$$\frac{6er\lambda\, d\lambda}{(r^2 + \lambda^2)^{2.5}\epsilon} \quad \text{(A-3)}$$

so that for the variation of field radially

$$(\partial E/\partial r)_\lambda = 2e(\lambda^2 - 2r^2)/(r^2 + \lambda^2)^{2.5}\epsilon \quad \text{(A-4)}$$

and for the dependence on separation $\lambda$

$$(\partial E/\partial \lambda)_r = -6er\lambda/(r^2 + \lambda^2)^{2.5}\epsilon \quad \text{(A-5)}$$

The field at $r$ hence continuously diminishes as $\lambda$ increases as may be expected; however, it is of interest to note that the radial variation of field for a given charge separation evidently exhibits a maximum at $\lambda = \sqrt{2}\, r$ as may be seen from eq A-4. At this point

$$E_\mathrm{m} = 4e/3^{1.5}\lambda^2\epsilon \quad \text{(A-6)}$$

is the maximum field; alternatively, in terms of $r$

$$E_\mathrm{m} = 2e/3^{1.5}r^2\epsilon \quad \text{(A-7)}$$

Introduction of dielectric saturation effects (cf. ref 18) increases the field at short ranges but the general trend of the relations shown above will be maintained. Detailed numerical calculations for the rigid polyion model have been given previously[18] taking into account dielectric saturation effects.

In terms of the integral electrostriction caused by the charges, either the low-field or high-field cases of the previously published equations[16] may be used (they have the same form but different constants). Thus, in a cylindrical element of solution, length $\Delta l$, about the charged rod the relative electrostriction $v/v_0$ is given by

$$\frac{v}{v_0} = \frac{\displaystyle\int_0^r 2\pi r\Delta l\, \rho_0/\rho_r\, dr}{\displaystyle\int_0^r 2\pi r\Delta l\, dr} \quad \text{(A-8)}$$

where $\rho_r/\rho_0$ is the density ratio function[16]

$$\frac{\rho_r}{\rho_0} = \left[\frac{A(1 - A)\epsilon_0 E_r^2}{8\pi\beta D} + 1\right]^{D/1 - A} \quad \text{(A-9)}$$

dependent on field $E_r$ at $r$. A numerical solution is possible using $E_r$ given by eq A-1 and the high- or low-field forms of eq A-9. The constants $A$ and $D$ define the variation of compressibility and dielectric constant, respectively, with pressure[16] and $\epsilon_0$ is the static dielectric constant.

(18) B. E. Conway, J. E. Desnoyers, and A. C. Smith, *Phil. Trans. Roy. Soc. London, Ser. A*, 256, 389 (1964).

# Heats of Dilution and the Thermodynamics of Dissociation

# of Uranyl and Vanadyl Sulfates

## by Allen R. Bailey and John W. Larson*

*Department of Chemistry, Marshall University, Huntington, West Virginia  25701*    (*Received December 10, 1970*)

*Publication costs borne completely by The Journal of Physical Chemistry*

Heats of dilution of aqueous solutions of uranyl and vanadyl sulfates have been measured.  These data have been used to calculate the heats of dissociation of their respective ion pairs.  For the reaction $UO_2SO_4(aq) \rightleftharpoons UO_2{}^{2+}(aq) + SO_4{}^{2-}(aq)$, the results are $\Delta G° = 3.71$ kcal/mol, $\Delta H° = -4.98$ kcal/mol, and $\Delta S° = -29.1$ gibbs/mol.  The corresponding results for $VOSO_4$ are $\Delta G° = 3.38$ kcal/mol, $\Delta H° = -4.12$ kcal/mol, and $\Delta S° = -25.2$ gibbs/mol.  The standard heat of solution of $UO_2(NO_3)_2 \cdot 6H_2O(c)$ has been determined and the $\bar{S}_2°$ of the $UO_2{}^{2+}(aq)$ ion calculated to be $-23.1$ gibbs/mol.  The partial molal entropies of the $UO_2SO_4$ and $VOSO_4$ ion pairs are calculated from these results and explained in terms of the primary hydration of these ion pairs.

The theory of ion-pair dissociation has been of considerable importance in providing an adequate theoretical description of electrolyte solutions.  There are two major factors that affect the thermodynamics of ion-pair dissociation: the long-range electrostatic forces between the ions and the specific solvation of the solute species.  We have undertaken the present investigation of the thermodynamics of dissociation of the uranyl sulfate and vanadyl sulfate ion pairs because of the unusual structure of the $UO_2{}^{2+}$ and $VO^{2+}$ ions.  These ions have a highly nonspherical distribution of charge and therefore might provide useful information on the limitations of the electrostatic theory of ion-pair dissociation.  In addition, the oxy groups of these cations would restrict the primary hydration of the metal ion.  This study might, therefore, also give some information on the effect of specific solvation on the thermodynamics of ion-pair dissociation.

Previously measured heat of dilution data for six divalent metal sulfates do not approach the Debye–Hückel limiting law even at concentrations as low as $10^{-4}$ $m$.[1]  This has recently been shown to be the result of ion-pair formation[2] and from these data calculations of the enthalpy and entropy of dissociation of these divalent metal sulfates were made.  In order to provide data that can be used to calculate enthalpies and entropies of dissociation of the uranyl and vanadyl sulfates, heats of dilution of their aqueous solutions have been measured.  No such data are presently available in the literature.

## Experimental Section

The calorimeter used in the present work has been described previously.[3]  Several modifications were made for the present study.  A 100-l. water bath has been used instead of the aluminum block bath.  The thermometer circuit consisted of two 1000-ohm thermistors obtained from the Yellow Springs Instrument Co. connected in two of the arms of a transposed Maier Bridge circuit similar to a previously described circuit.[4]  A Leeds and Northrup K-4 potentiometer and D-C null detector were used to measure the bridge potentials.  All of the calorimetric data reported here were obtained with 300 ml of water in the dewar at $25.00 \pm 0.1°$.

Diuranyl sulfate heptahydrate was obtained from the Poly Research Corp. with a minimum specified purity of $99.5\%$.  This compound was analyzed for $UO_2{}^{2+}$ by precipitation with $NH_3$, followed by ignition to $U_3O_8$; for $SO_4{}^{2-}$ by precipitation as $BaSO_4$; and for $H_2O$ by heating to $300°$.  The determined percentages were: $UO_2$, $62.2\%$; $SO_4$, $22.8\%$; and $H_2O$, $14.9\%$.  The calculated percentages based on the formula $UO_2SO_4 \cdot {}^7/_2H_2O$ were $62.9$, $22.4$, and $14.7\%$, respectively.

Certified ACS uranyl nitrate hexahydrate was obtained from the Fisher Scientific Co.  This compound was allowed to come to equilibrium in a vacuum desiccator with a $40\%$ sulfuric acid solution to ensure a hydration of six.[5]  This compound was analyzed for $UO_2{}^{2+}$.  The determined per cent $UO_2$ was found to be $53.6\%$, compared with the calculated $53.8\%$.

Purified vanadyl sulfate trihydrate was obtained from the Fisher Scientific Co.  Preliminary analysis for

(1) E. Lange in "The Structure of Electrolyte Solutions," W. J. Hamer, Ed., Wiley, New York, N. Y., 1959; E. Lange and J. Monheim, *Z. Phys. Chem.*, **150A**, 349 (1930); E. Lange and H. Streeck, *ibid.*, **157A**, 1 (1931); E. Lange and W. Miederer, *Z. Elektrochem.*, **60**, 34 (1956); E. Lange, J. Monheim, and A. L. Robinson, *J. Amer. Chem. Soc.*, **55**, 4733 (1933).

(2) J. W. Larson, *J. Phys. Chem.*, **74**, 3392 (1970).

(3) R. N. Goldberg and L. G. Hepler, *ibid.*, **72**, 4654 (1968).

(4) W. F. O'Hara, C. H. Wu, and L. G. Hepler, *J. Chem. Educ.*, **38**, 512 (1961).

(5) L. C. Coulter, K. S. Pitzer, and W. M. Latimer, *J. Amer. Chem. Soc.*, **62**, 2845 (1940).

$VO^{2+}$ and $SO_4^{2-}$ indicated an excess of $SO_4^{2-}$ of approximately 30%. This crude material was therefore washed between five and eight times with 95% ethanol, followed by washing several times with diethyl ether. The resulting compound was then dried in a vacuum desiccator. Two samples were prepared in this way. Analysis for $SO_4^{2-}$ by precipitation as $BaSO_4$ and for $VO^{2+}$ by titrating with standardized $KMnO_4$ gave a molar ratio of $SO_4^{2-}$ to $VO^{2+}$ of 0.996 and 1.002 for samples I and II, respectively. These two samples gave identical thermochemical results. The hydration number calculated from the average of all of the analyses was $2.98 \pm 0.01$.

Concentrated aqueous solutions (0.4 to 0.08 $m$) of $UO_2SO_4$ and $VOSO_4$ were made up by weight in glass bulbs of 4 to 15 ml total volume. Sample entry was effected by breaking the bulb.

## Results and Calculations

*Enthalpy of Dissociation of $UO_2SO_4$.* The results of our measured heats of solution of concentrated aqueous $UO_2SO_4$ solutions into a 0.00018 $m$ aqueous $H_2SO_4$ solution are given in Table I. The dilute acid solutions were used instead of pure water in order to suppress the hydrolysis of the $UO_2^{2+}$(aq) ion. Lange's measured heats of dilution of $UO_2(NO_3)_2$ solutions indicate that an acid of this concentration effectively prevents any appreciable hydrolysis.[6] The measured apparent molal heat of dilution, $\Delta\phi_H$, between the initial and final concentration is arrived at by dividing the measured heat (2 to 4.5 cal) by the number of moles of $UO_2SO_4$ in the sample.

**Table I:** Heats of Dilution of $UO_2SO_4$

| Initial molality | Final molality | $\Delta\phi_H$, kcal/mol | $-\Delta H,^a$ kcal/mol |
|---|---|---|---|
| 0.240 | 0.00618 | $1.62_5$ | 4.92 |
| 0.150 | 0.00337 | $1.78_6$ | 4.87 |
| 0.262 | 0.00632 | $1.68_8$ | 5.13 |
| 0.0652 | 0.00284 | $1.61_4$ | 4.99 |

$^a$ Average $\Delta H_1 = -4.98 \pm 0.10$ kcal/mol.

The enthalpy of reaction 1, $\Delta H_1^\circ$, may be calculated

$$UO_2SO_4(\text{ion pair, aq}) \rightleftharpoons$$

$$UO_2^{2+}(\text{aq}) + SO_4^{2-}(\text{aq}) \quad (1)$$
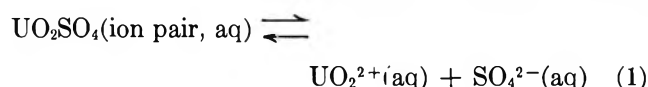
from these results by a method similar to that described previously.[2] The equilibrium constant for reaction 1 is taken from the literature as $K_1 = 0.00191$.[7] The equilibrium expression for reaction 1 is given by eq 2

$$K = (\gamma_\pm^{2-2})^2 m_{SO_4^{2-}} m_{UO_2^{2+}} / m_{UO_2SO_4} \quad (2)$$

where $\gamma_\pm^{2-2}$ is the mean activity coefficient of the

dissociated $UO_2SO_4$ and the activity coefficient of $UO_2SO_4$ is assumed to be one.

The molalities of the aqueous solutes and the total ionic strength, $I$, of the solution are given by eq 3 and 4, where $m$ is the total molality of $UO_2SO_4$. The value

$$m_{UO_2^{2+}} = \alpha m, \; m_{SO_4^{2-}} = \alpha m + m_{H_2SO_4},$$

$$m_{UO_2SO_4} = (1 - \alpha)m \quad (3)$$

$$I = 4\alpha m + 3m_{H_2SO_4} \quad (4)$$

for $\gamma_\pm^{2-2}$ is estimated using an extended Debye-Hückel theory, eq 5.[8] Using eq 2–5, $\alpha$ can be calculated at any concentration of $UO_2SO_4$ by a method of

$$\log \gamma_\pm = -0.5115 z_1 z_2 \sqrt{I}/$$

$$(I + 0.3291a\sqrt{I}) + 0.1z_1z_2 I \quad (5)$$

successive approximations.

The apparent molal heat of dilution is assumed to be made up of two parts, the heat of dilution of the dissociation $UO_2SO_4$, $\Delta H_d^{\circ 2-2}$, and the heat of dissociation of the $UO_2SO_4$ ion pairs.[9,10] $\Delta H_1$ then can be calculated using eq 6[2] if $\Delta H_d$ is estimated using eq 7

$$\Delta H_1^\circ = \frac{\Delta\phi_H}{\Delta(1 - \alpha)} - \frac{\Delta H_d^{2-2}}{\Delta(1 - \alpha)} \quad (6)$$

$$H_d = 0.477\left(\frac{\nu_1 z_1^2 + \nu_2 z_1^2}{\nu}\right)\sqrt{I}/$$

$$(1 + 0.3291a\sqrt{I}) \text{ kcal/mol}^{1/2} \quad (7)$$

Taking $a = 4$ Å, the calculated values of $\Delta H_1^\circ$ using the above equations are reported in Table I. The validity of eq 5 and 7 in these calculations rests on the constant value of $\Delta H_1^\circ$ calculated over an extensive concentration range. Although the concentration range covered in this work is rather limited, the values for the enthalpies of dissociation of six divalent metal sulfates calculated using these equations remained unchanged over the concentration range between $10^{-4}$ $m$ and 0.4 $m$.[2] It is assumed here that $UO_2SO_4$ behaves in a similar manner.

As a check on the validity of the assumptions made in our calculations, our choice of $K_1$, and our experimental procedure, $\Delta H_1^\circ$ was determined by a different path also. Heats of solution of $UO_2(NO_3)_2 \cdot 6H_2O$ were made into a solution of 0.0004 $m$ HNO$_3$ (reaction 8). These values are reported in Table II. Values of $\Delta H_8^\circ$ were

(6) E. Lange and W. Miederer, *Z. Elektrochem.*, **61**, 407 (1957).

(7) L. G. Sillen and A. E. Martell, "Stability Constants of Metal-ion Complexes," Special Publication No. 17, The Chemical Society, London, 1964.

(8) R. A. Robinson and R. H. Stokes, "Electrolyte Solutions," 2nd ed, revised, Butterworths, London, 1965.

(9) H. P. Hopkins, Jr., and C. A. Wulff, *J. Phys. Chem.*, **69**, 6, 9 (1965).
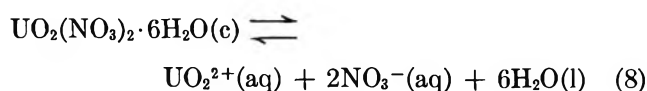
(10) H. P. Hopkins, Jr., C.-H. Wu, and L. G. Hepler, *ibid.*, **69**, 2244 (1965).

**Table II:** Heats of Solution of $UO_2(NO_3)_2 \cdot 6H_2O(c)$ in 0.0004 $m$ $HNO_3$

| Final molality | $\Delta H_8$, kcal/mol | $H_8°,$[a] kcal/mol |
|---|---|---|
| 0.0079 | 4.73 | 4.66 |
| 0.0075 | 4.75 | 4.66 |
| 0.0066 | 4.78 | 4.71 |
| 0.0043 | 4.72 | 4.65 |
| 0.0031 | 4.72 | 4.65 |

[a] Average $H_8° = 4.67 \pm 0.03$ kcal/mol.

$$UO_2(NO_3)_2 \cdot 6H_2O(c) \rightleftharpoons$$

$$UO_2{}^{2+}(aq) + 2NO_3{}^-(aq) + 6H_2O(l) \quad (8)$$

obtained from the measured $\Delta H_8$ by using the heats of dilution of $Ba(NO_3)_2$.[11]

Heats of solution were also determined for this compound in a 0.00018 $m$ $H_2SO_4$ solution with various amounts of $K_2SO_4$. This reaction may be written

$$m_1(UO_2(NO_3)_2 \cdot 6H_2O(c) + m_2K_2SO_4(aq') =$$

$$\alpha m_1 UO_2{}^{2+}(aq') + m_2 - (1-\alpha)m_1SO_4{}^{2-}(aq) +$$

$$(1-\alpha)m_1UO_2SO_4(aq') + 2m_1NO_3{}^-(aq') +$$

$$2m_2K^+(aq') \quad (9)$$
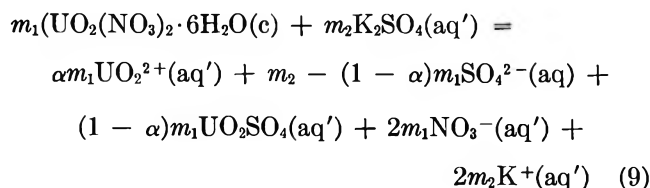
The molalities of the aqueous species and the total ionic strength of the solution are given by eq 10 and 11.

$$m_{UO_2{}^{2+}} = \alpha m_1, \quad m_{SO_4{}^{2-}} = m_2 - (1-\alpha)m_1,$$

$$m_{UO_2SO_4} = (1-\alpha)m_1 \quad (10)$$

$$I = 4\alpha m_1 + 3(m_2 - m_1) + 2m_1 \quad (11)$$

The heat given off during reaction 9, $q_9$, can be expressed as

$$q_9 = m_1\Delta H_8° + (1-\alpha)m_1\Delta H_1° -$$

$$m_2H_d{}^{21} + \alpha m_1 H_d{}^{22} + (m_2 - m_1) \times$$

$$H_d{}^{21} + 2m_1H_d{}^{11} \quad (12)$$

Taking the heat per mole of $UO_2(NO_3)_2$ as $\Delta H_9 = q_9/n$ and rearranging eq 12

$$\Delta H_1° = \frac{1}{1-\alpha}(\Delta H_9 - \Delta H_8° -$$

$$2H_d{}^{11} + H_d{}^{12} - \alpha H_d{}^{22}) \quad (13)$$

The $\Delta H_1°$ values arrived at by this path are reported in Table III. There is good agreement between this value and the value obtained from the heat of dilution measurements, even though it depends in a very different way on $K_1$ and $\alpha$.

*Enthalpy of Dissociation of $VOSO_4$.* Heat of dilution measurements have been made for $VOSO_4$ solutions.

**Table III:** Heats of Solution of $UO_2(NO_3)_2 \cdot 6H_2O$ in Aqueous $K_2SO_4$

| $m_1 \times 10^3$ | $m_2 \times 10^2$ | $\Delta H_9$, kcal/mol | $-\Delta H_1°,$[a] kcal/mol |
|---|---|---|---|
| 5.15 | 1.18 | 8.94 | 5.03 |
| 5.23 | 2.07 | 9.14 | 4.96 |
| 6.18 | 1.50 | 8.94 | 4.88 |
| 8.42 | 1.26 | 8.95 | 5.00 |

[a] Average $\Delta H_1° = -4.97 \pm 0.07$ kcal/mol.

The enthalpy of reaction 14, $\Delta H_{14}$[4], has been arrived at in the same way as for $UO_2SO_4$. $K_{14}$ is taken as

$$VOSO_4(\text{ion pair, aq}) \rightleftharpoons$$

$$VO^{2+}(aq) + SO_4{}^{2-}(aq) \quad (14)$$
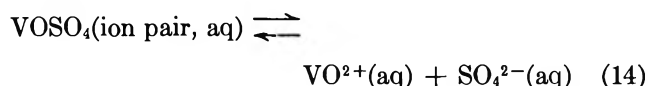
0.0033.[12] These results are reported in Table IV.

**Table IV:** Heats of Dilution of $VOSO_4$

| Initial molality | Final molality | $\Delta\phi_h$, kcal/mol | $\Delta H_{14}°,$[a] kcal/mol |
|---|---|---|---|
| 0.315 | 0.00580 | 1.643 | 4.05 |
| 0.275 | 0.00408 | 1.677 | 4.11 |
| 0.273 | 0.00423 | 1.743 | 4.11 |
| 0.269 | 0.00475 | 1.624 | 3.96 |
| 0.163 | 0.00455 | 1.537 | 4.26 |
| 0.158 | 0.00309 | 1.730 | 4.27 |

[a] Average $\Delta H_{14}° = -4.12 \pm 0.12$ kcal/mol.

*Entropy of $UO_2{}^{2+}(aq)$.* The entropy of the $UO_2{}^{2+}$-(aq) ion is calculated here by a method identical with that used by Coulter, Pitzer, and Latimer.[5] Using data from a more extensive study of the activity of aqueous $UO_2(NO_3)_2$ solutions[8] and the solubility of $UO_2(NO_3)_2 \cdot 6H_2O(c)$ in water at 25°,[13] we calculate a free energy change for reaction 8 of 3.20 kcal/mol. This value in combination with the value of $\Delta H_8°$ determined here gives $\Delta S_8° = 26.4$ gibbs/mol. The value of $\Delta H_8°$ obtained in this work is 0.58 kcal/mol less than that determined by Coulter, Pitzer, and Latimer[5] from the heat of solution of $UO_2(NO_3)_2 \cdot 6H_2O(c)$ in pure water. To ensure that the difference between these determinations was due primarily to the hydrolysis of $UO_2{}^{2+}$ and not sample differences, we have made several determinations of the heat of solution of this compound in pure water. Although very concentration dependent, the heats of solution determined in this way are higher than those reported in Table II by 0.3 to

(11) H. S. Harned and B. B. Owen, "The Physical Chemistry of Electrolytic Solutions," Reinhold, New York, N. Y., 1958.

(12) H. Strehlow and H. Wendt, *Inorg. Chem.*, 2, 6 (1963).

(13) A. Seidell, "Solubilities of Inorganic and Metal Organic Compounds," 3rd ed, D. Van Nostrand, New York, N. Y., 1940.

0.7 kcal/mol. $\Delta S_8°$ is then combined with the entropies of $H_2O(l)$,[14] $NO_3^-(aq)$,[14] and $UO_2(NO_3)_2 \cdot 6H_2O$-(c)[5] to give the partial molal entropy of $UO_2^{2+}(aq)$, $\bar{S}_2° = -23.1$ gibbs/mol. This value is 6 gibbs/mol more negative than the value arrived at by Coulter, Pitzer, and Latimer.[5] It is in good agreement with the average value of $-22.5$ gibbs/mol estimated by Brand and Cobble.[15]

*Entropies of the $UO_2SO_4$ and $VOSO_4$ Ion Pairs.* The values for $K_1$ and $\Delta H_1°$ have been used to calculate the values of $\Delta G_1°$ and $\Delta S_1°$ reported in Table V. These may be compared with the values $\Delta G_1° = 3.71$ kcal/mol, $\Delta H_1° = -2.35$ to $-5.19$ kcal/mol, and $\Delta S_1° = -20.4$ to $-29.9$ gibbs/mol arrived at from the temperature dependence of solubility of $Ag_2SO_4$ in $UO_2SO_4$ solutions[16] and the values $\Delta G_1° = 4.30$ kcal/mol, $\Delta H_1° = -5.10 \pm 0.43$ kcal/mol, and $\Delta S_1 = -31$ gibbs/mol from a temperature-dependent study of $K_1$ by Donnan membrane equilibrium.[17] Values for the thermodynamics of dissociation of $VOSO_4$ are also given in Table V. No previous measurements have been made on the $\Delta S°$ and $\Delta H°$ for this compound.

**Table V:** Thermodynamics of Dissociation of $UO_2SO_4$ and $VOSO_4$

| | $\Delta G°$, kcal/ mol | $\Delta H°$, kcal/ mol | $\Delta S°$, gibbs/ mol |
|---|---|---|---|
| $UO_2SO_4$ | 3.71 | $-4.98$ | $-29.1$ |
| $VOSO_4$ | 3.38 | $-4.12$ | $-25.2$ |
| Average values for six metal sulfates[a] | 3.16 | $-1.58$ | $-15.9$ |

[a] Reference 2.

$\Delta S_1°$ is combined with the entropies of $UO_2^{2+}(aq)$ and $SO_4^{2-}(aq)$ to obtain a partial molal entropy for $UO_2SO_4$(ion pair, aq), $\bar{S}_2° = 10.8$ gibbs/mol. $\Delta S_{14}°$ is combined with the entropies of $VO^{2+}(aq)$[18] and $SO_4^{2-}$-(aq)[14] to give $\bar{S}_2^0 = -2.0$ gibbs/mol for $VOSO_4$ (ion pair, aq).

## Discussion

The thermodynamics of dissociation of the sulfates of the oxy cations reported in Table III are apparently different from that for divalent metal sulfates for which data are available. Both the enthalpy and entropy of dissociation of the oxy cation sulfates are much more negative than the corresponding functions for divalent metal sulfates, but because these make opposite contributions to the free energy, this function is only slightly different. Such "compensation" is characteristic of reactions greatly affected by solute–solvent[19–21] interactions.

Electrostatic theories, that do not take into account the local charge distribution on the cations, do not pro-

vide an adequate description of the thermodynamics of the $UO_2SO_4$ and $VOSO_4$ ion pairs. For example, Fuoss's theory, that accounted well for the relative values of $\Delta G°$ and $\Delta S°$ of dissociation of divalent metal sulfates,[22] would require that the $UO_2SO_4$ ion pair had a distance of closest approach of 3.5 Å to account for $\Delta G°$, while a distance of 2 Å would be required to account for $\Delta S°$. Qualitatively, the high oxidation state of the metals in the oxy cations would result in a highly positive localized charge on the metal atom that would result in a higher value of $\Delta G°$. Such a charge distribution would also be expected to be accompanied by greater solvent orientation on dissociation and thus a more negative $\Delta S°$.

The partial molal entropies of the ion pairs are of particular interest with respect to solute–solvent interactions. Because these solutes are uncharged, the differences in their values would be expected to result mainly from differences in the primary solvation of these solutes. Assuming that the oxy groups block possible hydration sites of the octahedral coordination of the metal atom, the maximum cation hydration of $UO_2^{2+}$ ion in the sulfate ion pair is 4 and that of the $VO^{2+}$ ion in the sulfate ion pair is 5. The partial molal entropy of the $UO_2SO_4$ ion pair should be equal to or greater than the entropies of the $CaSO_4$ and $CdSO_4$ ion pairs that have previously been assumed to have cation hydration of 4. The data given in Table VI[23,24] clearly confirm this expectation. The significantly larger value of the $\bar{S}_2°$ of the $UO_2$ ion pair compared with the Ca and Cd ion pair indicates that additional water of hydration has been lost by the U atom on forming the sulfate ion pair and thus exists in solution as a mixture of contact and solvent-separated ion pairs. This conclusion is consistent with the fact that $UO_2SO_4$ forms only crystalline hydrates with less than four waters of hydration and that the visible spectrum of $UO_2^{2+}$ is affected by the addition of $SO_4^{2-}$.[25] Both of these results would indicate that at least some of the

(14) D. D. Wagman, W. H. Evans, V. B. Parker, I. Halow, S. M. Bailey, and R. H. Schuum, National Bureau of Standards Technical Note 270-3, U. S. Government Printing Office, Washington, D. C., 1968.

(15) J. R. Brand and J. W. Cobble, *Inorg. Chem.*, 9, 912 (1970).

(16) M. H. Lietzke and R. W. Stroughton, *J. Phys. Chem.*, 64, 816 (1960).

(17) R. M. Wallace, *ibid.*, 71, 1271 (1967).

(18) G. L. Bertrand, G. W. Stapelton, C. A. Wulff, and L. G. Hepler, *Inorg. Chem.*, 5, 1283 (1966).

(19) J. E. Prue, *J. Chem. Educ.*, 46, 12 (1969).

(20) M. G. Evans and M. Polanyi, *Trans. Faraday Soc.*, 32, 1333 (1936).

(21) L. G. Hepler, *J. Amer. Chem. Soc.*, 85, 3089 (1963).

(22) R. M. Fuoss, *ibid.*, 80, 5059 (1958).

(23) J. W. Larson, P. Cerutti, H. K. Garber, and L. G. Hepler, *J. Phys. Chem.*, 72, 2902 (1968).

(24) W. M. Latimer, "Oxidation Potentials," 2nd ed, Prentice-Hall, Englewood Cliffs, N. J., 1952.

(25) E. S. Davies and C. B. Monk, *Trans. Faraday Soc.*, 53, 442 (1957).

**Table VI:** The Entropies and Microscopic Structure of Some Sulfate Ion Pairs

| Ion pair | $\bar{S}_2°$ [$M^{2+}$(aq)], gibbs/mol | $\bar{S}_2°$ (ion pair), gibbs/mol | Predominant cation hydration number | Predominant type of ion pair |
|---|---|---|---|---|
| $UO_2SO_4$ | $-23.1$ | $10.8$ | 3 and 4 | Mixed |
| $CaSO_4$ | $-13.2^a$ | $7.2^b$ | 4 | Contact |
| $CdSO_4$ | $-17.4^c$ | $5.2^b$ | 4 | Contact |
| $VOSO_4$ | $-32^d$ | $-2$ | 5 | Solvent separated |
| $CuSO_4$ | $-23.6^c$ | $-2.2$ | 5 | Contact$^e$ |
| $ZnSO_4$ | $-26.9^c$ | $-6.9^b$ | 6 | Solvent separated |
| $MgSO_4$ | $-28.2^a$ | $-8.7^b$ | 6 | Solvent srparated |
| $NiSO_4$ | $-31.6^c$ | $-11.1^b$ | 6 | Solvent separated |

$^a$ Reference 24.   $^b$ Reference 2.   $^c$ Reference 23.   $^d$ Reference 18.   $^e$ $SO_4$ ion acting as a monodentate ligand.

$UO_2SO_4$ in solution would exist as a contact ion pair. More recently it has been shown that the $UO_2^{2+}$ ion is hydrated by a maximum of four waters in water–acetone mixtures.[26]

The partial molal entropy of the $VOSO_4$ ion pair should be greater than or equal to the entropy of the $CuSO_4$ ion pair that had previously been assumed to

have a primary hydration number of 5. Because these two ion pairs have almost identical entropies, we would conclude from this work that the $VOSO_4$ ion pair predominantly exists in solution as a solvent-separated ion pair. This conclusion is not in agreement with a pressure-jump kinetic study of $VOSO_4$ solutions, from which it was concluded that approximately 30% of the $VOSO_4$ ion pairs exist in aqueous solutions as solvent-separated ion pairs and 70% as contact ion pairs.[12] It is also not in agreement with the results one would expect from the crystal structure of $VOSO_4 \cdot 5H_2O$ in which the sulfate is in contact with the $VO^{2+}$ ion and the cation has a hydration number of 4.[27]

Although the partial molal entropies of these ion pairs appear to be predominantly determined by differences in the primary hydration of the cation, contributions from long-range electrostatic interactions may also be significant.

(26) A. Fratiello, V. Kubo, R. E. Lee, and R. E. Schuster, *J. Phys. Chem.*, **74**, 3726 (1970).

(27) C. J. Ballhausen, B. F. Djurinskij, and K. J. Watson, *J. Amer Chem. Soc.*, **90**, 3305 (1968).

# Rapid Preequilibria as a Cause for Change of Activation Energy with Temperature[1]

## by Ruth Koren and Berta Perlmutter-Hayman*

*Department of Physical Chemistry, Hebrew University, Jerusalem, Israel*   (*Received December 17, 1970*)

*Publication costs assisted by the Department of Physical Chemistry, Hebrew University, Jerusalem*

A reaction scheme is considered where the substance taking part in the rate-determining step is present in two forms which are in mobile equilibrium (isomers; or differently solvated or protonated species). Equations are developed which show that if only one of the two forms is kinetically active, while both are present at comparable concentrations, the apparent energy of activation decreases with temperature. On the other hand, if the two forms are present at different concentrations, but nevertheless contribute about equally to the observed reaction rate, having different, independent, rate constants, the apparent energy of activation is shown to increase with increasing temperature. The meaning of the results, and their possible applicability, are discussed.

## Introduction

The apparent energy of activation of a chemical reaction, defined by the expression

$$E_a = -R\, d \ln k / d(1/T) \qquad (1)$$

is frequently found to change with temperature; in

other words, what we may formally define as the specific heat of activation, *viz.*
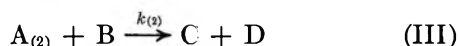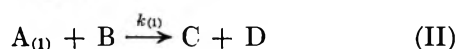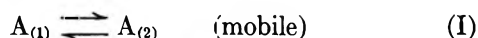
$$\Delta C_p^{\ddagger} \equiv dE_a/dT \qquad (2)$$

is found to be nonzero. Negative values of $\Delta C_p{}^{\ddagger}$ have been reported for many hydrolysis reactions[2-4] and have recently been discussed.[3-5] Positive values are less frequent and are usually ascribed to the existence of two or more different mechanisms.[5,6] At sufficiently low temperatures, they may occur as a consequence of proton tunneling.[7] In the present paper we shall show how the existence of a rapid preequilibrium can lead to both negative and positive values of $\Delta C_p{}^{\ddagger}$. Our calculations predict that these values may be strongly temperature dependent.

## Negative Values of $\Delta C_p{}^{\pm}$

Let is consider a reaction scheme

$$A_{(1)} \rightleftharpoons A_{(2)} \quad \text{(mobile)} \quad \text{(I)}$$

$$A_{(1)} + B \xrightarrow{k_{(1)}} C + D \quad \text{(II)}$$

$$A_{(2)} + B \xrightarrow{k_{(2)}} C + D \quad \text{(III)}$$

where $A_{(1)}$ and $A_{(2)}$ are isomers, or, for reactions in solution, substances which differ by their degree of solvation or protonation. The rate constant observed for the disappearance of B is

$$k_{\text{obsd}} = [k_{(1)}A_{(1)} + k_{(2)}A_{(2)}]/[A_{(1)} + A_{(2)}]$$

$$= (k_{(1)} + Kk_{(2)})/(1 + K) \quad (3)$$

where $K$ is the equilibrium constant of reaction I. From eq 3, together with the definition of $E_a$ (eq 1), we get

$$E_a = E_{(1)} - \frac{K}{K+1}\Delta H + $$

$$\frac{Kk_{(2)}/k_{(1)}}{1 + Kk_{(2)}/k_{(1)}}[\Delta H - (E_{(1)} - E_{(2)})] \quad (4)$$

where $E_{(1)}$ and $E_{(2)}$ are the "true" activation energies of reactions II and III, and $\Delta H$ is the heat of reaction of reaction I, all, for the sake of simplicity, assumed temperature independent.

Consider the limiting case where only one of the two species makes an appreciable contribution to the observed rate. When this species is $A_{(2)}$, i.e., $Kk_{(2)} \gg k_{(1)}$, eq 4 takes the form

$$E_a = E_{(2)} + \Delta H/(K+1) \quad (5a)$$

Conversely, when $k_{(1)} \gg Kk_{(2)}$ and thus only $A_{(1)}$ contributes, we have

$$E_a = E_{(1)} - K\Delta H/(K+1) \quad (5b)$$

In both cases, $E_a$ decreases with increasing temperature, and to the same extent. This becomes evident when we differentiate eq 5 to get

$$\Delta C_p{}^{\pm} = -\frac{\Delta H^2}{RT^2}\frac{K}{(K+1)^2} \quad (6)$$

For any given value of $\Delta H$ and $T$, the effect is at its
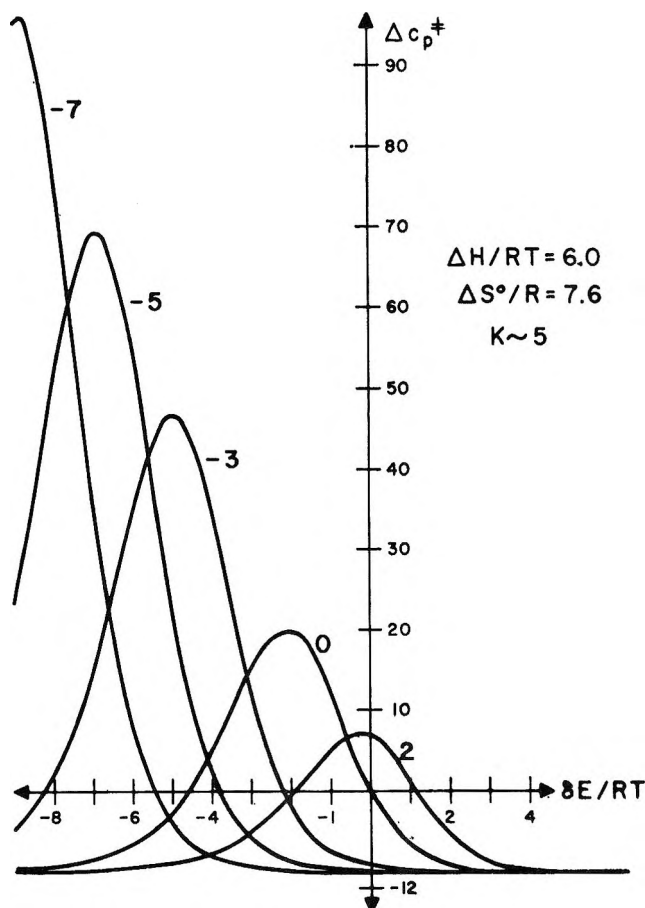


Figure 1. The dependence of $\Delta C_p{}^{\ddagger}$ on $\delta E/RT$, for various values of $\delta \Delta S^{\ddagger}/R$, indicated by a number alongside the appropriate curve.

maximum when $K = 1$. When $K$ differs considerably from unity, $\Delta C_p{}^{\ddagger}$ tends to zero and $E_a$ approaches temperature-independent values. For instance, when the kinetically active species is $A_{(2)}$, we get from eq 5a that $E_a = E_{(2)} + \Delta H$ when this species is present at very low concentration (small $K$) and $E_a = E_{(2)}$ when it is predominant. Similarly, when $A_{(1)}$ is kinetically active we get from eq 5b that $E_a = E_{(1)}$ and $E_a = E_{(1)} - \Delta H$ for small and large values of $K_1$, respectively.

It should be noted that $\Delta C_p{}^{\ddagger}$ is negative, irrespective of the algebraic sign of $\Delta H$. This means that it does not matter whether the relative concentration of the kinetically active species increases or decreases with increasing temperature. This can be understood from

(2) E. A. Moelwyn-Hughes, "The Kinetics of Reactions in Solution," Oxford University Press, London, 1947, Chapter 2.

(3) R. E. Robertson, *Progr. Phys. Org. Chem.*, **4**, 213 (1967).

(4) (a) B. Perlmutter-Hayman and Y. Weissmann, *J. Phys. Chem.*, **71**, 1409 (1967); (b) B. Perlmutter-Hayman, *Israel J. Chem.*, in press.

(5) J. R. Hulett, *Quart. Rev.*, **18**, 227 (1964).

(6) S. W. Benson, "The Foundations of Chemical Kinetics," McGraw-Hill, New York, N. Y., 1960, p 27.

(7) E. Caldin, *Chem. Rev.*, **69**, 130 (1969).

the following considerations. If, for instance, $A_{(2)}$ is kinetically active (see eq 5a) and $\Delta H$ is positive, then the observed rate constant increases with temperature because both the rate constant *and* the relative concentration of the active species increase. Therefore, $E_a$ is higher than the activation energy of the rate-determining step. This effect decreases as the temperature increases and $A_{(2)}$ therefore becomes more predominant. Conversely, if $\Delta H$ is negative, a rise in temperature represses $A_{(2)}$. Therefore, the observed rate constant rises with increasing temperature less than does the rate constant of the rate-determining step; $E_a$ is lower than $E_{(2)}$, and may even be negative. The effect is more pronounced as the relative concentration of $A_{(2)}$ decreases, *i.e.*, as the temperature increases. An analogous reasoning holds when $A_{(1)}$ is the kinetically active species.

## Positive Values of $\Delta C_p^{\pm}$

Let us now consider the case when $A_{(1)}$ and $A_{(2)}$ make comparable contributions to the observed rate. From eq 3 we see that the condition for this to happen is

$$k_{(1)} \sim K k_{(2)} \quad \text{or} \quad K k_{(2)}/k_{(1)} \sim 1 \quad (7)$$

For this case, eq 4 is valid (provided reactions II and III are independent, *i.e.*, proceed *via* different transition states: otherwise $[\Delta H - (E_{(1)} - E_{(2)})]$ is obviously zero). Differentiating that equation with respect to temperature and introducing

$$\delta E \equiv E_{(1)} - E_{(2)} \quad (8)$$

we get

$$\Delta C_p^{\pm} = -\frac{\Delta H^2}{RT^2}\frac{K}{(K+1)^2} + \frac{(\Delta H - \delta E)^2}{RT^2}\frac{K k_{(2)}/k_{(1)}}{[1 + K k_{(2)}/k_{(1)}]^2} \quad (9)$$

This expression is composed of two terms having opposite algebraic sign and may therefore be either negative or positive. Let us first consider the dependence of $\Delta C_p^{\pm}$ on $\delta E$, while all the other parameters have some constant, arbitrary values.

An arbitrary example is shown in Figure 1. Here $K \sim 5$, with $\Delta H/RT = 6.0$, and $\Delta S^\circ/R = 7.6$ (where $\Delta S^\circ$ is the standard entropy change of reaction I). The quantity $\delta \Delta S^{\pm}$ is defined as $\Delta S^{\pm}_{(1)} - \Delta S^{\pm}_{(2)}$, where $\Delta S^{\pm}$ is the entropy of activation. At very high values of $|\delta E|$ the first, negative term is seen to predominate. In a certain, fairly narrow range of $\delta E$ the second term predominates, and $\Delta C_p^{\pm}$ becomes positive.

Before determining the mathematical condition for $(\Delta C_p^{\pm})_{max}$ as a function of $\delta E$, we remember that

$$K k_{(2)}/k_{(1)} = \exp\left[-\frac{\Delta H - \delta E - T(\Delta S^\circ - \delta \Delta S^{\pm})}{RT}\right] \quad (10)$$

Differentiating eq 9 with respect to $\delta E$ and equating the result to zero, we see that $\Delta C_p^{\pm}$ has a maximum when the condition

$$\frac{\Delta H - \delta E}{2RT} = \coth\left[\frac{\Delta H - \delta E - T(\Delta S^\circ - \delta \Delta S^{\pm})}{2RT}\right] \quad (11)$$

is fulfilled. Mathematically, this can hold at two values of the argument. At one of them, $\Delta H - \delta E$ and $T(\Delta S^\circ - \delta \Delta S^{\pm})$ have opposite algebraic sign, and at the other, they have the same sign. Only the latter solution is of interest for our considerations. (Inspection of eq 10 shows that it is this solution which is compatible with condition 7.) From eq 9 it is clear that the value of $(\Delta C_p^{\pm})_{max}$ increases as $|\Delta H - \delta E|$ increases. At the same time, $|T(\Delta S^\circ - \delta \Delta S^{\pm})|$ must also increase for the maximum condition 11 to remain valid. This is brought out in Figure 1, where $\Delta S^\circ$ is positive; large negative values of $\delta \Delta S^{\pm}$ are seen to be accompanied by high values of $(\Delta C_p^{\pm})_{max}$. At the same time, the position of the maximum is shifted to more negative values of $\delta E$.

So far for the dependence of $\Delta C_p^{\pm}$ on $\delta E$, at constant $\Delta H$, and varying values of the parameter $T(\Delta S^\circ - \delta \Delta S^{\pm})$. If, on the other hand, we consider $\Delta C_p^{\pm}$ at a given value of $(\Delta H - \delta E)$, we find it to have a maximum when $(\Delta H - \delta E) = T(\Delta S^\circ - \delta \Delta S^{\pm})$, *i.e.* (see eq 9), when condition 7 becomes an equality and the two species make exactly equal contributions. Theoretically, there is thus no limit to increasing positive values of $\Delta C_p^{\pm}$. (In fact, the maximum conditions for dependence on $\delta E$ at constant $\Delta H$ and on $T(\Delta S^\circ - \delta \Delta S^{\pm})$ at constant $(\Delta H - \delta E)$ are simultaneously fulfilled when $(\Delta H - \delta E) \to \infty$.)

To get a better understanding of the physical meaning of the mathematical condition for positive values of $\Delta C_p^{\pm}$, let us again consider the example where $k_{(2)} \gg k_{(1)}$; this usually means that $\delta E > 0$. This must be accompanied by a particular, small value of $K$ for condition 7 to hold. We can then rewrite eq 4 to get

$$E_a = E_{(1)} + \frac{K k_{(2)}/k_{(1)}}{1 + K k_{(2)}/k_{(1)}}(\Delta H - \delta E) \quad (12)$$

When $(\Delta H - \delta E) < 0$, $E_a$ is smaller than $E_{(1)}$, the activation energy of the slower reaction (and may even be negative). However, the negative term decreases in value with increasing temperature, because, under the conditions we have chosen, $k_{(2)}/k_{(1)}$ decreases more strongly than $K$ increases. Finally, as the contribution of $A_{(2)}$ to the observed rate becomes negligible, $E_a \to E_{(1)}$. Conversely, when $(\Delta H - \delta E) > 0$, $E_a$ is higher than $E_{(1)}$ for the reason discussed in the previous section. This effect increases with increasing temperature, as the relative contribution of $A_{(2)}$ to the observed rate increases. When this becomes predominant, $E_a \to E_{(2)}$

$+ \Delta H$. The argument for the case where $k_{(2)} \gg k_{(1)}$ is completely analogous.

If, however, instead of $k_{(2)} \gg k_{(1)}$ and $K \ll 1$, we have merely $k_{(2)} > k_{(1)}$ and $K < 1$ (or *vice versa*), the positive and the negative terms on the right-hand side of eq 9 will always be of comparable magnitude, and $\Delta C_p{}^\ddagger$ does not attain high values.

## Applications

An argument similar to that outlined above has been adduced by Liebhafsky[8] to explain the negative values of $\Delta C_p$ in the hydrolysis of halogens. Negative values of $\Delta C_p{}^\ddagger$ for the same reaction may be explained on a similar basis.[9]

The negative values of $\Delta C_p{}^\ddagger$ for the uncatalyzed hydrolysis of dichromate have been tentatively explained on the assumption that a dichromate ion in the neighborhood of hydrogen-bonded or "icelike" water might be hydrolyzed more slowly than one situated in "free" water.[4]

Several years ago, in connection with a different topic, we measured[10] the esterification of acetic acid in methanol in the presence of $\sim 3.7$ $M$ chloroform, and in its absence; in both cases, varying small amounts of water were added to the reaction mixture. We found the observed rate constant $k_{obsd}$ to decrease, and $E_a$ to increase, with increasing water concentration. Furthermore, in the presence of chloroform, $E_a$ decreased with increasing temperature.

The retarding influence of small quantities of water on acid-catalyzed ester reactions has been known for a long time. Goldschmidt[11] explained this effect on the assumption that the catalytic effect of the proton present as $H_3O^+$ is small in comparison with that of the proton present as $ROH_2^+$. Various authors[12,13] have subsequently used the "Goldschmidt equation" to interpret their results on esterification reactions and to determine the equilibrium constant between the two forms of the proton from kinetic data.

The Goldschmidt mechanism in fact implies that $ROH_2^+$ should be the kinetically active species. This, however, is at variance with the $A_{AC}2$ mechanism now universally accepted for the hydrolysis of simple esters like methyl acetate.[14,15] According to that mechanism, it is the protonated acid (and not the protonated alcohol) which is involved in the rate-determining step of the esterification reaction.

We do not feel in a position to comment on this discrepancy, and we therefore derived expressions for $E_a$ for both the Goldschmidt and the $A_{AC}2$ mechanisms. On the very reasonable assumption that only a small fraction of the catalyzing proton is present as $CH_3COOH_2^+$, we found the two expressions to differ only by the heat of reaction of the protonation of acetic acid in ROH solution.[16] They both contain the temperature-dependent term

$$\frac{\Delta H}{1 + K[ROH]/[H_2O]} \quad (13)$$

where $\Delta H$ and $K$ refer to the reaction $H_3O^+ \rightarrow CH_3OH_2^+$. This may be compared with eq 5a; at a given water concentration, $K[ROH]/[H_2O]$ is a constant, and we get the temperature dependence of $E_a$ as given by eq 6. On the other hand, if we increase $[H_2O]$ from zero to a sufficiently high value, expression 13 increases from zero to $\Delta H$.

The Goldschmidt mechanism would thus constitute a straightforward application of our formulas: the active $ROH_2^+$ and the inactive $H_3O^+$ are present at comparable concentrations, and the equilibrium between them changes with temperature. According to the $A_{AC}2$ mechanism, the temperature dependence of $E_a$ arises in a more subtle way. The kinetically active substance is present at very low concentration; this usually leads to a temperature-independent $E_a$. In the present case, however, that substance is simultaneously in equilibrium with two other substances, $ROH_2^+$ and $H_3O^+$, whose equilibrium, in turn, changes with temperature.

To test the agreement between our expression for $E_a$ and the experimental results, we determined[11] $K$ in the presence of chloroform at different temperatures,[17] and hence $\Delta H$. We found it to be fairly constant in the range between 0 and 45°, and equal to $\sim 4.1$ kcal mol$^{-1}$. Our results are presented in Table I. The condition that $E_a$ at high water concentration should differ from

(8) H. A. Liebhafsky, *Chem. Rev.*, **17**, 89 (1935).

(9) A. Lifshitz, Ph.D. Thesis, Jerusalem, 1961; B. Perlmutter-Hayman, unpublished results.

(10) B. Perlmutter-Hayman, unpublished results, 1952.

(11) H. Goldschmidt and O. Udby, *Z. Phys. Chem.*, **60**, 728 (1907); see also R. P. Bell, "The Proton in Chemistry," Cornell University Press, Ithaca, N. Y., 1959, p 21.

(12) A. T. Williamson and C. N. Hinshelwood, *Trans. Faraday Soc.*, **30**, 1145 (1934).

(13) H. Goldschmidt and R. S. Melbye, *Z. Phys. Chem.*, **143**, 139 (1929); C. N. Hinshelwood and A. R. Legard, *J. Chem. Soc.*, 1586 (1935); R. J. Hartmann, H. M. Hoogsteen, and J. A. Moede, *J. Amer. Chem. Soc.*, **66**, 1714 (1944); H. A. Smith and J. Burn, *ibid.*, **66**, 1494 (1944), and several earlier papers by Hartmann and coworkers, by Goldschmidt and coworkers, and by Smith.

(14) See, *e.g.*, C. K. Ingold, "Structure and Mechanism in Organic Chemistry," 2nd ed, Cornell University Press, Ithaca, N. Y., 1969, Chapter 15, Section 58.

(15) We are indebted to one of the referees for drawing our attention to this fact.

(16) The dependence of the observed rate constant on $[H_2O]$ is, in principle, different for the two mechanisms, but the two expressions remain indistinguishable as long as the change in $[CH_3OH]$ is negligible, *i.e.*, at low water concentration, where the Goldschmidt equation was applied.[12–14]

(17) For this purpose we used the expression

$$\frac{[H^+]}{k_{obsd}} = \frac{1}{k} + \frac{[H_2O]}{[ROH]} \frac{1}{Kk}$$

and plotted $1/k_{obsd}$ *vs.* $[H_2O]$ for a series of experiments. At the lowest water concentration, where $[H_2O]$ cannot be considered constant during the experiment, a suitable correction was applied. The meaning of $k$ is $k_{ROH_2^+}$ or $K_{(ROH_2^+ \rightarrow H_2Ac^+)}k_{H_2Ac^+}$, according to the mechanism we assume.

**Table I:**  Apparent Energy of Activation in kcal mol$^{-1}$ for Esterification of Acetic Acid in Methanol Solution in the Presence of Chloroform; $[CH_3COOH]_0 = 8 \times 10^{-2} M$; $[HCl] = (1-3) \times 10^{-2} M$

|  | $[H_2O]$, M | | | | |
|---|---|---|---|---|---|
|  | $\geq 1.7$ | 1.1 | 0.83 | 0.55 | 0 |
| $E_a$ (273 → 289°K) |  |  | 14.0 | 13.6 |  |
|  | $14.7 \pm 0.1$ | 14.3 |  |  | 10.2[a] |
| $E_a$ (298 → 318°K) |  |  | 13.2 | 12.7 |  |

[a] See ref 13.

that at zero water concentration by $\Delta H$ is fulfilled as accurately as can be expected from the quality of our experiments.

It remains to explain why we did *not* find the expected temperature dependence of $E_a$ in the absence of chloroform.  This may be ascribed to the fact that the corresponding $\Delta H$, as calculated from data given in the literature,[13] increases with increasing temperature, thus masking the effect.  A more detailed investigation of the esterification reaction would be outside the scope of the present paper.

# Nuances of the ECE Mechanism.  III.  Effects of Homogeneous

# Redox Equilibrium in Cyclic Voltammetry[1]

## by Stephen W. Feldberg

*Brookhaven National Laboratory, Upton, New York  11973  (Received January 7, 1971)*

*Publication costs assisted by Brookhaven National Laboratory*

The ECE mechanism is generally presented as:   $e^- + A \rightleftarrows B$ (1);   $B \xrightarrow{k_2} C$ (2);   $e^- + C \rightleftarrows D$ (3).   It has been demonstrated previously that it is necessary to consider the redox reaction:   $B + C \underset{k_{-4}}{\overset{k_4}{\rightleftarrows}} A + D$ (4); which is related to the $E^0$'s of reactions 1 and 3 according to:   $K_4 = k_4/k_{-4} = \exp\{(F/RT)(E_3^0 - E_1^0)\}$ (5). The objective of this theoretical study is a qualitative assessment of the effect of reaction 4 on cyclic voltammograms of systems exhibiting ECE behavior.   Two limiting conditions are assigned to reaction 4:   (A) equilibrium is always maintained or (B) attainment of equilibrium is infinitely slow.   The effects of these two limiting conditions are observed in theoretical cyclic voltammograms of three representative ECE situations:   (1) $E_3^0 = E_1^0 + 0.3$ V $[K_4 (\approx 10^6) \gg 1]$; (2) $E_3^0 = E_1^0$ $(K_4 = 1)$; (3) $E_3^0 = E_1^0 - 0.3$ V $[K_4 (\approx 10^{-6}) \ll 1]$.   The heterogeneous reactions are assumed to be reversible one-electron transfers.   Qualitative diagnostic criteria are established which distinguish type "A" and type "B" ECE mechanisms.   The theory of Marcus, which correlates heterogeneous and homogeneous redox rate parameters, is used to estimate when condition A or B is likely to prevail.

The ECE mechanism has received much attention in the electrochemical literature[2-24]—partly because of the challenge of mathematically unraveling a myriad of coupled phenomena (diffusion, heterogeneous electron transfers, homogeneous electron transfers, and homogeneous chemical kinetics).   More important is that the ECE mechanism is probably quite common in organic electrochemistry in spite of the literature which might lead one to conclude (erroneously) that reductions of nitrosophenols are the only known examples.[2,6,8,9,11,12,16,17]   They are not, of course.[13,18,21-24]

The ECE mechanism is generally presented as[25]

$$e^- + A \rightleftarrows B \qquad (1)$$

$$B \xrightarrow{k_2} C \qquad (2)$$

$$e^- + C \rightleftarrows D \qquad (3)$$

It has been demonstrated previously[10,13] that it is necessary to consider the redox reaction

$$B + C \underset{k_{-4}}{\overset{k_4}{\rightleftarrows}} A + D \qquad (4)$$
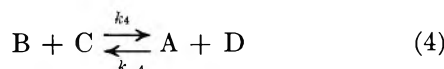
which is related to the $E^0$'s of reactions 1 and 3 according to

$$K_4 = \frac{k_4}{k_{-4}} = \exp\left\{\frac{F}{RT}(E_3^0 - E_1^0)\right\} \qquad (5)$$

The status of the present theory for chronoamperometric evaluation of $k_2$ [10] requires that either one of two conditions prevail:   (A) equilibrium of reaction 4 is maintained at all times;   or (B) attainment of equilibrium is infinitely slow.   If chronoamperometric

data are obtained over an adequately large time range it is often possible to deduce which type of behavior (A or

(1) This work was performed under the auspices of the United States Atomic Energy Commission.

(2) (a) D. Stocesova, *Collect. Czech. Chem. Commun.*, **14**, 615 (1949); J. Koutecky, R. Brdicka, and V. Hanus, *ibid.*, **18**, 611 (1953).

(3) A. C. Testa and W. H. Reinmuth, *J. Amer. Chem. Soc.*, **83**, 784 (1961).

(4) A. C. Testa and W. H. Reinmuth, *Anal. Chem.*, **33**, 1320 (1961).

(5) B. Kastening and L. Holleck, *Z. Elektrochem.*, **63**, 166 (1959).

(6) G. S. Alberts and I. Shain, *Anal. Chem.*, **35**, 1859 (1963).

(7) R. S. Nicholson and I. Shain, *ibid.*, **37**, 178 (1965).

(8) R. S. Nicholson and I. Shain, *ibid.*, **37**, 190 (1965).

(9) H. B. Herman and A. J. Bard, *J. Phys. Chem.*, **70**, 396 (1966).

(10) M. D. Hawley and S. W. Feldberg, *ibid.*, **70**, 3459 (1966).

(11) P. A. Malachesky, L. S. Marcoux, and R. N. Adams, *ibid.*, **70**, 4068 (1966).

(12) R. S. Nicholson, J. M. Wilson, and M. L. Olmstead, *Anal. Chem.*, **38**, 542 (1966).

(13) R. N. Adams, M. D. Hawley, and S. W. Feldberg, *J. Phys. Chem.*, **71**, 851 (1967).

(14) J. M. Savéant, *Electrochim. Acta*, **12**, 753 (1967).

(15) S. Karp, *J. Phys. Chem.*, **72**, 1082 (1968).

(16) H. N. Blount and H. B. Herman, *ibid.*, **72**, 3006 (1968).

(17) H. B. Herman and H. N. Blount, *ibid.*, **73**, 1406 (1969).

(18) D. L. Ehman and D. T. Sawyer, *Inorg. Chem.*, **9**, 204 (1970).

(19) H. R. Sobel and D. E. Smith, *J. Electroanal. Chem.*, **26**, 271 (1970).

(20) T. Mizoguchi and R. N. Adams, *J. Amer. Chem. Soc.*, **84**, 2058 (1962).

(21) Z. Galus and R. N. Adams, *ibid.*, **84**, 2061 (1962).

(22) S. Feldberg, *J. Phys. Chem.*, **73**, 1238 (1969).

(23) L. S. Marcoux, R. N. Adams, and S. W. Feldberg, *ibid.*, **73**, 2611 (1969).

(24) R. F. Nelson and S. W. Feldberg, *ibid.*, **73**, 2623 (1969).

(25) This mechanism represents a first-order or pseudo-first-order ECE mechanism. The qualitative discussion in this paper, however, is applicable to second-order ECE (see ref 20–24).
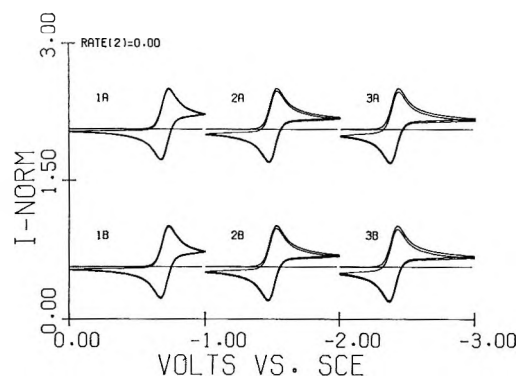
Figure 1. RATE(2) = $k_2(F/RT)^{-1}(dE/dt)^{-1}$ = 0. Abscissa and ordinate indicate scale rather than absolute values:
$I$-NORM = $i/nFAC_A\sqrt{D(F/RT)(dE/dt)}$ and $E_{rev}$ = $E_{start}$ − 1.0 V. For 1A and 1B ECE's: $E_1^0$ = $E_{start}$ − 0.7 V and $E_3^0$ = $E_{start}$ − 0.4 V. For 2A and 2B ECE's: $E_1^0$ = $E_3^0$ = $E_{start}$ − 0.5 V. For 3A and 3B ECE's: $E_1^0$ = $E_{start}$ − 0.4 V and $E_3^0$ = $E_{start}$ − 0.7 V. Heterogeneous one-electron transfers are infinitely fast.
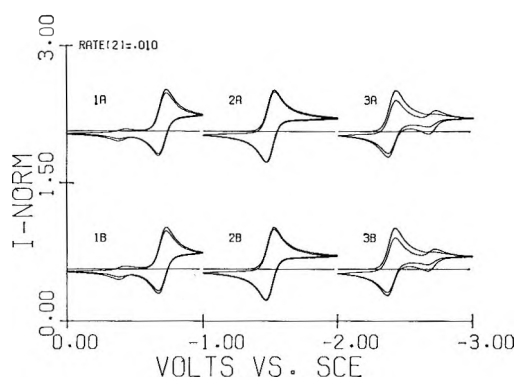


Figure 2. RATE(2) = 0.01. See Figure 1 caption for details.



Figure 3. RATE(2) = 0.02. See Figure 1 caption for details.
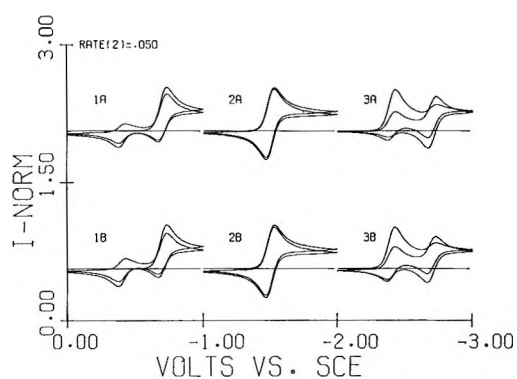


Figure 4. RATE(2) = 0.05. See Figure 1 caption for details.

B) obtains.[10,13] Often, however, the time range of the data is inadequate for this distinction, but adequate for evaluation of $k_2$ *if* some other method can be devised to distinguish type "A" and "B" behavior. Cyclic voltammetry can, in some cases, make the distinction. The objective of the present theoretical study is a qualitative assessment of the effect of reaction 4 on cyclic voltammograms of ECE systems. The effects of type "A" and type "B" behavior are evaluated for theoretical cyclic voltammograms of three representative ECE situations

1.      $E_3^0$ = $E_1^0$ + 0.3 V [$K_4$ ($\approx 10^6$) ≫ 1]

2.      $E_3^0$ = $E_1^0$ [$K_4$ = 1]

3.      $E_3^0$ = $E_1^0$ − 0.3 V [$K_4$ ($\approx 10^{-6}$) ≪ 1]

(Although voltammograms can be calculated for any value of $K_4$, the three values selected are adequate for this discussion.) Thus, six voltammograms were calculated for several different values of the rate constant $k_2$; the results are shown in Figures 1–8. Calculations

were carried out using the technique of digital simulation[26] with the following assumptions: diffusion coefficients of all species are the same; semiinfinite linear diffusion obtains; and the heterogeneous one-electron transfers are infinitely fast.

### Discussion of Results

The potentials of the peaks clearly distinguish type "1", "2", and "3" behavior.[7] In type "1" behavior a peak corresponding to reaction 3 appears only after the first cathodic scan, whereas in type "3" behavior a cathodic peak (the second one) appears on the first cathodic scan (Figures 2–8). Type "2" behavior is characterized by a single pair of peaks since $E_1^0$ = $E_3^0$.

Only subtle differences exist between cyclics of corresponding type "A" and type "B" ECE mechanisms. There appear to be no distinguishing phenomena quite as dramatic as the "peaked" working curves obtained for chronoamperometry of a "2A" or "3A" ECE.[10] Nevertheless, there are some distinguishing features. In the "1A" voltammograms note that as the normalized rate constant [RATE(2) = $k_2(F/RT)^{-1}(dE/dt)^{-1}$] increases [RATE(2) ≥ 0.2, Figures 6–8] the current on the anodic sweep (just after reversal) returns to zero and stays there until the potential is sufficiently anodic for species D to be reoxidized back to species C.

(26) S. W. Feldberg, "Electroanalytical Chemistry," Vol. 3, A. J. Bard, Ed., Marcel Dekker, New York, N. Y., 1969, p 299 ff.
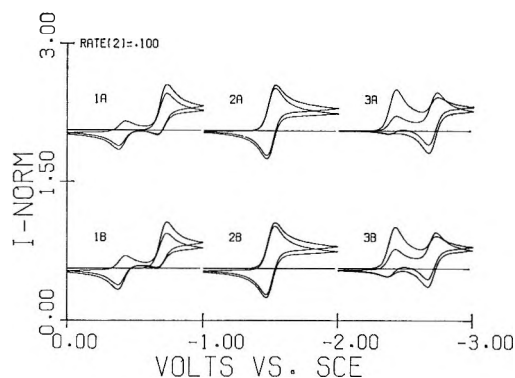
Figure 5. RATE(2) = 0.10. See Figure 1 caption for details.
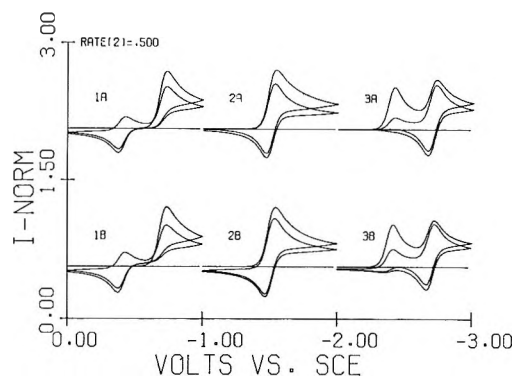


Figure 7. RATE(2) = 0.50. See Figure 1 caption for details.
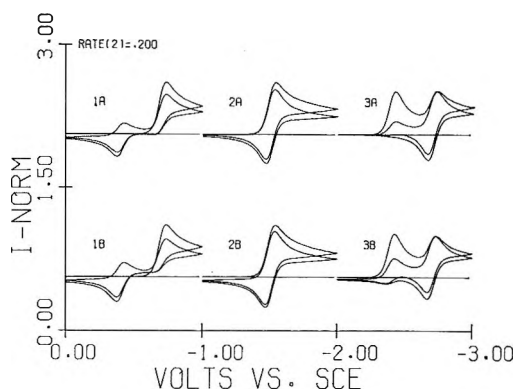


Figure 6. RATE (2) = 0.20. See Figure 1 caption for details.
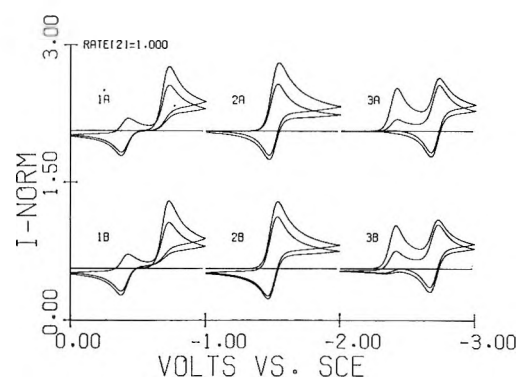


Figure 8. RATE(2) = 1.00. See Figure 1 caption for details.

Inspection of the mechanism (reactions 1–4) will indicate that in a type "1A" ECE, species C cannot exist until it is generated by oxidation of species D. In the corresponding "1B" voltammograms the anodic current just after reversal approaches zero but then levels off at a small cathodic current. At the potential where this occurs the only electroactive species present in solution is species C which is produced by reaction 2. In principle, then, this phenomenon distinguishes between the "1A" and "1B" ECE. It is particularly important that the double-layer current be eliminated from the experimental voltammograms. The type "3" ECE's exhibit distinguishable behavior when RATE(2) $\geq$ 0.1 (Figures 5–8). At potentials anodic to the first couple the current is zero in the "3A" voltammogram [RATE(2) $\geq$ 0.2] while in the type "3B" voltammogram (at the corresponding potentials) there is always an anodic current (except, of course, on the first cathodic sweep). The reason for this is quite straightforward. The anodic current in the "3B" voltammogram is due to the oxidation of species D. However, when type "3A" behavior prevails species D and A annihilate (reaction 4) to produce species C and B. Species B rapidly converts to C (reaction 2). Thus, there is no oxidizable species at these potentials.

Type "2A" and type "2B" ECE voltammograms exhibit virtually no distinguishing phenomena. A very subtle effect is the diminished anodic current toward the end of the first and second cycles of the "2A" voltammogram (compared to the "2B") when RATE(2) > 0.2. This is caused by the lability of reaction 4: species A and D react to form B and C just as in the "3A" voltammogram. Arguments in the subsequent section of this paper, however, suggest that it is highly unlikely that homogeneous electron transfer kinetics (reaction 4) will ever be sufficiently rapid for type "2A" behavior to be observed.

*Prediction of the Nature of the ECE on the Basis of Heterogeneous Rate Parameters.* We have already presented the very straightforward relationship between $K_4$ and the $E^0$'s for reactions 1 and 3 (eq 5). Marcus[27] has developed a theory relating the rates of heterogeneous electron transfer and corresponding homogeneous electron transfer. His theory assumes that electron transfer is outer sphere. (It is doubtful that this would apply to those cases involving multiple electron transfers interspersed with proton transfers.) On the basis of Marcus' theory[28]

$$k_4 \sim 10^3 k_{\text{hs}_1} k_{\text{hs}_3} K_4^{1/2} \qquad (6)$$

or

$$k_{-4} \sim 10^3 k_{\text{hs}_1} k_{\text{hs}_3} K_4^{-1/2} \qquad (7)$$

(27) R. A. Marcus, *J. Phys. Chem.*, **67**, 853 (1963).

(28) Units of eq 6 and 7 are such that when $k_{\text{hs}}$ is expressed as cm sec$^{-1}$, $k_4$ will be in l. mol$^{-1}$ sec$^{-1}$. Consequently, in eq 8 $C_A$ is in mol l.$^{-1}$.

In order for type "A" behavior to obtain the *rate* of reaction 4 in the appropriate direction must be significantly larger than the *rate* of reaction 2. Expressed mathematically

$$\frac{10^3 C_A k_{\text{hs}_1} k_{\text{hs}_3} \exp\left\{\dfrac{F}{2RT}|E_1^0 - E_3^0|\right\}}{k_2} > 10 \qquad (8)$$

where $C_A$ is the bulk concentration of species A. Conditions for a type "B" ECE exist when the left-hand side of eq 8 [LHS(8)] is small, *i.e.*

$$\text{LHS}(8) < 0.1 \qquad (9)$$

Equation 8 indicates that when $k_2 \sim 0.1 \text{ sec}^{-1}$, $C_A = 10^{-3} M$ and $|E_1^0 - E_3^0| = 0.3$ V, then in order for type "A" behavior to prevail

$$k_{\text{hs}_1} k_{\text{hs}_3} > 3 \times 10^{-3} \text{ cm}^2/\text{sec}^2 \qquad (10)$$

As $k_2$ increases or as $|E_1^0 - E_3^0|$ decreases, the product $k_{\text{hs}_1} k_{\text{hs}_3}$ must increase in order to maintain the condition prescribed by eq 8 for type "A" behavior. An extremely interesting conclusion may be drawn for the type "2" ECE ($K_4 = 1$). Here the Marcus relationships indicate that if $C_A = 10^{-3} M$ and $k_2 \sim 0.1 \text{ sec}^{-1}$, type "A" behavior requires

$$k_{\text{hs}_1} k_{\text{hs}_3} > 1 \text{ cm}^2 \text{ sec}^{-2} \qquad (11)$$

This suggests that the heterogeneous rate constants must approach a mean high value of about 1 cm sec$^{-1}$. Perusal of the tables of Tanaka and Tamamushi[29] indicates that values of $k_{\text{hs}}$ seldom exceed 1 cm sec$^{-1}$.

On the basis of these considerations it seems reasonable to conclude that type "2A" behavior is highly unlikely. As the term $|E_1^0 = E_3^0|$ increases, the probability of type "A" behavior increases. Thus, the chronoamperometric working curves previously calculated for type "A" behavior[10] are in principle correct. However, as the term $|E_1^0 - E_3^0|$ approaches zero ($K_4 \rightarrow$

1) it is considerably more probable that the Alberts and Shain working curve[5] which is valid for any type "B" ECE would correspond to the experimental phenomena. Conversely, as the term $|E_1^0 - E_3^0|$ increases, the working curves describing type "A" behavior are more and more likely to represent the experimental phenomena.

I have intentionally avoided detailed quantitative analysis of the various voltammograms since the conditions for the generation of the simulated cyclics are rather specific (*e.g.*, reversible one-electron transfer, specific $E^0$'s, $E_{\text{start}}$, $E_{\text{reverse}}$, etc.). The reader is referred to Nicholson and Shain[7] for a more detailed discussion of type "B" voltammograms of ECE mechanisms. The main objective of the present work is to show that cyclic voltammetry can, in some cases, elucidate the nature of reaction 4, and thereby help to interpret kinetic data obtained by the technique of choice.

Although the effect of reaction 4 on the nature of the cyclic voltammograms is at most subtle it has a dramatic effect upon the distribution of species in the diffusion layer. (The reader may satisfy himself on this point by sketching concentration profiles that would exist in the absence of reaction 4 and then considering the effects of reaction 4 for $K_4 = \infty$ and $K_4 = 0$.) By using transparent electrodes[30-34] or reflecting electrodes[35] it might be possible to monitor the spectral characteristics of species in the diffusion layer and thus elucidate the nature of reaction 4 in a direct way.

(29) N. Tanaka and R. Tamamushi, *Electrochim. Acta*, 9, 963 (1964).

(30) J. W. Strojek, T. Kuwana, and S. W. Feldberg, *J. Amer. Chem. Soc.*, 90, 1353 (1968).

(31) J. W. Strojek and T. Kuwana, *J. Electroanal. Chem.*, 16, 471 (1968).

(32) T. Kuwana and J. Strojek, *Trans. Faraday Soc.*, 45, 134 (1968).

(33) A. Prostak, H. B. Mark, and W. N. Hansen, *J. Phys. Chem.*, 72, 2576 (1968).

(34) D. R. Tallant and D. H. Evans, *Anal. Chem.*, 41, 835 (1969).

(35) P. T. Kissinger and C. N. Reilley, *ibid.*, 42, 12 (1970).

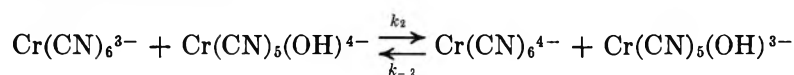# Chromium (II)-Catalyzed Aquation of Hexacyanochromate(III)

# to Pentacyanomonohydroxychromate(III)[1]

**by Ljubomir Jeftić[2] and Stephen W. Feldberg***

*Brookhaven National Laboratory, Upton, New York 11973* (*Received December 17, 1970*)

*Publication costs assisted by Brookhaven National Laboratory*

The chromium(II)-catalyzed aquation of hexacyanochromate(III) has been studied in aqueous alkaline cyanide media as a function of cyanide and hydroxide ion concentrations with sodium perchlorate as the inert electrolyte (ionic strength $= 1.0\ M$). When the concentrations of NaCN and NaOH are each greater than 0.1 $M$ and when the ratio [NaOH]/[NaCN] is less than 2 an equilibrium is established between the hexacyanochromate(III) and pentacyanomonohydroxychromate(III) complexes [no other chromium(III) complexes can be detected]. The kinetics can be explained on the basis of a simple outer-sphere electron transfer between the chromium(III) and chromium(II) complexes.

$$\text{Cr(CN)}_6{}^{3-} + \text{Cr(CN)}_5(\text{OH})^{4-} \underset{k_{-2}}{\overset{k_2}{\rightleftharpoons}} \text{Cr(CN)}_6{}^{4-} + \text{Cr(CN)}_5(\text{OH})^{3-}$$

Assuming the rapid lability (relative to the rates of the above reaction) of the Cr(II) complexes

$$K_3 = \frac{[\text{Cr(CN)}_5(\text{OH})^{-4}][\text{CN}^-]}{[\text{Cr(CN)}_6{}^{4-}][\text{OH}^-]}$$

and that $K_3 \ll 1$ (based on spectrophotometric studies of Cr(II) at different NaOH and NaCN concentrations), the following rate expression can be written: $d[\text{Cr(CN)}_6{}^{3-}]/dt = [\text{Cr(II)}]\{k_{-2}[\text{Cr(CN)}_5\text{OH}^{3-}] - k_2 K_3 \cdot [\text{Cr(CN)}_6{}^{3-}][\text{OH}^-][\text{CN}^-]\}$, where $K_3 k_2 = 150 \pm 9\ M^{-1}\ \text{sec}^{-1}$, $k_{-2} = 184 \pm 9\ M^{-1}\ \text{sec}^{-1}$, and the equilibrium constant $K_3 K_2 = K_3 k_2/k_{-2} = 0.81 \pm 0.03$. The proposed mechanism is shown to be consistent with electrochemical experiments (cyclic voltammetry). The heterogeneous rate parameters for the pentacyanomonohydroxychromate(III–II) couple are estimated: $E^0 < -1.48$ V, $k_{hs} > 4 \times 10^{-3}$ cm sec$^{-1}$, and $\alpha = 0.75$.

## Introduction

In this paper we report the results of our investigation of the chromium(II)-catalyzed aquation of the hexacyanochromate(III) complex to the pentacyanomonohydroxychromate(III) complex in aqueous alkaline cyanide media. The purpose of this study is the elucidation of the kinetics and mechanism of the catalyzed aquation.

In recent years there has been a great deal of interest in the cyanoaquochromate(III) complexes having the general form $\text{Cr(CN)}_n(\text{H}_2\text{O})_{6-n}{}^{3-n}$. Schaap and his coworkers[3-5] have reported the preparation, isolation, and spectra (300–700 nm) of all the complexes ($n = 0$ to $n = 6$). Very recently, however, we reported[6] that the complex characterized by Schaap, *et al.*,[3-5] as the tetracyanodiaquochromate(III) complex is in fact the pentacyanomonoaquochromate(III) complex. The spectral characteristics and the preparation techniques of the pentacyano complex are those formerly assigned to the tetracyano complex. Some doubt remains as to the exact nature of the complex identified by Schaap, *et al.*, as the pentacyano complex; the tetracyano complex has yet to be prepared and/or isolated.

The six coordinating positions of chromium(III) are equivalent; thus there are no isomers of either the hexa-

cyano or pentacyano complexes.[7] Ligand exchange of the hexacyano and pentacyano complexes is slow and the aquation kinetics have been investigated.[4,5] In acidic media the aquation rates increase with decreasing pH. Although no quantitative experiments were reported for aquation in alkaline media, Krishnamurthy[4] points out that the hexacyano complex is stable in dilute base even on heating. Our own preliminary spectrophotometric experiments have indicated that the pentacyano complex is stable for at least an hour in dilute base at room temperature. Heating in this medium will aquate the pentacyano complex to the

(1) This work was performed under the auspices of the U. S. Atomic Energy Commission.

(2) On leave from the Rudjer Bošković Institute, Zagreb, Yugoslavia.

(3) R. Krishnamurthy, W. B. Schaap, and J. R. Perumareddi, *Inorg. Chem.*, 6, 1338 (1967).

(4) R. Krishnamurthy, Ph.D. Thesis, Indiana University, 1966.

(5) W. B. Schaap, R. Krishnamurthy, D. K. Wakefield, and W. F. Coleman in "Coordination Chemistry," S. Kirschner, Ed., Plenum Press, New York, N. Y., 1969, p 177.

(6) L. Jeftić and S. Feldberg, *J. Amer. Chem. Soc.*, 92, 5272 (1970).

(7) Cis–trans isomers of the tetra-, tri-, and dicyano complexes should exist; however, no tetracyano and only cis forms of tri- and dicyano complexes have been isolated. Trans labilization by the cyanide ligand is put forth as the reason for absence of trans forms (see ref 4).

aquohydroxy complex and will ultimately form the chromic oxide precipitate.[4] Thus base-catalyzed aquation of the hexacyano or pentacyano complex can be ignored in our experiments, which required less than 10 min to execute and were carried out at 25°.

Photoaquation of the hexacyanochromate(III) complex has been studied by Chiang and Adamson.[8] Their spectra clearly show photoinduced conversion of the hexacyano complex into the pentacyano complex. The quantum efficiency for the conversion is low (~0.09) and our own observations indicate that negligible photoaquation is caused in the laboratory by artificial or natural light or by the light source in the Cary 14 spectrophotometer.

The distribution of the cyanoaquochromate(II) species as a function of cyanide and hydroxide ion concentrations is, of course, relevant to the mechanism of the chromium(II)-catalyzed reactions. Some spectrophotometric data have been reported.[9-11] Davies, Sutin, and Watkins[11] have studied the kinetics of chromium(II) oxidation by hydrogen peroxide and from their kinetic data deduce an equilibrium constant for the reaction

$$Cr(CN)_5H_2O^{3-} + CN^- \underset{}{\overset{K_1}{\rightleftarrows}} Cr(CN)_6^{4-} + H_2O \quad (1)$$
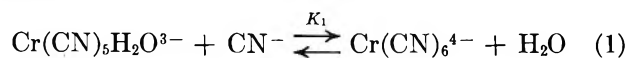
where $K_1 = 9.55\ M^{-1}$. They note that the spectrum of the chromium(II) species is independent of cyanide and hydroxide concentration when the ratio $(CN^-)/(OH^-) \geq 20$ and the concentration of cyanide is greater than $0.5\ M$.

Electrochemical experiments carried out previously have not attempted to elucidate the chromium(II)-catalyzed aquation of the hexacyanochromate(III) complex. Hume and Kolthoff[12] established that the hexacyanochromate(III-II) couple has an $E^0 = -1.39$ V (vs. the standard calomel electrode, sce) and several workers[13,14] have evaluated the rate parameters for the couple: $k_{hs} \approx 0.25$ cm sec$^{-1}$ and $\alpha \approx 0.5$. This is a relatively fast reaction, i.e., in a cyclic voltammetric experiment it would begin to exhibit irreversibility as the sweep rate approached 20 V/sec.

## Experimental Section

*Materials.* Stock solutions of sodium perchlorate were prepared from the anhydrous salt (G. F. Smith, analytical reagent grade). Sodium hydroxide stock solutions were prepared from commercially standardized Acculute (Anachemia Chemicals Ltd.). An appropriate quantity of sodium cyanide (Allied Chemical, reagent grade) was weighed out for each experiment. Analysis of the sodium cyanide by silver nitrate titration indicated that the salt was about 95% sodium cyanide.

Tripotassium hexacyanochromate(III) (Potassium chromicyanide, City Chemical Corp., New York) was analyzed on the basis of its spectrum (300-600 nm). With one batch the spectrum checked exactly with that

reported in the literature.[3-5] Other batches, however, required recrystallization from aqueous solution with methanol. The pentacyanomonoaquochromate(III) complex was prepared according to Schaap, et al.[4,5] The ion exchange resins used to isolate the complex were Dowex 1-X8, an anion resin (Baker analyzed reagent, J. T. Baker Chemical Co.) and AG 50W-X8, a cation resin (analytical grade, Bio Rad Laboratories).

A chromium(II) stock solution was prepared by zinc amalgam reduction of $1.60 \times 10^{-3}\ M$ tripotassium hexacyanochromate(III) in 0.016 M sodium hydroxide and 0.36 M sodium cyanide. The solution was in series with an argon purification train.

Argon for deaeration of solutions was passed through a concentrated acidic chromium(II)-zinc amalgam reducing solution [5 M HClO$_4$, 1 M Cr(II)], water, and finally the stock alkaline cyanide solution of chromium(II) just described.

*Analysis of Solutions.* The concentrations of the chromium(III) complexes were determined by spectrophotometric measurements (with a Cary 14) from 300 to 700 nm. Cyanide ion was titrated with standard silver nitrate solution; pCN was measured with the Orion cyanide electrode[15] (hydroxide interferes when its concentration exceeds 0.2 M).

*Characterization of Spectra.* Schaap and coworkers[3-5] have characterized the spectra for the cyanoaquochromate(III) complexes in the aquo form (not the hydroxy form). Our kinetic studies, however, were carried out at pH >13 (NaOH $\gtrsim$ 0.1 M); thus, it was necessary to determine the spectra of the hexacyano and pentacyano complexes at these higher pH values. Spectra of the hexacyano complex obtained between pH 5 and pH 14 were identical, exhibiting no pH effect.

The spectrum of the pentacyano complex changes with increasing pH (starting at pH 7) until pH 11. Increasing pH further causes no perceptible changes. A pH titration indicates that one proton is removed and that the $pK_a$ for the acid-base reaction is about 9. The spectra for the pentacyanomonoaquo- and the pentacyanomonohydroxychromate(III) are shown in Figure 1.

Spectra of the hexacyanochromate(II) were obtained by reduction of the hexacyanochromate(III) with zinc amalgam. A solution of 0.010 M K$_3$Cr(CN)$_6$ and desired concentrations of NaOH, NaCN, and zinc amalgam

(8) A. Chiang and A. W. Adamson, *J. Phys. Chem.*, **72**, 3827 (1968).

(9) R. Samuel, A. Khan, and N. Ahmad, *Z. Phys. Chem., Abt. B*, **22**, 431 (1933).

(10) R. Samuel and A. Despande, *Z. Phys.*, **80**, 395 (1933).

(11) G. Davies, N. Sutin, and K. Watkins, *J. Amer. Chem. Soc.*, **92**, 1892 (1970).

(12) D. N. Hume and I. M. Kolthoff, *ibid.*, **65**, 1897 (1943).

(13) J. E. B. Randles and K. W. Somerton, *Trans. Faraday Soc.*, **48**, 957 (1952).

(14) D. E. Smith, Ph.D. Thesis, Columbia University, 1961.

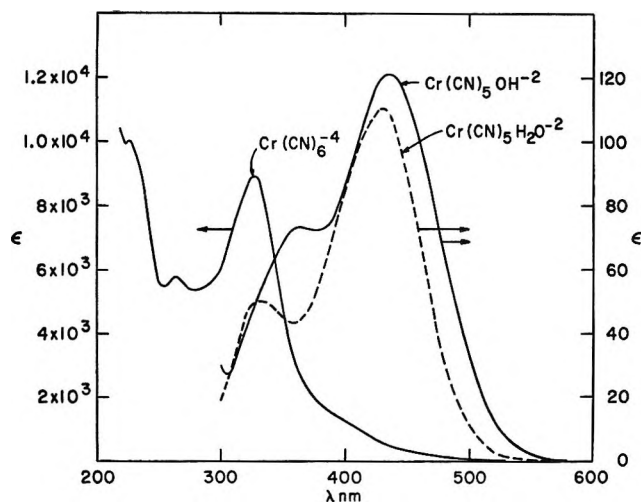(15) Orion Research Inc., Cambridge, Mass.

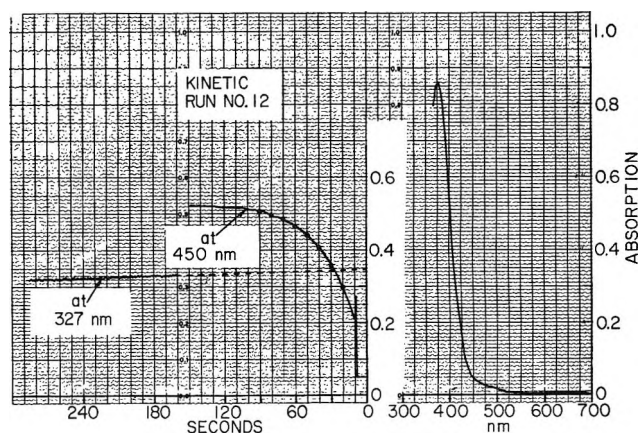Figure 1.  Extinction coefficients for $Cr(CN)_6^{4-}$ (left scale) and for $Cr(CN)_5H_2O^{2-}$ and $Cr(CN)_5OH^{3-}$ (right scale).



Figure 2.  Sample experimental run (see Table II, run 12, for details).  Theoretical points were calculated according to eq 6.

was sealed in a 0.125-cm optical cell.  With 1 $M$ NaCN and no NaOH, and with 0.5 $M$ NaCN and 0.5 $M$ NaOH, identical spectra were obtained.  This spectrum which we assume to be that of hexacyanochromate(II) is shown in Figure 1.  Three peaks at 227, 265, and 327 nm have extinction coefficients of $1.01 \times 10^4$, $5.8 \times 10^3$, and $9.0 \times 10^3$ l. $mol^{-1}$ $cm^{-1}$ in good agreement with the values reported by Davies, et al.[11]  When the ratio [NaOH]/[NaCN] was greater than unity the efficiency of reduction diminished; no discernible chromium(II) was produced when the ratio was greater than 3.  The green aquohydroxychromate(III) (which is *not* reduced by zinc amalgam) appeared in solution produced by the chromium(II)-catalyzed aquation of hexacyanochromate(III).  At a ratio of 5 where $c_{NaOH}$ = 2.5 $M$ and $c_{NaCN}$ = 0.5 $M$ the sodium hydroxide concentration was increased from 0.5 $M$ to 2.5 $M$ *after* reduction.  In spite of our efforts to avoid introducing air into the system we lost more than 30% of the chromium(II).  Nevertheless the resulting spectrum could be completely rationalized using the extinction coefficients for the hexacyanochromate(II) and aquohydroxychromate(III) complexes.

Relevant extinction coefficients of the chromium(III and II) complexes are summarized in Table I.  At 450 nm the extinction coefficients of the pentacyanomonohydroxychromate(III) and hexacyanochromate(III) complexes have the maximum difference.

**Table I:**  Extinction Coefficients for Chromium Species at Wavelengths Used for Evaluating Kinetic Data

| $\lambda$, nm | $\epsilon$ for $Cr(CN)_6^{3-}$ | $\epsilon$ for $Cr(CN)_5OH^{3-}$ | $\epsilon$ for $Cr(CN)_6^{4-}$ |
|---|---|---|---|
| 327 | 38.3 | 48.7 | 9000[a] |
| 380 | 86[a] | 72.4 | |
| 450 | 3.0 | 112.9 | 315 |

[a] Denotes major absorption peak.

*Kinetic Measurements.*  The kinetics of the chromium(II)-catalyzed aquation of hexacyanochromate(III) were observed by combining the chromium(III) and chromium(II) species and then following the change in optical density at 450 nm, where the difference between $\epsilon_{Cr(CN)_6^{3-}}$ and $\epsilon_{Cr(CN)_5OH^{3-}}$ is maximized (see Figure 1).  When the chromium(II) concentration is $\sim 10^{-4}$ $M$ the rate of aquation is slow enough for changes in optical density to be easily followed on the Cary 14 strip-chart pen and ink recorder.  The reaction vessel was a standard 1-cm quartz cuvette.  A rubber septum cap was mounted so that a mercury pool (on the cap) acted as an air seal to minimize air leaks when a hypodermic needle was introduced into the cuvette.  Stirring was effected with a magnetic stirrer and a small Teflon-coated stirring bar.

*Procedure.*  A cuvette was filled with 2.50 ml of a solution containing appropriate quantities of $K_3Cr(CN)_6$, NaCN, NaOH, and $NaClO_4$ (see Table II).  After purging with argon for 15 min, a partial spectrum was taken to determine the exact concentration of the hexacyano complex (Figure 2).  Then, with the wavelength set at 450 nm, the *strip-chart moving*, the pen control off, and the magnetic stirrer on, chromium(II) stock solution (0.1–0.4 ml) was introduced into the cuvette with a 1-ml hypodermic syringe.  By the time the Cary cell compartment cover was replaced, the magnetic stirrer turned off, and the pen turned on, approximately 10 sec had elapsed (see Figure 2).  The change in optical density was followed until equilibrium was reached.  Then, without stopping the strip-chart, the wavelength was changed to 327 nm.  A slow linear decrease in optical density was observed.  Since the chromium(III) species were virtually at equilibrium and since $\epsilon_{Cr(CN)_6^{3-}} - \epsilon_{Cr(CN)_5OH^{3-}}$ at 327 nm is only about 10 $M^{-1}$ $cm^{-1}$, the decay in optical density must have been due to oxidation of the chromium(II).  Extrapolation back to zero time allowed us to calculate the zero-time concentration of chromium(II).  It is this

**Table II:** Summary of Kinetic Data ($T = 25°$, Ionic Strength $= 1.00\ M^a$)

| Run | [NaOH], $M$ | [NaCN], $M$ | [NaClO$_4$], $M$ | [Cr-(CN)$_6$$^{3-}$], $M \times 10^{-3}$ | [Cr-(CN)$_5$OH$^{3-}$], $M \times 10^{-4}$ | [Cr(II)], $M \times 10^{-4}$ | $\dfrac{[\text{NaOH}]}{[\text{NaCN}]}$ | $K_3k_2$, $M^{-1}\,sec^{-1}$ | $k_{-2}$, $M^{-1}\,sec^{-1}$ | $K_3K_2$ |
|---|---|---|---|---|---|---|---|---|---|---|
| 1 | 0.092 | 0.117 | 0.73 | 8.9 | 1.3 | 1.19 | 0.79 | 167 | 199 | 0.83 |
| 2 | 0.23 | 0.46 | 0.23 | 9.1 | 1.1 | 1.04 | 0.50 | 156 | 196 | 0.78 |
| 3 | 0.23 | 0.68 | 0 | 8.4 | 1.0 | 1.08 | 0.34 | 154 | 197 | 0.78 |
| 4 | 0.23 | 0.24 | 0.46 | 9.0 | 1.4 | 1.02 | 0.96 | 142 | 178 | 0.80 |
| 5 | 0.46 | 0.24 | 0.23 | 9.5 | 0.9 | 1.00 | 1.92 | 144 | 181 | 0.79 |
| 6 | 0.46 | 0.33 | 0.14 | 9.5 | 1.2 | 1.04 | 1.39 | 145 | 176 | 0.83 |
| 7 | 0.46 | 0.46 | 0 | 9.6 | 1.3 | 1.03 | 1.00 | 136 | 175 | 0.77 |
| 8 | 0.46 | 0.46 | 0 | 17.8 | 1.9 | 1.02 | 1.00 | 150 | 178 | 0.85 |
| 9 | 0.46 | 0.46 | 0 | 4.4 | 0.5 | 1.09 | 1.00 | 155 | 192 | 0.80 |
| 10 | 0.43 | 0.46 | 0 | 8.6 | 0.9 | 2.00 | 0.93 | 163 | 190 | 0.86 |
| 11 | 0.48 | 0.47 | 0 | 9.6 | 1.1 | 0.51 | 1.02 | 149 | 177 | 0.84 |
| 12 | 0.46 | 0.46 | 0 | 9.1 | 1.7 | 1.05 | 1.00 | 148 | 181 | 0.82 |
| 13 | 0.094 | 0.113 | 0.74 | 9.1 | 1.5 | 1.04 | 0.83 | 148 | 178 | 0.83 |
| 14$^a$ | 0.094 | 0.113 | 0 | 8.8 | 1.1 | 0.98 | 0.83 | 58 | 81 | 0.72 |
| 15$^b$ | 0.46 | 0.46$^b$ | 0 | 9.1 | 1.04 | 1.06 | 1.00 | 262 | 287 | 0.91 |
|  |  |  |  |  |  |  |  | 150 ± 9$^c$ | 184 ± 9$^c$ | 0.81 ± 0.03$^c$ |

$^a$ Ionic strength for run 14 was 0.26 $M$ (average for all other runs was 0.99 ± 0.025 $M$). Ionic strength $=$ [NaCN] $+$ [NaOH] $+$ [NaClO$_4$] $+$ 6[Cr(CN)$_6$$^{3-}$]. $^b$ KCN instead of NaCN. $^c$ Average for runs 1–13.

concentration which is reported in Table II. The decay rate of the chromium(II) was always less than $10^{-3}$ sec$^{-1}$, but varied from experiment to experiment. It did increase with stirring, suggesting that there was a slight air leak. This is why the stirring was stopped as soon as possible. The decay rate (without stirring) was considered when calculating the rate constants for the catalyzed aquation. In a final step the chromium-(II) was oxidized by aeration and the spectrum of the equilibrium mixture of the chromium(III) species was taken.

*Electrochemical Measurements.* Cyclic voltammograms[16] were obtained at a hanging mercury drop[17] using a three-electrode system with solid-state potentiostat and functional generator.[18] Data were recorded from the oscilloscopic CRT display with a Polaroid camera. The cell[16] used permitted thorough deaeration and exclusion of oxygen. Repetitive cyclic voltammograms were recorded for the hexacyanochromate(III) and pentacyanomonohydroxychromate(III) complexes. The only results which we shall discuss in this paper were obtained with a supporting electrolyte of 0.05 $M$ NaCN, 0.05 $M$ NaOH, and 0.9 $M$ NaClO$_4$, and sweep rates varying from 0.2 to 20 V/sec. The potential range of the scan was between $-0.8$ and $-1.7$ V *vs.* sce. Although preliminary cyclic voltammetric studies gave us some insight as to the general nature of the reactions, we could not quantitate the homogeneous rate constants with sufficient precision. Once the kinetic data had been obtained by a more classical approach the electrochemical behavior was easily rationalized.

### Results and Discussion

The kinetic data are shown in Table II. The con-

stants reported were evaluated using a nonlinear least-square program which minimizes the error between the theoretical and experimental absorbances (at 450 nm) for a given kinetic run. Since the concentration of hexacyanochromate(III) complex is at least 0.005 $M$ in order to obtain reasonable optical densities (in a 1-cm cell), aquation effects a significant variation in the cyanide and hydroxide ion concentrations. Thus, assumptions based on a proposed stoichiometry and mechanism for the reaction were introduced into the calculation.

*Mechanism.* Two reactions are considered: an electron transfer

$$Cr(CN)_6{}^{3-} + Cr(CN)_5OH^{4-} \underset{k_{-2}}{\overset{k_2}{\rightleftharpoons}}$$

$$Cr(CN)_6{}^{4-} + Cr(CN)_5OH^{3-} \quad (2)$$

and a rapid equilibrium

$$Cr(CN)_6{}^{4-} + OH^- \overset{K_3}{\rightleftharpoons} Cr(CN)_5OH^{4-} + CN^- \quad (3)$$
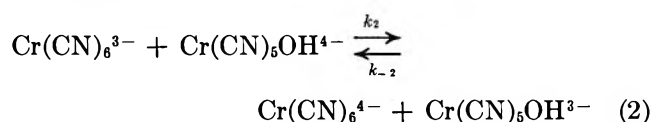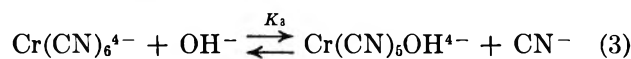
Since the p$K_a$ for the pentacyanomonoaquochromate-(III) complex is about 9, it seems reasonable that the hydroxy form predominates at pH $>11$. Although the p$K_a$ for the pentacyanomonoaquochromate(II) complex has not been determined, we assume that the fraction of chromium(II) present as the aquo form is negligible and that it is the hydroxy form which reacts

(16) For a description and theory of the technique of cyclic voltammetry, see R. S. Nicholson and I. Shain, *Anal. Chem.*, **36**, 706 (1964), and references cited therein.

(17) Metrohm-Brinkman Instruments, Inc., Westbury, N. Y.

(18) See, as an example, T. R. Muller and H. C. Jones, *Chem. Instrum.*, **2**, 65 (1969), or J. L. Huntington and D. G. Davis, *ibid.*, **2**, 83 (1969), and references cited therein.

with the hexacyanochromate(III). The kinetic data show that the backward rate of reaction 2 is independent of the cyanide and hydroxide ion concentrations, while the forward rate is proportional to the $[OH^-]/[CN^-]$ ratio. Since the spectrum of $Cr(CN)_6^{4-}$ does not seem to change even when the ratio $[OH^-]/[CN^-] = 5$, the implication is that

$$K_3 = \frac{[Cr(CN)_5OH^{4-}][CN^-]}{[Cr(CN)_6^{4-}][OH^-]} \ll 1 \qquad (4)$$

and

$$[Cr(CN)_6^{4-}] \approx [Cr(II)] \qquad (5)$$

Combining eq 2–5 gives the rate expression

$$\frac{d[Cr(CN)_6^{3-}]}{dt} = [Cr(II)]\{k_{-2}[Cr(CN)_5OH^{3-}] -$$

$$k_2K_3[Cr(CN)_6^{3-}][OH^-][CN^-]\} \qquad (6)$$

The values for the rate parameters based on runs 1–13, Table II are: $K_3k_2 = 150 \pm 9$ $M^{-1}$ sec$^{-1}$, $k_{-2} = 184 \pm 9$ $M^{-1}$ sec$^{-1}$, $K_3K_2 = K_3k_2/k_{-2} = 0.81 \pm 0.03$.

Run 14 (Table II) demonstrates the effect of decreasing the ionic strength from 1 $M$ to 0.26 $M$. The decrease in both $K_3k_2$ and $k_{-2}$ is to be expected, since the reacting species are all negatively charged. Run 15, in which KCN has been used rather than NaCN, demonstrates that the potassium ion enhances electron transfer. We were particularly concerned about this point, since we were using the potassium salt of the hexacyanochromate(III) complex. In light of the data of run 15 and the low concentrations of potassium ion in all other runs we feel safe in ignoring this effect.

The range of concentrations for these studies was limited by several factors: when the cyanide concentration was $<0.1$ $M$ we noted the appearance of the aquohydroxychromate(III) as an aquation product. The same phenomenon was also noted when the ratio $[OH^-]/[CN^-]$ exceeded 2. It is rather surprising that the next aquation product to appear is the aquohydroxy form rather than any of the intermediate cyanoaquohydroxy species. The tricyanotrihydroxychromate(III) species will spontaneously aquate to the aquohydroxy complex, but this process is considerably slower than the rate of appearance we observe for the aquohydroxy complex.[4] The implication is that there is enough aquohydroxychromate(II) to effect a significant rate of aquation of chromium(III) to the aquohydroxychromate(III). This phenomenon will be the subject of a future publication. Because of the limited range of experimental conditions the seemingly straightforward mechanism that we deduce may be considerably oversimplified.

The question of inner- vs. outer-sphere mechanism cannot be unambiguously resolved. There are a number of facts which circumstantially support an outer-sphere electron transfer mechanism but which do not preclude an inner-sphere mechanism. The kinetics exhibit a first-order dependence on both chromium(II) and chromium(III) species, but of course a short-lived bridged intermediate could be introduced without changing the overall mechanism. Replacing the sodium cation with potassium cation (run 15, Table II) causes a threefold increase in the rates—this seems in accord with the effect described by Shporer, Ron, Loewenstein, and Navon[19] in their studies of the outer-sphere ferricyanide–ferrocyanide electron transfer kinetics. There were indications that the presence of mercury metal in the reaction vessel caused an apparent increase in the reaction rates—this would certainly support an outer-sphere mechanism unless one postulated an inner sphere type electron transfer between chromium species and the mercury surface.[20] There is no spectrophotometric evidence for Cr–NC linkages, but these isomers are clearly less stable (or they would appear as products) and may exist as short-lived intermediates.

Birk and Espenson[21] have argued that electron transfer between Cr(II) and $Cr(CN)(H_2O)_5^{2+}$ proceeds by an inner-sphere mechanism in acidic media. Their argument states that since there is no loss of bound cyanide from the chromium(III) complex (i.e., no aquation) that cyanide must act as a bridging ligand. In our reaction such a mechanism would also preclude aquation if cyanide were the bridging ligand, and if the bridging reaction involved displacement of the hydroxide from the pentacyanomonohydroxychromate(II) species. It is certainly possible that this nonaquating inner-sphere electron transfer parallels our proposed mechanism and could be detected by isotope exchange studies of the type described by Birk and Espenson.

If the mechanism we have presented is essentially correct we can speculate on the distribution of the chromium(II) species. Although we had hoped to be able to measure $K_3$ spectrophotometrically, efforts here were thwarted by the previously described difficulties of generating Cr(II) when $[OH^-]/[CN^-] > 2$. The spectral and kinetic data do indicate, however, that when $[OH^-]/[CN^-] \leq 5$ it is reasonable to assume that the chromium(II) is nearly 100% in the form of the hexacyanochromate(II) complex. In the context of the precision of our data we can estimate

$$\frac{Cr(CN)_5OH^{4-}}{Cr(CN)_6^{4-}} < 0.10 \qquad (7)$$

Since the ratio $[OH^-]/[CN^-]$ did not exceed 5 we can state

$$K_3 < 0.02 \qquad (8)$$

(19) M. Shporer, G. Ron, A. Loewenstein, and G. Navon, Inorg. Chem., 4, 361 (1965).

(20) D. J. Barclay, E. Passeron, and F. C. Anson, ibid., 9, 1024 (1970).

(21) J. P. Birk and J. H. Espenson, J. Amer. Chem. Soc., 90, 2266 (1968).

One can define

$$K_9 = K_w \frac{[Cr(CN)_5OH^{4-}]}{[Cr(CN)_5H_2O^{3-}][OH^-]} \qquad (9)$$

where $K_w = 10^{-14} \, M^{-2}$. Combining eq 9 with the expressions for $K_1$ and $K_3$ gives

$$K_1 = \frac{K_9}{K_3 K_w} \qquad (10)$$

If we were to assume $K_9$ is $10^{-11}$ (the $K_a$ for pentacyanomonoaquochromate(III) is $10^{-9}$) and that 0.1 is an upper limit for $K_3$, we would conclude that $K_1 = 10^4 \, M^{-1}$. This is at odds with the estimate of 9.55 $M^{-1}$ by Davies, et al.[11]

*Description and Rationalization of the Electrochemical Results.* The most dramatic cyclic voltammograms were obtained with pentacyanomonohydroxychromate-(III) as the starting material (Figure 3). On the first cathodic sweep a single cathodic wave is observed with a peak potential at $-1.62$ V (vs. sce). This wave corresponds to the irreversible reduction

$$e^- + Cr(CN)_5OH^{3-} \xrightarrow{k_{hf_{11}}, \alpha_{11}} Cr(CN)_5OH^{4-} \qquad (11)$$
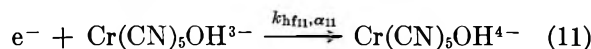
Labile pentacyanomonohydroxychromate(II) is rapidly converted (by reaction 3) into the hexacyanochromate-(II) complex. Thus, on the anodic cycle we observe a peak corresponding to the reversible oxidation of hexacyanochromate(II) to hexacyanochromate(III).

$$e^- + Cr(CN)_6^{3-} \underset{\longleftarrow}{\overset{k_{hs_{12}}, \alpha_{12}}{\longrightarrow}} Cr(CN)_6^{4-} \qquad (12)$$
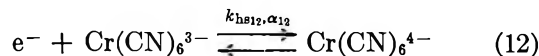
On subsequent cycles we see the development of the cathodic wave corresponding to the reduction of the hexacyanochromate(III). In the steady-state voltammogram the reversible process (reaction 12) predominates. The second cathodic reaction manifests itself as a small bump on the tail of the first cathodic peak.

The addition of a small amount of surfactant ($<0.01\%$ gelatin) effected a marked cathodic shift in the position of the irreversible wave while having a much smaller effect on the position of the reversible couple. This is good evidence that the irreversibility of reaction 11 is due to a slow, heterogeneous process (electron transfer or adsorption) rather than to a rapid, irreversible, homogeneous chemical reaction following a reversible electron transfer.

Analysis of the shape of the irreversible peak[16] indicated that the transfer coefficient, $\alpha_{11}$, is about 0.75, and from the potential of the peak we calculated that $k_{hf_{11}} = 5.9 \times 10^{-22}$ cm sec$^{-1}$ (based on potential vs. sce and $\alpha_{11} = 0.75$). Using the literature values for the heterogeneous parameters for reaction 12,[12-14] and our experimental results for $k_{hf_{11}}$, $\alpha_{11}$, $k_2K_3$, and $k_{-2}$, we calculated[22] a theoretical cyclic voltammogram (Figure
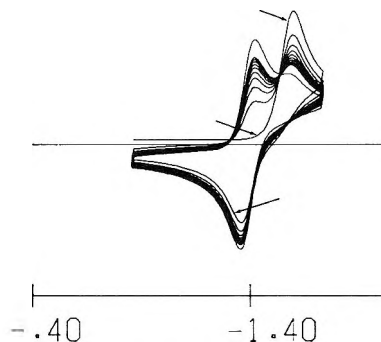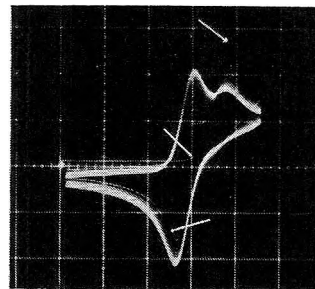
Figure 3. Top: experimental repetitive cyclic voltammogram, $[Cr(CN)_5OH^{3-}] = 0.0032 \, M$, $[NaCN] = 0.05 \, M$, $[NaOH] = 0.05 \, M$, $[NaClO_4] = 0.9 \, M$, scan rate = 16.0 V sec$^{-1}$, $T = 25°$. Bottom: theoretical cyclic voltammogram of the same system as above. Shown here are the first ten cycles followed by a single cycle obtained at steady state. Arrows denote the first cycle. The rate parameters are $K_3k_2 = 150 \, M^{-1}$ sec$^{-1}$, $k_{-2} = 184 \, M^{-1}$ sec$^{-1}$, $k_{hf_{11}} = 5.9 \times 10^{-22}$ cm sec$^{-1}$, $\alpha_{11} = 0.75$, $E_{12}^0 = -1.39$ V (vs. sce), $k_{hs_{12}} = 0.25$ cm sec$^{-1}$, $\alpha_{12} = 0.5$, diffusion coefficients for all species = $7 \times 10^{-6}$ cm$^2$ sec$^{-1}$, and differential double layer capacitance = $20 \times 10^{-6}$ F cm$^{-2}$. Scales: horizontal, 0.2 V/graticule division; vertical, $3.3 \times 10^{-3}$ amp cm$^{-2}$ graticule division.

3). The similarity to the experimental voltammogram is striking; we believe that it is added verification of the mechanism we have proposed.

Cyclic voltammetry of hexacyanochromate(III) as the starting material exhibited much less dramatic behavior. The first cycle exhibited peaks corresponding to the reversible couple only; the second cathodic peak appeared only gradually on subsequent cycles. The steady-state voltammogram was the same as the steady state obtained for the pentacyanomonohydroxychromate(III) complex (Figure 2).

It is possible to express the parameters $k_{hs_{11}}$ and $E_{11}^0$ in terms of equilibrium constant $K_3$ and $E_{12}^0$. On the basis of reactions 2, 11, and 12

$$E_{11}^0 = E_{12}^0 - \frac{RT}{F} \ln K_2 \qquad (13)$$

Thus

$$k_{hs_{11}} = k_{hf_{11}} K_2^{+\alpha_{11}} \exp\left(\frac{-\alpha_{11}F}{RT}E_{12}^0\right) \qquad (14)$$

(22) S. Feldberg, "Electroanalytical Chemistry," Vol. 3, A. J. Bard, Ed., Marcel Dekker, New York, N. Y., 1969, p 199.

and since

$$K_3 K_2 = 0.8 \qquad (15)$$

$$k_{\mathrm{hs_{11}}} = k_{\mathrm{hf_{11}}} \times 0.8^{+\alpha_{11}} K_3^{-\alpha_{11}} \exp\!\left(\frac{-\alpha_{11} F}{RT} E_{12}{}^0\right) \qquad (16)$$

In the basis of our "guesstimate" that $K_3 < 0.02$ (eq 8), then

$$k_{\mathrm{hs_{11}}} > 4 \times 10^{-3} \ \mathrm{cm \ sec^{-1}} \qquad (17)$$

$$E_{11}{}^0 < -1.48 \ \mathrm{V} \qquad (18)$$

# Donor–Acceptor Complexes of Phenothiazine and Phenoxazine

# with Nickel Thiete[1]

by William E. Geiger, Jr.,*[2] and August H. Maki

*Department of Chemistry, University of California, Riverside, California 92502* (*Received February 16, 1971*)

*Publication costs borne completely by The Journal of Physical Chemistry*

Molecular complexes of bis-*cis*-(1,2-perfluoromethylethylene-1,2-dithiolato)nickel (nickel thiete) with phenothiazine and phenoxazine were prepared and studied by a variety of physical methods, including electron spin resonance, magnetic susceptibility, and electronic absorption spectroscopy. The solid complexes are ionic, but solvent-dependent equilibria between ionic and neutral materials exist in solution. In dichloromethane solutions complicated ion-pairing phenomena are found, and evidence is presented for the existence of a donor–acceptor complex with an ionic ground state in certain solutions of phenothiazine–nickel thiete. Solid phenothiazine–nickel thiete also shows a strong charge-transfer band. Differences in the magnetic susceptibilities and optical spectra of the solid complexes are interpreted to result from differences in their crystal packing.

## Introduction

Complexes between $\pi$ donors (D) and $\pi$ acceptors (A) in which the ground state is ionic (D$^+$A$^-$) are well known.[3] Cases in which D$^+$ and A$^-$ are both radical ions have been investigated,[4] but these studies, particularly those which have dealt with the solution properties of these complexes, have usually been hindered by the instability of one or more of the species involved.[5–11] Electron spin resonance (esr) studies of such complexes have frequently been unable to distinguish between paramagnetism indigenous to the complex and that due to decomposition products frequently undergoing resonance in the same region ($g \approx 2.00$). Furthermore, if D$^+$ and A$^-$ are both organic free radicals their esr signals are usually difficult to distinguish. This paper presents a study of the complexes formed between the organic donors phenothiazine (PTZ) and phenoxazine (POZ) and the metal complex acceptor bis-*cis*-(1,2-perfluoromethylethylene-1,2-dithiolato)-nickel, or nickel thiete (NiTh).[12]
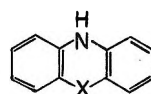


X=S, PTZ
X=O, POZ
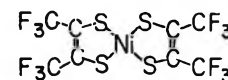
NiTh

The work was undertaken because NiTh offers several advantages over previously investigated acceptors. It

(1) Abstracted from the Ph.D. Thesis of William E. Geiger, Jr., Cornell University, Ithaca, N. Y., Jan 1970.

(2) Department of Chemistry, Southern Illinois University, Carbondale, Ill. 62901.

(3) R. S. Mulliken and W. B. Person, "Molecular Complexes," Wiley-Interscience, New York, N. Y., 1969.

(4) For leading references see R. Foster, "Organic Charge-Transfer Complexes," Academic Press, New York, N. Y., 1969, Chapter 11, and ref 3, Chapter 16.

(5) R. E. Miller and W. F. K. Wynne-Jones, *J. Chem. Soc.*, 2375 (1959).

(6) R. Foster and T. J. Thomson, *Trans. Faraday Soc.*, 58, 860 (1962).

(7) W. Liptay, G. Briegleb, and K. Schindler, *Z. Elektrochem.*, 66, 331 (1962).

is an extremely powerful oxidizing agent, is stable in air when neutral and as mono- and di-negative ions, has an esr signal (as a monoanion) displaced from the free spin value ($g = 2.06$), and has rich and characteristic electronic spectra in all oxidation states.

## Experimental Section

Phenothiazine–nickel thiete (PTZ–NiTh) was formed by mixing dichloromethane solutions containing equimolar amounts of NiTh[13] and phenothiazine (Eastman, three times recrystallized from toluene). The dark brown precipitate was washed repeatedly with pentane, dried *in vacuo*, and purified by recrystallizations from either benzene or chloroform. Analysis was satisfactory for a 1:1 complex (Calcd: C, 33.8; S, 22.6; H, 1.3. Found: C, 33.6; S, 21.0; H, 2.0). Phenoxazine (Aldrich, recrystallized from ethanol–water)–nickel thiete (POZ–NiTh) was made similarly and recrystallized from benzene (Calcd: C, 34.6; S, 18.5; H, 1.3. Found: C, 34.9; S, 18.7; H, 2.1). Tetrabutylammonium nickel thiete[14] and phenothiazonium perchlorate[15] were prepared using literature methods. Other materials were reagent grade, and used as commercially available.

Absorption spectra were recorded over the range 2600 to 250 nm ($3.85 \times 10^3$ to $40 \times 10^3$ cm$^{-1}$) on a Cary Model 14 spectrophotometer. Solid state spectra were obtained as pressed KBr or NaCl disks. Nujol mulls gave spectra which were qualitatively similar, but of poorer resolution. Solution spectra at ambient temperatures were obtained in matched 10-mm quartz cells using pure solvent in the reference compartment. Extinction coefficients and band maxima were determined for the donors and acceptor in their neutral and monoionic oxidation states in all solvent systems studied, except for POZ$^+$, which was only studied in sulfuric acid, the medium used for its generation. The values obtained agreed with literature values, whenever a comparison was possible. Low-temperature solution spectra were obtained by inserting the sample cell contained in a brass holder into a dewar which was cooled by pouring a small amount of liquid nitrogen into it. The cooled sample was allowed to warm slowly and the temperature was monitored by means of a glass-encased thermocouple wire inserted into the sample solution.

Esr data were obtained with a Varian V-4500 esr spectrometer. Relative spin concentration measurements were made by integrating the first derivative esr signal using a Philbrick integrator, Model UPA-2, and then integrating a second time using a planimeter. Absolute determinations of spin concentrations in dichloromethane solutions of the complexes were made by comparing signal intensities of solutions containing the complexes with the signal intensity of a standard solution of tetrabutylammonium nickel thiete, under the identical experimental conditions. The values

obtained were reproducible and were practically identical to values obtained using the free radical diphenylpicrylhydrazyl as a quantitative internal standard.

Magnetic susceptibility measurements were made on a Faraday balance using a Varian V-4007 6-in. magnet and V-4086-5 pole caps in conjunction with a Cahn electrobalance. The temperature was varied by blowing cold nitrogen at a controlled rate past a tube sheathing the sample, and was monitored by means of a thermocouple close to the sample. Calibration was achieved using HgCo(CNS)$_4$ as a standard.[16]

## Results

*A. Solid Complexes.* McConnell[17] has shown theoretically that the crystalline form of a donor–acceptor complex should have either a neutral (D–A) or ionic (D$^+$A$^-$) ground state, but that mixtures of the two forms are not expected. The spectrum of the complex of phenothiazine with nickel thiete (PTZ–NiTh) in a KBr matrix is shown in Figure 1 and indicates the presence of an ionic ground state for the solid material, *i.e.*, a structure composed of PTZ$^+$ and NiTh$^-$. The very intense band centered at about 1300 nm is not observed in the spectra of the possible components in the complex ground state (NiTh, NiTh$^-$, PTZ, or PTZ$^+$) and is assigned as a *reverse* charge-transfer band (D$^+$A$^-$ → D·A).[18] This is not without precedent, for Anex and Hill have reported such a band in the spectrum of crystalline tetramethylphenylenediamine–chloranil.[19]

The spectrum of solid phenoxazine–nickel thiete (POZ–NiTh) in KBr (Figure 2) is dominated by ionic bands at 810 nm (NiTh$^-$) and 547 nm (POZ$^+$). Bands were present at 720 and 1250 nm which were absent from the solid-state spectra of NiTh, NiTh$^-$, and POZ, and the solution spectrum of POZ$^+$. Since the solid spectrum of POZ$^+$ was not obtained, these two bands

(8) I. Isenberg and S. L. Baird, Jr., *J. Amer. Chem. Soc.*, **84**, 3803 (1962).

(9) J. W. Eastman, G. Englesma, and M. Calvin, *ibid.*, **84**, 1339 (1962).

(10) G. T. Pott and J. Kommandeur, *Mol. Phys.*, **13**, 373 (1967).

(11) D. Romans, W. H. Bruning, and C. J. Michejda, *J. Amer. Chem. Soc.*, **91**, 3859 (1969).

(12) The following abbreviations are used in this paper: PTZ (phenothiazine), PTZ$^+$ (phenothiazonium free radical ion), POZ (phenoxazine), POZ$^+$ (phenoxazonium free radical ion), NiTh (nickel thiete), NiTh$^-$ (nickel thiete anion), TBAP (tetrabutylammonium perchlorate), NiTh–PTZ or NiTh–POZ (molecular complex formed between nickel thiete and phenothiazine or phenoxazine), and TBA-NiTh (tetrabutylammonium nickel thiete).

(13) A. Davison, N. Edelstein, R. H. Holm, and A. H. Maki, *Inorg. Chem.*, **2**, 1227 (1963).

(14) A. Davison and R. H. Holm, *Inorg. Syn.*, **10**, 19 (1967).

(15) J-P. Billon, *Ann. Chim.*, **7**, 204 (1962).

(16) B. N. Figgis and R. S. Nyholm, *J. Chem. Soc.*, 4190 (1958).

(17) H. M. McConnell. B. M. Hoffman, and R. M. Metzger, *Proc. Nat. Acad. Sci.*, **53**, 46 (1965).

(18) Reference 3, p 254 ff.

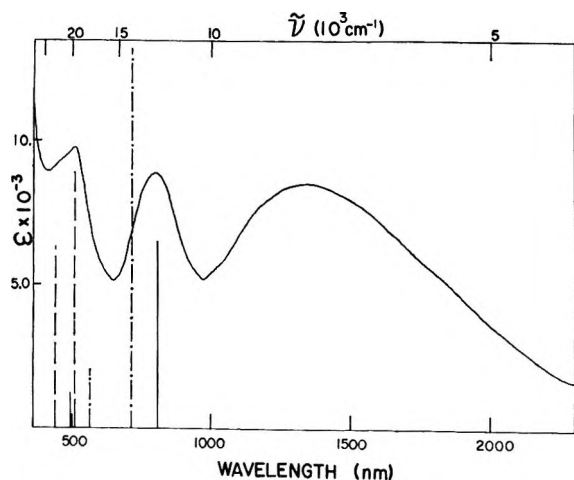(19) B. G. Anex and E. B. Hill, *J. Amer. Chem. Soc.*, **88**, 3648 (1966).

Figure 1. Optical absorption spectrum of PTZ–NiTh in KBr at +29°. The vertical lines denote the positions of band maxima of: ——, TBA–NiTh in KBr; –·–·, NiTh in KBr; – – – –, PTZ$^+$ClO$_4^-$ in KBr. Extinction coefficients were derived from dichloromethane solutions except for PTZ–NiTh, which is plotted on an arbitrary scale.
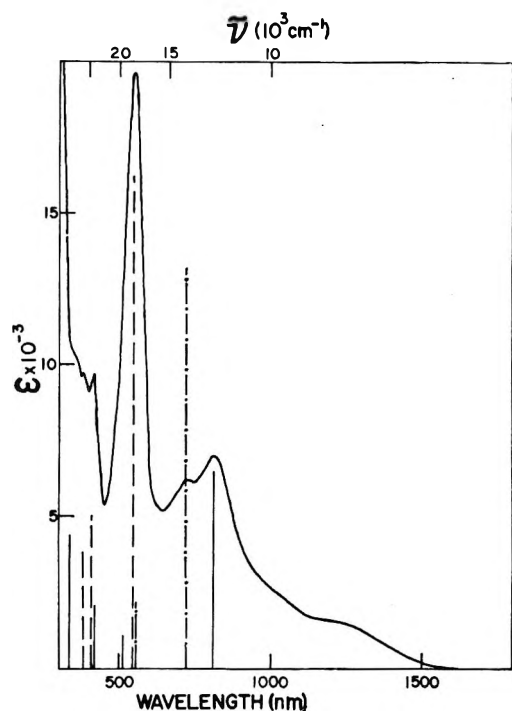


Figure 2. Optical absorption spectrum of POZ–NiTh in KBr at 29°. The vertical lines denote positions of band maxima of: ——, TBA–NiTh in KBr; –·–·, NiTh in KBr; – – – –, POZ$^+$ in H$_2$SO$_4$. Extinction coefficients were derived from solution studies, except for POZ–NiTh, which is plotted on an arbitrary scale.

must be considered unassigned, but the longer wavelength absorption is probably a charge transfer transition, although of considerably weaker intensity than that observed for PTZ–NiTh. Possible assignment of the 720-nm band to neutral nickel thiete is considered unlikely both from McConnell's results[17] and from pre-

liminary X-ray crystallographic data[20] on POZ–NiTh which indicate one molecule per unit cell, ruling out the possibility of a "mol-ionic" lattice, consisting of complexes in both neutral and ionic ground states.[10]

The esr spectra of both complexes showed a broad (~250 G wide) structureless single line at room temperature, having a $g$ value near 2.030. This $g$ value is approximately an average of the isotropic donor and acceptor $g$ values, and is indicative of an exchange interaction between electrons on donor and acceptor sites which is large compared with the difference in Zeeman energies ($J \gg \Delta g\beta H \approx 2 \times 10^{-2}$ cm$^{-1}$) of the two sites. The integrated intensity of the esr line for the phenothiazine complex decreases with decreasing temperature, in qualitative agreement with the results of bulk susceptibility measurements (vide infra). Spectra of PTZ–NiTh at 77°K and 4°K reveal only a weak residual three-line signal, the features of which are identical to those reported for polycrystalline samples of NiTh$^-$.[13] The low-temperature esr spectrum of the phenoxazine complex was not investigated.

The bulk magnetic susceptibility properties of these complexes were very dissimilar (Table I). The phenothiazine complex was weakly paramagnetic at room temperature and became even less so at lower temperatures. However, the phenoxazine complex followed a Curie–Weiss law dependence down to $T = 77°$K with two unpaired spins per ion pair.

Table I: Values of $X_M^C$, the Molar Magnetic Susceptibility (Corrected for Diamagnetism), vs. $T$ for Phenothiazine–Nickel Thiete and Phenoxazine–Nickel Thiete (the diamagnetic corrections to the susceptibilities were calculated from Pascal's constants[a] as $X_M$(PTZ) $= -118 \times 10^{-6}$, $X_M$(POZ) $= -108 \times 10^{-6}$, $X_M$(NiTh) $= -195 \times 10^{-6}$)

| | $X_M^C$, emu/mol $\times 10^6$ | |
|---|---|---|
| $T$, °K | PTZ–NiTh | POZ–NiTh |
| 295 | 370 | 2080 |
| 279 | 333 | 2180 |
| 255 | 277 | 2340 |
| 226 | 222 | 2580 |
| 183 | 169 | 3020 |
| 143 | 153 | 3580 |
| 104 | 150 | 4310 |
| 77 | 147 | 5170 |

[a] P. W. Selwood, "Magnetochemistry," Interscience, New York, N. Y., 1956, p 91.

B. *Solution Behavior.* The dissolved complexes are best treated in terms of the equilibria

$$D + NiTh \underset{}{\overset{K_1}{\rightleftarrows}} D^+ \cdot NiTh^- \underset{}{\overset{K_2}{\rightleftarrows}} D^+ + NiTh^- \quad (1)$$
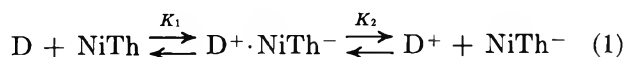
where D and NiTh denote the neutral components (D is either phenothiazine or phenoxazine); the ions, D$^+$

(20) We are grateful to Dr. Richard Schmitt for performing these measurements for us.
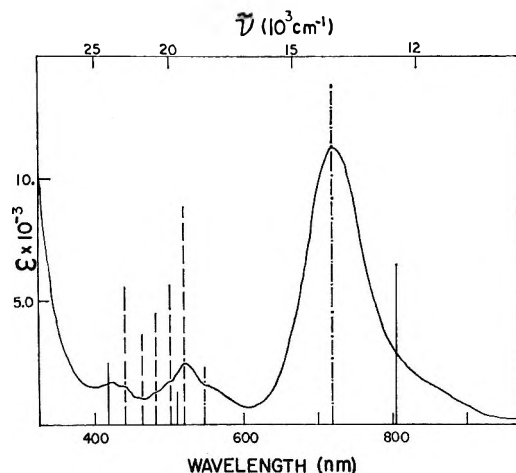
Figure 3. Optical absorption spectrum of a $10^{-4}$ $F$ solution of PTZ–NiTh in dichloromethane at 29°. The vertical lines denote positions and intensities of band maxima in dichloromethane of: ———, TBA–NiTh; ····, NiTh; – – –, PTZ$^+$ ClO$_4^-$.

and NiTh$^-$, are "free" or solvated, and D$^+$·NiTh$^-$ denotes a complex having an ionic ground state.

*Optical Spectra of Phenothiazine–Nickel Thiete.* The electronic absorption spectrum of a $1 \times 10^{-4}$ $F$ solution of PTZ–NiTh in dichloromethane at ambient temperature ($T \sim 29°$) is shown in Figure 3. This spectrum indicates the presence of NiTh and NiTh$^-$ as well as PTZ$^+$. Neutral PTZ is transparent in this region, but was identified by a strong band at 254 nm. Thus the spectrum is a composite arising from bands due to both neutral and ionic components. A quantitative estimate of the relative concentrations of these components was made by noting that the apparent extinction coefficient of the band at 720 nm due to neutral nickel thiete is 0.86 times that of the corresponding band in a standard solution of nickel thiete in dichloromethane. We take this to mean that at this temperature about 86% of the acceptor is present as neutral molecules, and that, by difference, 14% is ionic. It is important to note that a change-transfer band (not shown in Figure 3) is present in this solution as a broad, weak absorption centered at about 1220 nm. The assignment of an ionic ground state (*i.e.*, D$^+$·A$^-$) to the charge-transfer complex was made on the basis of the spectra observed at this and lower temperatures. It must be noted that the charge-transfer complex will give an optical spectrum identical to that of the ground state components (*i.e.*, either D and A or D$^+$ and A$^-$) in addition to showing the charge-transfer band. Therefore the nature of the complex ground state can be assigned by observing how the temperature-dependent intensity of the charge-transfer band relates to the temperature-dependent intensities of the neutral and ionic bands. Figure 4 shows that at lower temperatures the band intensities originating from ionic species increase and those assigned to the neutral materials decrease. Concomitant with this in-
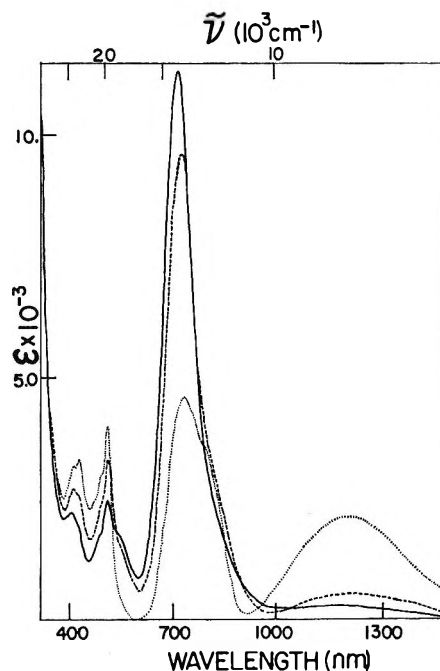
Figure 4. Optical absorption spectra of a $10^{-4}$ $F$ solution of PTZ–NiTh in dichloromethane at ———, 29°; – – – –, 13°; and ····, −31°.

crease in the ionic bands at lower temperatures is an increase in the charge-transfer band intensity, indicating that the complex has an ionic ground state.

The ionic concentrations vary greatly with solvent composition. For example, by employing procedures identical to those above, we find for the PTZ–NiTh complex at 29° about 2 mol % ions in toluene (dielectric constant, $\epsilon = 2.4$), 8% in chloroform ($\epsilon = 4.1$), and 100% in nitrobenzene ($\epsilon = 34.9$).

*Optical Spectra of Phenoxazine–Nickel Thiete.* The phenoxazine complex was expected to exhibit behavior similar to the phenothiazine complex because of the similarity of the structures and oxidation potentials of the donors.[21] Indeed, techniques identical to those applied to PTZ–NiTh gave the following estimates of mole per cent ions (either POZ$^+$ or NiTh$^-$) in various solvents at 29°: toluene, less than 1%; dichloromethane, 8% (Figure 5); nitrobenzene and acetonitrile, 100%. Spectra at reduced temperatures again indicated an increase in the ionic concentrations at the expense of the neutral materials. These changes were large enough to allow us to derive the pertinent thermodynamic quantities for the equilibria, as discussed below. The most significant difference in the spectra of the two complexes is the absence of a charge transfer absorption in all solutions of the phenoxazine complex which were studied.

*Esr Studies.* It was expected that the solution esr studies would give only the spectra of the free ions, D$^+$

(21) We measure polarographic half-wave potentials *vs.* the sce in dichloromethane–0.1 $M$ TBAP of +0.69 V for phenoxazine and +0.71 V for phenothiazine.
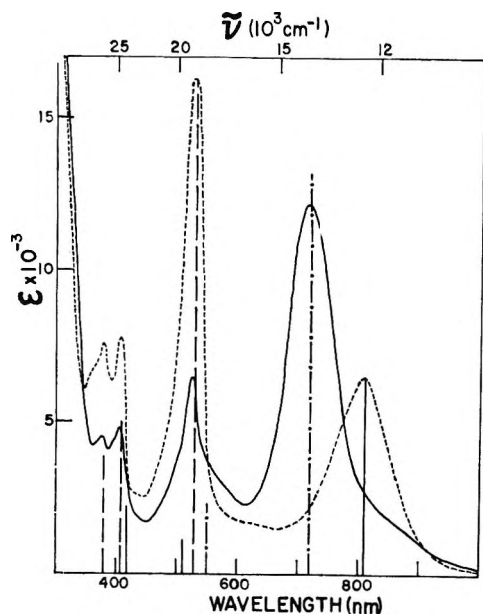
Figure 5. Optical absorption spectra at 29° of $10^{-4}$ $F$ POZ–NiTh in dichloromethane (solid line) and $10^{-4}$ $F$ POZ–NiTh in dichloromethane with $10^{-2}$ $M$ TBAP added (dashed line). The vertical lines give positions and intensities of band maxima observed for ———, TBA–NiTh in dichloromethane; -·-·, NiTh in dichloromethane; and - - -, POZ$^+$ in $H_2SO_4$.



Figure 6. First derivative esr spectra of a $10^{-4}$ $F$ PTZ–NiTh solution in dichloromethane at $+11°$ (top) and $-86°$ (bottom).

and NiTh$^-$ in eq 1, and no observable spectrum associated with the D·A complex, which would be either in a singlet or triplet state. A $1 \times 10^{-4}$ $F$ solution of PTZ–NiTh in dichloromethane solution at 11° exhibits the esr spectrum shown in Figure 6. The low-field line has $g = 2.061$, the isotropic $g$ value of NiTh$^-$,[13] and was assigned to the free acceptor anion. The quartet of lines at $g = 2.0048$ was characteristic of PTZ$^+$ spectra under conditions of low resolution and was assigned to the free donor cation ($g = 2.0051$[22]). The inter-
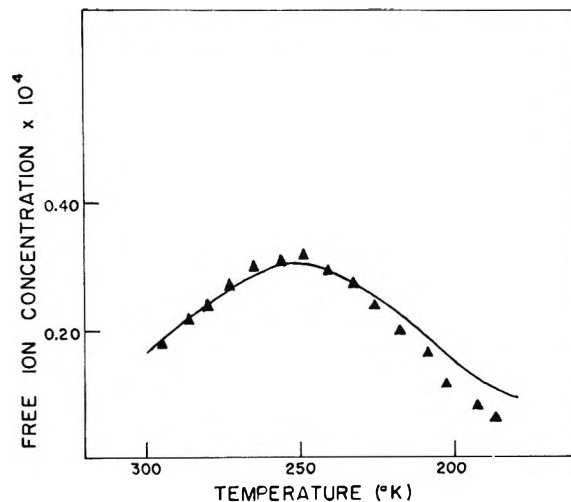


Figure 7. The temperature dependence of the free ion concentration ([NiTh$^-$] = [PTZ$^+$]) of a $10^{-4}$ $F$ solution of PTZ–NiTh in dichloromethane as measured by esr (▲). The curved line gives the free ion concentrations calculated using eq 2 together with the thermodynamic data listed in Table II.

grated intensities of the separated signals are nearly equal (measured 1 NiTh$^-$:1.1 PTZ$^+$). Vacuum degassing of the solution had no effect on the spectrum (PTZ$^+$ClO$_4^-$ yields a similar poorly-resolved four-line spectrum in dichloromethane at concentrations down to $10^{-5}$ $M$). By a measurement of the absolute number of spins in this sample, the concentrations of free ions NiTh$^-$ and PTZ$^+$ at 22° were each determined to be 18 mol % of the formal concentration of the complex. The intensity of the esr lines due to PTZ$^+$ at first increases as the temperature is lowered, but then decreases after reaching a maximum at $-23°$ (Figure 7). This concentration behavior of the free ions as measured by esr means that the monotonically increasing ionic band intensities which were observed at decreasing temperatures in the optical absorption spectra must be due to increasing amounts of a complex with an ionic ground state (PTZ$^+ \cdot$NiTh$^-$), and not merely to increasing free ion concentrations.

From room temperature to about $-20°$ the esr line due to NiTh$^-$ follows the same quantitative dependence as the PTZ$^+$ lines, but at still lower temperatures these measurements are complicated by the asymmetric broadening of the line (see Figure 6 for an example). Simple NiTh$^-$ salts with diamagnetic counterions (e.g., tetrabutylammonium nickel thiete) do not show asymmetric spectra under these conditions. Possible sources of this peculiar line shape are discussed below.

The esr spectra associated with $10^{-4}$ $F$ phenoxazine–nickel thiete in dichloromethane again showed the presence of donor and acceptor radical ions but showed no asymmetry over the investigated temperature range,

(22) B. C. Gilbert, P. Hanson, R. O. C. Norman, and B. T. Sutcliffe, Chem. Commun., 161 (1966).
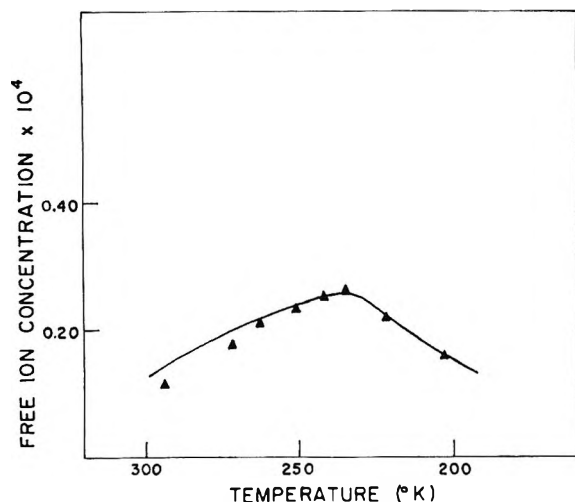
Figure 8. The temperature dependence of the free ion concentration ([NiTh⁻] = [POZ⁺]) of a $10^{-4}$ $F$ solution of POZ–NiTh in dichloromethane as measured by esr (▲). The curved line gives the free ion concentrations calculated using eq 2 together with the thermodynamic data listed in Table II.

from $+21$ to $-90°$. A quantitative experiment established that at $21°$ POZ⁺ (observed $g = 2.0040$) and NiTh⁻ were each present at 11.5 mole % of the formal complex concentration. The free ion concentration (Figure 8) passed through a maximum at about $-38°$.

*Effect of Added Electrolyte.* When a 100-fold excess of tetrabutylammonium perchlorate is added to dichloromethane solutions of the complexes the only species detectable by either optical absorption spectroscopy or esr are the free ions, D⁺ and NiTh⁻. Figure 5 shows the optical spectrum of a dichloromethane solution which is $10^{-4}$ $F$ in phenoxazine–nickel thiete and $10^{-2}$ $F$ in tetrabutylammonium perchlorate. There is apparently total conversion to the free ions. The same situation obtains for the case of excess tetrabutylammonium perchlorate added to a phenothiazine–nickel thiete solution in dichloromethane; only ionic bands are detected, at an intensity corresponding to 100% ions. No charge-transfer band is present, indicating that the excess of "innocent" counterions precludes any significant concentration of radical–radical ion pairs. The effect of excess tetrabutylammonium perchlorate on the esr spectra of dichloromethane solutions of the phenothiazine complex was also striking. In the presence of the electrolyte, the esr lines are symmetrical from room temperature down to the freezing point of the solvent. This is strong evidence that the line asymmetry observed in the absence of added electrolyte arises from ion pairing phenomena between the radical ions, PTZ⁺ and NiTh⁻.

*Calculation of Thermodynamic Parameters.* Quantitative measurements of the esr and optical spectra allow calculation of the equilibrium constants which

are involved in eq 1. The intensities of the sharp esr lines measure the free ion concentrations, whereas the ionic bands in the optical spectra measure the sum of the free ion and complex ion pair concentrations. The difference between these two quantities at any particular temperature was taken to give the complex ion pair concentration at that temperature. The assumption was made that complex ion pairs do not contribute to the esr sharp line signal intensity. Evidence for this assumption is presented below. Since by mass balance the neutral molecule concentrations at each temperature also can be determined, it is possible to derive the temperature dependence of the equilibria, and thus to obtain the thermodynamic parameters for these systems.

At $286°$K, the concentration of either NiTh⁻ of PTZ⁺ from phenothiazine–nickel thiete in dichloromethane as measured by optical spectroscopy is about $0.28$ $F$, where $F$ is the formal concentration of the complex ($1 \times 10^{-4}$). The esr experiment indicates the free ion concentration to be $0.22$ $F$, leaving $0.06$ $F$ as the concentration of ion pairs (PTZ⁺·NiTh⁻). By difference, $[PTZ] = [NiTh] = 0.72$ $F$. At $242°$K, we estimate from the intensities of the PTZ⁺ and NiTh⁻ optical bands that the ionic concentrations are $0.75$ $F$. Coupled again with the esr data (Figure 7), this yields $[PTZ⁺] = [NiTh⁻] = 0.30$ $F$, $[PTZ] = [NiTh] = 0.25$ $F$, and $[PTZ⁺·NiTh] = 0.45$ $F$. Since the optical estimate of the total ionic concentrations at $242°$K is subject to some error due to the overlapping bands, it is satisfying to note that the observed increase in the charge-transfer band intensity (a factor of 5.7) from 286 to $242°$K parallels the calculated increase in ion pairs over this range (a factor of 7.5). The thermodynamic parameters derived *via* this treatment are presented in Table II. These were calculated using $K_1 = 1.16 \times 10^3$ and $K_2 = 8.12 \times 10^{-5}$ at $286°$K, and $K_1 = 7.20 \times 10^4$, $K_2 = 2.00 \times 10^{-5}$ at $242°$K.

**Table II:** Thermodynamic Data for Eq 1

|  | PTZ–NiTh | POZ–NiTh |
|---|---|---|
| $\Delta H_1°$, kcal | $-12.8$ | $-7.9$ |
| $\Delta H_2°$, kcal | $4.4$ | $5.4$ |
| $\Delta G_1°$ (300°K), kcal | $-3.5$ | $-2.7$ |
| $\Delta G_2°$ (300°K), kcal | $5.4$ | $4.5$ |
| $\Delta S_1°$, cal/deg | $-30.8$ | $-17.2$ |
| $\Delta S_2°$, cal/deg | $-3.3$ | $+3.2$ |

These equilibrium constants were used to calculate the temperature dependence of the free-ion concentrations, which from simple considerations of the equilibria and mass balance conditions can be expressed as

$2[PTZ⁺] = 2[NiTh⁻] =$

$[K_2(K_2 + K_1^{-1} + 2K_2^{1/2}K_1^{-1/2} +$

$4 \times 10^{-4})]^{1/2} - K_2 - K_2^{1/2}K_1^{-1/2}$　(2)

A comparison between the calculated curves and the experimental data appears in Figure 7, and the agreement is satisfactory.

In a similar analysis of the phenoxazine–nickel thiete complex in dichloromethane ($10^{-4}$ $F$), 248 and 228°K were chosen as the reference temperatures, and the treatment yielded $K_1 = 1.64 \times 10^3$, $K_2 = 7.85 \times 10^{-5}$ at the higher temperature, and $K_1 = 6.60 \times 10^3$ and $K_2 = 3.00 \times 10^{-5}$ at the lower one. These values were obtained using total ion concentrations of 0.32 $F$ at 248°K and 0.45 $F$ at 228°K, together with the free ion concentrations from esr (Figure 8). The thermodynamic parameters are again given in Table II, and the calculated and experimental plots of the free ion concentrations appear in Figure 8.

We did not consider a least-squares fit of the calculated curves of Figures 7 and 8 to the esr intensity data to be worthwhile because of the considerable error in the optical data due to overlapping bands. Also, there is evidence from the low-temperature esr line shapes that chemical species other than those included in eq 1 are present (*vide infra*). The derived thermodynamic data in Table II should consequently be considered only as semiquantitative. The basic agreement with the temperature dependence of the free radical concentration based upon only two data points for each complex is, however, good evidence for the validity of the equilibria postulated in eq 1.

## Discussion

The formation of ions is favored in solvents of higher dielectric constant, consistent with expectations based on simple electrostatic considerations, and with the results of other investigators.[6,7] The technique of forcing complete dissociation of the radical–radical ionic complex by addition of tetrabutylammonium perchlorate may be useful for measuring physical characteristics (*e.g.*, optical extinction coefficients) for ions which are difficult to isolate. The low energy optical band detected for PTZ–NiTh in dichloromethane is noteworthy, for it is apparently the first reported observation of a charge-transfer transition for a dissolved radical ion complex pair in an ionic ground state. When conditions are such that the number of ion pairs between NiTh$^-$ and PTZ$^+$ are small (*e.g.*, in nitrobenzene solutions in which the complex is a fairly strong electrolyte, and in dichloromethane solutions doped with tetrabutylammonium perchlorate) no charge-transfer band is observed, even though the ionic optical band intensities are high.

The calculated entropy changes in $K_1$ are comparable to those typical of a dissociation into singly charged ions[23,24] and argue strongly that the complex has an ionic ground state with a large dipole moment, thus producing a significant ordering of the solvent dipoles.

The peculiar asymmetry of the NiTh$^-$ signal at low temperatures in dichloromethane solutions of the phenothiazine complex is not understood well. This line shape (Figure 6, $T = -86°$) must be related in some manner to the presence of ion pairs which are the dominant species present at $-86°$. As mentioned earlier, addition of $10^{-2}$ $M$ TBAP which breaks up the PTZ–NiTh ion pairs leads to esr spectra with normal symmetrical line shapes down to the freezing point of $CH_2Cl_2$. No esr signal which could be attributed to the ion pair is found in a 1:1 v/v $CH_2Cl_2$–$CH_3CHCl_2$ glass containing $10^{-4}$ $F$ PTZ–NiTh at 77°K. The ground state of the ion pair is thus presumably a singlet having no detectable population of a higher triplet state at 77°K. Consequently, ion pairs should not contribute directly to the esr spectrum in solution unless the excited triplet state were thermally accessible at $-86°$. The mere presence of ion pairs does not necessarily give rise to the peculiar line shape since POZ–NiTh solutions which contain principally ion pairs at comparably low temperatures show completely normal esr spectra. Exchange effects between free PTZ$^+$ and NiTh$^-$ ions seem an unlikely cause of the line shape since only the NiTh$^-$ signal is asymmetrically broadened. The most reasonable explanation which we can advance at the present time is that the solution of PTZ–NiTh contains at reduced temperatures not only strongly interacting ion pairs, but weakly interacting pairs of PTZ$^+$ and NiTh$^-$ ions as well. The latter pairs are essentially biradicals with very weak exchange interactions. The low-temperature spectrum shown in Figure 6 is assumed to be a superposition of free ion spectra and a spectrum due to the weakly interacting pairs. If a symmetric spectrum of equimolar PTZ$^+$ and NiTh$^-$ is subtracted from the low-temperature spectrum of such an intensity as to just eliminate the sharp PTZ$^+$ lines, the difference spectrum resembles that expected from weakly exchanging pairs of NiTh$^-$ and PTZ$^+$ with $\nu_{ex} \sim 10^8$ Hz. A physical model for the weakly coupled ions might be a four-molecule unit, for instance, in which a PTZ$^+$ and NiTh$^-$ are associated with a tightly bound donor–acceptor complex.

It should be emphasized that in the case of the phenoxazine–nickel thiete complex no esr line shape asymmetry or optical charge-transfer band was observed, suggesting that the structures of the POZ–NiTh ion pairs and the PTZ–NiTh ion pairs may be rather dissimilar. Differences between the donors themselves may at first appear subtle, but could still account for the observed differences in behavior if it is noted that metal atoms in square-planar dithiolene complexes have a strong affinity for five-coordination with sulfur,[25] and it is possible that the PTZ–NiTh

(23) G. N. Lewis and M. Randall, "Thermodynamics," 2nd ed, K. Pitzer and L. Brewer, Ed., McGraw-Hill, New York, N. Y., 1961, p 524.

(24) M. Szwarc, *Accounts Chem. Res.*, **2**, 87 (1969).

(25) J. A. McCleverty, *Progr. Inorg. Chem.*, **10**, 49 (1968), and references contained therein.

ion pair is stablized by a weak interaction between the nickel atom and the phenothiazine sulfur atom. This probably would lead to a "stacked" structure with parallel aromatic planes of the donor and acceptor, a configuration favorable to the appearance of a charge-transfer band.

Results for the solid complexes support this possibility. Because of the strong charge-transfer band and spin coupling characteristic of the phenothiazine complex, we think that in this complex the donor and acceptor ions lie alternately along the stacking axis, in a configuration which allows maximum possible

overlap of the donor and acceptor $\pi$ systems. The absence of a strong charge-transfer band for the phenoxazine complex and the lack of observable antiferromagnetic coupling of the unpaired electrons on the donor and acceptor sites suggest relatively small $\pi$-electron interactions between the radical ions.

# Radiation-Induced Isomerization of the 1,2-Diphenylpropenes in Polar Liquids

## by Robert R. Hentz* and H. G. Altmiller

*Department of Chemistry and the Radiation Laboratory,[1] University of Notre Dame, Notre Dame, Indiana 46556*
*(Received February 24, 1971)*

Radiation-induced cis-trans isomerizations of the 1,2-diphenylpropenes have been studied in acetone, ethanol, diethyl ether, and 1,2-dimethoxyethane. Singlet excitation transfer between acetone and *trans*-1,2-diphenylpropene was not detectable in a study of acetone fluorescence from solutions excited at 3130 Å. Consequently, results for the photosensitized isomerization are attributed to transfer of triplet excitation from acetone. Such results give $\chi = 1.0 \pm 0.1$ for the efficiency of intersystem crossing from the lowest excited singlet of liquid acetone and $k\tau = 9 \times 10^2 \, M^{-1}$ as the product of the specific rate of excitation transfer and lifetime for the lowest triplet of liquid acetone. Results for $\gamma$-irradiated solutions of the 1,2-diphenylpropenes in acetone indicate that solute excitation, with subsequent isomerization, occurs entirely by transfer of triplet excitation from acetone to solute at concentrations below about 0.01 $M$. Such results give $k\tau = 9 \times 10^2 \, M^{-1}$, in agreement with the photosensitization results, and a yield of lowest triplets of acetone of $^3G = 1.5$ which agrees well with values determined in pulse-radiolysis studies. Isomerization yields in ethanol and the two ethers are lower than those in acetone and decrease in the order 1,2-dimethoxyethane, diethyl ether, and ethanol. It is suggested tentatively that solute excitation in the two ethers occurs, as previously proposed for cyclohexane solutions, in charge-neutralization reactions in which solute ions (formed by electron and positive-hole capture) are involved. The low isomerization yields obtained in ethanol and the two ethers and the variation in yield with solvent are ascribed to the occurrence with varying degrees of rapidity of the proton-transfer reaction (which precludes solute excitation) between a solvent cation and solvent molecule.

## Introduction

In a series of papers, we have reported studies of the yields and behavior of solute excited states in $\gamma$ radiolysis of benzene,[2-5] cyclohexane,[4-7] and pyridine[8] solutions. The stilbenes,[2-4,7] 1,2-diphenylpropenes,[5,8] *trans*-1,3-pentadiene,[8] 3,5-cycloheptadienone,[2] *p*-terphenyl,[6] and 2,5-diphenyl-1,3,4-oxadiazole[6] have been used as solutes because of the well characterized and suitable properties of their excited states. Our object has been to elucidate the mechanism of formation of solute excited states and to determine the yields of precursors in each solvent. From such studies it was concluded that for solute concentrations less than

about 0.1 $M$ in benzene[3-5] and pyridine,[8] solute excited states are formed almost entirely by energy transfer

(1) The Radiation Laboratory of the University of Notre Dame is operated under contract with the U. S. Atomic Energy Commission. This is AEC Document No. COO-38-687.

(2) R. R. Hentz and L. M. Perkey, *J. Phys. Chem.*, **74**, 3047 (1970).

(3) R. R. Hentz and W. V. Sherman, *ibid.*, **73**, 2676 (1969).

(4) R. R. Hentz, D. B. Peterson, S. B. Srivastava, H. F. Barzynski, and M. Burton, *ibid.*, **70**, 2362 (1966).

(5) R. R. Hentz and H. G. Altmiller, *ibid.*, **74**, 2646 (1970).

(6) R. R. Hentz and R. J. Knight, *ibid.*, **72**, 1783 (1968).

(7) R. R. Hentz and H. P. Lehmann, *ibid.*, **73**, 4283 (1969).

(8) R. R. Hentz, H. G. Altmiller, and L. J. Sharp, *Int. J. Radiat. Phys. Chem.*, in press.

from the lowest triplet and excited singlet states of the solvent. For liquid benzene, a yield[9] of $^1G = 1.5^2$ was determined for the lowest excited singlet state and $^3G = 4.1^{2,5}$ was obtained as the yield of lowest triplets which do not have the lowest excited singlet as a precursor; consequently, with an intersystem crossing efficiency of $\chi = 0.58,^2$ the total yield of lowest triplets in neat benzene is $^3G = 5.0$. For liquid pyridine, $^3G = 2.9^8$ was obtained for the total yield of lowest triplets; because $\chi = 0.056^8$ in liquid pyridine, such a value probably corresponds closely to the yield of lowest triplets that do not have the lowest excited singlet as a precursor. In contrast to the mechanism of solute excitation in $\gamma$-irradiated benzene and pyridine solutions, it was concluded from results obtained for $\gamma$-irradiated cyclohexane solutions[4-7] that solute excitation occurs in charge-neutralization reactions of solute anions and cations, formed by electron and positive-hole capture, with no discernible contribution *via* energy transfer from solvent excited states.

In the work reported in this paper, we have extended our study to solute excitation in $\gamma$ radiolysis of solutions of the polar solvents acetone, ethanol, diethyl ether, and 1,2-dimethoxyethane. The 1,2-diphenylpropenes were used as solutes because their photo- and radiation-induced cis–trans isomerizations have been shown to provide a convenient direct measure of the yield of solute excited states.[5,10] A study of the radiation-induced cis–trans isomerizations of the stilbenes in acetone and 2-propanol has been reported by Lehmann.[11] Solute triplet yields in a number of polar solvents have been determined by pulse radiolysis.[12-16]

## Experimental Section

Sources and purification procedures for the 1,2-diphenylpropenes were the same as in previous work.[5] Purification of $N_2O$ (Matheson Co.) has been described.[6] Acetone (Fisher Certified) and ethanol (Gold Shield, Commercial Solvents Corp.) were purified by distillation. Diethyl ether (Union Carbide) and 1,2-dimethoxyethane (Eastman Kodak) were purified by distillation from $LiAlH_4$. All distillations were performed with a Nester-Faust spinning-band column. Solvents were stored over anhydrous calcium sulfate which was removed by a final bulb-to-bulb distillation on the vacuum line. No unsaturates or peroxides were detected by uv spectrophotometry in the purified ethers or ethanol.

Sample preparation and the cells, procedures (including actinometry and dosimetry), and equipment used in the radiolysis, photolysis, spectrophotometric, and luminescence work have been described.[2,5] Nitrous oxide was added to acetone solutions by condensation of the desired amount of $N_2O$ (determined by pressure measurement in a calibrated volume) onto the deaerated solution at 77°K. The cells were sealed, shaken thoroughly after warming to room temperature,

and allowed to stand overnight prior to irradiation. The concentration of $N_2O$ in solution was calculated from the known amount of gas in the cell, the volumes of cell and solution, and an Ostwald solubility coefficient of $5.95^{17}$ at 25°.

All experiments were performed with deaerated solutions at ~25°. Dose rates in $^{60}Co$ irradiations were near $1.0 \times 10^{18}$ eV ml$^{-1}$ min$^{-1}$ throughout the course of the work. Gas chromatographic determination of the 1,2-diphenylpropenes has been described.[5] Yields of $N_2$ from irradiated acetone solutions containing $N_2O$ were determined by collection of gas volatile at 77°K with a standard Toepler pump and gas buret arrangement.[6] The gas was analyzed on a Beckman GC-5 gas chromatograph with a $^1/_8$-in. $\times$ 6-ft column of molecular sieve (Linde 5A), operated at room temperature, and a helium-ionization detector.

## Results

*Acetone Solutions.* For all the acetone solutions studied, initial quantum yields and $G$ values were obtained from the slopes of yield–dose plots that were linear through the origin; the concentration of product isomer never exceeded 5% of the total isomer concentration.

The photoinduced isomerization of *trans*-1,2-diphenylpropene in acetone was studied at 3130 Å. For the concentrations used, there is an appreciable contribution to the isomerization *via* light absorption by the solute. Quantum yields, $\Phi_s$, for the sensitized isomerization were calculated from measured quantum yields, $\Phi$, with eq I. The molarity of *trans*-1,2-diphe-

$$\Phi_s = \Phi + (\Phi - {}^1\phi)\epsilon_t[t]/\epsilon[A] \qquad (I)$$

nylpropene is denoted by $[t]$ and acetone molarity by $[A]$; extinction-coefficient values of $\epsilon_t = 2.64 \times 10^3$ $M^{-1}$ cm$^{-1}$ and $\epsilon = 1.93$ $M^{-1}$ cm$^{-1}$ were determined for *trans*-1,2-diphenylpropene and acetone, respectively, at 3130 Å; $^1\phi = 0.54_5$ is the quantum yield for the photoexcited isomerization of *trans*-1,2-diphenylpropene at 3130 Å.[5] The results are presented in Figure 1

(9) The symbol $G$ denotes a yield in molecules per 100 eV absorbed by the system.

(10) G. S. Hammond, J. Saltiel, A. A. Lamola, N. J. Turro, J. S. Bradshaw, D. O. Cowan, R. C. Counsell, V. Vogt, and C. Dalton, *J. Amer. Chem. Soc.*, **86**, 3197 (1964); R. A. Caldwell, D. G. Whitten, and G. S. Hammond, *ibid.*, **88**, 2659 (1966).

(11) H. P. Lehmann, *J. Phys. Chem.*, **73**, 20 (1969).

(12) S. Arai and L. M. Dorfman, *ibid.*, **69**, 2239 (1965).

(13) J. P. Keene, T. J. Kemp, and G. A. Salmon, *Proc. Roy. Soc., Ser. A*, **287**, 494 (1965).

(14) T. J. Kemp and J. P. Roberts, *Trans. Faraday Soc.*, **64**, 2106 (1968).

(15) T. J. Kemp, J. P. Roberts, G. A. Salmon, and G. F. Thompson, *J. Phys. Chem.*, **72**, 1464 (1968).

(16) E. Hayon, *J. Chem. Phys.*, **53**, 2353 (1970).

(17) J. Horiuti, *Bull. Inst. Phys. Chem. Res., Tokyo*, **7**, 119 (1931); *cf.* W. F. Linke, "Solubilities of Inorganic and Metal Organic Compounds," 4th ed, Vol. 2, American Chemical Society, Washington, D. C., 1965, p 803.
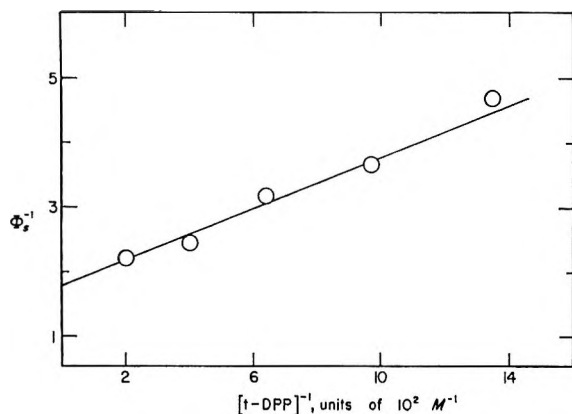
Figure 1. Concentration dependence of the quantum yield for acetone-sensitized isomerization of trans-1,2-diphenylpropene at 3130 Å.
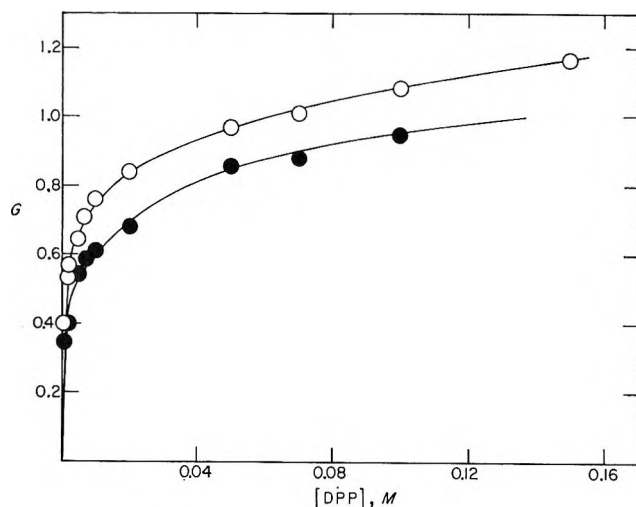


Figure 2. Radiation-induced isomerization of the 1,2-diphenylpropenes in acetone: O, $G(t \rightarrow c)$; ●, $G(c \rightarrow t)$.

in the form of a plot of $\Phi_s^{-1}$ vs. $[t]^{-1}$. No change in total concentration of the 1,2-diphenylpropenes was detectable in the photochemical experiments, and no peaks other than the isomer peaks were seen in the glc traces.

Acetone solutions of trans-1,2-diphenylpropene were excited at 3130 Å, and acetone fluorescence was measured at 4150 Å. For each of the five solutions studied, with concentrations in the range 0.4–5 m$M$, the ratio of fluorescence intensity from the solution to that from neat acetone was within experimental error of the calculated fraction of light absorbed by acetone. Thus, there is no quenching of the excited singlet of acetone by trans-1,2-diphenylpropene and no singlet excitation transfer from the solute to the solvent.

Figure 2 shows the concentration dependence of $G$ for the γ-induced isomerizations of the 1,2-diphenylpropenes in acetone. From the small decreases in total isomer concentration that were detectable for the 1 and 2 m$M$ solutions of trans-1,2-diphenylpropene, $G$ values

of 1.1 and 1.5, respectively, were estimated for consumption of the diphenylpropenes. Though such values indicate that consumption is the dominant process, the glc traces contained only the isomer peaks and one other peak which immediately followed the cis peak and had an area of about 5% of that of the cis peak. Table I gives isomerization and nitrogen yields

Table I: Radiolysis of Acetone Solutions Containing $N_2O$ and 0.01 $M$ trans-1,2-Diphenylpropene

| [N$_2$O]., m$M$ | $G(t \rightarrow c)$ | $G(N_2)$ |
|---|---|---|
| 0 | 0.79 | |
| 7 | | 0.32 |
| 35 | 0.74 | 0.56 |
| 70 | 0.68 | 0.97 |
| 105 | 0.65 | |

obtained in γ radiolysis of acetone solutions containing $N_2O$ and 0.01 $M$ trans-1,2-diphenylpropene.

*Ether and Ethanol Solutions.* Figure 3 shows the concentration dependence of $G$ for the γ-induced isomerization of trans-1,2-diphenylpropene in diethyl ether and in 1,2-dimethoxyethane. By use of doses less than $2 \times 10^{19}$ eV ml$^{-1}$ and analysis of the samples immediately after irradiation, linear yield–dose plots with small positive intercepts were obtained. The $G$ values in Figure 3 were calculated from the slopes of such plots. For the 1, 5, and 10 m$M$ solutions in 1,2-dimethoxyethane, $G$ values of 0.5, 1.3, and 2, respectively, were estimated for consumption of the diphenylpropenes.

Study of the γ-induced isomerization of trans-1,2-diphenylpropene in ethanol is limited by solubility to a maximum concentration of 0.01 $M$. Values of $G$ again were calculated from the slopes of linear yield–dose plots with small positive intercepts. For four concentrations over the range 3–10 m$M$, $G(t \rightarrow c)$ was found to be independent of concentration with an average value of 0.16 ± 0.01, and $G \approx 2$ was estimated for consumption of the diphenylpropenes.

## Discussion

*Acetone Solutions.* The first absorption band of acetone extends from about 3300 to 2200 Å with a maximum at 2750 Å and corresponds to a forbidden transition to a $^1(n,\pi^*)$ state.[18] Acetone fluorescence,[18] for which $\phi = 0.0014$,[19] extends from about 3400 to 5500 Å with a maximum at 4050 Å. The onset of absorption in the 1,2-diphenylpropenes is near 3300 Å and corresponds to an allowed transition to a $^1(\pi,\pi^*)$ state which does not fluoresce.[5] Thus, efficient singlet excitation

(18) R. F. Borkman and D. R. Kearns, *J. Chem. Phys.*, **44**, 945 (1966).

(19) A. M. Halpern and W. R. Ware, *ibid.*, **54**, 1271 (1971).
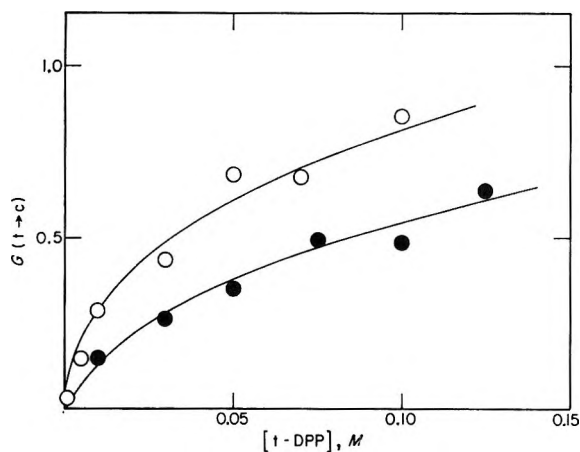
Figure 3. Radiation-induced isomerization of
trans-1,2-diphenylpropene in diethyl ether (●) and in
1,2-dimethoxyethane (O).

transfer between acetone and trans-1,2-diphenylpropene is not expected. However, with $\tau = 1.7$ nsec,[19] even were singlet excitation transfer from acetone to occur with a diffusion-controlled $k \approx 10^{10}$ $M^{-1}$ sec$^{-1}$, a value of only 17 $M^{-1}$ would be obtained for $k\tau$ for singlet excitation transfer. That the results in Figure 1 are not attributable to singlet excitation transfer is established by the failure to detect quenching of acetone fluorescence over the same range of concentrations. Consequently, the results in Figure 1 are attributed to transfer of triplet excitation from acetone ($E_T{}^{18} = 80$ kcal mol$^{-1}$) to trans-1,2-diphenylpropene ($E_T{}^{10} = 48$ kcal mol$^{-1}$) and, therefore, should conform to eq II. In eq II, $\chi$ is the intersystem crossing efficiency for the

$$\Phi_s{}^{-1} = (\chi \cdot {}^3\phi)^{-1}\{1 + (k\tau[t])^{-1}\} \quad (II)$$

lowest excited singlet of liquid acetone; ${}^3\phi = 0.54_5$ is the quantum yield of isomerization for triplet excitation of trans-1,2-diphenylpropene;[5] $k\tau$ is the product of the specific rate of excitation transfer and lifetime for the lowest triplet of liquid acetone. From the slope and intercept of the line in Figure 1, $\chi = 1.0$ and $k\tau = 9 \times 10^2$ $M^{-1}$ are obtained. The value obtained for $\chi$ is identical with that obtained by Borkman and Kearns[20] from a study of the acetone-sensitized isomerizations of the 2-pentenes. The value of $\phi = 0.0014$ for acetone fluorescence[19] is well within the experimental error (~10%) of such $\chi$ determinations.

Values of $G(t \rightarrow c)/G(c \rightarrow t)$ calculated for each concentration in Figure 2 give an average value and average deviation of $1.19 \pm 0.05$. Such a value is experimentally indistinguishable from the corresponding quantum-yield ratio of 1.20 obtained in both photoexcitation and triplet-sensitization experiments.[5,10] Thus, for all concentrations in Figure 2, the radiation-induced isomerization appears to occur entirely via excited states of the solute.

The results in Figure 2 are similar to those previously obtained for radiation-induced isomerization of

the 1,2-diphenylpropenes in benzene[5] in that, with increase in solute concentration, a rather large initial rate of increase in $G$ is followed by an apparent approach to an upper limit near 0.01 $M$ (~0.1 $M$ in benzene) which merges into a gradual increase above 0.01 $M$. For the benzene solutions, the large initial rate of increase in $G$ was attributed to energy transfer from the lowest triplet and excited singlet states of the solvent. Similarly, it seems reasonable to attribute the results for acetone solutions with diphenylpropene concentrations below about 0.01 $M$ to energy transfer from the lowest triplet of acetone (transfer from the lowest excited singlet having been shown not to occur in this system).

The yield of free ion pairs (i.e., those sibling ion pairs whose members escape geminate recombination) in acetone is considerably greater than $G_{fi} = 0.05$ in benzene,[21] but apparently the neutralization of such free ions in acetone does not yield excited states. Values of $G_{fi} = 1.7$[12] and $G_{fi} = 1.2$[16] have been obtained from pulse-radiolysis studies of $5 \times 10^{-3}$ $M$ anthracene in acetone. However, Arai and Dorfman[12] find that the kinetics of anthracene-triplet formation and of anthracene-anion decay are not related and, therefore, rule out the free anion as a precursor of the triplet.

For solute concentrations below 0.01 $M$, positive-charge transfer from an acetone cation to a solute molecule is probably precluded by the rapidity of reaction 1

$$(CH_3)_2CO^+ + (CH_3)_2CO \longrightarrow$$
$$CH_3COCH_2 + (CH_3)_2COH^+ \quad (1)$$
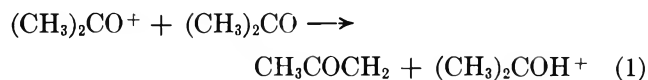
(observed in the mass spectrometer and in $\gamma$-irradiated acetone at 77°K[22]). Thus, for such solute concentrations, free solute anions are neutralized by $(CH_3)_2COH^+$ and proton transfer to the anion is expected to occur with no concomitant excitation. However, recombination of some geminate ion pairs may be sufficiently rapid to compete to some extent with reaction 1, and neutralization of $(CH_3)_2CO^+$ by an acetone anion may be sufficiently exothermic to produce excitation. The possibility of such an ionic contribution to the yield of excited states is indicated by the results in Table I. Nitrous oxide is not expected to quench excited states of acetone and diphenylpropene[23] but has been shown to suppress solute excitation that presumably is a consequence of ionic processes.[6,7,24]

Lehmann, in unpublished work at this laboratory, has obtained values somewhat lower than those in Table

(20) R. F. Borkman and D. R. Kearns, J. Amer. Chem. Soc., 88, 3467 (1966).

(21) W. F. Schmidt and A. O. Allen, J. Chem. Phys., 52, 2345 (1970).

(22) T. Shida and W. H. Hamill, J. Amer. Chem. Soc., 88, 3683 (1966).

(23) A. Morikawa and R. J. Cvetanović, Can. J. Chem., 46, 1813 (1968); M. W. Schmidt and E. K. C. Lee, J. Amer. Chem. Soc., 92, 3579 (1970).

(24) C. Capellos and A. O. Allen, J. Phys. Chem., 72, 4265 (1968).

I for $G(N_2)$ at corresponding concentrations of $N_2O$ as the only solute in acetone. Thus, for the concentrations in Table I, 0.01 $M$ trans-1,2-diphenylpropene does not compete significantly with $N_2O$ (apparently one of the best electron scavengers[25]) for the acetone electron. Consequently, from the result that 35 m$M$ $N_2O$ suppresses $G(t \rightarrow c)$ by only 6%, it is concluded that neutralization of diphenylpropene anions contributes negligibly to excitation of diphenylpropene at concentrations of 0.01 $M$ and less. The suppression of $G(t \rightarrow c)$ by $N_2O$ is attributed plausibly to suppression of a contribution to acetone excitation from geminate recombination of cations and anions of acetone.

In summary, the evidence and arguments presented indicate that processes other than energy transfer from the lowest triplet of acetone make a negligible contribution to radiation-induced isomerization of the diphenylpropenes at concentrations below about 0.01 $M$. For such concentrations, then, the results should conform to eq III in which $G$ is the isomerization yield and

$$G^{-1} = ({}^3G \cdot {}^3\phi)^{-1}\{1 + (k\tau[t])^{-1}\} \qquad (III)$$

${}^3G$ is the yield of lowest triplets of acetone. A plot of $G^{-1}$ vs. $[t]^{-1}$ is presented in Figure 4 for the concentration range $10^{-3}$ to $10^{-2} M$. From the slope and intercept of the line in Figure 4, ${}^3G = 1.5$ and $k\tau = 9 \times 10^2 M^{-1}$ are obtained. Agreement of the latter value with that obtained from study of the photosensitized isomerization provides strong support for the assumed mechanism. The gradual increase in isomerization yield with increase in diphenylpropene concentration above 0.01 $M$ may reflect, among other factors,[5] an increase in charge scavenging by diphenylpropene (as reflected for $N_2O$ by the increase in nitrogen yield shown in Table I) with a consequent increased involvement of diphenylpropene ions in charge-neutralization processes and, thereby, in solute-excitation processes.

In a pulse-radiolysis study of acetone solutions of anthracene, naphthalene, and benzanthracene, Arai and Dorfman[12] have determined solute triplet yields for complete scavenging of excited acetone. Assuming that scavenging was entirely by triplet excitation transfer, such solute triplet yields correspond to ${}^3G$. Thus, with the triplet extinction coefficients determined by Land,[26] the results of Arai and Dorfman for anthracene, naphthalene, and benzanthracene give 1.4, 1.3, and 1.7, respectively, for ${}^3G$. Similarly, the results of Hayon[16] for pulse radiolysis of 0.05 $M$ naphthalene in acetone give ${}^3G = 1.2$.[27] Such values are in reasonably good agreement with ${}^3G = 1.5$ from the present study. Lehmann[11] gives yields of the radiation-induced isomerization of trans-stilbene in acetone for four concentrations over the range 0.005-0.1 $M$ and calculates ${}^3G = 2.3$ from $G(t \rightarrow c) = 1.15$ at 0.1 $M$ and ${}^3\phi = 0.5$ for trans-stilbene. With ${}^3\phi = 0.55$ for trans-stilbene,[28] the calculated yield of solute triplets at 0.1 $M$ is 2.1 which agrees well with the value 2.0 calculated from
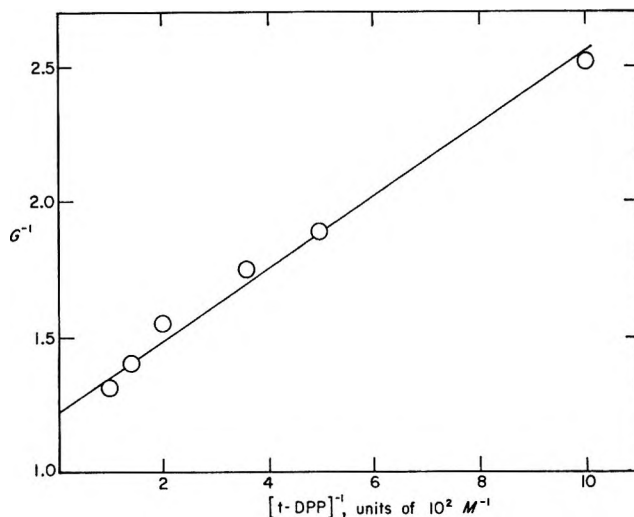
Figure 4. Reciprocal of the trans to cis isomerization yield vs. the reciprocal of solute concentration for $\gamma$ radiolysis of acetone solutions of trans-1,2-diphenylpropene.

$G(t \rightarrow c) = 1.08$ at 0.1 $M$ (cf. Figure 2) and ${}^3\phi = 0.545$ for trans-1,2-diphenylpropene. However, agreement between the isomerization studies is poor for the 0.005 $M$ solutions.

With anthracene as the triplet acceptor, Arai and Dorfman obtained $k = 6.2 \times 10^9 M^{-1} sec^{-1}$ for triplet transfer and $\tau = 8.3 \mu sec$ for the lowest triplet of acetone; with naphthalene, values of $k = 4.5 \times 10^9 M^{-1} sec^{-1}$ and $\tau = 6.3 \mu sec$ were found. Such values give $k\tau = 5.2 \times 10^4 M^{-1}$ and $k\tau = 2.8 \times 10^4 M^{-1}$ for anthracene and naphthalene, respectively. Thus, the value of $k\tau = 9 \times 10^2 M^{-1}$ obtained for trans-1,2-diphenylpropene (with $E_T$ about 30 kcal mol$^{-1}$ less than that of acetone) is surprisingly small; for $\tau \approx 7 \mu sec$, $k \approx 1.3 \times 10^8 M^{-1} sec^{-1}$ which indicates some barrier or forbiddenness in the triplet transfer. A similarly small value of $k = 5 \times 10^8 M^{-1} sec^{-1}$ has been reported[29] for triplet transfer from acetone to biphenyl ($E_T{}^{30} = 65$ kcal mol$^{-1}$). The presence of $\sim 10^{-3} M$ of an impurity that is an efficient quencher of the lowest triplet of acetone could account for the small $k\tau$ obtained in the present work. However, there was no evidence of such an impurity in the absorption spectrum or in gas-chromatographic analysis of the purified acetone; also, identical results were obtained with acetone from different stocks and with unpurified acetone.

(25) J. M. Warman, K. -D. Asmus, and R. H. Schuler, Advan. Chem. Ser., No. 82, 25 (1968).

(26) E. J. Land, Proc. Roy. Soc., Ser. A, 305, 457 (1968).

(27) In contrast with our results, the presence of $N_2O$ at 1 atm (0.24 $M$) was found to have no effect on the yield of naphthalene triplets.

(28) H. A. Hammond, D. E. De Meyer, and J. L. R. Williams, J. Amer. Chem. Soc., 91, 5180 (1969).

(29) L. M. Dorfman, N. E. Shank, and S. Arai, Advan. Chem. Ser., No. 82, 58 (1968).

(30) G. N. Lewis and M. Kasha, J. Amer. Chem. Soc., 66, 2100 (1944).

Because $\chi = 1.0$ for acetone, $^3G = 1.5$ corresponds to the total yield of lowest excited singlets and lowest triplets which do not have the lowest excited singlet as a precursor. A value of 5.6 has been obtained for such a total yield in liquid benzene.[2,5] The low yield of excited states in liquid acetone is probably a consequence, in large part, of the inefficiency with which charge-neutralization processes yield excited states. That inefficiency is attributed to the occurrence of reaction 1 prior to neutralization for all the free ion pairs and a major fraction of the geminate ion pairs. Consequently, ionic processes in acetone probably are manifested largely in the relatively high yield for consumption of the diphenylpropenes.

*Ether and Ethanol Solutions.* From the value $G(t \rightarrow c) = 0.16$ for 3–10 mM trans-1,2-diphenylpropene in ethanol, and with $^1\phi = ^3\phi = 0.54_5$ for trans-1,2-diphenylpropene,[5] $G = 0.29$ is obtained for the yield of solute excited states. Such a small value is consistent with the small yields of solute triplets observed in pulse-radiolysis studies of alcohol solutions;[13,16,31] e.g., Hayon[16] reports $G = 0.09$ for the yield of naphthalene triplets at 0.05 M naphthalene in ethanol. Evidently, excited states of ethanol are formed in low yield or are too short-lived for excitation transfer to be significant at the solute concentrations used or both. The yield of solvent or solute excitation via charge-neutralization processes in ethanol should be negligible because of the rapidity of proton transfer from $C_2H_5OH^+$ to $C_2H_5OH^{32}$ (the analog of reaction 1 in acetone). Neutralization of $C_2H_5OH_2^+$ is expected to occur with no concomitant excitation. Moreover, proton transfer from $C_2H_5OH$ to solute anion may be sufficiently rapid to preclude participation of *free* solute anions ($G_{fi} = 1.0^{16}$) in charge-neutralization processes.[31] Thus, ionic processes in ethanol are expected to make a major contribution to $G \approx 2$ for consumption of the diphenylpropenes and to yield little or no isomerization.

The results for diethyl ether and 1,2-dimethoxyethane solutions in Figure 3 are similar to those previously obtained for radiation-induced isomerization of the 1,2-diphenylpropenes in cyclohexane[5] and do not exhibit the large initial rate of increase in isomerization yield that was obtained with benzene[5] and acetone (cf. Figure 2) solutions and was identified with energy transfer from excited states of the solvent. Isomerization yields for the ether solutions in Figure 3 fall between those obtained for ethanol and cyclohexane solutions. The foregoing comparisons suggest that excited states of diethyl ether and 1,2-dimethoxyethane, like those of

ethanol, may be too short-lived for energy transfer to be significant at the solute concentrations used and that solute excitation occurs, as previously proposed for cyclohexane solutions,[4,7] via charge-neutralization reactions involving solute cations or solute anions or both. Such an interpretation requires that the proton transfer from solvent cation to solvent molecule (which precludes excitation in charge neutralization) be somewhat slower in diethyl ether than in ethanol and still slower in 1,2-dimethoxyethane. Then, for a particular solute concentration, the probabilities of positive-charge transfer to the solute and of neutralization of solute anions by solvent or solute cations (with concomitant solute excitation and subsequent isomerization) will increase with change in solvent from ethanol to diethyl ether to 1,2-dimethoxyethane to cyclohexane.

Though results for the ether solutions in Figure 3 are suggestive in relation to results obtained with other solvents, such results clearly are not sufficient for establishment of the mechanism of solute excitation in diethyl ether and 1,2-dimethoxyethane. For such a purpose, additional studies of various kinds are needed. It is quite possible that the results in Figure 3 are in part or entirely a consequence of energy transfer from a solvent excited state of appropriate lifetime. In uv[33] and high-energy electron[34] irradiations of liquid 1,4-dioxane, fluorescence from an excited state with a lifetime of $\sim 2$ nsec has been observed. On the other hand, Baxendale, et al.,[34] could find no evidence for an excited state of tetrahydrofuran. We are not aware of any definitive information on lifetimes of excited states of diethyl ether or 1,2-dimethoxyethane.

It is of interest to compare some relative yields obtained for triphenylamine triplets by pulse radiolysis of various solvents containing $10^{-2}$ M solute[15] with relative yields obtained for isomerization of $10^{-2}$ M trans-1,2-diphenylpropene in the same solvents (ref 6 and this work). Such triplet yields normalized to unity for cyclohexane and with the corresponding isomerization yields in parentheses are 0.07(–), 0.11-(0.27), 0.54(0.53), 0.93(–), 1(1), and 3.2(2.4) for tetrahydrofuran, diethyl ether, 1,2-dimethoxyethane, 1,4-dioxane, cyclohexane, and benzene, respectively.

(31) S. Arai and L. M. Dorfman, *J. Chem. Phys.*, **41**, 2190 (1964).

(32) J. W. Sieck, F. P. Abramson, and J. H. Futrell, *ibid.*, **45**, 2859 (1966); T. Shida and W. H. Hamill, *J. Amer. Chem. Soc.*, **88**, 3689 (1966).

(33) A. M. Halpern and W. R. Ware, *J. Phys. Chem.*, **74**, 2413 (1970).

(34) J. H. Baxendale, D. Beaumond, and M. A. J. Rodgers, *Chem. Phys. Lett.*, **4**, 3 (1969).

# NOTES

## Protolysis Kinetics of Diamines in Sulfuric Acid

by Donald E. Leyden* and J. M. McCall, Jr.

*Department of Chemistry, University of Georgia,
Athens, Georgia 30601*   (*Received January 25, 1971*)

Except for several papers concerned with protonation thermodynamics,[1,2] previous study of acid–base reaction kinetics of amines has been almost exclusively concerned with monoamines and amino carbonylates. Considerable work has been done on the protolysis kinetics of tertiary amines using high-resolution nuclear magnetic resonance and spin-echo techniques.[3-9] Considering these systems fairly well known, there should be similarities between these results and the protolysis reactions of diamines when the amino groups are separated by long chain lengths. Yet significant influence of the second amino group may be expected as the separation of the amino groups is decreased. These differences could arise from steric and coulombic effects and possibly proton chelate formation. Accordingly, the protolysis kinetics of $N,N,N',N'$-tetramethyl-1,2-diaminoethane (I) and its monoquaternary methyl sulfate (II), $N,N,N',N'$-tetramethyl-1,3-diaminopropane (III), and $N,N,N',N'$-tetramethyl-1,4-diaminobutane (IV) were studied. The acid dissociation constants of these compounds vary sufficiently to require a wide range of acidity for the study. The study was undertaken using a sulfuric acid–water solvent system to take advantage of Hammett acidity values in the highly acidic region.[10] The investigation yielded kinetic parameters and dissociation constants for these compounds and interesting observations related to the chain length.

## Experimental Section

All spectra were recorded using a Hitachi-Perkin-Elmer R-20 high-resolution nuclear magnetic resonance spectrometer equipped with a variable temperature probe. A standard temperature of 25° was chosen for all the compounds and was checked frequently to ensure accuracy to ±1°. Care was taken to avoid saturation during each experiment.

The compounds used, with the exception of I and II, were obtained from Aldrich Chem. Co. I was obtained from Eastman Organic Chemicals. No further purification was necessary. The quaternary salt (II) was prepared from the tetramethylamine and methyl iodide. The resulting iodide quaternary salt was then treated with silver oxide to form a quaternary hydroxide. This, when mixed with sulfuric acid, gave the desired quaternary sulfate salt in a solution of known acidity. Stock solutions of sulfuric acid were prepared by dilution of 96% sulfuric acid (J. T. Baker, AR), and standardized with potassium hydroxide.

All $pK_a$ values were determined by potentiometric titration using a Corning Model 12 pH meter and NBS standard buffers. The titrant used was standardized, carbon dioxide-free potassium hydroxide. The temperature was maintained at 25.0 ± 0.1°.

Exchange rate values were calculated by matching computer simulated curves to the experimental spectra. The equation used to simulate the curves was similar to those given by Arnold for spin-coupled systems in which the coupling is small relative to the chemical shift difference of the coupled nuclei.[11] In all cases the line shape of the methyl proton resonance was used to calculate the proton exchange rate. The value of $T_2$ was measured frequently as the line width at half-height of the methyl protons in solutions of low acidity and was assumed to be controlled by inhomogeneities in the magnetic field. Computer processing was done on an IBM 360/65 remote terminal Model 2741.

Kinetic data were taken for I and II over a concentration range of 0.1–0.7 $M$. The concentration dependence of the rate of exchange was nonlinear and the apparent rate increased only slightly at low concentration and rapidly increased above 0.4 $M$. The change in rate with concentration was not related to concentration or viscosity in any simple manner. It was concluded that an accurate representation of the acidity could not be made using acidity function values under these conditions. Therefore, the apparent rate was determined over the above concentration range and extrapolated to zero concentration. The rate constants reported were calculated from the extrapolated data.

## Results and Discussion

A number of reactions have been shown to apply to the study of proton exchange in aqueous solu-

(1) F. Holmes and D. R. Williams, *J. Chem. Soc., A*, 478 (1967).

(2) A. Vacca and D. Arenare, *J. Phys. Chem.*, **71**, 1495 (1967).

(3) A. Loewenstein and S. Meiboom, *J. Chem. Phys.*, **27**, 1067 (1957).

(4) E. Grunwald, *J. Phys. Chem.*, **67**, 2211 (1963).

(5) E. Grunwald, *ibid.*, **67**, 2208 (1963).

(6) Z. Luz and S. Meiboom, *J. Chem. Phys.*, **39**, 366 (1963).

(7) E. K. Ralph and E. Grunwald, *J. Amer. Chem. Soc.*, **89**, 2963 (1967).

(8) E. Grunwald and A. Y. Ku, *ibid.*, **90**, 29 (1968).

(9) E. Grunwald and E. K. Ralph, III, *ibid.*, **89**, 4405 (1967).

(10) E. M. Arnett and G. W. Mach, *ibid.*, **86**, 2671 (1964).

(11) J. T. Arnold, *Phys. Rev.*, **102**, 136 (1956).

tions.[3,5,9,12-15] The potentially significant reactions for diamines are

$$^+HBBH^+ + H_2O \xrightarrow{k_1} {}^+HBB + H_3O^+ \quad (1)$$

$$^+HBBH^+ + OH^- \xrightarrow{k_2} {}^+HBB + H_2O \quad (2)$$

$$^+HBBH^+ + {}^+HBB \xrightarrow{k_3} {}^+HBB + {}^+HBBH^+ \quad (3)$$

$$^+HBBH^+ + H_2O + {}^+HBB \xrightarrow{k_4}$$

$$^+HBB + H_2O + {}^+HBBH^+ \quad (4)$$

$$^+HBB \xrightarrow{k_5} BBH^+ \quad (5)$$
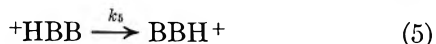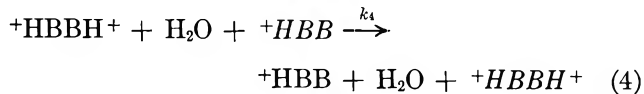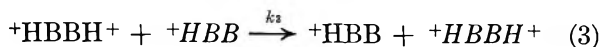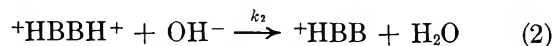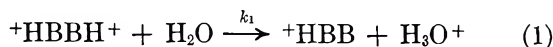
where $^+HBBH^+$ represents the diprotonated amine. Since the system also contains sulfuric acid, other mechanisms of proton exchange involving sulfate and bisulfate ions acting as bases should also be considered.[16]

$$^+HBBH^+ + HSO_4^- \xrightarrow{k_6} {}^+HBB + H_2SO_4 \quad (6)$$

$$^+HBBH^+ + SO_4^{2-} \xrightarrow{k_7} {}^+HBB + HSO_4^- \quad (7)$$
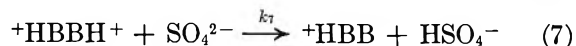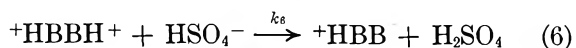
Consideration of the medium enables us to immediately reject several of these reactions. Reaction 2 has been shown to be negligible in solutions of very low pH because of the extremely low concentration of hydroxide ions.[16] Also, reaction 3 has been shown to be negligible for trialkyl monoamines due to steric factors.[8] Reactions 6 and 7 were considered even though a 10–100-fold greater amount of water is present. However, the protolysis rate was observed to increase sharply as the concentration of both $HSO_4^-$ and $SO_4^{2-}$ decreased; thus they could not play an important part in determining the overall rate. Experimentally, a variation in the concentration of the amine at constant acidity produced no effect on the observed rate which demonstrated that no mechanism second order in amine was important. Therefore, reactions 3 and 4 may be neglected.

Reaction 5 represents the transfer of a proton from one side of the diamine to the other by formation of a ring structure. This is deemed unlikely since in strongly acidic solutions even one side of the diamine would not be likely to be completely deprotonated for very long. However, ring formation could take place incorporating a water molecule. At any rate these possibilities could not be ruled out without further investigation. We reasoned that if reaction 5 were important, a significant drop in the rate would occur upon quaternization of one side of I. An investigation of the monoquanternary salt (II) showed the protolysis rate actually increased slightly. This ruled out any sort of intramolecular exchange mechanism.

Thus reaction 1 is found to be the mechanism which significantly contributes to the total rate observed. Reaction 1 represents the net process of proton exchange with water, but several workers have found it more meaningful to divide this total process into a two-step

reaction[7,9,15,17-19] The first step is a transfer of the proton from a hydrated amine molecule to the solvent water with retention of the $N\cdots HOH$ hydrogen bond. This is followed by complete breakage of the $N\cdots HOH$ bond in a second step. The two steps are shown in the following equations.

$$^+HBBH^+\text{---}HOH + H_2O \underset{k_{-a}}{\overset{k_a}{\rightleftarrows}}$$

$$^+HBB\text{---}HOH + H_3O^+ \quad (8a)$$

$$^+HBB\text{---}HOH \xrightarrow{k_H} {}^+HBB + HOH \quad (8b)$$
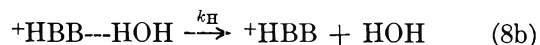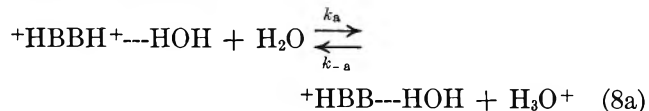
The first equilibrium is that process identified with the acid dissociation constant of the compound. The second step is the process detected using nmr observation of the amine. Equation 9 may be obtained from eq 8 after applying a steady-state approximation to the concentration of $^+HBB\text{---}HOH$

$$\frac{\text{rate}}{[^+HBBH^+]} = 1/\tau = \frac{k_a k_H}{k_H + k_{-a}[H_3O^+]} \quad (9)$$

where $[^+HBBH^+]$ represents the total concentration of the diprotonated species. This equation together with a second term in cases where reaction 4 is important have been successfully used to describe the protolysis kinetics of a wide variety of amines.[7,9,15] Depending upon the relative magnitudes of $k_H$ and $k_{-a}[H_3O^+]$, one may be able to simplify the denominator in the preceding rate expression by neglecting one or the other term.

A plot of $1/\tau$ vs. $1/a_H$ (or $1/h_0$) at several concentrations of amine gave a straight line with an intercept of zero within experimental error for I, II, and III. Assuming $k_{-a}[H_3O^+] \gg k_H$, the first term in the denominator of eq 9 can be neglected and we can calculate $k_H$ from the slope and known $K_a$. However, IV gave a curve as shown in Figure 1. This curve may be divided into three regions; the first is at high acidity where $k_{-a}[H_3O^+] \gg k_H$. After neglecting $k_H$ in the denominator we may estimate $k_H$ from the slope and $K_a$. In the curved central region $k_{-a}[H_3O^+] \approx k_H$ and both are important. In the limit of low acidity, $k_{-a}[H_3O^+] \ll k_H$ and $1/\tau$ approaches a value given by

$$1/\tau = \frac{k_a k_H}{k_H} = k_a \quad (10)$$

(12) E. Grunwald, A. Loewenstein, and S. Meiboom, J. Chem. Phys., 27, 630 (1957).

(13) M. T. Emerson, E. Grunwald, and R. A. Kromhout, ibid., 33, 547 (1960).

(14) E. Grunwald, P. J. Karabatsos, R. A. Kromhout, and E. L. Purlee, ibid., 33, 556 (1960).

(15) D. E. Leyden and W. R. Morgan, J. Phys. Chem., 73, 2924 (1969).

(16) D. E. Leyden and J. F. Whidby, ibid., 73, 3076 (1969).

(17) M. T. Emerson, E. Grunwald, M. T. Kaplan, and R. Kromhout, J. Amer. Chem. Soc., 82, 6307 (1960).

(18) M. Sheinblatt, J. Chem. Phys., 36, 3103 (1962).

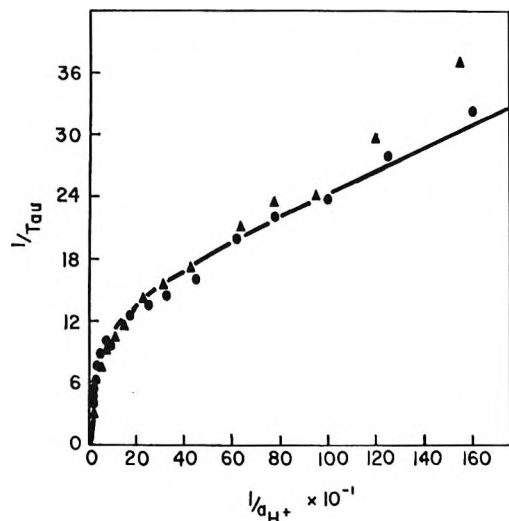(19) M. Sheinblatt and H. S. Gutowsky, J. Amer. Chem. Soc., 86, 4814 (1964).

Figure 1. $1/\tau$ vs. $1/a_{H^+}$ for $N,N,N',N'$-tetramethyl-1,4-diaminobutane.

The middle and low acidity region of the curve is easily fitted by variation of $k_a$ in eq 9, assuming a value of 1 $\times$ $10^{10}$ for $k_{-a}$. The results for all compounds studied are shown in Table I. In the case of I, II, and III, only the linear portion of the $1/\tau$ vs. $1/a_{H^+}$ was available. Therefore $k_a$ and $k_{-a}$ could not be determined. A statistical correction has been applied to account for the two exchangeable sites in each molecule.[20]

**Table I:** Summary of Kinetic Parameters

| Compd | $pK_{a_1}$ | $pK_{a_2}$ | $k_H \times 10^{-9}$ | $k_a$ | $k_{-a} \times 10^{-10}$ |
|---|---|---|---|---|---|
| I | 5.75 | 9.17 | 4.52 | | |
| II | 5.92 | | 7.47 | | |
| III | 7.85 | 9.80 | 0.145 | | |
| IV | 8.77 | 10.30 | 0.085 | 17 | 1.0 |

Considering the values obtained for I, III, and IV, we note a sharp increase in the magnitude of $k_H$ for I, compared with the other two compounds. Apparently the interaction between the two amino groups increases in importance as the separating chain length is decreased. The interaction between amino groups in these diamines is also apparent in the difference between the first and second stepwise protonation constant in each compound, $\Delta pk_A$, which is 3.56 for I, while only 1.95 for III, and 1.56 for IV. This interaction between amino groups has also been noted for primary aliphatic diamines, for which it was found that the difference in the successive enthalpies for stepwise protonation decreases appreciably as the distance between the amino groups increases.[1,2] The dissociation of the N$\cdots$HOH moiety does not involve charged species. However, a correlation was found between the value of $k_H$ and the separation between the amino groups.

The distance between these groups was obtained using molecular models assuming an orientation which gave maximum separation of the amino groups. A plot of $1/R^2$ vs. $k_H$, where $R$ is the distance between the amino groups, is essentially linear. This correlation is at least in part explained by simple charge–dipole repulsion between the protonated amino group on the one end and the dipole of the N$\ldots$HOH which is broken during exchange at the other end. Such forces predict a $1/R^2$ dependence.

In a recent review article, Grunwald and Ralph reported a study of the protolysis kinetics of $N,N,$-$N',N'$-tetraethyl-1,2-diaminoethane.[21] Two processes were detected which were attributed to exchange from trans and gauche isomers with $k_H$ values of $3 \times 10^9$ and $3 \times 10^7$ sec$^{-1}$, respectively. Our methods only detected the faster process. The agreement of the larger $k_H$ between the tetraethyl and tetramethyl compounds is quite good.

(20) J. E. Leffler and E. Grunwald, "Rates and Equilibria of Organic Reactions," Wiley, New York, N. Y., 1963, p 133.

(21) E. Grunwald and E. K. Ralph, *Accounts Chem. Res.*, **4**, 107 (1971).

# Shock-Tube Study of $C_2H_2$–$O_2$ Reaction. Acceleration of Reaction in the Presence of Trace Amounts of $Cr(CO)_6$

by Shimpei Matsuda*

*Department of Chemistry, Harvard University, Cambridge, Massachusetts 02138*

and David Gutman

*Department of Chemistry, Illinois Institute of Technology, Chicago, Illinois 60616 (Received March 4, 1971)*

The effect of metallic additives on the combustion of hydrocarbons, in particular the antiknocking effect of tetraethyl lead, has been extensively studied by kinetic spectroscopy in a flash photolysis system.[1] It was found that hydrocarbon combustions were retarded in the presence of $Pb(C_2H_5)_4$ and $Te(CH_3)_2$.[2] In the case of $Pb(C_2H_5)_4$ this effect was explained by assuming a chain-breaking process involving PbO. Erhard[3] studied the effect of metal carbonyls on the flash-initiated combustion of $C_2H_2$–$O_2$ mixtures. Contrary to the case of $Pb(C_2H_5)_4$, the combustion was greatly accel-

(1) For a review see, R. G. W. Norrish, *Symp. (Int.) Combust. [Proc.] 10th*, 1 (1965).

(2) K. H. L. Erhard and R. G. W. Norrish, *Proc. Roy. Soc., Ser. A*, **259**, 297 (1960); **234**, 178 (1956); A. B. Callear and R. G. W. Norrish, *ibid.*, **259**, 304 (1960).

(3) K. Erhard, *Z. Phys. Chem. (Frankfurt am Main)*, **36**, 126 (1963).

erated in the presence of $Ni(CO)_4$, $Fe(CO)_5$, and $Cr(CO)_6$. Erhard suggested the formation of reactive species of the type $Cr(CO)_5(C_2H_2)$ on the photodissociation of $Cr(CO)_6$ and questioned whether the acceleration of combustion reactions was also observed in thermal reaction systems.[3] Recently, the oxidation of carbon monoxide in the presence of trace amounts of $Cr(CO)_6$ has been studied in shock waves.[4] It has been observed that CO oxidation is greatly accelerated in the presence of $Cr(CO)_6$ (gas-phase homogeneous catalysis by transition metal compounds). This note describes the effect of $Cr(CO)_6$ on the shock-initiated $C_2H_2$–$O_2$ reaction.

The shock-tube apparatus used in this study has been described previously.[5] Argon gas was saturated with $Cr(CO)_6$ vapor by passing Ar through the $Cr(CO)_6$-packed column.[6] The reaction gas mixtures were prepared by adding the $Cr(CO)_6$ saturated Ar to the $C_2H_2$–$O_2$–Ar mixtures. The vapor pressure of $Cr(CO)_6$ was taken from the literature.[7] All reaction gas mixtures used in this study are listed in Table I.

**Table I**

| Mixture | $C_2H_2$, % | $O_2$, % | $Cr(CO)_6$, ppm | Ar, % |
|---|---|---|---|---|
| I | 0.5 | 1.0 | | 98.5 |
| II | 0.5 | 1.0 | 10 | 98.5 |
| III | 0.5 | 1.0 | 25 | 98.5 |
| IV | 0.5 | 1.0 | 50 | 98.5 |

The reaction course was followed by monitoring the emissions at 308 nm (OH* plus continuum)[8] and 314 nm (CH* $C^2\Sigma^+ - X^2\pi$) simultaneously by the end-on detection technique.[5,8] Experiments were performed at about 1700°K with a total concentration in the reflected shock zone of $1.4 \times 10^{-3}$ mol/l. Oscillograms from two experiments performed under nearly identical conditions, one with mixture I and the other with mixture II, are shown in Figure 1 and the emission intensities are plotted against reaction time in Figure 2. As shown in Figure 2 the emission intensity displays an exponential growth of about one decade when the $Cr(CO)_6$ concentration is 10 ppm. It can be seen in Figure 2 that the reaction is greatly accelerated in the presence of only 10 ppm of $Cr(CO)_6$. The induction time (defined as the time when the falloff from the exponential growth occurs) is reduced to almost $1/2$ in the presence of 10 ppm of $Cr(CO)_6$. When the reaction gas mixtures containing more than 25 ppm of $Cr(CO)_6$, i.e., mixtures III and IV, are shock heated, the reaction proceeds extremely fast and exponential growth of the emissions is no longer observed. The emissions were over within 130 and 200 $\mu$sec with mixtures IV and III, respectively, under the same experimental conditions as given in Figure 1. It should be noticed in Figure 2 that the exponential growth constant of the
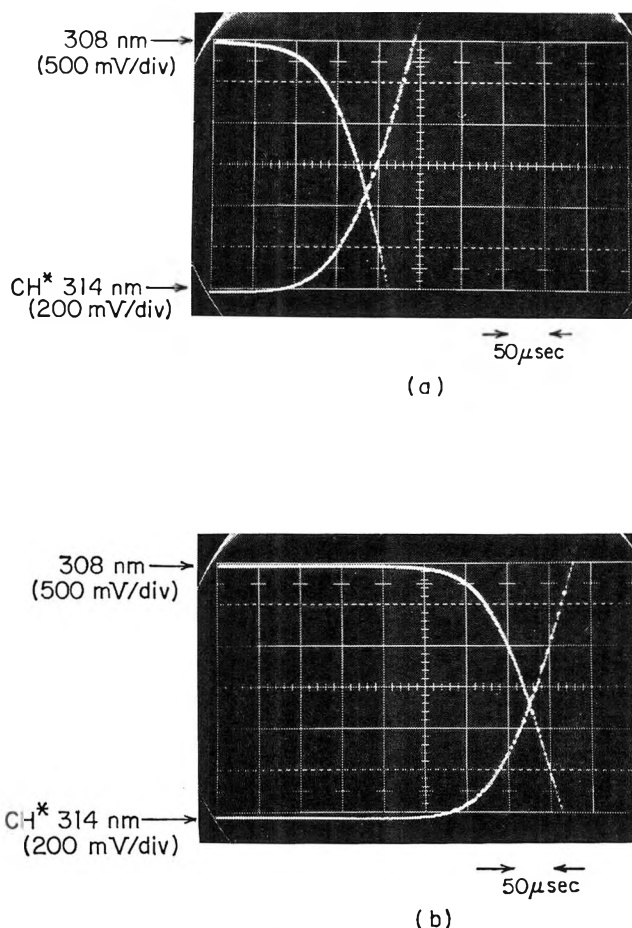


Figure 1. Oscillograms obtained from two experiments. Reaction time increases from left to right: (a) mixture II, $T = 1645°K$, $C = 1.40 \times 10^{-3}$ mol/l.; (b) mixture I, $T = 1650°K$, $C = 1.40 \times 10^{-3}$ mol/l.

emission is not altered in the presence of $Cr(CO)_6$, and that the falloff from the exponential growth occurs at the same emission intensity whether the reaction gas mixture contains $Cr(CO)_6$ or not.

The $C_2H_2$–$O_2$ reaction is one of the chain-branching reaction systems whose induction period is characterized by the exponential growth of chain carriers,[9] for example $(OH) = (OH)_0 \exp(\alpha t)$. The exponential growth constant, $\alpha$, is a characteristic function of the reactant concentrations and the rate constants in the chain-branching reactions and independent of initiation

(4) S. Matsuda, T. P. J. Izod, and G. B. Kistiakowsky, submitted for publication in *J. Chem. Phys.*

(5) D. Gutman, E. A. Hardwidge, F. A. Dougherty, and R. W. Lutz, *ibid.*, **47**, 4400 (1967).

(6) W. L. Schakleford, Ph.D. Thesis, California Institute of Technology, Pasadena, Calif., 1964.

(7) (a) T. D. Wilkerson, Ph.D. Thesis, University of Michigan, Ann Arbor, Mich., 1962; (b) A. A. Boni, *J. Electrochem. Soc.*, **113**, 1089 (1966).

(8) I. R. Slagle, D. Fife, S. Matsuda, J. Marquart, and D. Gutman, submitted for publication in *J. Chem. Phys.*

(9) (a) D. Gutman and S. Matsuda, *ibid.*, **52**, 4122 (1970); (b) G. P. Glass, G. B. Kistiakowsky, J. V. Michael, and H. Niki, *ibid.*, **42**, 608 (1965).
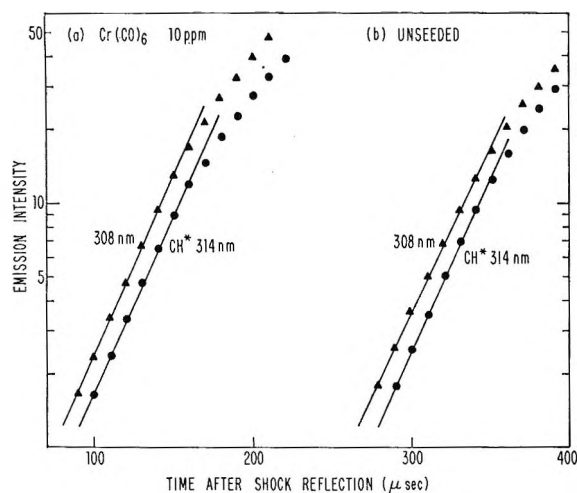
Figure 2. Plots of emission intensities vs. reaction time from two oscillograms shown in Figure 1. The exponential growth constant calculated is for (a) $3.35 \times 10^4$ sec$^{-1}$ and for (b) $3.20 \times 10^4$ sec$^{-1}$.

reactions.[10] The initial concentration of chain carriers, $(OH)_0$ in the above example, is linearly proportional to the initiation rate.[10]

In the present study it has been found that the exponential growth constant is not affected substantially, but the reaction time is greatly reduced in the presence of $Cr(CO)_6$. From these observations it can be said that Cr or some species containing Cr is not involved in the main chain branching reactions but enhances the chain initiation process. It could be suggested that the Cr compound(s) form some activated complex with $C_2H_2$ which produces chain carriers either by reaction with $O_2$ or by thermal decomposition. The activated complex of the type $Cr(CO)_5(C_2H_2)$ as suggested in the flash photolysis system,[3] however, is not probable at all, because under the present experimental conditions the decomposition of $Cr(CO)_6$ is known to be very fast.[4] In the shock-tube study of the $Cr(CO)_6-O_2$ and $Cr(CO)_6-CO-O_2$ reaction systems by a time-of-flight mass spectrometer, the formation of $CrO$, $CrO_2$, and $CrO_3$ is observed.[4] Therefore, it seems more likely that Cr atom formed by the decomposition of $Cr(CO)_6$ is oxidized to $CrO$, $CrO_2$, and $CrO_3$ in the present reaction system and the $CrO_3$ (or $CrO_2$) reacts with $C_2H_2$ to form chain carriers. Since a very low concentration of $Cr(CO)_6$ is used in the present study, the possibility of solid particle formation (chromium oxides) is completely eliminated.[4]

(10) J. N. Bradley, *Trans. Faraday Soc.*, **63**, 2945 (1967).

# N-H···π Hydrogen Bonding

by S. Mukherjee, S. R. Palit,*

*Physical Chemistry Department, Indian Association for the Cultivation of Science, Jadavpur, Calcutta-32, India*

and Sadhan K. De

*Chemistry Department, Indian Institute of Technology, Kharagpur, West Bengal, India* (Received February 1, 1971)

Although hydrogen bonding of hydroxylic compounds (that is, phenols and alcohols) with π-electron systems of olefins and aromatics has been studied by various workers in the recent years,[1-5] there has been but little investigation on N-H···π-type hydrogen bonding.[6] This note presents the results of our investigations on the hydrogen-bonding interaction where N-H of α-naphthylamine acts as proton donor and π-electron systems of aromatics act as proton acceptors. We have utilized Nagakura and Baba's suggestions that π-π* transitions of organic molecules with suitable chromophores undergo a red shift in proton-accepting solvents due to solute-solvent hydrogen-bonding interaction and also spectral measurements at the shifted peak can be used to evaluate the equilibrium constant for the complex formation.[7-8]

## Experimental Section

The α-naphthylamine (B.D.H.) was recrystallized before use. The π bases (Eastman Kodak) were purified by standard methods[9] and distilled before use. The nonhydrogen bonding solvent used was n-heptane (E. Merck) which showed cutoff at 220 mμ. The details of spectral measurements made on a Hilger uv spectrophotometer were same as described previously.[8]

## Results and Discussion

The π-π* band of α-naphthylamine in n-heptane at 318 mμ undergoes a red shift to 322 mμ in the π bases. Figure 1 shows the absorption spectra of α-naphthyl amine in n-heptane and in mesitylene.

(1) (a) R. West, *J. Amer. Chem. Soc.*, **81**, 1614 (1959); (b) W. Beckering, *J. Phys. Chem.*, **65**, 206 (1961); (c) M. Oki and H. Iwamura, *J. Amer. Chem. Soc.*, **89**, 567 (1967).

(2) P. J. Krueger and H. D. Mette, *Can. J. Chem.*, **42**, 288 (1964).

(3) B. Ghosh and S. Basu, *Trans. Faraday Soc.*, **61**, 2097 (1965).

(4) M. R. Basila, E. L. Saier, and L. R. Cousins, *J. Amer. Chem. Soc.*, **87**, 1665 (1965).

(5) (a) Z. Yoshida and E. O. Sawa, *ibid.*, **87**, 1467 (1965); **88**, 4019 (1966); (b) Z. Yoshida and N. Ishibe, *Bull. Chem. Soc. Jap.*, **42**, 3254 (1969).

(6) B. Chakravorty and S. Basu, *J. Chim. Phys.*, **64**, 950 (1967).

(7) (a) S. Nagakura and H. Baba, *J. Amer. Chem. Soc.*, **74**, 5693 (1952); (b) S. Suzuki and H. Baba, *J. Chem. Phys.*, **35**, 1118 (1961).

(8) (a) S. K. De and S. R. Palit, *J. Phys. Chem.*, **71**, 444 (1967); (b) S. Mukherjee, S. R. Palit, and S. K. De, *ibid.*, **74**, 1389 (1970).

(9) "Techniques of Organic Chemistry," A. Weissberger, Ed., Vol. VII, Interscience, New York, N. Y., 1955.
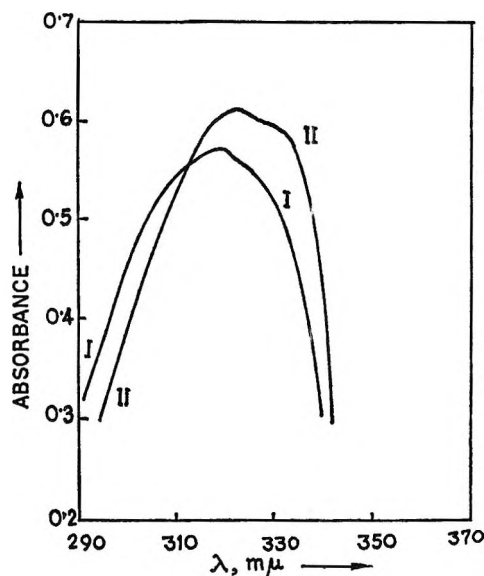
Figure 1. Long wavelength absorption spectra of
$\alpha$-naphthylamine in I, $n$-heptane ($\lambda_{max}$ 318 m$\mu$, $\epsilon$ 3920) and in
II, mesitylene ($\lambda_{max}$ 322 m$\mu$, $\epsilon$ 8710).

Optical density measurements were made on mixtures
of the proton donor and the different $\pi$ bases at various
concentrations of the latter at the shifted peak (322 m$\mu$).
The results were then examined for possible 1:1 com-
plex formation. In the hydrogen bonding of $\alpha$-naph-
thylamine (B) and $\pi$ bases (A)

$$A + B \rightleftharpoons AB$$
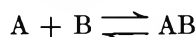
when [A] $\gg$ [B], the equilibrium constant may be
calculated using the following equation[3,8]

$$\frac{[A]}{\bar{\epsilon} - \epsilon_0} = \frac{1}{\epsilon_1 - \epsilon_0}\left(\frac{1}{K}\right) + \frac{[A]}{\epsilon_1 - \epsilon_0} \qquad (1)$$

where [A] and [B] are the concentrations of the $\pi$ base
and the proton donor, respectively, $\epsilon_1$ and $\epsilon_0$ are the
extinction coefficients of the complexed and free $\alpha$-
naphthylamine, respectively, $K$ is the equilibrium con-
stant, $\bar{\epsilon}$ is the formal extinction coefficient of the solu-
tion, given by $\bar{\epsilon} = D/[B]l$, where $D$ is the measured
optical density of the solution containing an initial
concentration of [B] in moles per liter, and $l$ is the path
length in centimeters.

**Table I:** Equilibrium Constants for 1:1 Hydrogen-Bonded
Complex Formation between $\alpha$-Naphthylamine
and the $\pi$ Bases at 25°

| Base | Equilibrium constant, $K$, $M^{-1}$ |
|---|---|
| Chlorobenzene | 0.109 ± 0.040 |
| Benzene | 0.147 ± 0.030 |
| Toluene | 0.254 ± 0.040 |
| Ethylbenzene | 0.244 ± 0.050 |
| Cumene | 0.608 ± 0.080 |
| $p$-Xylene | 1.300 ± 0.100 |
| Mesitylene | 2.220 ± 0.150 |
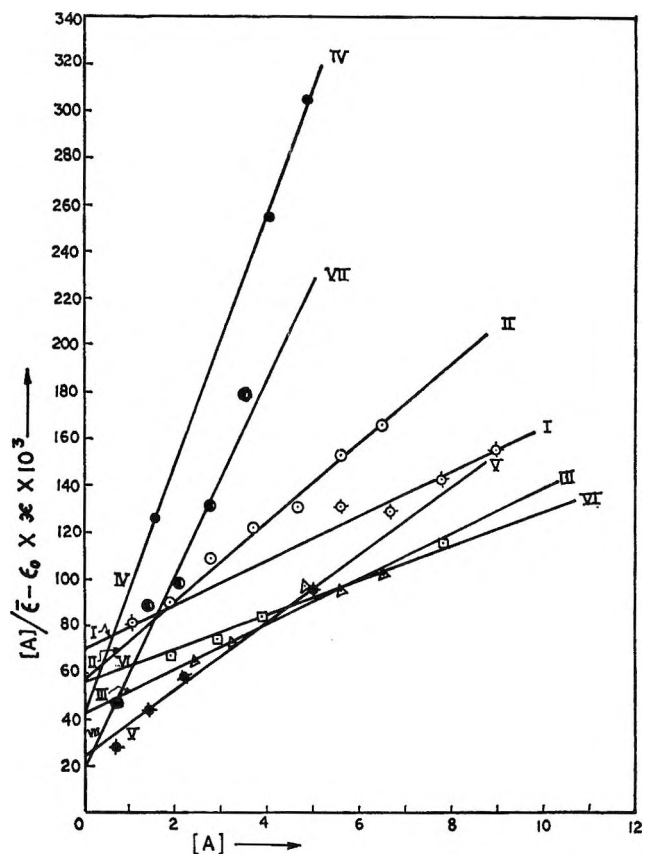


Figure 2. Plots of [A]/($\bar{\epsilon} - \epsilon_0$) vs. [A] for different bases:
I, benzene (7.94); II, toluene (8.55); III, ethylbenzene
(7.81); IV, $p$-xylene (8.33); V, cumene (7.15); VI, chlorobenzene
(7.81); VII, mesitylene (7.15). Numbers in parentheses
indicate values of $x$ in the ordinate where $x \times 10^3 = 1/[B]$.

The observed linear plots of [A]/$\bar{\epsilon} - \epsilon_0$ vs. [A] (Figure
2), according to eq 1, show the formation of 1:1 hydro-
gen-bonded complex between $\alpha$-naphthylamine and the
$\pi$ bases. The equilibrium constants (Table I) increase
with the increase in the number of alkyl groups in the
series of aromatics studied. Possible steric effects due
to substituted groups in the alkylbenzenes[2] are absent
in the present system of hydrogen bonding. Our results
can be explained on the basis of inductive effects alone,
where alkyl substitution increases the basicity of the $\pi$
bases, while halogen substitution, as in chlorobenzene,
decreases the same. Our findings are similar to the ob-
servations on O–H$\cdots\pi$ interaction.[1,3-5]

## Low-Energy Electron Radiolysis of Methane

by C. D. Finney and H. C. Moser*

*Department of Chemistry, Kansas State University,
Manhattan, Kansas 66502 (Received July 14, 1970)*

Several electron radiolysis studies have shown that
information on mechanisms may result when the im-

pacting electron energy is defined.[1-5] Melton and Rudolf[3-5] have well established the relationship between impacting electron energies and product yields. It is the purpose of this note to report additional information, obtained by an independent experimental method, on the low-energy electron radiolysis of methane. Some results pertaining to product thresholds differ from those previously reported.

## Experimental Section

Photoelectrons as opposed to thermionic electrons were used so that static gas phase experiments could be performed without the complication of pyrolytic background products. The radiolysis cell is a modification of one developed by Williams.[1,6,7] A positive-ion measuring capability originated by Compton and van Voorhis[8] was also incorporated. The method is limited only by the fact that the gas under study (and the radiolysis products) must be transparent to the light which produces the photoelectrons.

A schematic representation of the tetrode radiolysis cell and auxiliary equipment is shown in Figure 1. Experiments were performed in a glass vacuum system capable of attaining ultimate pressures of less than $5 \times 10^{-6}$ Torr. The potentials on the various electrodes were then applied. The grid and collector electrodes were always at ground potential. The cathode was set at the desired negative accelerating potential. The bias on the ion-collecting electrodes was always 1.5 V more negative than that on the photocathode. Voltages applied in this mannern esured that neither primary nor secondary electrons would be collected on the ion measuring system. The reaction period was 45 min. During runs the currents at the anode and ion-collecting wires were recorded. The currents typically decreased by a few per cent during the reaction period. The current at the anode was about $5 \times 10^{-7}$ A. Reactant consumption did not exceed 5%. After reaction the gases were quantitatively transferred to a sampler and analyses were performed on an F & M Model 810 chromatograph equipped with an HFI detector.
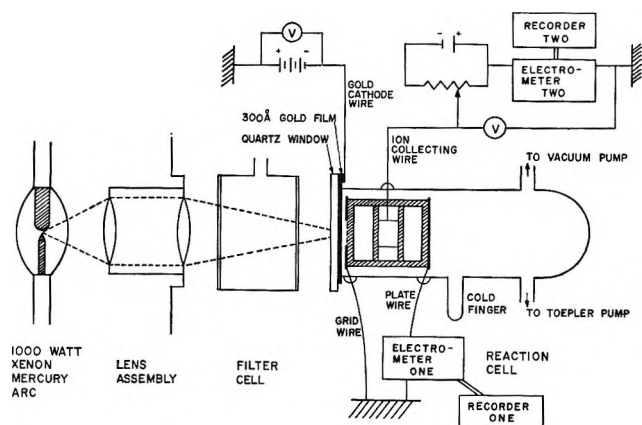


Figure 1. Schematic representation of the tetrode radiolysis cell and auxiliary equipment.
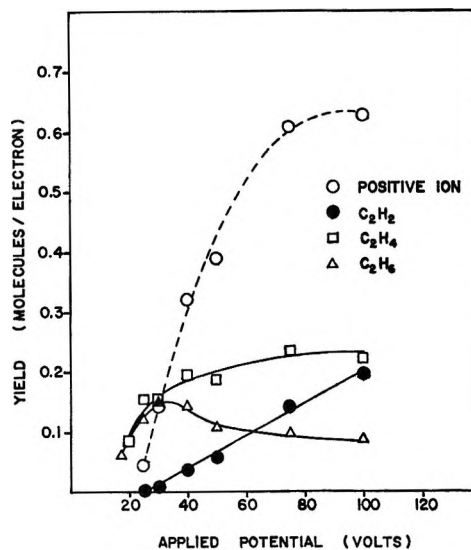
Figure 2. Total ionic and neutral product yields per anode electron as a function of applied potential.

## Results and Discussion

The product yields are presented in Table I and are plotted in Figure 2. The units are molecules of product (ionic or neutral) per anode electron. From Figure 2 it is seen that the experimental threshold for ion formation occurred in the region of an applied potential of 20 V. This value is clearly much greater than the electron impact ionization energy of 12.7 eV recently reported by Lossing and Semeluk.[9] The latter may be taken as the

**Table I:** Product Yields[a] with Methane Reactant (0.025 Torr; Reacted for 45 min)

| Applied potential, V | Positive ion | $C_2H_2$ | $C_2H_4$ | $C_2H_6$ |
|---|---|---|---|---|
| 100 | 0.627 | 0.197 | 0.222 | 0.087 |
| 75 | 0.609 | 0.141 | 0.237 | 0.098 |
| 50 | 0.389 | 0.058 | 0.190 | 0.106 |
| 40 | 0.321 | 0.039 | 0.196 | 0.142 |
| 30 | 0.139 | 0.007 | 0.155 | 0.148 |
| 25 | 0.047 | 0.003 | 0.156 | 0.122 |
| 20 | | | 0.085 | 0.089 |
| 17.5 | | | 0.063 | 0.066 |

[a] The yields presented are in units of molecules of product per electron collected at the plate.

(1) R. R. Williams, Jr., *J. Phys. Chem.*, **63**, 776 (1959); **66**, 372 (1962).

(2) J. E. Manton and A. W. Tickner, *Can. J. Chem.*, **38**, 858 (1960).

(3) C. E. Melton and P. S. Rudlof, *J. Chem. Phys.*, **47**, 1771 (1967).

(4) P. S. Rudolf and C. E. Melton, *J. Phys. Chem.*, **71**, 4572 (1967).

(5) P. S. Rudolf, *Advan. Chem. Ser.*, No. **82**, 101 (1968).

(6) C. D. Finney, Ph.D. Thesis, Kansas State University, Manhattan, Kans., 1970.

(7) J. L. Moruzzi, *Rev. Sci. Instrum.*, **38**, 1284 (1967).

(8) K. T. Compton and C. C. van Voorhis, *Phys. Rev.*, **26**, 436 (1925).

(9) F. P. Lossing and G. P. Semeluk, *Int. J. Mass Spectrom. Ion Phys.*, **2**, 408 (1969).

effective upper limit of the electron energy spectrum at an applied potential of 20 V. The margin between the two must be due principally to the perturbation of the electric field caused by the ion-collecting electrodes in the collision region. Compton and van Voorhis[8] analyzed the effect of such a field on a beam of electrons and found that it caused a spread in impact energies ranging from about 0.6 to 1 times the applied potential and thus shifted the electron spectrum to lower energies. Two other effects in our system which caused the electron spectrum to be broadened less extensively were the initial spread in photoelectron energies and the inhomogeneity of the electric field between the cathode and grid.

Figure 2 illustrates a major result of our investigation. Ethane and ethylene were produced at energies below the threshold for ionization, while acetylene had a threshold about equal to that for ionization. In physical studies of the direct scattering of low-energy electrons, Bowman and Miller[10] observed a threshold for methane at 7.5 eV. Using higher energy electrons, Lassettre and Francis[11] reported an energy loss threshold at 8.0 eV. In chemical studies, however, Rudolf[5] has reported product thresholds of 12.7, 12.7, and 12.9 eV for ethane, ethylene, and acetylene, respectively.

The formation of significant yields of $C_2H_6$ and $C_2H_4$ at applied potentials where no ions were detected is evidence for primary excitation being a principal contributor to these yields. However, some ethane and ethylene were probably formed from ionic precursors at voltages where ionization was important. The appearance of acetylene at the threshold for the formation ions signifies that it was formed entirely from ionic and/or superexcited[12] precursors.

*Acknowledgments.* Informative discussions with Professors A. G. Harrison, C. E. Melton, R. L. Platzman, and D. W. Setser were greatly appreciated. C. D. F. is indebted to the Phillips Petroleum Co. for a fellowship. The work was supported by the United States Atomic Energy Commission.

(10) C. R. Bowman and W. D. Miller, *J. Chem. Phys.*, 42, 681 (1965).

(11) E. N. Lassettre and S. A. Francis, *ibid.*, 40, 1208 (1960).

(12) R. L. Platzman, *Vortex*, 23, 373 (1962).

## Reactions of Fast $T_2$ Molecules with 1-Butene[1]

by J. W. Beatty, L. G. Pobo, and S. Wexler*

*Argonne National Laboratory, Argonne, Illinois 60439*
*(Received February 22, 1971)*

Chemical reactions in the gas phase of species with hyperthermal energies have mainly been studied by the nuclear recoil technique.[2a,b] In particular, recoil tritium atoms are observed to react with 1-butene by addition to the double bond followed by decomposition of the excited butyl radical, by direct displacement of a hydrogen atom or a radical, and by abstraction of a hydrogen atom.[3-6] Atomic tritium with thermal energy distributions also insert into the double bond of 1-butene with the eventual formation of tritiated decomposition products of the transient butyl radical.[7] The reactions of molecular tritium have not been studied, but the addition of $H_2$ to a double bond is forbidden by molecular orbital symmetry rules,[8] and therefore, the reaction should require a rather high activation energy. The only presently known method of causing molecular hydrogen to react with unsaturated hydrocarbons is by exposing them to freshly prepared catalysts.[9] Under proper conditions, hydrogen exchange, addition to the double bond, and isomerization are prominent reactions.

We wish to report some observations on the reactions of accelerated $T_2$ molecules with 1-butene molecules, the experiments being conducted with a "chemical accelerator." $T_2^+$ ions are produced in a low-voltage arc, extracted and accelerated, separated from other species by a zero deflection mass filter, decelerated to a well-defined energy between 5 and 100 eV, and then neutralized by near resonance charge exchange. A beam of the accelerated $T_2$ molecules collides with a crossed beam (actually a broad sheath) of 1-butene molecules, and the products are collected and later analyzed by radiogas chromatography. A detailed description of the apparatus has been given.[10]

In Figure 1 are the yields of the major products formed by reactions of fast $T_2$ molecules with 1-butene molecules as functions of the initial kinetic energy of tritium. Note that the products are 1-butene, *n*-bu-

(1) Work performed under the auspices of the U. S. Atomic Energy Commission. One of us (J. W. B.) received partial support from the National Science Foundation under NSF Grant No. GY8428.

(2) (a) F. S. Rowland in "Molecular Beams and Reaction Kinetics," Ch. Schlier, Ed., Academic Press, New York, N. Y., 1970, pp 108-116; (b) A. G. Maddock and R. Wolfgang in "Nuclear Chemistry," Vol. II, L. Yaffe, Ed., Academic Press, New York, N. Y., 1968, pp 186-248.

(3) E. K. C. Lee and F. S. Rowland, *J. Amer. Chem. Soc.*, 74, 439 (1970).

(4) D. Urch and R. Wolfgang, *ibid.*, 83, 292 (1961); *Chem. Eff. Nucl. Transform. Proc. Symp.*, 2, 99 (1961).

(5) J. K. Lee, B. Musgrave, and R. S. Rowland, *J. Amer. Chem. Soc.*, 82, 3545 (1960); R. S. Rowland, J. K. Lee, B. Musgrave, and R. M. White, *Chem. Eff. Nucl. Transform. Proc. Symp.*, 2, 67 (1961).

(6) F. Schmidt-Bleek and F. S. Rowland, *Angew. Chem. Int. Ed. Engl.*, 3, 769 (1964).

(7) W. M. Ollison and J. Dubrin, *Radiochim. Acta*, 14, 111 (1970).

(8) R. G. Woodward and R. Hoffman, "The Conservation of Orbital Symmetry," Academic Press, New York, N. Y., 1969; for a popular review, see R. G. Pearson, *Chem. Eng. News*, 48 (41), 66 (1970).

(9) See the following reviews for examples: G. C. Bond and P. B. Wells, *Advan. Catal.*, 15, 92 (1964); J. J. Rooney, *Chem. Brit.*, 2, 242 (1966); A. Clark, "The Theory of Adsorption and Catalysis," Academic Press, New York, N. Y., 1970.

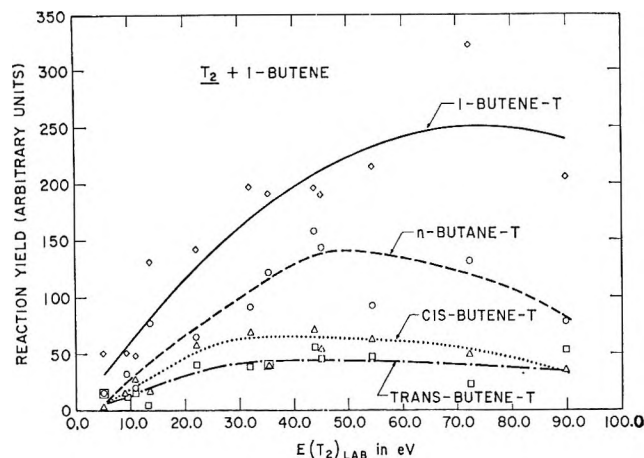(10) J. W. Beatty and S. Wexler, *J. Phys. Chem.*, in press.

Figure 1. Reaction yields of major tritiated products from reactions with 1-butene of $T_2$ molecules with initial kinetic energies in the range from 5 to 90 eV.

tane, cis-2- and trans-2-butene, and that their yields increase from thresholds below 5 eV to plateaus or broad maxima at high energies. The yields are in the approximate proportion 1-butene-$t$/$n$-butane-$t$/cis-2-butene-$t$/trans-2-butene-$t$, 4:2:1:1.

A mechanism that can account for our observations is the addition of the energetic $T_2$ to the double bond (the kinetic energy of the $T_2$ supplying the activation energy for the reaction) forming an excited tritiated butane, which then dissociates into one of the butenes or is stabilized by collision. The energy of activation for isomerization of alkenes (double bond movement or cis–trans transformation) is 2.7 eV,[11] a value below that attainable in our experiment, but which in the laboratory system of coordinates (3.0 eV) appears to be approached by three of the curves in Figure 1. Furthermore, if we assume equal probability of abstraction of adjacent hydrogen pairs from the excited doubly tritiated butane, the proportion of labeled butene products is calculated to be 1-butene-$t$/cis-2-butene-$t$/trans-2-butene-$t$, 6:1:1, values not too dissimilar from those observed. The relative yields differ greatly from those found in the recoil studies, in which the tagged parent is by far the most prominent organic product.[3-6] The differences may be accounted for by the contrasting chemical behaviors of atomic and molecular tritium and the much lower gas densities existing in this experiment, which precludes extensive gas phase collisional stabilization of the intermediates of reactive encounters.

Though the yields of the tritiated products remain high even at high initial kinetic energies of $T_2$ (Figure 1), it should not be concluded that chemical reactions actually take place in this range. Since the reactions occur in a collision chamber, the $T_2$ molecules may pass through the 1-butene sheath several times, being degraded in energy between passes by collisions with the walls of the chamber. Analysis of the yield curves by Porter's theory,[12] which takes into account kinetic

energy moderation of fast species, indicates that chemical reactions take place when the $T_2$ energy is below 20–30 eV.

(11) L. G. Pratt, "Gas Kinetics," Wiley, London, 1969, p 156.
(12) R. N. Porter, J. Chem. Phys., 45, 2284 (1966).

## Infrared Study of Aluminum-Deficient Zeolites in the Region 1300 to 200 cm$^{-1}$

by O. Lahodny-Šarc*

Institute of Physical Chemistry, Technological Department,
University of Zagreb, Zagreb, Yugoslavia

and J. L. White

Department of Agronomy, Purdue University,
Lafayette, Indiana 47907   (Received March 16, 1971)

There is considerable interest currently in the nature and properties of Al-deficient zeolites. Several authors[1-6] have recently described changes in composition and adsorption properties resulting from removal of aluminum from the zeolite framework but very little infrared evidence for structural changes has been published. This note reports an infrared study of synthetic zeolites A, 13X, and Y in the 1300 to 200-cm$^{-1}$ region with the objective of obtaining information about structural changes induced by removal of aluminum.

### Experimental Section

Linde Type 4A, 13X, and Y zeolites were treated with $H_2CO_3$ for various time periods in one series of experiments and with ethylenediaminetetraacetic acid in a second series of experiments.

Infrared spectra were obtained using the KBr pellet technique with a Perkin-Elmer 521 double-beam grating infrared spectrophotometer.

### Results and Discussion

Infrared spectra of the three zeolites and the two series of experiments are shown in Figure 1.

(1) R. M. Barrer and M. B. Makk, Can. J. Chem., 42, 1981 (1964).
(2) S. P. Zdanov and B. G. Novikov, Dokl. Akad. Nauk SSSR, 166, 1107 (1966).
(3) G. T. Kerr, J. Phys. Chem., 71, 4155 (1967).
(4) G. T. Kerr, ibid., 72, 2594 (1968).
(5) D. Barthomeuf and R. Beaumont, C. R. Acad. Sci., Ser. C, 269, 1345 (1969).
(6) W. L. Kranich, Y. H. Ma, L. B. Sand, A. H. Weiss, and I. Zwiebel, Second International Conference on Molecular Sieve Zeolites, Worcester, Mass., 1970, p 802.
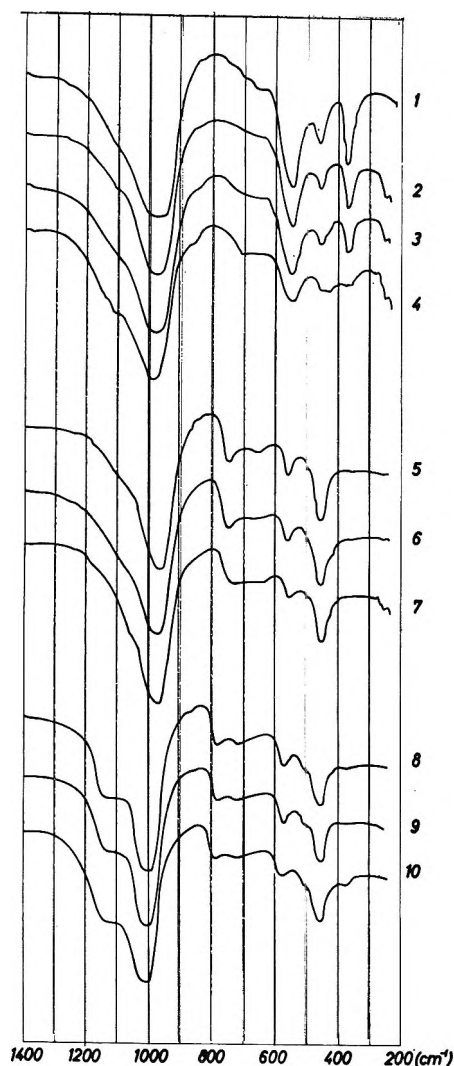
Figure 1. Infrared spectra of zeolites before and after
aluminum-removal treatments: spectrum 1, 4A zeolite (original
sample); spectrum 2, 4A zeolite treated with H4EDTA 2 hr;
spectrum 3, 4A zeolite treated with H2CO3 1 hr; spectrum 4,
4A zeolite treated with H4EDTA 12 hr; spectrum 5, 13X
zeolite (original sample); spectrum 6, 13X zeolite treated
with H4EDTA 13 hr; spectrum 7, 13X zeolite treated with
H2CO3 1/2 hr; spectrum 8, Y zeolite (original sample);
spectrum 9, Y zeolite treated with H4EDTA 2 hr; spectrum
10, Y zeolite treated with H4EDTA 12 hr.

The interpretation of the spectra is greatly facilitated
by the classic publication of Flanigen and Khatami.[7]
According to these authors, the infrared spectra of zeo-
lites in the 1300–200-cm$^{-1}$ region appear to consist of
two classes of vibrations: (1) those caused by internal
vibration of the framework TO$_4$ tetrahedron (950–
1250 cm$^{-1}$) and (2) the vibration related to the external
linkages between tetrahedra (500–600 and 300–420
cm$^{-1}$). Thus, removal of aluminum from tetrahedral
sites should cause changes in both classes of vibrations.

The most intense absorption band occurs in the 950–
1050-cm$^{-1}$ region and is related to the T–O asymmetric
stretching vibration; this vibration is sensitive to the

Si–Al ratio as has been shown for the Linde 4A zeolite.[8]
This band is shifted to higher frequency with increasing
content of Si and the same shift is observed for the
samples of the A zeolite series treated with acid to give
Al-deficient zeolites.

There is a shoulder at about 1100 cm$^{-1}$ for the A
zeolite; this shoulder occurs at about 1150 cm$^{-1}$ for the
Y zeolite which has a higher content of Si than the A
zeolite. This shoulder appears to be more pronounced
for all Al-deficient specimens in this study. Flanigen[7]
suggests that this shoulder is related to the framework
topology of the zeolites and assigned it to an external
linkage mode.

The symmetric stretching vibration which occurs at
780 cm$^{-1}$ in the Y zeolite series, at 750 cm$^{-1}$ in the 13X
series, and is very faint at about 720 cm$^{-1}$ for the 4A
series, has been assigned to external linkage modes;[7]
this band also shifts toward higher frequencies for sam-
ples having a higher Si/Al ratio.

A linear increase in frequency with decrease of Si con-
tent is quite distinct for the double six-ring band at
about 570 cm$^{-1}$ for Y zeolite and at about 560 cm$^{-1}$ for
13X zeolite; the double four-ring band occurs at about
550 cm$^{-1}$ for the 4A zeolite.

The band at about 460 cm$^{-1}$ in all three types of
zeolites was assigned by Flanigen[7] to a T–O bend-
ing mode. This band does not change with the Si–Al
ratio except in the 4A series, where a decrease in inten-
sity and broadening of this band was observed for Al-
deficient samples. This band has a high-frequency
shoulder (about 500 cm$^{-1}$) in the spectra of the Y
zeolite but is only very faint in the 13X zeolite and is
absent in the 4A zeolite series. A low-frequency
shoulder at about 430 cm$^{-1}$ is present in the spectra of
all three zeolites.

The band at 370 cm$^{-1}$ in the A zeolite (assigned to a
"pore opening" by Flanigen[7]) is very distinct.
It decreased with increasing Si content and is greatly
reduced in intensity for the most Al-deficient A zeolite
sample. This feature is very faint in the X and Y zeo-
lites. Removal of aluminum from the A zeolite by
treatment with H4EDTA for 12 hr produced the follow-
ing spectral changes: a decrease of approximately
50% in the intensity of the external linkage band at
550 cm$^{-1}$; almost complete disappearance of the "pore
opening" band at 370 cm$^{-1}$; and broadening of the band
in the T–O stretching region (460 cm$^{-1}$). It is specu-
lated that removal of the aluminum from the framework
of the A zeolite may have produced framework distor-
tion and changes in symmetry of the ring cages similar
to that described by Flanigen[7] for cation move-
ment and framework distortion in a Ca-exchanged Y
zeolite. There is a very distinct shoulder at about 620

(7) E. M. Flanigen and H. Khatami, Second International Confer-
ence on Molecular Sieve Zeolites, Worcester, Mass., 1970, p 460.
(8) O. Lahodny-Šarc and D. Došen, Bull. Groupe Fr. Argiles, 22,
167 (1970).

cm$^{-1}$ which we postulate may be due to a partial shift of the vibration at 550 cm$^{-1}$. The broad band in the 430-460-cm$^{-1}$ region may be due to a shift of the "pore opening" band at 370 cm$^{-1}$ to about 430 cm$^{-1}$ as a result of aluminum removal.

The most dramatic shift was observed for the absorption band assigned to asymmetric stretching of T-O in the 950-1050-cm$^{-1}$ region. The frequency shift of infrared stretching bands with changes in the Si-Al ratio in tetrahedra in aluminosilicate frameworks has been reported by several authors;[9,10] Flanigen[7] has recently reported new information on a large number of synthetic zeolites and has established excellent relationships between Si-Al content and frequency shifts in several classes of infrared bands.

The effect of aluminum removal treatments on the position of the T-O asymmetrical stretching bands in the three zeolites examined in this study is shown in Table I. Using the data reported by Flanigen[7] for the slope of the lines relating the T-O stretching frequency with atom fraction of aluminum in the framework, we have estimated the atom fraction of Al removed by the treatments (Table I).

**Table I:** Effect of Aluminum-Removal Treatments on the Asymmetric T-O Stretching Band of 4A, 13X, and Y Zeolites

| Zeolite | Treatment | Frequency $\nu_{asym}$, cm$^{-1}$ | Frequency shift, cm$^{-1}$ | Atom fraction of Al removed[a] |
|---|---|---|---|---|
| 4A | Untreated | 980 | | |
| 4A | H$_4$EDTA 12 hr | 994 | +14 | 0.07 |
| 13X | Untreated | 970 | | |
| 13X | H$_4$EDTA 13 hr | 976 | +6 | 0.03 |
| 13X | H$_2$CO$_3$ 30 min | 979 | +9 | 0.045 |
| Y | Untreated | 1004 | | |
| Y | H$_4$EDTA 2 hr | 1008 | +4 | 0.02 |
| Y | H$_4$EDTA 12 hr | 1015 | +11 | 0.055 |

[a] For A zeolite the slope = 19 cm$^{-1}$/0.1 atom fraction of Al; for X and Y zeolites the slope = 20 cm$^{-1}$/0.1 atom fraction of Al.[7]

Comparison of estimates in Table I with results of chemical analyses shows qualitative agreement between these values within a given series. The infrared estimates tend to be consistently higher than the chemical results.

In conclusion, we have shown that removal of aluminum from the zeolite framework within a series of any given zeolite of the A, 13X, or Y type results in an intensification of frequencies assigned to external linkage modes in the 1120-1140-cm$^{-1}$ region. This is somewhat parallel but less marked than the shifts to higher frequencies observed for external linkage mode assignments in the 1100-1150, the 720-800, and the 550-580-cm$^{-1}$ regions in going from a high to low alu-

minum content in the sequence A, 13X, and Y zeolites.

Removal of aluminum from the zeolite framework caused the asymmetric stretch of the T-O to be shifted to higher frequencies for the A, 13X, and Y zeolites.

The spectral features of the A zeolite were affected most strongly. Framework distortion and changes in symmetry of the ring cages are suggested as possible explanations for spectral changes produced by aluminum removal.

(9) R. G. Milkey, *Amer. Mineral.*, **45**, 990 (1960).

(10) K. Oinuma and H. Hayashi, *J. Tokyo Univ. Gen. Educ.*, **8**, 1 (1967).

# High Molecular Weight Boron Sulfides.
# VII.   Lower Temperature Studies and
# Metastable Decompositions

by Jimmie G. Edwards, James M. Leitnaker,

Heribert Wiedemeier, and Paul W. Gilles*

*Department of Chemistry, University of Kansas, Lawrence, Kansas 66044*   (Received October 5, 1970)

In their studies of the high molecular weight boron sulfides, arising from slightly sulfur-rich diboron trisulfide, B$_2$S$_3$, Greene and Gilles[1,2] reported the discovery of more than 30 boron sulfide ions observed mass spectrometrically. They were not able to identify the neutral molecules, but suggested that the parent molecules are polymers of BS$_2$(g). Chen and Gilles[3] and Edwards, Wiedemeier, and Gilles[4,5] have reported several metastable decompositions. In the present paper we report experiments performed at lower temperatures which confirm the presence of neutral BS$_2$ polymers through the identification of their parent ions, and experiments which yield additional metastable decompositions.

Chen and Gilles[3] in studying stoichiometric B$_2$S$_3$, rather than the sulfur-rich samples used by most of the other workers, found five metastable decompositions of B$_2$S$_3$ and its polymers at natural boron $m^*$ values of 47.7, 62.7, 110.0, 330, and 450. These were

$$B_2S_3^+ \longrightarrow BS_2^+ + BS \tag{1}$$

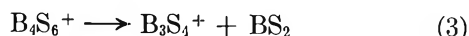$$B_2S_3^+ \longrightarrow B_2S_2^+ + S \tag{2}$$
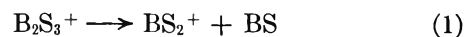
(1) F. T. Greene and P. W. Gilles, *J. Amer. Chem. Soc.*, **84**, 3598 (1962).

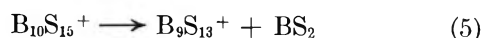(2) F. T. Greene and P. W. Gilles, *ibid.*, **86**, 3964 (1964).

(3) H. Y. Chen and P. W. Gilles, *ibid.*, **92**, 2309 (1970).

(4) J. G. Edwards, H. Wiedemeier, and P. W. Gilles, *ibid.*, **88**, 2935 (1966).

(5) J. G. Edwards and P. W. Gilles, *Advan. Chem. Ser.*, **No. 72**, 211 (1968).

$$B_4S_6^+ \longrightarrow B_3S_4^+ + BS_2 \qquad (3)$$

$$B_8S_{12}^+ \longrightarrow B_7S_{10}^+ + BS_2 \qquad (4)$$

and

$$B_{10}S_{15}^+ \longrightarrow B_9S_{13}^+ + BS_2 \qquad (5)$$
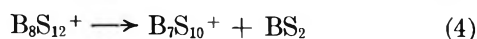
Except in the second of these reactions, $BS_2$ is always involved, and the charge remains on the larger assembly of atoms. Edwards, Wiedemeier, and Gilles[4,5] have reported six metastable decompositions among the thioboric acids in the H–B–S system, at [10]B-enriched $m^*$ values of 38.5, 46.8, 48.5, 71.3, 89.7, and 100.0.

The mass spectrometer and procedure have been previously described.[1-5] Boron sulfide was prepared from both naturally occurring and [10]B-enriched boron as previously described by the reaction between boron and dried $H_2S$ at temperatures of about 700° in Vycor tubes. The white, needle-shaped crystals of $HBS_2$ were subsequently thermally decomposed in graphite containers under high vacuum at temperatures between 100 and 150°. The decomposed product was heated in the mass spectrometer in a graphite crucible. Ions were identified by their masses and by their isotopic distributions. The metastable decomposition reactions were recognized and identified in the usual way.

Samples similarly prepared have been analyzed[2,3] to be sulfur-rich, and the present samples are believed to be similarly sulfur-rich.

Spectra obtained at progressively increasing temperatures up to 300° from samples that had never been heated to a higher temperature revealed the presence of $B_8S_{16}^+$ as the most important boron sulfide ion. Two additional polymer ions of $BS_2$, $B_7S_{14}^+$, and $B_6S_{12}^+$, as well as polymers of sulfur were observed. No ion with more than four boron atoms contained more than twice as many sulfur atoms as boron atoms.

Table I lists the metastable reactions observed in samples prepared with enriched boron. All metastable decompositions given in Table I produce either $S_2$ or $BS_2$ as a neutral fragment. In each instance the charge remains on the larger particle, as is the case for the previously reported decompositions.[3]

**Table I:** Metastable Decompositions of Boron Sulfides

| Mass ([10]B) | | Number of atoms per molecule | | | | | | T, |
| --- | --- | --- | --- | --- | --- | --- | --- | --- |
| | | Parent | | Fragment | | Neutral | | |
| Obsd | Calcd | B | S | B | S | B | S | °C[a] |
| 325 | 326 | 6 | 12 | 6 | 10 | 0 | 2 | 465 |
| 359 | 359 | 8 | 13 | 7 | 11 | 1 | 2 | 400 |
| 367 | 367 | 7 | 13 | 7 | 11 | 0 | 2 | 400 |
| 391 | 391 | 8 | 14 | 7 | 12 | 1 | 2 | 370 |
| 408 | 408 | 8 | 14 | 8 | 12 | 0 | 2 | 400 |
| 425 | 422 | 8 | 15 | 7 | 13 | 1 | 2 | 510 |
| 440 | 440 | 8 | 15 | 8 | 13 | 0 | 2 | 370 |
| 471 | 471 | 8 | 16 | 8 | 14 | 0 | 2 | 370 |
| 505 | 505 | 10 | 17 | 9 | 15 | 1 | 2 | 510 |

[a] Lowest temperature at which metastable decomposition reaction was observed, on charts 5040, 1, 5.

Unidentified metastables are observed in [10]B-enriched samples at masses 63, 83, 115, 149, 193, and 453, and in natural boron samples at masses 239 and 251. Reactions accounting for these metastable transitions could not be unambiguously identified; possibly they involve doubly charged precursors.

The appearance potentials for the metastable decomposition at mass 471 and the ions $B_8S_{16}^+$ and $B_8S_{14}^+$ were measured as 11.0, 8.5, and 11.0 eV, thus substantiating the identification.

The nine metastable reactions listed in Table I when added to the previously reported 11 raise the number of identified metastable decompositions in the boron sulfide and H–B–S systems to 20. Eight remain yet unidentified. The reactions reported here involve more sulfur-rich species than those reported earlier from stoichiometric samples.[3] Four chains of metastable decompositions involving two or more reactions are recognizable.

The low appearance potential of $B_8S_{16}^+$ and its metastable decomposition to $B_8S_{14}^+$ indicate the existence of neutral $B_8S_{16}(g)$. The existence of the polymers $B_6S_{12}^+$ and $B_7S_{14}^+$ and the absence of metastable reactions yielding them may indicate that they arise from neutral molecules of the same composition. The ion $B_8S_{15}^+$ has been shown to have a source other than $B_8S_{16}^+$. The ion $B_8S_{14}^+$ grew in intensity with time and temperature relative to $B_8S_{16}^+$. Earlier appearance potential measurements[2] give a much lower value, 8.3 ± 0.8 eV, than that reported here. Thus not only is it a fragment of $B_8S_{16}^+$, but also it has another source as well.

In the work of Greene and Gilles[1,2] neither the $(BS_2)_n^+$ polymers nor the metastables appeared. The most likely reason is that the mass spectrometric source conditions of repeller and drawout potentials were such as to retain the ions sufficiently long that they decomposed.

The chemical reactions producing the gaseous polymers of $BS_2$ from samples of "sulfur-rich" $B_2S_3$ are not clear. Two suggestions can be proposed, but the choice cannot be made at the present time. The analysis does not completely distinguish between excess sulfur and excess $H_2S$. On the first basis, that sulfur is present, the reaction will be, as Greene and Gilles[2] suggested

$$B_2S_3(gl) + S(soln) = 2/n(BS_2)_n \qquad (6)$$
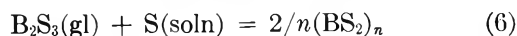
On the second basis, that the impurity is $H_2S$, the presence of $H_2B_2S_5$, previously reported,[4,5] can be accounted for, and a succession of condensation reactions of $H_2B_2S_5$ with the elimination of $H_2S$ at each stage may occur to produce $B_8S_{16}(g)$.

The structure of the important species $B_8S_{16}(g)$ has not been deduced but we suggest that a ring of boron atoms lies between two rings of sulfur atoms.

States Atomic Energy Commission under Contract AT(11-1)-1140. They also are pleased to acknowledge the help of the University of Kansas Computation Center for the calculations of the metastable masses.

# Laser-Produced Oxygen From Silicon Dioxide

by J. P. Biscar*

*Department of Physics, University of Wyoming, Laramie, Wyoming 82070*

and F. Miknis

*Laramie Energy Research Center, Bureau of Mines, U. S. Department of Interior, Laramie, Wyoming 82070*
*(Received December 29, 1970)*

We report the production of a relatively large amount of oxygen by focusing a Q-switched ruby laser on a fused silica sample. Approximately $10^{17}$ molecules of oxygen were produced per shot. To our knowledge this physicochemical effect has not been previously reported, although laser-induced damage in glasses and subsequent radiation has been observed.[1-7]

Considering the energy per photon (1.78 eV) and the number of photons per pulse ($10^{18}$), the ratio of ten photons for each molecule of oxygen produced suggests a relatively high efficiency taking into account the binding energy of the silicon dioxide. This is probably due to the localized, rapid heating of the sample to several thousand degrees Kelvin initiated by a multiphoton ionization process. The high temperature also provides the kinetic energy for an extremely rapid plasma expansion, minimizing the probability of silicon-oxygen recombination.

A water-cooled ruby laser was used for these experiments. A superior internal quality ruby crystal, 4 in. $\times$ $9/16$ in. with uncoated flat ends was sand-blasted on its cylindrical surface for uniform optical pumping. Optical pumping was achieved by discharging 4000 J into a helical flash lamp mounted between ceramic reflectors. The optical cavity consisted of a totally reflecting quartz prism and a sapphire etalon. A 20-nsec Q-switched pulse was achieved with a solution of kryptocyanine dye in methanol. The passive dye cell had an optical path of 1 cm. Under these conditions the peak output power exceeded 100 MW, and single pulses were obtained by adjusting the dye concentration. Since the laser operated in a multimode, some mode-locking and picosecond effects are not to be excluded. The output of the laser was focused in the center of a spherical Pyrex bulb (50 to 100 cc) by a lens of 42-mm focal length, where a fused silica plate was placed. This was to avoid large power densities at the bulb surface and prevent its damage. For smaller bulbs (10 to 25 cc), a 20-mm focal length lens was used.

We report here only the data obtained with fused silica samples because fused silica is much less contaminated with impurites than glasses. Samples of two different sources of fused silica gave the same results. Each sample was first rinsed with acetone and distilled water, then heated at a high temperature with a flame to desorb any water and surface impurities. The sample was placed in an evacuated bulb and thoroughly degassed. The pressure inside the bulb was monitored with a thermocouple gauge.

In a volume of 20 cc, each laser shot produced an average pressure rise of 200 mTorr. An independent check was made on a powdered fused silica sample. To verify that the pressure rise was due to liberated oxygen, several laser shots were focused into the powdered sample and the contents were examined on a time-of-flight mass spectrometer. The mass spectral results indicated the presence of oxygen. A pressure rise of 200 mTorr corresponds to approximately $10^{17}$ molecules of oxygen released by the dissociation of silicon dioxide. It also includes other liberated gases and probably water which is eventually readsorbed. These contaminants must, however, be negligible in proportion to the amount of oxygen produced based on mass spectral evidence and the small volume of silica irradiated. A small portion of the fused silica surface is vaporized after each shot, owing to the high temperature attained. The volume of the craters depends both on the output power and focusing of the laser. Repetitive lasing on the same crater reduces the amount of oxygen released because of the large amount of scattering from the rough surface and less photon penetration into the sample. The pressures recorded were usually 100 to 150 mTorr from the rough surface. However, with higher laser outputs and better quality optics the amount of oxygen liberated per shot should increase substantially. With the same pumping power and in the conventional mode, no appreciable oxygen was liberated, although a large surface damage was noted on a previously created crater. Even though the amount of energy per pulse was an order of magnitude more in the conventional mode, it produced no damage on a transparent fused silica surface because the threshold of multiphoton ionization was not reached. The Q-switched mode seems to be the most efficient, providing the maximum release of oxygen for the minimum amount of sample.

(1) R. A. Miller and N. F. Borelli, *Appl. Opt.*, **6**, 164 (1967).
(2) J. P. Buding and J. Raffy, *Appl. Phys. Lett.*, **9**, 291 (1966).
(3) M. P. Lisitsa and I. V. Fekeshgazi, *Ukr. Fiz. Zh. (Ukr. Ed.)*, **12**, 1698 (1967).
(4) J. Davit, J. Decoux, J. Gautier, and M. Soulie, *Rev. Phys. Appl.*, **3** (2), 118 (1968).
(5) J. Martinelli, *Jour, Appl. Phys.*, **37**, 1939 (1966).
(6) B. S. Sharma and K. Rieckhoff, *Can. J. Phys.*, **48**, 1178 (1970).
(7) D. W. Harper, *Brit. J. Appl. Phys.*, **16**, 751 (1965).

An interesting step in these experiments was to be able to replace gas chromatrography and mass spectroscopy techniques of detection by a pressure measurement because of the relatively large amounts of oxygen produced. Before laser irradiation the bulb is pumped at a pressure below 10 mTorr which is sufficient for the precision of these experiments. Immediately following the laser shot, one expects to find in the gas mixture $SiO_2$, $SiO$, $Si$, $O$, $SiO_2^+$, $SiO^+$, $Si^+$, $O^+$, and some of these species ionized several times. However, as a stable gas product only molecular oxygen will remain, $SiO$, $SiO_2$, and $Si$ decreasing rapidly as impurities in suspension by condensation on the walls where microcrystals start to grow. Not all the laser energy is spent to heat the plasma. Amounts of solid materials of different size are also ejected from the target acquiring part of the available energy for their kinetic energy and temperature increase. Additional energy is also required to raise the temperature of the solid target. The oxygen production efficiency reported here is due to the minimization of the ejected solid particles.

In order to increase the recuperation of oxygen from silica, the use of a hydrogen atmosphere was advised, since it is easy to electrolytically decompose the produced water while $H_2$ is recycled. Conducting a different research, we had suspected oxygen hydrogen recombination near a glass surface. Attempting to reproduce some data on hydrogen vibrational lifetimes,[8] we found an unexpected fluorescence. This fluorescence decayed exponentially, and its lifetime became shorter with increasing hydrogen pressure. Although the laser was not focused directly into a glass surface, as in the original experiments,[8] the emission was traced to a laser–glass–hydrogen interaction, possibly with oxygen extracted from glass and hydrogen recombination.

Experiments of decomposition of fused silica under hydrogen atmosphere by focusing a Q-switched laser on its surface were conducted. Attempts to identify water by gas chromatography after lasing fused silica in a hydrogen atmosphere were not reproducible due to the condensation of the water in the bulb and sampling syringe, although some water production was indicated. To build up a sizeable quantity of water for analysis a V-shaped fused silica target was constructed and placed in a 100-cc bulb filled with 15 lb of hydrogen above atmospheric pressure. We decided to fire 100 shots onto the target and analyze the mixture for water. The bulb exploded after 60 shots, producing a dense fog inside the bulb which later condensed on the sides. This result indicated that molecular oxygen was liberated from the fused silica, which upon achieving a high enough concentration explosively combined with hydrogen to produce water under the action of the next laser spark. Qualitatively, indications are that only relatively small amounts of oxygen are converted in water at each laser shot and that the hydrogen ap-

proach might not be very interesting to increase the oxygen production from silica. In order to determine if more oxygen is recuperated under hydrogen atmosphere, the gas mixture has to be circulated through cold traps in order to remove and measure the amount of oxygen and water produced.

In these experiments, the overall efficiency is lost in the ruby laser itself. A carbon dioxide laser at a pressure of one atmosphere or more could produce a 100-MW output per pulse, with an efficiency of 18 to 20%. If it can further be made to operate at a repetition rate of 100 pulses/sec, laser-produced oxygen from silicon dioxide will be largely improved.

(8) F. De Martini and J. Ducuing, *Phys. Rev. Lett.*, **17**, 117 (1966).

## Effects of Solvents on Molecular Complex Formation Equilibria. Use of Nonpolar Analogs for Polar Solutes

by Sherril D. Christian,* Kwang Ok Yeo, and Edwin E. Tucker

*Department of Chemistry, The University of Oklahoma, Norman, Oklahoma 73069 (Received December 31, 1970)*

Recent research from this laboratory has been directed toward elucidating the effects of solvents on reactions of the type $D + A = DA$ where DA is a molecular complex stabilized by electron donor–acceptor interaction between a donor (D) and an acceptor (A) molecule.[1] It has been emphasized that significant progress in our ability to predict the effects of various media on the thermodynamics of complex formation reactions will require improved methods for predicting energies and free energies of transfer of individual D, A, and DA molecules from the ideal gaseous state into the ideal dilute solution state in solvents of interest. The molecules involved in complex formation reactions are often quite polar; unfortunately, current theories of liquids and solutions are generally inadequate for predicting transfer energies and free energies of polar solutes.

We have developed a simple model of dilute solutions of polar solutes in nonpolar solvents which appears to be quite generally applicable to relate energies and free energies of transfer of solutes from the ideal gaseous

(1) (a) S. D. Christian, J. R. Johnson, H. E. Affsprung, and P. J. Kilpatrick, *J. Phys. Chem.*, **70**, 3376 (1966); (b) J. R. Johnson, P. J. Kilpatrick, S. D. Christian, and H. E. Affsprung, *ibid.*, **72**, 3223 (1968); (c) S. D. Christian, A. A. Taha, and B. W. Gash, *Quart. Rev. Chem. Soc.*, **24**, 20 (1970); (d) S. D. Christian, Office of Saline Water Research and Development Progress Report, in press; (e) S. D. Christian and J. Grundnes, *Acta Chem. Scand.*, **22**, 1702 (1968).
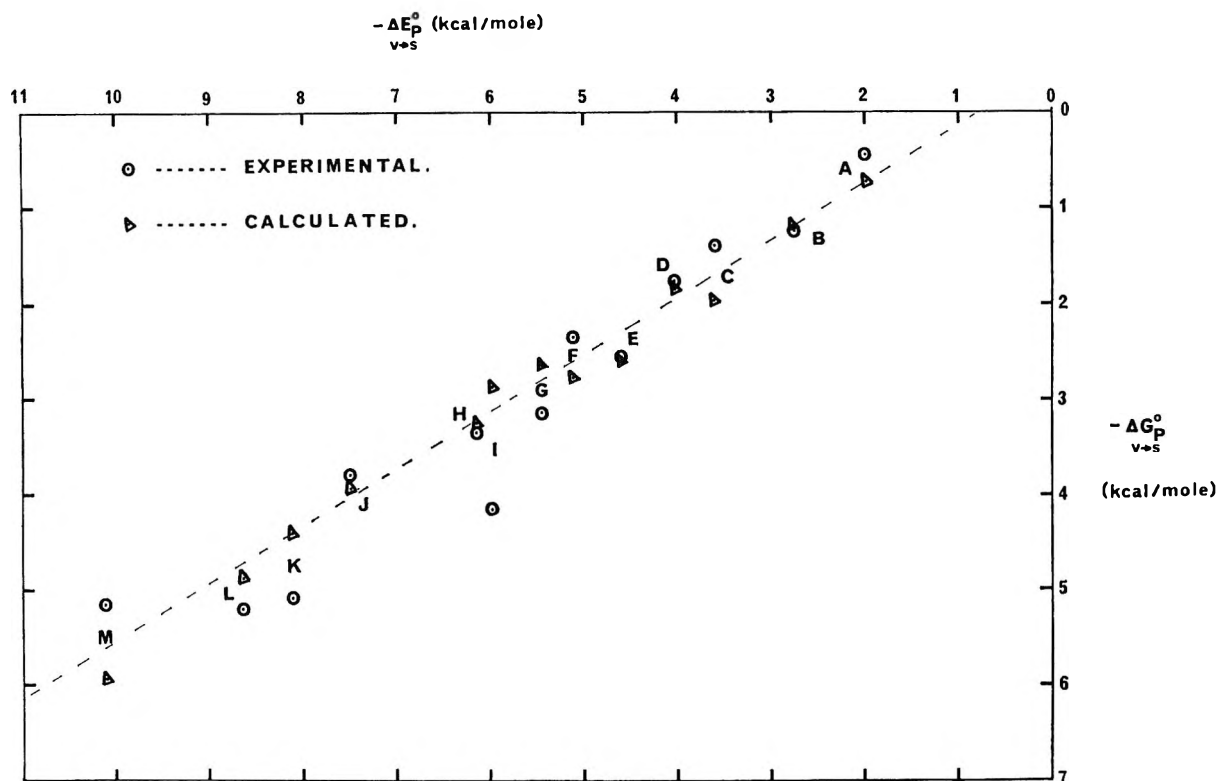
Figure 1. Correlation of energy and free energy of transfer of polar solutes into infinitely dilute solution in nonpolar solvents at 25°; systems: A, water (W) in hexadecane (HX); B, methanol (M) in HX; C, $SO_2$ in heptane (HP); D, W in diphenylmethane (DPM); E, trimethylamine (TMA) in HP; F, M in DPM; G, diethylamine (DEA) in HX; H, DEA in DPM; I, M·DEA in HX; J, W·DEA in HX; K, M·DEA in DPM; L, W·DEA in DPM; M, TMA·$SO_2$ in HP. Data from E. E. Tucker, Ph.D. Dissertation, University of Oklahoma, 1969, and ref 1e.

state into the ideal infinitely dilute solution state. For the purpose of calculating thermodynamic properties, we propose that the polar solute (P) be replaced by a hypothetical molecule which serves as its nonpolar analog (NPA); the NPA molecule is selected to have the same molecular volume and the same total energy of interaction with the solvent as P. We assume that dispersive interactions between the NPA molecule and the nonpolar solvent (S) will contribute to the free energy or entropy of the ideal dilute solution to the same extent as the combined dispersive and inductive interactions between P and S. Implicit in this approach is the assumption that a dilute solution of P in S is not ordered, since the immediate environment of every P molecule consists solely of solvent molecules, with which P interacts via nonspecific van der Waals forces. No attempt is made to relate properties of dilute solutions of P in S to those of pure liquid P, in which orientation effects are important and difficult to handle theoretically.[2]

Although the NPA model is independent of any other model or theory of solutions, it is informative to examine the consequences of employing it together with solubility parameter theory[3] in correlating $\Delta G°_P$ with $\Delta E°_P$ (where these terms represent, respectively, the free energy and energy of transfer of one mole of P from

the ideal gaseous state at unit molarity into the ideal dilute solution in S, also at unit molarity).[1] $\Delta E°_P$ may be equated to the difference between the internal energy change for transferring one mole of NPA from pure liquid NPA into its infinitely dilute state in solvent S and the molar internal energy of vaporization of pure liquid NPA. Applying results from solubility parameter theory (and neglecting volume changes on mixing) this difference may be written $\Delta E°_P = \bar{V}_P(\delta_S - \delta_{NPA})^2 - \delta_{NPA}^2 \bar{V}_P$, from which

$$\delta_{NPA} = \frac{1}{2}\left(\delta_S - \frac{\Delta E°_P}{\delta_S \bar{V}_P}\right) \qquad (1)$$

where $\delta_{NPA}$ and $\delta_S$ are the solubility parameters of the

(2) Various attempts have been made to calculate properties of polar solutions by using models involving the substitution of homomorphic (i.e., geometrically similar) molecules for polar molecules of interest. [Cf. A. Bondi and D. J. Simkin, J. Chem. Phys., 25, 1073 (1956); D. E. Martire and P. Riedl, J. Phys. Chem., 72, 3478 (1968).] Generally the homomorph has been chosen so as to have the same molecular polarizability as the polar molecule, but no permanent dipole. In the present model, the NPA molecule must have a molecular polarizability greater than that of the polar solute in order to compensate for the total interaction of P with the medium through both inductive and dispersive forces.

(3) J. H. Hildebrand, J. M. Prausnitz, and R. L. Scott, "Regular and Related Solutions," Van Nostrand-Reinhold, Princeton, N. J., 1970.

nonpolar analog and the solvent, respectively, and $\bar{V}_P$ and $\bar{V}_S$ are the limiting partial molar volume of P and the molar volume of pure S. Similarly, an expression for $\Delta G^\circ_{P_{v \to s}}$ may be developed by considering the isothermal transfer of the NPA molecule from the ideal gaseous state to the pure liquid state at the equilibrium vapor pressure and then to the ideal dilute solute state in solvent S at unit molarity. This derivation leads to the result

$$\Delta G^\circ_{P_{v \to s}} = \bar{V}_P(\delta_S - \delta_{NPA})^2 + RT \ln (p^\circ_{NPA} \bar{V}_S / RT) \quad (2)$$

where $p^\circ_{NPA}$ is the vapor pressure of pure liquid NPA at the temperature $T$.[4]

Figure 1 shows results of applying eq 1 and 2 to predict $\Delta G^\circ_{P_{v \to s}}$ from $\Delta E^\circ_{P_{v \to s}}$ for various polar donor, acceptor, and complex molecules transferred into nonpolar solvents at 25°. For simplicity, $\bar{V}_P$ for each donor and acceptor has been equated to the molar volume of the pure liquid, and $\bar{V}_P$ for each complex is taken to be the sum of the molar volumes of pure donor and acceptor; moderate changes in $\bar{V}_P$ produce only slight changes in calculated thermodynamic properties. Values of $p^\circ_{NPA}$, in Torr, were obtained from the empirical relation

$$\log p^\circ_{NPA} \text{ (at 25°)} =$$
$$-1.038 \times 10^{-4}(\delta^2_{NPA} \bar{V}_P)^{1.15} + 4.889$$

which provides an excellent fit of vapor pressure data for the nonpolar liquids for which $\delta$ values are available.[3] Calculated and experimental values of $\Delta G^\circ_{P_{v \to s}}$ in general agree to within a few tenths of a kilocalorie; the calculated results are in somewhat better agreement with an empirical linear free energy–energy correlation proposed previously[1e] (represented by the dashed line in Figure 1) than are the experimental values.

Attempts are being made to provide a satisfactory theoretical basis for the NPA model[5] and to apply it conjointly with several theories of nonpolar liquids and solutions. The model is also being used to predict limiting activity coefficients of polar solutes at infinite dilution in nonpolar solvents, referred to the pure polar liquid standard state; this prediction requires merely that experimental thermodynamic properties of the polar liquid be combined with results of calculations based on eq 1 and 2, using known values of $\Delta E^\circ_{P_{v \to s}}$.

(4) Strictly speaking, $p^\circ_{NPA}$ should be replaced by the fugacity of pure liquid NPA, but the effect of this correction on calculated free energies is usually negligible.

(5) R. Frech, unpublished work.

# COMMUNICATIONS TO THE EDITOR

## Modification of Nitrobenzene Photochemistry by Molecular Complexation

*Sir:* One of the intriguing possibilities for photochemists today is the modification of photochemistry *via* inter- or intramolecular perturbations, *i.e.*, protonation, complexation, heavy atom effects, etc. In previous investigations from this laboratory we demonstrated that nitrobenzene in its lowest triplet n,$\pi^*$ state undergoes hydrogen abstraction from isopropyl alcohol and stannane, resulting in the formation of phenylhydroxylamine.[1,2] In the presence of acidic solutions, photoreduction of nitrobenzene and nitronaphthalene is observed, the latter showing no reactivity in alcoholic solutions.[3,4]

In this report we present the results of a novel photochemical process involving nitrobenzene, after formation of the 1:1 donor acceptor complex with $BCl_3$, *i.e.*, $C_6H_5NO_2^{\delta+} \cdot BCl_3^{\delta-}$, in cyclohexane solutions. The complex was prepared by bubbling $BCl_3$ through solutions having known concentrations of nitrobenzene in cyclohexane.[5,6] Photolysis of these solutions does not lead to photoreduction of nitrobenzene, but rather photooxidation to nitrosobenzene is observed. Irradiation of 366 nm of a vacuum degassed cyclohexane solution of $2.5 \times 10^{-2}$ $M$ nitrobenzene complexed

(1) R. Hurley and A. C. Testa, *J. Amer. Chem. Soc.*, **88**, 4330 (1966).

(2) W. Trotter and A. C. Testa, *ibid.*, **90**, 7044 (1968).

(3) R. Hurley and A. C. Testa, *ibid.*, **89**, 6917 (1967).

(4) W. Trotter and A. C. Testa, *J. Phys. Chem.*, **74**, 845 (1970).

(5) H. C. Brown and R. R. Holmes, *J. Amer. Chem. Soc.*, **78**, 2174 (1956).

(6) E. F. Mooney, M. A. Qaseem, and P. H. Winson, *J. Chem. Soc. B*, 224 (1968).

with $BCl_3$ (0.58 $M$) undergoes a photochemical change resulting in formation of a white precipitate and a reddish brown coloration of the solution. The white precipitate was identified by its ir spectrum to be $H_3BO_3$, while disappearance of nitrobenzene is accompanied by the formation of nitrosobenzene. Photolysis after 130 min resulted in 11% disappearance of nitrobenzene, and the quantum yield was determined to be 3.9 $\pm$ 0.3 $\times$ $10^{-2}$, based on polarographic analysis of the remaining nitrobenzene. The identification of nitrosobenzene was made by comparison of its uv spectrum and gas chromatographic behavior with that of an authentic sample. The photochemical process most likely involves oxygen atom transfer from nitrobenzene to $BCl_3$, concomitant with formation of a chlorine atom, which initiates a free radical attack on the solvent, cyclohexane, the source of hydrogen atoms for formation of $H_3BO_3$, to form chlorocyclohexane. The presence of chlorocyclohexane was confirmed by gas chromatography using a 20% Carbowax 20M column. Unphotolyzed solutions could be kept clear for a considerable length of time without any trace of hydrolysis of $BCl_3$. Thus, it is reasonable to consider that electronic excitation results in weakening of the N–O bond and strengthening of the O–B bond of the complex. Nmr studies have shown that the effect of coordination is confined to the nitro group and that one of the two initially equivalent oxygen atoms is the donor.[6] There are no significant new peaks or shifts evident in the absorption spectrum upon complexation, although the 1:1 complex is isolable as a yellow solid. Nitrobenzene in cyclohexane when photolyzed is unreactive, with a hydrogen abstraction quantum yield of $\leq 10^{-4}$; consequently, it is clear that the excited complex is the source of modified photochemistry. The disappearance quantum yield for nitrobenzene increases with $BCl_3$ concentration, as is expected for an equilibrium process involving formation and dissociation of the complex. An alternate interpretation for the observations is that uncomplexed nitrobenzene excited to its lowest singlet or triplet state attacks $BCl_3$; however, we consider this process very unlikely since upon n,$\pi^*$ excitation electron migration within the nitrobenzene molecule results in the nitro group being electron deficient, whereas in the excited state of the complex it is an electron donor. Although

we have previously shown that the triplet state of nitrobenzene is responsible for hydrogen abstraction, it is difficult at present to identify which electronically excited state of the donor–acceptor complex is responsible for this new photochemical reaction.

On the basis of experimental evidence, the following scheme is presented to describe the photochemical process of the electronically excited donor–acceptor complex

$$\left[\begin{array}{c} O \\ \| \quad \delta^+ \quad \delta^- \\ Ph-N-O---BCl_3 \end{array}\right] \xrightarrow{h\nu} \left[\begin{array}{c} O \\ \| \quad \quad \ominus \\ Ph-N---O \rightarrow BCl_3 \\ \oplus \end{array}\right] \longrightarrow$$

$$PhNO + \cdot O\text{-}BCl_2 + Cl\cdot \quad (1)$$

$$Cl\cdot + \langle S \rangle \longrightarrow \langle S \rangle\text{-}Cl + H\cdot \quad (2)$$

$$H\cdot + \cdot O\text{-}BCl_2 \longrightarrow (HO)BCl_2 \quad (3)$$

$$3(HO)BCl_2 \longrightarrow H_3BO_3 + 2BCl_3 \quad (4)$$
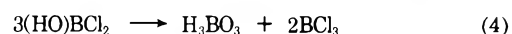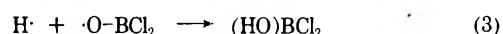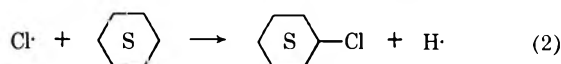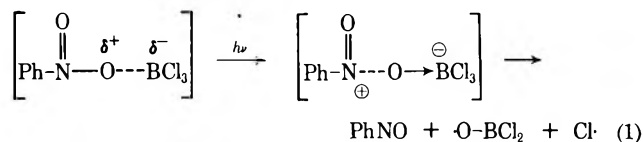
Reaction 2 is a known free radical reaction,[7] while reaction 4 is a known rapid disproportionation reaction in which unsymmetrical boron compounds generally decompose to afford symmetrical products.[8,9]

Since $BCl_3$ is a strong Lewis acid capable of forming donor–acceptor complexes with many aromatic molecules, it becomes interesting to consider the photochemistry of aromatic molecules isolated and when complexed. Further photochemical studies using $BCl_3$ as an acceptor are currently in progress.

(7) W. A. Pryor, "Free Radicals," McGraw-Hill, New York, N. Y., 1966, pp 185–188.
(8) M. F. Lappert, *Chem. Rev.*, **56**, 959 (1956).
(9) W. Gerrard and M. F. Lappert, *ibid.*, **58**, 1087 (1958).

DEPARTMENT OF CHEMISTRY                                W. TROTTER
ST. JOHN'S UNIVERSITY                                   A. C. TESTA*
JAMAICA, NEW YORK   11432

# Journal of Chemical and Engineering Data

## July 1971, Vol. 16, No. 3

## TABLE OF CONTENTS

# Keep pace with the new...

through these basic research journals of the American Chemical Society

## The Journal of the American Chemical Society
The premier American chemistry journal publishing original research papers in every field. Biweekly.

| | | |
|---|---|---|
| *ACS members: U.S. $22.00 | Canada, PUAS $26.50 | Other nations $27.50 |
| Nonmembers: U.S. $44.00 | Canada, PUAS $48.50 | Other nations $49.50 |

## The Journal of Organic Chemistry
Embraces the field, from synthesis to structure to behavior. Biweekly publication.

| | | |
|---|---|---|
| *ACS members: U.S. $20.00 | Canada, PUAS $24.50 | Other nations $25.50 |
| Nonmembers: U.S. $40.00 | Canada, PUAS $44.50 | Other nations $45.50 |

## The Journal of Physical Chemistry
Maintains a balance between classical areas of chemistry and modern structural quantum oriented areas. Biweekly.

| | | |
|---|---|---|
| *ACS members: U.S. $20.00 | Canada, PUAS $24.00 | Other nations $25.00 |
| Nonmembers: U.S. $40.00 | Canada, PUAS $44.00 | Other nations $45.00 |

## Biochemistry
Covers enzymes, proteins, carbohydrates, lipids, nucleic acids and their metabolism, genetics, biosynthesis. Biweekly.

| | | |
|---|---|---|
| *ACS members: U.S. $20.00 | Canada, PUAS $23.00 | Other nations $23.50 |
| Nonmembers: U.S. $40.00 | Canada, PUAS $43.00 | Other nations $43.50 |

## The Journal of Agricultural and Food Chemistry
Places special emphasis on the chemical aspects of agricultural and food chemistry. Bimonthly.

| | | |
|---|---|---|
| *ACS members: U.S. $10.00 | Canada, PUAS $13.00 | Other nations $13.50 |
| Nonmembers: U.S. $20.00 | Canada, PUAS $23.00 | Other nations $23.50 |

## The Journal of Medicinal Chemistry
Emphasis is on synthesis, mode of action and pharmacology of medicinal agents. Monthly.

| | | |
|---|---|---|
| *ACS members: U.S. $15.00 | Canada, PUAS $18.00 | Other nations $18.50 |
| Nonmembers: U.S. $30.00 | Canada, PUAS $33.00 | Other nations $33.50 |

## The Journal of Chemical and Engineering Data
Quarterly journal presenting data on properties and behavior of both new and known chemical systems.

| | | |
|---|---|---|
| *ACS members: U.S. $15.00 | Canada, PUAS $18.00 | Other nations $18.50 |
| Nonmembers: U.S. $30.00 | Canada, PUAS $33.00 | Other nations $33.50 |

## Inorganic Chemistry
Publishes original research, both experimental and theoretical, in all phases of inorganic chemistry.

| | | |
|---|---|---|
| *ACS members: U.S. $18.00 | Canada, PUAS $21.00 | Other nations $21.50 |
| Nonmembers: U.S. $36.00 | Canada, PUAS $39.00 | Other nations $39.50 |

## Macromolecules
Presents original research on all fundamental aspects of polymer chemistry. Bimonthly publication.

| | | |
|---|---|---|
| *ACS members: U.S. $12.00 | Canada, PUAS $15.00 | Other nations $15.50 |
| Nonmembers: U.S. $24.00 | Canada, PUAS $27.00 | Other nations $27.50 |

# Platinum Group Metals and Compounds

ADVANCES IN CHEMISTRY SERIES
NO. 98



Eleven papers from a symposium by the Division of Inorganic Chemistry of the American Chemical Society chaired by U. V. Rao.

What new complexes of the platinum group metals have been synthesized? Here is a collection of papers presenting data on chalcogenides, oxides, nitrido and hydrido complexes, as well as the catalytic properties of these metals and their alloys. Information is included on

- synthesis
- structure
- magnetic susceptibility
- double bond migration

The platinum group metals are considered from the viewpoints of both industry and research. Their magnetic and thermodynamic properties are explored, as well as recent chemistry of $\sigma$- and $\pi$-bonded complexes. Crystal structure is discussed by several authors, with data presented in the form of

- x-ray scattering data
- absorption spectra
- crystal spectra
- infrared spectra
- Mossbauer spectra
- vibrational spectra

165 pages with index. Cloth bound (1971) $9.00 Postpaid in U.S. and Canada; plus 35 cents elsewhere.

Set of L. C. cards with library orders upon request.

Other books in the ADVANCES IN CHEMISTRY SERIES of interest to inorganic chemists include:

**No. 89   Isotope Effects in Chemical Processes**
278 pages      Cloth bound      (1969)      $13.00

**No. 82   Radiation Chemistry — II**
558 pages      Cloth bound      (1968)      $16.00

**No. 81   Radiation Chemistry — I**
616 pages      Cloth bound      (1968)      $16.00

**No. 81 and No. 82 ordered together $30.00**

**No. 78   Literature of Chemical Technology**
732 pages      Cloth bound      (1968)      $17.50

**No. 73   Trace Inorganics in Water**
396 pages      Cloth bound      (1968)      $12.50

**No. 72   Mass Spectrometry in Inorganic Chemistry**
329 pages      Cloth bound      (1968)      $12.00

Order from:
**Special Issues Sales**
**American Chemical Society**
**1155 16th St., N. W.**
**Washington, D. C. 20036**